Design, Synthesis and Studies of Radical and Radical Ion Probes: From Enzyme Investigations to Electroactive Surfactants

DISSERTATION

zur Erlangung des Grades eines Doktors

der Naturwissenschaften

vorgelegt von

Mukul Lal M.Sc.

geb. am 28.Mai 1973 in Hyderabad, Indien.

eingereicht beim Fachbereich 8

der Universität Siegen

Siegen 2004

Gutachter: Prof. Dr. M. Schmittel
Prof. Dr. H. Ihmels

Tag der mündlichen Prüfung: 21-01-2005

urn:nbn:de:hbz:467-1954

Ph. D. Thesis of Mukul Lal

Design, Synthesis and Studies of Radical and Radical Ion Probes: From Enzyme Investigations to Electroactive Surfactants

Abstract

The present work is centered at understanding the mechanistic details of the coenzyme B_{12} dependent enzymes such as diol and glycerol dehydratase that are known to involve radical and radical ionic intermediates in transforming vicinal diols to carbonyl compounds. The work aims on translating such reactive intermediates to relatively long lived ones (making use of beta cleavage leading to persistent radical or electron transfer processes) thereby enabling their spectroscopic detection. A number of modified enzyme substrates attached with groups such as ferrocene, quinone and 2,2,6,6-tetramethylpiperidinoxy were synthesised and were investigated. The efficacies of electrophores to probe radical ions at the active site of the enzyme inherently rely on the electron transfer process. Modulation of the oxidising/reducing property of radical cation/radical anion formed at the active site invariably effects the trapping efficiency of the electrophore. Cyclic voltammetry investigations on the model compounds based on Fuson enols revealed that hydrogen bonding can indeed alter oxidation potentials of enols by up to 500 mV_{Fc} cathodically. The concept was also tested in solution by generating and trapping radical cations in solution via inter as well as intramolecular electron transfer from ferrocene as a donor to enol/enol ether radical cation. Use of stable and reversible redox systems can set a precedent to the development of not only radical ion clocks, they can additionally prove pivotal in areas of nano-technology requiring transfer of small volumes (nano litre range) of solutes in a well defined manner. Thus a couple of redox active compounds were synthesised and investigated for their surfactant property, electrochemical and chemical stability.

Zusammenfassung

Die vorliegende Arbeit beschäftigt sich mit mechanistischen Details der Coenzym B12-abhängigen Enzyme, z.B. Diol- und Glyceroldehydratase. Im Verlauf der Umwandlung vicinaler Diole in Carbonylverbindungen treten Radikale und Radikalionen als Zwischenstufen auf. Es wurde versucht diese reaktiven Zwischenstufen in langlebigere Modelle zu übersetzen, um so spektroskopische Untersuchungen zu ermöglichen. Dabei wurden ß-Spaltungs- und Elektronentransferreaktionen eingesetzt. Zahlreiche modifizierte Enzymsubstrate (mit zusätzlichen Ferrocen-, Chinon- und 2,2,6,6-Tetramethylpiperidinoxy-Substituenten) wurden synthetisiert und untersucht.. Die Wirksamkeit der Elektrophore bei der Untersuchung von Radikalionen im aktiven Zentrum des Enzyms hängt wesentlich vom Elektronentransferprozeß ab. Veränderungen der Oxidations-/Reduktionseigenschaften der gebildeten Radikalkationen/-anionen beeinflussen die Effizienz des Elektroneneinfangs der Elektrophore. CV-Messungen an Modellverbindungen, die auf Fuson Enolen basierten, zeigten, daß Wasserstoffbrückenbindungen die Oxidationspotentiale der Enole bis zu 500 mV_{Fc} kathodisch verschieben. Dieses Konzept wurde auch in Lösung getestet, indem sowohl inter- als auch intramolekularer Elektronentransfer von Ferrocen zu Enol- bzw. Enolether-Radikalkationen untersucht wurde. Die Verwendung von stabilen reversiblen Redoxsystemen kann eine Schlüsselfunktion in der Nanotechnologie einnehmen, wenn es um den Transfer kleinster Flüssigkeitsvolumina (Nanoliter-Maßstab) geht. Daher wurden einige redoxaktive Verbindungen hergestellt und ihre Oberflächeneigenschaften sowie ihre elektrochemische und chemische Stabilität untersucht.

For Ritika

The Present work was carried out under the guidance of

Prof. Dr. Michael Schmittel

I take the present opportunity to extend my sincere and deepest gratitude to Prof. Dr. M. Schmittel for providing me an opportunity to carry out the present work under his expertise. I would also like to thank him for the constant encouragement that I had received from him all throughout this work.

I would also like to thank Dr. Demuth, Ms. Hatzig and Mr. Bodenstedt for providing technical assistance throughout this work. I would also like to thank Prof. B. Schink, Britta Müller from University of Konstanz (phenoxyethanol dehydratase) and Prof. J. Rétey, C. Weber (diol and glycerol dehydratase) for their help in enzymatic investigations. I would like to thank Prof. G. Bucher from University of Bochum for LFP investigations. It gives me a pleasure to thank Dr. T. Mukherjee and Dr. S. Adhikari from BARC (India) for pulse radiolysis investigations.

I thank the group members, W. Henn, V. Kalsani, R. Kishore, Atul Mahajan, H. Lin, B. He and V. Chandrasekhar for all the help that they have extended during this work. I would also like to thank Ms. U. Ulrike for the help that she had extended to me throughout this work. I would also like to thank Hisham and Deena for correcting the manuscript.

I would like to thank my parents, Dr. Mani Lal and Dr. Asha Rani. I am very much obliged to my parents-in-law, Mr. Anil Marathe and Mrs. Vrishali Marathe for their constant support in all ways.

Finally I would like to thank my wife Rupali Lal for her constant support and encouragement during the research.

Publications

1) M. Lal, A. Langels, H.-J. Deiseroth, J. Schlirf, M. Schmittel, The Role of Hydrogen Bonding in the Oxidation Potential of Enols, *J. Phys. Org. Chem.* **2003**, 16, 373-379.

2) M. Schmittel, M. Lal, M. Schlosser, H.-J. Deiseroth, Unusual ladder like supramolecular arrangement by cooperative effect of bifurcated O-H…O hydrogen bonding in crystals of racemic 4-ferrocenylbutan-1,2-diol, *CrystEngComm.* **2003**, 5, 294-299.

3) M. Schmittel, M. Lal, W. A. Schenk, M. Hagel, N. Burzlaff, A. Langels, Synthesis and One-Electron Oxidation Chemistry of Stable ß,ß-Dimesityl Enols with Heteroaryl Substituents, *Z. Naturforschg. B* **2003**, 58b, 877-884.

4) M. Schmittel, M. Lal, M. Schlosser, H.-J. Deiseroth, A Supramolecular Ladder Motif in 2-(2,2,6,6-Tetramethylpiperidin-1-yloxy)propane-1,3-diol, *Acta Cryst. C* **2004**, C60, o589-o591.

5) M. Schmittel, M. Lal, K.-H. Graf, I. Suske, N,N'-Dimethyl-2,3-dialkylpyrazinium Salts as Redox-Switchable Surfactants? Redox, Spectral, EPR and Surfactant Properties, *Chem. Commun*. **2005**, *45*, 5650-5652.

Manuscript in Preparation

6) M. Schmittel, M. Lal, R. Lal, M. Röck, A. Langels, Z. Rappoport, J. Schlirf, H.-J. Deiseroth, M. Keller, G. Gescheidt, U. Flörke, A Comprehensive picture of the one-electron oxidation chemistry of enols, enolates and α-carbonyl radicals-Oxidation potentials and characterisation of radical intermediates.

7) M. Schmittel, M. Lal, G. Bucher, Ferrocene as reporter molecule of enol radical cations in solution.

8) M. Schmittel, M. Lal, J. Schlirf, H.-J. Deiseroth, Non-covalent interaction motifs in the crystal structure of β,β-dimesitylenols with heterocylic substituents.

9) M. Schmittel, M. Lal, M. Schlosser, H.-J. Deiseroth, Crystal structure of diethyl-2-methyl-2-(2,2,6,6-tetramethyl-piperidin-1-yloxy)malonate.

Poster presentations

1) "*Design and synthesis of substrates to probe radical and radical ionic intermediates in coenzyme B_{12} dependent enzymes such as diol and glycerol dehydratase*"-Postgraduate Winter School on Organic Reactivity-WISOR, Bressanone, Jan., **2003**.

2) "*Design and synthesis of substrates to probe radical and radical ionic intermediates in coenzyme B_{12} dependent enzymes such as diol and glycerol dehydratase*"-Gordon Research Conference on "Free Radical Reactions", New-Hampshire, July, **2003**.

3) "*Design and synthesis of substrates to probe radical and radical ionic intermediates in coenzyme B_{12} dependent enzymes such as diol and glycerol dehydratase*"-6th International Symposium of the Volkswagen-Stiftung on Intra- and Intermolecular Electron Transfer, Köln, Oct. 29-Nov. 1, **2003**.

4) "*Design and synthesis and studies of 2,3-disubstituted pyrazinium tetrafluoroborates-towards redox modulated surfactants*"-6th International Symposium of the Volkswagen-Stiftung on Intra- and Intermolecular Electron Transfer, Köln, Oct. 29-Nov. 1, **2003**.

Abbreviations Used

Abs	Absorbance
Ad	Adenosyl
B3LYP	Becke Lee Yang Parr
BuLi	*t*-Butyl lithium
BP	Boiling Point
CIDNP	Chemically Induced Dynamic Nuclear Polarisation
DABCO	1,4-Diazbicyclo[2,2,2]octan
DCM	Dichloromethane
DFT	Density Functional Theory
DMAP	4-*N*,*N*-Dimethylaminopyridine
DME	Dimethoxyethane
DMF	Dimethyl formamide
DMSO	Dimethyl sulfoxide
E. coli	*Escherichia coli*
Eq.	Equivalents
EPR	Electron Pair Resonance Spectroscopy
ESI-MS	ElectroSpray Ionisation Mass Spectroscopy
ESR	Electron Spin Resonance Spectroscopy
Fc	Ferrocene
HOMO	Highest Occupied Molecular Orbital
HPLC	High Performance Liquid Chromatography
HRMS	High Resolution Mass Spectrometry
IR	Infrared Spectrometry
KIE	Kinetic Isotope Effects
LAH	Lithium aluminium hydride
LDA	Lithium diisopropylamide
LFP	Laser Flash Photolysis
LUMO	Lowest Occupied Molecular Orbital
MCPBA	m-Chloroperoxybenzoic acid
MO	Molecular Orbital
MP	Melting Point
Pd-C	Palladium-Carbon
PTOC	Pyridine-thione carboxylic acid

RNR	Ribonucleotide Reductases
S_N2	Nucleophilic Substitution
SOMO	Singly Occupied Molecular Orbital
SPh	Thiophenyl
TBAP	Tetra-(*n*-butyl) ammonium hexafluoro phosphate
TPBA	*tris*-(4-Bromophenyl)-aminium hexachloroantimonate
TEMPO	2,2,6,6-Tetramethyl-piperidin-1-yloxy radical
TFA	Trifluoroacetic acid
THF	Tetrahydrofuran
TIM	Triose-Phosphate Isomerase
TMSCl	Trimethylsilylchloride

Index

Summary

Radical and radical ions are important reactive intermediates frequently encountered in chemical as well as biological transformations. Intermediacy of such reactive intermediates in chemical systems can be established by various methods ranging from chemical methods (kinetic investigations, employing radical clocks etc.), spectroscopic investigations (UV-Vis, EPR and mass spectrometry) to theoretical methods. Establishing the intermediacy of radical and radical ions in biological systems is a big challange. However, in many instances the above techniques while providing useful insights, fail to give conclusive evidence primarily due to the fleeting existence of radical and radical ions at the active site of the enzymes.

The present work was mainly aimed at scrutinising the mechanistic details of coenzyme B_{12} dependent enzymes and ether-bond cleaving enzymes. All these enzymes employ a protein based radical in their catalytic cycle. Additionally, application of stable radical ion forming compounds were synthesised and investigated for their probable application in modulating surface wetting properties for nanotechnology application.

Radical and Radical Ion Probes for Enzymatic Investigations

Coenzyme B_{12} dependent enzymes such as diol, glycerol dehydratase and ribonucleotide reductases and some ether-bond cleaving enzymes (phenoxyethanol dehydratase) are known to carry out transformation of vicinal diols (α-hydroxyethers) into their corresponding carbonyl derivatives.

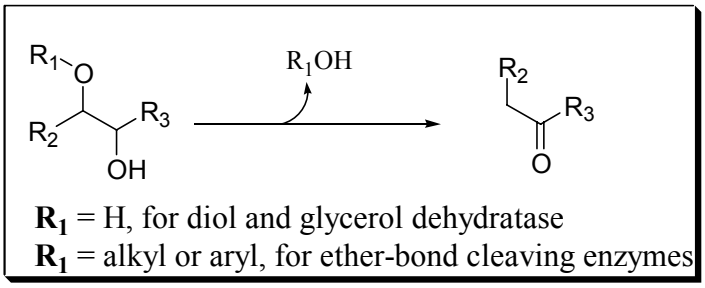

R_1 = H, for diol and glycerol dehydratase
R_1 = alkyl or aryl, for ether-bond cleaving enzymes

A large diversity exists in these enzymes, both in their distribution in biological systems and the substrate requirements. However, a common mechanistic scheme is thought to be operative in these enzymes. The transformation in these enzymes is initiated by a hydrogen atom abstraction from the subsrate, which is then (by unknown reactions) transformed into the product radical. The product radical reabstracts the hydrogen atom thereby regenerating the active enzyme (Scheme I).

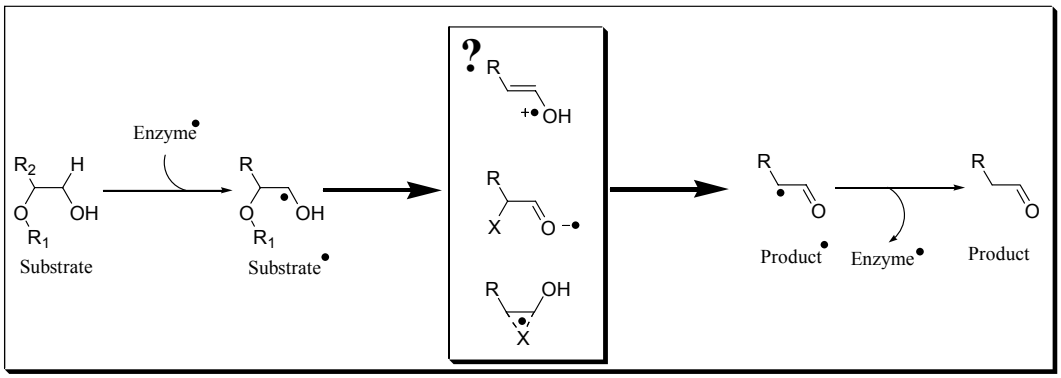

Scheme I: General accepted mechanism for the eliminase reaction carried out by diol, glycerol and phenoxyethanol dehydratase.

The transformation of the substrate radical to product radical is still not well understood but has drawn immense interest. However, the various reactive intermediates invoked during the transformation of the substrate radical to the product radical range from radical ions to neutral radicals.

Conceptual basis of the present work was to utilise the reactivity patterns of these reactive intermediates to detect them directly at the active site of the enzyme. Since radical ions are strong oxidants (radical cation) or strong reductants (radical anion), the short-lived radical ions can be investigated directly at the active site of the enzymes by translating them into long-lived ones by an intramolecular electron transfer process. Similarly, for probing neutral radicals the concept was to translate such reactive radicals into relatively long-lived or persistent ones directly at the active site. The above concept has the advantage in the fact that it would allow for a direct detection of reactive intermediates at the active site of the enzyme, additionally long-lived radical and radical ions could be investigated by simple spectroscopic methods such as UV-Vis and EPR spectrocopy.

To start with we chose to investigate the mechanistic details of phenoxyethanol dehydratase, however, the concept could be applied to various other enzymes. Phenoxyethanol dehydratase was chosen since this enzyme is known to accept bulky substrate such as low molecular weight PEG´s. Secondly the microorganism from which it was extracted also contained the other coenzyme B_{12}-dependent enzymes such as diol and glycerol dehydratase. However, the enzyme was not available in pure form, hence we also investigated the electronic and hydrophobic tolerance of the enzyme by synthesising a number of phenoxyethanol derivatives.

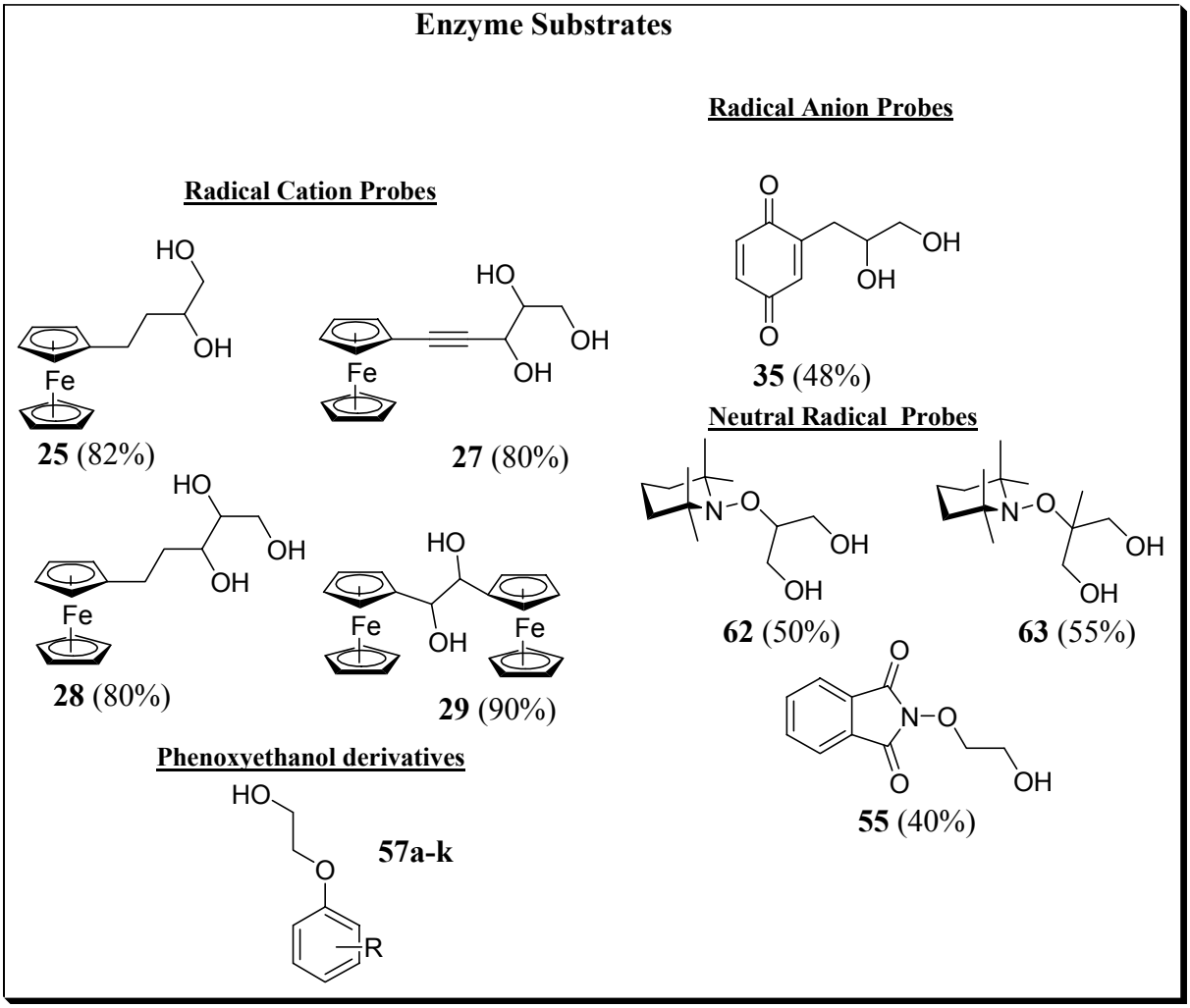

A number of radical, radical ion probes and phenoxyethanol derivatives were synthesised and investigated. The enzymes used were pure diol and glycerol dehydratase expressed in *E. Coli*. and cell free extract of phenoxyethanol dehydratase. None of the radical and radical ion probes were accepted by diol and glycerol dehydratase. Among the various radical and radical ion probes only radical cation probe **25** was found to have an inhibitory effect on the phenoxyethanol dehydratase. Kinetic investigations revealed that the inhibitory effect was mainly due to irreversible tight binding of the substrate **25** to the enzyme.

Investigations on phenoxyethanol dehydratase with various phenoxyethanol derivatives **57a-h** provided important insights into the mechanistic details of the enzymatic transformation. All phenoxyethanol derivatives showed low activity when compared with the phenoxyethanol, which is the natural substrate. Interestingly the 4-bromo derivative (**57h**) showed the highest activity (14%). 4-Methoxy derivative (**57j**), 2,6-dimethyl (**57a**) and 2-*tert*-butylphenoxyethanol (**57g**) showed similar activity ~4-8%.

The above results are in stark disagreement with the proposed radical anion mechanism based on investigations by Schink *et. al*. Based on the stereochemcial considerations and the results from the enzymatic investigations with **57a-h** it was concluded that a radical ionic pathway

would require an additional step of recombination of the phenolate to the product derived radical which after hydrogen atom abtraction and hydrolysis yields the product.

Translating Short-Lived Radical Cations into Long-Lived Ones in Solution

The concept was tested in solution by initially trapping an enol radical cation (**E1**$^{+\bullet}$) with ferrocene as the donor with a $k_{ET} = 10^7$ s^{-1}. Barton ester **75** was synthesised to generate ethenol radical cation in solution under mild conditions. **75** upon photolysis in the presence of TFA and ferrocene gave a long absorbing species at around $\lambda_{max} = 620$ nm, which is a band characteristic for ferrocenium ion. HPLC investigation for the product analysis indicates that the formation of **99** (an expected rearranged product) decreased by 30% in presence of TFA. The initial radical **104** formed after decarboxylation was characterised by TR-EPR. LFP experiments on **75** in presence of TFA do indicate the formation of a strong oxidant, which was assigned to **105** (ethenol radical cation) based on the $\lambda_{max} = 305$ nm obtained in the transient spectrum and which was close to the theoretical spectrum $\lambda_{max} = 315$ nm, calculated by density functional theory (B3LYP/ 6-31g**).

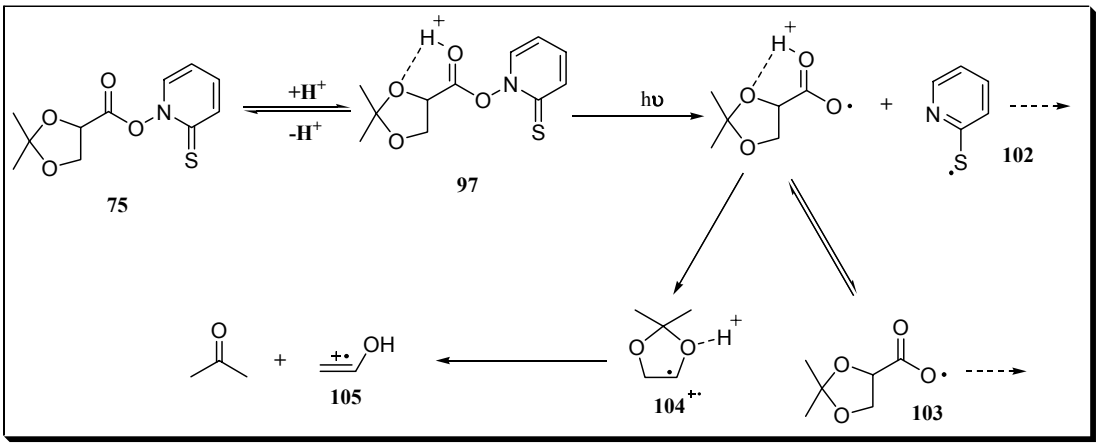

Mimicking the eliminase reaction with the diol **25** attached with a ferrocene as the donor. was carried out by pulse radiolysis method. Pulse radiolysis of **25** indeed showed the formation of ferrocenium ion in the transient spectrum at ~ 620 nm. The formation constant for the formation of ferrocenium ion was found to be $k_{ET} = 8.5 \times 10^{10}$ s^{-1}. Thus, the intramolecular electron transfer process was found to be 1000 times faster than the intermolecular electron transfer.

Design, Synthesis and Cyclic Voltammetric Investigation of β,β-Dimesityl Enols

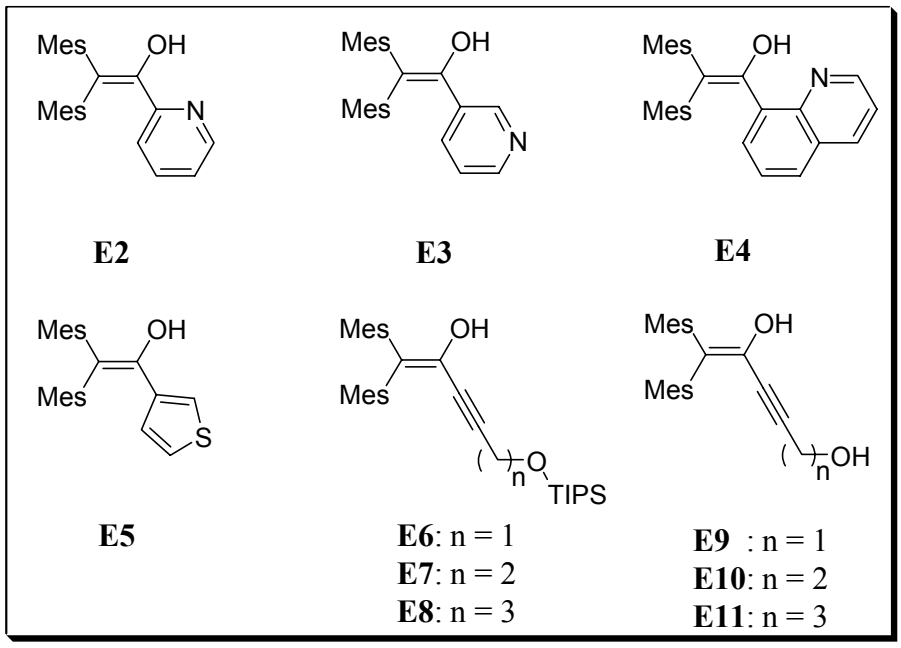

β,β-Dimesityl enols **E2**-**E4** were synthesised to investigate the effect of hydrogen bonding on the oxidation potential of enols. As expected all the three enols showed N···HO type of hydrogen bonding in solution as well as in the solid state. In solution **E2** and **E4** showed intramolecular hydrogen bonding via five and six membered rings respectively. Solvent dependence studies and UV-Vis spectroscopic investigations showed a partial proton transfer in **E4**. In **E3**, as expected only intermolecular hydrogen bonding was observed both in solution and in the solid state. Cyclic voltammetric investigations revealed that hydrogen bonding could shift the oxidation potentials of enols by almost 500 mV. This also suggests that the enol radical cations formed by such hydrogen bonded enols would be much weaker oxidants than expected.

β,β-Dimesityl enol **E5** was synthesised to study the effect of 5-membered heterocycle in the α-position. Cyclic voltammetric investigations (cathodic shift of the oxidation wave) coupled with UV-Vis and ^{1}H-NMR spectroscopic investigations revealed that presence of a 5-membered heterocycle in the α-position of β,β-dimesityl enols stabilises the carbocation formed after oxidation.

A number of β,β-dimesityl enols containing propargyl alcohol and homologs in the α-position were synthesised and their cyclic voltammetric behaviour was investigated. Enols **E9** and **E10** showed the normal behaviour for a β,β-dimesityl enol while enol **E11** showed an unusual behaviour where in a 5-exodig mode of cation stabilisation was observed. This was further confirmed by synthesis of **E12** where in the alcoholic OH group was converted to an ester

showing the normal behaviour.

Enolates of all the enols were generated and their cyclic voltammetric investigations were carried out. It was found that the enolates showed a completely reversible wave, which was cathodically shifted by 1-1.5 V compared to the enols. Oxidation wave for the α-carbonyl radicals was also observed in majority of the enols. Since α-carbonyl radicals are one of the potential reactive intermediates in conenzyme B_{12} dependent enzymes and a number of other flavin dependent enzymes, it was found essential to determine the oxidation potentials of some biologically relavent α-carbonyl radicals. However, simple carbonyl compounds usually are in their *oxo* form under normal conditions, hence we went on to develop a correlation between the adiabatic ionisation potentials of carbon centered radicals (after solvent correction) *vs* the oxidation potential of these carbon centered radicals in solution. A good linear correlation was obtained with a correlation coefficient of 0.97. This correlation was then used to predict the oxidation potentials of a number of important α-carbonyl radical.

Interestingly it was found that the oxidation potentials of hydrated form of α-carbonyl radicals are much lower in oxidation than their non hydrated forms. Thus, the hydrogen atom abstraction by the product derived radical in coenzyme B_{12} and ether-bond cleaving enzymes must be occuring in the hydrated form.

Design, Synthesis and Studies of Electroactive Surfactants for Modulation of Surface Wetting Properties

Wetting phenomenon is observed in our day-to-day life and in recent times has found wide application in moving small volumes of liquid on a surface popularly known as "microfluidics". While electroactive surfactants have previously been synthesised and studied, however, the investigations were restricted to understand the dynamics of the micellisation. Our objective was to design and investigate novel electroactive surfactants having both chemical as well as electrochemical stability. Thus a number of 1,4-dimethyl-2,3-dialkylpyrazinium tetrafluoroborates (**167a-d**) and ferrocene based surfactants (**172-174**) were designed, synthesised and investigated.

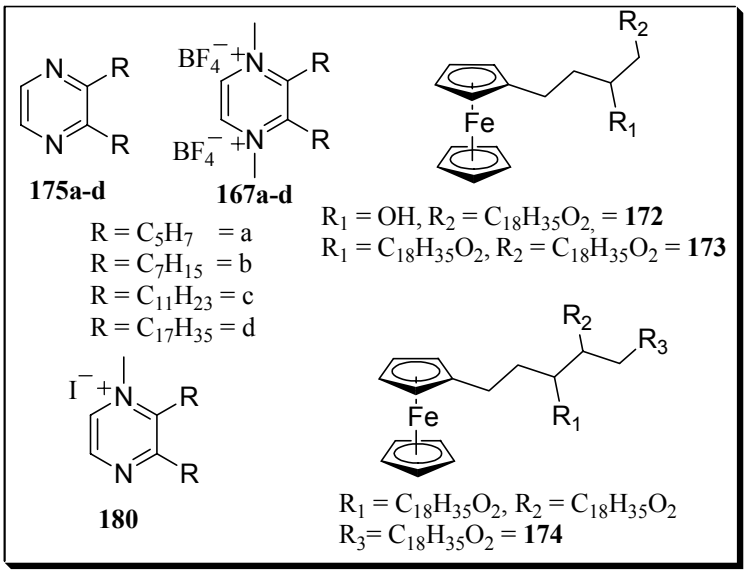

Cyclic voltammetric investigations in acetonitrile and dichloromethane showed two completely reversible waves for **167a-d**. Upon addition of 2000 eq. of water to **167b** the second wave completely disappeared. The first wave showed a small 70 mV cathodic shift. This wave was completely reversible and showed a $E_{rev}C_{cat}$ electrode kinetics determined by Nicholson-Shain criteria. UV-Vis investigations showed that upon addition of water to a solution of **167b** an immediate colour change was observed and the colour darkened with time (in line with the literature report). However, for the first time it was shown that product formed (characterised and compared with the authentic sample by ^{1}H-NMR) after addition of water to these pyrazinium salts are the diketones, formed after hydrolysis. It was also found that the 1,4-dimethyl-2,3-dialkylpyrazinium tetrafluorobotrates when stored in strongly acidic solution (pH = 2) were not attacked by water. The radical cations of **167c-d** were also investigated by EPR spectroscopy.

Langmuir-Blodgett film balance experiments were carried out on **175d**, **167d** and **180**. To our expectation only **180** showed a stable thin-film forming behaviour, while **167d** showed an unusual behaviour, which could be explained to the degradation of the sample on the trough.

1 Introduction

1.1 Mechanistic Investigations on Coenzyme B_{12}-Dependent Enzymes

Enzymes are proteins that are required for all metabolic activity in a living cell (both plants and animals). They are biocatalysts and carry out various transformations by providing an alternative pathway requiring a low activation barrier (Figure 1–1). The transformations carried out by enzymes range from redox reactions,[1] substitution reactions,[2] to eliminations[3] etc.

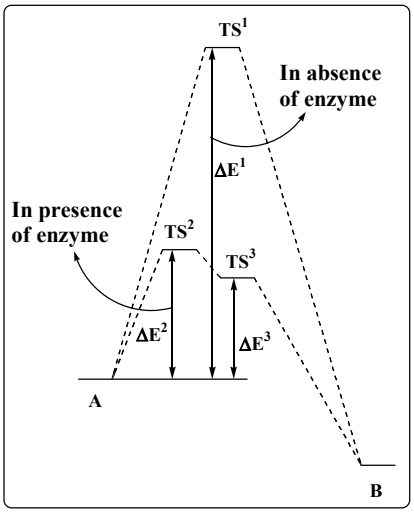

Figure 1–1: A simplified schematic representation of enzyme catalysed and uncatalysed reactions.

The ease with which enzymes carry out such wide range of transformations in aqueous media (cytosol in cells) is attributed to its micro-environments, popularly known as the "*active site"*. The active site of the enzymes plays a vital role in the catalytic cycle by providing appropriate stabilisation to the reactant, transition state/intermediate and the product.

While radicals are reactive odd-electron intermediates of growing importance in enzymatic catalysis[4], radical enzymes are a class of enzymes utilising stable or transient radicals in their catalytic cycle. Usually such enzymes require a metallic cofactor (transition metals) as radical reservoir,[5] such as cobalt in coenzyme B_{12} dependent enzymes (such as diol dehydratase, glycerol dehydratase, ribonucleotide reductase, glutamine mutases etc), iron[5b] (cytochrome P-450 enzymes, lipoxygenases[5d]) and copper in galactose oxidase.[5c]

The classical organic radicals encountered in biochemistry are the resonance-stabilised semiquinone radicals of flavin and coenzyme Q. These flavin types of organic radicals facilitate one-electron transfer reactions of oxygen and metals in the electron-transport chain of living cells. However, there are many enzymatic reactions known, involving radical

intermediates other than the semiquinone radicals that involve rearrangements or eliminations. Such enzymes, in which unreactive C-H bonds are cleaved, employ stable protein-based radicals.[6] The most common of these reactions are the adenosylcobalamin dependent rearrangements,[5a] and cytochrome P-450 dependent monooxygenations of hydrocarbons.

1.2 Charged Radicals

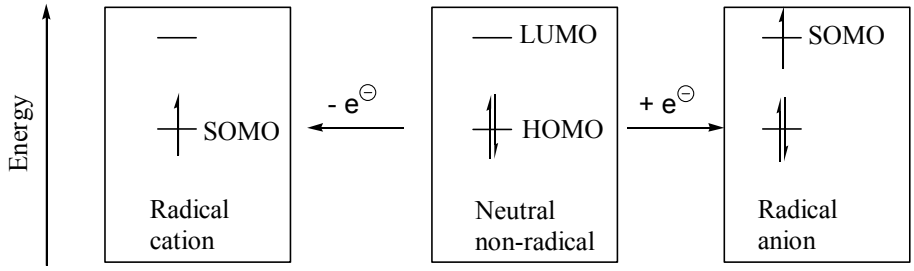

Scheme 1–1: One-electron-transfer reduction and oxidation of neutral non-radical compounds to radical ions.

Although the intermediacy of radical and ionic species can be established in solution, proof of intermediacy of radicals (radical clocks), especially radical ions, in biological systems pose a very big challenge. Unlike their neutral counterparts, radical ions are odd electron species with a positive or negative charge that are called radical cations or radical anions. Radical ions are usually generated by one-electron oxidation or reduction processes starting from neutral compounds. For radical cations an electron is lost from the highest occupied molecular orbital (HOMO) (Scheme 1–1), and in radical anions an electron is accepted in the lowest unoccupied molecular orbital (LUMO) of a neutral non-radical precursor. A simple MO picture suggests that the two radical-ion intermediates should share some common features that will determine their chemical fate:[7]

a) Both species carry an unpaired electron and a charge; hence they will behave either as nucleophiles or electrophiles or likewise as radicals.

b) By electron injection into an antibonding orbital or electron removal from the bonding orbital characteristic bonds are weakened; as a consequence a plethora of bond cleavage processes are typical for both radical anions and cations.

Some of the chemical reactions that involve radical anions include the reduction of aromatics or carbonyls with metals such as sodium or potassium (pinacol coupling, acyloin condensation, Bouveault-Blanc reduction).[8] In organic synthesis, radical cations are encountered during the oxidation of aromatic compounds in presence of oxidising metal ions such as Mn(III), Co(III), or Ag(II). They are also generated by electron impact in mass spectrometry. Radical cations or radical anions can also be formed by the addition of a radical

to a cation or an anion (Scheme 1–2).

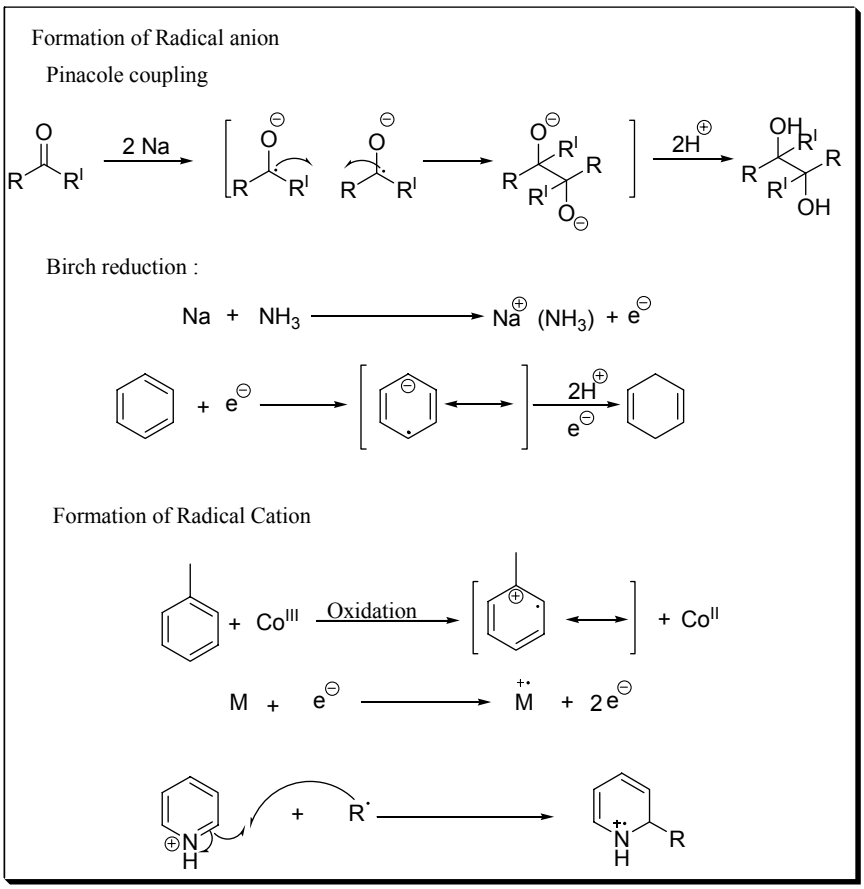

Scheme 1–2: Examples of radical ions in Organic transformations.

Interestingly, radical ions have also been postulated in important biological transformations carried out by certain enzymes.[4,5,6] The most extensively investigated radical enzyme processes include adenosylcobalamin dependent rearrangements and eliminations, such as ribonucleotides to deoxyribonucleotides by ribonucleotide reductases.

Diol dehydratase is one such enzyme, which is mechanistically related to ribonucleotide reductase, and carries out fermentation of vicinal alcohols to their aldehyde equivalents, via radical or radical ion intermediate.

2 Radical Enzymes

2.1 Present State of Knowledge

2.1.1 Ribonucleotide Reductase

Ribonucleotide reductases (RNR) are a class of adenosylcobalamin dependent anaerobic enzymes catalysing the reduction of ribonucleotides to deoxyribonucleotides in DNA biosynthesis (Scheme 2–1), thus playing a key role in nucleic acid metabolism.

They are abundant in all living cells and produce four deoxyribonucleotides required for DNA replication and repair.[9] One of the interesting features of the RNR´s is that they all use a protein free radical to activate the substrate.

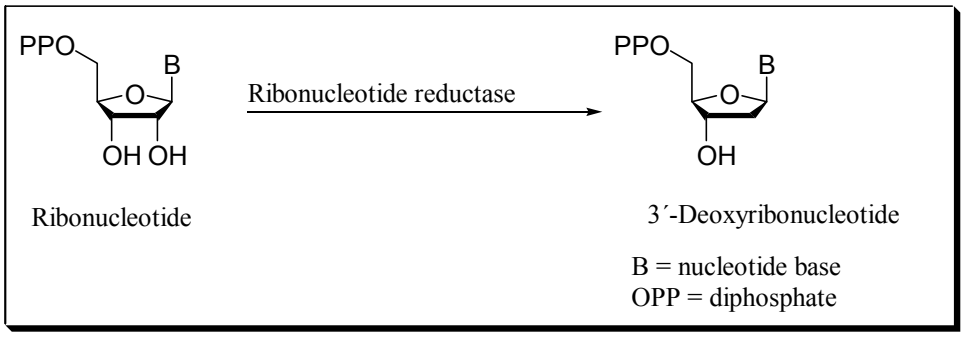

Scheme 2–1: Transformation of ribonucleotide to deoxyribonucleotide by RNR.

2.1.1.1 Classification

Ribonucleotide reductases have been classified[6] (Figure 2–1) into four classes based on the cofactors essential for catalysis:

Class I reductases, being found in eukaryotes, eukaryotic viruses, eubacteria, and bacteriophages, require oxygen for the radical generation. They use only nucleo-diphosphates as substrates and possess a stable tyrosyl substituent adjacent to a diferric cluster (Reichard[10]).

Class II reductases have been found in eubacteria, archaebacteria and bacteriophages, and can utilise both nucleo-triphosphates and diphosphates as substrates. The holoenzyme is a α_2 protein and requires adenosylcobalamin (Blakley[11] and Beck[12]) as cofactor. Since the initial formation of radical starts by homolysis of cobalt-carbon bond of adenosylcobalamin, the reaction is neither dependent nor sensitive to oxygen, hence they are found in both aerobic and anaerobic organisms.

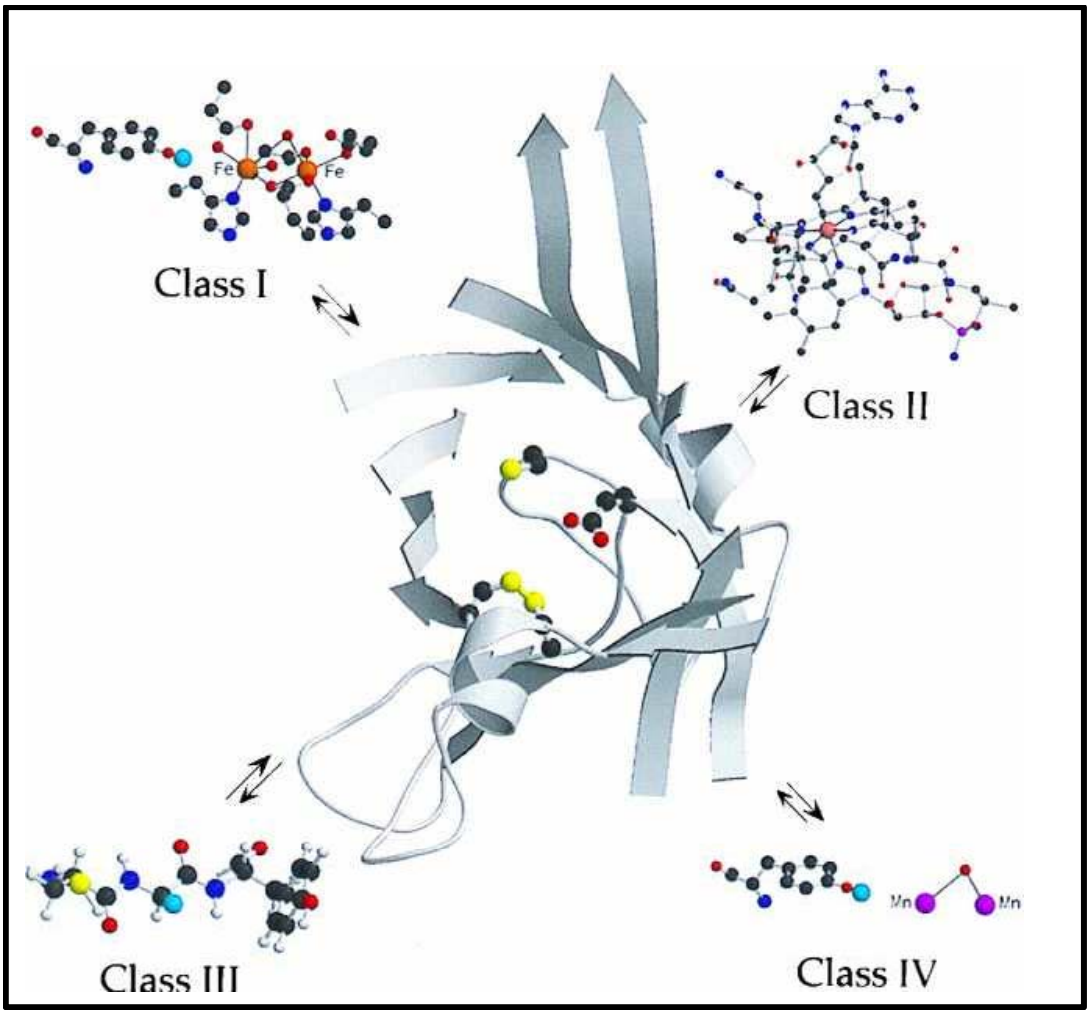

Figure 2–1: Classification of ribonucleotide reductases based on the cofactor.[9b]

Class III reductases found in eubacteria, archaebacteria and bacteriophages (Fontecave, Eliasson and Reichard[13]) are similar to Class I in the fact that the holoenzyme is a $\alpha_2\beta_2$ protein. They are very sensitive to oxygen and hence found only in prokaryotes. They utilise only nucleo-triphosphate as substrates and have a glycyl and a FeS cluster as the radical source in the R2 subunit.

Class IV reductases[14] possess a putative dimanganese cluster and a tyrosyl group.

2.1.1.2 Mode of Action

Despite dramatic differences in structure and cofactor requirements, Stubbe (Scheme 2–2) postulated a common mechanistic scheme for all ribonucleotide reductases.[6] The cascade mechanism involves a hydrogen atom abstraction from the 3′-position of the substrate by thiyl radical (C439). The subsequent elimination of the 2′-hydroxyl group as water occurs along with deprotonation of the 3′-hydroxyl leading to **1**.[15]

Alternatively, it may involve a radical cation or anion (i.e., general acid or general base catalysis respectively).[16] Reduction of the intermediate α-carbonyl radical **1** via oxidation of

two cysteines (C462 and C225) to the corresponding disulfide generates a 3´-deoxynucleotide radical **2**. Finally, the originally removed hydrogen atom from the cysteine (C439) is re-abstracted by **2** providing the product and regenerating the thiyl radical (C439). The above working model was a result of extensive investigations supported by biochemical studies,[17] use of mechanism based inhibitors,[18] side directed mutagenesis,[19,20] model studies in solutions (Giese),[21] and crystallographic studies.[22]

2.1.1.3 Biomimetic and Theoretical Modelling Studies

The mechanism of the RNR catalysed reduction of ribonucleotides to the corresponding deoxyribonucleotides with its unusual interplay of homolytic and heterolytic bond cleavage steps is still a subject of controversy. Theoretical studies by Siegbahn[23] suggest involvement of only neutral radicals in the entire conversion, with the oxaallyl radical (**1**) (Scheme 2–2) as the most stable (stabilised by -10.7 kcal/mol) of all the radicals formed in the reduction sequence. The overall conversion was exothermic by 18.9 kcal/mol.

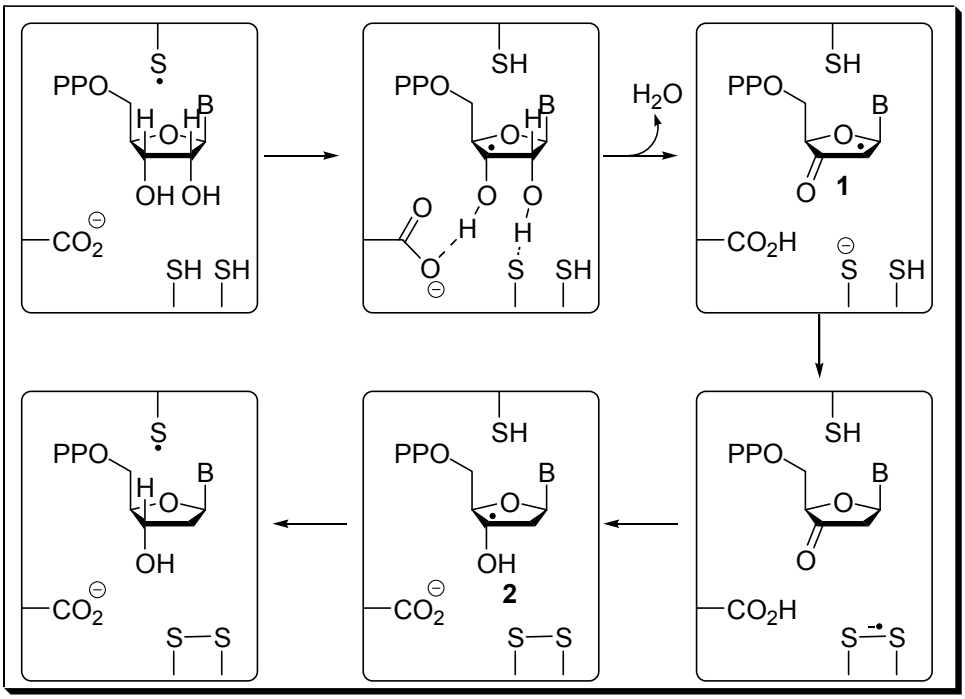

Scheme 2–2: Mechanism proposed for the enzymatic conversion of ribonucleotide reduction to deoxyribonucleotide.[6]

A very conclusive mechanistic study by Giese[21] using 3´-selenocarbonyl nucleotides favour base catalysis involving radical anion intermediates, proved by product distribution and kinetic data (Scheme 2–3). The key argument in favour of the base catalysis is the large pK_a value difference between **3** and **4**, favouring the deprotonation of **3→5** and not the protonation of **3→4**. Presence of a Glutamate 441 in the active site of the enzyme favours this

observation. The overall rate for base catalysis was found to be $k_{cat} \approx 10^6$ M^{-1} s^{-1}. Theoretical studies by Zipse[24] favour a base catalysed concerted loss of a water molecule in ribonucleotide reduction.

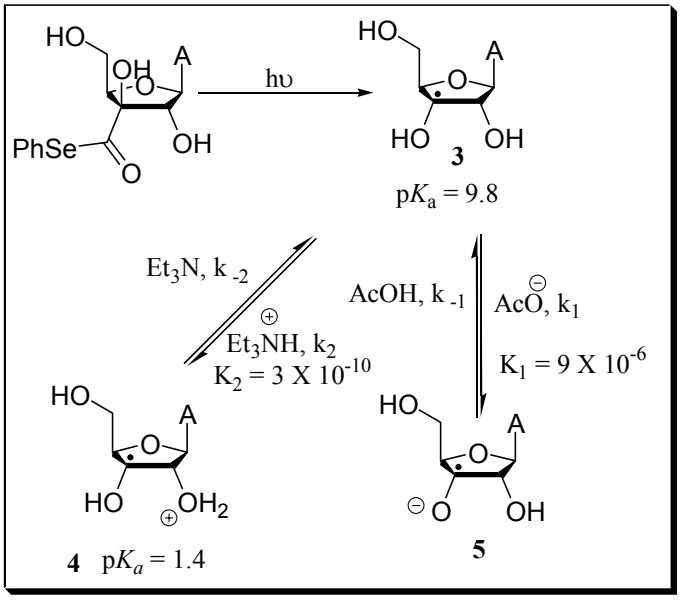

Scheme 2–3: Model studies favouring the general base catalysis involved in ribonucleotide reduction.[21]

2.1.2 Diol Dehydratase

Since the isolation of Vitamin B_{12} in 1947 by Folkers,[25] it has been found to serve as a cofactor in many enzymatic reactions, which include carbon skeleton rearrangements, heteroatom eliminations[26] and intramolecular amino group migrations.[27] Diol dehydratase is one such enzyme that depends on Vitamin B_{12} for its catalytic activity.[28] The enzyme catalyzes the dehydration of short-chain vicinal diols to the corresponding carbonyl derivatives (Scheme 2–4). The enzyme is produced by some genera of Enterobacteriaceae, e.g. *Klebsiella*[29] and *Citrobacter*[30]. The physiological role of the enzyme is to transform vicinal diols (1,2-propanediol, 1,2-ethanediol) or triols (glycerol) into aldehydes or β-hydroxyaldehydes. The aldehydes formed serve as metabolic intermediates in the fermentation process as well as electron acceptors.

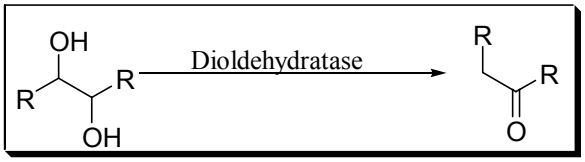

Scheme 2–4: General transformation carried out by the enzyme diol dehydratase.

2.1.2.1 Active Site Description and Binding of the Adenosylcobalamin

The crystal structure[31] of the enzyme indicates that it exists as a dimer of a heterotrimer $(\alpha\beta\gamma)_2$ in which the 5,6-dimethylbenzimidazole nucleotide moiety of the corrin ring is coordinated to the cobalt atom of cobalamin[32] ("base-on" mode of cobalamin binding to proteins). Such a binding of cobalamin prevents the enzyme from mechanism based inactivation. Each heterotrimer ($\alpha\beta\gamma$) binds to one molecule of the cobalamin.

The secondary structure of the enzyme reveals that the α subunit contains a centrally placed $(\beta/\alpha)_8$ barrel-like structure called the triose-phosphate isomerase (TIM) barrel, also found in methylmalonyl-CoA and glutamate mutase.[33] The cobalamin molecule is located between α and β subunits. The α subunit consists mainly of the α helices with few β strands and surrounds the outer parts of the barrel. The main function of the γ subunit is to provide support to the α subunit in maintaining the overall barrel structure. The β subunit has a unique topology at the centre i.e. a Rossmann-fold-like structure and plays an important role in the contact with the lower axial ligand of the cobalamin. It mainly consists of α helices and few anti-parallel β strands.

It was found that a phosphate group in the cobalamin is very important for the tight binding of the adenosylcobalamin to the apoenzyme, which was based on the inactivation brought by the binding of adesonylcobinamide methyl phosphate. A lengthening of the bond between Co of the corrin and the *N*-3 of the 5,6-benzimidazole was found (about 2.5 Å), due to steric repulsions between the flattened corrin ring and the bulky 5,6-dimethylbenzimidazole moieties.

The long Co-N bond suggests favourable homolysis of Co-C bond rather than its heterolysis. Thus the active site of the enzyme is barrel shaped with the lower end occupied by the corrin ring. In some diol dehydratase enzymes the upper part of the active site accommodates the substrate and a potassium ion. It was found that the potassium ion was essentially required as a cofactor for the binding of the cobalamin at the active site.[34] The potassium ion binds to the negatively charged inner part of the barrel cavity and the cobalamin covers the cavity to isolate the active site from solvent molecules.

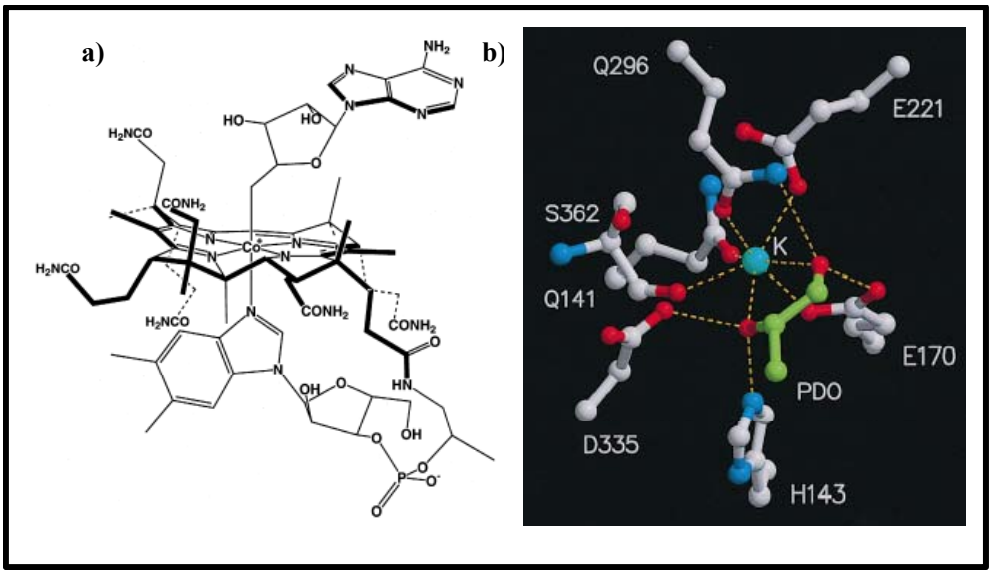

Figure 2–2: a) Structure of adenosylcobalamine (coenzyme B_{12}), b) A stereo view depicting the interaction of K^+ with the active.[31]

It was found that the distance between the potassium ion and cobalt was about 11.7 Å, with a hexa-coordinated K^+ in absence of the substrate. It is well established that a deficiency of potassium ion in the active site causes deformation of the TIM barrel.

2.1.2.2 Mechanism of Action

The common feature shared by a large and diverse variety of coenzyme B_{12} dependent enzymes is the hydrogen atom migration (Scheme 2–5) from one carbon atom of the substrate to an adjacent carbon atom in exchange of a group X which moves in the opposite direction. In case of diol or glycerol dehydratase, X is a hydroxyl group; hence there is a loss of water molecule from a geminal diol, forming the aldehyde or ketone.[26, 31]

Large kinetic isotope effects (KIE) of k_H/k_D = 10-13 identify the hydrogen atom transfer as the rate limiting step in the catalysis.[35] Dependence on adenosylcobalamin (which is the radical source) and inactivation of the enzyme by coenzyme analogs demonstrates the involvement of radicals in the catalytic cycle.[36] The formation of cobalamin (II) during catalysis was observed by optical and electron paramagnetic resonance spectroscopy. In EPR a high-field doublet and low-field broad signals were observed and assigned to organic radical and low-spin Co (II) of cobalamin (II).[37]

Based on a model study, a minimum distance of about 8 Å was suggested between the Co and C1 and C2 of 1,2-propanediol, which is in close agreement with the value estimated by EPR (~ 10 Å). It was found that in absence of the substrate only a small fraction of the coenzyme is in the dissociated form. Binding of the substrate shifts the equilibrium such that a major fraction of the coenzyme exists as dissociated form. Thus binding of the substrate to the active site not only accelerates the homolysis of adenosylcobalamin, it additionally lowers the

activation barrier for homolysis by 10 kcal/mol.

The overall stereochemical course[38] of the reaction requires that the migrating hydrogen atom and the leaving hydroxy group are *trans* to each other. Finally, the migrating hydroxy group is eliminated during the course of product formation.[39]

Based on the above mentioned arguments a mechanistic working model was suggested.[31] Accordingly, the catalysis starts with an initial homolysis of the Co-C bond of adenosylcobalamin in presence of the substrate (**S**). The adenosyl radical thus formed abstracts a hydrogen atom from the substrate (**S**) forming the substrate radical (**S**$^{\bullet}$), which rearranges to the product derived radical (**P**$^{\bullet}$). The product radical (**P**$^{\bullet}$) then abstracts a hydrogen atom from the adenosine, leading to the formation of product (**P**) and regeneration of the coenzyme (Scheme 2–5).

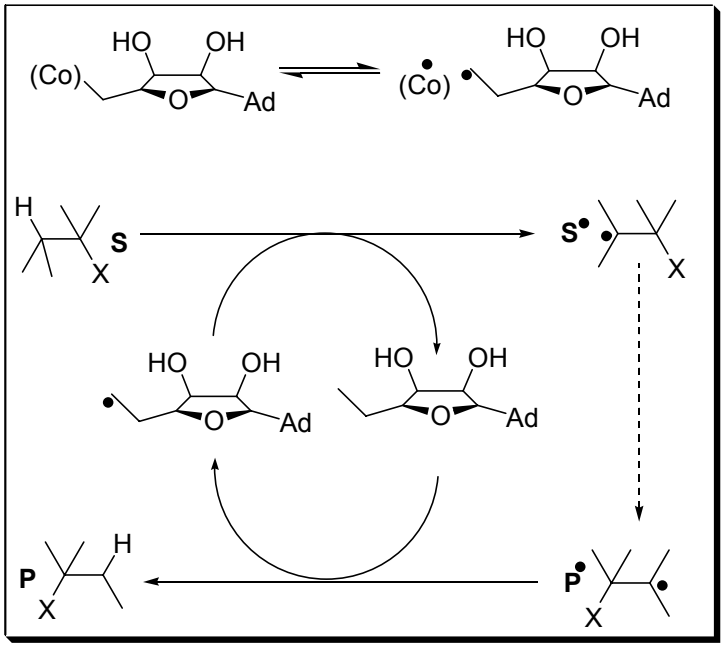

Scheme 2–5: The minimal mechanism for adenosylcobalamine-dependent rearrangements.[31]

However, the type of radical intermediates involved during the rearrangement of the substrate radical (**S**$^{\bullet}$) into the product radical (**P**$^{\bullet}$) is still a subject of persistent controversy.[40,41,42]

2.1.2.3 Biomimetic Modelling Studies

Although the enzyme diol dehydratase has attracted attention of many biochemists and microbiologists, the mechanism of the enzyme is still a subject of immense interest and persistent controversy.[40,41,42] A number of theoretical modelling studies intended to analyse the various mechanistic scenarios ranging from ionic, radical-like to radical ion intermediates, fall short of a clear picture of the mechanism. Earlier mechanistic investigations by Golding *et*

al. [40a] invoked a cyclic radical cationic species (Scheme 2–6) having a protonated migrating group. It was shown that 1,2-shifts in simple radicals occur via a dissociation-recombination mechanism, whereas an intramolecular rearrangement is favoured when the radicals are protonated. It was also shown that protonation of the migrating hydroxyl group lowers the rearrangement barrier from 100 kJ/mol to 18 kJ/mol.[40] The reaction mechanism bears resemblance to certain reactions that occur nonenzymatically, such as conversion of vicinal diols to aldehydes when treated with hydroxyl radicals.[105] The strength of the above mechanism (Scheme 2–6) relies on the fact that the acidity of the α-hydroxyl radicals is 5 pK_a units lower than that of alcohols.[40d] Further support to the above mechanism comes from the fact that some of the diol dehydratase enzymes have a potassium ion in the active site. The potassium ion was found necessary not only for the binding of the substrate but is also considered to play a very important role in stabilisation of the transition states and the product. The key finding of theoretical investigations made by Toraya *et al*.[40c] was that the potassium ion acts as an inhibitor of intramolecular hydrogen bonding thereby decreasing the activation energy by 4 kcal/mol.

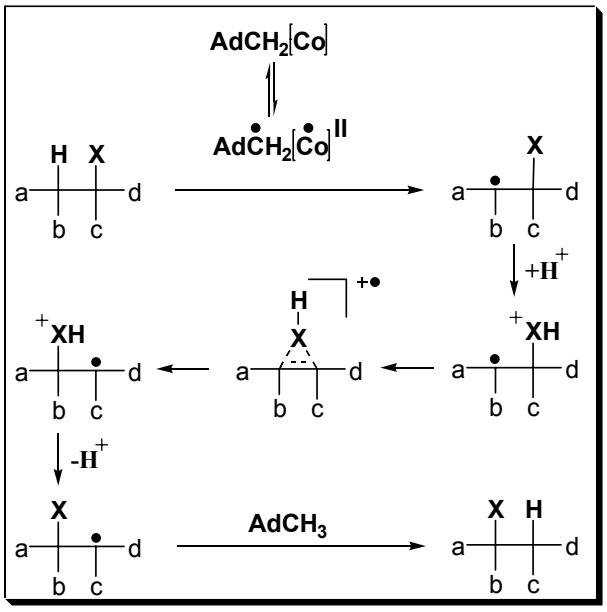

Scheme 2–6: Mechanistic model involving a cyclic radical cation intermediate as proposed by Golding *et al*.[40] based on theoretical calculations.

Cyclic radical cationic species were ruled out by Glusker *et al*[40b] based on their theoretical investigations, who instead suggested the involvement of a hydrated form of acetaldehyde radical cation **6** (equivalent to hydrogen bonded enol radical cation (Scheme 2–7). The latter can yield acetaldehyde either via path **A** or path **B**. Another interesting mechanism termed as retro-push-pull approach was suggested by Radom *et al*.[40g] where partial protonation of the

migrating hydroxy and partial deprotonation of the spectator hydroxy group had shown to facilitate the migration and a barrier reduction of 100 kJ/mol.

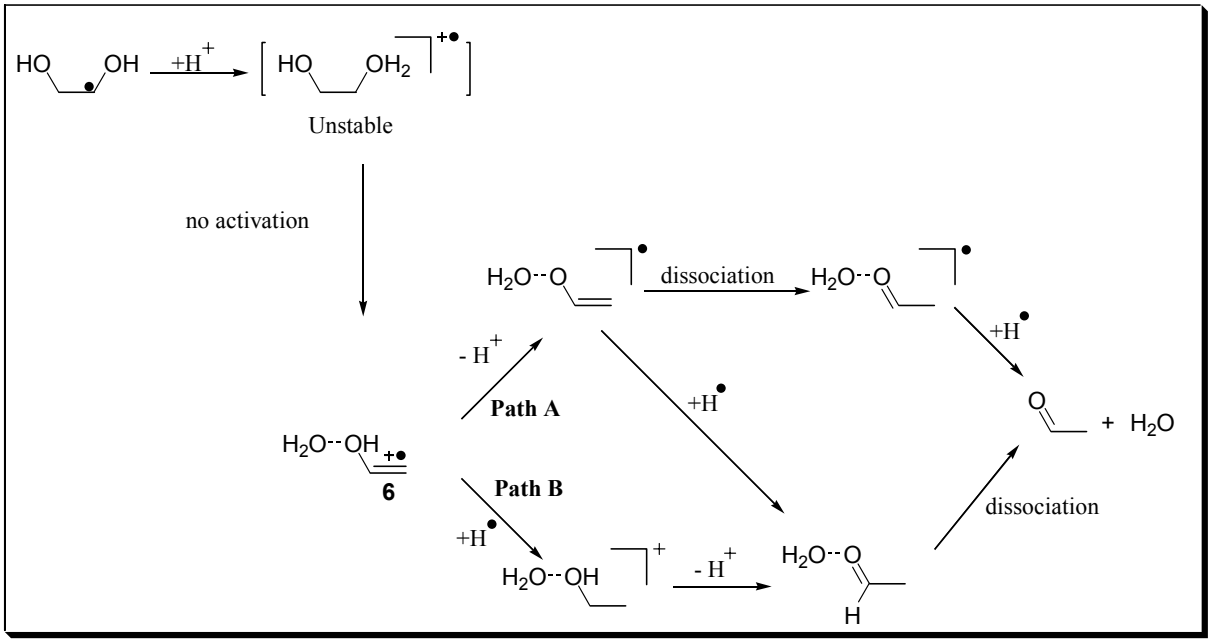

Scheme 2–7: Mechanism of diol dehydratase elimination based on the modelling studies by Glusker *et al*.[40b]

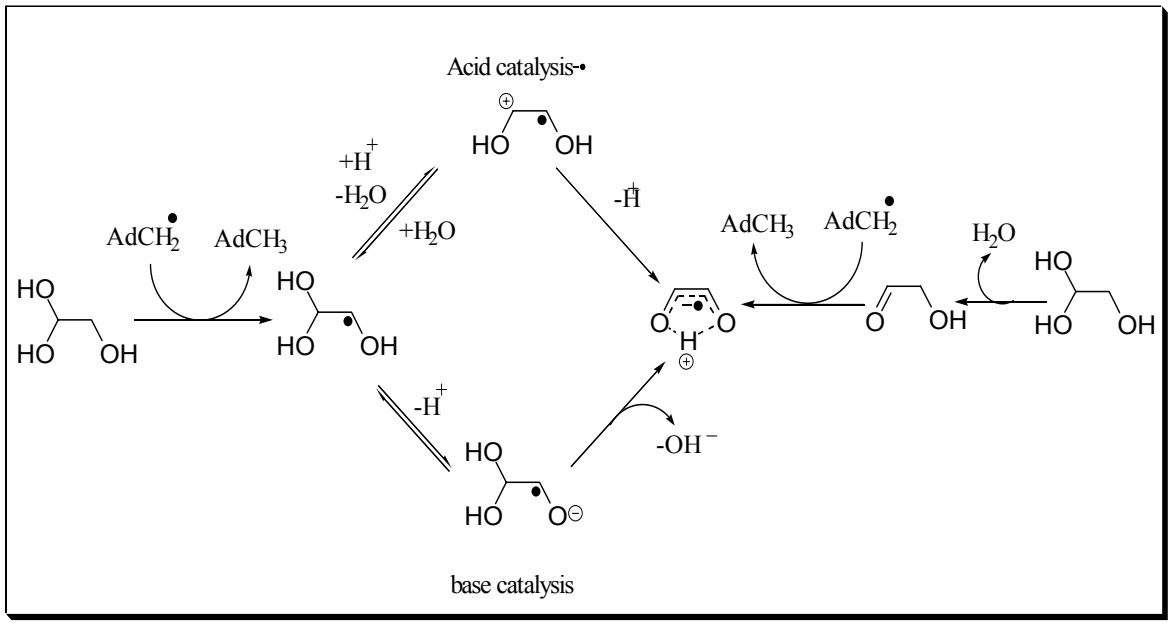

Scheme 2–8: Proposed[41] radical (ion) intermediates in the reduction mediated by diol dehydratase.

Recent EPR investigations by Frey *et al*.[41] on the inactivation of diol dehydratase and ethanolamine ammonialyase by glycolaldehyde led to the identification of a semidione radical, which itself can be formed via the intermediacy of a radical cation or radical anion (general acid or general base catalysis Scheme 2–8).

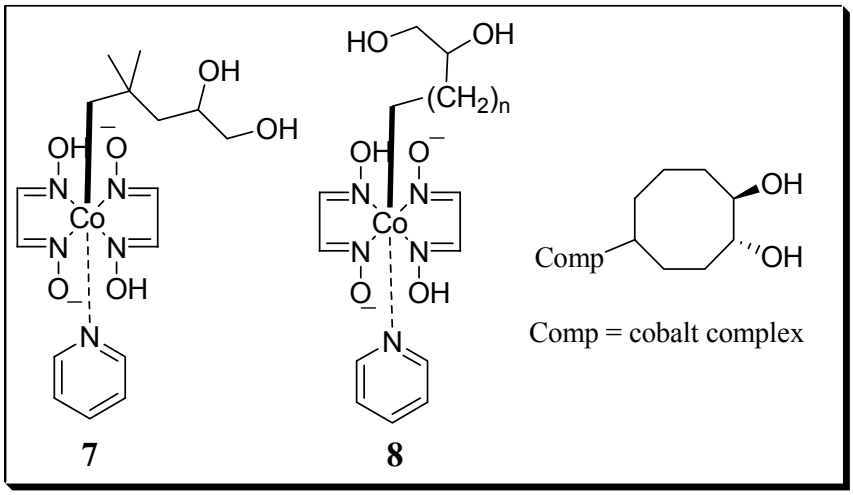

Scheme 2–9: Model compounds developed for biomimetic modelling studies[42] for the enzyme diol dehydratase.

Biomimetic modelling studies for the enzyme have not been able to provide clear mechanistic details. Model compounds **7** and **8** (Scheme 2–9) based on cobalt complexes[42] of terminal dihydroxy alkyl chains with variation in the chain lengths could mimic part of the mechanism involved, however, no conclusive evidence for the intermediates or transition states could be obtained.

2.1.3 Scission of Ether Bonds by Enzymes

2.1.3.1 Introduction

Ether linkages pose a considerable problem for microbial degradation (since the cleavage of the C-O ether bond requires ~360 kJ/mol of energy).[43] A group of xenobiotic ether compounds, like linear polyether PEG and its derivatives are released in nature as lubricants, solubility mediators, anti-freeze formulations, wetting agents, non-ionic surfactants and household detergents and as a constituent of cosmetics and pharmaceutical preparations. A number of microorganisms are known to degrade such ether linkages both in presence and in absence of molecular oxygen, such as species of *Corynebacterium*, *Nocardia*, *Achromobacter*, *Arthobacter* and *Flavobacterium* etc.[43]

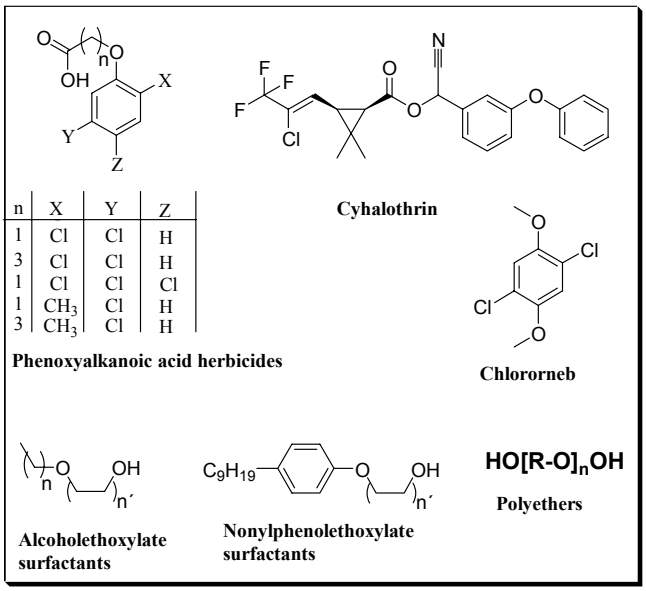

Scheme 2–10: Ether containing compounds released in nature in the form of herbicides, insecticides, rodenticides, and as constituents of household detergents.[43]

2.1.3.2 Mechanism

Although compounds containing ether linkages have found wide application, little is known about the mechanistic details of their bio-degradation both by aerobic and anaerobic microorganisms (Scheme 2–10). Almost all conceivable mechanisms have been invoked ranging from oxygenation[44a] (methanemonoxygenase of *Methylococcus capsulatus*), demethylations by cytochrome P-450[44b] (*Rhodococcus rhodochrous*), hydroxyl shifts[43b,c] (species from *Acinetobacter*), hydrolysis[44c] (*Aerobacter aerogenes*), oxidation to carboxylic acids[44d] (*Flavobacterium sp*. and *Pseudomonas sp*.) and to reductions[44e] (*Pseudomonas paucimobilis* SYK-6).

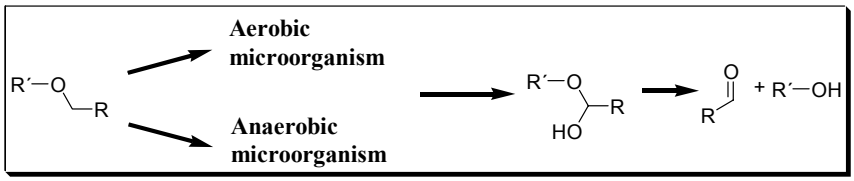

Scheme 2–11: General mechanistic scheme for the bio-degradation of ether linkages by microorganism in nature.

With such wide diversity both in microbial distribution as well as in degradation mechanism, the generally accepted working model includes primarily the conversion of the ether linkage to a hemiacetal form, which undergoes spontaneous hydrolysis to an alcohol and the corresponding carbonyl derivative (Scheme 2–11).

Interestingly, bio-degradation of ether linkages by enzymes of some anaerobic microorganisms requires a β-hydroxyl group to the ether bond. It is suggested that during the

degradation of the PEG by these enzymes there is a shift of the α-hydroxyl group to yield the hemiacetal. The overall reaction mechanism is similar to transformations carried out by diol dehydratase and other coenzyme B_{12} dependent eliminases, involving radical and radical ionic intermediates.

Another alternative mechanism postulated involves 1,2-elimination activated by either a suitable base or a suitable radical source (Scheme 2–12).

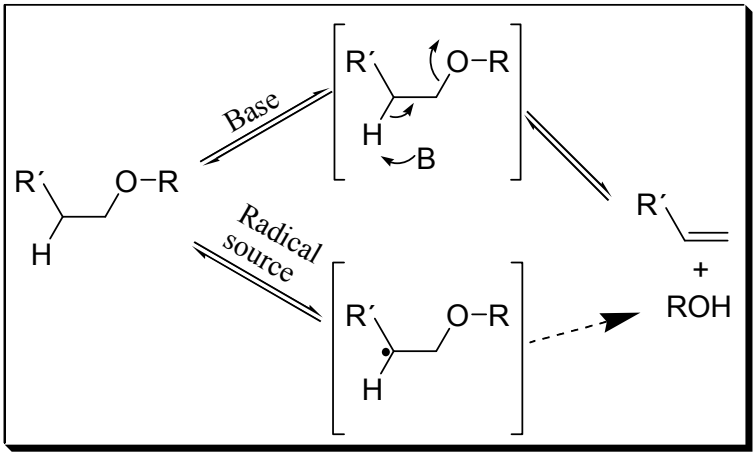

Scheme 2–12: Proposed mechanism for the cleavage ether bond cleavage in microorganisms.

2.1.4 Methods of Detection of Radicals and Radical Ions

Radical and radical ions are reactive species encountered both in chemical as well as biological transformations as reactive intermediates. Despite the short lifetimes of radical and radical ions, a wide range of techniques are available to investigate them. These techniques range from UV-Vis spectroscopy to highly sensitive methods such as ESR, LFP.

The methods of studying reactive intermediates in general (radical and radical ions) are classified into spectroscopic methods and chemical methods. Spectroscopic methods are direct or indirect methods of detecting reactive species usually in lifetime regimes of the order 10^{-3} to 10^{-9} s. However, the chemical methods are indirect method which make use of those aspects of the reactive intermediates wherein the chemical reactivity of the species involved serves as a marker of its detection.

2.1.4.1 Spectroscopic Methods

All radicals are paramagnetic since they have one or more unpaired electrons. Mass spectrometry and infrared spectroscopy can be used to provide structural information for a very limited range of radicals. UV-Visible spectroscopy can be used for the detection of radicals (radical ions), as the radical (radical ions) often absorbs at higher wavelength (λ_{max})

with increased molar extinction coefficient or molar absorptivity (ε) than the non radical precursor or products. The most important method for the detection of radicals is the electron spin resonance (ESR) spectroscopy and, to a lesser extent, chemically induced dynamic nuclear polarisation (CIDNP). Radical ions can also be detected by electrospray ionisation mass spectrometry.

2.1.4.2 Chemical Methods and Radical Clocks[45]

Chemical methods are based on competition kinetics and require irreversible partitioning of the radical intermediate between a reaction whose rate constant is known and the reaction of interest with unknown rate. The chemical method is an indirect method and requires product analysis. Most bimolecular competition methods are based on one of the three methods, the tin hydride method,[46] the PTOC-thiol method,[47] or the nitroxyl radical coupling method.[48]
These methods are used when a) the rate constant for a reaction of a given radical is comparable with the rate constant of another structurally related radical, and b) the rate constants are relatively insensitive to solvent effects.
Another competition method that is widely applied for providing insight into radical reactions is the unimolecular rearrangement reaction, popularly known as radical clock reaction (Scheme 2–13). Any unimolecular radical reaction with known rate constant can be used as a radical clock. Most of the clocks are based on cyclisations (5-hexenyl radical), ring opening of small ring "carbinyl" radicals (reverse of cyclisation), and 1,2-migrations that proceed by cyclisation followed by ring opening. The most known radical cyclisation is the 5-hexenyl radical to cyclopentylmethyl radical reaction with a rate constant of 2.3×10^5 s^{-1} at 25 °C.[49]
Cyclopropylcarbinyl radical ring openings are the best known radical clocks in unimolecular radical rearrangements with a rate constant of 1.8×10^8 s^{-1} at 25 °C.[50]

2.1.4.3 Cyclopropylmethyl Radical as Probe for Reaction Mechanisms in Enzyme Catalysed Reactions[51]

The efficiency of the ring opening of the cyclopropylmethyl radical has resulted in the wide spread use of cyclopropane rings as a probe of reaction mechanism both in chemical and enzyme catalysed reactions. The formation of ring opened products from substrates containing the cyclopropylmethyl group has been widely used as an indication that a particular reaction proceed via a radical intermediate. It has been applied to a number of enzymes postulated to have radical intermediates or transition state such as hydroxylations of alkanes[52] and monoxygenase-catalyzed epoxidation of alkenes by cytochrome P-450,[53] mechanism of inhibition of monoamine oxidase by cyclopropylamines[54], hydrogen transfer by

nicotinamide co-enzyme,[55] mechanism of penicillin biosynthesis,[56] mechanism of coenzyme B_{12} modified rearrangements,[57] and mechanism of dephosphorylation of organophosphates by *Escherichia coli.*[58]

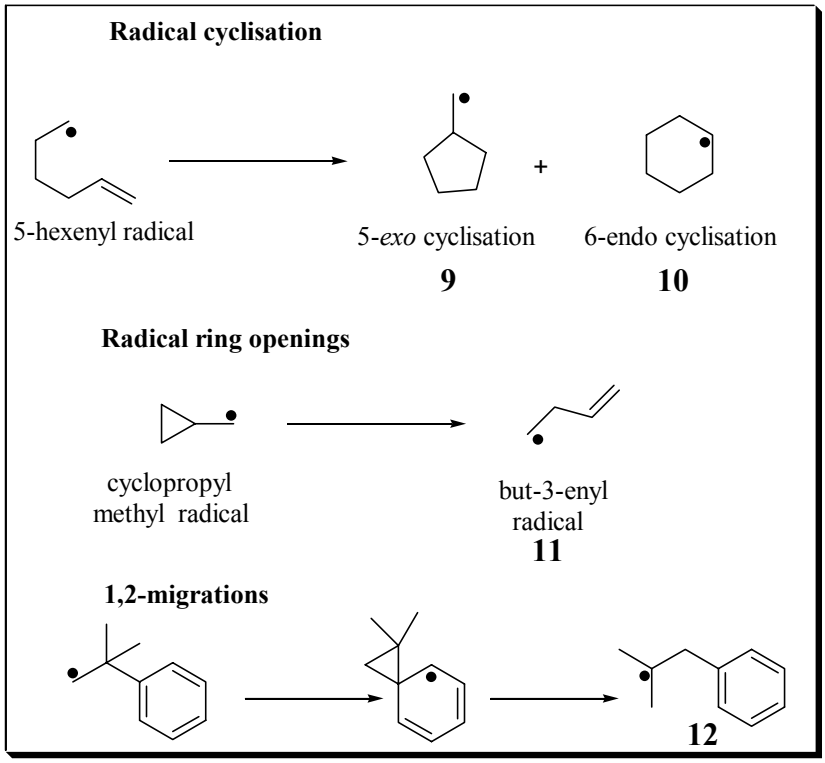

Scheme 2–13: Examples of radical clocks used in studying reactions involving radical intermediates based on radical cyclisations, radical rearrangements and radical-1, 2-migrations.

Results had been quite encouraging for some case studies such as with cytochrome P-450, nicotinamide coenzyme, and monoamine oxidase, but in other cases conflicting results were obtained[55]. The success of the above technique stems from the fact that the ring opening of the cyclopropylmethyl radical should be more rapid than any competing reactions. Although the above technique can give information about the involvement of radical intermediates in an enzyme catalysed reaction, however, such clock reactions for testing the intermediacy of radical ions are still at a stage of infancy.

2.2 Objective

With the ever increasing number of enzymes being classified as radical enzymes, there is a growing interest to understand these enzymes and to characterise the reactive intermediates that are involved in the catalytic cycle. Coenzyme B_{12} dependent enzymes are one such class of radical enzymes that carry out various transformations ranging from carbon skeleton rearrangements, heteroatom eliminations, to intramolecular amino group migrations. These enzymes depend on intermediate radicals for catalysis. Despite the differences in their substrates they follow a general motif ($S^{\bullet} \rightarrow P^{\bullet}$), wherein the reaction is initiated and terminated by hydrogen atom abstraction and addition, respectively. Thus, a common mechanistic scheme is thought to be operative (Scheme 2–14) in most of the eliminases that is described below:

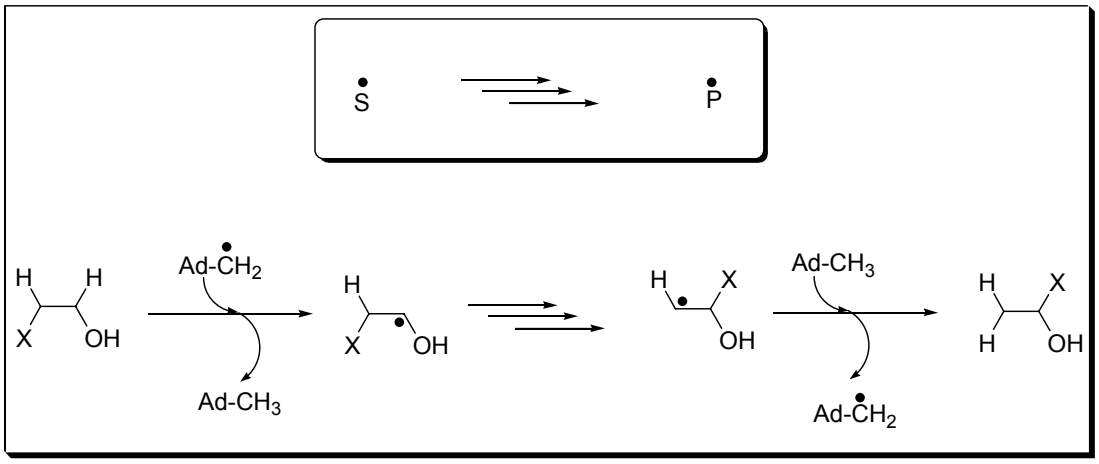

Scheme 2–14: General mechanistic scheme outlined for adenosylcobalamine mediated heteroatom elimination and rearrangement.

Three different approaches have been used in the literature to address the transformation of the substrate radical to the product radical ($S^{\bullet} \rightarrow P^{\bullet}$); a) isotopic labelling methods probing directly part of the enzymatic process (usually involves product isolation), b) use of appropriate compounds to model the enzymatic reaction in solution, and c) theoretical investigations involving high-level calculations.

All of the above approaches had been utilised in the past for mechanistic investigations. They have been useful in providing insights into the mechanistic details of these enzymes; and in many cases gave conflicting results.

The objective of the present work was to provide insights into the mechanistic details of the transformation from substrate derived radical ($S^{\bullet}$) to product derived radical ($P^{\bullet}$) in coenzyme B_{12} dependent and phenoxyethanol dehydratase.

2.3 Conceptual Basis of the Present Work

A wide spectrum of reactive intermediates (Scheme 2–15) ranging from neutral radicals to charged radicals have been invoked in adenosylcobalamin mediated rearrangements and eliminations. In contrast, our approach was to develop appropriate methods that would test for the intermediacy of various reactive species directly at the active site of the enzyme.

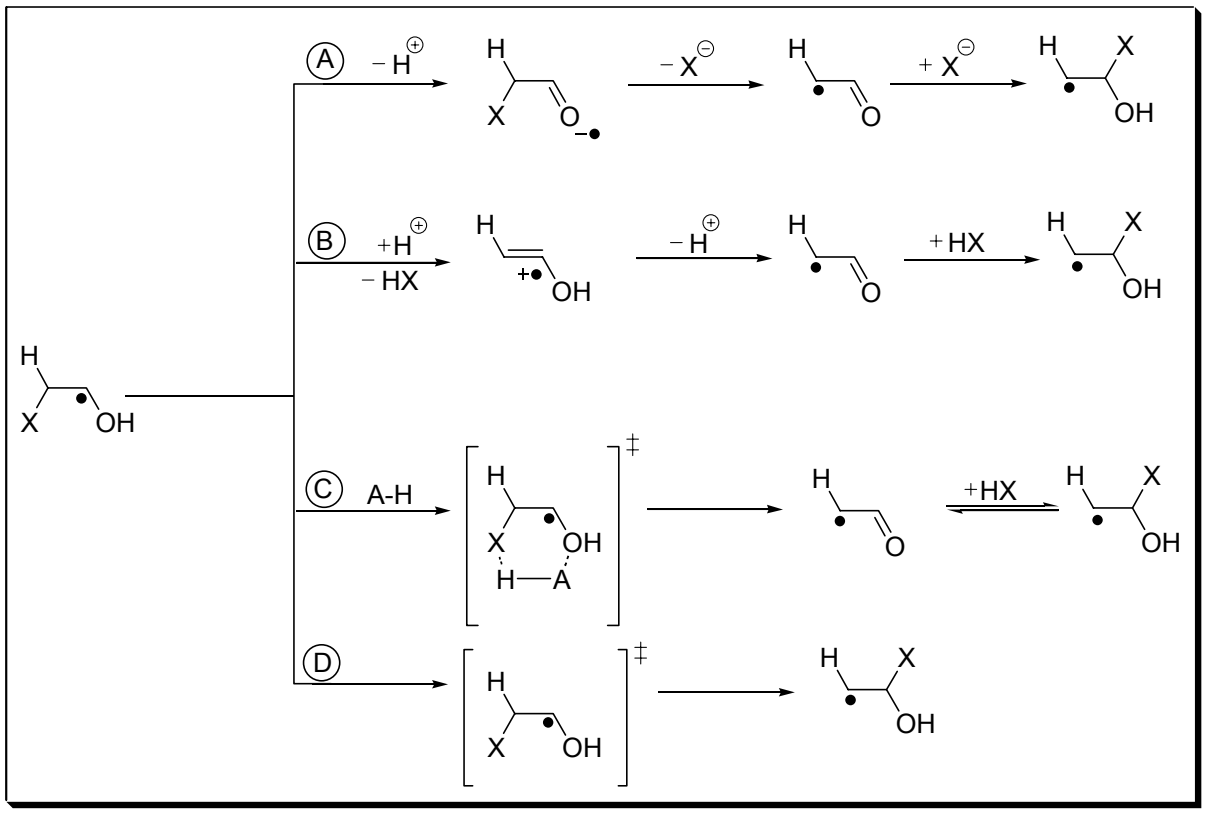

Scheme 2–15: Radical (ion) intermediates possibly involved in the adenosylcobalamine mediated heteroatom eliminations.

2.3.1 Concept to Investigate Radical Ionic Species Directly at the Active Site of the Enzyme

Radical ions due to the unpaired electron and the charge present can behave both as radical as well as an electrophile or a nucleophile (radical cations and radical anions, respectively). One of the main deactivating routes of radical ions is the one-electron transfer to the neutral species, hence, they can act as strong oxidants (radical cations) /reductants (radical anions).
Intramolecular electron transfer processes between enol radical cations/ ketyl radical anions to a suitable donor or acceptor was conceptualised for translating reactive radical ions into long-lived ones directly at the active site of the enzyme (Scheme 2–16). Since the radical ions of the donor and acceptor have distinct absorption spectra the entire process can be followed by

UV-Vis or EPR spectroscopy.

The feasibility of such a process would depend on the potential difference between the donor and the acceptor functionalities given by the equation below: (e.g. feasibility of electron transfer between an acceptor radical cation [$A^{+\bullet}$] and the donor [D]).

$$D + A \underset{}{\overset{K}{\rightleftharpoons}} D^{+\bullet} + \bar{A}^{\bullet}$$

$$\Delta G° = -nF(E°_{A/A^{-\bullet}} - E°_{D^{+\bullet}/D}) = -RTlnK$$

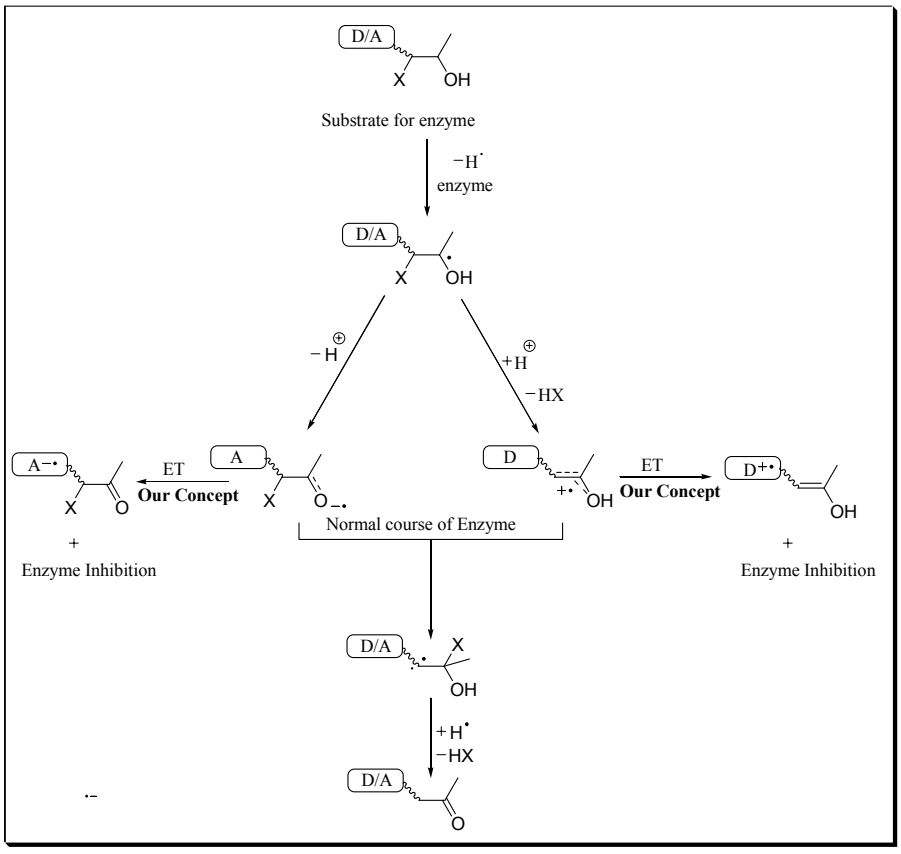

Scheme 2–16: Schematic representation of the concept of translating short-lived radical ions into long-lived ones by electron transfer.

2.3.2 Concept to Investigate Radical Intermediates Directly at the Active Site of the Enzyme

Radicals unlike cations and anions are neutral and paramagnetic. The chemical fate of radicals primarily range from homo-coupling i.e. dimerisation, or reaction with non-radicals. In solution such dimerisation reactions occur within diffusion controlled rates, but can be slowed down either by stabilising electronic effects (stable radicals) or by steric effects (persistent radicals).

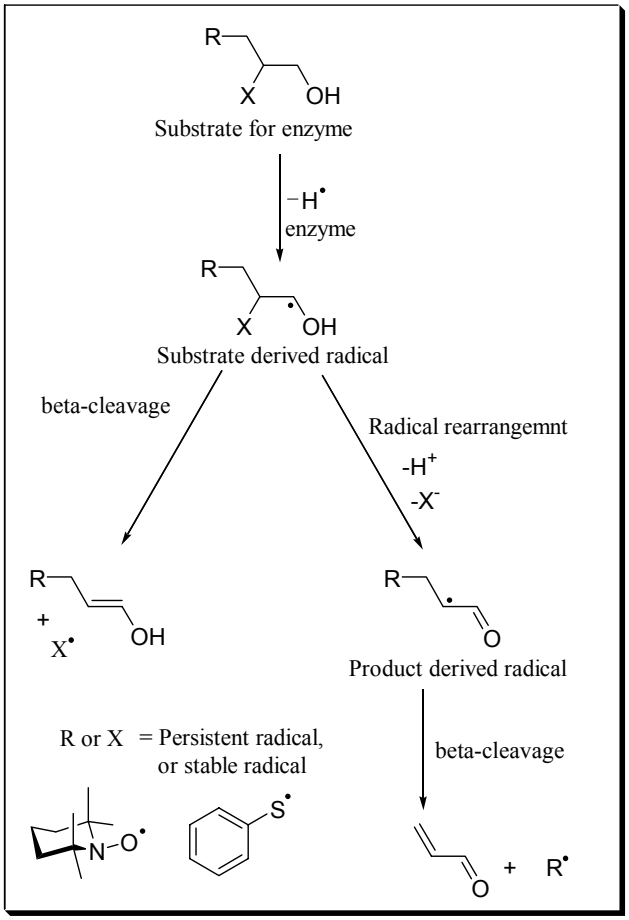

Scheme 2–17: Concept of translating short-lived radical intermediates directly at the active site of the enzyme based on the β-cleavage process.

Since many enzymes are able to generate, stabilise and utilise radicals and radical intermediates in their catalytic cycles, a lot of efforts are being made in developing methods to probe their intermediacy. Most of the methods described involve radical rearrangements such as ring opening reactions of cycloproylcarbinyl types etc. popularly known as "radical clocks".[45] Most of these methods provide indirect evidence and usually require product analysis. Our approach to test for neutral radicals directly at the active site of the enzyme is to translate these short-lived radicals into long-lived ones. The present method would provide firm evidence for involvement of radical intermediates and would additionally allow an easy detection (EPR) of such reactive intermediates.

Effectively this could be achieved by placing a fast β-cleaving group (TEMPO or SPh) to the radical being formed (Scheme 2–17).

Thus β-cleavage reaction was formulated as an approach of translating short-lived radicals into persistent ones (kinetically stable ones), directly at the active site of the enzymes.

2.4 Work Plan

As a test case we chose initially to develop probes for the phenoxyethanol dehydratase, however the above concept can be potentially extended to other coenzyme B_{12} dependent eliminases. The reason for choosing phenoxyethanol dehydratase was the ability of the enzyme to accept large molecules (unlike diol and glyceroldehydratase, which have small active sites) such as polyethyleneglycol. This indicates a relatively tolerant active site.[28b] Additionally, the cell extract also showed some diol and glycerol dehydratase activity also making it a suitable candidate for parallel testing of other enzymes.

In order to obtain further insight into the mechanistic details of phenoxyethanol dehydratase the following work plan was mapped out:

1) Development and testing of radical and radical ion probes on coenzyme B_{12} dependent enzymes (diol/glycerol) and phenoxyethanol dehydratase.

2) Development of phenoxyethanol derivatives to probe the active site tolerance of the enzyme.

3) Design and development of solution substrates to check the ability of hydrogen bonding phenomena in modulating oxidation potentials of enols.

4) Design and investigation of probes to test our concept of translating short-lived radicals and radical ions into long-lived ones in solution.

2.4.1 Mechanistic Probes for Diol, Glycerol and Phenoxyethanol Dehydratase

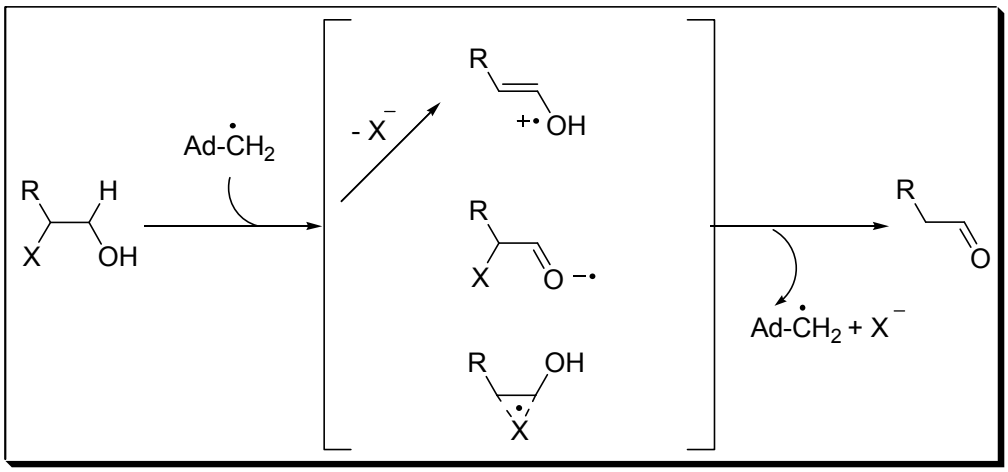

Scheme 2–18: General scheme depicting the heteroatom (X = OH, NH_2) elimination in coenzyme B_{12} dependent enzymes.

The design of probes to test for reactive intermediates, (shown in Scheme 2–18) directly at the active site of the enzyme requires substrates modified with a donor, acceptor or persistent

radical forming species. The choice of electrophore and persistent radical species can be made from a series of well-known electron donors, acceptors and persistent radicals listed in Chart 2–1.

The cell free extract that was available for enzyme investigations was a soup of various enzymes including diol, glycerol and phenoxyethanol dehydratase. Designing mechanistic probes for each and every individual enzyme would be time consuming, especially in the absence of any knowledge of the active site (except for the fact that the phenoxyethanol dehydratase accepts bulky substrates such as polyethylene glycol). The practical approach therefore was to first develop general probes that would allow us to conduct parallel testing for all three enzymes.

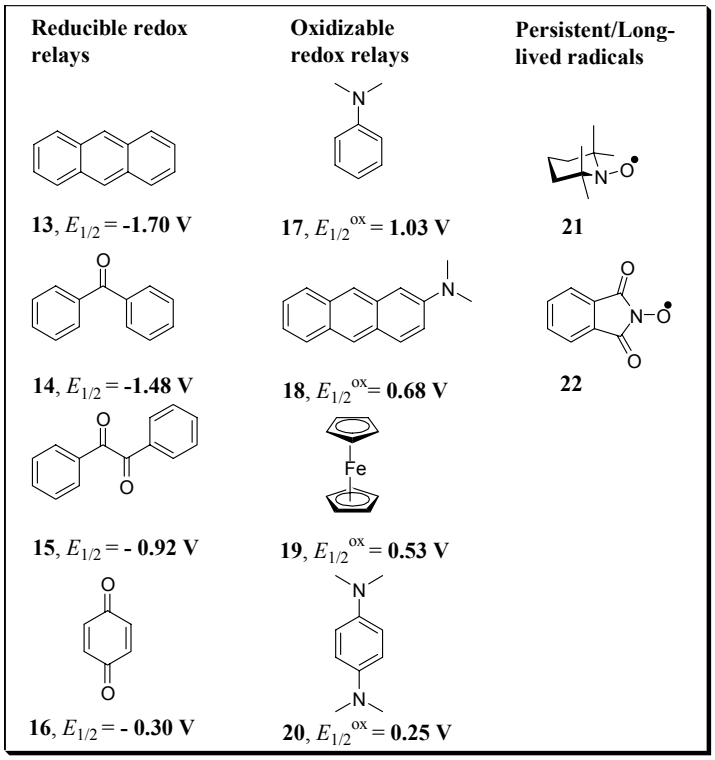

Chart 2–1: List of electrophores and persistent radical/ long-lived radical forming groups that can be attached to the natural substrate enzymatic investigations.

2.4.2 Design and Retrosynthesis of Radical and Radical Ion for Enzymatic Investigations

2.4.2.1 Design and Retrosynthesis of Radical Cation Probes for Enzymatic Investigations

The choice of ferrocene as the redox mediator stems from its stable redox property [Fe(II)/Fe(III)], and the spectroscopic properties [UV-Vis absorption of ferrocene

(λ_{max} = 450 nm), of ferrocenium ion (λ_{max} = 620 nm)]. Use of ferrocene as a redox mediator had been applied successfully on glucoseoxidase,[59] alcohol dehydrogenase,[60] and as electrochemical sensors in nucleic acid analysis.[61]

A series of vicinal diols and triols (**23**-**29**) was designed (Chart 2–2) as enzyme substrates and a retrosynthetic analysis was carried out. The strong electron donating ability of ferrocene makes it a very labile group for oxidation; hence synthetic procedures were designed to avoid any oxidising conditions.

From the retroanalysis (Scheme 2–19), **23** and **26** can be prepared by the addition of ferrocene anion to protected α-hydroxyaldehydes, leading to ferrocene and α-benzyloxy acetaldehyde/ [D]-2,3-isopropylideneglyceraldehyde (**34**) as the desired synthons. The above retro-analysis has the advantage that at no point during the synthesis a strong oxidative step is involved (deprotection conditions for benzyloxy group and acetonide are mild, requiring neutral [H_2/Pd-C] to acidic conditions).

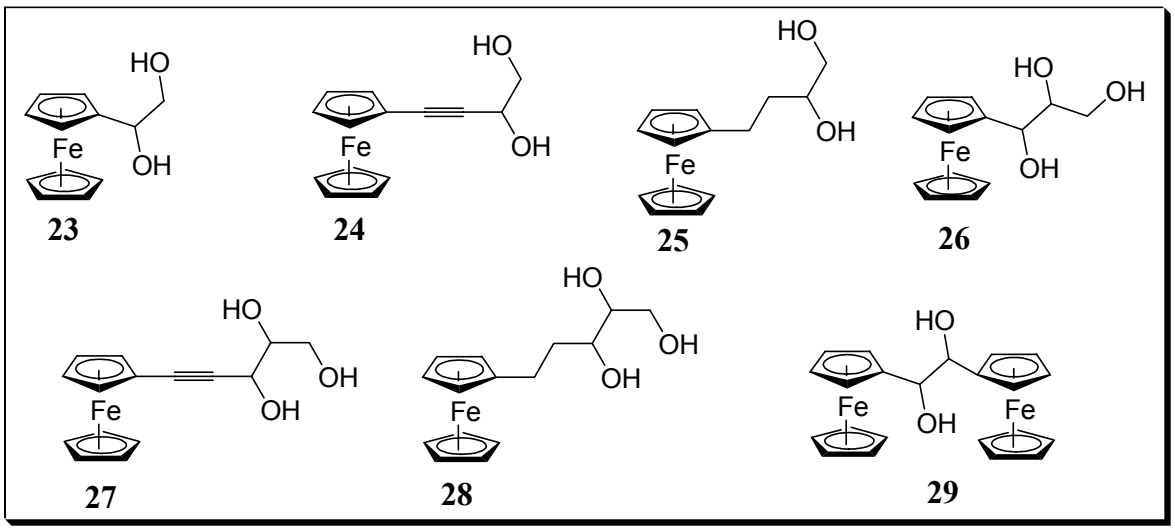

Chart 2–2: Enzyme substrates containing a ferrocene unit designed to test for radical cationic intermediates.

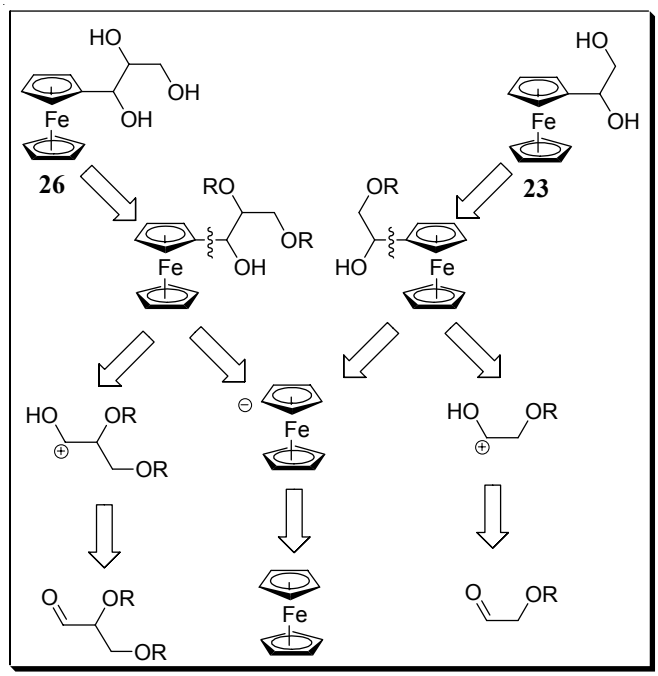

Scheme 2–19: Retrosynthesis of enzyme substrate **23** and **26** based on ferrocene as the radical cation probe.

Enzyme substrates **24** and **27** require ethynylferrocene (**32**) and α-benzyloxy acetaldehyde (**33**)/ [D]-2,3-isopropylideneglyceraldehyde (**34**) as desired synthons with **30** and **31** as important intermediates (Scheme 2–20). The initial step would then be a Grignard addition of 1-(ferrocenyl)ethynyl magnesium bromide to α-benzyloxyacetaldehyde/[D]-2,3-isopropy-lideneglyceraldehyde. A reductive cleavage of the benzyloxy group in **30** can be effected using Ca/ NH_3 (liq.) for the preparation of **24** keeping the triple bond intact. In the case of **27**, it can be prepared by deprotection of the acetonide group of **31** under mild acidic conditions. Retrosynthesis of **25** and **28** becomes straightforward, hydrogenation (H_2/Pd-C) of **30** would not only cause the reduction of the triple bond but additionally would lead to the cleavage of the benzyloxy group yielding **25**. A similar approach on **31** followed by mild acid treatment would render **28**.

Substrate **29** can be synthesised by a well known procedure involving a pinacol type of coupling of ferrocenealdehyde in the presence of samarium iodide.[62]

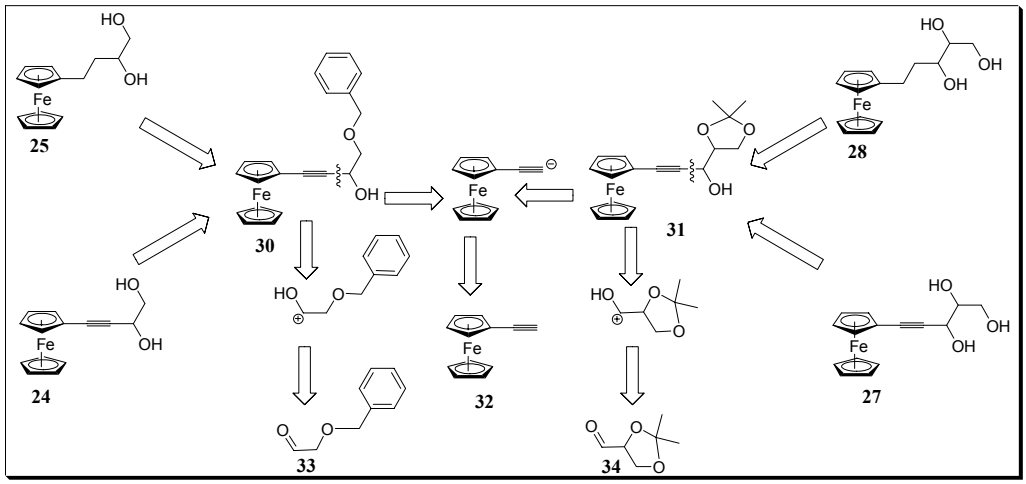

Scheme 2–20: Retroanalysis of **24**, **25**, **27** and **28** radical cation probes for enzyme investigations.

2.4.2.2 Design and Retrosynthesis of Radical Anion Probes for Enzymatic Investigations

In order to translate reactive radical anionic intermediates to relatively long-lived ones directly at the active site of the enzyme, a few substrate derivatives containing an electron acceptor were designed. For preliminary investigations quinone and fluorene based (tetranitrofluorene etc.) probes were designed and their synthesis was attempted (Chart 2–3).

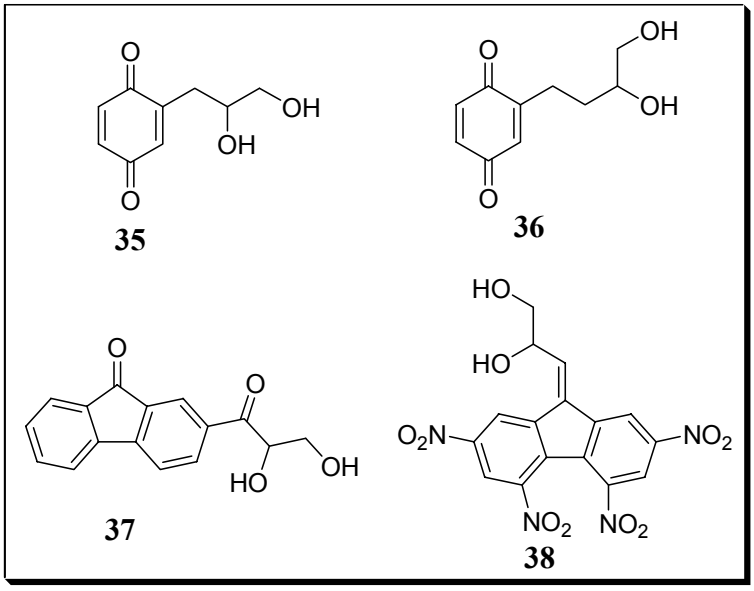

Chart 2–3: Enzyme substrates **35**-**38** designed to probe for radical anionic intermediates in the catalytic cycle of diol, glycerol or phenoxyethanol dehydratase.

Quinone containing substrates with varying chain lengths were designed. A literature known compound,[63] **35** required 2-allylphenylacetate (**40**) as the desired synthon. The latter can be readily prepared by acylation of 2-allylphenol. Epoxidation of **40** followed by ring opening

and deprotection would yield **39**. The desired product **35** can be obtained by oxidation of **39** with Fremy´s salt. Similarly, the homologue **36** would require the protected diol **41** that can be readily prepared by hydrogenolysis of the benzyloxy protected **42**. Preparation of **42** would require a Grignard coupling between the 2-(1,4-dimethoxyphenyl)ethynyl-1-magnesium bromide with benzyloxyacetaldehyde **33**. Thus, the overall synthesis for **36** requires dimethoxyacetophenone and benzyloxyacetaldehyde as synthons (Scheme 2–21).

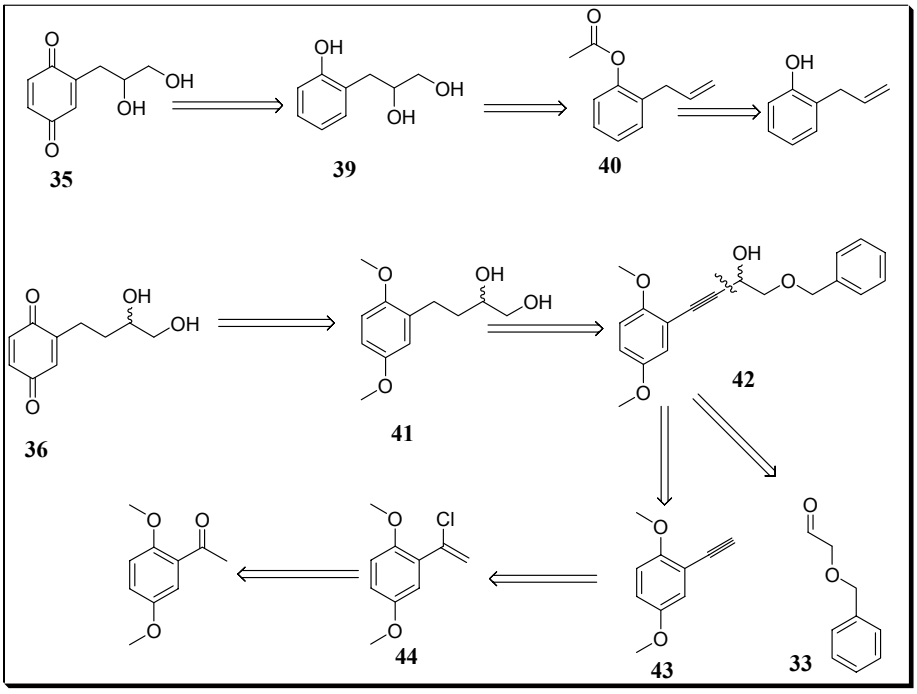

Scheme 2–21: Retroanalysis for the synthesis of **35**, **36** i.e. quinone based radical anion probe substrates for enzyme investigation.

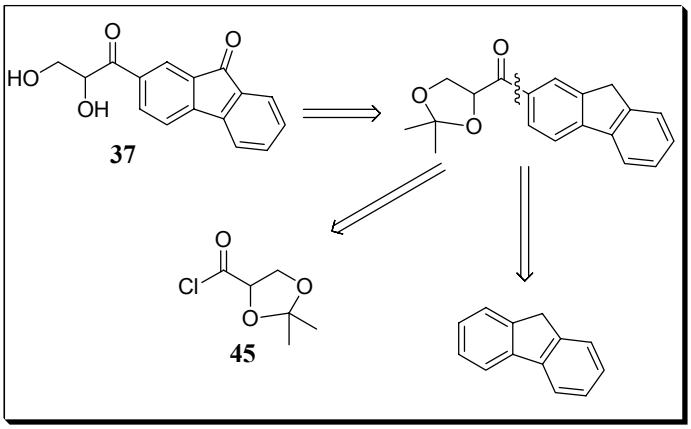

Scheme 2–22: Retroanalysis of fluorenone based radical anion probe **37**.

The radical anion probe containing fluorenone as acceptor, requires fluorene and 2,3-isopropylideneglyceroylchoride (**45**) as the key synthons (Scheme 2–22). A Friedel-Crafts

acylation followed by oxidation with a phase transfer catalyst (tetrabutylammoniumhydrogen-sulfate) would yield the desired substrate **37**.

A further extension to fluorene based radical anion probe was to utilise tetranitrofluorene as the acceptor (Scheme 2–23). The desired synthons for the synthesis of **38** were tetranitrofluorene (**47**) and [D]-2,3-isopropylideneglyceraldehyde (**34**).

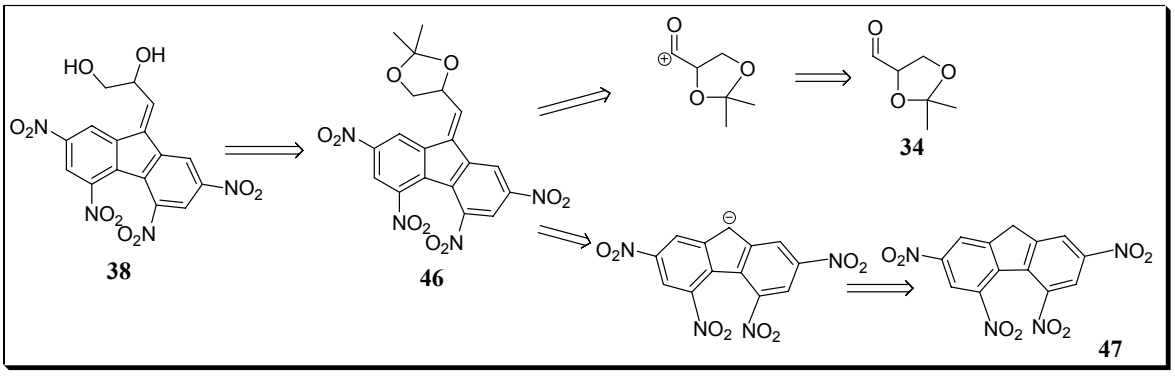

Scheme 2–23: Retroanalysis of tetranitrofluorene based radical anion probe **38** for enzyme investigations.

2.4.2.3 Design and Retrosynthesis of Neutral Radical Probes for Enzymatic Investigations

To test the intermediacy of neutral radicals directly at the active site of the enzyme it was our approach to translate short-lived radicals into a long-lived /persistent radicals. This could be achieved via β-cleavage of a group that would form a persistent radical. The essence of this approach relies on the fact that the β-cleavage process must occur at a faster rate than any other competing reactions (such as deprotonation etc.).

Nitroxide free radicals exhibit a chemical inertness, which is quite uncharacteristic of other free radicals. This feature of nitroxides is responsible for their role and application as reporter molecules in the study of biological systems by electron spin resonance spectroscopy. McConnell[64] first introduced spin labelling in 1965, and since then it has evolved into one of the most powerful and versatile tools in the hands of biophysicists. For spin labelling, the formed nitroxide free radical must be stable, and thus a number of secondary *N*-oxylamines of the general structure **48** devoid of any α-hydrogen were developed.[65]

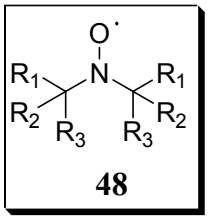

48

Substituents on the α-carbon not only prevent the disproportionation reaction but also diminish the tendency towards dimerisation.[66] The most commonly used nitroxides as spin labels are derived from 4-hydroxy-2,2,6,6-tetramethylpiperidine-*N*-oxyl, 2,2,5,5-tetramethyl-pyrroline-*N*-oxyl and 4,4-dimethyloxazolidine-*N*-oxyl (doxyl nitroxide) (Chart 2–4).

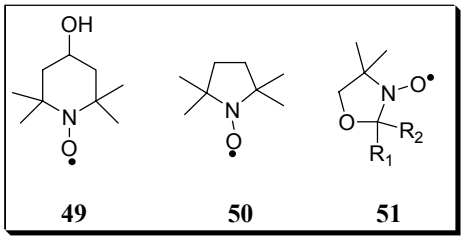

Chart 2–4: List of kinetically stable nitroxide radicals used as spin labels.

These radicals have also found wide application as catalysts in alcohol oxidation and living radical polymerisations.[67] Based on the above features of nitroxide radicals, radical probes with TEMPO residues attached at suitable positions onto the substrate molecule were designed (Chart 2–5).

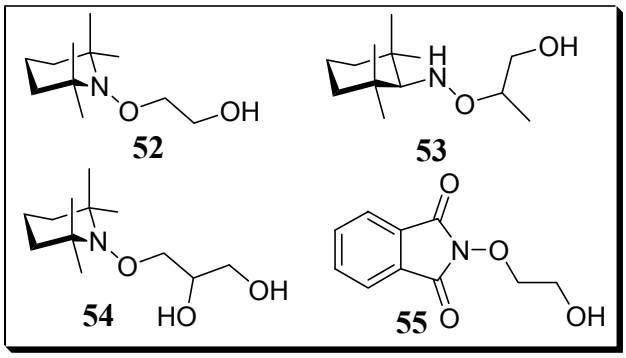

Chart 2–5: List of compounds **52-55** designed to probe for neutral radical formation directly at the active site of the enzyme.

Retroanalysis of the above probes **52-54** suggests that they can be prepared either by the ionic pathway involving nucleophilic substitution by 2,2,6,6-tetramethylpiperidinoxide anion or by trapping of carbon centred radicals by TEMPO (Scheme 2–24).

Neutral radical probe **55**, an already known substance, can be prepared by reacting potassium-*N*-hydroxyphthalamide with 2-bromoethanol.

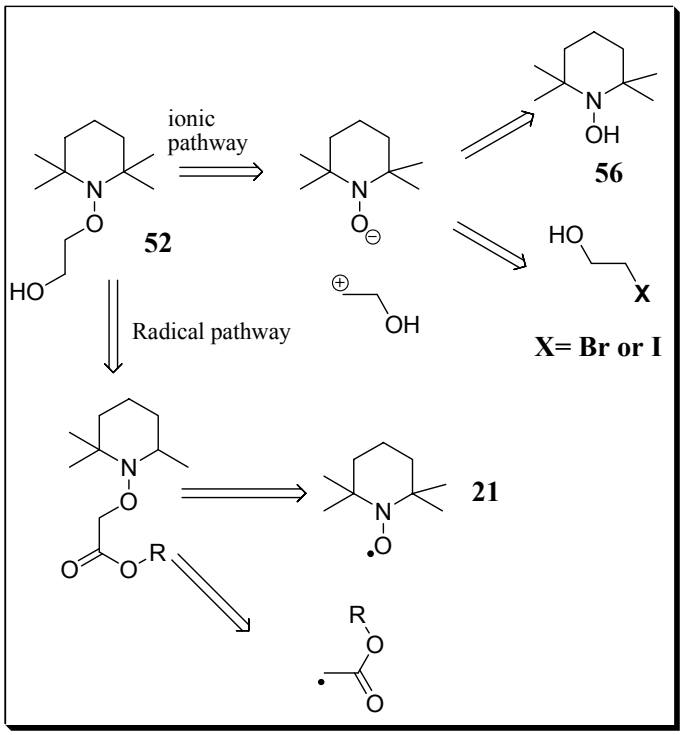

Scheme 2–24: Retroanalysis for the synthesis of neutral radical probes **52-54** for enzyme investigations.

2.4.2.4 Design and Retrosynthesis of Probes for Phenoxyethanol Dehydratase to Test the Hydrophobic and Electronic Tolerance of the Active Site

The cleavage of an ether bond poses a considerable challenge for enzymes; only certain enzymes are able to break them down by converting ether into hemiacetals, primarily via oxidative/ reductive mechanisms or via migration involving radical intermediates. phenoxyethanol dehydratase is one such enzyme known to degrade low molecular weight polyethylene glycols.

The unique properties of these enzymes have attracted a lot of attention; however, a large number of these enzymes have not been isolated, or are not available in pure form. Due to the inability to isolate these enzymes in pure form (due to stability reasons), little is known about their mechanism and their active site.

The rational approach to gain insight into the active site of phenoxyethanol dehydratase enzymes would be to prepare derivatives of the enzymes original substrate, in order to probe for the active site tolerance. In all two types of substrates were designed:

a) A substrate derivative containing varying degrees of alkyl substituents. These substrates would prove vital in recognising the path towards the active site of the enzyme and help in estimating the size of the active site.

b) Substrate derivatives with an electron donor/ acceptor that would help in estimating the

electronic requirements for the substrate in the overall catalytic cycle.

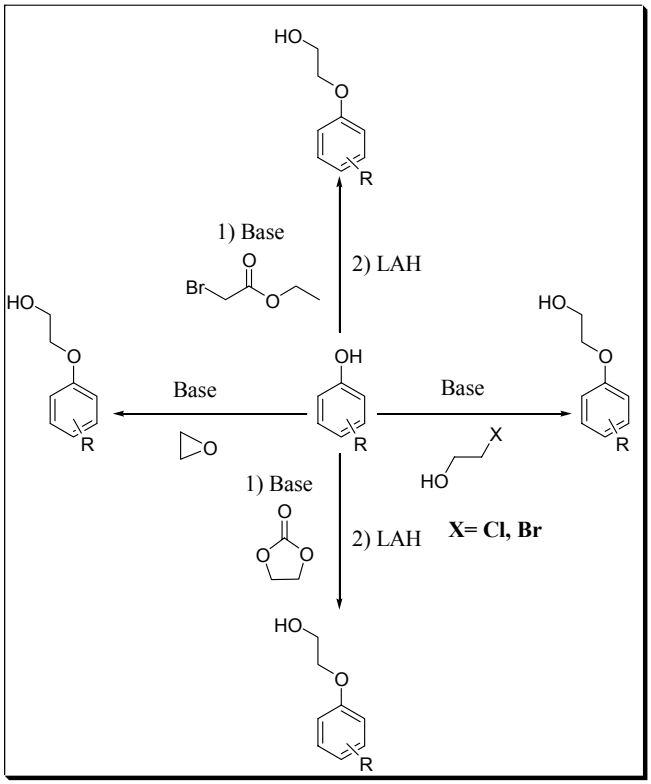

Scheme 2–25: Known methods for synthesis of phenoxyethanol derivatives.

Thus, a number of phenoxyethanol derivatives **57a-k** closely resembling the natural substrate i.e. phenoxyethanol, were designed. Substituted phenoxyethanol derivatives are usually prepared by one of the four different approaches as described in Scheme 2–25. All of the approaches described above involve the nucleophilic attack (S_N2) of a phenolate anion on to a suitable functionality. In direct methods, the substitution of a halogen[68] or ring opening of epoxide[69] or [1,4]-dioxolan-2-one,[70] leads to phenoxyethanol derivatives. However, in the indirect route, phenoxyacetates[71] are prepared initially followed by LAH reduction,[72] which then yields the desired phenoxyethanol.

The latter approach was utilised (Scheme 2–36) in the present work for the synthesis of substituted phenoxyethanols.

2.5 Results

2.5.1 Synthesis of Enzmye Probes

2.5.1.1 Synthesis of Radical and Radical Ion Probes for Enzymatic Investigations

Based on the retroanalysis, attempts were made to make the enzyme substrates containing ferrocene as the electron donor.. The synthesis of four of the radical cation probes was successfully realised. The ferrocene containing substrate **24**, **25** and **29** with vicinal diol and **26** and **27** with vicinal triol were synthesised. They were characterised by various spectroscopic methods and their radical cations were generated and observed by UV-Vis and ESI-MS.

2.5.1.1.1 Synthesis of 4-Ferrocenyl-butane-1,2-diol (25)

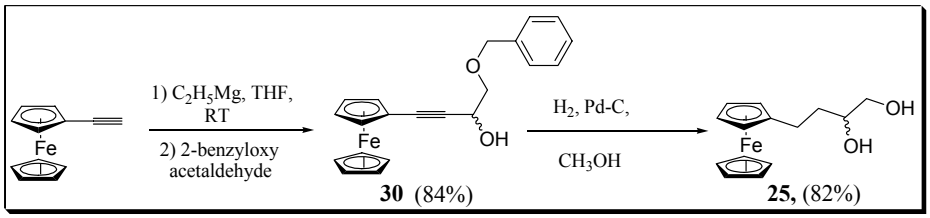

Scheme 2–26: Synthesis of radical cation probe **25** starting from ferrocenylethyne and benzyloxyacetaldehyde.

25 was synthesised by an initial Grignard reaction between ferrocenylethyne **32** and benzyloxyacetaldehyde **33** (Scheme 2–26). The adduct **30** was obtained in 84% yield and had a melting point of 84-85 °C. The IR of **30** exhibited a broad band at 3391 cm^{-1} (OH) and a characteristic acetylenic stretching at 2226 cm^{-1} (C≡C). A characteristic doublet at $\delta = 2.56$ (OH) and a singlet at $\delta = 4.6$ ppm (CH_2) in the ^{1}H-NMR were observed that were absent in the product **25**. Adduct **30** under hydrogenation conditions (H_2/Pd-C, 5-7 bar, 12 h) in methanol furnished the desired product **25** in 82% yield.

Compound **25** had a melting point of 92 °C and was characterised by absence of acetylenic stretching 2226 cm^{-1} (C≡C) in the IR, the singlet at $\delta = 4.6$ ppm (CH_2) and the signals in aromatic region in the ^{1}H-NMR. Appearance of new signals at $\delta = 1.5$-1.6 ppm (CH_2), 2.3-2.4 ppm (CH_2) and 2.4-2.5 ppm (CH_2), 3.37-3.41 ppm (CH_2) in the ^{1}H-NMR further confirmed product formation.

Suitable single crystals for **25** were obtained by slow evaporation of dichloromethane and analysed by X-ray diffraction. Single crystal analysis indicated that **25** crystallises in the monoclinic system with the space group $P2_1/c$, with one molecule in the asymmetric unit. A

molecular view of **25** is depicted with its atom-labelling scheme (Figure 2–3).

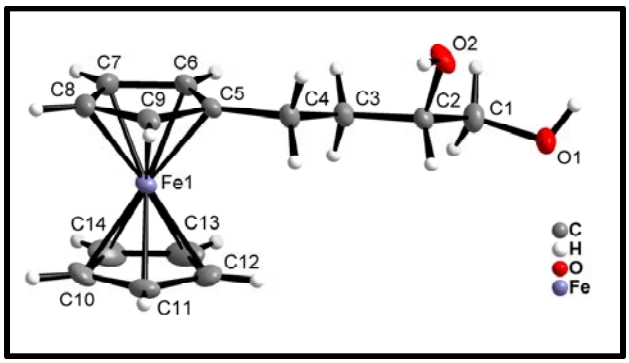

Figure 2–3: Molecular view of **25** as obtained from X-ray single crystal analysis.

The ferrocene group adopts a rather unstrained geometry with only a small tilt of the two cyclopentadienyl (cp) rings *vs*. each other. The cyclopentadienyl rings were found in the eclipsed conformation (very small deviation of 1.6-2.1 °) with the iron placed at the centre in a sandwich structure (angle [centroid-Fe-Centroid]: 170.22 [1] °).

The cp rings were characterised by C-C bond distances in the range of 1.419 (2) to 1.434 (2) Å and Fe-C_{cp} distances of ca. 2.04 Å. An average bond of ca. 1.52 Å was observed for the alkyl chains. Interestingly intermolecular hydrogen bondings were observed in the crystal structure of **25**.

2.5.1.2 Synthesis of 5-Ferrocenylpent-4-yn-1,2,3-triol (27)

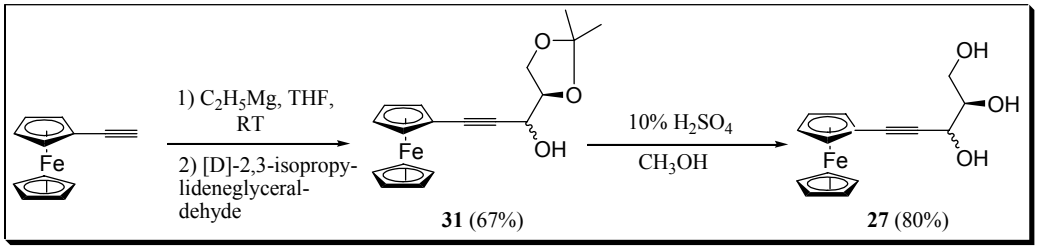

Scheme 2–27: Synthesis of enzyme substrate **27** starting from ferrocenylacetylene and [D]-2,3-isopropylidene glyceraldehyde.

For the synthesis of **27** (Scheme 2–27) initial Grignard reaction between 1-(ferrocenyl)-ethynyl magnesium bromide and [D]-2,3-isopropylideneglyceraldehyde **34** resulted in the adduct **31** as a brown solid in 67% yield. It had a melting point of 95 °C, a characteristic broad stretching band at 3389 cm^{-1} (OH) and a sharp band at 2231 cm^{-1} (C≡C) in the IR.

Deprotection of the acetonide in **31** with trifluoroacetic acid/ acetic acid solution gave the

desired product **27** as a red solid in low yields (30%) with a number of by-products. However, when the deprotection was carried out in acidified methanol (10% sulphuric acid*) **27** was obtained in quantitative yields (80%, MP = 70 °C) within 5 min. A characteristic OH band at 3369 cm^{-1} (OH) and a C≡C 2227 cm^{-1} were observed in the IR. Disappearance of signals at 1.40 and 1.49 ppm in ^{1}H-NMR was indicative of deprotection, which was further confirmed by ^{13}C-NMR.

2.5.1.3 Synthesis of 5-Ferrocenylpentan-1,2,3-triol (28)

Hydrogenation of **31** with palladium over charcoal (10%) in methanol gave the reduced product **59**. It was obtained as yellow oil in 92% yield. It was characterised by the disappearance of the acetylenic stretching band at 2227 cm^{-1} (C≡C) in the IR and an up-field shift of the proton from 4.60 ppm in adduct **31** to 3.5 ppm in product **59** by ^{1}H-NMR.

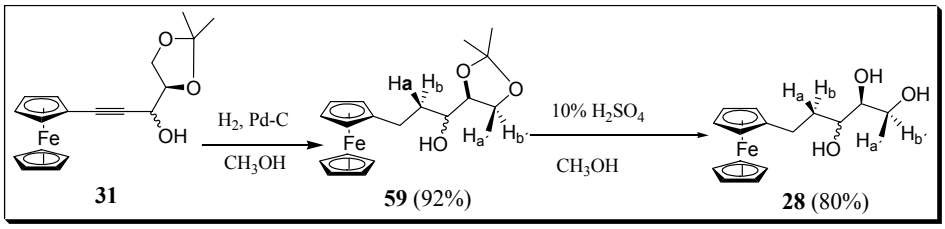

31 **59** (92%) **28** (80%)

Scheme 2–28: Synthesis of the ferrocene containing enzyme substrate **28**.

Deprotection of the acetonide in **59** with 10% sulphuric acid in methanol gave the desired product **28** in 80% yield as a yellow coloured solid with a melting point 71 °C (Scheme 2–28. The product was characterised by disappearance of the methyl protons at 1.35 and 1.43 ppm in the ^{1}H-NMR.

2.5.1.4 Synthesis of 1, 2-Diferrocenylethane-1,2-diol (29)

The vicinal diol **29** was synthesised in 90% yield by a pinacol type of coupling between ferrocenealdehyde in the presence of samarium iodide (Scheme 2–29). The compound was found to be very sensitive to temperature and decomposed above 40 °C.

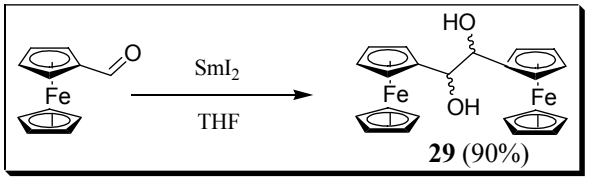

29 (90%)

Scheme 2–29: Synthesis of **29** via a pinacole type coupling of ferrocenealdehyde in the presence of samarium iodide.

* Procedure from Dr. Dilip Dhawale (Pune University), private communication.

It was further characterised by various spectroscopic techniques such as IR, ^{1}H-NMR, ^{13}C-NMR, ESI-MS, and elemental analysis.

2.5.1.5 Attempted Synthesis of 1-Ferrocenylethane-1,2-diol (23) and 1-Ferrocenyl-propane-1,2,3-triol (26)

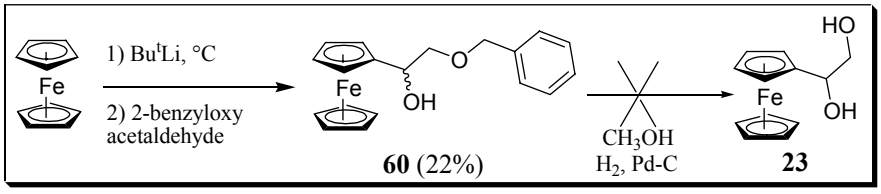

Scheme 2–30: Attempted synthesis of substrate **23** starting from ferrocene and benzyloxyacetaldehyde.

For the synthesis of **23**, an initial addition between monolithiated ferrocene and benzyloxy-acetaldehyde furnished the adduct **60** as a brown oil in 22% yield (Scheme 2–30). A characteristic signal at 4.61 ppm for the benzylic CH_2 protons in ^{1}H-NMR was consistent with the formation of **60**. All attempts to deprotect the benzyloxy group under hydrogenolysis conditions led to the decomposition of the product as well as the formation of small amounts of ferrocenealdehyde and ferrocene. Other methods of deprotection such as boron tribromide and Ca/NH_3 (liq) also led to decomposition of the adduct **60**.

For the synthesis of **26** (Scheme 2–31), the addition of monolithiated ferrocene to [D]-2,3-isopropylidene glyceraldehyde gave the adduct **61** in 20% yield as a yellow solid. Presence of signals at 1.34, 1.37, 1.42 and 1.44 ppm for methyl protons (four signals due to diastereomer formation) in ^{1}H-NMR, and a broad band at 3438 cm^{-1} in the IR were indicative of the adduct formation.

Deprotection of the acetonide group in **61** using various methods including treatment with I_2 in methanol, trifluoroacetic acid in dichloromethane and Dowex 50-W resulted in the decomposition of the adduct. With 10% sulphuric acid in methanol, only a trace amount of the product was obtained within 5 min of reaction time. Longer reaction times as well as column conditions caused product decomposition.

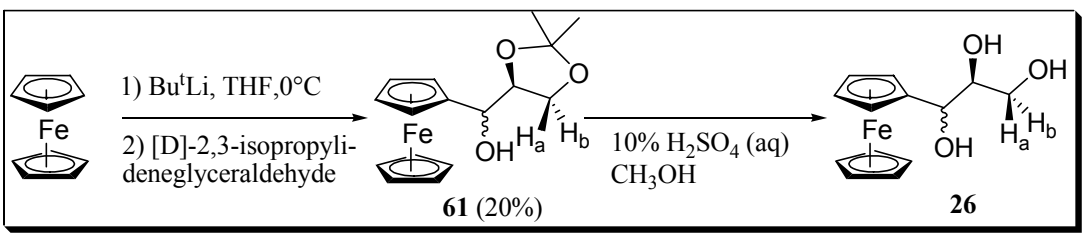

Scheme 2–31: Attempted synthesis of enzyme substrate **26** starting from ferrocene and [D]-2,3-isopropylidene glyceraldehyde.

2.5.1.6 Synthesis of 3-(1,4-Benzoquinoyl)propane-1,2-diol (35)

Synthesis of substrate **35** was achieved as described in the literature,[63] with the initial step involving acylation of 2-allylphenol to 2-allylphenoxyacetate **40** with acetic anhydride in presence of pyridine and catalytic amounts of DMAP. The product **40** was obtained as a colourless oil (90%) having a boiling point of 62-65 °C/2 mbar. The IR of the compound had a strong band at 1762 cm^{-1} which is characteristic for ester bonds (C=O). Presence of a new signal at 2.33 ppm in the ^{1}H-NMR was in agreement with the assignment for **40** (Scheme 2–32).

Peroxidation, epoxide ring opening and deprotection of the phenol were all effected in one step starting with, hydrogen peroxide in formic acid followed by the addition of the base (NaOH) yielding **39** as a colourless oil (11%). Characteristic absorption at 3349 cm^{-1} in the IR and disappearance of signals at 5.18 ppm (terminal alkene, CH2) and 5.99 ppm (alkene, CH) and appearance of new signals at 2.56 ppm and at 3.27 ppm in the ^{1}H-NMR further confirmed the formation of **39**.

Fremy´s salt mediated oxidation of **39** in water containing potassium dihydrogenphosphate gave the desired product **35** as a reddish brown solid (48%). The pure product had a melting point at 79-80 °C (Lit:[63] 81-82 °C), and a strong band at 1651 cm^{-1} (C=O) in the IR. The compound was not stable under mass spectrometric conditions; however, the fragmentation pattern was in agreement with the expected m/z values at 152 (loss of CH_2O), 123 (loss of CH_3O_2) etc. The product was characterised by ^{1}H-NMR, ^{13}C-NMR, and elemental analysis.

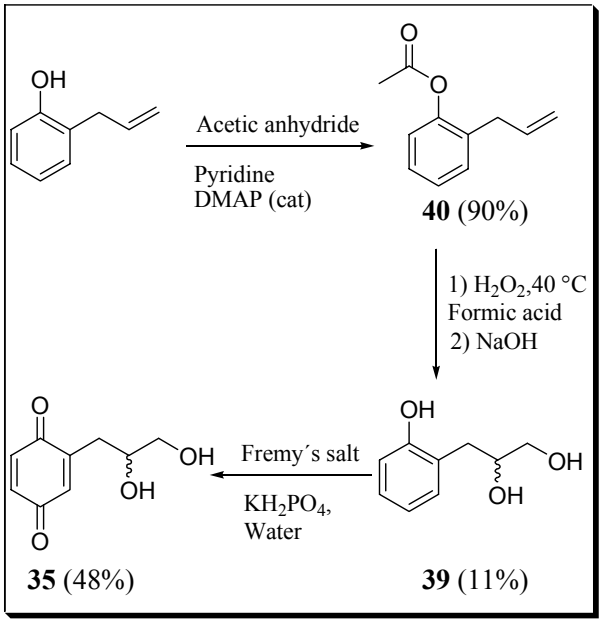

Scheme 2–32: Synthesis of modified enzyme substrate **35** containing quinone as the acceptor group.

2.5.1.7 Attempted Synthesis of Radical Anion Probes 36, 37 and 38 for Enzymatic Investigations

For the synthesis of substrate **36**, a sequence of steps starting with the synthesis of 1-(2,5-dimethoxyphenyl)ethyne was desired. 2,5-Dimethoxyacetophenone was converted initially into 2-(1-chloro-vinyl)-1,4-dimethoxyphenyl benzene (**44**) with PCl_5 in benzene. The product was obtained as a colourless liquid (84-87 °C/1 mbar, 80%). Presence of a strong band at 1578 cm^{-1} in the IR with new signals at 5.73 and 5.79 ppm in the ^{1}H-NMR further confirmed the formation of the product. Refluxing **44** with ethanolic potassium hydroxide for four days gave **43** as a colourless solid (53%, MP = 39-40 °C). Presence of bands at 2106 cm^{-1} in the IR for the acetylenic group and appearance of a signal at 3.31 ppm in ^{1}HNMR for the terminal alkyne were consistent with product formation.

Addition of the corresponding Grignard reagent of **43** onto benzyloxyacetaldehyde gave a colourless oil (85%), having signals at 4.67 ppm for the benzylic protons in ^{1}H-NMR indicating the formation of **42**. Under hydrogenating (H_2/ Pd-C) conditions the diol **41** (81%) was formed from **42** with both deprotection of the alcohol and reduction of the triple bond occuring smoothly. Disappearance of signals at 4.67 ppm and in the aromatic region in ^{1}H-NMR confirmed the assignment. Ceric ammoniumnitrate oxidation of **41** to **36** failed, leading to the decomposition of the product (probably due to polymerisation).

Attempts to synthesise the substrate **37** by Friedel-Crafts reaction between fluorene and [D]-2,3-isopropylideneglyceroylchloride (**45**) in CS_2 failed to generate the acylated product.

Tetranitrofluorene (**47**), the radical anion trap, was prepared by nitration of fluorene, resulting in a cream coloured solid in 84% yield. However, attempts to couple the tetranitrofluorene with the aldehyde failed due to the poor solubility of the tetranitrofluorene in various organic solvents.

2.5.1.8 Attempted Synthesis of Neutral Radical Probes 52-54 Containing TEMPO as the Persistent Radical Source

The synthesis of neutral radical probes **52-54** containing TEMPO as the persistent radical source required 2,2,6,6-tetramethylpiperidin-1-ol (**56**). TEMPO **21** was prepared by refluxing tetramethylpiperidin in benzene with MCPBA for 24 h. The TEMPO radical (**21**) was obtained in 32% overall yield as a low-melting deep red coloured solid. Suitable single crystals of **21** were obtained and analysed by X-ray crystallography.[73] For the synthesis of the neutral radical probes by an ionic pathway, radical **21** was first reduced quantitatively to the corresponding alcohol **56** with ascorbic acid in water for 15 min (disappearance of red colour). The crude alcohol was extracted using ether and concentrated at room temperature in

an inert atmosphere yielding **56** as a colourless solid. The stability of **56** in air was very low as evidenced by a slow appearance of an orange colour when exposed to air. A sharp band at 3440 cm^{-1} (OH) in the IR, and appearance of a signal at 3.5 ppm (OH, 1H) in the ^{1}H-NMR were indicative of product formation.

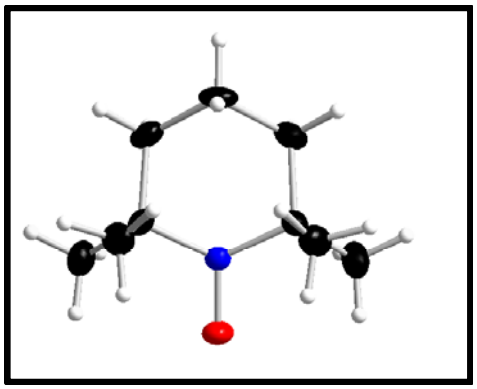

Figure 2–4: Molecular structure of **21** as obtained by X-ray single crystal analysis.

Deprotonation of the alcohol **56** with one equivalent of sodium hydride in dry THF, followed by the addition of 2-bromoethanol yielded no product even when the reaction was stirred for a long duration (over 1 day). Although, such an approach had successfully been utilised in literature for the synthesis of a number of compounds by Fisher *et al.*[74] in their case the bromo group was activated by a phenyl or an allyl group (private communication of *Prof. A. Studer*). Thus, the second approach of trapping a carbon-centred radical was thought to be more appropriate for preparing TEMPO derivatives for enzymatic investigations. However, efforts to trap the α-carbonyl radical of ethyl acetate did not yield the desired product. This could be due to fast dimerisation of the α-carbonyl radical (or due to over-oxidation of the α-carbonyl radical by the oxidant).

Having failed to synthesise enzyme substrates **52-54** to investigate for neutral radical, new probes with TEMPO as the persistent radical source were designed and their synthesis was realised (Chart 2–6).

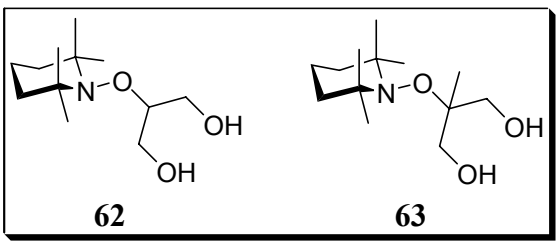

Chart 2–6: List of neutral radical probes designed for enzymatic investigations.

2.5.1.8.1 Synthesis of radical probe 2-(2,2,6,6-tetramethylpiperidinoxy)-propane-1,2-diol (62)

and 2-methyl-2-(2,2,6,6-tetramethylpiperidinoxy)propane-1,2-diol (63)

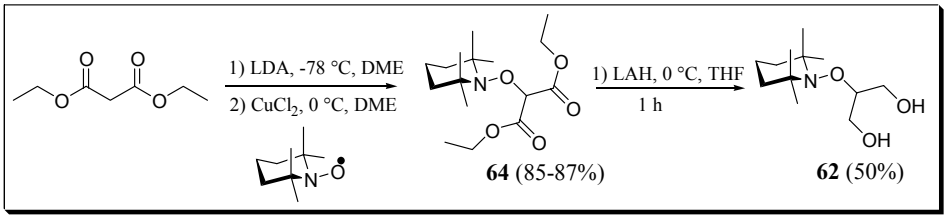

Scheme 2–33: Synthesis of **62** starting from diethylmalonate and the TEMPO radical.

The achiral diol **62** was prepared by LAH mediated reduction of the corresponding diester **64** in 50% isolated yield (Scheme 2–33).[75] The diester precursor itself was prepared by the trapping of the carbon centred radical, obtained by oxidation of the enolate of diethylmalonate at 0 °C, by TEMPO as a colourless low melting solid (85-87%, M.P = 28-30 °C). Presence of a strong IR band at 1767 and 1746 cm^{-1} and methyl signals at 1.08 ppm, 1.20 ppm, 1.29 ppm and methylene signals in ^{1}H-NMR were indicative of product formation. The product was further confirmed by elemental analysis.

The LAH reduction of **64** gave **62** showing a strong band at 3310 cm^{-1} (OH) and bands at 1767 cm^{-1} and 1746 cm^{-1} in the IR. The signals at 1.08 ppm (CH_3) and a shift of the signal at 4.92 ppm (in **64**) to 4.38 ppm (CH) were observed in the ^{1}H-NMR of **62**. The radical probe was further confirmed by elemental analysis.

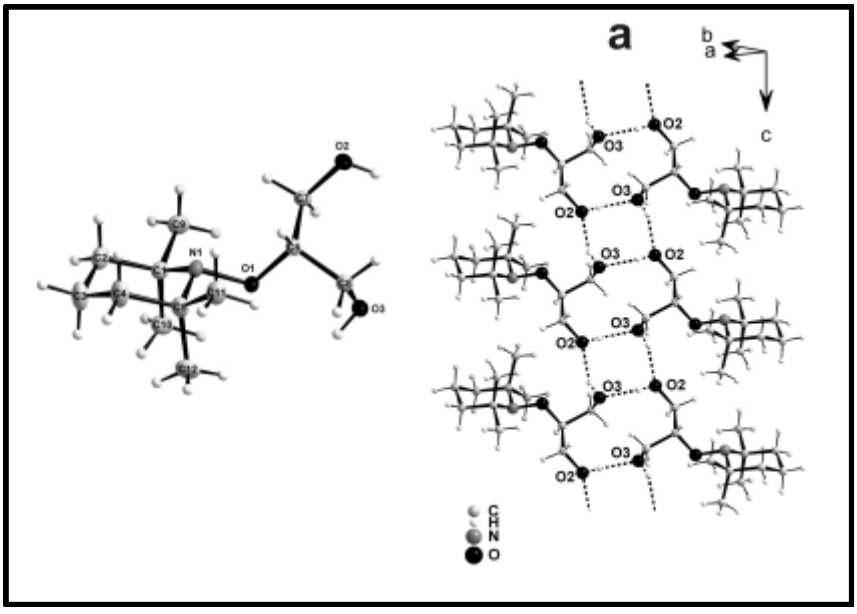

Figure 2–5: Molecular view of **62** as obtained by X-ray single crystal analysis.

Suitable single crystals were obtained for **62** and were analysed by X-ray spectroscopy (Figure 2–5). The title compound crystallises in space group $P2_1/n$ with one molecule in the formula unit. The piperidinoxy ring in **62** adopted the usual chair conformation. The oxygen atom O2 was found staggered with respect to O1 while it was gauche with O3 in the solid

state. Intermolecular hydrogen bonding was observed in the crystal structure of **62**.

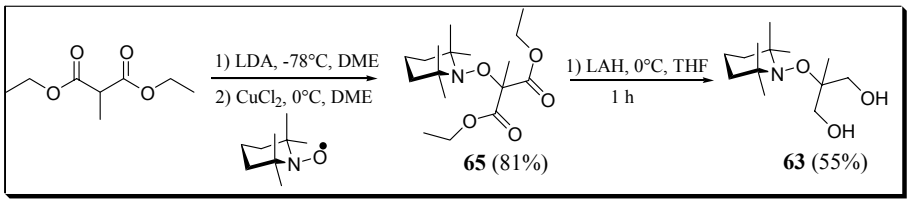

Scheme 2–34: Synthesis of **63** starting from diethyl methyl malonate.

Similarly, radical probe **63** was synthesised by trapping of an α-carbonyl radical,[75] generated by oxidation of the enolate of methyl malonate with copper (II) chloride in dimethoxyethane (Scheme 2–34) with TEMPO. Product **65** was obtained in 81% yield and was further characterised by IR, ^{1}H-NMR, ^{13}C-NMR etc. Suitable single crystals of **65** were obtained and analysed.

Based on X-ray crystallography, **65** was found to crystallise in the monoclinic system with the piperidinoxy ring in the usual chair conformation (Figure 2–6). Intramolecular CH···N and CH···O bonding was observed in the crystal structure with a bond distance of 2.344 (H14-O4)-2.771 Å (H2-N1).

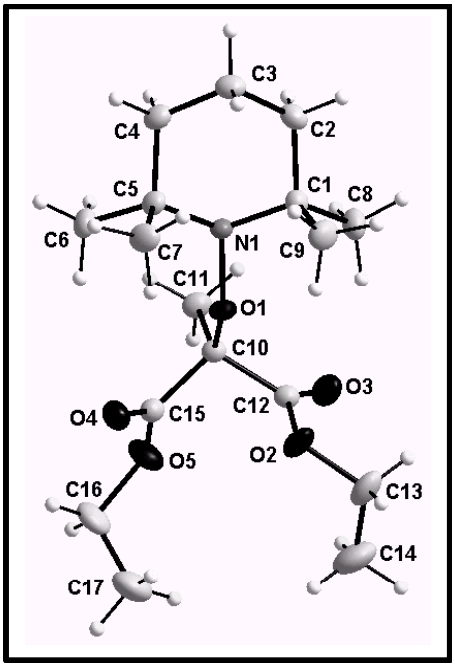

Figure 2–6: Molecular structure of **65** showing the thermal ellipsoids with 50% probability.

LAH reduction of **65** yielded the radical probe **63** in 50-55% yield as a colourless solid, characterised by the appearance of a broad band at 3399 cm^{-1} and the disappearance of a band at 1760 cm^{-1} (C=O) in the IR. Disappearance of signals at 1.08 ppm for the ester methyl and the methylene protons at 3.6 ppm in the ^{1}H-NMR further supported product formation.

Radical probe **55** was synthesised as described in the literature[76] by a coupling of the sodium salt of N-hydroxyphthalimide with 2-bromoethanol in DMF (Scheme 2–35). The product was obtained as a white coloured solid (40%, 82-84 °C). Presence of a sharp band at 3537 cm^{-1} and broad strong bands at 1793 and 1736 cm^{-1} in the IR indicates product formation.

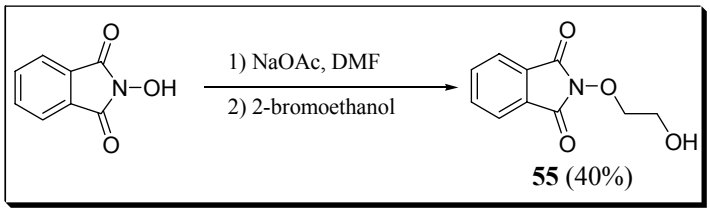

Scheme 2–35: Synthesis of phthalimido derivative **55** as radical and radical anion probe for enzymatic studies.

2.5.1.9 Synthesis of Phenoxyethanol Derivatives for Enzymatic Investigations

Based on the strategy in Scheme 2–36 various substituted phenoxyacetates (**58a-j**) were synthesised in good to moderate yields (48-89%) by treating phenols with ethylbromoacetate in acetone and K_2CO_3.

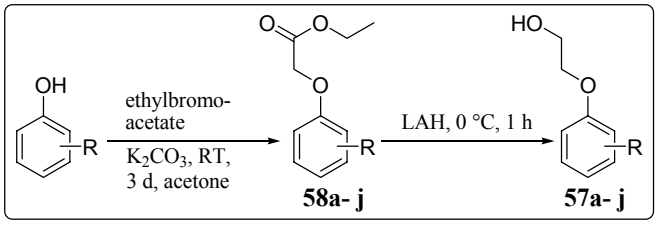

Scheme 2–36: Strategy utilised in the synthesis of various substituted phenoxyethanol derivatives for probing the tolerance of the active site for phenoxyethanol dehydratase from *Acetobacterium sp*.

The formation of the phenoxyacetates was confirmed by various spectroscopic methods. Typically, C=O stretching bands between 1756-1762 cm^{-1} were observed by IR spectroscopy. The presence of signals between 1.26-1.33 ppm (t, CH_3), 4.24-4.27 (q, CH_2) and 4.37-4.76 ppm (s, CH_2) in ^{1}H-NMR were indicative of the formation of phenoxyacetates.

Reduction of the phenoxyacetates **58a-j** with LAH gave the corresponding phenoxyethanols **57a-j** in yields between 31-92%.

Table 2–1: Various phenoxyethanol derivatives **57a-k** prepared from phenoxyesters by LAH reduction (except **58k**).

S. No.	substituents	Ester (% yield, R_f*)	Phenoxyethanol (% yield, R_f*)

a	2,6-Me	**58a** (80, 0.38)[77]	**57a** (79.0, 0.23)[78]
b	2,4-Me	**58b** (87, 0.34)[77]	**57b** (75.0, 0.15)[78]
c	2,4,6-Me	**58c** (89, 0.34)[79]	**57c** (92, 0.15)
d	2-Propyl^{n}	**58d** (48, 0.57)	**57d** (49, 0.36)
e	2-Propyl^{i}	**58e** (89, 0.65)	**57e** (86, 0.19)
f	2-Butyl^{s}	**58f** (84, 0.67)	**57f** (92, 0.19)
g	2-Butyl^{t}	**58g** (84, 0.64)	**57g** (91, 0.23)[80]
h	4-Bromo	-	**57h** (32, 0.08)
i	2-Nitro	**58i** (87, 0.23)[81]	-
j	4-Methoxy	**58j** (83, 0.13)[82]	**57j** (81, 0.38)[83]
k	4-Nitro		**57k** (31, 0.38)[84]

*R_f values obtained on SiO_2 in 20% ether in hexane.

Formation of the products was further confirmed by the disappearance of the band at 1750 cm^{-1} band for (C=O) and the appearance of an OH vibration between 3500-3300 cm^{-1} in the IR. Disappearance of signals between 1.26-1.33 ppm (t, CH_3) and 4.24-4.27 (q, CH_2) with the appearance of new signals between 3.89, 4.18 ppm and 3.96-4.65 ppm (CH_2) by ^{1}H-NMR as well as the disappearance of a signal at 200 ppm (C=O) in ^{13}C-NMR were indicative of product formation.

2.5.2 Synthesis of Mechanistic Probes for Solution Studies

To test the concept of translating short-lived radical cations both via intra as well as intermolecular electron transfer process, substrates were designed to mimic the complete enzymatic eliminase reaction in solution. The essential components necessary to mimic the enzymatic eliminase reactions are, i) a radical source (**RS**) which would lead to α,β-dihydroxyethyl radical under mild conditions, ii) a vicinal diol group and c) an electrophore (donor [**D**] or acceptor [**A**]) attached somewhere in the molecule.

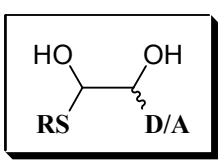

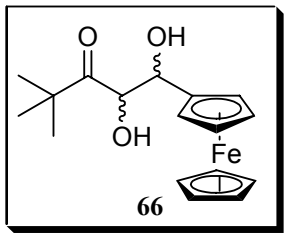

Thus compound **66** was designed containing a *t*-butylketone as the radical precursor with a vicinal diol and ferrocene as donor.

2.5.2.1 Design and Synthesis of Substrates to Mimic Eliminase Reactions with Ketones as Radical Precursors

Use of ketones as radical precursors has been successfully applied by Giese *et al*.[85] The retroanalysis for the synthesis of **66** (Scheme 2–37) reveals that it can be prepared by an aldol type of reaction between a protected *t*-butyl-α-hydroxymethylketone and ferrocenealdehyde as the desired synthons. The deprotection of the hydroxyl group would lead to the desired product **66**.

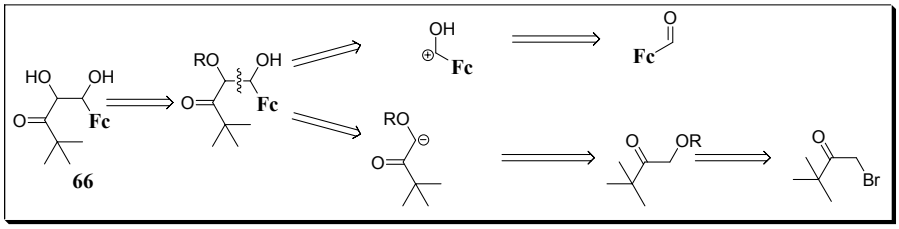

Scheme 2–37: Retrosynthesis of **66**, a solution probe to mimic eliminase reaction.

For the synthesis of **66** the methodology required a very labile protecting group of the hydroxy group. Protecting groups such as trimethylsilyl[86] or benzyloxy[87] groups are desired, as these functional groups can be cleaved off easily under mild acidic or neutral hydrogenolysis conditions.

The synthesis of **66** containing ferrocene as the donor, initially required the synthesis of *t*-butyl-α-trimethylsilyloxyketone (**68**), which was prepared by converting *t*-butylmethylketone into 3,3-dimethyl-2-trimethylsilyloxybutene-1 (**67**) with DABCO and trimethylsilylchloride. **67** was obtained in 75% yield as a colourless liquid (45-48 °C/19 mbar [Lit:[86a] 140-142 °C]).

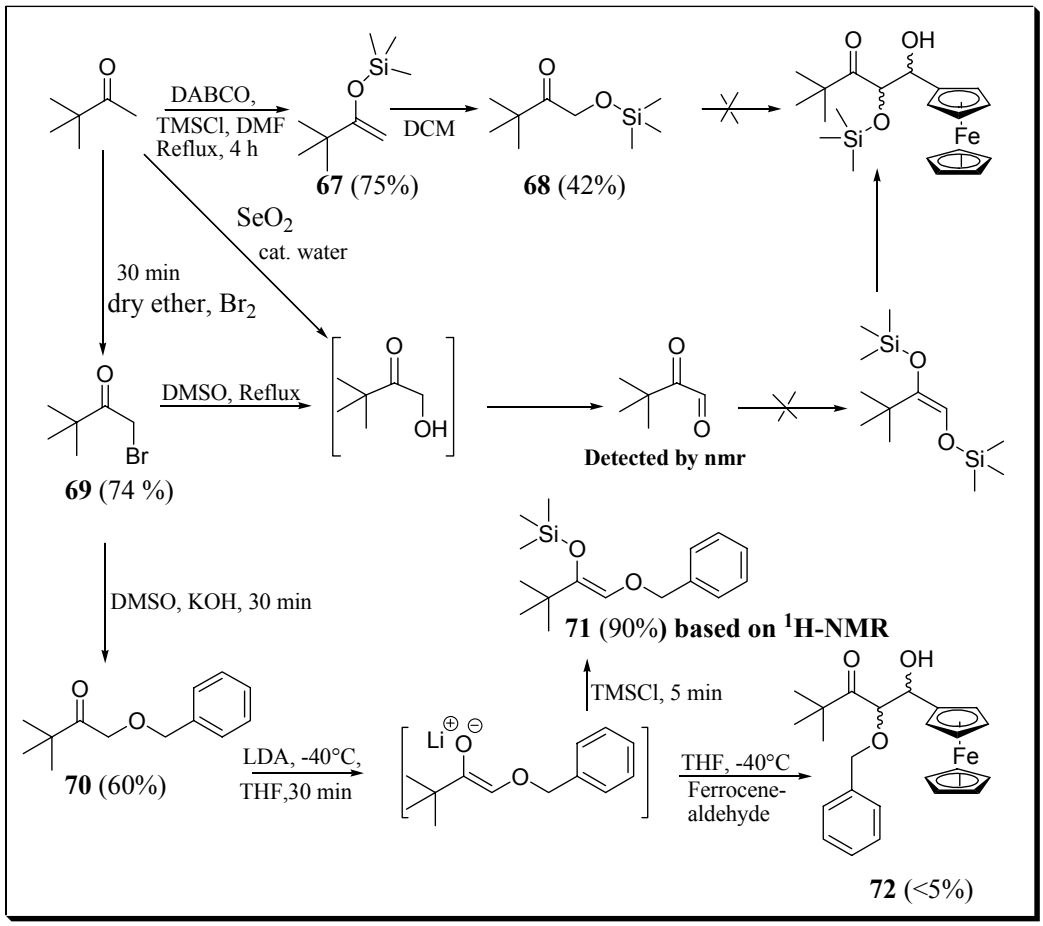

Scheme 2–38: Attempted synthesis of **66** by various routes starting from *tert*-butylmethylketone.

The IR showed a strong absorption at 1619 cm^{-1} (C=C). 3,3-Dimethyl-2-trimethylsilyloxybutene-1 (**67**), when treated with MCPBA in DCM, gave 3,3-dimethyl-1-trimethylsilyloxybutane-2-one (**68**)[86a] as a colourless liquid in 42% yield. A strong absorption at 1725 cm^{-1} (C=O) in the IR and the presence of a signal at 0.1 ppm (9H) in the ^{1}H-NMR confirmed the product formation. Aldol condensation between **68** and ferrocenealdehyde did not yield the desired adduct. ^{1}H-NMR of the reaction mixture (after workup) showed a complete disappearance of the silylether group at 0.1 ppm, suggesting the deprotection of the hydroxyl group under these reaction conditions (Scheme 2–38). Thus, substitution of the protecting group with the more versatile benzyloxy group was chosen (as in **70**).

For the synthesis of 1-benzyloxy-3,3-dimethyl-2-butanone (**70**), 1-bromo-3,3-dimethyl-2-butanone (**69**)[88] was synthesised according to the literature procedure (74%). Treatment of **69** with powdered potassium hydroxide in dry DMSO in presence of benzylalcohol gave the desired product **70** in 60% yield as a colourless liquid. The IR showed an absorption at 1720 cm^{-1} (C=O) and had two distinct signals in ^{1}H-NMR at 4.3 and 4.5 ppm for the two methylene protons.

Aldol condensation between ferrocenealdehyde and **70** failed to give the desired Aldol adduct at low temperatures, however, when the reaction was allowed to stir at room temperature for nearly two days, a yellow crystalline solid was isolated in less than 5% yields. The solid showed a carbonyl stretching at 1700 cm^{-1} (C=O) in the IR, disappearance of the signal at 4.3 ppm in the ^{1}H-NMR for the methylene proton, and the appearance of signals for ferrocene confirmed the formation of **72**. Mass spectroscopic investigations revealed a molecular ion peak at m/z = 422 for $\mathbf{M}^{+}$, which corresponded to **72**.

Trapping the enolate of **70** by trimethylsilylchloride showed the trimethylsilyl derivative **71** in over 90% yield, which was quantified by ^{1}H-NMR. The above experiment indicated that the low product formation was not because of low enolate content but because of the low coupling reaction. This could be due to strong steric repulsions between the benzyloxy group of the enolate and the ferrocenealdehyde in the transition state. This was further confirmed by the formation of the aldol product (**73**) in over 81% yield between t-butylmethyl ketone and ferrocenealdehyde.

Another approach to prepare **66** was then to introduce the diol functionality towards the end of the synthesis, which would allow one to avoid any protection and deprotection steps. One such approach is epoxidation of double bonds followed by base catalysed ring opening (Scheme 2–39).

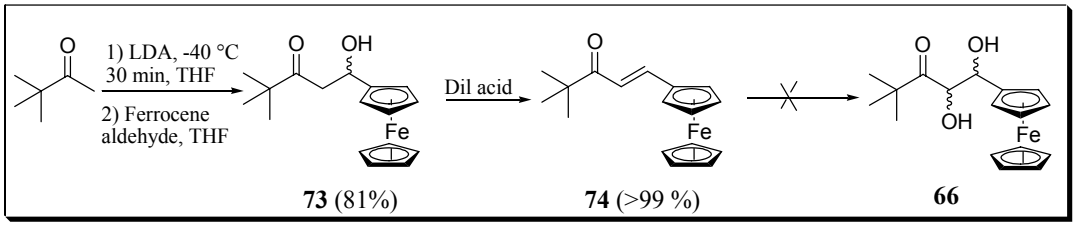

Scheme 2–39: Attempted synthesis of **66** via epoxidation of double bond in **74.**

An aldol condensation between ferrocenealdehyde and *t*-butylmethylketone upon acidic work up gave the desired dehydrated product **74** in quantitative yield (99%). The product was characterised by IR, ^{1}H-NMR, ^{13}C-NMR and elemental analysis. Epoxidation of **74** with MCPBA led to the decomposition of the starting material.

2.5.2.2 Design and Synthesis of Substrate Mimic 75 for Eliminase Reaction using Barton ester as Radical Initiator

For the synthesis of Barton ester **75** we started with the initial preparation of the diacetonide of D-mannitol (Scheme 2–40). The [D]-1,2,5,6-diisopropylidenemannitol (**77**) was prepared by treating D-mannitol with fused zinc chloride in dry acetone at room temperature for 10 h.

The diacetonide **77** was obtained in 72% (MP 120-122 °C) yield as a colourless solid. While the D-mannitol was insoluble in dichloromethane or chloroform, the acetonide **77** dissolved easily in organic solvents such as dichloromethane and chloroform. The presence of signals at δ = 1.34 and 1.39 ppm (s) for the methyl protons in the ^{1}H-NMR confirmed the formation of **77**. Sodium metaperiodate oxidation of the diacetonide **77** gave the aldehyde **34** ([D]-2,3-isopropylideneglyceraldehyde) in 62% (BP 42-44 °C/11 mbar) as a colourless oil. The presence of a band at 1735 cm^{-1} (C=O) in IR and signal at 9.68 ppm in ^{1}H-NMR and 202.8 ppm (C=O) in ^{13}C-NMR confirms assignment to **34**.

Aldehyde **34** was further oxidised to the potassium salt **76** (potassium-[D]-2,3-isopropylideneglycerate) as a colourless solid in 46% (softens above 60 °C). A shift in the C=O band in the IR from 1735 cm^{-1} in **34** to 1620 cm^{-1} in **76**,[89] and the disappearance of the aldehydic signal at 9.28 ppm in ^{1}H-NMR indicated the product formation. **76** was found to dissolve easily in water and other protic solvents such as ethanol and methanol. Acid chloride **45** was prepared by treating **76** with oxalylchloride in dry ether with catalytic amounts of pyridine. The pure product was obtained in 43% yield as a colourless liquid (71-72 °C/25 mbar). The presence of a band at 1777 cm^{-1} for the C=O in IR and a signal at δ = 174.2 ppm in the ^{13}C-NMR confirmed formation of **45**.

Barton ester **75** was prepared by treating the acid chloride **45** with the sodium salt of *N*-hydroxy-2-pyridinethione in dry ether with catalytic amounts of DMAP in 83% as a cream coloured solid (MP 62 °C). Barton ester **75** showed a band at 1810 (C=O) and 1736 cm^{-1} (C=S) in IR. The compound was further characterised by ^{1}H-NMR ^{13}C-NMR and elemental analysis.

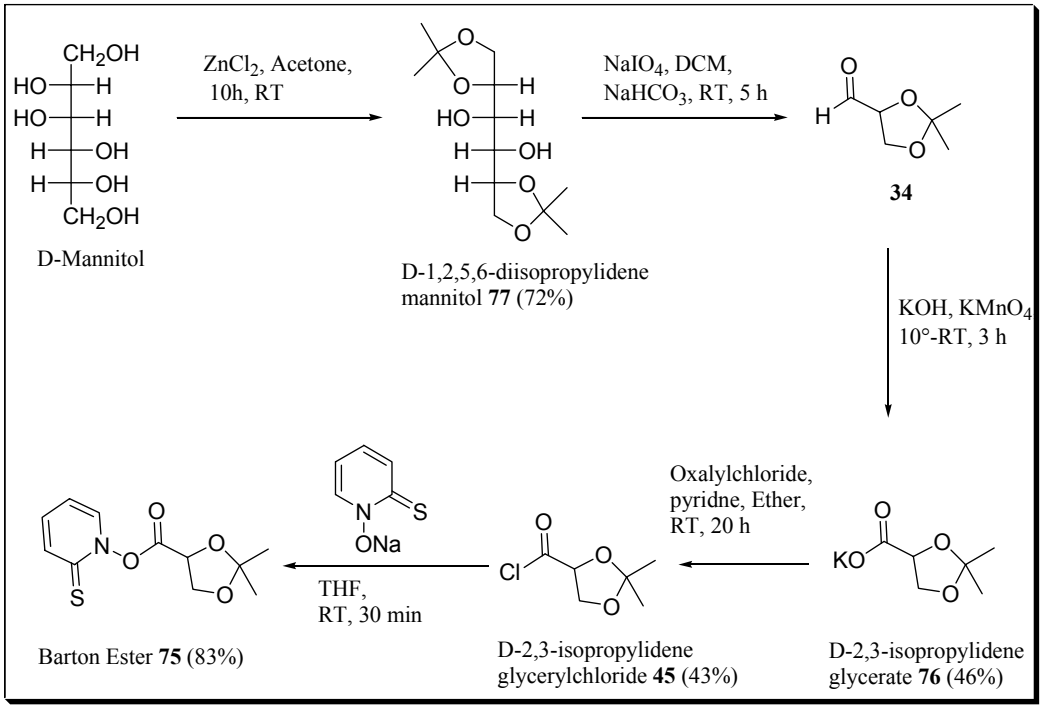

Scheme 2–40: Synthesis of **75** starting from D-mannitol.

2.5.2.3 Synthesis of Barton Ester 78

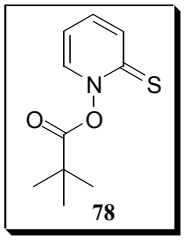

Barton ester **78**[90] was prepared in a way similar to the synthesis of **75**, involving reaction between 2, 2-dimethlypropanoylchloride and the sodium salt of *N*-hydroxy-2-pyridinethione. The product was obtained in quantitative yield as a cream coloured crystalline solid and was characterised by various techniques such as IR, ^{1}H-NMR, ^{13}C-NMR and HRMS.

2.5.2.4 Synthesis of Substrates to Mimic Eliminase Reaction using Fluorenoneoxime Derivatives as Radical Precursors

Acyl radicals, an important class of reactive intermediates have been generated from fluorenoneoxime esters under flash photolytic conditions by Bucher *et al.*[91] Their advantage is that they are easy to synthesise and that they show excellent thermal stability. To mimic only the radical cationic intermediate pathway for an eliminase reaction in solution, **79** was designed, based on the fluorenoneoxime as the radical precursor.

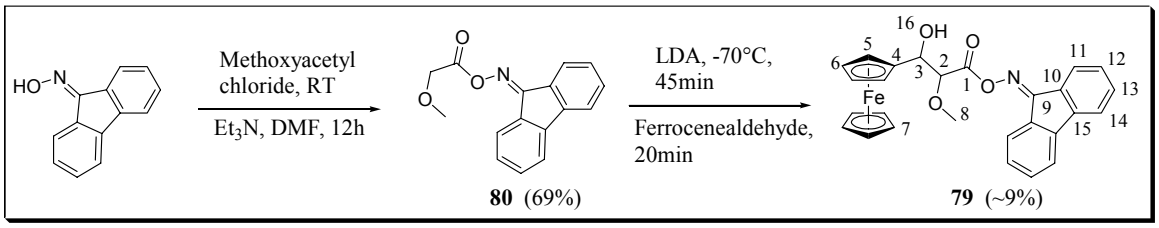

Scheme 2–41: Synthesis of **79** starting from fluorenoneoxime.

For the synthesis of **79**, initially fluorenoneoxime was reacted with methoxyacetyl chloride in dry DCM at room temperature to yield **80** (69%) as a cream-yellow solid. The product was characterised by IR and ^{1}H-NMR. Aldol condensation of **80** with ferrocenealdehyde at -70 °C gave a mixture of compounds, along with **79** as a reddish brown solid in about 9% yield (decomposes above 95 °C, Scheme 2–41). The product was characterised by IR, ^{1}H-NMR, ^{13}C-NMR and HRMS. The experimentally found isotope splitting in ESI-MS was found to be in agreement with the theoretical isotope splitting (Figure 5–2).

2.5.2.5 Synthesis of Substrate to Mimic Eliminase Reaction Based on Cobalt-Carbon Bond Homolysis

Cobalamin is commonly used as a co-reactant for carrying out enzymatic reactions with coenzyme B_{12} dependent enzymes such as diol and glyceroldehydratase. Co-C bond homolysis has also been used to generate carbon centred radicals for synthetic applications[92] as well as for biomimetic modelling studies.[42] Thus, substrate **81** after the Co-C bond homolysis (photochemical/thermal) was designed to undergo a fast intramolecular hydrogen atom abstraction via a six membered ring giving rise to a more stable protected hydroxyalkyl radical.

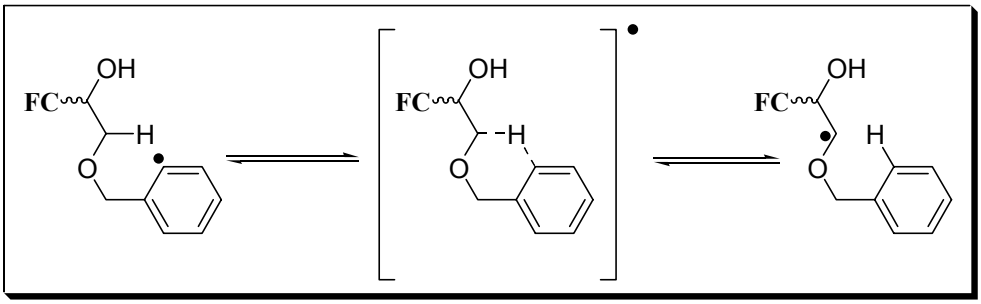

Retroanalysis for the synthesis of **81**, gave **82** and **83** as the main precursors (Chart 2–7). Synthesis of **82** can be achieved via a Grignard reaction between ethylnylferrocene and (2-iodo-benzyloxy)-acetaldehyde.

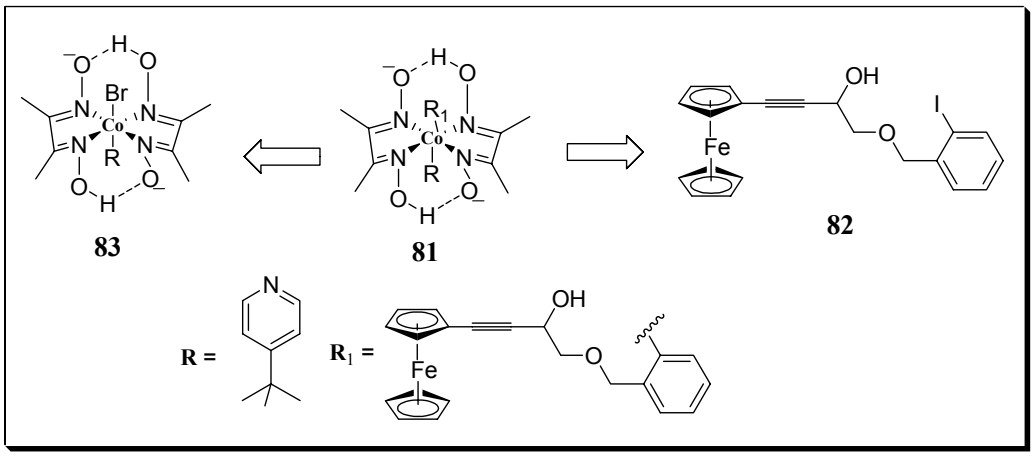

Chart 2–7: Retroanalysis for the synthesis of **81**.

Synthesis of (2-iodobenzyloxy)-acetaldehyde required an initial photochemical bromination of acetaldehyde diacetal with *N*-bromosuccinamide. The 2-bromo acetaldehyde diethylacetal (**86**)[93] was obtained as a colourless liquid in 47% yield (Scheme 2–42).

The bromoacetaldehyde diethylacetal (**86**) was then converted into 1-(2,2-diethoxy-ethoxymethyl)-2-iodo-benzene (**85**) in the presence of powdered potassium hydroxide in DMSO. A colourless liquid was obtained in 44% yield, and the presence of signals below 6 ppm in the ^{1}HNMR for the aryl protons confirmed the product formation. Product **85** was then converted into (2-iodobenzyloxy)-acetaldehyde (**84**) with trifluoroacetic acid[94] in chloroform.

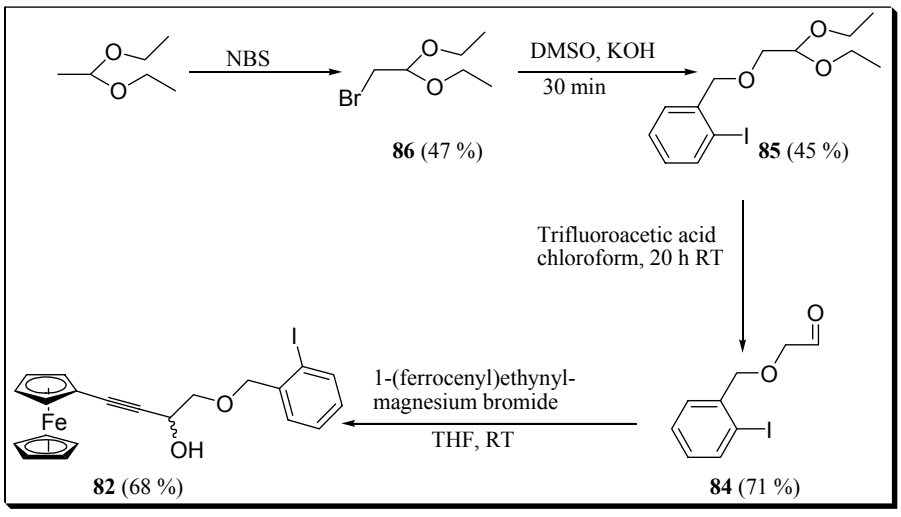

Scheme 2–42: Synthesis of **82** starting from acetaldehyde dimethylacetal and ferrocenylethyne.

The aldehyde formed had two stretching bands in the IR spectrum at 1736 cm^{-1} (C=O) and 1711 cm^{-1} (C=O) for the aldehyde. All the products were characterised by ^{1}H-NMR, ^{13}C-NMR and DEPT.

Grignard reaction between the aldehyde **84** and ethynylferrocene **32** gave a brown liquid in

68% yield. The product **82** was characterised by ^{1}H-NMR, ^{13}C-NMR, DEPT and HRMS.
For the synthesis of **83**, dimethyl glyoxime was initially reacted with cobalt (II) bromide in acetone to give a green coloured solid in quantitative yield. From the elemental analysis the product was assigned to **87**.[95] The green coloured solid **87** upon treatment with 4-*t*-butylpyridine in methanol gave a brown crystalline solid **83** in 98% yield. It was characterised by ^{1}H-NMR having a characteristic signal for the *t*-butyl at 1.29 ppm and by elemental analysis. Attempts to couple **82** with **83** under literature known procedures gave either the starting materials or led to decomposition of **82** under the reaction conditions giving rise to products that could not be characterised.

2.5.3 Cyclic Voltammetry and UV-Vis Spectroscopic Investigation of Mechanistic Probes

After having synthesised a representative number of radical and radical ion probes for enzyme studies, their electrochemical properties (i.e. the redox potentials etc) were investigated. Furthermore, UV-Vis spectroscopic investigations of the ferrocene radical cations was undertaken in solution.

2.5.3.1 Cyclic Voltammetric Investigations

Cyclic voltammetric measurements were made at room temperature using freshly distilled dry acetonitrile. For radical cation probes a reversible wave was observed for the ferrocene and similarly two reduction waves were observed for the quinone based radical anion probe. The difference in the anodic to cathodic current was between 55-60 mV, which was close to the theoretical value (56 mV) for a one-electron reversible system having Nernstian behaviour (except the second wave of **35**). The anodic to cathodic current ratio was found to be one, which further confirmed the E_{rev} electrode kinetics, as expected for such systems (Table 2–2).
The oxidation potentials observed for the ferrocene-based radical ion probes clearly show that simple saturated alkyl substitution on the ferrocene ring causes a cathodic shift of the wave by 50 - 70 mV (**25**, **28** and **29**). The presence of two waves in **29** could be due to the diastereomeric composition of the sample, which could not be obtained in a single diastereomer due to the instability of the product.

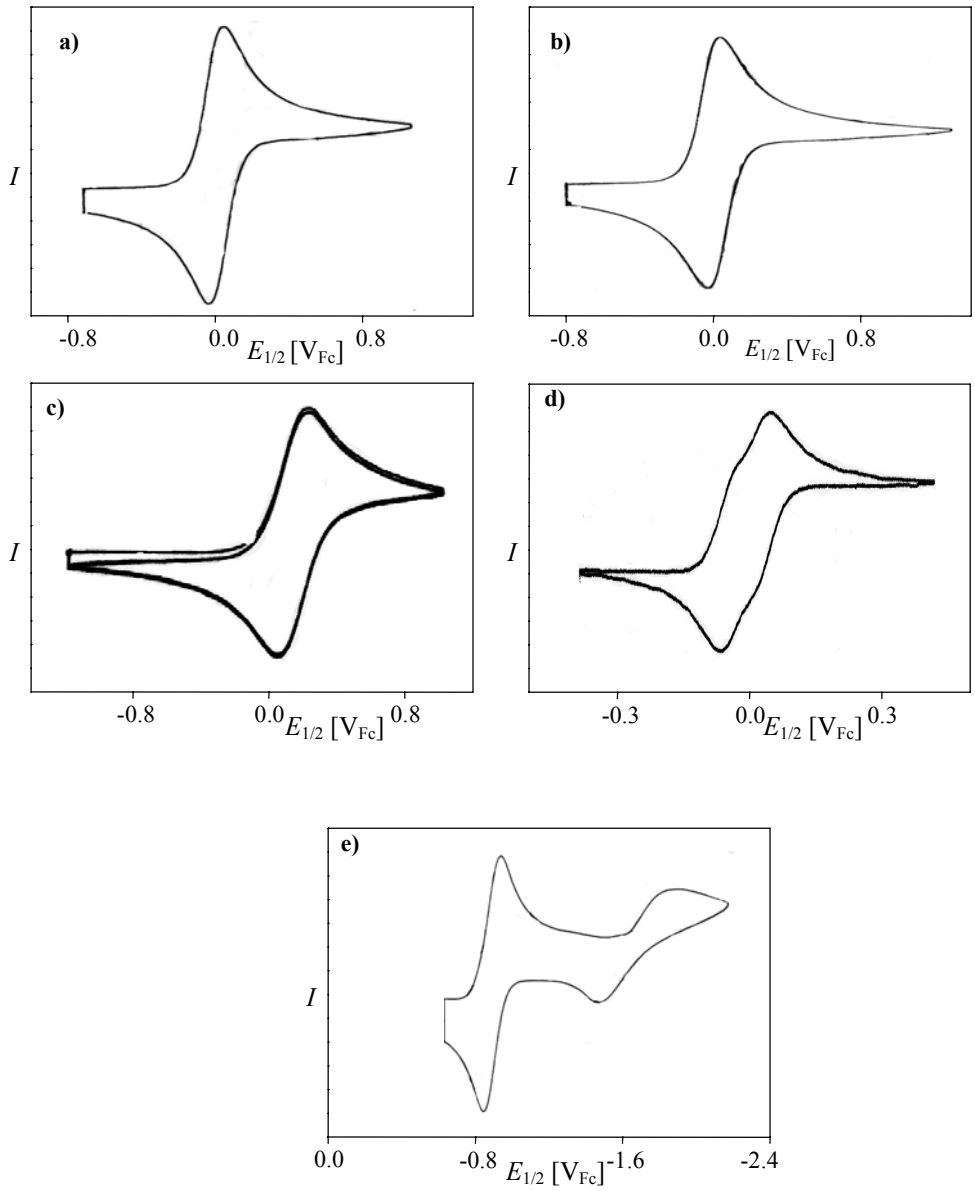

Figure 2–7: Cyclic voltammograms of various substrates for enzymatic investigations, a-d are ferrocene based radical cation probes, a) **25**, b) **28**, c) **27** and d) **29** respectively, e) quinone based radical anion probe **35**.

When the ferrocene ring was attached to a triple bond, an anodic shift of about 50 mV was observed as in **28**. The radical anion probe **35** showed two reduction waves at -0.87 V_{Fc} and -1.71 V_{Fc}, of which the first wave was found to be completely reversible (E_{pc}-E_{pa} = 60 mV, I_c/I_a = 1) while the second wave was found to be partially reversible (the effect could be due to intramolecular hydrogen bonding between the ketone part of the molecule with that of the alcohol part of the side chain).

Table 2–2: $E_{1/2}$ [V_{Fc}] values obtained for various radical ion probes for enzymatic investigations by cyclic voltammetry in acetonitrile at 100 mV/s scan rate.

Radical ion probe	$\Delta E = E_{pa} - E_{pc}$ (mV)	$E_{1/2}$ (V_{Fc})
25	55	– 0.05
27	60	+ 0.12
28	60	– 0.05
29	55, 60	– 0.07, + 0.05
35	60	–0.87, –1.71

2.5.3.2 Cyclic Voltammetric Investigation of 79

Cyclic voltammetry investigations of **79** revealed a completely reversible wave for the ferrocene moiety at $E_{1/2}$ = -0.06 V_{Fc} and two irreversible waves at E_{pc}^{1} = -1.82 V_{Fc} and E_{pc}^{2} = -2.17 V_{Fc} (Figure 2–8a and Figure 2–8b). The two reduction waves must originate from the reduction of the fluorenoneoxime residue, which was in agreement with the cyclic voltammetric investigation of **80** (E_{pc}^{1} = -1.83 V_{Fc} and E_{pc}^{2} = -2.16 V_{Fc}, Figure 2–8c, Table 2–3).

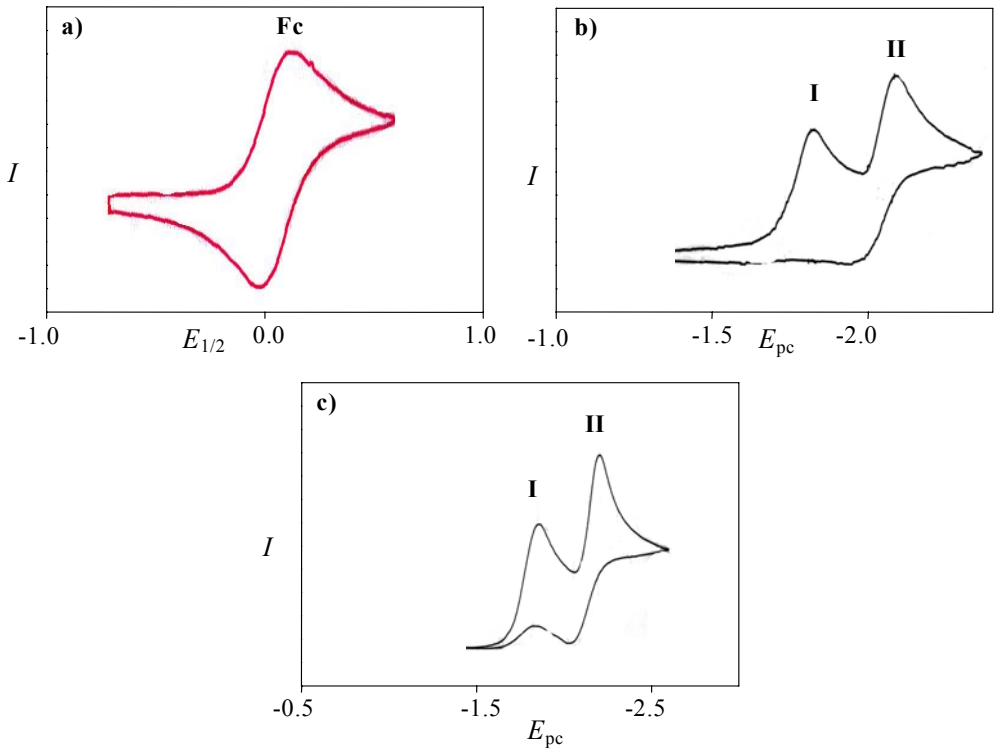

Figure 2–8: Cyclic voltammogram in acetonitrile at 100 mV/s scan rate, a) anodic side of **79**, b) cathodic side of **79** and c) cathodic side of **80**.

Table 2–3: Electrochemical data for **79** and **80** as observed by cyclic voltammetry in acetonitrile.

Substrate	$E_{1/2}$ [V_{Fc}]	E_{pc}^{1} [V_{Fc}]	E_{pc}^{2} [V_{Fc}]
80	-	-1.83	-2.16
79	-0.06	-1.82	-2.17

2.5.3.3 UV-Vis Spectroscopic Investigation of the Radical Cation of Ferrocene-based Enzyme Probes

The UV-Vis spectrum of various ferrocene-based enzyme substrates was measured. Typically, for the probes containing saturated alkyl chain (**25**, **28**, and **29**) three absorption maxima were obtained (λ_{max} = 229-232 nm, 330-334 nm and 446-450 nm, Figure 2–9). However, probe **27** had an additional absorption at λ_{max} = 267 nm that was also observed in all the precursors containing the triple bond (**30** and **31**).

Ferrocene-based enzyme probes were then oxidised chemically with a saturated solution of ferric chloride as oxidant. UV-Vis spectroscopy and ESI-MS spectroscopy monitored the entire process of oxidation. Ferrocene and its oxidised form (ferrocenium ion) have distinct UV-Vis spectra with the latter (λ_{max} = 450 nm) being more bathochromically shifted than (λ_{max} = 620 nm) the neutral form.

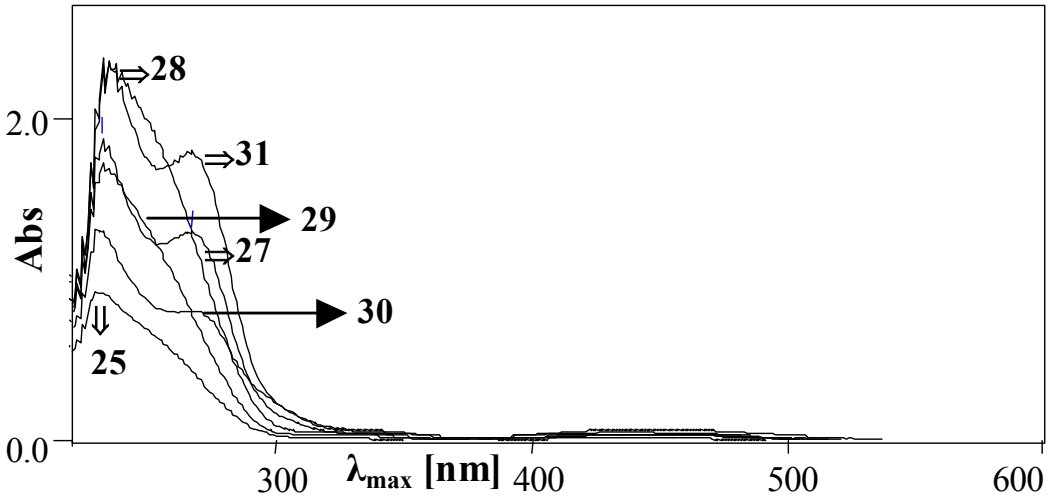

Figure 2–9: UV-Vis spectrum of ferrocene based enzyme probes (including precursors).

2.5.3.4 UV-Vis Study to Check the Solubility of Phenoxyethanol Derivatives 57a-g in Buffer Solution at pH 8

The substituted phenoxyethanol derivatives **57a-g** were tested for water solubility at pH 8, required for the enzyme investigation. The quantification was performed using UV-Vis spectroscopy.

Initially, the determination of the ε values was made in a known solvent wherein the solubility was complete (Lambert-Beer behaviour). This was followed by a concentration determination at pH 8 using the ε value determined earlier.

The ε values were obtained by the UV-Vis spectroscopic dilution method (obeying Beer-Lambert law), where a known quantity of phenoxyethanol derivative was dissolved in chloroform and the concentration was varied by successive dilution.

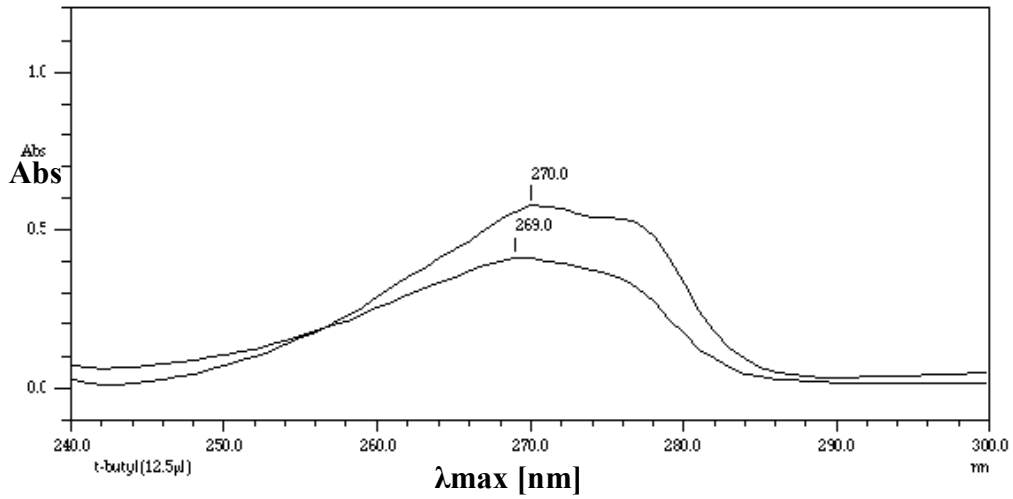

Figure 2–10: UV-Vis spectrum of 2-*t*-butylphenoxyethanol in dichloromethane and at pH = 8.

Table 2–4: UV-Vis spectroscopic determination of the solubility of the various phenoxyethanol derivatives in DCM and at pH 8.

Substrate	λ_{max} [nm] in DCM	ε	λ_{max} [nm] at pH 8	Conc. [mM] at pH 8
57a	265	328.7	263	0.8
57b	279	230.5	272	2.4
57c	272	555.0	269	1.7
57d	272	1466	272	0.6
57e	272	1461.3	269	0.7
57f	272	1417.2	271	0.2
57g	270	1760.8	271	0.2

The UV-Vis spectroscopic investigations revealed that the λ_{max} values in the **57a-g** series

remained more or less in the same range 265-279 nm in DCM; however, the ∈ value increases with an increase in the bulk of the substituents at the 2-position (Table 2–4).

To achieve solubility in the buffer solution (pH 8) a known quantity of the phenoxyethanol derivative was suspended in 0.5 ml of the buffer solution and warmed in a water bath at 80 °C for 5-6 min. After the solution had cooled to room temperature (~20-22 °C), 50 µl of the aliquote was diluted to a final volume of 3 ml with the buffer and its absorption determined. The concentration was then obtained from the ε values determined in chloroform (no significant shift in λ_{max} was observed for **57a-g** in buffer solution from chloroform, Figure 2–10).

Thus, it was observed that all the phenoxyethanol derivatives **57a-g** form a mM solution in buffer solution at pH-8. A 10-fold decrease in the solubility was observed upon increasing the bulk at position-2.

2.5.4 Enzymatic Testing of Radical and Radical Ion Probes

The substrate derivatives were tested on diol and glyceroldehydratase isolated from an over-expressed enzyme in *E. Coli* and also on phenoxyethanol dehydratase from *Acetobacterium sp*. The studies were carried out in collaboration with Prof. J. Rétey´s group at the University of Karlsruhe (diol and glyceroldehydratase) and with Prof. B. Schink´s group at University of Konstanz (phenoxyethanol dehydratase).

2.5.4.1 Testing of Radical and Radical Ion Probes on Diol and Gylceroldehydratase from *E. Coli*.

Materials for enzyme studies

The enzyme diol and glyceroldehydratase were obtained in pure form by purifying the protein expressed in *E. Coli*. The enzymes were found to be stable in air and required propane-1,2-diol as their natural substrate. The enzymes were active at pH 8, and all tests were carried out at 37 °C. The enzymes diol and glyceroldehydratase were adenosylcobalamine (coenzyme B_{12}) dependent.

Apart from 1,2-propanediol, the enzymes were also known to accept 2,3-butanediol, however, with lower activity when compared to the natural substrate. Gel filtration was performed on the enzyme material to get rid of the 1,2-propanediol used as a stabiliser before testing the substrate derivatives.

The various probes tested on these enzymes include the radical (**55**, **62**, **63**) and radical ion probes (**25**, **27**, **28** and **35**) synthesised as described earlier. Apart from these 2-

(methylthio)ethanol (**88**), 2-mercaptoethanol (**89**), 2-(methanesulphonyl)ethanol (**90**) and glycidol (**91**) were used as radical probes which were obtained from commercial sources (Acros/Aldrich).

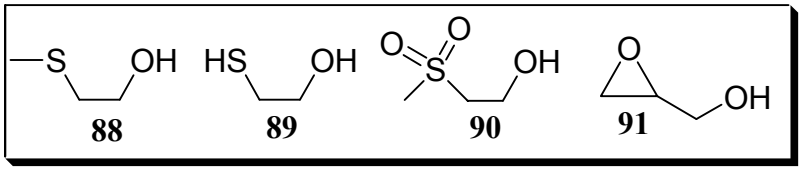

2.5.4.2 Enzyme Assay

The enzyme assay used for the present investigations was an indirect activity assay according to which the product of one enzyme becomes the substrate for another enzyme. Thus, the product of the diol or glyceroldehydratase, i.e. an aldehyde or ketone, becomes the substrate for the alcohol dehydrogenase, which transforms the carbonyl derivatives into the corresponding alcohol. In doing so, the enzyme consumes NADH which can be easily monitored by following a decrease in the absorption at λ_{max} = 350 nm (Scheme 2–43).

Typically, an enzyme test involved incubation of a known amount of the diol dehydratase, substrate/substrate derivative, NADH and alcohol at 37 °C, in a buffer solution at pH 8 for 3 min. A known amount of adenosylcobalamine was then added and the decrease in absorption at λ_{max} = 350 nm for consumption of NADH was monitored over a period of 5 min.

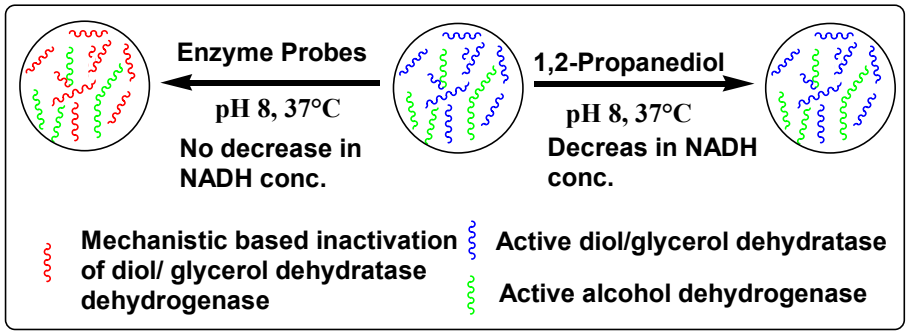

Scheme 2–43: Schematic representation of the enzyme assay used.

Any inhibitory effect by radical or radical ionic intermediates could easily be detected by no change in the absorption of NADH even after the addition of a natural substrate.

First, pure enzymes (diol and glycerol dehydratase) were treated with the natural substrate 1,2-propanediol. The substrate concentration varied between 1 mM to 1 µM and the initial velocity was measured. The kinetic data for the diol dehydratase showed a V_{max} = 0.198 mM/s and K_m = 0.004 mM which were obtained by plotting the change in initial velocity/ rate against the concentration of the substrate (Table 2–5, Figure 2–11).

Table 2–5: Effect of 1,2-propanediol concentration on the initial velocity in diol dehydratase expressed in *E. Coli*.

Substrate [mM]	Initial Velocity [mM/s]	1/Substrate [mM^{-1}]	1/Rate [$mM^{-1}s$]
1	0.174	1	5.75
0.5	0.211	2	4.74
0.25	0.185	4	5.41
0.1	0.209	10	4.78
0.05	0.193	20	5.18
0.025	0.186	40	5.38
0.001	0.144	1000	6.94

The treatment of diol and glycerol dehydratase from *E. Coli* with substrate derivatives to probe radical cationic intermediates showed no change in absorption for the consumption of NADH. The addition of 1,2-propanediol to the above mixture showed an immediate decrease in concentration of NADH (similar to the one observed only for 1,2-propanediol).

Similarly, for radical anionic and neutral radical probes no change at $\lambda_{max} = 350$ nm was observed when they were incubated with the enzyme. After the addition of the natural substrate an immediate decrease in the NADH concentration was observed (Table 2–6, Scheme 2–44).

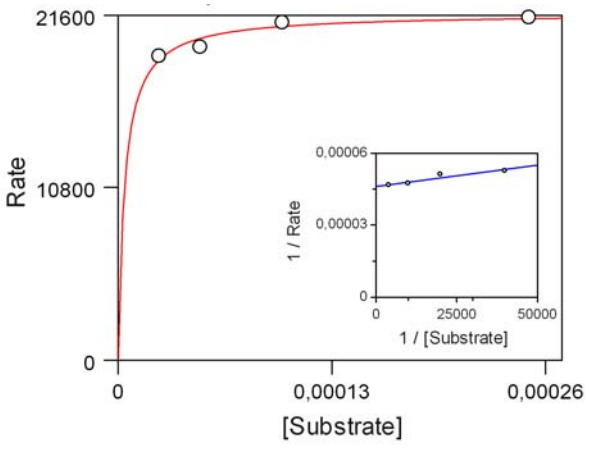

Figure 2–11: Michaelis-Menten plot of the rate as a function of [S] from the data in Table 2–5. Inset is the Lineweaver-Burk plot.

Table 2–6: Various radical and radical ion probes tested on diol and glyceroldehydratase expressed in *E. Coli*.

Substrate	Enzyme Activity (without 1,2-propane diol)	Enzyme Activity (with 1,2-propane diol)
25-28	No activity	Activity found*
35	No activity	Activity found*
55	No activity	Activity found*
62-63	No activity	Activity found*
88-91	No activity	Activity found*

* Activity similar to pure 1,2-propanediol

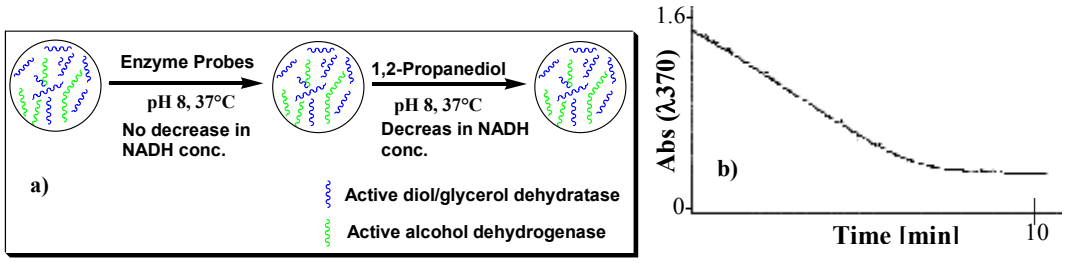

Scheme 2–44: a) Enzymatic assay for testing the radical and radical ion probes, b) typical decay at λ_{max} = 350 nm observed after addition of 1,2-propanediol.

The major implications of the above enzyme investigations are a) the investigated active site of the enzymes diol and glycerol dehydratase are very small (known from the crystal structure data, and b) the retention of the activity in the presence of 1,2-propanediol and the substrate derivatives suggests that the radical and radical ion substrate derivatives are no inhibitors of the enzyme. Since the present method is an indirect method there is the possibility that the carbonyl derivatives of the diol dehydratase enzyme are not accepted by alcohol dehydrogenase (from yeast).

In order to rule this out, investigations were also carried out with alcohol dehydrogenase from horse liver (known to accept large and bulky aldehydes and ketones as substrates). For radical cation probes no decrease in NADH was observed indicating that they were indeed not accepted by the diol/glycerol dehydratase. With radical anion probes, a small activity was observed, and the activity was only dependent on the alcoholdehydrogenase enzyme and NADH. The addition of 1,2-propanediol showed an immediate decrease in NADH, hence no deactivation of the enzymes by the radical anion probes was observed. Similar results were obtained when the neutral radical probe glycidol was used as a substrate in the enzyme assay.

The inability of the above enzymes to accept 2-mercaptoethanol, 2-(methylthio)ethanol, 2-

(methylsulphonyl)ethanol also reinforced the fact that the enyzme required the two OH-group for its activity.

2.5.4.3 Testing of Radical, Radical Ion Probes and Phenoxyethanol Derivatives on Phenoxyethanol Dehydratase from *Acetobacterium sp.*

Enzyme assays similar to the ones used in diol and glyceroldehydratase, were run with phenoxyethanol dehydratase with the main difference being that the enzyme was not available in pure form. Substrate derivatives to probe the hydrophobic and electronic factors were tested in addition to the radical and radical ion probes.

2.5.4.3.1 Materials

The enzymes used for the investigations included the cell free extract from the Acetobacterium strain *LuPhet 1*. The cells grown in the lactate were harvested after achieving a certain size (Figure 2–12) determined by transmittance of the solution and checking of the samples under microscope.

The cells were washed once with a potassium phosphate buffer, centrifuged and stored at liquid nitrogen temperature. The harvested cells were then resuspended in a phosphate buffer (pH = 8) containing 2.5 mM titanium (III) citrate. The latter was found essential for the stability of the enzyme. The cells were ruptured using a French press technique. The ruptured cells were then centrifuged giving a supernatant free of cell extract. The supernatant was a cocktail of various enzymes including the diol, glycerol and phenoxyethanol dehydratase (confirmed by the enzyme assay).

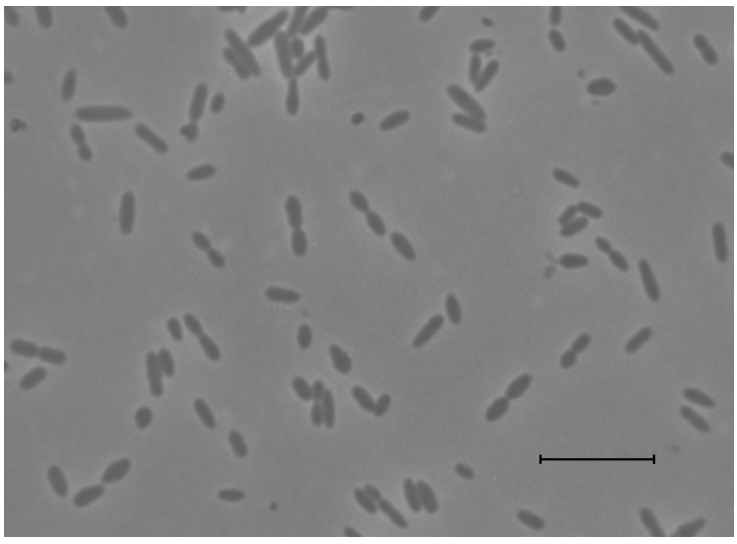

Figure 2–12: Photo showing the growth of *Acetobacterium sp*. culture used for the preparation of cell free extract.

The enzyme was found to be very unstable in oxygen, thus, all solutions for the assay were

prepared and handled under anoxic conditions. All the probes to map out the active site of the enzyme **57a-j** including the radical and radical ion probes used for diol dehydratase were investigated.

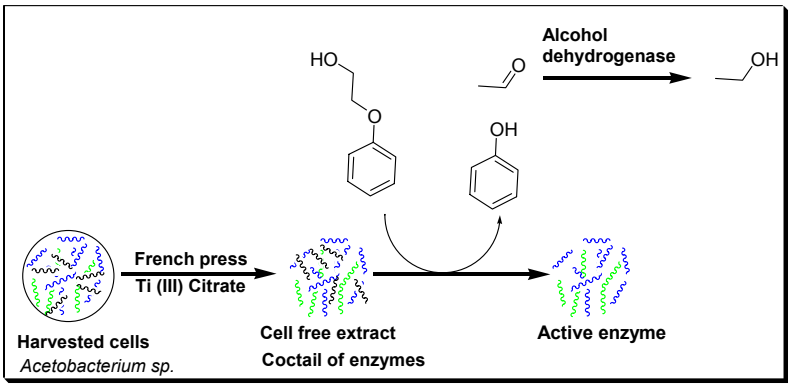

Scheme 2–45: Assay used to test radical, radical ion and various phenoxyethanol derivatives for activity in phenoxyethanol dehydratase.

A typical enzyme assay involved an initial incubation of the alcohol dehydrogenase, NADH and a substrate derivative for 2-3 min followed by the addition of the cell free extract of the phenoxyethanol dehydratase (Scheme 2–45). The enzyme kinetics was monitored by UV-Vis spectroscopy at λ_{max} = 350 nm for the consumption of NADH. The activity of the enzymes in growing cells was measured *in-vivo* and was calculated with the assumption of 5 mg/ml of protein concentration in the cell extract. With this procedure an activity of the crude cell extract was found to be 9.7 µmol/mg /min.

The radical and radical ion probes gave millimolar solutions when dissolved in a pH 8 phosphate buffer. However, the presence of titanium (III) citrate was found to lower the solubility of these substrates in the buffer. To dissolve the substrates, initially a stock solution of the substrate was prepared in ethanol, which was then added to the buffer (without the enzyme); the solution was then warmed for about 20-25 min at 50 °C to remove the alcohol.

Phenoxyethanol was used as control and its activity was assigned arbitrarily to 100%. The activity of the radical and radical ion probes and phenoxyethanol derivatives was positioned accordingly.

Testing the radical and radical ion probes with phenoxyethanol dehydratase

The cell free extract was initially screened with the radical and radical ion probes using the assay described in Scheme 2–45. Only with radical cation probe **25** was the inhibition of the enzyme observed, while with other probes retention of the enzyme activity was observed (activity observed after the addition of phenoxyethanol, which was similar to, when only phenoxyethanol was used, Table 2–7).

The loss of activity for the **25** can arise due to a) mechanism based inhibition or b) due to substrate based inhibition. The presence of ethanol could also be the cause for the inhibition. To get further insights into the nature of the inhibition, control experiments only with ethanol were also performed.

Table 2–7: Activity of various substrates on phenoxyethanol dehydratase.

Enzyme Probe	Enzyme activity (no phenoxyethanol)	Enzyme activity (in presence of phenoxyethanol
25	No activity	No activity
27, **28**, **35, 55**, **62**, **63**	No activity	Activity found

Testing the Hydrophobic and Electronic Tolerance of Phenoxyethanol Dehydratase

The phenoxyethanol derivatives **57a-j** were also tested on the cell-free extract containing the phenoxyethanol dehydratase. Additionally 2-phenylthioethanol (**92**) and 2-ethylthioethanol (**93**) were also tested for phenoxyethanol dehydratase activity.

The assay was similar to the one used earlier. The activity was measured for the substrate derivatives and was positioned relative to phenoxyethanol, which was arbitrarily assigned 100% activity (Table 2–8).

Table 2–8: Activity of phenoxyethanol dehydratase in presence of various phenoxyethanol derivatives.

Substrate derivative	Concentration [mM]	Activity [%age]
2,6-Dimethyl [**57a**]	0.50, 0.15	1-2, 3.4-7.8
2,4,6-Trimethyl [**57c**]	0.53	0.71
2-^{n}Propyl [**57d**]	0.14	No activity
2-^{i}Propyl [**57e**]	0.14	1-3
2-^{i}Butyl [**57f**]	0.09	No activity
2-^{t}Butyl [**57g**]	0.14	4-8
4-Bromo [**57h**]	0.53	14.2
4-Methoxy [**57j**]	0.53	6.6
2-ethylthioethanol [**93**]	2.7	11
2-phenylthioethanol [**92**]	1.7	1

Substrate derivatives containing hydrophobic groups such as methyl, propyl and butyl groups showed very low activity except for **57b**, **57d** and **57g** where no activity was observed. Substrates probing for electronic effects with a methoxy or bromo group as in **57j** and **57h**

showed activity which was lower than the natural substrate. Interestingly 2-ethylthioethanol showed relatively high activity than 2-phenylthioethanol. Interestingly the activity of **57a**, **57g** and **57j** had very similar activity. The most interesting of the three is the **57g** which has a very bulky *t*-butyl group in the *ortho* position.

2.5.4.4 Kinetic Investigations to Determine the Nature of the Inhibition of Phenoxyethanol Dehydratase by Racemic4-Ferrocenylbutane-1,2-diol (25)

Typically, the assay involved variations of the concentration of **25**. Three such assays were carried out with 1 mM, 0.1 mM and 0.01 mM of **25**. For each concentration of inhibitor four sets of experiments were run forming a "bundle". The bundle was further subdivided into "sets" wherein the concentration of the phenoxyethanol added after the addition of **25** (concentration constant) was varied (7.14 mM, 3.57 mM, 1.43 mM and 0.71 mM). For the purpose of comparison control experiments with above concentrations of phenoxyethanol were carried out without **25**. Control experiments with ethanol addition were also performed. Within each set three measurements were carried out, one for phenoxyethanol without **25** (Table 2–9) one for phenoxyethanol added to an already incubating solution of enzyme + **25** (Table 2–10) and finally one for phenoxyethanol added to an incubating solution of enzyme + ethanol (Table 2–11).

Table 2–9: Control assays containing only phenoxyethanol with variation of initial velocity with concentration.

Final Phox conc. [mM]	Avg Velocity 10^{-6} [mol L^{-1} min^{-1}]	1/Phox	1/Velocity
Bundle-A			
7.14	639.79	140.06	1563.01
3.57	368.39	280.11	2714.51
1.43	391.09	699.30	2556.94
0.71	281.20	1408.45	3556.16
Bundle-B			
7.14	462.75	140.06	2161.00
3.57	317.56	280.11	3149.03
1.43	220.89	699.30	4527.14
0.71	116.86	1408.45	8557.16
Bundle-C			
3.57	608.18	280.11	1644.26

1.43	503.99	699.30	1984.17
0.71	357.06	1408.45	2800.67

Table 2–10: Addition of phenoxyethanol to the assay containing known concentration of **25**.

Final Phox conc. [mM]	Avg Velocity 10^{-6} [mol L^{-1} min^{-1}]	1/Conc.	1/Velocity
Bundle-A	Final concentration of **26** = 15.71 μM		
7.14	96.63	140.06	10349
3.57	43.91	280.11	22774
1.43	20.64	699.30	48456
0.71	11.20	1408.45	89311
Bundle-B	Final concentration of **26** = 8.57 μM		
7.14	310.49	140.06	3221
3.57	190.96	280.11	5237
1.43	73.08	699.30	13683
0.71	43.21	1408.45	23141
Bundle-C	Final concentration of **26** = 1.43 μM		
3.57	614.93	280.11	1626.21
1.43	420.24	699.30	2379.57
0.71	265.51	1408.45	3766.41

Table 2–11: Control assays containing known concentration of ethanol as inhibitor.

Final Phox conc. [mM]	Avg Velocity 10^{-6} [mol L^{-1} min^{-1}]	1/Conc.	1/Velocity
Bundle-A	Final concentration of ethanol = 15.71 μM		
7.14	228.31	140.06	4380.08
3.57	215.93	280.11	4631.06
1.43	182.31	699.30	5485.20
0.71	108.05	1408.45	9255.04
Bundle-B	Final concentration of ethanol = 8.57 μM		
7.14	300.41	140.06	3328.83
3.57	238.92	280.11	4185.43

1.43	113.91	699.30	8778.90
0.71	73.87	1408.45	13719.90
Bundle-C	Final concentration of ethanol = 1.43 μM		
3.57	570.36	280.11	1753.29
1.43	438.11	699.30	2282.54
0.71	326.38	1408.45	3063.95

2.5.5 Generation and Intermolecular Trapping of Enol Radical Cations

Relatively long-lived enol radical cations (half-life of few milliseconds to microseconds) based on β,β-dimesityl enols have been reported by our group some time ago.[96] Here, the translation of radical cations of the above type, into long-lived ones such as ferrocene radical cation was attempted. While the generation of enol radical cation usually requires an undesired oxidation step (which could lead to a direct oxidation of ferrocene), a rather different approach was adopted here. The approach for generating enol radical cations involved the transformation of enols to enolates (the oxidation potentials of enolates are approximately 1-1.5 V cathodically shifted as compared to the enols) which allows a selective one-electron oxidation to α-carbonyl radicals. Additionally, it allows the use of mild oxidising agents such as ferrocenium hexafluorophospahte instead of *tris*-(4-bromophenyl)aminium salt. The α-carbonyl radicals generated by this method are kinetically stable due to the presence of two bulky mesityl groups. The enolates under cyclic voltammetric conditions showed complete reversibility and were also characterised by EPR.These α-carbonyl radicals can be converted into enol radical cations via protonation using strong organic acids such as trifluoroacetic acid (Scheme 2–46). The advantage being that the whole process could be followed by UV-Vis spectroscopy.

The utility of the ferrocene not only as oxidant but as a reporter molecule for enol/ enol ether radical cation is further enhanced by the fact that both the ferrocene and its oxidised form have a distinct UV - Vis absorption spectrum, with the latter being more bathochromically shifted (ferrocene: λ_{max} = 450 nm, and ferricenium ion: λ_{max} = 620 nm).

Enol **E1** was chosen as the model compound and was deprotonated with tetramethylammonium hydroxide between -10 to-15 °C leading to enolate **A1**.

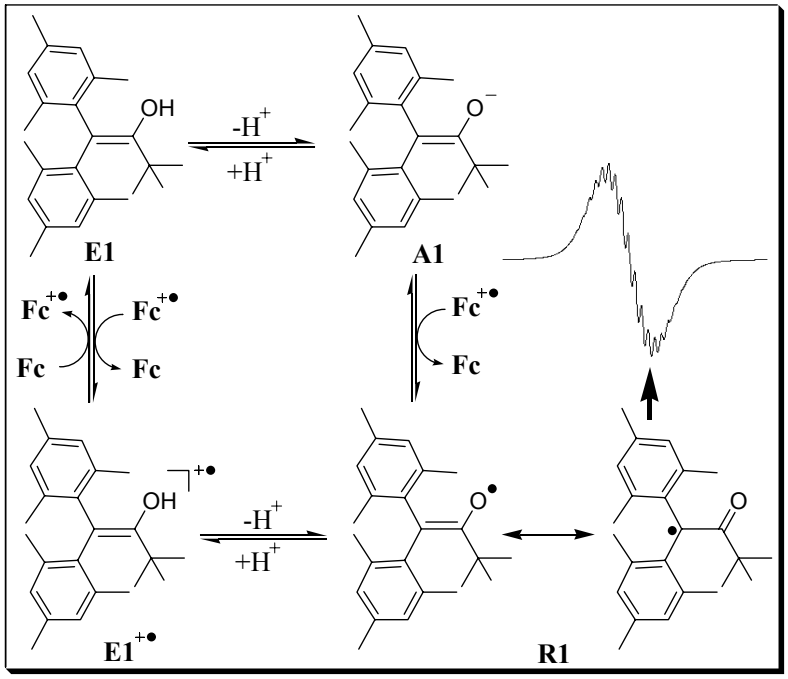

Scheme 2–46: Depicts the procedure used for generation of the kinetically stable α-carbonyl radical **R1** and trapping the enol radical cation (**E1**$^{+\bullet}$) by ferrocene in an intermolecular fashion. The EPR spectra for **R1** were taken from thesis of M. Röck.

Enolate **A1** when oxidised with 1eq. of ferrocene radical cation (**Fc**$^{+\bullet}$) gave the α-carbonyl radical **R1** and ferrocene (**Fc**). The disappearance of the 620 nm band for the ferrocene radical cation was indicative of the one-electron reduction of the ferrocenium ion.

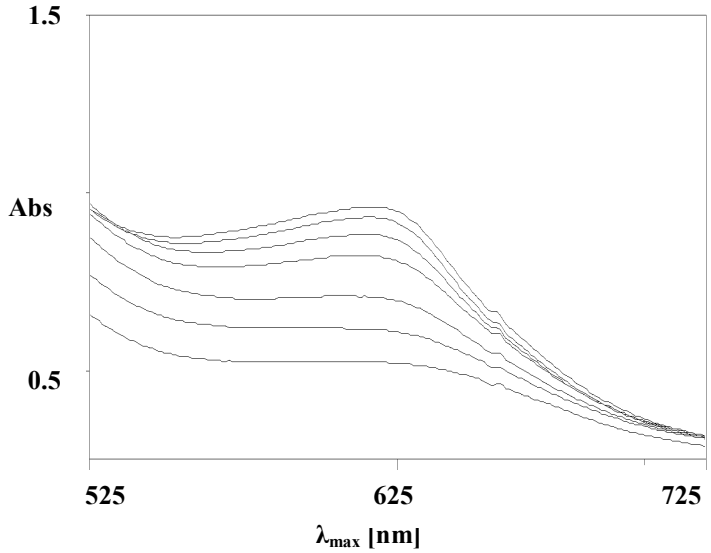

Figure 2–13: Formation of ferrocenium ion observed upon addition of trifluoroacetic acid to a solution containing ferrocene and **R1**.

The slow addition of trifluoroacetic acid to the solution containing **R1** and **Fc** showed the emergence of the 620 nm band for the **Fc**$^{+\bullet}$ indicating the conversion of **R1** into enol radical cation (**E1**$^{+\bullet}$) which oxidised the ferrocene intermolecularly (Figure 2–13). The increase in the band at 620 nm was observed till 1. eq. of the TFA was added. The oxidation potential of the

α-carbonyl radical **R1** was found to be +0.14 V_{Fc}. Hence, it could not be further oxidised to α-carbonyl cation by $\mathbf{Fc^{+\bullet}}$.

2.5.6 Photochemical Studies on Barton Ester 75

The concept of generating ethenol radical cation from **75** would require acidic conditions; hence, it was necessary to know the acid sensitivity of **75**, which shows a typical absorption at λ_{max} = 360 nm. This absorption band can be used as a marker and any change by protonation can easily be follwed by monitoring the changes of this band.

The acid sensitivity test was performed with trifluoroacetic acid. The ratio of the absorption in the presence of the acid to the retention in absorption after the addition of a little excess pyridine was taken as a measure of acid lability. The experiments were further divided into two categories:

a) Dependence of the absorption at λ_{max} = 360 nm on the concentration of acid, b) time dependence of the absorption at λ_{max} = 360 nm with known concentration of the acid.

2.5.6.1 Effect of TFA Concentration on Absorption at λ_{max} = 360 nm for Barton Ester 75

An increasing amount of trifluoroacetic acid (10 µl at each step from a stock solution of TFA 38.5 mM and 219 mM) was added to a solution of **75** (0.10 mM). By adding an equimolar quantity of TFA to **75**, a very small decrease in absorption was observed at λ_{max} = 360 nm (Figure 2–14a). A further increase in acid concentration not only induced a decrease in the absorption at λ_{max} = 360 nm but additionally led to a 12 nm shift of the chromophore to λ_{max} = 348 nm (Figure 2–14c).

Interestingly, a plateau was reached after the addition of 28 equivalents of the acid (Figure 2–15, Table 2–12). This was further supported by the fact that no change in the spectrum was observed even after the addition of 70 equivalents of the acid (Figure 2–14b). The original spectrum of the acid-free **75** was retained after the addition of a slight excess of pyridine as base to the acidified solution clearly showing a reversible protonation of the chromophore (Figure 2–14c).

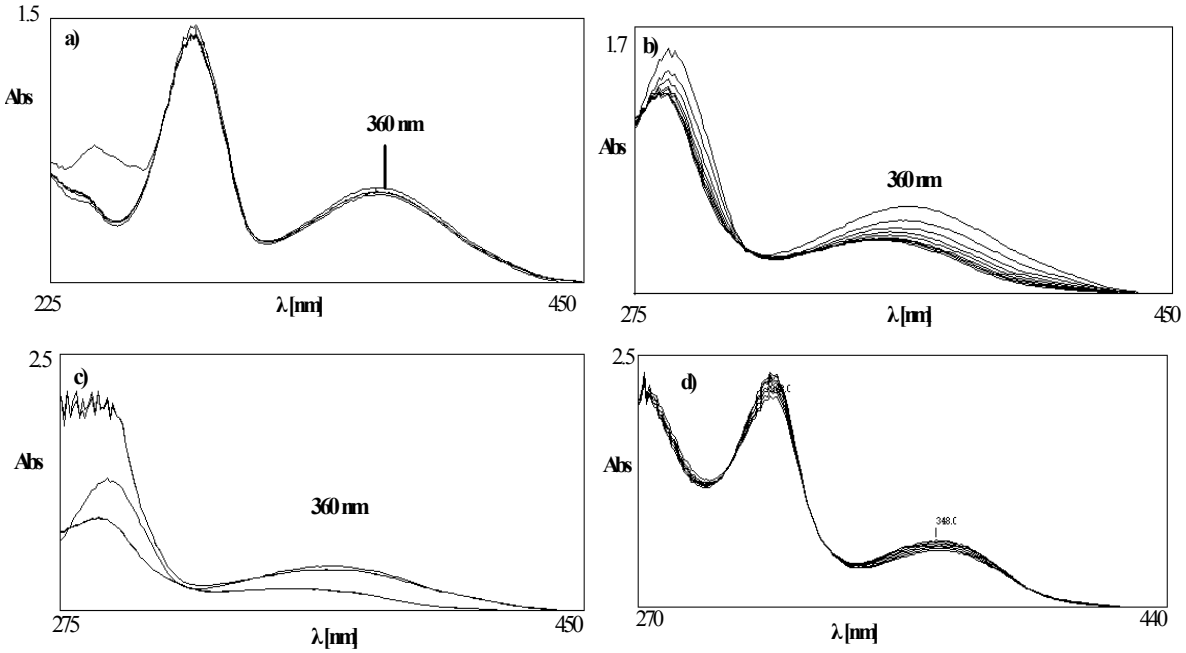

Figure 2–14: Addition of TFA to **75**, a) 1 eq. of TFA followed by addition of 1.1eq. pyridine, b) serial addition of TFA upto 70eq. of TFA, c) addition of 70 eq. of TFA followed by addition of 1.1eq. pyridine, d) time dependent measurement (over 5 h) over the decay of **75** with 56eq. of TFA.

TFA addition up to 5 eqs. showed no substantial decay over time (Abs at 360 nm was 0.646 after 2 min and it was 0.645 after 4 h). Even with 70 eq. of TFA the decay of **75** was not extensive after 5 h (Abs at 360 nm was 0.669 after 2 min and it was 0.638 after 5 h, Figure 2–14d).

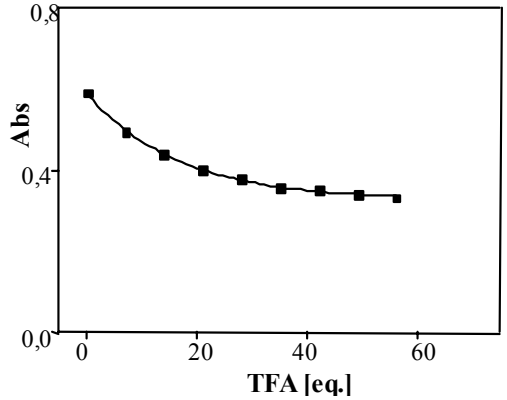

Figure 2–15: UV-Vis spectrum showing the changes observed upon addition of increasing amount of TFA to **75** (0-56 eq. of TFA).

Table 2–12: Changes observed in the absorption of **75** (0.1 mM) upon addition of TFA.

Eq. of TFA added	TFA [mM]	Abs at 360 nm
0	0	0.590
7.3	0.73	0.494
14.5	1.45	0.438
21.7	2.17	0.403
28.8	2.88	0.379
35.9	3.59	0.356
42.9	4.29	0.351
49.9	4.99	0.341
56.9	5.69	0.332

The above experiments with the addition of TFA to **75** clearly showed that it was not very sensitive to the TFA at low concentrations. The process of protonation was reversible in the time frame of about 3-4 h, which was confirmed by the retention of the absorption and the λ_{max} upon the addition of pyridine as base.

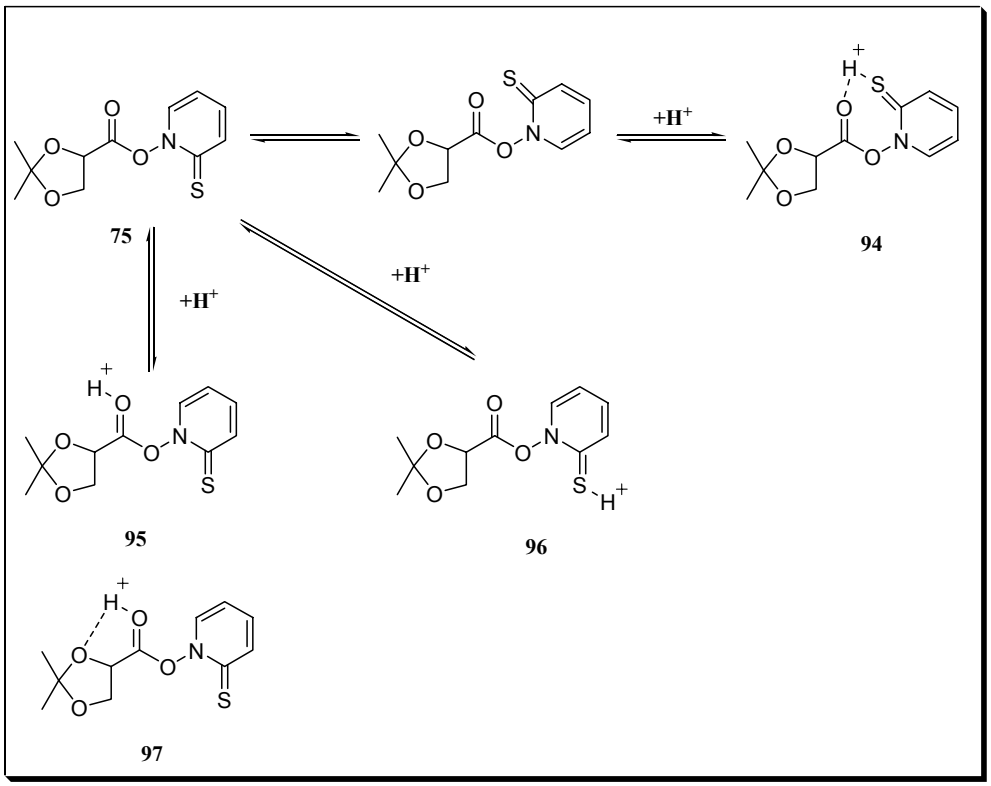

Scheme 2–47: The various possible sites of protonation in **75** upon addition of TFA.

The above acid addition experiments indicated that protonation of **75** predominantly occured

at the chromophore part of the molecule as evidenced from the UV-Vis spectral changes. While protonation at the dioxolane moiety could occur even at low concentration of acid, any relevance to degradation of **75** at least at low conc. (upto 5 eq.) of acid can be ruled out.

At low concentration of TFA, the possible sites that could undergo reversible protonation are either the carbonyl carbon or the thiocarbonyl part of the molecule giving rise to the protonated species **95, 96** and **97** respectively (Scheme 2–47). A syn-orientation of both the chromophores would give **94**.

2.5.6.2 Photochemical Investigation of Barton Ester 75

The *O*-acyl derivatives of thiohydroxamic acid (*N*-hydroxypyridine-2-thione) undergo facile reaction not only with stannyl radicals but also with thiyl, alkyl and many other thiophilic radicals.[97] The most elementary radical reaction undergone by the *O*-acyl thiohydroxamates is decarboxylative rearrangement to alkyl 2-pyridyl sulphides. The decarboxylative rearrangement of *O*-acyl-thiohydroxamates to alkyl-2-pyridyl sulphides has been reported and occurs via a radical chain mechanism.[98] The rate for such a rearrangement for a primary radical was found to occur at 10^6 $M^{-1}s^{-1}$ (n-octyl).

A similar decarboxylative rearrangement was carried out with **75** in benzene with a 300 W UV lamp. The photolysis was monitored by both UV-Vis spectroscopy and ^{1}H-NMR. The photolysis of **75** is expected to yield three products, of which two are dimerisation products of the corresponding 2-pyridylthiyl radical and **104**. The third product is the rearranged product formed by decarboxylative radical rearrangement (Scheme 2–48).

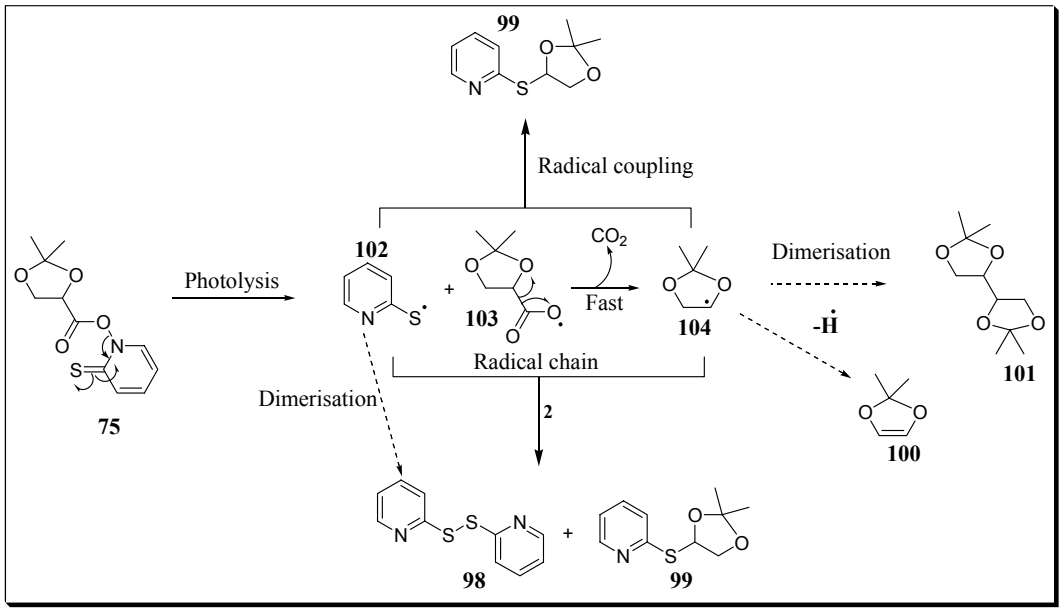

Scheme 2–48: Most feasible mechanism for the photo-rearrangement of **75→99** and possible pathways for other side reactions leading to **98**, **100** and **101**.

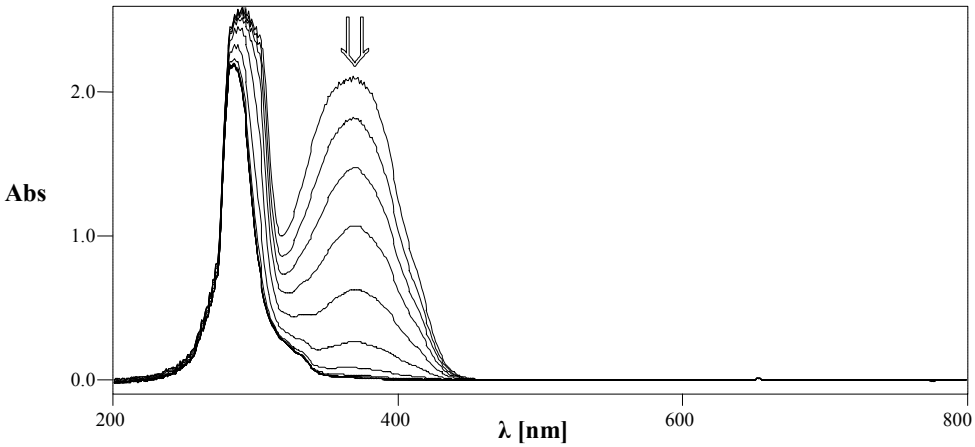

Figure 2–16: UV-Vis spectrum showing the changes observed when a solution of **75** (0.2 mM) in dry benzene was exposed to a 300 W UV-lamp. The spectrum is an overlay of measurements carried out over a period of 90 s with each spectrum measured at every 10 s.

When **75** (0.2 mM) was exposed to a 300 W UV-lamp it underwent a dramatic change in the UV-Vis spectrum. The band at 360 nm, characteristic of the **75** disappeared completely in 60 s (Figure 2–16). In ^{1}H-NMR spectrum, a clean conversion from **75→99** was observed (Figure 2–17).

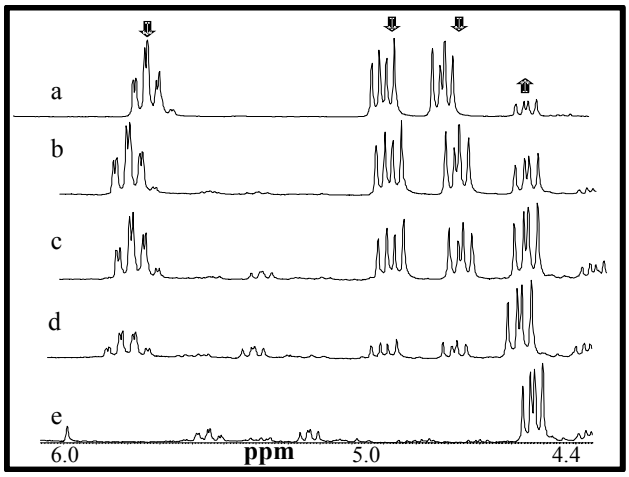

Figure 2–17: Photorearrangement of **75→99**, as observed by ^{1}H-NMR when **75** (0.2 M) was photolysed in dry C_6D_6, a) before photolysis, b)-e) ^{1}H-NMR measured after every 5 min exposure to light.

At higher concentrations (used for ^{1}H-NMR experiments) the formation of product **99** was also observed and compared to the authentic samples.

2.5.7 Photolysis of 75 in Presence of Organic Acids

The clean conversion of **75** to **99** under mild photolytic conditions coupled with the small reaction time (maximum 1-2 minutes) needed for the conversion, its stability to TFA (1-5eq.) and the ease with which the conversion could be followed, made **75** ideal for photolytic investigations in the presence of acid.

Photolysis experiments were carried out in formic as well as in trifluoroacetic acid (TFA). For all photolysis experiments equimolar amounts of **75** (490 μM) with or without the acid/acid + ferrocene were made.

2.5.7.1 Photolysis of 75 in Presence of Formic Acid

Upon the addition of an equimolar quantity of formic acid to **75**, a slight decrease in the absorption maximum at 360 nm was observed (due to protonation of the chromophore). Photolysis of **75** in the absence of acid (Figure 2–16) or in the presence of only acid (Figure 2–18a) or only ferrocene (Figure 2–18b) did not produce any bands above 400 nm. However, when **75** was photolysed in the presence of an equimolar amount of acid and ferrocene a new band at ~620 nm appeared (Figure 2–18c). The band at 620 nm is typical of the ferrocenium ion, suggesting that some oxidants were produced during the process of photolysis. The whole photolysis experiment required 90 s. Photolysis of ferrocene or ferrocene with an equimolar amount of formic acid failed to produce a band at 620 nm (even after 10 min of photolysis).

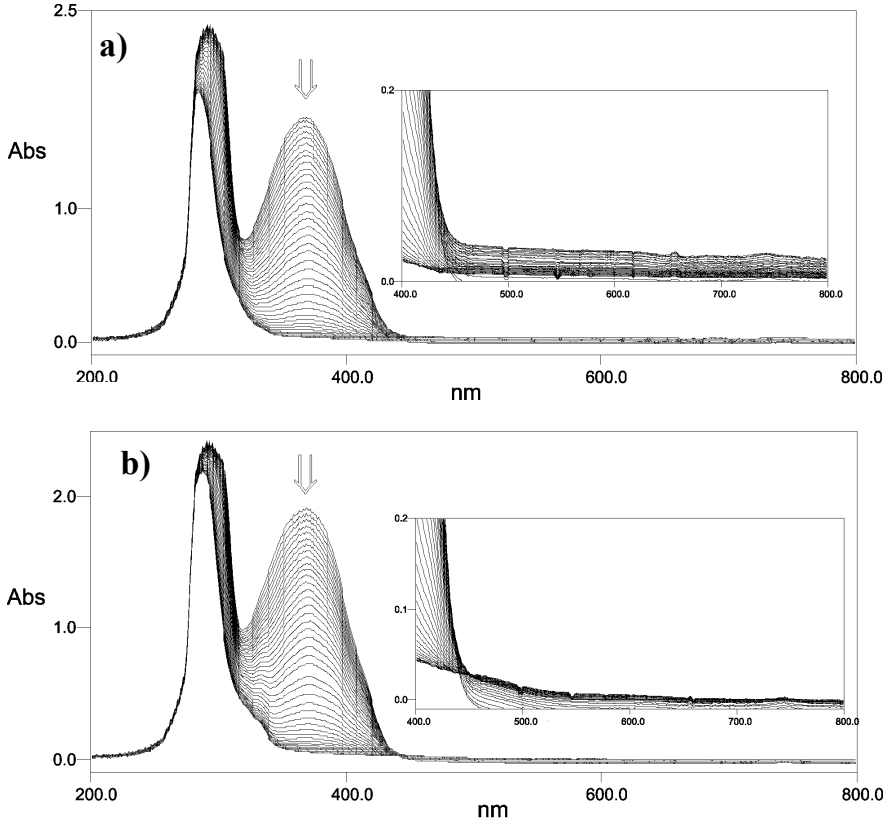

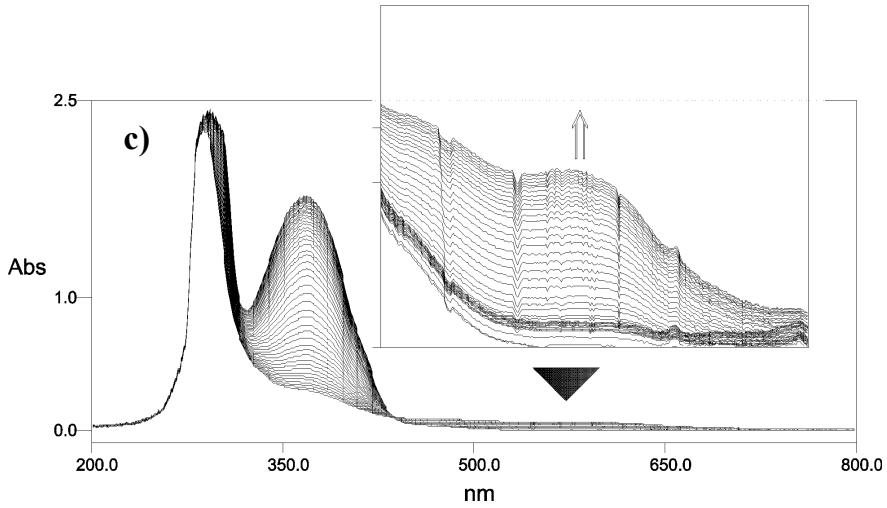

Figure 2–18: UV-Vis spectrum showing changes upon photolysis of Barton ester **75** (490 μM), a) in presence of formic acid (490 μM), b) ferrocene (490 μM) and c) both formic acid (490 μM) and ferrocene (490 μM) in dry benzene. The UV-Vis spectrum is an overlay of spectra measured every second over a span of 90 s.

2.5.7.2 Photolysis of 75 in Presence of TFA

Barton ester **75** when treated with equimolar amounts of TFA showed a relatively larger decrease of its band at 360 nm than after treament with formic acid. Upon photolysis of **75** alone, or in the presence of TFA or ferrocene (Figure 2–19a), no long absorbing species were observed.

However, the photolysis of **75** in the presence of both TFA and ferrocene (equimolar concentrations), afforded a new band at ~620 nm band (Figure 2–19b). The photolysis was monitored by UV-Vis spectroscopy over a period of 90 s. By adding a strong acid, such as TFA, the photolysis of **75** was slowed down suggesting that protonation of the chromophore (**97)** slows down the photo-degradation.

The formation of the new band at ~620 nm is much clearer in TFA than in the experiments using formic acid. The photolysis experiments in TFA and ferrocene further supported the experiment carried out in formic acid and clearly suggested the formation of a strong oxidant, possibly arising from one of the photoproducts of the Barton ester.

The most obvious of the oxidants that can be generated from **75** upon photolysis in the presence of acid are $\mathbf{98}^{+\bullet}$, $\mathbf{102}^{+\bullet}$ and **106** (ethenol radical cation, Scheme 2–49). The intermediacy of oxidants $\mathbf{98}^{+\bullet}$ and $\mathbf{102}^{+\bullet}$ can easily be tested by photolysing a Barton ester without a leaving group in the presence of acid as well as both acid and ferrocene. Thus Barton ester **78** was designed to test for the formation of $\mathbf{98}^{+\bullet}$ and $\mathbf{102}^{+\bullet}$ during the photolysis of **78** in acid and ferrocene.

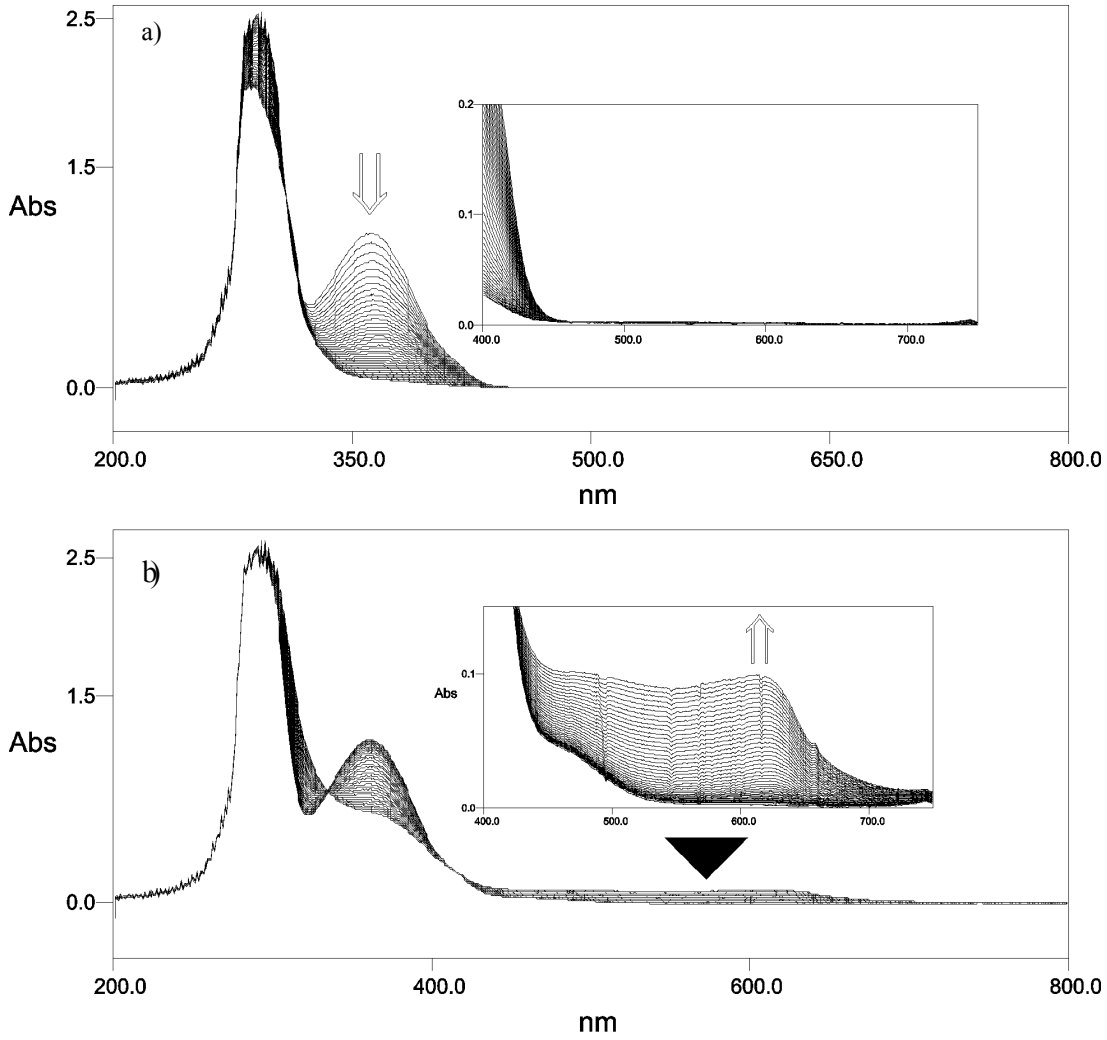

Figure 2–19: UV-Vis changes observed upon photolysis of Barton ester **75** (490 µM), a) in TFA (490 µM) and b) in presence of 490 µM both of TFA and ferrocene in dry benzene (25 ml). The UV-Vis spectrum is overlay of spectra measured every second over a period of 90 s.

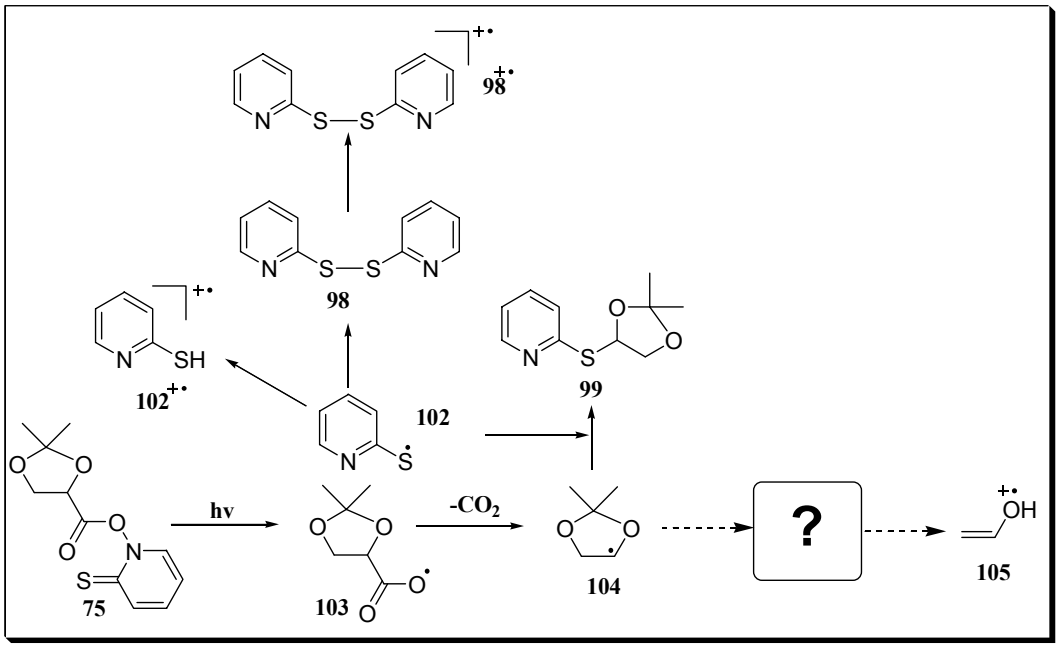

Scheme 2–49: Possible oxidants that could be formed upon photolysis of **75** in presence of formic acid or TFA.

2.5.7.3 Photochemical Investigations on Barton Ester 78

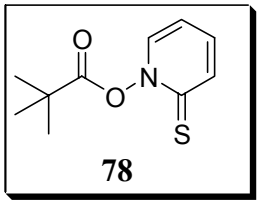

78

Photolysis of **78** (568 μM) in the presence of an equimolar concentration of ferrocene and TFA showed a decrease in the 370 nm band but no formation of any long absorbing species above 400 nm. Even with 9 eq. of TFA (5.19 mM) no formation of any long absorbing species was observed (Figure 2–20).

The above experiments clearly indicated that $\mathbf{98}^{+\bullet}$ and $\mathbf{102}^{+\bullet}$ are either not formed during the photolytic conditions or have very transient life times not sufficient enough to allow for intermolecular electron transfer with ferrocene. Laser flash photolysis of **98** in various solvents carried out by Osamu Ito *et al*.[99] indicated no formation of $\mathbf{98}^{+\bullet}$ and $\mathbf{102}^{+\bullet}$.

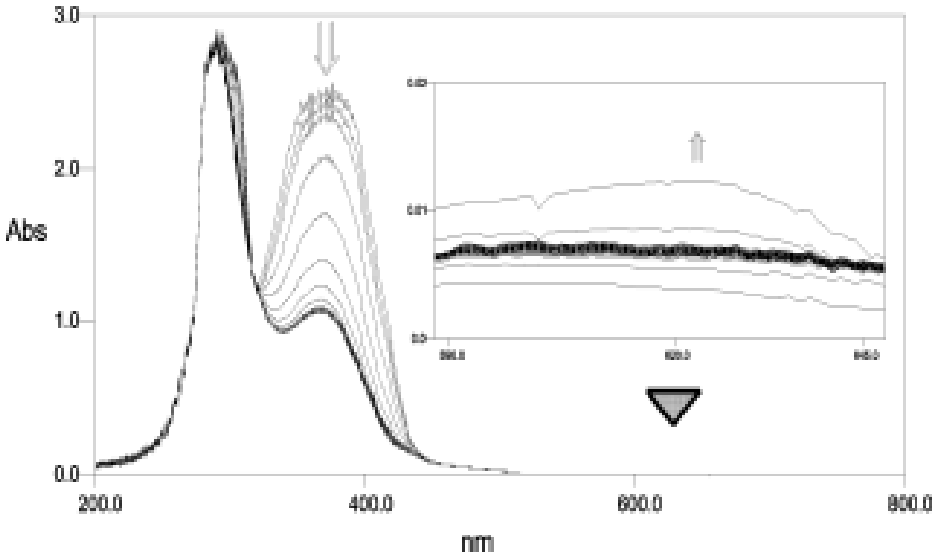

Figure 2–20: UV-Vis changes observed during the photolysis of **78** (568 μM) in presence of both ferrocene (567.9 μM) and TFA (5.19 mM). The overall UV-Vis spectrum is an overlay of measurements made at every second over a period of 90 s.

2.5.7.4 Product Distribution after Photolysis in 75 and 78

Preparative scale photolysis was carried out for **75** and **78** in dry benzene. The products of the photolysis were purified by column chromatography with hexane and ethyl acetate as eluent. Alkyl-2-pyridylsulfides **99** (20% ethyl acetate in hexane, $R_f = 0.35$) and **106** (10% ethyl acetate in hexane, $R_f = 0.72$) were obtained. A substantial amount of **98** was also obtained as a by-product when photolysis was carried out at high concentrations of the Barton ester due to the involvement of $\mathbf{102}^{\bullet}$ in the radical chain propagation step.[100] The products were characterised by various spectroscopic methods IR, ^{1}H-NMR, and ^{13}C-NMR.

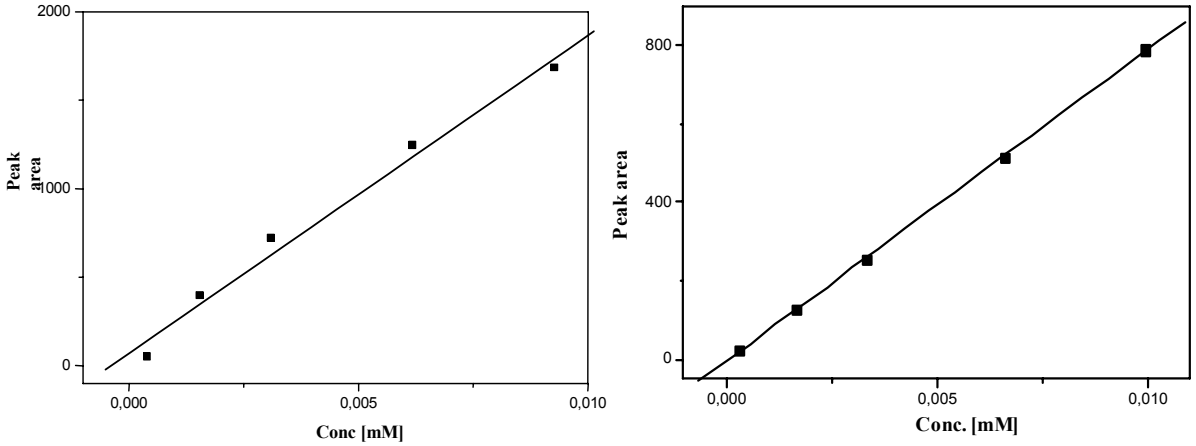

Figure 2–21: HPLC calibration curves for **98** and **99** with 15% ethyl acetate and 85% hexane over a concentration range of 0.4 to 9.3 mM at 290 nm.

Photolysis of Barton ester **75** (1.57 mM) was carried out both in the absence and in the presence of an equimolar amount of TFA (1.57 mM) and the products were analysed by HPLC. The chromatograms typically had four peaks at 4.78, 5.24 (**99**), 7.26 and 9.25 min (**98**) (both in acid and in absence of acid). Interestingly, the peak area for **98** remained more or less unchanged in both the experiments. The peak area of **99**, on the other hand decreased by about 30% (Figure 2–22, Table 5–2). Based on the calibration curves the overall conversion of **75**→**99** in the absence of acid was calculated to be 89% and 59% in the presence of acid.

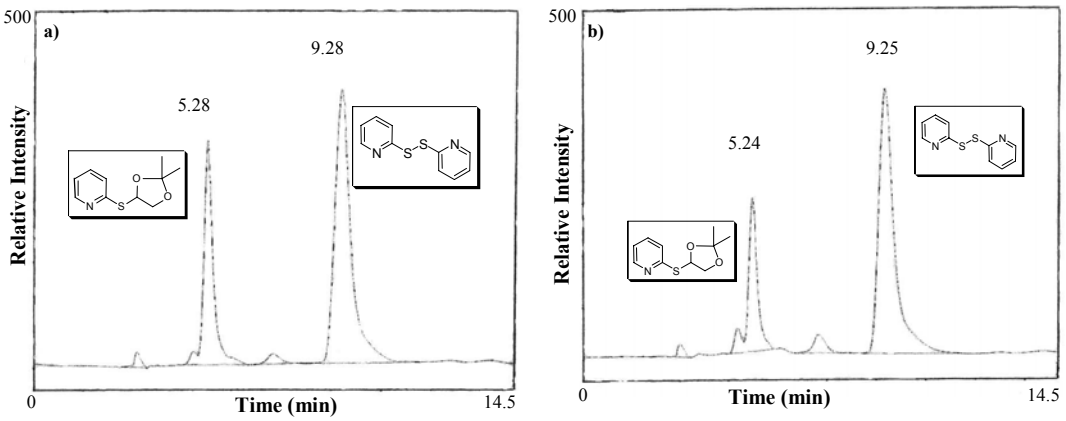

Figure 2–22: HPLC chromatograms of photolysed **75** (1.57 mM, for 15 min), a) without TFA, b) with TFA (1.57 mM). The shift in the retention time was due to a change (lowering) in the pressure of the pump.

The photolysis of **99** (0.95 mM) in the presence of TFA (0.93 mM) for 15 min or in the absence of acid did not lead to measurable changes in the product yields (Table 5–3). Interestingly, upon photolysis of **75** both in presence and absence of TFA two additional signals at 7.26 min and 9.25 min were observed. The peak area of these new products doubled in presence of TFA (Figure 2–23).

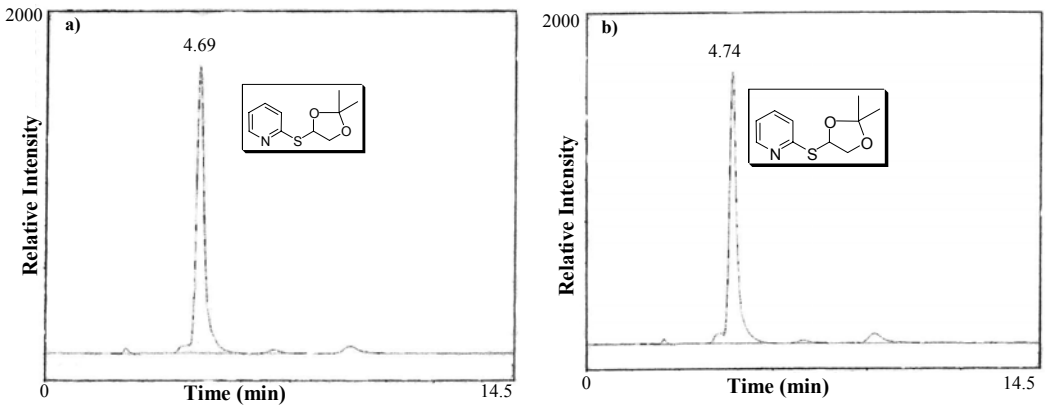

Figure 2–23: HPLC chromatograms of **75** (0.95 mM) after photolysis (15 min), a) without TFA and b) in presence of TFA (0.93 mM).

A summary of the above UV-Vis and HPLC investigations indicated that the oxidation of ferrocene during the photolysis of **75** in the presence of TFA could arise from ethenol radical cation. In order to get a closer look at the conversion from **104→105** we resorted to time resolved measurements.

2.5.7.5 Characterisation of 104 by TR-ESR (In collaboration with Dr. G. Bucher)

Electron spin resonance spectroscopy has been widely used to characterise 1,3-dioxolan-4-yl radicals.[101] Most of the methods used di-*t*-butyl peroxides for the radical formation or photo-ionisation.

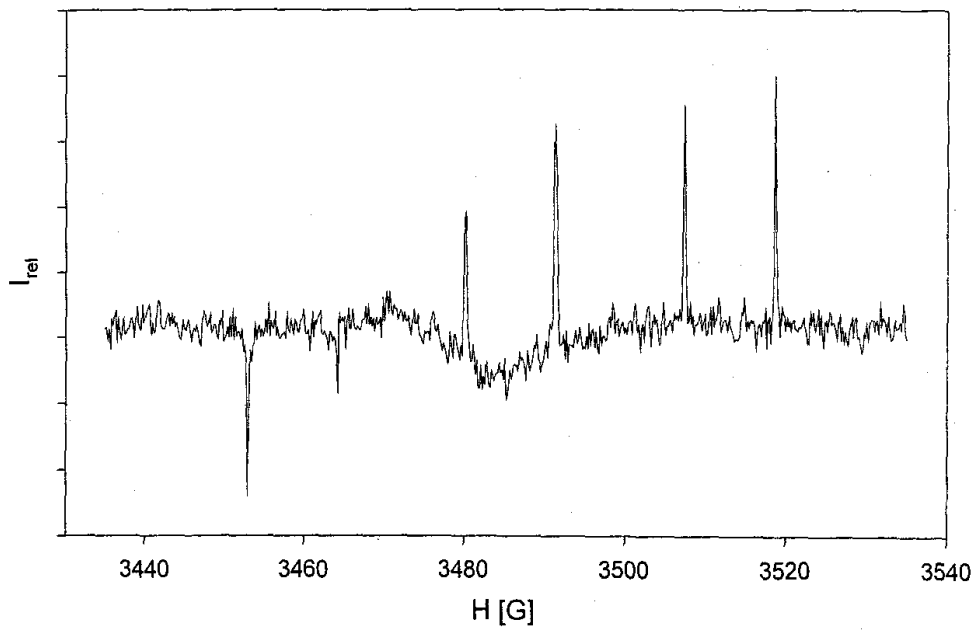

Figure 2–24: Time resolved EPR spectrum of **104** obtained by photolysis of **75** in benzene.

Time resolved ESR spectrum for **104** was observed upon photolysis of **75** in benzene. The

ESR results showed inequivalence of the β-protons due to fast torsional oscillations. For **104** a literature reported g value was 2.0032. The spectrum showed a doublet and a quartet, as expected for **104** (Figure 2–24). The g value was found to be 2.0035, which is in close agreement to the earlier literature reported value, with a coupling constant of 11.2 G (d) and 27.2 G (q). Having characterised the formation of **104**, the conversion of **104→105** was investigated by laser flash photolysis.

2.5.7.6 Laser Flash Photolysis Investigations on 75 and 78

Laser flash photolysis (355 nm, laser beam "attenuated" to ca. 20 mJ/pulse at the sample by widening) of a deaerated benzene solution containing ~0.1 mM of **78** gave a transient with λ_{max} = ~480 nm (second order decay with a half life in μs range). The species was assigned to pyridine-2-thiyl radical. Addition of 0.5 mM of TFA had no effect on the transient spectrum and no additional new transients were observed (Figure 2–25).

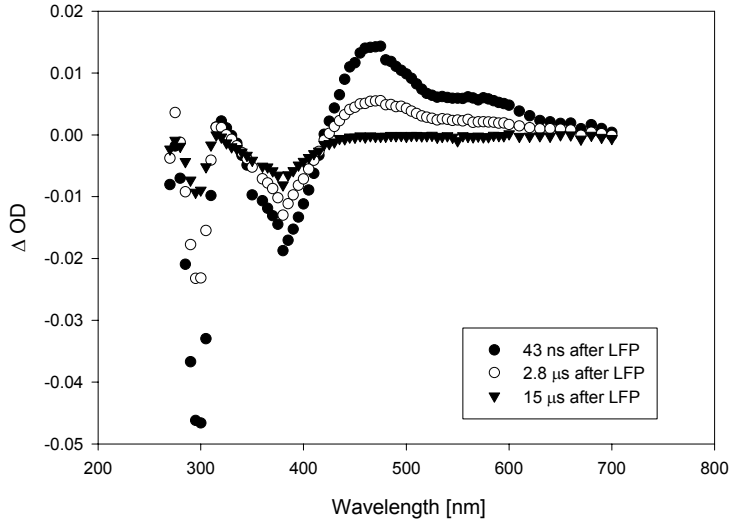

Figure 2–25: Transient spectrum after photolysis of **78** (0.1 mM) observed in benzene with LFP (355 nm laser beam).

Interestingly, at λ_{max} = 295 nm and λ_{max} = 375 nm bleaching and recovery was observed occuring with a first order rate constant k = 7.4 X 10^4 s^{-1}. The trace at λ_{max} = 295 nm is given above in the Figure 2–26. Such a bleach and recovery is often observed when a long-lived triplet excited state returns to the ground state replenishing the precursor. However, this is not the case in **78** and could occur only if the resulting radical reacted with the precursor replenishing the *t*-butyl radical (radical chain process).

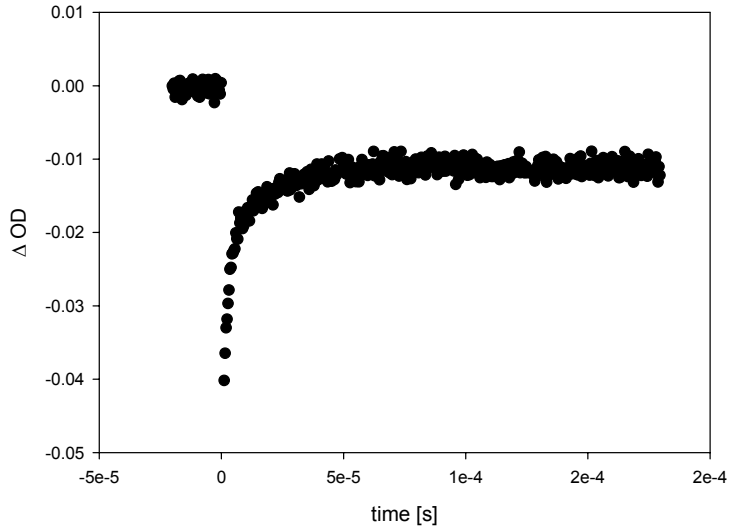

Figure 2–26: Trace showing bleach and recovery at λ_{max} = 295 nm for **78** under LFP conditions (both in absence and presence of TFA).

LFP of **75** in acetonitrile and benzene gave a complex spectrum with transients observed at λ_{max} 305, 350, 480 and 600 nm, the decay constants of which are summarised in Table 2–13. The absorbance at λ_{max} = 305 nm was tentatetivly assigned to the ethenol radical cation,[101c] λ_{max} = 350 nm to a distonic radical cationic species (**107**),[117] and λ_{max} = 480 nm to the 2-thiopyridyl radical (**102**).[99]

Table 2–13: Decay constants observed for various transients generated by photolysis of **75** under LFP conditions.

Transient (LFP)	λ_{max} [nm]	k [10^5/sec]	$t_{1/2}$ [µs]
104	305	2.1	3.3
107	350	1.3	5.3
102	480	2.9	2.4
103	580	1.3	5.3

TFA addition under LFP conditions also show saturation above 0.05% (TFA, close to 30 eq., Figure 2–27b) which is in agreement with our earlier TFA addition experiments observed by UV-Vis spectroscopy. Quenching of the transients (λ_{max} = 350 and 580 nm) by methanol and TBAP [tris-(4-bromophenyl)amine] with the formation of $TBAP^{+\bullet}$ (λ_{max} = 700 nm) indicate radical cationic nature of these species. The assignment of transient species at 580 nm could not be made to the distonic radical cation although it has a similar decay to 350 nm.

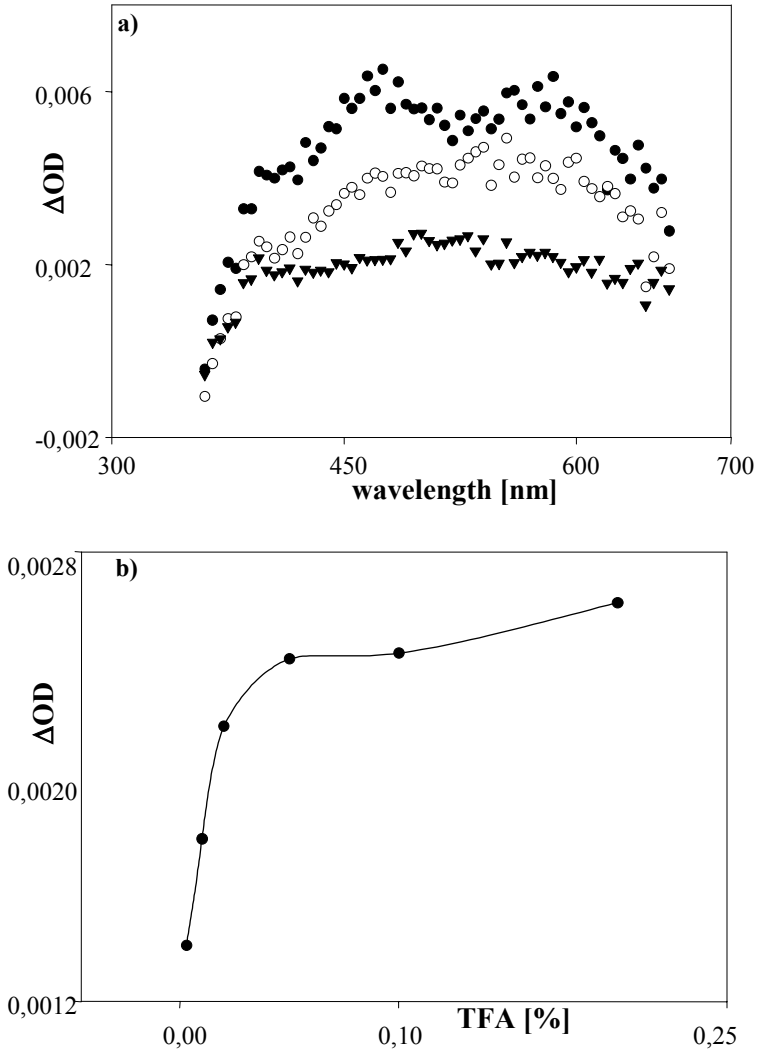

Figure 2–27: a) Transient spectra in benzene with 1% TFA upon photolysis of **75**, b) plot of transient intensity at 580 nm vs. TFA addition, showing the saturation above 0.05% of TFA.

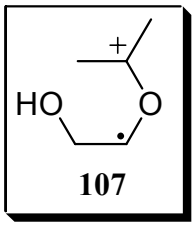

One is easily inclined to postulate an excited form of protonated **75**, i.e. [**75**+**H**]*, because of its long wavelength absorption. However, this is in contrast to the quenching experiment (**TBAP**→**TBAP**$^{+\bullet}$ [700 nm]) which suggests a radical cationic nature of the 580 nm transient. LFP of **75** (355 nm laser beam with a laser output of 120 mJ/pulse) in benzene gave a transient spectrum similar to that observed in the LFP of **78**. A transient was observed at λ_{max} = 445 and 485 nm, assigned to the pyridine-2-thiyl radical (second order kinetics). Additionally, a transient with λ_{max} = 315 nm (first order, τ = 170 ns) was observed (Figure 2–

28). Upon lowering the laser energy (hitting the sample) a bleach and recovery at λ_{max} = 295 and 375 nm similar to the LFP of **78** was observed. The bleach and recovery occured with a lifetime of 170 ns, which is equal to the decay rate constant of the λ_{max} = 315 nm transient. It therefore appears likely that the 315 nm transient reacts with the precursor. On a much shorter time-scale another transient at λ_{max} = 500 nm was observed, which appears to have been formed in a monophotonic process showing a linear dependence on the laser power (Figure 2–29, Figure 2–30).

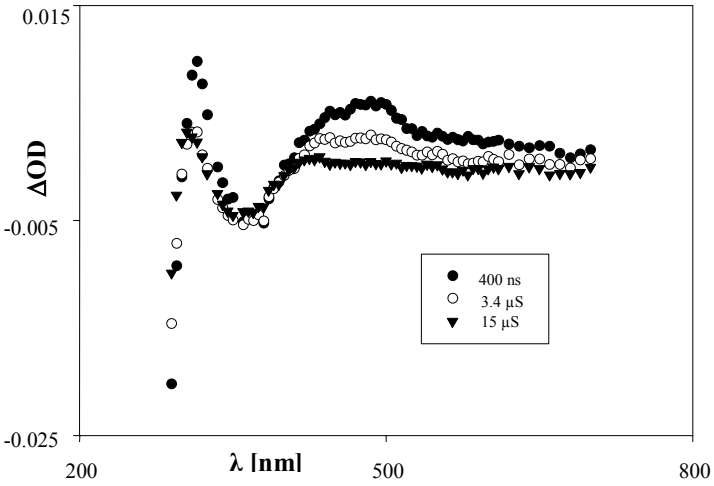

Figure 2–28: Transient spectrum as observed by LFP of **75** in benzene with a 355 nm laser beam and a laser output of 120 mJ/pulse.

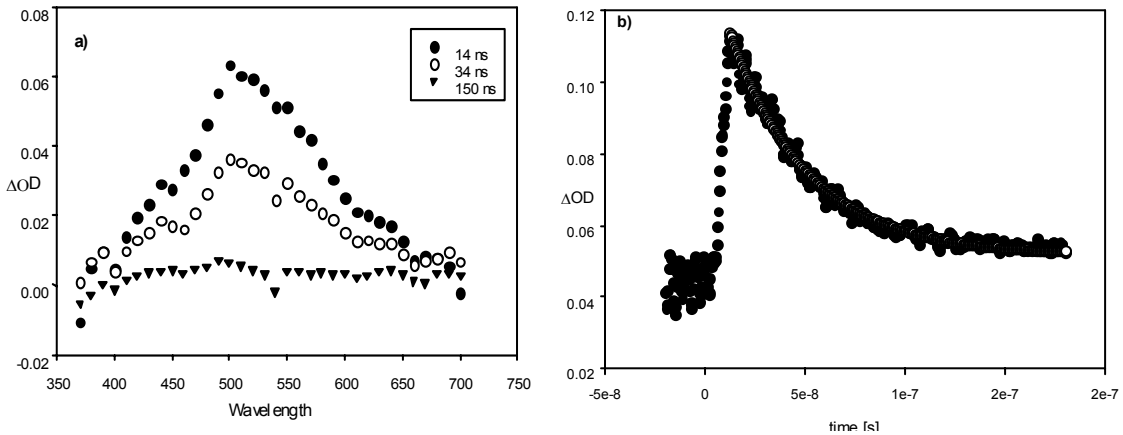

Figure 2–29: LFP of **75** depicting a) the transient spectra observed in benzene and b) trace observed at 500 nm (black is the experimental trace while white is the first order5 fit to the experimental data).

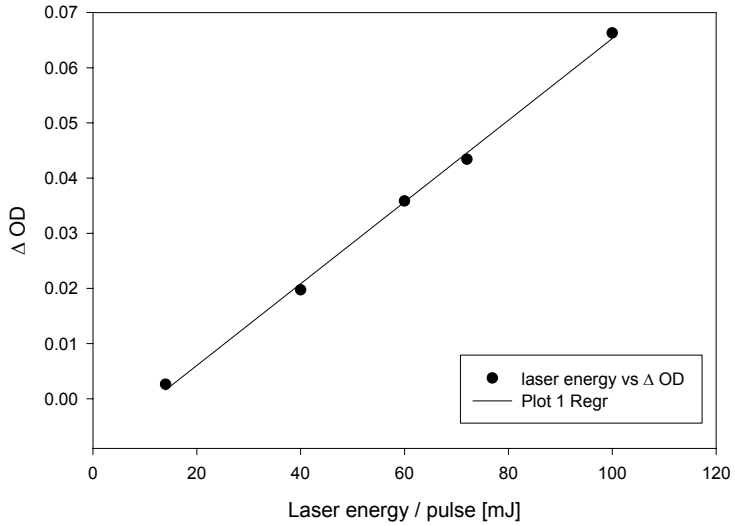

Figure 2–30: Linear dependence of transient intensity at λ_{max} = 500 nm on laser power.

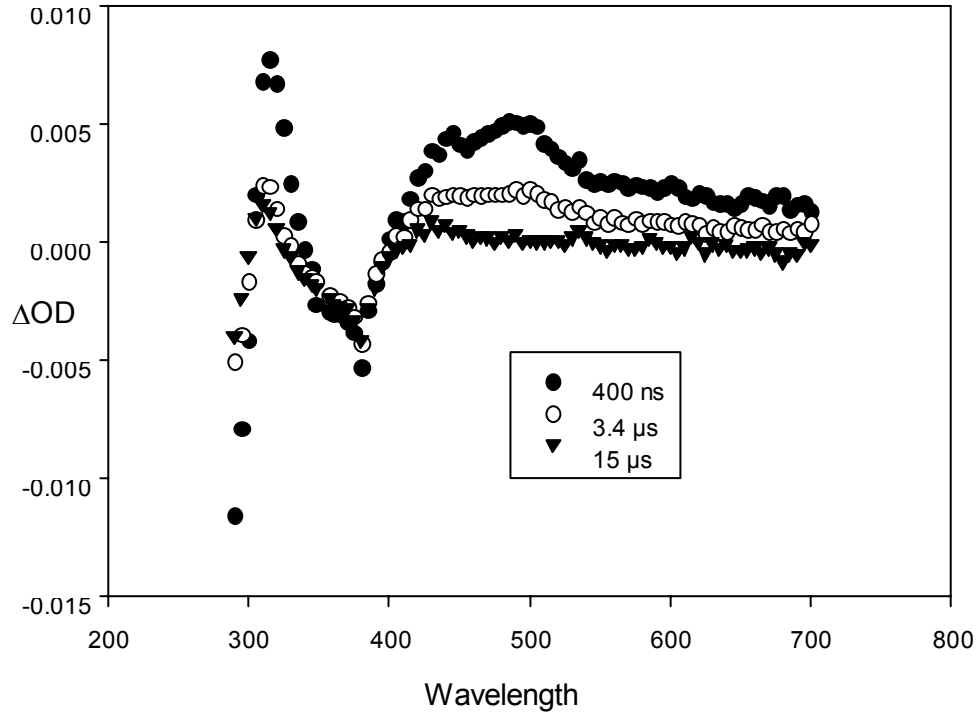

Figure 2–31: Transient spectra of **75** containing 0.5 mM TFA with a laser beam at 355 nm and purged with argon.

The transient with λ_{max} = 315 nm showed the same lifetime as in the absence of TFA (τ = 160 ns, Figure 2–31). Quenching experiments were carried out in benzene to figure out the nature of the 500 nm transient. Addition of 0.03 % TFA increased its reactivity with all the quenchers used (1,2,3-trimethoxybenzene, anisole, diphenylether and tri-n-butylstannane, Figure 2–32a). The reactions of the 500 nm transient with quenchers in presence of 0.03% of TFA were found to be diffusion controlled. With diphenylether a new transient around 630 nm was observed in addition to the transient at 500 nm (Figure 2–32b).

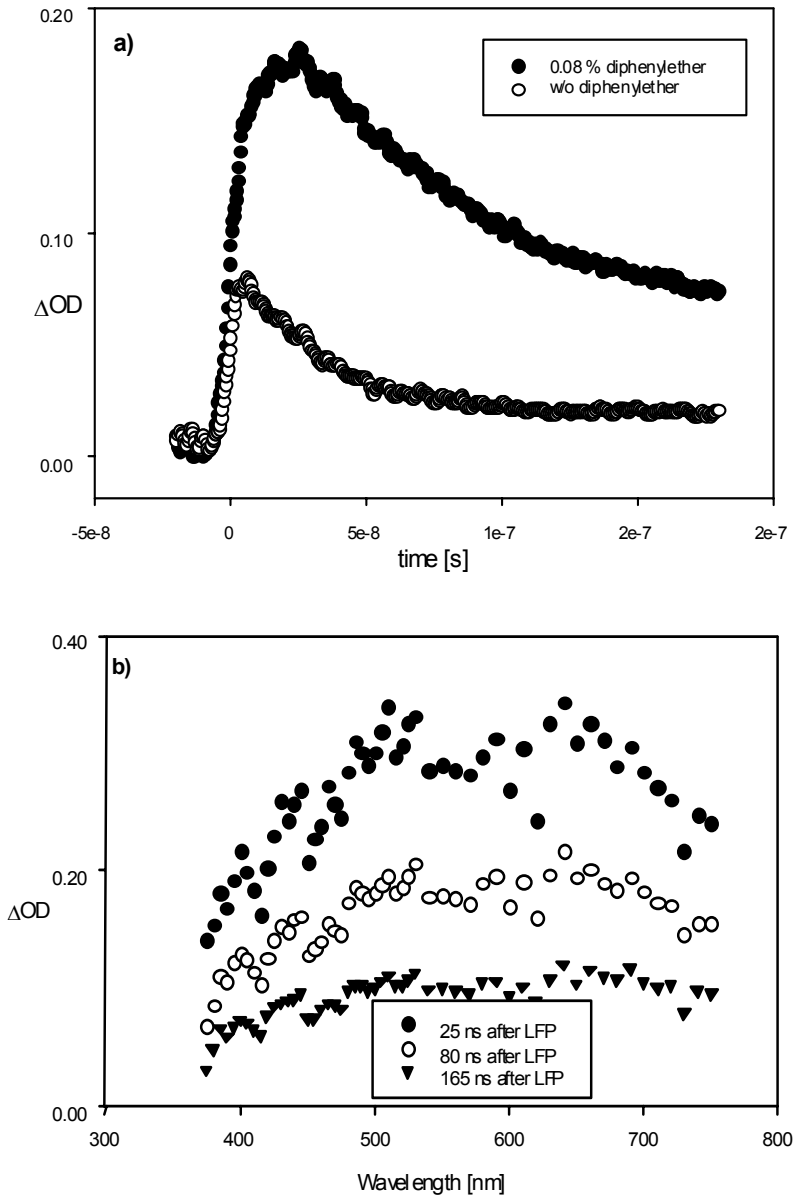

Figure 2–32: LFP experiments showing the behaviour of transient at 500 nm a) Transient trace monitored at 500 nm upon LFP (355 nm) on **75** and b) transient spectrum showing the 500 and 630 nm band upon LFP of **75** in presence of diphenylether and TFA.

Table 2–14: Effect of quencher on the reactivity of the transient at 500 nm.

Quencher	Rate constant in benzene	Rate constant in benzene + 0.03 % TFA
1,2,3-trimethoxybenzene	8.2×10^9 l mol^{-1} s^{-1}	1.1×10^{10} l mol^{-1} s^{-1}
anisol	4.9×10^9 l mol^{-1} s^{-1}	8.9×10^9 l mol^{-1} s^{-1}
diphenylether	lifetime increases!	1.4×10^{10} l mol^{-1} s^{-1}
tri-*n*-butylstannane	1.6×10^9 l mol^{-1} s^{-1}	not measured

In summary, a translation of a short-lived enol radical cations was successfully achieved via

an intermolecular electron transfer between ferrocene and an enol/enolether radical cation. The various spectroscopic methods and HPLC investigations suggests the formation of an enol/enol ether radical cation during the photolysis of **75** in the presence of acid. However, LFP results were inconclusive regarding the nature of the enol radical cation or any other oxidant involved. The species at 500 nm, due to its short lifetime (34 ns), was assigned to a carbonyloxy radical **103** formed after the initial homolytic cleavage upon photolysis of **75**. This species could potentially undergo a facile proton coupled electron transfer in presence of trifluoroacetic acid.

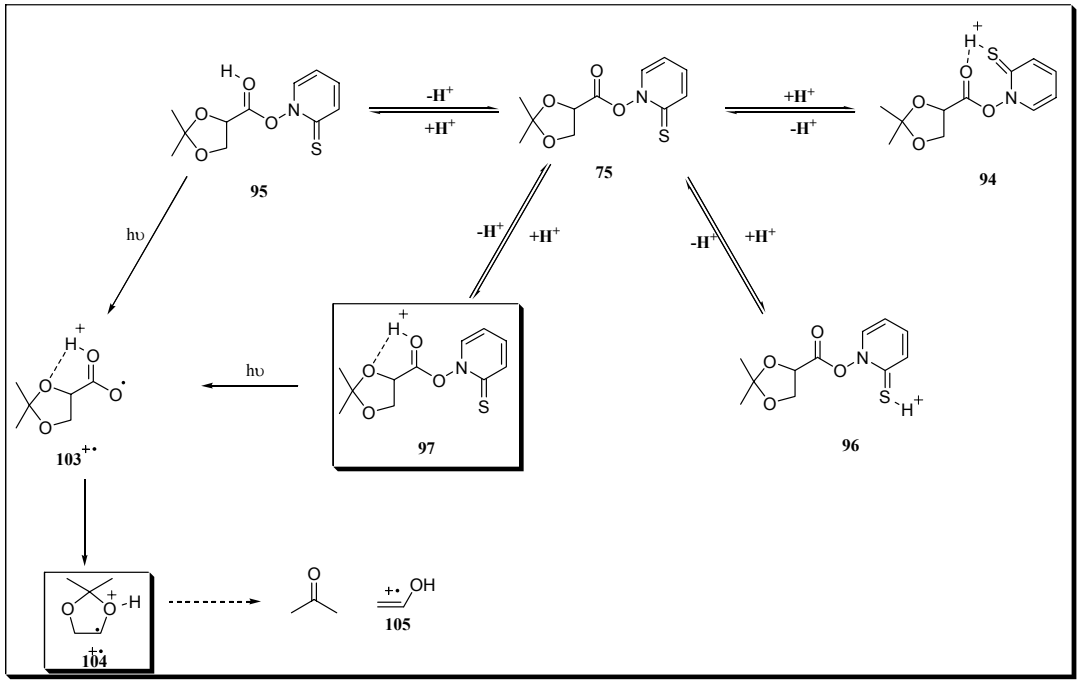

Scheme 2–50: Possible mechanism for the formation of ethenol radical cation from the protonated **75** upon photolysis.

The nature of the transient at 315 nm was temporarily assigned to the radical **104**, however this has to be confirmed by generation of **104** independently (the experiments are in progress in collaboration with Dr. Bucher at University of Bochum). The identification of the enol/enol ether radical cation by LFP is further complicated by absence of any good chromophore on **104** or the radical cation formed. Quenching of the 500 nm species did not change with addition of TFA (since the reaction in absence itself is close to diffusion controlled) indicating that formation of **104** is the primary reaction pathway of its decay (if it is carbonyloxy radical). In presence of acid (TFA or formic acid) the most likely conformation of the protonated species could be the **97**. Upon photolysis it directly goes to $\mathbf{104}^{+\bullet}$ which according to DFT calculations would break down into acetone and ethenol radical cation. This could be the most prefferred pathway. The 315 nm transient could be the ethenol radical cation (this is

the reason it did not show any change in reactivity upon addition of incremental amount of TFA, the formation of which can also occur if trace amounts of water is also present in the benzene and acetonitrile).

2.5.8 Generation and Intramolecular Trapping of Enol Radical Cation: A Pulse Radiolysis Investigation

Pulse radiolysis[102] is a branch of chemistry dealing with the study of chemical changes brought about by the interaction of ionising radiation with matter. The mechanism by which ionising radiation transfers energy on collision with matter depends on the type and energy associated with them. The general classification is into three types; i) charged particles (electrons, protons, deuterons), ii) neutral particles (neutrons), and iii) electromagnetic radiations (X-rays, γ-rays, UV, etc).

The interaction of ionising radiation with water has been extensively investigated and primarily leads to the formation of presolvated electrons (ejection of electrons from water).[103] These electrons further loose energy by ionising and exciting molecules along their path and finally get thermalised and solvated (λ_{max} = 720 nm).

$$e^- \rightarrow e^-_{therm} \rightarrow e^-_{aq.}$$
$$H_2O^{+\bullet} + H_2O \rightarrow OH^\bullet + H_3O^+ \qquad \text{Equation 2–1}$$

The secondary species that are formed include the hydrogen atom and hydroxyl radical. While hydrogen atoms are reducing in nature, hydroxyl radicals (λ_{max} = 230 nm, $\varepsilon_{235\ nm}$ = 540 $dm^3mol^{-1}cm^{-1}$) are oxidising with a standard reduction potential of +2.8 V_{NHE} in mild acidic conditions and +1.8 V_{NHE} under neutral conditions.[102]

There are procedures for generating exclusively reducing radical species or exclusively oxidising species in pulse radiolysis experiments. The common method used to generate reducing species involves the addition of high concentrations of sodium formate in water. The formate reacts with the hydroxyl radical forming the carbon dioxide radical anion ($CO_2^{-\bullet}$).

$$OH^\bullet + HCO_2^- \rightarrow H_2O + CO_2^{-\bullet} \qquad \text{Equation 2–2}$$

One method for generating an exclusively oxidising radical species is to irradiate water in the presence of nitrous oxide. Nitrous oxide converts the solvated electrons into the hydroxyl radicals (up to 90%) as shown in eq. below:

$$N_2O + e^-_{aq} + H_2O \rightarrow N_2 + OH^\bullet + OH^- \qquad \text{Equation 2–3}$$

The hydroxyl radicals are characterised by their ability to do various reactions with solute molecules such as a) electron transfer leading to the formation of hydroxide ion, b) hydrogen atom abstraction of C-H bonds, c) addition reactions to double bonds, and d) displacement reactions.

2.5.9 Pulse Radiolysis Investigations on Ethylene Glycol

Reactions of polyhydric alcohols[104] with hydroxyl radicals in aqueous solution have been extensively investigated mainly due to their close resemblance to the more complicated carbohydrate substrates.

The reaction of hydroxyl radicals with carbohydrates occurs at a rate of about 10^9 $dm^3mol^{-1}s^{-1}$ by C-H hydrogen bond abstraction.[104b] In deoxygenated solutions, the main reaction is the dehydration by elimination of water. This part of the reaction has been extensively investigated with ethylene glycol as the model compound.[104b-d] Pulse radiolysis investigations have revealed that the α,β-dihydroxyethyl radical undergoes an acid-catalysed dehydration to give the α-carbonyl radical with the ethenol radical cation as a reactive intermediate.[105] For the formation of a α-carbonyl radical under base catalysis, the ketyl radical anion intermediate has been proposed.[106] It has been shown that the presence of alkyl substituents markedly increase the dehydration under acid catalysis (second order rate constants for dehydration of the radicals from ethane-1,2-diol and butane-2,3-diol are 9×10^6 and 1.3×10^8 $dm^3mol^{-1}s^{-1}$).[105b] Pulse radiolysis investigations on ethylene glycol by Janata *et al.*[105] revealed that at pH = 6.0 the transient spectrum was dominanted by the initial α,β-dihydroxyethyl radical (up to 100 μs), however, at higher pH (8.5 and above) as well as at a lower pH (1.5), a transient was observed. This transient showed an initial fast decay which was attributed to the loss of water from the α,β-dihydroxyethyl radical (Scheme 2–51).

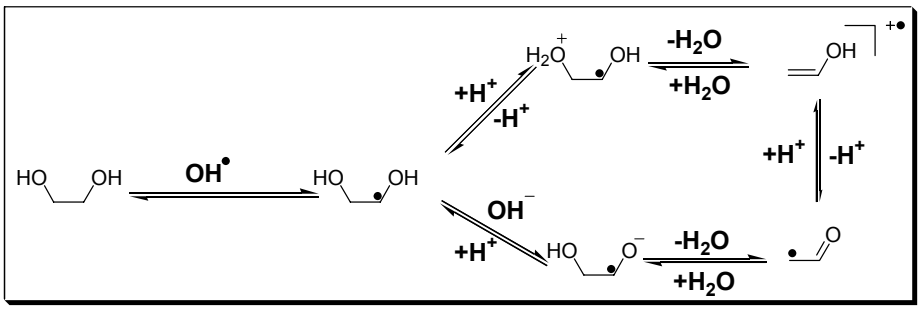

Scheme 2–51: Proposed mechanism for the decay of the α,β-dihydroxyethyl radical under general acid and base catalysis.

2.5.9.1 Pulse Radiolysis Investigation of 25 and 27

Ferrocene-based diol and triol compounds (**25** and **27**, Chart 2–8) can serve not only as enzyme substrates but also for substrates in pulse radiolysis experiments.

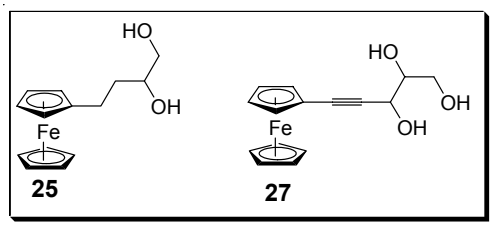

Chart 2–8: Ferrocene-based diol and triols used for pulse radiolysis investigations.

For pulse radiolysis, a 50 ns pulse was used (electron). The dose was determined using chemical dosimetry with the thiocyanate method (0.05 u, KSCN). The dose obtained for the hydroxyl radical was ≅ 5.8 G (G = no of species/100 eV). The substrate solutions were prepared by dissolving the corresponding solute in 100 ml water (0.5 mM). The transient spectrum was recorded between 290 nm to 700 nm. Traces were obtained at both 290 (decay for all carbon-centred radicals and ethenol radical cation) as well as 620 nm (for the formation of the ferrocene radical cation).

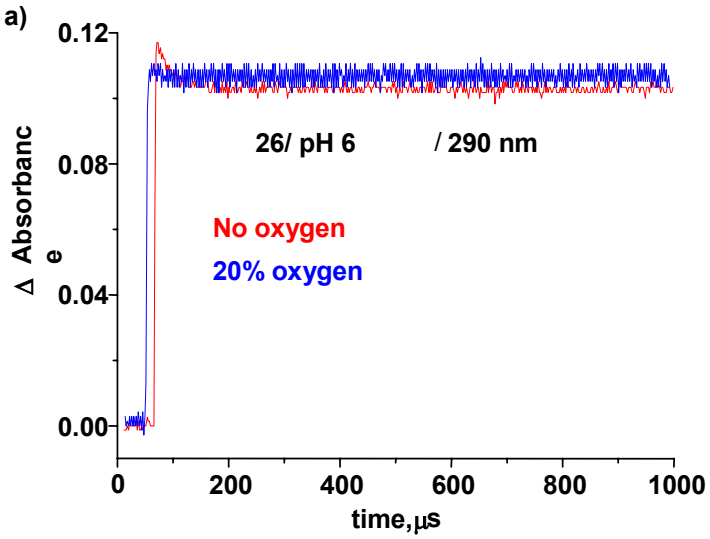

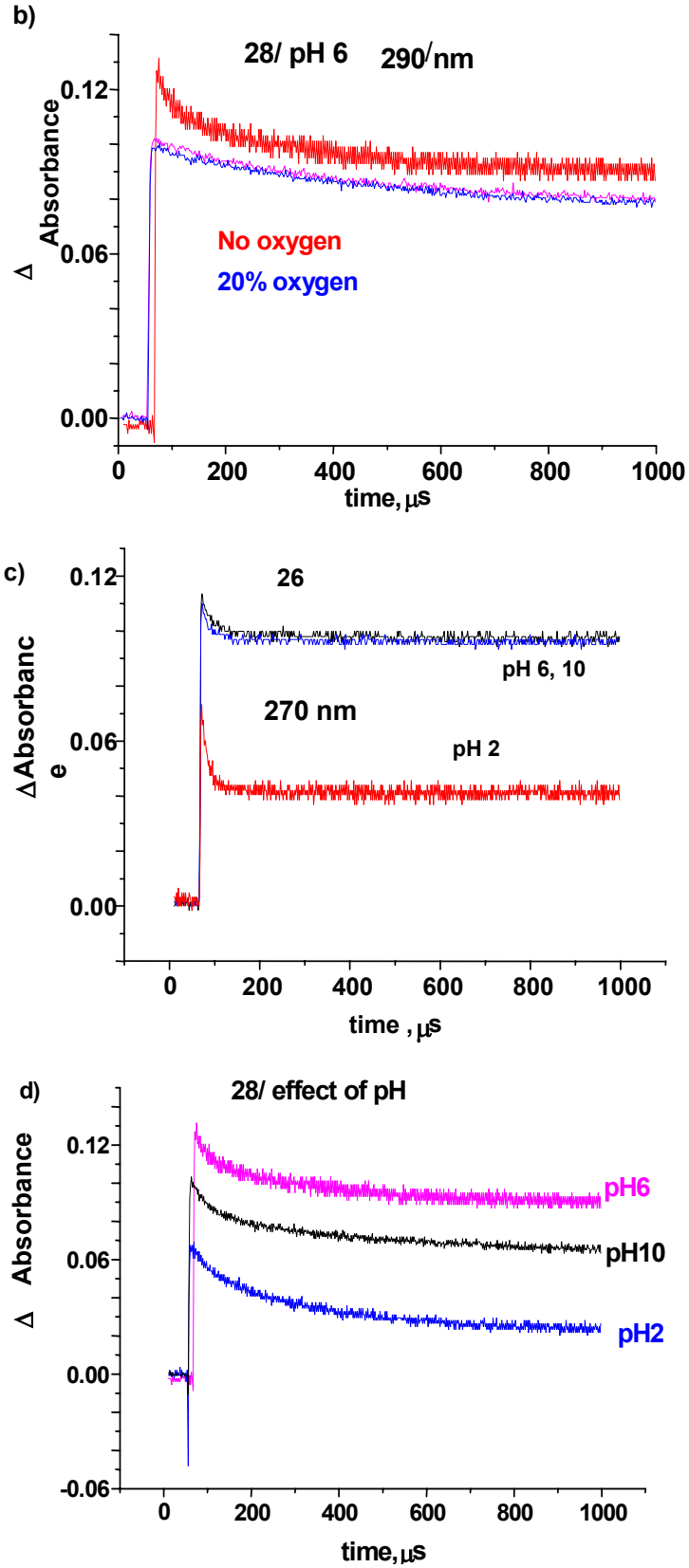

Figure 2–33: Traces obtained for **25** and **27** under pulse radiolysis conditions, a) and b) are traces obtained for **26** and **28** at pH = 6 in presence and absence of oxygen. Traces c) and d) are for **25** and **27** at different pH (6, 10 and 2) in absence of oxygen.

Pulse radiolysis of **25** in presence of nitrous acid (without oxygen) at pH 6 showed traces (290 nm), similar to the ones observed earlier. It was characterised by an initial fast decay

which reached a plateau after 100 µs. When the radiolysis was carried out in presence of oxygen no such decay process was observed indicating a fast quenching of the carbon centred radicals formed (Figure 2–33a). At 290 nm a strong overlap of the absorbances of carbon centred radicals and ferrocenium ion was observed resulting in a plateau formation. As a result the decay of all carbon-centred radical could not be analysed.

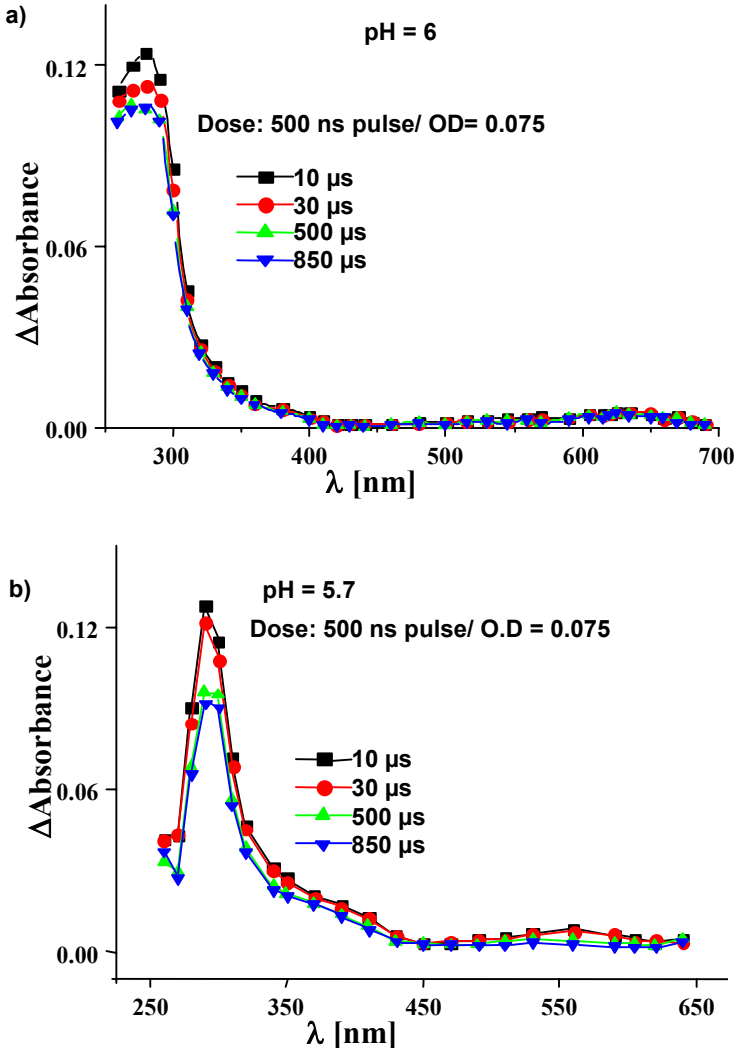

Figure 2–34: Transient spectrum of a) **25** and b) **27** obtained by pulse radiolysis.

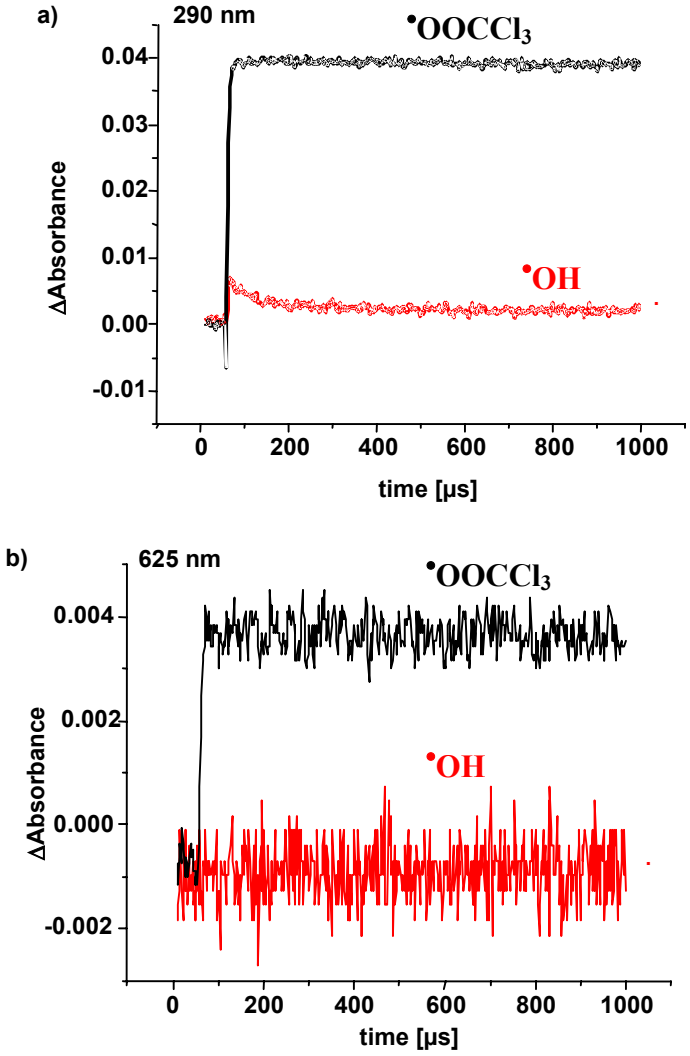

Figure 2–35: Pulse radiolysis of ferrocene. a) Trace at 290 nm, b) trace at 620 nm.

An overall bimolecular decay ($2k$) of about 1.5 x 10^{10} $dm^3mol^{-1}s^{-1}$ at 290 nm for **25** was observed. At 620 nm formation of ferrocenium ion was observed (Figure 2–34a) with a unimolecular formation constant of 8.5 x 10^{10} s^{-1}, which amounts to 74% of the radical cation formed (assuming ε_{620} = 340 [ethanol]). As predicted, at pH 2 the initial fast decay (attributed to dehydration of the α,β-dihydroxyethyl radical) is very fast leading to the appearance of the plateau at much shorter times than at pH = 6. At pH = 10 a similar very fast initial decay was observed that could be attributed to dehydration (loss of hydroxide ion from the initial radical, Figure 2–33c). Pulse radiolysis of **27** revealed a transient having no absorption above 600 nm; instead a band at around 550 nm was observed (Figure 2–34b). Interestingly, the trace at 270 nm showed a decay similar to that of carbon centred radicals (270 nm = 1.2 x 10^{10} $dm^3mol^{-1}s^{-1}$, at 290 nm = 9.0 x 10^9 $dm^3mol^{-1}s^{-1}$, Figure 2–33b and d).

Direct formation of ferrocenium ion under pulse radiolysis conditions could not be ruled out (direct interaction of hydroxide ion with ferrocene moiety of the molecule). Hence, control

experiments with ferrocene (1 mM) under similar conditions of pulse radiolysis were investigated. Pulse radiolysis of ferrocene showed no formation of radical or radical cationic species (at 290 and 625 nm). However, ferrocene solutions purged with oxygen, containing CCl_4 immediately showed formation of the stable radical cation (one electron reduction of peroxyradicals by ferrocene, Figure 2–35).

2.6 Discussion

2.6.1 Enzymatic Investigations on the Radical, Radical Ion Probes and Phenoxyethanol Derivatives

Radical enzymes are a class of enzymes such as diol, glycerol[25,27,28,29] and penoxyethanol dehydrates,[43] that utilise reactive radical intermediates in their catalytic cylce. A number of approaches ranging from isotopic labelling,[35] product distribution,[39] ESR[37] and theoretical methods[40,41] has been applied in the past to gain insights into the nature of reactive intermediates involved in their catalytic cycle. Despite such extensive investigations no conclusive picture has emerged regarding the type of reactive intermediates involved in the transformations carried out by diol, glycerol and phenoxyethanol dehydratase. However, a general motif for the transformation has been accepted,[31] wherein the reaction is initiated and terminated by hydrogen atom abstraction and addition respectively. Thus, a common mechanistic scheme is thought to be operative in most of the eliminases.

Our approach was mainly to translate such short-lived reactive intermediates into long-lived ones directly at the active site of the enzyme. The principle behind our approach was to exploit the reactivity patterns of reactive intermediates at the active site of the enzyme. The various reactive intermediates that have been invoked in the elimination reactions carried out by diol, glycerol and phenoxyethanol dehydratase range from neutral radicals to charged radicals.

Intramolecular electron transfer process between enol radical cations/ketyl radical anions to a suitable donor or acceptor was conceptualised for translating short-lived radical ions into long-lived ones directly at the acitve site of the enzyme. β-Cleavage reaction was formulated as an approach of translating short-lived radicals into persistent ones directly at the active site of the enzyme.

Thus, synthesis of a number of substrate derivatives was realised sucessfully. For translating short-lived enol radical cations to long-lived ones a number of ferrocene based substrate derivatives were synthesised in excellent yields (90-80 %). Cyclic voltammetric investigation on these probes reveal a completely reversible wave between -0.07 to +0.12 V_{Fc} for the ferrocene in these substrates depending on the substitution pattern of the side chain.

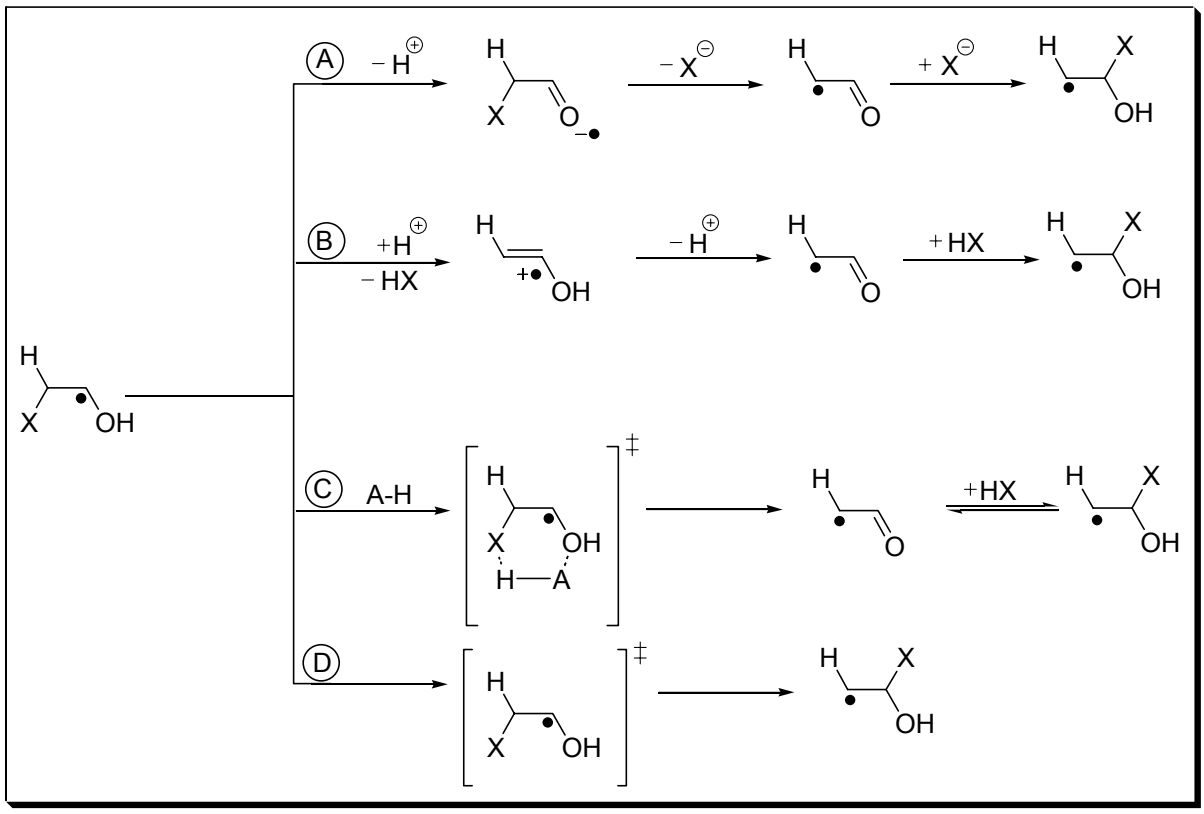

Scheme 2–52: Radical [ion] intermediates possibly involved in the eliminations reactions carried out by diol, glycerol and phenoxyethanol dehydratase.

UV-Vis absorption spectrum of the ferrocene based enzyme substrates with saturated alkyl chain typically had three absorption maxima λ_{max} = 229-232 nm, 330-334 nm and 446-450 nm. The enzyme substrates with a triple bond had an additional band at λ_{max} = 267 nm.

Quinone based enzyme substrate **35** for translating a short-lived radical anion into long-lived one was synthesised in reasonable yield (48 %). Under cyclic voltammetric conditions two reduction waves were observed out of which the first wave was observed at -0.81 V_{Fc} and a partially reversible wave at -1.71 V_{Fc}.

Neutral radical enzyme probes **62** and **63** bearing a TEMPO group were synthesised in moderate yields (50-55%). **62** was further characterised by X-ray single crystal analysis. An interesting hydrogen bonded ladder motif was observed in the crystal structure of **62**. Enzyme probe **55** containing *N*-hydroxyphthalimide was synthesised in moderate yield (40%). **55** can potentially be used both as a neutral radical as well as a radical anion probe. In addition to radical and radical ion probes a number of phenoxyethanol derivatives **57a-k** were synthesised to probe for the electronic and hydrophobic tolerance of phenoxyethanol dehydratase.

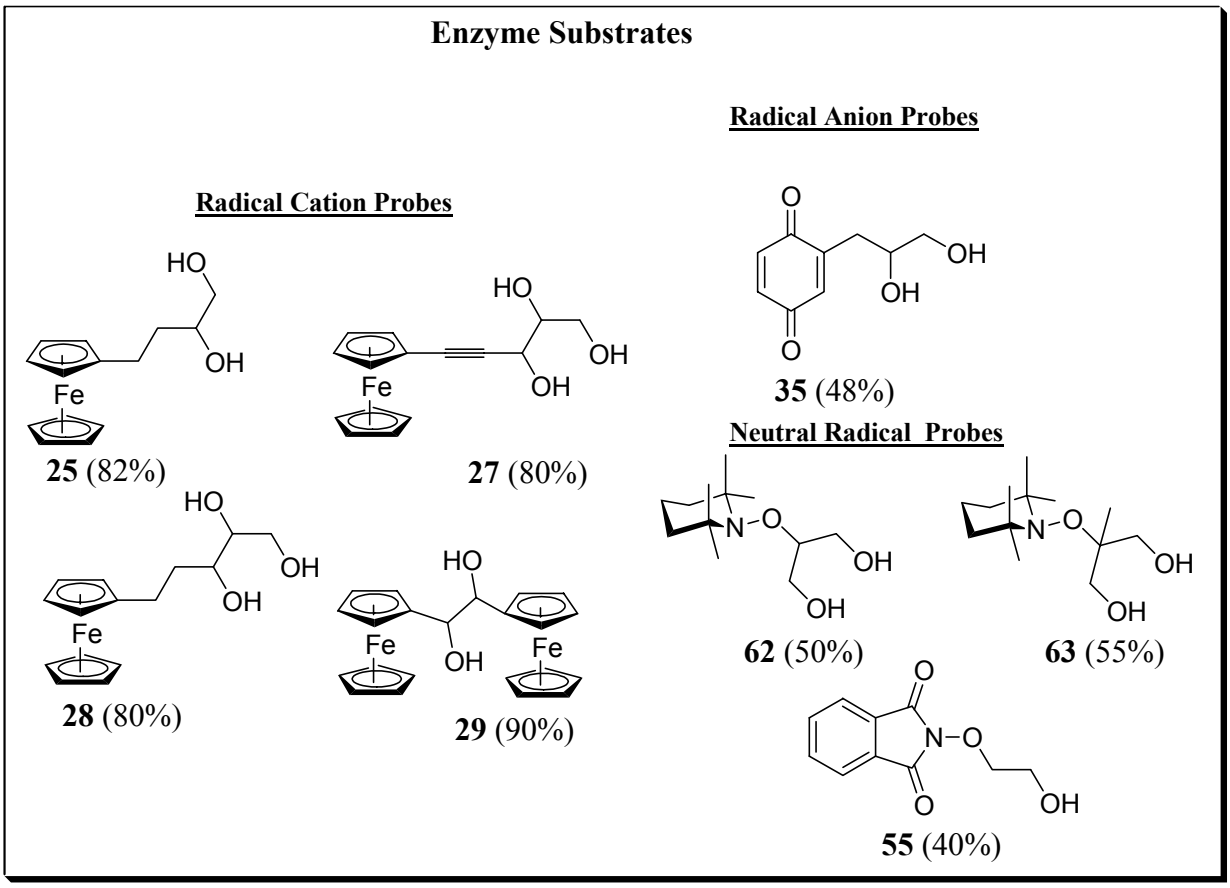

Chart 2–9: Radical and radical ion probes synthesised for enzymatic investigations

2.6.2 Enzymatic Investigations of Radical and Radical Ion Probes

The radical and radical ion probes were tested on pure diol and glycerol dehydratase. The results indicated that these probes were not accepted by the enzyme as no change in the concentration of NADH was observed with time. Radical and radical ion probes did not show any kind of inhibitory effect on the diol and glycerol dehydratase as observed by retention in activity upon addition of 1,2-propanediol (natural substrate).

This indicates that the active site path of the enzyme is small, which is in agreement with the crystal structure of some enzymes of the same family. Interestingly, when the enzyme probes were treated on phenoxyethanol dehydratase, only the radical cation probe **25** showed an inhibitory effect. In order to determine the nature of inhibition structural based or mechanistic based, kinetic investigations were carried out. Typically, the assay involved variations of the concentration of **25**. Three such assays were carried out with 1 mM, 0.1 mM and 0.01 mM of **25**. For each concentration four sets of experiments were run forming a bundle. The bundle was further subdivided into sets wherein the concentration of the phenoxyethanol added after the addition of **25** was varied. For the purpose of comparison control experiments with the

above given concentrations of phenoxyethanol were carried out without **25**. Control experiments with ethanol addition were also performed.

Enzyme activity for phenoxyethanol was determined and the V_{max} = 600.81 mM and K_m = 0.001 mM was obtained. The kinetic investigations on **25** were basically carried out with the assumption that the inhibitiory effect was purely structural based and that it was reversible. It is quite apparent from Table 2–9,Table 2–10, and Table 2–11 that a lot of variation was observed from one bundle to the other just for phenoxyethanol itself. The inhibition of the enzyme by ethanol was not very dramatic as observed from the initial velocity. In contrast to the assay containing ethanol, a distinct effect of **25** on the initial velocities of the enzyme activity could be observed which is further dependent on the concentration of **25**

Apparently, the enzyme activity varies from one bundle to the other although the concentration of the phenoxyethanol was kept constant. This effect was attributed either to the ageing of the enzyme extract or to oxygen seeping into the cuvette (a typical measurment time for one bundle required 3-3.5 h). In order to determine the nature of inhibition caused by **25** the values V_{max} and K_m were obtained by plotting the initial rate vs. the substrate concentration (here the phenoxyethanol was added after allowing the enzyme to incubate with the inhibitor for about 10-15 min).

As expected of an inhibitor, a significant decrease in the initial velocity was observed when the enzyme was pre-equilibrated with varying concentrations of **25** (Figure 2–36c and Figure 2–36d) prior to the addition of phenoxyethanol. Additionally, the decrease in the initial velocity showed a direct relationship with the concentration of **25**, which was further expressed in the V_{max} and K_m values. For "bundle A" having the highest concentration of **25** (15.1 µM), unusual low values for the V_{max} and K_m were obtained from the kinetic evaluation of the above data (a linear dependence on the phenoxyethanol concentration was obtained).

Double reciprocal plots for **25** showed a pattern of lines that did not match the known diagnostic features of a reversible inhibition. Only at a lower concentration of 1.43 µM a competitive inhibition could be speculated, since no dramatic change in the K_m value was observed, although the V_{max} value changed (criteria for a competitive inhibition). However, overall the pattern of the double-reciprocal plot appeared to be one of a non-competitive type. The Dixon plot (Figure 2–37b) failed to fit in any of the above given reversible inhibition modes suggesting that the inhibition of **25** probably does not arise from any reversible type of inhibition (assuming that no enzyme decay occurs over the entire

measurement time).

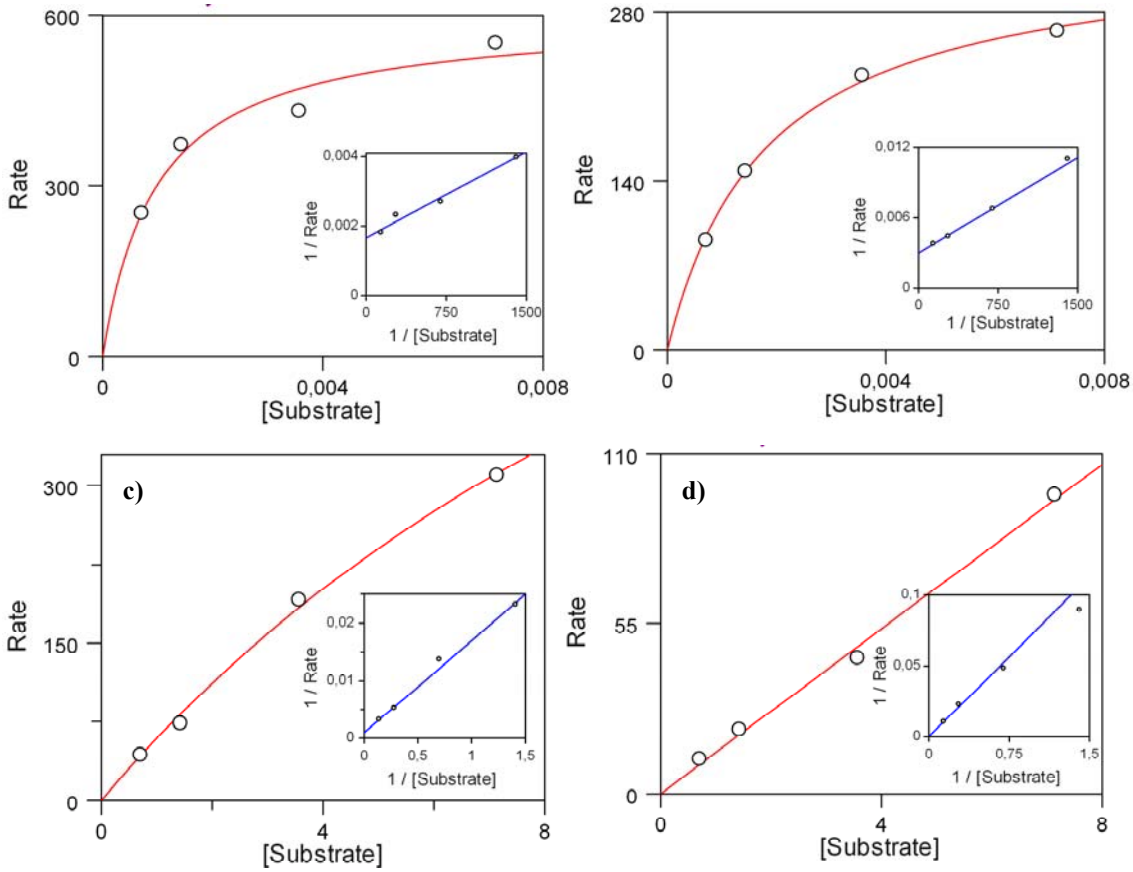

Figure 2–36: Michaelis-Menten plots showing the dependence of substrate concentration on the enzyme activity, a) only phenoxyethanol, b) phenoxyethanol + ethanol (8.57 µM), c) 4-ferrocenylbutane-1,2-diol (**25**, 8.57 µM) + phenoxyethanol and d) 4-ferrocenylbutane-1,2-diol (15.1 µM) + phenoxyethanol. Inset shows the Lineweaver-Burk plot for each measurement.

It is well known that when inhibitors have high affinity for the enzyme then the resulting inhibition is of the type "*tight binding inhibition*". While steady state approximations are valid for reversible inhibition of the enzyme, they are no longer valid for tight binding inhibition (Dixon and Webb[107]) leading to the failure of the double reciprocal plots. However, it was suggested that tight binding inhibitors display double-reciprocal plots that appear similar to the classical pattern of non-competitive inhibitors (Figure 2–37a), regardless of their true mode of interaction with the enzyme.

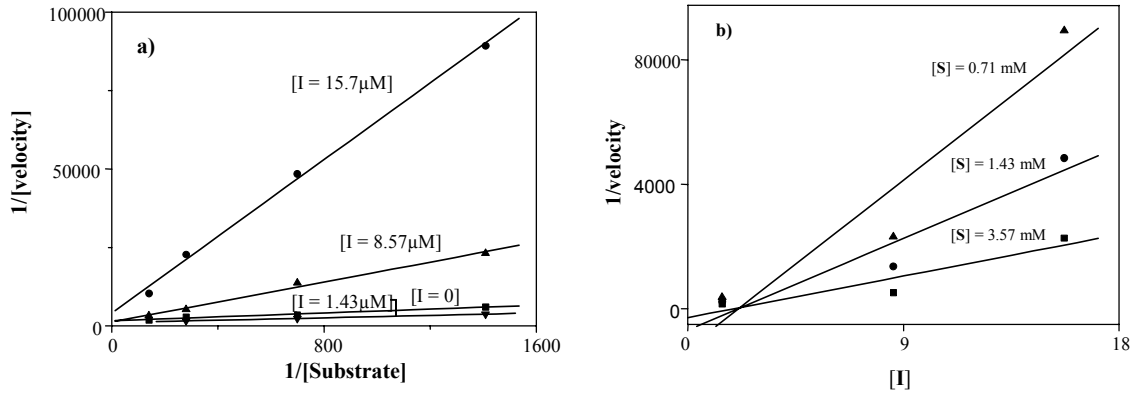

Figure 2–37: Pattern of lines observed upon addition of phenoxyethanol to a pre-incubated enzyme with **25** [I], a) double-reciprocal plot and b) Dixon plot ([I] = 15.71, 8.57 and 1.43 μM).

Table 2–15: Enzyme kinetics determined for phenoxyethanol dehydratase with phenoxyethanol, **25** and ethanol. The V_{max} and K_m values were obtained from the data in Table 2–9, Table 2–10, and Table 2–11.

Experiment set	V_{max} (mM/s)	K_m (mM)
Phenoxy ethanol		
Average	600.8	0.0011
Inhibitor 25		
Bundle B	1037.7	0.0166
Bundle C	906.5	0.0017
Ethanol as Inhibitor		
Avg.	335.5	0.0018

2.6.3 Testing of Hydrophobic and Electronic Tolerance of Phenoxyethanol Dehydratase

With the radical cation probe **25** acting as the inhibitor of the enzyme it was essential to get a much clearer understanding of the active site of the enzyme. Owing to the absence of any structural proof and the inability to isolate the phenoxyethanol dehydratase in pure form, we resorted to the more classical approach of developing a number of phenoxy ethanol derivates to probe for the hydrophobic and electronic tolerance of the active site.

It was found that the substrate derivatives containing hydrophobic groups such as methyl, propyl and butyl groups showed very low to no activity except for 2,6-dimethyl and *t*-butyl substituted phenoxyethanol (at low concentrations). Overall, substrate derivatives containing hydrophobic groups showed low activity indicating that the active site is not very hydrophobic (Table 2–8).

Substrate derivatives containing 4-methoxy (**57j**) and 4-bromo (**57h**) groups interestingly show an activity, which would be consistent with the electronic effect. Assuming a radical

anionic mechanism the 4-bromo derivative (**57h**) an electron deficient derivative should have had more activity than phenoxyethanol and **57j** (4-methoxy group, an electron-donating group). The activity of **57h** was almost twice that of **57j** however, when we compare it to the activity of phenoxyethanol, it becomes more apparent that the effect is due to some factor other than electronic effects.[108]

Unlike the diol and glyceroldehydratase, phenoxyethanol dehydratase was able to utilise the substrate when an ethylthiyl group replaced the phenoxyl moiety. This result is quite intriguing, however, it is suggesting that there are at least two different enzymes present having eliminase activity. The presence of the two oxygen atoms in phenoxyethanol dehydratase is essential for activity, is reinstated by the low activity observed for substrate derivative **92**.

For the degradation of phenoxyethanol to phenol and acetaldehyde various mechanisms have been proposed.[109] Interestingly, all of the proposed mechanisms require an initial hydrogen atom abstraction from the substrate. Recent investigations by Schink *et. al*.[109] support a radical anion pathway based on isotope labelling experiments (path C in Scheme 2–53). The phenoxyethanol dehydratase enyzme was found to be independent of added cobalamine. This suggests that the radical initiation must come from a protein based radical such as a tyrosyl radical or a thiyl radical (as in ribonucleotide reductase[6]). The other two pathways involving migrations were ruled out based on ^{2}H and ^{13}C labelling experiments. Enzymatic investigations with various phenoxy ethanol derivatives **57a-j** do correlate well with the suggested radical anionic pathway. According to the latter pathway the initial step is the hydrogen atom abstraction from the substrate. Since the phenoxyethanol derivatives **57a-j** have substitutients only at the phenyl ring of the substrate, it would have a negligibile effect on the hydrogen atom abtraction and thus, on the follow up processes i. e. the formation of ketyl-radical anion and α-carbonyl radical. The only effect that these 2-substituted phenoxyethanol derivatives (**57a-j**) can have is on the binding of the substrate.

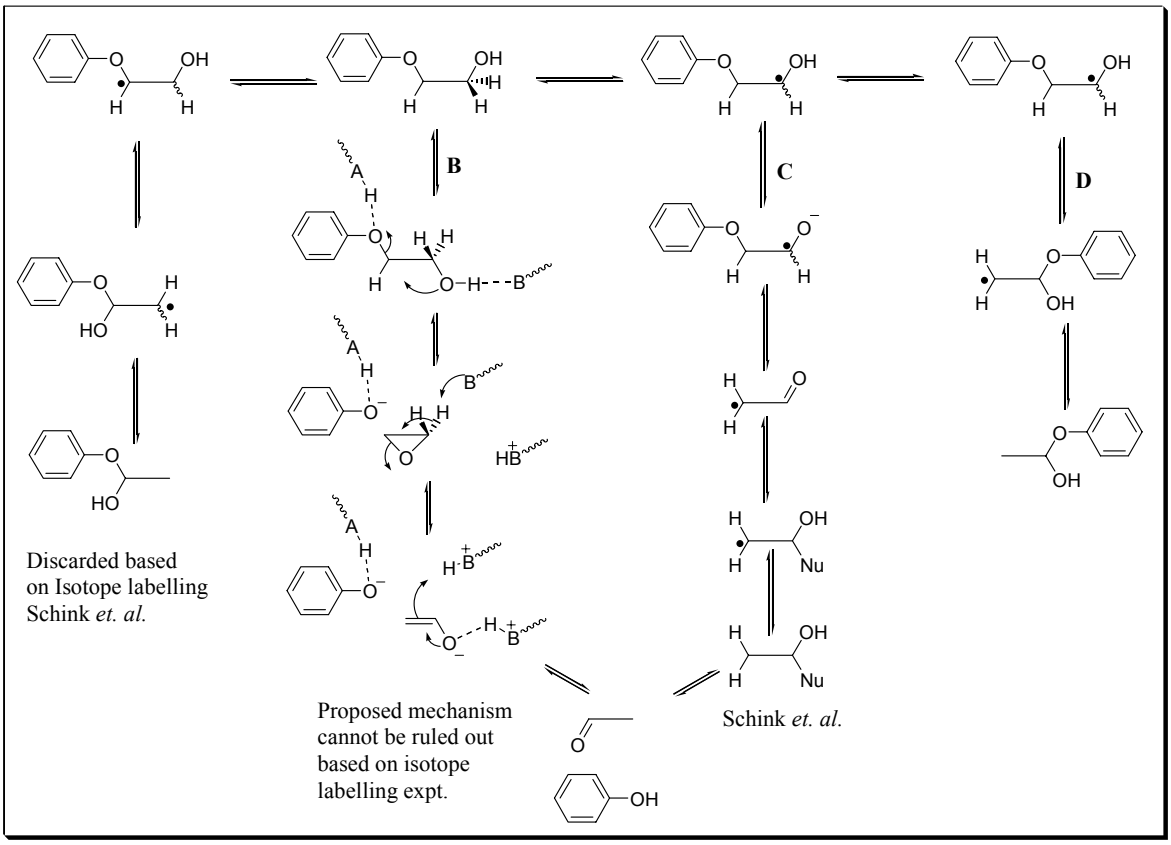

Scheme 2–53: Possible mechanistic scenarios in phenoxyethanol dehydratase for formation of acetaldehyde and phenol

One can argue over the sterics of the various 2-alkyl substituted phenoxyethanol derivatives **57a-j** and any pronounced effect on the binding of the substrate to the enzyme. However, **57h** which has a 4-bromo derivative stands out from the rest since the bromo group is not a very bulky substituent and is in the *p*-position. The activity with **57h** should have been at least similar to that observed with the phenoxyethanol derivative. Incontrast only 14% of the activity was found. The above observation raises some doubts about the radical anion pathway in the phenoxyethanol dehydratase.

An alternative mechanism that could be operative is a synergistic-push-pull mechanism (path B, Scheme 2–53). According to this pathway the entire transformation of phenoxyethanol to phenol and acetaldehyde can take place involving purely ionic reactive intermediates. Thus, an initial protonation of the oxygen atom of the phenoxy group and deprotonation of the oxygen atom of the OH group can take place by suitable acid and base at the active site of the enzyme. The rate determining step in this mechanism would be the deprotonation of the epoxide (pK_a <50) leading to the enolate formation. Another alternative ionic mechanism could be proposedinvolving acid catalysis. The initial step could be protonation of only the phenoxyl group by a suitable acid at the active site thus, generating a good leaving group

(Scheme 2–54).

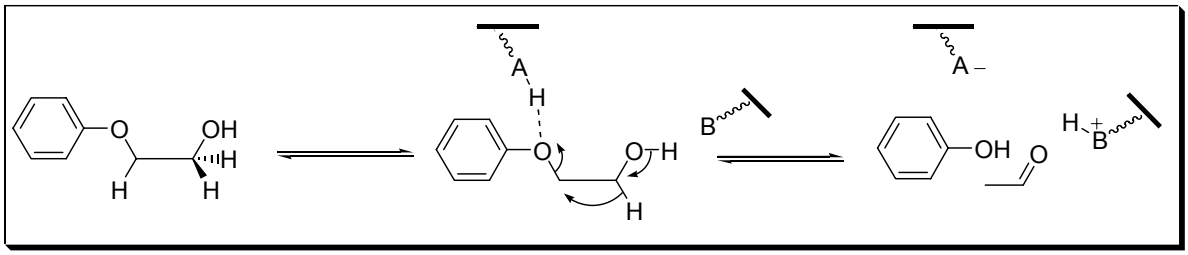

Scheme 2–54: Proposed acid-catalysed mechanism for degradation of phenoxyethanol by phenoxyethanol dehydratase.

A concerted follow up processes consisting of a cleavage of the ether bond, 1,2-migration of hydride ion and deprotonation the hydroxyl group would lead to the formation of phenol and acetaldehyde. Such acid catalysed rearrangements are well known in solution involving hydride/alkyl migration.[110] However the above mechanism requires that the migrating group (hydride ion) is *anti*-periplanar to the leaving group (phenoxy).

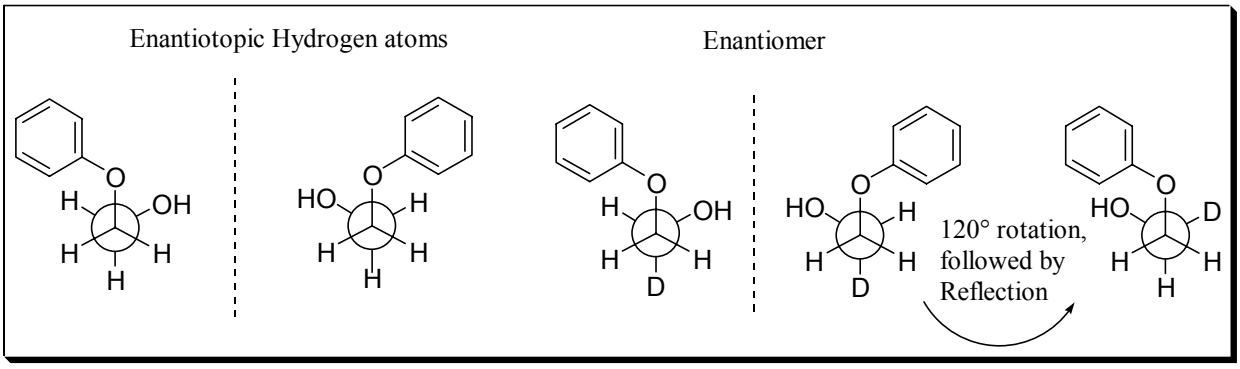

Scheme 2–55: Stereochemical course of the transformation in phenoxyethanol dehydratase.

Stereochemically seen in order to get the hydrogen atom *anti*-periplanar one would need a *syn*-orientation of the phenoxy and the OH group. From Scheme 2–55 it is clear that the two hydrogen atoms on C-1 are enantiotopic and hence should have a profound effect on the activity upon substitution at this position. Indeed this was reflected in the isotopic labelling studies by Schink *et. al.*[109] where in only the (S)-2-phenoxy(1-^{2}H)ethanol predominantly gave the monodeuterated product (*ca*. 2.5:1). When (R)-2-phenoxy(1-^{2}H)ethanol was fed to the enzyme only the nondeuterated product was formed (characterised as acetate). The syn-orientation of the two oxygen atoms would also help in binding of the substrate to the enzyme via a metal ion (such as potassium ion, similar to diol and glycerol dehydratase). This is further reflected in the inability of the enzyme to utilise **92** where the oxygen atom of the phenol was replaced by a sulfur. Binding of the phenoxyethanol to a metal ion at the active site should also enhance the 1,2-migration of a hydride ion as proposed in Scheme 2–54. The

syn-orientation of the two oxygens would also mean that substitution in the *o*-positions should dramatically affect the binding ability of the substrate, which was indeed observed with 2-phenoxyethanol derivatives **57a-j**.

The stereochemical analysis not only suits the ionic pathway. It should facilitate even the hydrogen atom abstraction. Isotope labelling experiments (^{13}C) by Schink *et. al*.[109] clearly show that the C-1 carbon bearing the OH group finally becomes the carbonyl carbon, which prompted them to propose radical anion mechanism and rule out the OH group migration (path A, Scheme 2–53). However in the light of our experiments, stereochemical analysis based on the isotopic labelling experiments by Schink *et. al*.[109] does indicate that, if radical intermediates are involved in the mechanism of phenoxyethanol dehydratase, then a phenoxyl group migration (path D, Scheme 2–53) is needed to fullfil the back hydrogen atom transfer. The migration of the phenoxyl group would then be similar to the one proposed by Toraya *et. al*.[31] and Radom *et. al*.[42] for diol dehydratase, involving predominantly cyclic transition states. The latter pathway should also be affected by substitution pattern on the phenyl ring, which is in line with our experiments with phenoxyethanol derivatives **57a-j**.

2.6.4 Solution Studies Using Various Solution Probes

In addition to the enzymatic investigations to understand the mechanistic details of diol, glycerol and phenoxyethanol dehydratase it was pertinent for us to test our concept in solution. Exploiting the redox behaviour of radical ions, we had conceptualised that, intramolecular electron transfer between a suitable donor/acceptor could be a means of translating short-lived radical ions into long-lived ones.

Enol radical cations are reactive intermediates that have been invoked in diol and glycerol dehydratase. Enol radical cations of simple enols, such as ethenol or propenol, have been extensively investigated by theoretical calculations[111,112] and observed in the gas phase.[113,114] Their chemical reactivity in the gas phase is dominated by unimolecular rearrangements. By contrast, the fate of enol radical cations in solution (on model compounds) is governed by two main reactions, one-electron transfer reduction (back electron transfer) or deprotonation ($k_{dep} = 10^6\ s^{-1}$).[7,115] Extensive investigations on enol radical cations derived from β,β-dimesityl enols indicate that in some cases these reactive intermediates have life times in millisecond range. Additionally, the α-carbonyl radicals obtained after deprotonation of these enol radical cations can serve as both a one-electron donor or an acceptor. The proton affinity of the α-carbonyl radical was found to be $k_{prot} = 10^{10}\ M^{-1}s^{-1}$.[115]

The long life times of enol radical cations of β,β-dimesityl enols coupled with the kinetic stability of the α-carbonyl radicals derived after deprotonation makes them the best candidates

to test our concept in solution.

Thus enol **E1** (3.42 mM) was transformed initially to the corresponding α-carbonyl radical (**R1**, Scheme 2–46) via a one electron oxidation of the enolate (**A1**) with ferrocenium ion. Since the oxidation potential of **R1** (+0.14 V_{Fc}) was higher than that of ferrocene overoxidation of **R1** with ferroceneium ion would not occur under the given conditions. The advantage of using ferrocene as a redox mediator was in the fact that ferrocene and its oxidised form have distinct UV-Vis absorption maxima (**Fc**, λ_{max} = 450 nm, **Fc**$^{+\bullet}$, λ_{max} = 620 nm). This allowed us to follow the whole transformation by UV-Vis spectroscopy. Incremental addition of TFA (up to 1 eq.) showed the reapprearence of the band at λ_{max} = 620 nm for the ferrocenium ion (**Fc**$^{+\bullet}$).

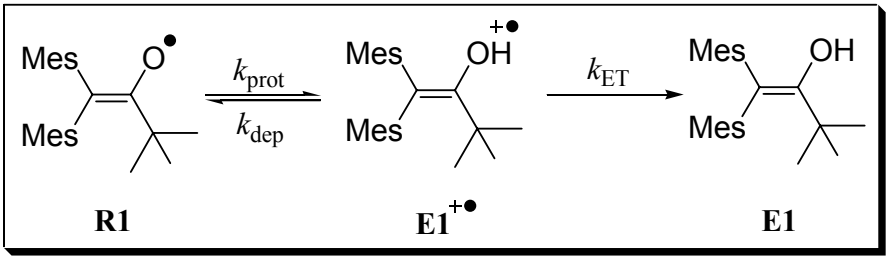

Scheme 2–56: Translating short-lived enol radical cation (**E1**$^{+\bullet}$) to long-lived-lived ferrocenium ion (**Fc**$^{+\bullet}$)in an intermolecular fashion in solution.

Using Scheme 2–56 the rate of electron transfer process is proportional to the concentration of the radical cation **E1**$^{+\bullet}$:

$$v_{ET} = k_{ET}\left[E1^{+\bullet}\right] \qquad \text{Equation 2–4}$$

Using steady state kinetics it follows that:

$$\left[E1^{+\bullet}\right] = k_{prot}\left[R1\right] - k_{dep}\left[E1^{+\bullet}\right] - k_{ET}\left[E1^{+\bullet}\right] \qquad \text{Equation 2–5}$$

$$\frac{d\left[E1^{+\bullet}\right]}{dt} \approx 0 = k_{prot}\left[R1\right] - k_{dep}\left[E1^{+\bullet}\right] - k_{ET}\left[E1^{+\bullet}\right] \qquad \text{Equation 2–6}$$

Assuming that the rate of deprotonation is negligible then the term $k_{dep}[E1^{+\bullet}]$ can be neglected. Rearrangement of the equation then leaves:

$$\Rightarrow k_{ET} = \frac{k_{prot}\left[R1\right]}{\left[E1^{+\bullet}\right]} \qquad \text{Equation 2–7}$$

Since the concentration of the **E1**$^{+\bullet}$ would be sufficiently low during the reaction, the denominator in the above equation can be negleted. Thus, the electron transfer is the directly proportional to the concentration of the radical **R1**.

$$\Rightarrow k_{ET} = k_{prot}\left[R1\right] \qquad \text{Equation 2–8}$$

Using Equation 2-8 the electron transfer rate constant (k_{ET}) for the above process was found to

be 10^7 s^{-1}. Having trapped relatively long-lived enol radical cations in solution in an intermolecular fashion, the obvious question then was, whether it is feasible to translate short-lived enol radical cations into long-lived ones? Can we generate ethenol radical cation (the radical cation thought to be formed at the active site of the enzyme) in solution and translate it into a long-lived radical cation?

Generation of the ethenol radical cation in solution would require ethenol in pure form. However, in solution it prefers the more stable tautomeric form "acetaldehyde" [K = enol/keto ≈3 X 10^{-7} at 25 °C].[116] A well known approach to enol ether radical cations under mild photochemical condition utilises the famous Barton-ester decarboxylation reactions.[117] Such mild conditions for the generation of ethenol radical cations in solution has not been reported. It was conceptualised by us that if we place a suitable leaving group in the α-position to the radical then a fast β-cleavage under mild acidic conditions would yield the ethenol radical cation. Hence, we chose to use the acetonide group as the protecting group which is labile to mild acidic conditions (k_{hyd} = 2.06 X 10^4 s^{-1} at 25 °C in formic acid).[118] Selective generation of radical **104** from a suitable precursor would undergo facile cleavage into the ethenol radical cation upon protonation with concomitant formation of acetone (Scheme 2–57).

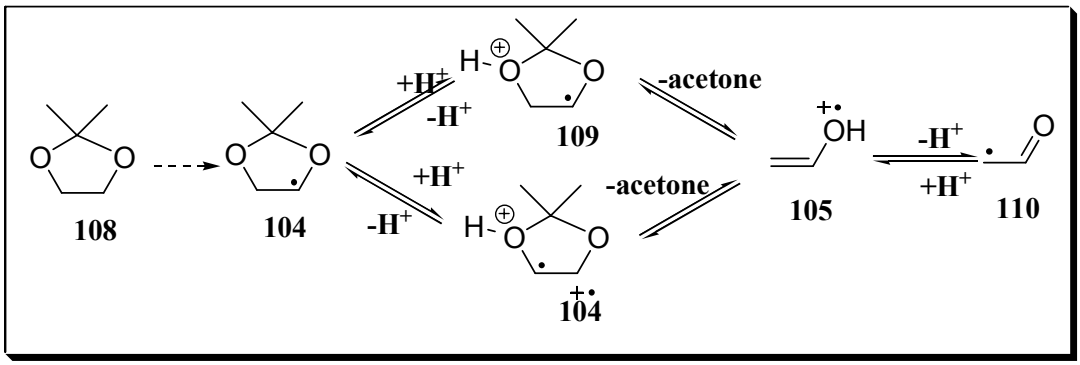

Scheme 2–57: Proposed mechanism for the formation of ethenol radical cation in solution.

Simple MO as well as DFT calculations suggest that protonation of the radical **104** at the distal position generates the distonic radical cation **109** while protonation of the proximal oxygen atom yields the radical cation $\mathbf{104}^{+\bullet}$ (Figure 2–38).

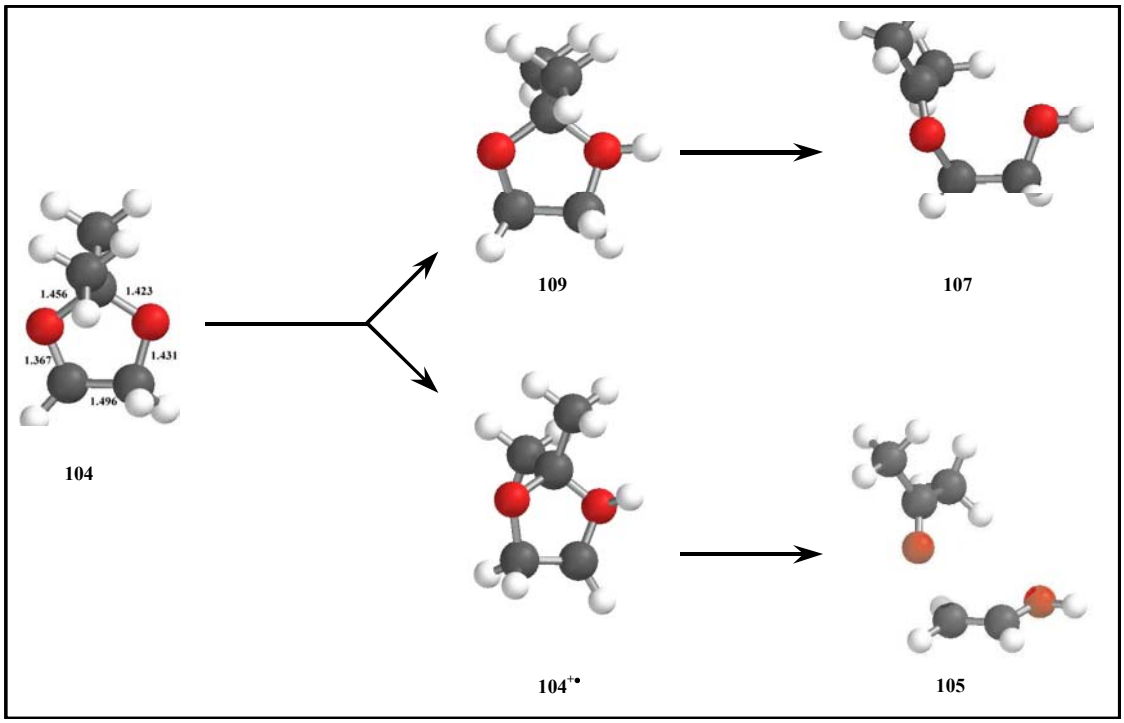

Figure 2–38: Protonation of **104** both at the proximal and distal position leads to the formation of the acetone and enol radical cation in former case and a distonic radical cation in the latter case. The optimistion of the structures were carried out at DFT/B3LYP (6-31g**) level (Calculations by Rupali Lal).

Interestingly, in the distonic radical cation **109** (1.423 Å) substantial lengthening of the C1-O2 bond between the carbon of diol and the oxygen atom was observed, equivalent to bond-cleavage leading to **107** (2.942 Å, Table 2–16). Protonation of the proximal oxygen yields **104**$^{+\bullet}$, which undergoes a simultaneous two bond dissociation giving rise to the expected ethenol radical cation and acetone.

Table 2–16: DFT/B3LYP (6-31g**) calculations results showing the total energy (gas phase) of various possible species required for prediction of cleavage of **104** in presence of acid (PhD thesis work of Rupali Lal).

Species	E_{Total} Hartrees	ΔE [E_{105+H}^{+}-E_X] (kcal/mol)
104	-346.34227	0
acetone	-153.49000	
ethenol radical cation	-193.16419	
water	-76.41973	
hydronium ion	-76.70564	
H^+	0.28591	
104 + H^+	-346.62818	
109	-346.67548	-29.68

$104^{+\bullet}$	-346.70139	-45.94
acetone + 105	-346.65419	-16.32

Interestingly the calculations indicate that protonation of the proximal oxygen in **104** was preferred over the distal oxygen (1.2 times) almost by 16 kcal mol^{-1}, with the overall conversion from **104** to acetone and ethenol radical cation being governed mainly by entropy. To generate the radical **104** under mild conditions the Barton ester **75** was designed and synthesised.

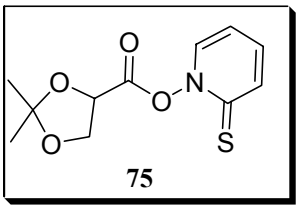

75

The UV-Vis spectrum of **75** showed a maximum absorption band at λ_{max} = 360 nm characteristic for a Barton ester. This band was further utilised to follow the acid stability of **75** with varying concentrations of trifluoroacetic acid. The acid stability test revealed that protonation of **75** in presence of TFA is reversible (for 1-5 eq. more than 24 h and 70 eq. ~5-6 h). Interestingly, a plateau was achieved after 28 equivalents of TFA addition which was similar to the observation by LFP. A number of possible modes of reversible protonation could be invoked. Of all the possible modes of protonation the most preferred one would be of **97**. The photochemical studies by contrast reveal that the photostability was not affected by addition of 1 eq. of TFA. This rules out a substantial amount of **94** and **96** upon addition of TFA to **75**.

Photolysis of **75** both in presence of TFA/formic acid and ferrocene gave a long absorbing band at λ_{max} = 620 nm typical for $\mathbf{Fc}^{+\bullet}$. This observation was in line with our expectation of formation of an enol radical cation. However, efforts to isolate acetaldehyde in the form of a Schiff base failed.

Thus, the prime objective then was to understand the nature of the oxidant. Photolysis of ferrocene itself or in presence of 1-5 eq. of TFA upon extended photolysis did not yield $\mathbf{Fc}^{+\bullet}$ which rules out the photo-oxidation of ferrocene in presence of TFA. The other potential oxidants ($\mathbf{102}^{+\bullet}$, $\mathbf{98}^{+\bullet}$) were ruled out by photochemical investigations on **78**. While acetaldehyde is the product formed from the one-electron reduction of ethenol radical cation by **Fc**, it might also undergo some side reactions making its identification difficult. However, it is known that Barton esters upon photolysis or thermolysis undergo a decarboxylative reagrrangement leading to the formation of alkylpyridylsuphides. Thus, presence of TFA can

have profound effect on the formation of **99** if ethenol radical cations are formed.

Quantification based on the HPLC method using hexane-ethyl acetate (85:15) as eluent revealed that indeed a decrease of about 30% in **99** was observed upon photolysis of **75** in presence of TFA. The photodegradation of **99** in presence/absence of TFA was about ~2-3%. This further supports our mechanism for the involvement of ethenol radical cation. Time resolved studies were carried out to characterise each step of photolysis. Using the TR-ESR we were able to characterise the radical **104** having a g value of 2.0035 which was in close agreement with the literature reported value Lit: 2.0032.[101] The coupling constants were found to be 11.2 G (d) and 27.2 G (q).

Laser flash photolysis of **75** in acetonitrile and benzene gave a complex spectra with transients at λ_{max} = 305, 350, 480 and 600 nm, the decay constants of which have been summarised in Table 2–13. The absorption maximum at λ_{max} = 305 nm was tentatively assigned to ethenol radical cation which is close to the theoretically calculated one λ_{max} = 315 nm (PhD work of Rupali Lal, private communication of Dr. G. Bucher, University of Bochum). From the kinetic data ethenol radical cation was found to decay with a unimolecular decay constant of 2.1 x 10^5 s^{-1}, giving rise to a half life of 3.3 μs.

Trapping experiments with relatively long-lived β,β-dimesitylethenol radical cations reveal an intermolecular electron transfer constant (k_{ET}) of 10^7 s^{-1}. With a half-life of 3.3 μs for ethenol radical cation the intermolecular k_{ET} should be between 10^6-10^7 s^{-1}.

Theoretical investigations, coupled with UV-Vis photolysis, HPLC quantification, TR-ESR and LFP investigations further indicate the formation of ethenol radical cation during the photolysis of **75** in presence of TFA. The formation of ethenol radical cation can be explained from the Scheme 2–58. The Barton ester **75** in presence of TFA, can undergo protonation at the ester-oxygen. The protonation of this site would be preferred as it would be further stabilised by the adjacent oxygen atom via a 5-membered cyclic ring. Photolysis of this intermediate would yield the desired radical cation **104**$^{+\bullet}$ after decarboxylation. The radical cation **104**$^{+\bullet}$ would form the ethenol radical cation **105** via a simultaneous two-bond dissociation. Formation of the ethenol radical cation can also occur via protonation of the distal oxygen however, it would be limited by the protonated precursor complex.

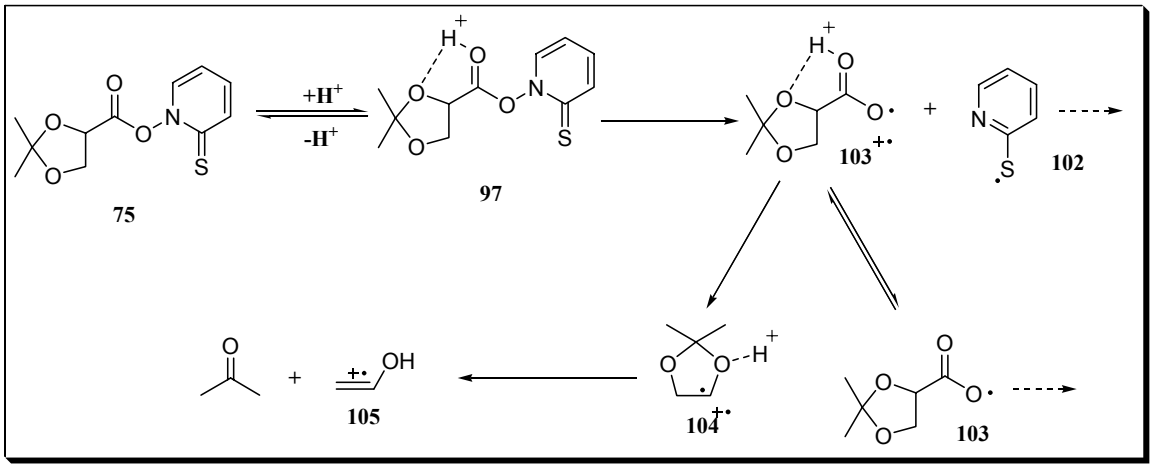

Scheme 2–58: Most probable mechanism for the formation of ethenol radical cation upon photolysis of **75** in presence of TFA.

Encouraged with the intermolecular trapping experiments a next step would be to test the concept in an intramolecular fashion. A number of attempts were made to synthesise probes bearing both a vicinal diol, a radical initiator and ferrocene coupled to a part of the moelcule. Compound **79** containing a fluoroenoneoxime ester as a radical source, a ferrocene as the donor, a methoxy and a OH group in vicinal position was synthesised sucessfully to mimic the dehydratase reaction.

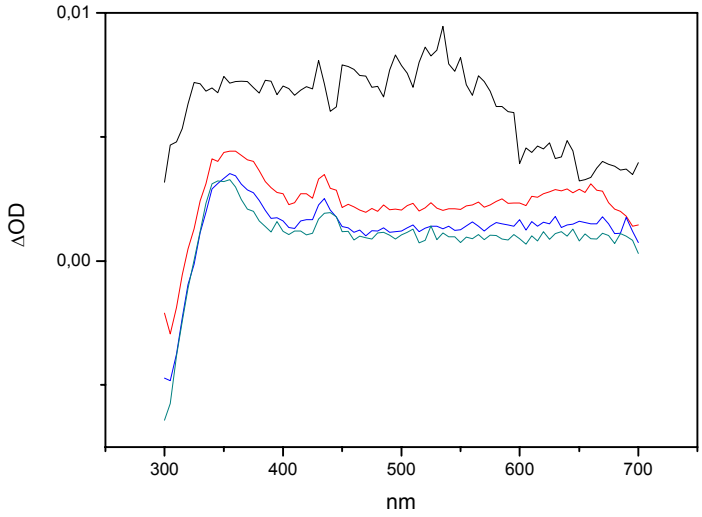

Figure 2–39: Changes observed during the laser flash photolysis of **79** in acetonitrile.

Preliminary investigations by laser flash photolysis of **79** showed the formation of the 9-fluoreneiminyl radical with a λ_{max} = 650, 430, 380, and 320 nm (Figure 2–39). However, no formation of radical cation was observed after addition of trifluoroacetic acid to the solution. A thorough investigation is still in progress.

The main bottleneck for the synthesis of substrates to mimic dehydratase reaction for both diol, glycerol and phenoxyethanol dehydratase was the introduction of a radical source. Thus, we resorted to pulse radiolysis investigations where a high energy radiation becomes the

source of the radical. Since we had sucessfully synthesised a number of probes containing a vicinal diol with ferrocene as donor (**25**, **27**, **28** and **29**), these can be used for investigating intramolecular trapping of enol radical cations in solution. It is well known in literature[105] that vicinal diols can be converted into an α-carbonyl radical in presence of $OH^{\bullet}$ generated under pulse radiolytic conditions. The formation of α-carbonyl radical was observed both under acidic as well as basic pH. Invovlement of enol radical cation and ketyl radical anion was suggested.

Pulse radiolysis experiments with substrate **25** and **27** were carried out with a 50 ns pulse (electron). The transient spectrum in **25** showed a strong absorption at 290 nm. In addition to that a band at 620 nm was observed at pH = 6. The band at 620 nm is a clear indication for the formation of the ferrocenium ion. The formation constant at 620 nm was found to be 8.5 x 10^{10} s^{-1}. The formation constant of the 620 nm under pulse radiolytic conditions can be considered similar to the k_{ET}, because the electron transfer rate constant for an intramolecular process is 1000 times faster than observed for intermolecular ones. This is in line with our expectations for an intramolecular process, and additionally supports our concept for translating short-lived radical ions into long-lived ones directly at the active site of the enzyme.

An overall bimolecular decay ($2k$) of about 1.5 x 10^{10} $dm3mol^{-1}s^{-1}$ was observed at the band at 290 nm for **25**. The decay of 290 nm band was strongly pH dependent, it is very fast at lower pH = 2.

In conclusion, the pulse radiolysis experiments with **25** clearly showed formation of a ferrocene radical cation, which could occur only when strong oxidants such as enol radical cations were formed.

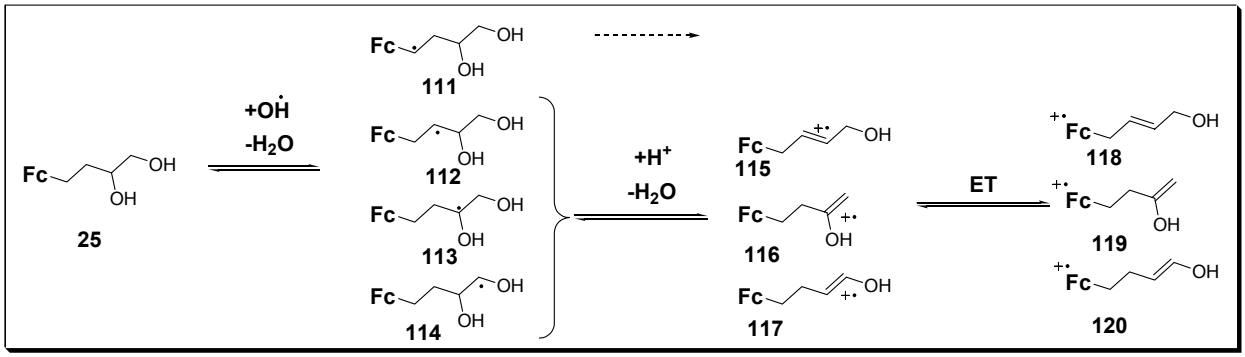

Scheme 2–59: Possible mechanism for the formation of ferrocenium ion from **25** (0.5 mM) under pulse radiolysis conditions in absence of oxygen and carbon tetrachloride.

The most possible mechanism would involve an initial formation of radicals via hydrogen atom abstraction by the hydroxyl radicals from **25** giving rise to all possible radicals **111-114**.

From a crude analysis based on the stability of the radicals, it would be fair to assume a substantial amount of **113** forming. Of the four various possible radicals only the latter three (**112-114**) can potentially form radical cations (**115-117**). A fast intramolecular electron transfer from the ferrocene to the radical cation would lead to formation of the ferrocene radical cation (**118-120**) and the corresponding alkene or carbonyl derivative.

The inability to observe such a radical cationic species for **27** could be due to the higher oxidation potential ($E_{1/2}$ = +0.12 V_{Fc}) of the ferrocenyl group in comparison to **25** ($E_{1/2}$ = -0.05 V_{Fc}). The pulse radiolysis experiment further supports our concept of translating short-lived enol radical cations into long-lived ones via a intramolecular electron transfer process.

2.7 Conclusion

The tests carried out with our first generation of enzyme probes designed to dissect and understand the various mechanistic scenarios in elimination reactions carried out by diol, glycerol and phenoxyethanol dehydratase provided useful information that can be used for further development of mechanistic probes for these enzymes.

Enzymatic investigations on diol and glyceroldehydratase (in collaboration with Prof. Dr. J. Rétey) were useful in the fact that the radical and radical ion probes are not structural inhibitors of the enzyme. The small active site rendered these probes ineffective for mechanistic scrutinisation.

Collaborative work with Prof. Dr. B. Schink on phenoxyethanol dehydratase clearly has provided some leads that could be followed up by developing new probes. The primary factor for the ineffectiveness of the radical and radical ion probes was their inability to seep into the active site of the enzyme probably due to the large steric bulk of these probes. This was further supported by the phenoxyethanol derivatives designed to test for the active site tolerance. Although radical cation probe **25** was able to effectively inhibit the enzyme, the inhibition could mainly be due to non-competitive binding as suggested before. A mechanistic based inhibition of the enzyme by **25** could be rule out in light of the results obtained from the various substrate derivatives (**57a-j**).

Results with phenoxyethnaol dehydratase using various phenoxyethanol derivatives clearly indicate that a radical anion mechanism cannot be denied. However, if involved, it would lead to a fragmentation of the corresponding radical anion into a phenolate and an α-carbonyl radical. The latter radical itself is an oxidant and would not be able to abstract a hydrogen atom unless it is converted into a acetal or a similar derivative. The isotope labelling experiments (^{1}H and ^{13}C) reported by Schink *et. al.*[109] clearly indicate that the carbon bearing the OH group becomes the carbonyl of the resulting aldehyde. It also suggests that a very selective "*Pro-S*" hydrogen atom migrates. While these results are interesting and help to understand the stereochemical course of the transformation, it does not rule out a purely acid/base catalysed mechanism. The acid/base catalysed mechanism postulated by us would also be able to explain the experimental results from labelling experiments. If in phenoxyethanol dehydratase the reaction involves radical or radical ionic intermediates we strongly believe that it should involve a phenoxy migration (similar to the mechanism proposed by Toraya *et. al.*[31] for diol and glycerol dehydratase or retro-push-pull mechanism proposed by Radom *et. al.*[42]). Investigations with various phenoxyethanol derivatives (**57a-j**) reveal that the substitution pattern at the phenoxy ring plays an

important role on the activity of this enzyme. The derivatives **57a-g** have substitution primarily on the *o*-position, which indicates that they could potentially affect either the binding of the substrate at the active site (*syn*-orientation of the oxygen atoms is needed) or the protonation of the phenoxy group. This was indeed reflected on the activity of the enzyme in presence of this substrate. **57h** is the most interesting case where a *p*-bromo derivative is used. The activity with this probe was about 14%, suggesting that presence of an electron withdrawing group probably lowers the electron density at the phenoxy oxygen atom. Hence, it can effect either the binding, protonation or migration of the substrate. A purely radical anionic mechanism would in fact have resulted in an enhanced activity of the enzyme with **57h**.

Experiments to translate short-lived radical cations into long-lived ones using ferrocene as donor were performed. Intramolecular translation was found to be 1000 times faster than intermolecular. Pulse radiolysis experiments on **25** reveal a k_{ET} of 10^{10} s^{-1} which is ideal for translating such reactive intermediates directly at the active site of the enzyme.

2.8 Future Perspectives

With regard to the above mentioned results that were obtained from various enzymatic investigations carried out in this work one is tempted to design and test new probes that could prove pivotal in getting insights into the mechanistic details of the eliminase reactions. Successful manipulation of substrates for mechanistic investigations in diol and glyceroldehydratase from *E. Coli* might not work due to the small active site of these enzymes. The design and synthesis of radical ion probes would be difficult for diol and glyceroldehydratase. One approach that can still be exploited and has not been addressed earlier is to hook a donor or acceptor close to the active site of these enzymes, by site-directed mutagenesis (Scheme 2–60).

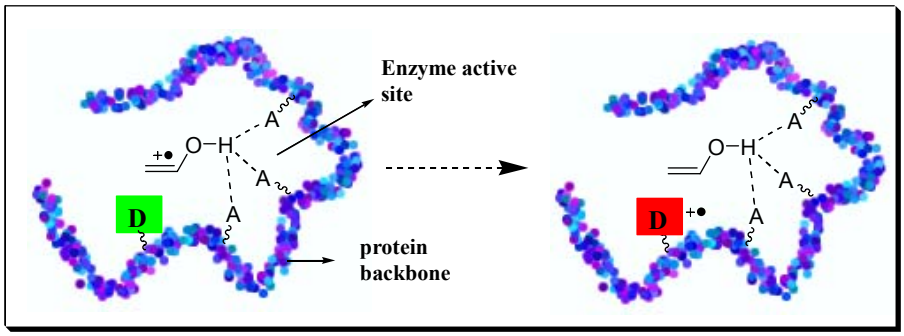

Scheme 2–60: A possible approach to understand the mechanistic details of coenzyme B_{12} dependent eliminase reactions.

As for testing the radical intermediates, the smallest and smartest way would be to attach a cyclopropyl ring to the substrate derivative. The presence of a cyclopropyl group would not pose a big steric challenge for the enzyme (Chart 2–10).

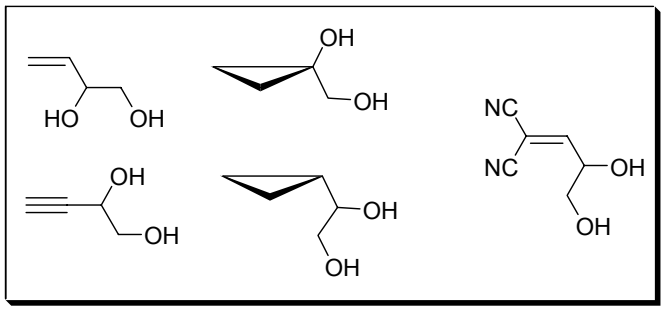

Chart 2–10: List of possible substrate derivatives to probe for neutral radical intermediates in diol and glyceroldehydratase.

While the size of the active site remains more challenging for diol and glyceroldehydratase, this is not the case for phenoxyethanol dehydratase, which makes it a suitable and promising candidate for developing mechanistic probes (Chart 2–11).

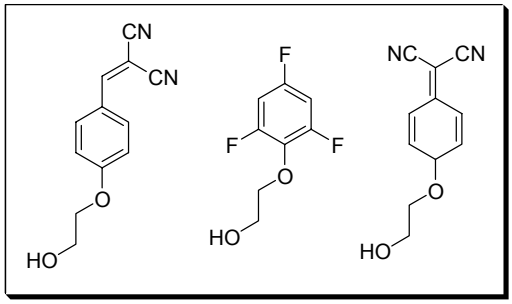

Chart 2–11: List of substrate derivatives to probe for radical anionic intermediates in phenoxyethanol dehydratase.

To further understand the mechanism of this enzyme one could also develop a series of 4-substituted phenoxyethanol derivatives. In addition to the functionalisation of the phenoxy group one can also functionalise the C1 position at the *Pro-R* centre and study the effect of the functional groups at this position. This might be of prime importance as presence of any bulky group here would hinder the migration. It would help in eliminating the phenoxy migration hypothesis proposed earlier.

Radical ions are important reactive intermediates in many biological transformations. However, not many methods (ESR) are available to investigate them directly in the protein. The approach of translating short-lived radical ions into the long-lived ones directly at the active site of the enzyme via fast electron transfer process would not only help in detecting them but would allow one to understand their reactivity directly at the active site of the enzyme. Although a clear understanding of some of the test probes is still required the applicability of the concept was demonstrated in homogenous solution both in an inter as well a intramolecularly.

While the successful translation of short-lived enol radical cations into long-lived ones was achieved, developing solution probes that would mimic the eliminase reaction still pose some serious problems for synthesis. The primary reason for the failure to prepare solution probes to mimic the eliminase reaction is that, in most of the cases the attachment of the radical source (iodide, Barton ester etc.) to free hydroxyl group was not compatible to the synthetic procedures. Tin based systems as radical source can be prepared, but, they are not stable to acidic conditions, which is required for the generation of enol radical cations.

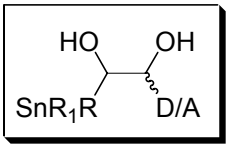

One compound that can have potential application as radical initiatior is the 2,3-di-*t*-butylphenoxy derivative[119] with a *p*-substitution. The radical initiation can be achieved chemically or electrochemically by reacting phenolates. The advantage of generating radicals

by this method is that one would be able to follow the cleavage process by UV-Vis spectroscopy, because the product of initial cleavage (quinonemethide) absorbs at a higher wavelength (350 nm in isooctane and 490 nm in TFA + isooctane)[120] than the reactant itself.

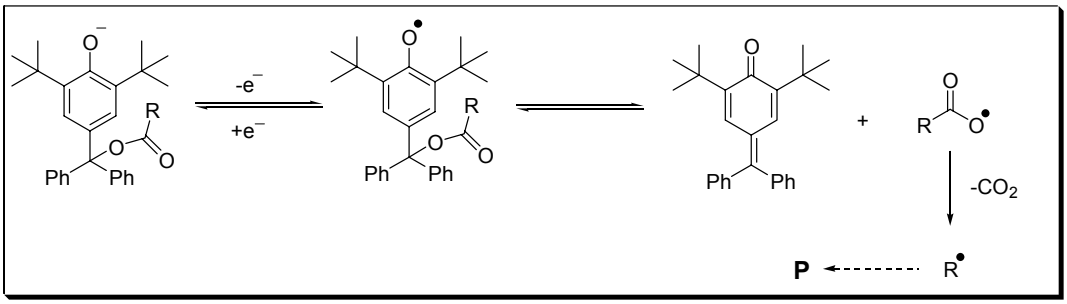

Scheme 2–61: New radical initiator based on 2,6-di-*t*-butylphenol.

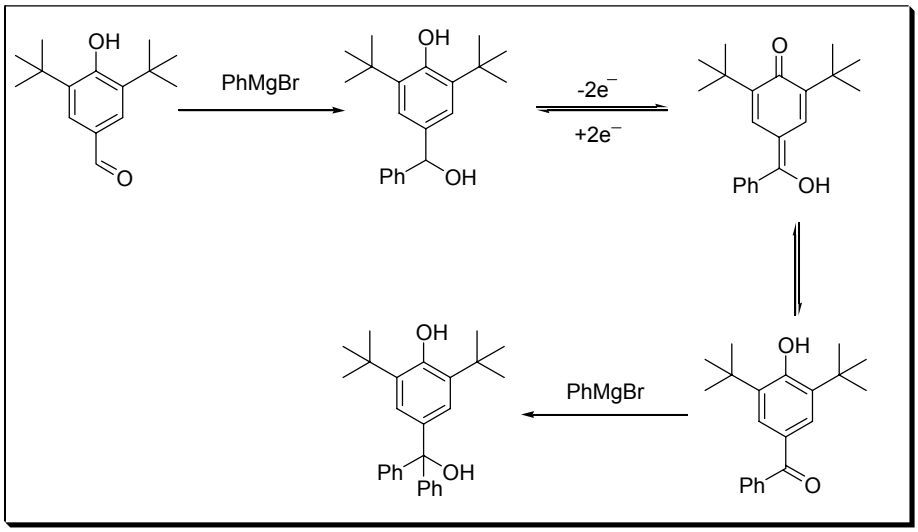

Scheme 2–62: Synthetic strategy to prepare derivatives of 2,6-di-tert-butylphenol.

The derivatives could be synthesised easily by an initial reaction between phenylmagnesium bromide with 3,5-di-tert-butyl-4-hydroxybenzaldehyde (Scheme 2–62). The product upon 2-electron oxidation would give the corresponding ketone. The ketone, when treated with phenylmagnesium bromide, would give the desired tri-arylalcohol which can further be derivatised.

3 One Electron Oxidation Chemistry of Enols

3.1 Introduction[121]

Electrochemistry can be defined as the study of chemical reactions to produce electric power or, alternatively, the use of electricity to affect chemical processes or systems. The first relates to *galvanic cells*, while the second to *electrolytic processes*. The science of electrochemistry has its origins in the fact that oxidation-reduction reactions can be performed in ways that allow the direct harvesting of the free energy released in these processes. The free energy is given by:

$$\Delta G° = -nFE^{0}_{cell} \qquad \text{Equation 3–1}$$

Electrochemical reactions are heterogeneous in nature and occur at interfaces usually referred to as electrodes. The electrode where reduction takes place is called *cathode* and where oxidation occurs as *anode*. A net electrochemical reaction implies the transfer of charge across the corresponding metal solution boundary and the flow of current across the electrode. An instantaneous measurement of the rate of the electrochemical reaction can be obtained from the basic electrical quantity current *i,* from the equation:

$$i = -nFAr \qquad \text{Equation 3–2}$$

where n is the number of electrons transferred in the interfacial reduction or oxidation process, F is the Faraday's constant, A is the surface area of the metal solution boundary, and r is the instantaneous reaction rate. Integration of the current over a period of time gives electrical charge, Q, which can be transformed into the amount of material in moles, N, converted in the electrochemical reaction using Faraday's law:

$$Q = nFN \qquad \text{Equation 3–3}$$

A third quantity of fundamental importance is the electrode potential, which can be considered as an adjustable driving force for the electrochemical reactions. Generally as the potential of an electrode is made more negative, the average energy of the electrons in the metal, which is approximately equal to its Fermi level, becomes higher, giving the electrode more reducing power. Similarly, the oxidising power of an electrode can be increased by making its potential more positive.

$$Ox + ne \Leftrightarrow \mathrm{Re}\,d$$

For a generalised process involving the transfer of n electrons, where the *Ox* and *Red* represent the oxidised and reduced partners of the redox couple, the thermodynamic potential, E, of the corresponding electrode is given by Nernst equation,

$$E = -E^0 + \frac{RT}{nF} \ln \frac{a_{Ox}}{a_{\mathrm{Re}d}} \qquad \text{Equation 3–4}$$

where $E°$ is the potential under standard conditions, a_{Ox} and a_{Red} are the activities of the oxidised and reduced species, respectively.

3.1.1 Movement of Ions in the Electrochemical Cell

In electrochemical cells, the movement of charged and neutral species occurs in three ways, *migration, convection and diffusion*. *Migration* is the movement of ions under the influence of an electric field. It can be removed by the addition of an ionisable salt called a *supporting electrolyte*.

Convection is mass transport resulting from movements of the solution as a whole. In shorter experiments, convection is not a factor in mass transport as long as the solution is quiescent and the electrodes are stationary.

Diffusion is mass transport driven by a gradient of chemical potential. The rate of diffusion of any chemical species is described by its diffusion coefficient *D*. Most small organic or inorganic molecules or ions have *D* values in the vicinity of 10^{-5} cm^2/s. This value usually decreases with molecular size.

3.1.2 Classification of Electrochemical Techniques

Electrochemical techniques can be divided in two classes, bulk and interfacial. *Bulk* techniques are based on phenomena that take place in the core of the solution, such as in conductometry. *Interfacial* techniques focus on phenomena taking place at the electrode-solution interface. Interfacial electrochemical methods can be further classified into equilibrium and dynamic methods. In *equilibrium* methods, measurements are taken under equilibrium conditions, that is, when there is no net flow of current through the cell, for example potentiometric methods. In *dynamic* methods, measurements are made in a cell that has been displaced away from equilibrium conditions. The measurements are done under conditions of potential or current control.

In potential controlled electrochemical methods, the working electrode is subjected to a so-called excitation function, that is, a potential that varies as a function of time. The simplest type of excitation function is the *potential step*. It implies that an abrupt change of the working electrode from an initial rest value, at which no current flows, to a final value, at which the Faradic process of interest takes place at an appreciable rate, such as in chronoamperometry and chronocoulometry.

In *potential sweep methods* the potential of the working electrode is varied continuously

according to a predetermined potential waveform, while the current is measured as a function of the potential, such as in linear sweep voltammetry and cyclic voltammetry.

3.2 Cyclic Voltammetry

Cyclic voltammetry (CV) is an *interfacial*, *dynamic, potential sweep* electrochemical method in which the potential of the working electrode is varied continuously according to a predetermined potential waveform, while the current is measured as a function of the potential. It is based on the same principle as linear sweep voltammetry (LSV). However, in CV the potential of the working electrode is scanned back after reaching a certain value E_S, called the switching potential. The key advantage of CV over simple LSV lies in the fact that a reverse scan is possible in the former. Reversing the scan after the electrochemical generation of a species is a direct and straightforward way to probe its stability. A stable electrogenerated species will remain in the vicinity of the electrode surface and yield a current wave of opposite polarity to that observed in the forward scan. An unstable species will react as it is formed and no current wave will be detected in the reverse scan. A typical cyclic voltammogram for the reversible reduction of *Ox* to *Red* is shown below (Figure 3–1). The electrochemical process is fast in the time scale of the experiment and the electrogenerated species *Red* is perfectly stable in the electrolytic solution.

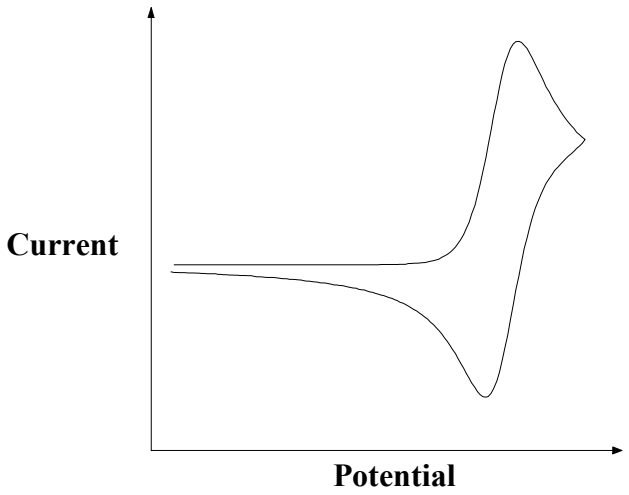

Figure 3–1: Typical cyclic voltammogram for a reversible electrode process.

Assuming that the solution is kept unstirred during the experiment, the ratio of the cathodic and anodic peak currents should be equal to one. Deviations from unity reveal the presence of chemical reactions involving either redox partner (Ox or Red) or both partners. The average of the two peak potentials affords the half-wave potential for the corresponding couple. At any potential, the difference between the cathodic and anodic current (Δi) is given by:

$$\Delta i = 2vC \qquad \text{Equation 3–5}$$

where v is the scan rate and C is the capacitance of the electrode at the potential of choice. This equation provides a simple method to determine the capacitance of the working electrode. Another method to assess the reversibility of a redox couple is the evaluation of the potential difference between the peak potentials of the anodic and cathodic peaks associated with the couple. Based on numerical solutions of the current-potential response in CV experiments, a value of 57/n mV (at 25 °C) is expected for a reversible redox couple.

The half-wave potential ($E_{1/2}$) can be readily obtained from the midpoint between the two peak potentials for a reversible or quasi-reversible redox couple. This value is characteristic of a redox couple and is typically within a few mV of the formal potential for the couple ($E^{0'}$) according to the equation:

$$E = E^{0'} - \frac{RT}{2nF}\ln\frac{C_{Ox}}{C_{\mathrm{Re}d}} \qquad \text{Equation 3–6}$$

Where the ratio of the diffusion coefficients C_{ox} and C_{Red} is usually very close to unity.

3.3 Electrode Kinetics[122]

Electrochemical reaction rates are governed by the rate with which the reactant arrives at the interface given by the expression:

$$\frac{i}{A} = i_0\left[\frac{C_O^{\,S}}{C_O^{\,b}}e(-\alpha f\eta) - \frac{C_R^{\,S}}{C_R^{\,b}}e(1-\alpha)f\eta\right] \qquad \text{Equation 3–7}$$

[i = current, i_0 = exchange current density, A = area, $C_O^{\,S}$, $C_O^{\,b}$, $C_R^{\,S}$, $C_R^{\,b}$ are the surface and bulk concentrations of oxidised and reduced species, α the transfer coefficient, f (F/RT) and η = activation over potential]. As described earlier, the three possible ways in which reactants are transported to the surface occurs are diffusion, convection and migration. The addition of excess of electrolyte prevents migration, while convection can be avoided by decreasing the measurement time. Fick´s first and second law controls movement of ions under the concentration gradient:

$$i_x = -D\left[\frac{\delta C}{\delta x}\right] \qquad \text{Fick´s first law} \qquad \text{Equation 3–8}$$

$$\left(\frac{\delta C}{\delta x}\right) = D\left[\frac{\delta^2 C}{\delta^2 x}\right] \qquad \text{Fick´s second law} \qquad \text{Equation 3–9}$$

When solving Fick´s second law for the diffusion layer model and applying it to simple electron transfer reactions two limiting case arise, a) when i_0 is small then the perturbation of diffusion layer is little and b) when i_0 is large (high potentials or intrinsically irreversible reactions). For large values of activation over potential the equation has the form:

$$\ln\frac{i}{A} - \ln i_0 = -\alpha n f \eta \quad \text{Tafel equation} \qquad \text{Equation 3–10}$$

In the presence of an electroactive material that undergoes reversible electron transfer, a typical cyclic voltammogram appears as in Figure 3–1. At non-Faradic current no change is observed, however as the potential becomes more positive, the current rises exponentially. While the current flows, a progressive depletion of material occurs near the electrode surface and when the peak current (i_p) is reached, the concentration of the reactant at the electrode surface becomes virtually zero. A subsequent decrease in current occurs until a diffusion-limited condition is obtained. When the potential is changed, (backward sweep) the product that was formed during the forward sweep that is still in the vicinity of the electrode gets reduced at the electrode surface (showing similar behaviour as in the forward sweep until a diffusion limit is reached).

For completely reversible systems the peak current (i_p) was found to be directly proportional to the sweep rate given by the equation:

$$i_p = 2.687\times10^5 n^{3/2} A D^{1/2} C \nu^{1/2} \qquad \text{Equation 3–11}$$

For a reversible system where the fast electron transfer process is not accompanied by any chemical reaction the ratio of the peak current for the cathodic process to the anodic process is equal to unity. The other criteria to check for the reversibility include the spacing for the peak potentials or half peak potentials (E_{pa}-E_{pc} = 60-65 mV), the dependence of current on the square root of the sweep rate ($i_p/\nu^{1/2}$) and independence of anodic peak potential E_{pa} with ν.

Integral equations solved by Nicholson and Shain[123] for linear-sweep voltammograms provide a much superior method for investigating dependence of various electrode reactions on the scan rate (reversible electron transfer process, irreversible electron transfer process, electron transfer followed by chemical reaction etc). The diagnostic curves were obtained either by plotting a) current function ($i_p/\nu^{1/2}$) *vs* scan rate (ν)or b) shift of peak potential ($\Delta E_{pa}/\Delta\log\nu$) with scan rate (ν) (Figure 3–2a). The third diagnostic criterion involves the variation of the ratio of anodic peak current to cathodic peak current with scan rate (Figure 3–2b).

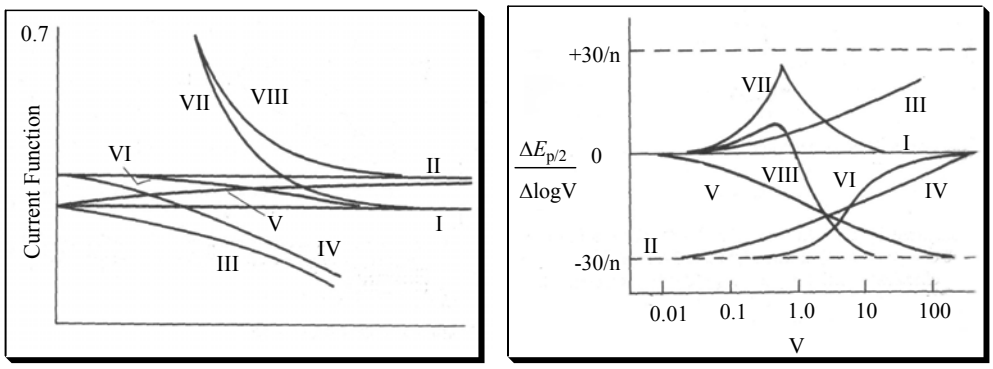

Figure 3–2: Diagnostic criteria given by Nicholson and Shain for linear sweep voltammograms for various electrode reactions given (see table below), a) variation of peak current functions (i_p /$\nu^{1/2}$) with scan rate (ν) and b) rate of shift of potential with scan rate.

I	E_{rev}	II	E_{irr}
III	CE_{rev}	IV	CE_{irr}
V	$E_{rev}C_{rev}$	VI	$E_{rev}C_{irr}$
VII	$E_{rev}C_{kat}$	VIII	$E_{irr}C_{kat}$

3.4 Reactivity Pattern of Enols

Enols, enolates and α-carbonyl radicals are important intermediates in many reactions and experimental knowledge on many of the fundamental properties of their simple derivatives such as electrochemical properties are not known due to their fleeting existance in solution. The main knowledge on these reactive intermediates usually comes from theoretical investigations and gas phase investigations using mass spectrometry. Theoretical and experimental investigations have established that the thermochemical stability order of keto/enol tautomers can be inverted upon one-electron oxidation both in the gas phase and in solution. As a consequence, enols are much more readily oxidized than the tautomeric ketones (E_{ox} [ketone] ≈ E_{ox} [enol] + 1.0 V). The enol forms of simple carbonyl compounds are present at exceedingly low concentration in solution ($K_{enol} = 10^{-8}$), however their concentrations in biological systems may approach unity (i.e. $K_{enol} = 1$) or even favour enol formation. Enols have been invoked in a number of reactions carried out by racemases e.g. mandalate racemase, proline racemase etc. Typically under biochemical conditions the enol/enolate breakdown occurs by one of the following three ways; a) reversible reaction with an electrophile leading to bond formation/cleavage (such as molecular oxygen,[124] carbonyl group,[125] decarboxylation[126]), b) eliminations leading to α,β-unsaturated carbonyl compounds,[127] and c) reduction reactions by losing one or two electrons.[128]

Although involvement of enols as electron donors are not yet known in biological systems, cation radicals of simple enols and enol ethers are known to play a vital role in DNA damage. Enol radical cations have been invoked in the transformations carried out by coenzyme B_{12} dependent enzymes such as ribonucleotide reductase,[5,6] diol and glycerol dehydratase and ethanolamine ammonia lyase.[27,30,31]

Extensive investigations in the gas phase indicate that enol radical cations are not only very stable in the gas phase over their oxo counterparts, it is accompanied by a complex reactivity predominantly consisting of unimolecular rearrangements, isomerisations and fragmentation processes.

However, in the last 20 years knowledge about the synthesis and structures of isolable and stable enols has steadily increased.[129,96] Two different modes of substituents, i.e. halogens and sterically bulky aryl groups, have found widespread use in stabilising enols and to rendering them isolable.

Electrochemical investigations on a number of such stable and isolable enols have enhanced our understanding of the reactivity pattern of enol radical cations in solution. In general the two main pathways that determine the fate of enol radical cations in solution are either one electron reduction processes to give neutral precursors or deprotonation to yield the α-carbonyl radicals (Scheme 3–1).[7]

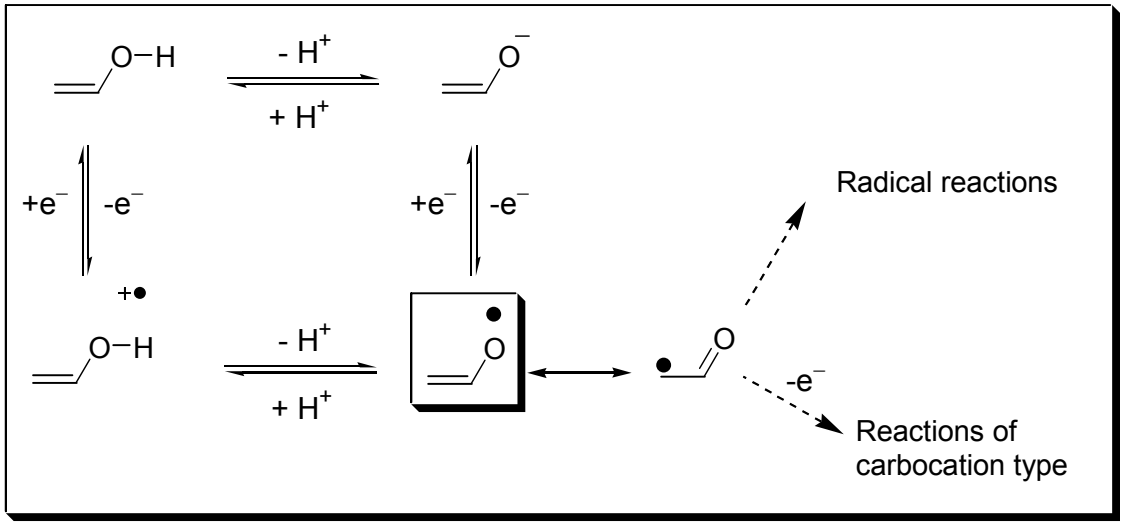

Scheme 3–1: One electron oxidation chemistry of enols, enolates and α-carbonyl radicals.

One-electron oxidation of enolates would also result in α-carbonyl radical. The reactivity of the latter could be modulated depending on the substitutent. α-Carbonyl radicals bearing electron withdrawing groups in the α-position are known to undergo radical type reactions,

while those bearing electron donating groups undergo typical carbocationic reactions upon further one-electron oxidation.

β,β-Dimesityl enols are kinetically stable enols bearing bulky mesityl groups in the β-position. One electron oxidation chemistry of which has been extensively investigated in our laboratory (Schmittel *et. al*.).[130,131] Mechanistic investigations with β,β-Dimesityl enols enabled for the first time to detect enol radical cations in solution. Oxidation of β,β-Dimesityl enols with two equivalents of sufficiently strong one-electron oxidant afforded the benzofuran derivatives. Mechanistic investigations by Schmittel *et. al*.[130,139] have led to a detailed understanding of these oxidative transformations. A fast deprotonation of the corresponding enol radical cations was observed after one electron oxidation. The resulting α-carbonyl radicals oxidize to α-carbonyl cation intermediates that cyclize intramolecularly and after a [1,2]-methyl shift 4,6,7-trimethylbenzofurans are formed (Scheme 3–2). Importantly, such oxidations are not restricted to stable enols, an almost identical mechanistic scheme should be valid for the oxidation of enolates (**A**).

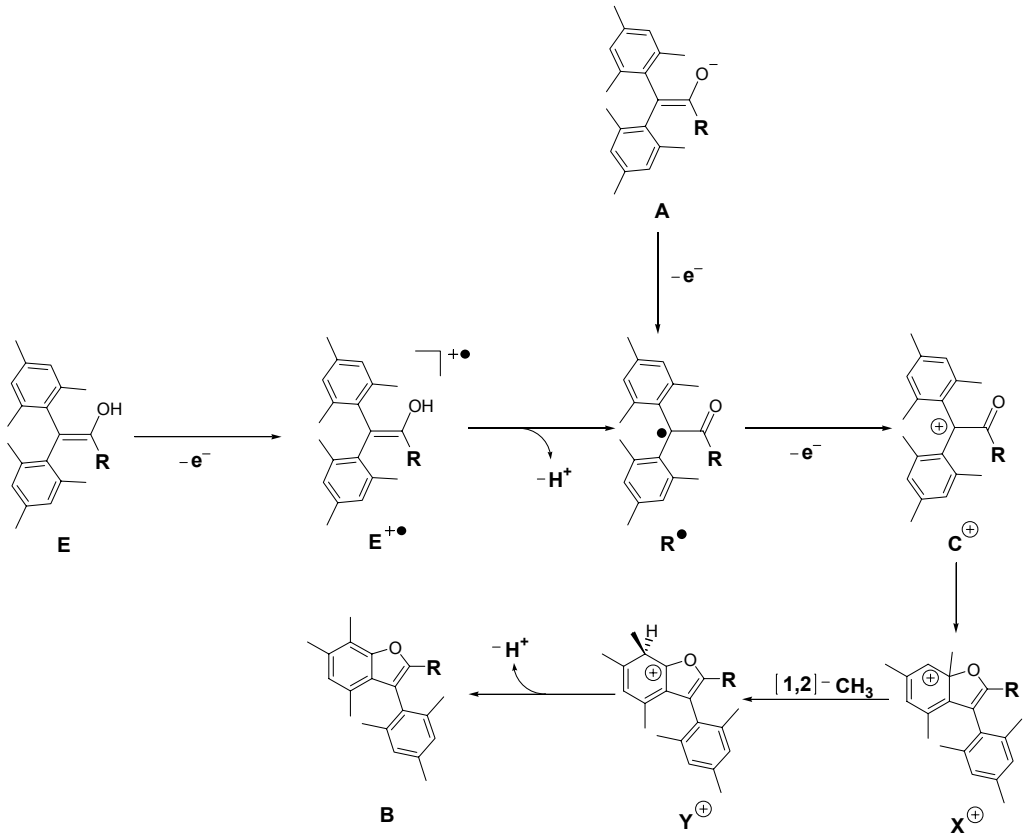

Scheme 3–2: Mechanism of the oxidation of stable β,β-dimesityl enols and enolates.

3.5 Objective

It has been found that hydrogen bonding at the active site of enzymes plays an important role not only in the stabilisation of a redox state, but it is additionally responsible for binding of a particular redox state.[132,133] A recent investigation shows that a profound effect on the reduction potentials of quinone was observed upon addition of alcohol even at very, low concentrations. Investigations on the reduction potentials of phthalimido esters in our laboratory had shown an anodic shift of about 100 to 200 mV for various hydrogen bonded *N*-substituted phthalimido esters.[134]

Extensive investigations of the hydrogen bonding effect on reduction potentials of quinone are well documented. However, little is known about the modulation of oxidation potentials of enols via hydrogen bonding.

Hydrogen bonding to enol radical cations should not only reduce their oxidation potential but should also enhance the deprotonation step leading to the α-carbonyl radical. Hence, modulation of the reactivity of enol radical cations at the active site of enzymes, through hydrogen bonding becomes crucial for developing probes that would test for such reactive intermediates during the catalytic cycle (Scheme 3–3).

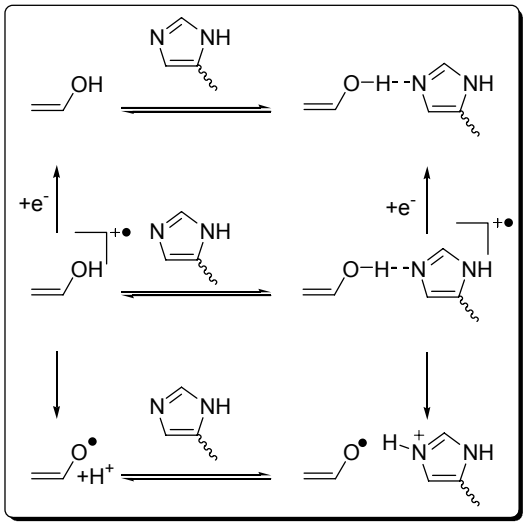

Scheme 3–3: Modulation of enol radical cation reactivity through hydrogen bonding, by imidazole moiety of protein residue.

Solution studies on simple enols are still difficult, which enable the of β,β-Dimesityl enols as model compounds to enhance insights into various aspects of enols, enolates, enol radical cations and α-carbonyl radicals. Additionally, it has the advantage that the enols can be prepared quantitatively in pure enol forms using simple starting materials. Thus the present objective of the work was to develop:

1) Model compounds that would provide useful insights on to the oxidising power of enol radical cations via hydrogen bonding.

2) Model compounds with various α-substituents to investigate their effect on the reactivity of α-carbonyl radical and α-carbonyl cations.

3.6 Results

3.6.1 Synthesis of Model Compounds Based on β,β-Dimesityl Enols

3.6.1.1 Synthesis of β,β-Dimesityl Enols E2-E4, with Six-membered Nitrogen Heterocycles

All the enols were prepared by a reaction of dimesitylketene[135] with the corresponding lithium or Grignard reagent. Enols **E2-E4** were prepared in moderate to good yields (29-44%, Scheme 3–4) by reacting the corresponding lithium reagent with dimesitylketene at –60-65 °C in dry THF (when the reactions were carried above these temperature, the reaction led to undesired products which could not be characterised).

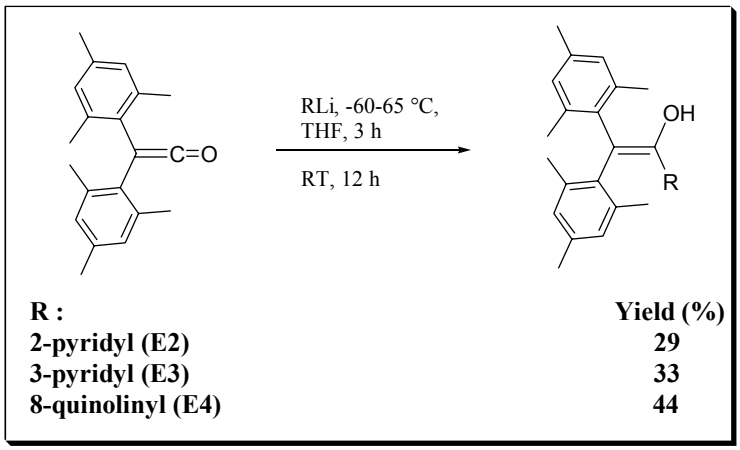

R :	Yield (%)
2-pyridyl (E2)	29
3-pyridyl (E3)	33
8-quinolinyl (E4)	44

Scheme 3–4: Synthesis of enols **E2-E4** prepared starting from dimesitylketene.

Characterisation of the enols was based on various spectroscopic data such as IR, ^{1}H-NMR, ^{13}C-NMR, and elemental analysis. The IR spectrum of enols showed a characteristic signal at 1609 cm^{-1} (C=C), and broad band at 3435 (OH) cm^{-1}. The ^{1}H-NMR of enols showed a characteristic OH signal for all the enols.

For enols **E2**, **E3**, and **E4** suitable single crystals were obtained and analysed. Single crystal measurements for enols **E2-E4** suggested that despite the difference in the aryl substitution, the hydrocarbon skeletons of these enols adopt a helical propeller conformation similar to various aryl substituted enols.[136] All the enols displayed a C=C distance of about 1.35 Å.

In the solid state OH···N hydrogen bonding was observed for all the enols **E2-E4** with intermolecular hydrogen bonding leading to a dimeric structure in **E2** (Figure 3–3a) and a chain like structure in **E3** (Figure 3–3b). In **E4** (Figure 3–3c) an intramolecular OH···N hydrogen bonding was observed. A dimeric structure was also observed for **E4** mainly because of the π-π stacking interactions. While a synclinal orientation for the enolic OH was

observed for **E2** and **E3**, the OH group in **E4** adopts an anticlinal orientation stabilised by OH···N interaction.

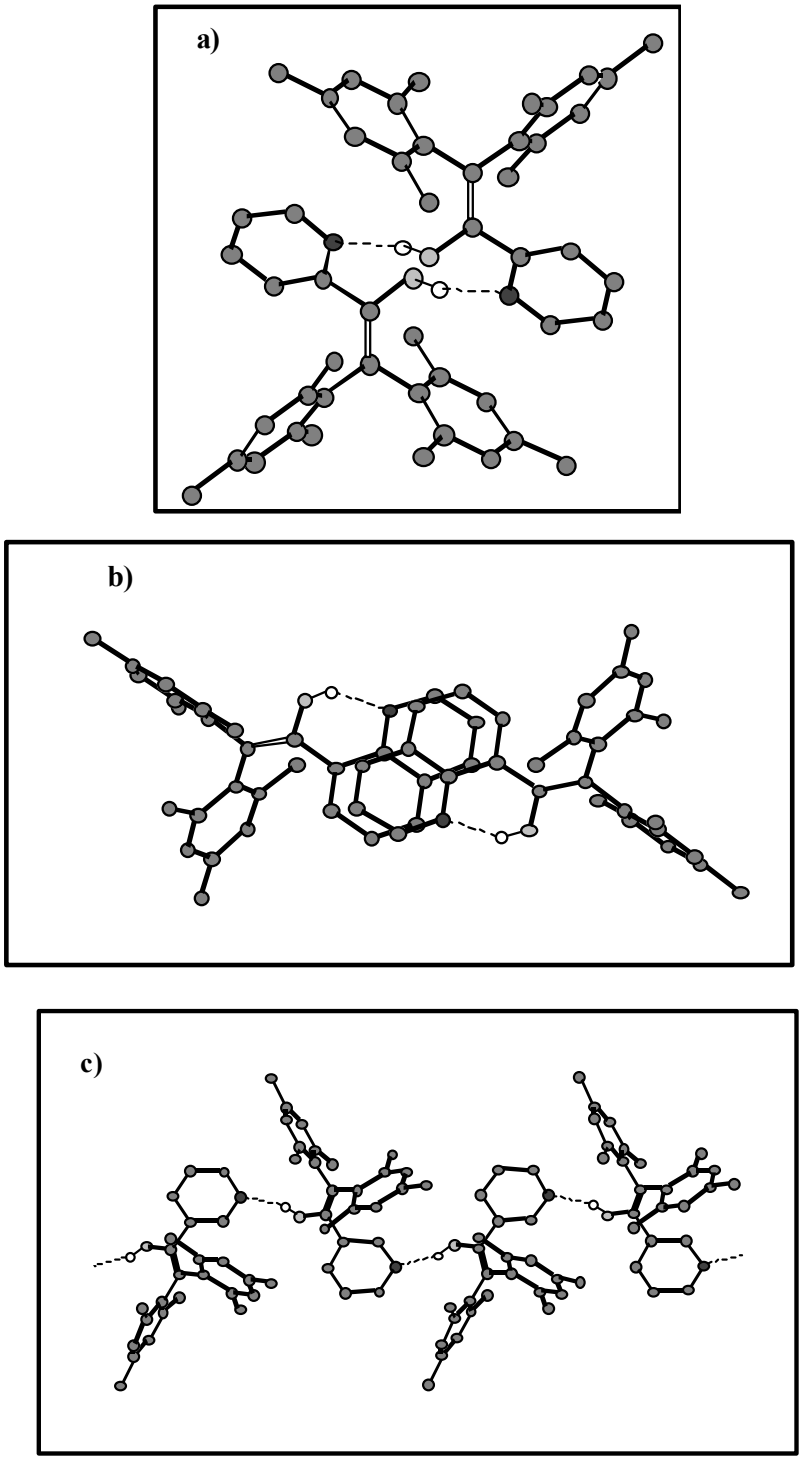

Figure 3–3: X-ray structures of **E2**, **E3** and **E4** depicting the OH···N type hydrogen bonding in the solid state.

3.6.1.2 Synthesis of β,β-Dimesityl Enol with 5-membered Heterocycle (3-Thiophenyl) E5

Enol **E5** was synthesised by addition of lithiated 3-thiophene with dimesitylketene in 78% yield (MP = 164-166 °C, Scheme 3–5). Characteristic OH signal at 3500 cm^{-1} was observed for **E5** in the IR spectra and a sharp signal at 5.09 ppm in the ^{1}H-NMR.

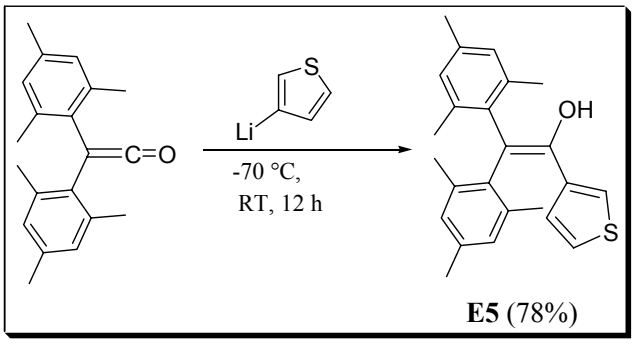

Scheme 3–5: Synthesis of **E5** starting from dimesitylketene and 3-bromothiophene.

3.6.1.3 Synthesis of β,β-Dimesityl Enols with Propargyl Alcohol and Homologues in α-Position E6-E11

Enols **E6-E11** (together with Rupali Lal) were prepared by the deprotection of the corresponding TIPS protected enols **E6-E8** with sulphuric acid in methanol at room temperature in 71-78% yields.

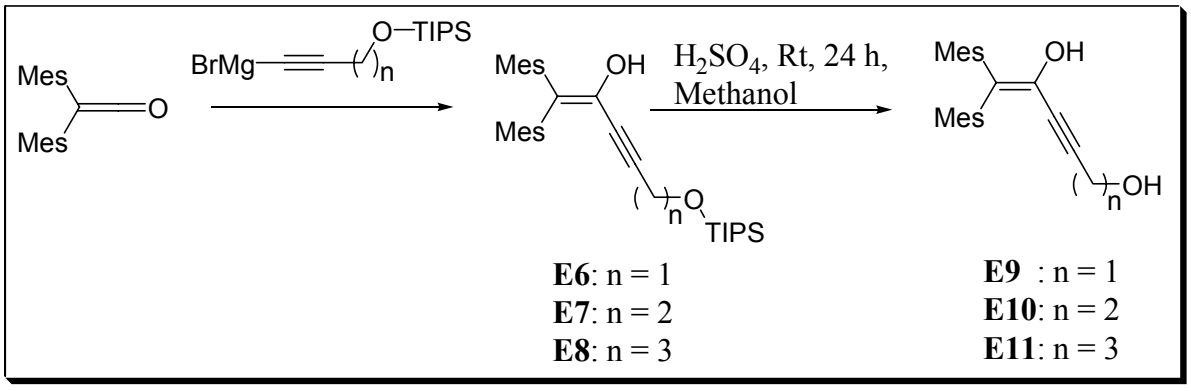

Scheme 3–6: Synthesis of enols **E6-E11** starting from dimesitylketene.

E6-E8 were prepared by a Grignard addition of the corresponding TIPS protected terminal alcohol (Scheme 3–6) to dimesitylketene in acceptable yields (30-80%). All the enols were characterised by various techniques such as IR, ^{1}H-NMR, ^{13}C-NMR and elemental analysis. Suitable single crystals for **E6** and **E11** were obtained and analysed by X-ray single crystal

analysis.

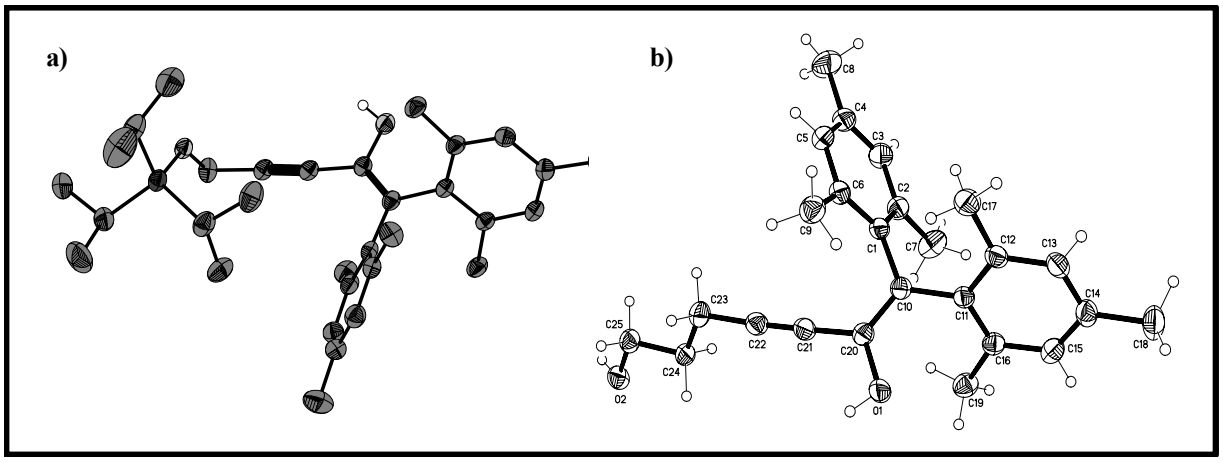

Figure 3–4: Molecular structures of **E6** and **E11** obtained by X-ray single crystal analysis.

X-ray single crystal analysis of **E6** reveals that it crystallises as triclinic with a space group P-1 with two formula unit in the asymmetric unit. Intermolecular hydrogen bonds leading to dimers of **E6** were observed. Interestingly, two different dimers were observed for each molecule of the asymmetric unit i.e., Si1 forms dimer with Si1 only and that Si2 forms dimer with Si2. No mixing of the dimers were observed. The hydroxyl group of enol acts as a hydrogen bond donor while the Si-O acts as an acceptor (Si-O···H-O), with a 195 Å between the acceptor and the hydrogen (H···A) [Table 3–1, Figure 3–4a].

Table 3–1: Selected bond distances for **E6** obtained from X-ray single crystal analysis.

Bond distances			
C3-C4	119.1(10)	C5-O2	142.8(17)
O2-SI1	167.2(11)	SI1-C24	188.1(13)
C2-O1	137.0(24)	SI1-C27	188.3(38)
O1-H1	82.0(12)	SI1-C30	187.5(30)
Bond angles			
C2-C3-C4	174.84(10)	C3-C4-C5	178.06(10)

E11 was also found to crystallise as triclinic with one molecule in the formula unit. A small deviation of the triple bond from planarity was observed (178.57 [14] Å), with the overall propeller orientation of the enol. Enolic OH group was found to be anticlinal showing an intermolecular hydrogen bonding network. Some selected bond angles and lengths are summarised in the table below (Table 3–2, Figure 3–4b).

Table 3–2: Selected bond angles and distances for **E11** obtained from X-ray single crystal analysis.

Bond distances			
O(1) C(20)	1.3727(15)	C(21) C(22)	1.1929(19)
O(2) C(25)	1.4296(16)	C(22) C(23)	1.4649(17)
C(24) C(25)	1.5051(17)	C(20) C(21)	1.4327(17)
C(23) C(24)	1.5255(19)	C(10) C(20)	1.3473(18)
Bond angles			
C22-C21-C20	178.57(14)	C23-C22-C21	177.22(14)

3.6.2 Role of Hydrogen Bonding on Oxidation Potential of Enol Radical Cations

3.6.2.1 OH···N Hydrogen Bonding Interactions in E2-E4 (Solid State and Solution)

The dilution and solvent dependent shifts of the hydroxy group (δ_{OH}) by ^{1}H-NMR are diagnostic for characterising the nature of hydrogen bonding in general.[137] A small δ_{OH} shift was observed for **E3** (0.5 ppm) upon dilution in chloroform, while for **E2** and **E4** no shift was observed even at 1000 times dilution (**Table 3–3**). This suggests intramolecular hydrogen bonding for **E2** and **E4** and intermolecular hydrogen bonding for **E3**. Dilution experiments for **E3** in DMSO showed no shift thus indicating that the intermolecular O-H···N hydrogen bonding was replaced by a (**E3)** OH···O=SMe$_2$ interaction.

Table 3–3: δ_{OH} values (ppm) for enols **E2-E4** upon dilution in $CDCl_3$.

Dilution factor	δ_{OH}(**E2**)	δ_{OH}(**E3**)	δ_{OH}(**E4**)
0	8.44[a]	5.69[b]	11.09[c]
10	8.43	5.31	11.08
100	8.42	5.24	11.05
1000	8.42	5.21	-

[a] Initial concentration: 0.14 M, [b] Initial concentration: 0.01 M, [c] Initial concentration: 0.06 M

While the dilution experiments convincingly indicated intramolecular hydrogen bonding for **E2** and **E4** and intermolecular hydrogen bonding for **E3**, the large upfield shift δ_{OH} of **E4** vs δ_{OH} of **E2** could not be ascertained solely by these ^{1}HNMR experiments and required further investigations, such as solvent dependence studies.

It is quite well known that δ_{OH} of triarly enols show a downfield shift with increasing solvent hydrogen accepting ability.[138] The interpretation was that in non-polar-non-hydrogen bonding solvents, the triaryl enols adopt a synclinal orientation while in polar-hydrogen bond accepting solvents they adopt anticlinal orientation. Weak OH-π interactions are thought to stabilise the synclinal orientation of the triarylenols. Only **E3** showed an analogous behaviour to the known triarylenols while **E2** and **E4** showed a completely different behaviour. The zwitterionic character in **E4** was further confirmed by UV-Vis spectroscopy.

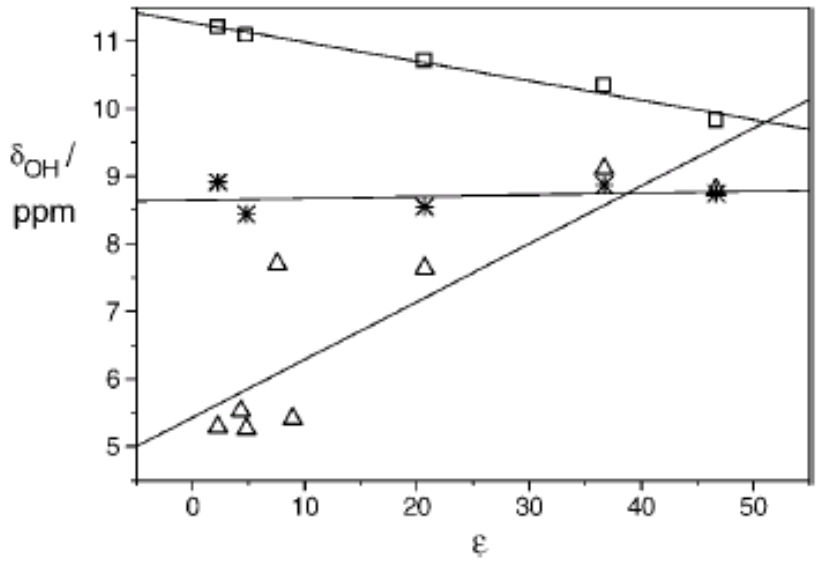

Figure 3–5: Plot of δ_{OH} values (ppm) versus the dielectric constant of the solvents for enols **E2** (∗), **E3** (Δ), and **E4** (□).

While **E1** showed a small but random δ_{OH} shift when the solvent polarity was increased, **E3** on the other hand showed a small but regular upfield δ_{OH} shift that correlated well with the solvent dielectric constant. The inverse relationship in **E4** suggested a strong intramolecular hydrogen bonding with zwitterionic character (Figure 3–5).

3.6.2.2 UV-Visible Spectroscopic Investigation for Enols E2-E4:

UV-visible spectroscopic investigations revealed that **E4** (λ_{max} = 379 nm) was much more bathochromically shifted than **E2** (λ_{max} = 320 nm) and **E3** (λ_{max} = 340 nm) or quinoline (λ_{max} = 313 nm). However, the shift was lower than in the protonated **E4** (λ_{max} = 433 nm) which indicated that the proton transfer is not complete.

3.6.2.3 Cyclic Voltammetric Investigations on Enols E2-E4

It is known that oxidation of β,β-dimesitylenols furnishes benzofuran derivatives via a two electron oxidation. Typically, two oxidation waves are expected in the cyclic voltammetric

experiments of β,β-dimesitylenols. Whereas the first wave was assigned to the two-electron oxidation of the enol, the second partially reversible wave was attributed to the oxidation of the benzofuran derivative.

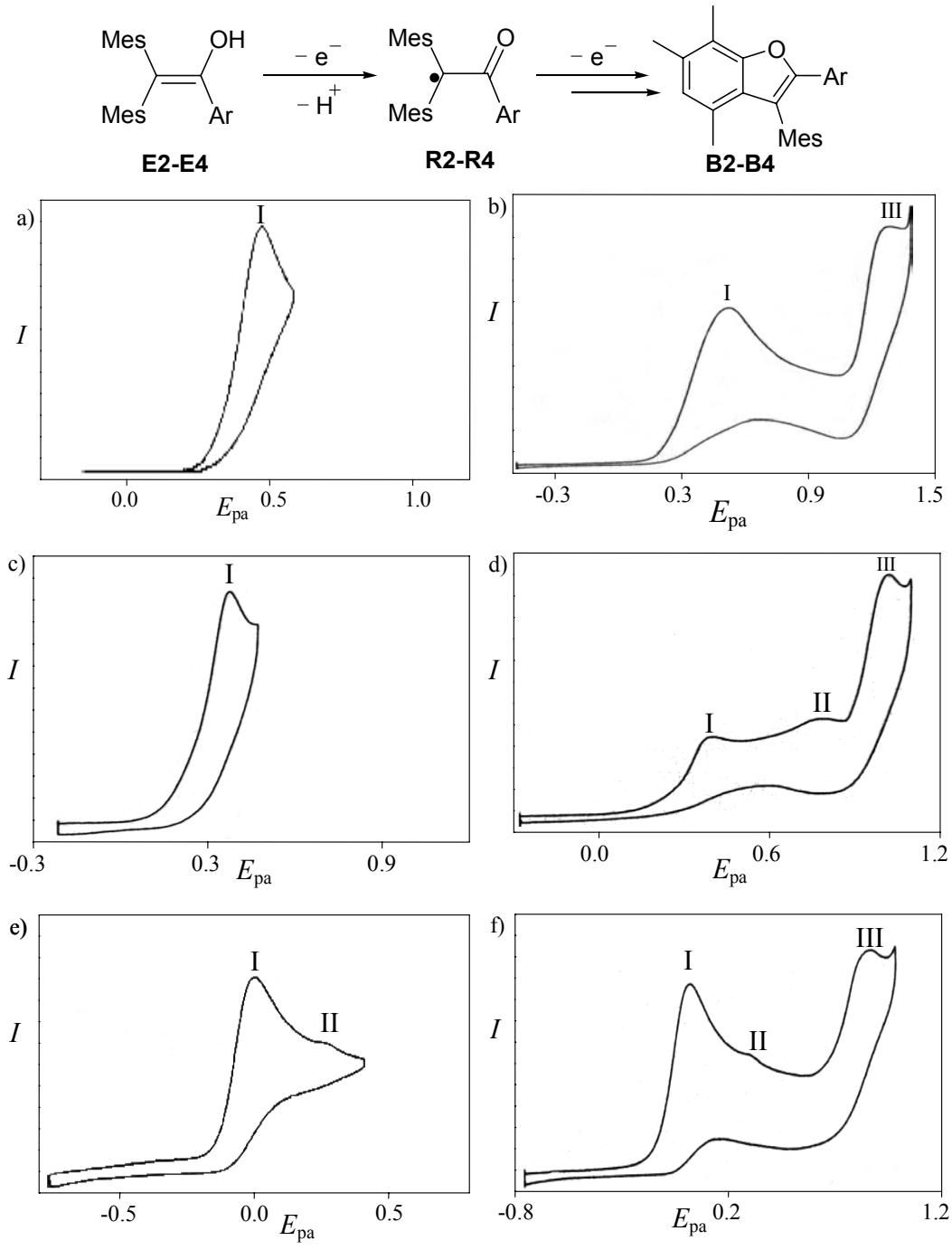

Figure 3–6: Cyclic voltammograms showing the enol oxidation waves in **E2-E4** in acetonitrile at 100 mV/s scan rate. I corresponds to the oxidation wave of the OH···N hydrogen bonded enols, II in **E3** corresponds to the free enol while in **E4** it could be due to the syn-rotamer. Wave III corresponds to the *N*-protonated enols.

Cyclic voltammetry investigations were carried out for enols **E2-E4** both in acetonitrile and dichloromethane. Enols **E2-E4** exhibited more than two oxidation waves in both solvents (Table 3–4). For **E2** two irreversible oxidation waves were observed at 100 mVs^{-1} scan rate (Figure 3–6a and b). Acid addition experiments shifted the oxidation wave from 0.53 V_{Fc} to

0.75-0.77 V_{Fc} (at 20 equivalents of trifluoroacetic acid); additionally a new wave appeared at 0.91 V_{Fc} that finally merged with wave **III**. Addition of 0.5 equivalents of pyridine led to the complete disappearance of the wave **III**.

For **E3** three irreversible oxidation waves were observed at E_{pa} = 0.36 (0.34), 0.76 (0.76), 1.04 (1.02) in acetonitrile (dichloromethane, Figure 3–6c and d). Dilution experiments showed a decrease for the peak current of the oxidation wave at 0.34 V while the intensities of the other waves (0.76 and 1.04) remained unchanged. Addition of 0.5 equivalents of base (pyridine) led to complete disappearance of the wave **III**.

Table 3–4: Oxidation potentials of enols **E2-E4** obtained by cyclic voltammetry in acetonitrile (dichloromethane) at 100 mV/s scan rate.

Enol	E_{pa} (I) (V_{Fc})	E_{pa} (II) (V_{Fc})	E_{pa} (III) (V_{Fc})
E2	0.46 (0.53)	-	1.20 (1.15)
E3	0.36 (0.34)	0.76 (0.76)	1.04 (1.02)
E4	0.02 (0.04)	0.27 (0.25)	0.80 (0.78)

Three irreversible waves were observed for **E4** at 100 mVs^{-1}, both in acetonitrile and dichloromethane (Figure 3–6e and f). While dilution experiments showed no change in the relative intensities between the oxidation waves, the acid addition experiments exhibited a complete disappearance of the first two waves was observed.

The various CV experiments performed on enols **E2-E4** confirmed the fact that in all the systems the lowest oxidation wave E_{pa} = 0.46 V_{Fc} (**E2**), 0.36 V_{Fc} (**E3**) and 0.02 V_{Fc} (**E4**) corresponded to the oxidation of the OH···N hydrogen bonded enol. The waves at 1.20 V_{Fc} (**E2**•H^+), 1.04 V_{Fc} (**E3**•H^+) and 0.80 V_{Fc} (**E4**•H^+) were assigned to the *N*-protonated enols, which is in accordance with the acid/base addition experiments

3.6.2.4 Cyclic Voltammetric Investigation of β,β-dimesitylethenol Containing 5-membered Heterocycles (E5) in the α-Position

Cyclic voltammetry investigation of **E5** exhibited two irreversible oxidation waves with the first appearing at E_{pa} = 0.58 V_{Fc} and the second at E_{pa} = 1.89 V_{Fc} (Figure 3–7). The first wave was assigned to the one-electron oxidation of the enol while the latter was assigned to the oxidation of dihydrofuranyl cations $\mathbf{X}^+$. The assignment of the second wave to $\mathbf{X}^+$ comes from the recent investigations on β,β-dimesitylenols containing electron donating groups in the α-

position (2,5-dimethoxy phenyl).[139] The oxidation waves in **E5** were in the similar range as **E13**, **E14** and **E15** (Table 3–5). Deprotonation of enol **E5** with tetramethylammonium hydroxide gave the enolate **A5** which exhibited a reversible wave at $E_{1/2}$ = -0.99 V_{Fc} (Table 3–5).

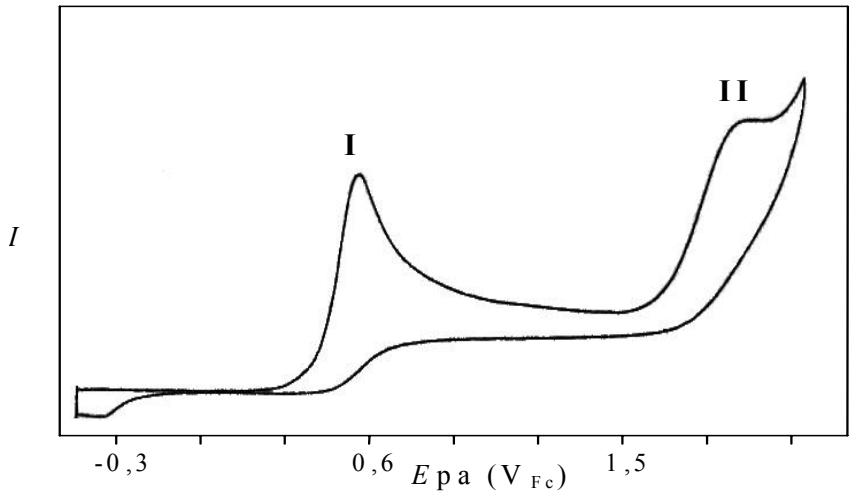

Figure 3–7: Cyclic voltammogram of **E5** in acetonitrile at 100 mV/s^{-1} scan rate.

Table 3–5: Oxidation potentials of β,β-dimesitylenols with 5-membered heterocycles in acetonitrile at 100 mV/s scan rate.

System	Enol E	Enolate A	Radical R	Cation X^+
	E_{pa} [V_{Fc}]	$E_{1/2}$ [V_{Fc}]	E_{pa} [V_{Fc}]	E_{pa} [V_{Fc}]
13	0.53	-0.78	0.24	1.80
14	0.46	-0.77	0.27	1.64
5	0.58	-0.99	nd	1.89
15	0.50	-0.78	0.27	1.79

3.6.2.5 UV-Vis Kinetic Investigation on Enol E5

The formation of an intensely coloured species upon oxidation of **E5** or **A5** (similar to **E13**, **E14** and **E15**) under cyclic voltammetric conditions or upon addition of copper (II) triflate was indicative of the formation of $\mathbf{X5}^+$. UV-Vis investigation revealed a persistent species with λ_{max} = 501 nm (Figure 3–8), which was assigned to cation $\mathbf{X5}^+$ based on earlier reports.

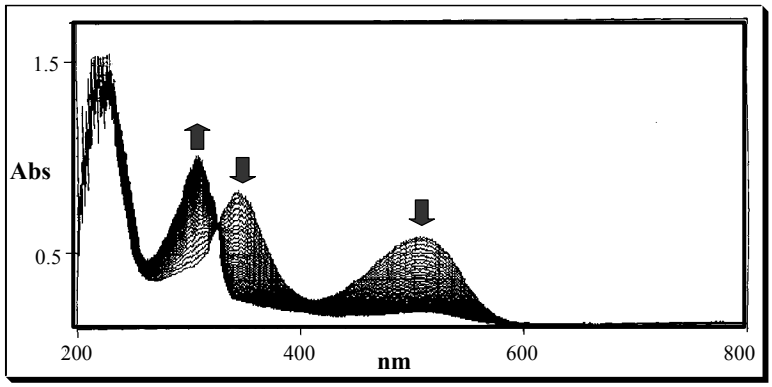

Figure 3–8: UV-Vis spectrum of decay of $\mathbf{X5}^+$ obtained by oxidising **E5** with copper (II) triflate.

The UV-Vis spectrum for the decay of $\mathbf{X5}^+$ showed an isosbestic point with the clean formation of the benzofuran **B5** derivative (Figure 3–8).

Table 3–6: Absorption, half-life and rate constant for cations $\mathbf{X}^+$ at room temperature.

cation	λ_{max} / nm	$t_{1/2}$ / min	k / 10^{-2} min^{-1}
$\mathbf{X13}^+$	512	18.4	3.78
$\mathbf{X5}^+$	501	7.2	9.60
$\mathbf{X15}^+$	509	17.3	4.00

The kinetic decay of the cation $\mathbf{X5}^+$ was monitored at room temperature and was found to have a half life of $t_{1/2}$ = 7.2 min (Table 5–4, Figure 5–3) which was less than the $t_{1/2}$ observed for $\mathbf{X13}^+$, $\mathbf{X15}^+$ (Table 3–6).

3.6.3 Cyclic Voltammetric Investigation of Novel β,β-Dimesitylethenols Containing Propargyl Alcohol and Homologues in the α-Position

As shown in the previous section the presence of an electron donating group or a 5-membered heterocycle in the α-position of enols renders stability to the carbocation formed thereby retarding the 1,2-methyl migration essential for benzofuran formation. In a novel approach to trap such $\mathbf{X}^+$**,** we substituted the α-position with propargyl alcohol in β,β-dimesitylethenol and investigated them by cyclic voltammetry (Chart 3–1).

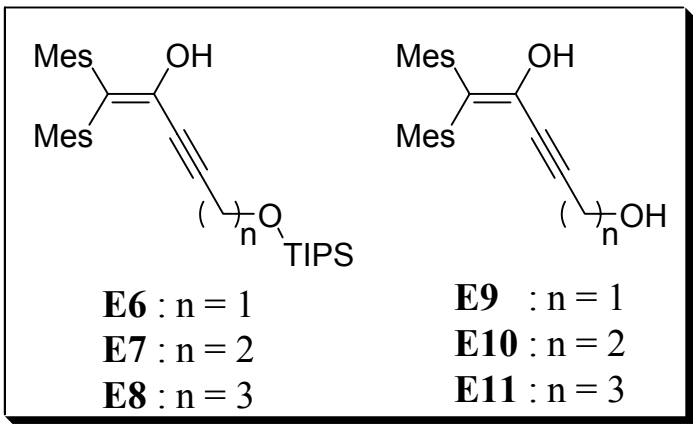

E6 : n = 1
E7 : n = 2
E8 : n = 3

E9 : n = 1
E10 : n = 2
E11 : n = 3

Ch**art 3–1**: Enols designed to trap intramolecularly the $\mathbf{X}^+$ by the alcohol group.

The cyclic voltammetric behaviour of enols **E6** (Figure 3–9a, b) and **E7** (Figure 3–9c, d) was typical of the Fuson enols with two characteristic oxidation waves. The first irreversible wave (E_{pa} = 0.69 and 0.67 V_{Fc}) was due to the oxidation of the enol while the second partially reversible wave (E_{pa} = 1.03 V_{Fc}) was due to the oxidation of the benzofuran derivative.

A similar behaviour was observed for enols **E9** (Figure 3–10a, b) and **E10** (Figure 3–10c, d): the oxidation wave for the enol was observed at E_{pa} = 0.84 and 0.71 V_{Fc} and for the benzofuran at E_{pa} = 1.1 and 1.0 V_{Fc}.

For **E11**, however, the oxidation wave for the enol (E_{pa} = 0.74 V_{Fc}) was followed by a completely irreversible wave at E_{pa} = 1.63 V_{Fc}. The latter irreversible oxidation wave was similar to the ones observed earlier in various β,β-dimesityl enols (with 5-membered heterocycles or electron donor substituents in the α-position).[139] Thus, the wave at E_{pa} = 1.63 V_{Fc} in **E11** was assigned to the oxidation of the dihydrofuranyl cation ($\mathbf{X}^+$, Chart 3–2b).

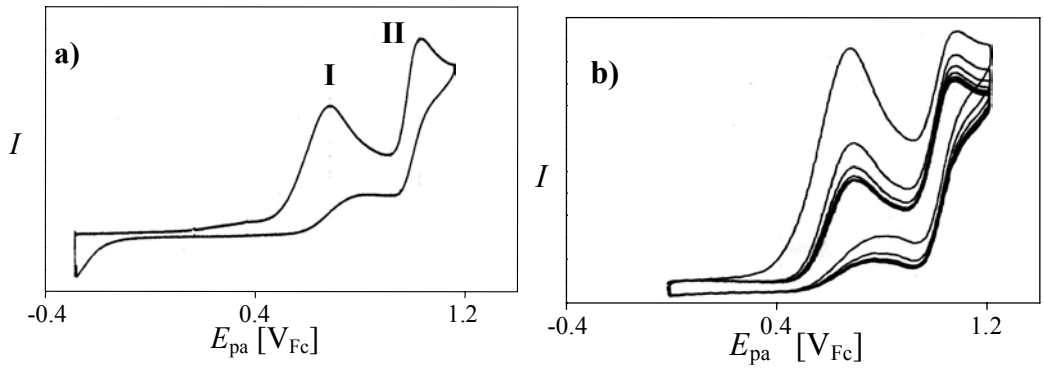

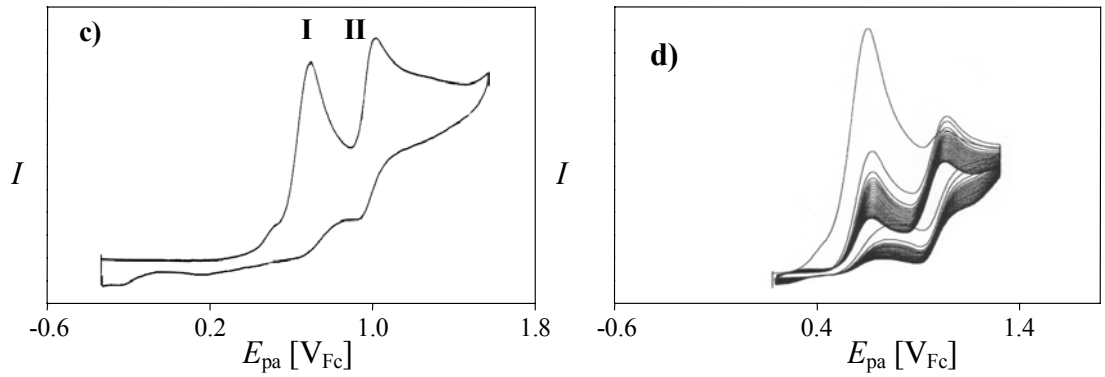

Figure 3–9: Cyclic voltammograms of a) **E6** and c) **E7** in acetonitrile at 100 mV/s scan rate. Figures b) and d) are the multiscans made on **E6** and **E7** respectively.

Table 3–7: Oxidation potentials of enols **E6-E11** from cyclic voltammetry in acetonitrile at 100 mV/s scan rate.

Enol	E_{pa} (V_{Fc})	E_{pa} (V_{Fc})
E6	0.69	1.03
E7	0.67	1.03
E9	0.84	1.11
E10	0.71	1.0
E11	0.74	1.63

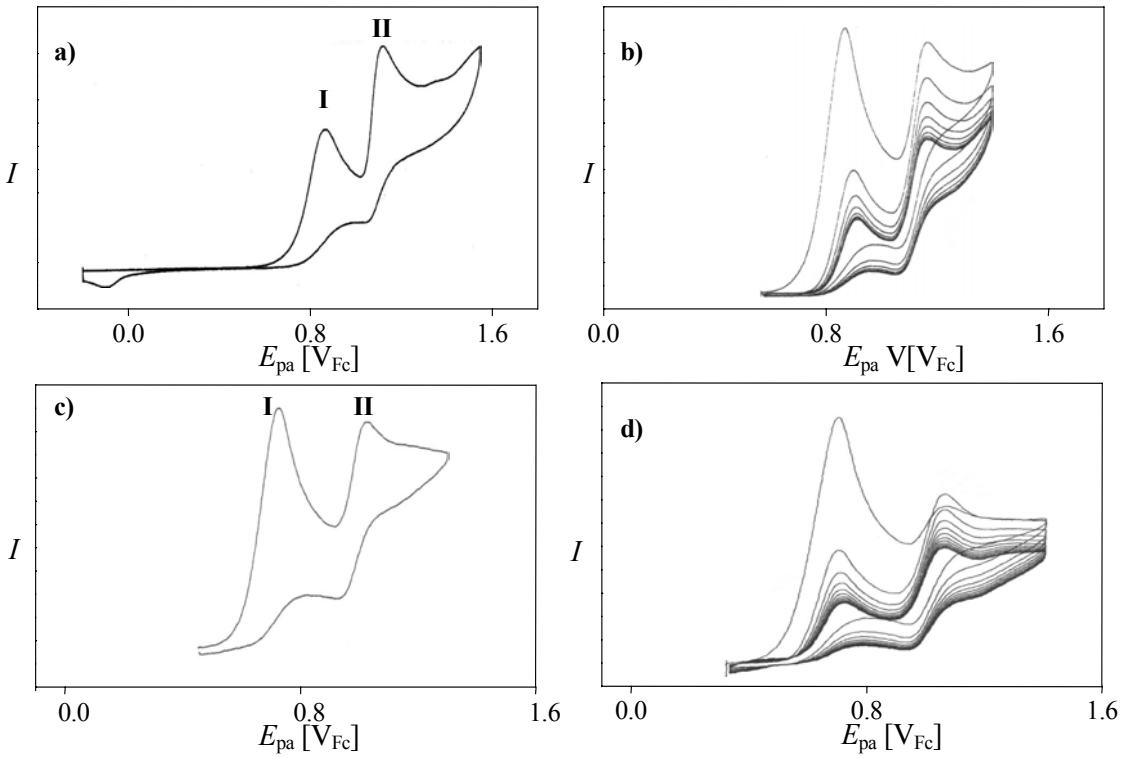

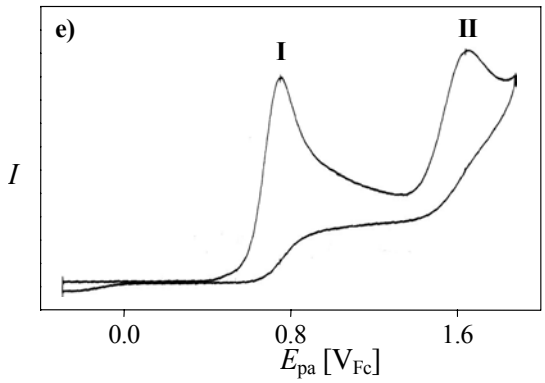

Figure 3–10: Cyclic voltammograms showing the oxidation waves of **E9** (a, b), **E10** (c, d) and **E11** (e) in acetonitrile at 100 mV/s scan rate.

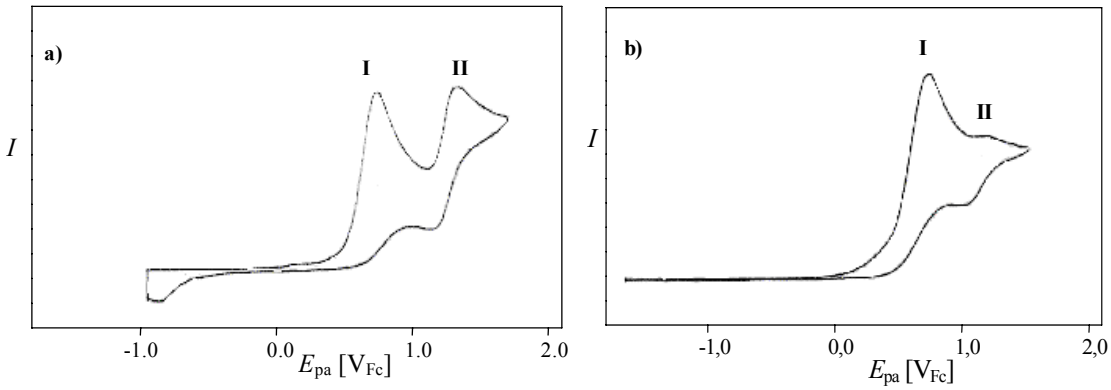

Figure 3–11: Cyclic voltammogram of **E12** showing two waves in the anodic side in a) acetonitrile b) DCM at 100 mV/s scan rate

A solvent dependence of **E12** was observed, and a cyclic voltammogram in acetonitrile showed a clean formation of benzofuran (Figure 3–11a) which was less predominant in dichloromethane (Figure 3–11b).

3.6.3.1 UV-Vis Investigation of Enols E9-E12

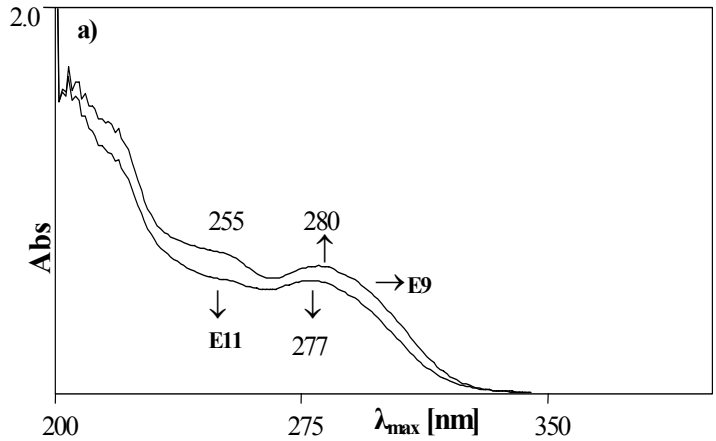

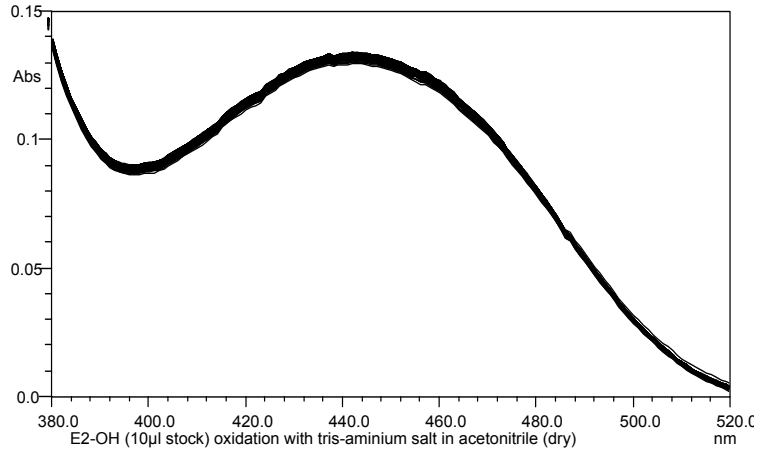

Figure 3–12: UV-Vis spectrum of a)overlay spectrum of **E9** (35.4 µM) and **E11** (29.6 µM) in acetonitrile, b) oxidation of **E11** (35.4 µM) with 2 eq. TBPA in dry acetonitrile (spectrum is an over lay of 100 measurements over a period of 25 min).

To get a closer look at the oxidative cyclisation, enols **E9**-**E11** were oxidised with 2 eq. of *tris*-(4-bromophenyl)aminium hexachloroantimonate (TBPA) in dry acetonitrile. The whole process was monitored by UV-Vis spectroscopy.

The UV-Vis spectra of enols **E9** and **E11** showed a absorption at λ_{max} = 280 and 277 nm, respectively (Figure 3–12a). A solution of **E9** (0.33 mM) when oxidised with freshly prepared 2 eq. of TBPA had a band at λ_{max} = 501nm which underwent fast decay. The band was not observed at lower concentrations (µM) were used. The band could be due to enol radical cations generated upon oxidation. The assignment was based on similar absorption observed in the time-resolved experiment for enol radical cation with aryl rings in the β-position.[140]

Aryl substituted enol radical cations were found to have a strong absorption maximum at λ_{max} = 340 nm and a much weaker band at λ_{max} = 500 nm and were long-lived under nitrogen-saturated conditions.[140] The oxidation of **E11** (29.6 µM) with 2 eq. of TBPA formed a pale yellow coloured solution with an absorption band at λ_{max} = 442 nm with little decay even after 30 min (Figure 3–12d). This band was tentatively assigned to an allene like product.

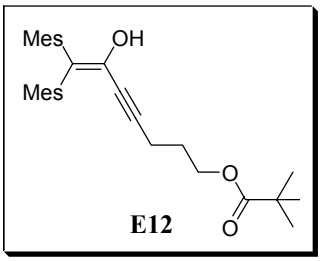

E12

The chemical oxidation of **E12** with copper (II) triflate was carried out both in DCM and acetonitrile. In acetonitrile, an absorption band was observed at λ_{max} = 285 nm that was

characterised by three isosbestic points (Figure 3–13a). In dichloromethane, however, no absorption at λ_{max} = 285 nm was seen; instead, two long absorbing bands at λ_{max} = 348 nm and 468 nm were observed (Figure 3–13b). Poor solubility of copper triflates in dichloromethane could have enhanced the complexation of the reduced copper to the benzofuran derivative acting as bidentate ligand.

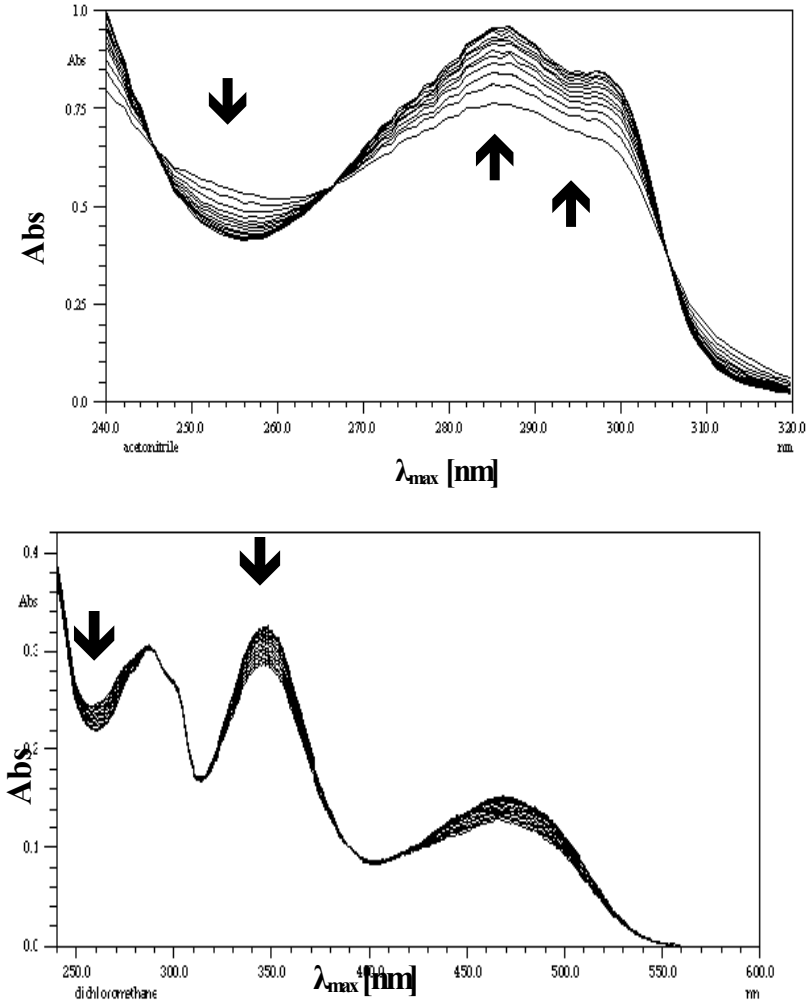

Figure 3–13: UV-Vis spectrum showing the changes observed during the chemical oxidation of **E12** in acetonitrile and dichloromethane with copper (II) triflate.

3.6.4 Generation and Investigation of Enolates and α-Carbonyl Radicals by Cyclic Voltammetry

Enolates were generated *in situ* by the addition of one equivalent of tetramethylammonium hydroxide (TMAH) solution in acetonitrile. For enols, **E2-E4**, **E6, E7** and **E9-E11** upon the addition of 1eq. of TMAH a reversible wave $E_{1/2}$ for the enolate was observed between –0.55 to –0.78 V_{Fc} under cyclic voltammetric conditions (Table 3–8).

Table 3–8: Electrochemical properties of enolates and α-carbonyl radicals as observed by cyclic voltammetry at 100 mV/s scan rate upon addition of 1eq of base (TMAH).

Enol	$E_{1/2}$ enolat (V_{Fc})	$E_{1/2}$ enolat ($V_{Ag/AgCl}$)	E_{pa} α-carbonyl radical (V_{Fc})	E_{pa} α-carbonyl radical ($V_{Ag/AgCl}$)
E2	-0.78	-0.59	+0.11	+0.30
E3	-0.72	-0.53	+0.37	+0.56
E4	-0.56	-0.37	+0.01	+0.21
E6	-0.61	-0.42	+0.35	+0.54
E7	-0.61	-0.42	+0.32	+0.51
E9	-0.55	-0.36	+0.34	+0.53
E10	-0.56	-0.37	+0.31	+0.50
E11	-0.63	-0.44	+0.30	+0.49

Cyclic voltammetric investigations reveal that in all the enolates the E_{pa}-E_{pc} was found to be between 0.68-0.70 V, close to the Nicholson-Shain criteria for reversibility. Dependence of the anodic current with scan rate was carried out to gain insights into the electrode kinetics (Figure 5–5). In all the enolates, a linear dependence of the cathodic current with the square root of the scan rate was observed (Figure 3–14) and was independent of the scan rate.

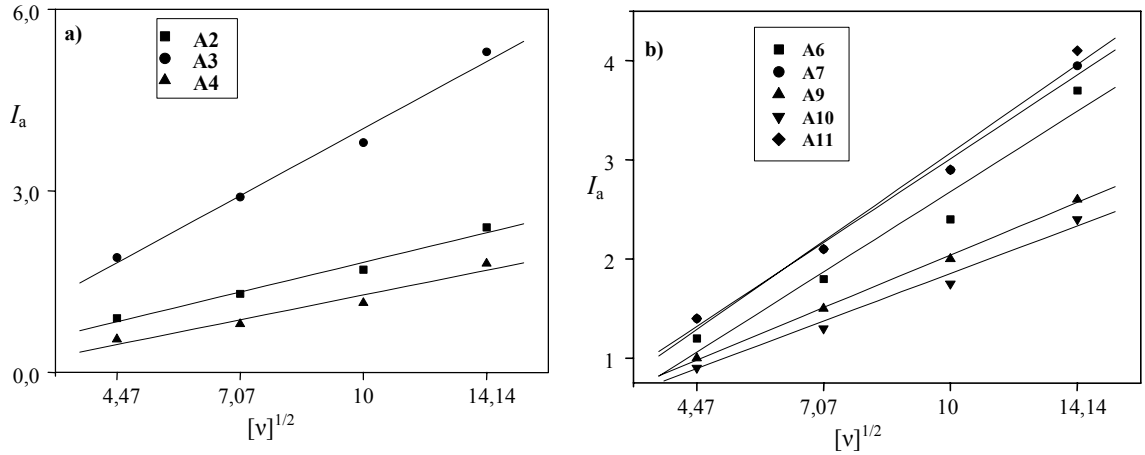

Figure 3–14: Plot showing dependence of anodic current with scan rate, a) for enolates **A2-A4** and b) for enolates **A6-A11** in acetonitrile.

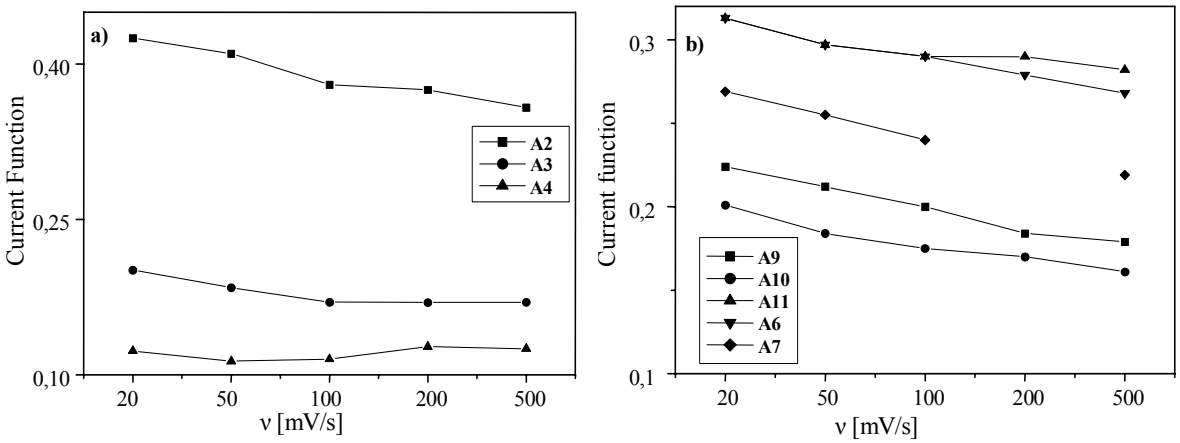

Figure 3–15: Plots showing the dependence of current function (ratio between anodic current vs [scan rate]$^{1/2}$) vs the scan rate, showing the E_{rev} behaviour of enolates, a) **A2-A4**, b) **A6-A11** (except **A8**) in acetonitrile.

A plot of the current function (I_a/[ν] $^{1/2}$ Vs ν) for the enolate wave indicated an E_{rev} electrode kinetics for all enolates (**A2-A4** (Figure 3–15a), **A6-A11** (Figure 3–15b), except for **A8** which was not measured). Irreversible oxidation waves for the α-carbonyl radicals were observed between E_{pa} = 0.02-0.37 V_{Fc} (Figure 3–16, Table 3–8). The irreversible wave for α-carbonyl radicals was due to the fast follow-up reaction of the α-carbocations leading to benzofuran derivatives Chart 3–2b.

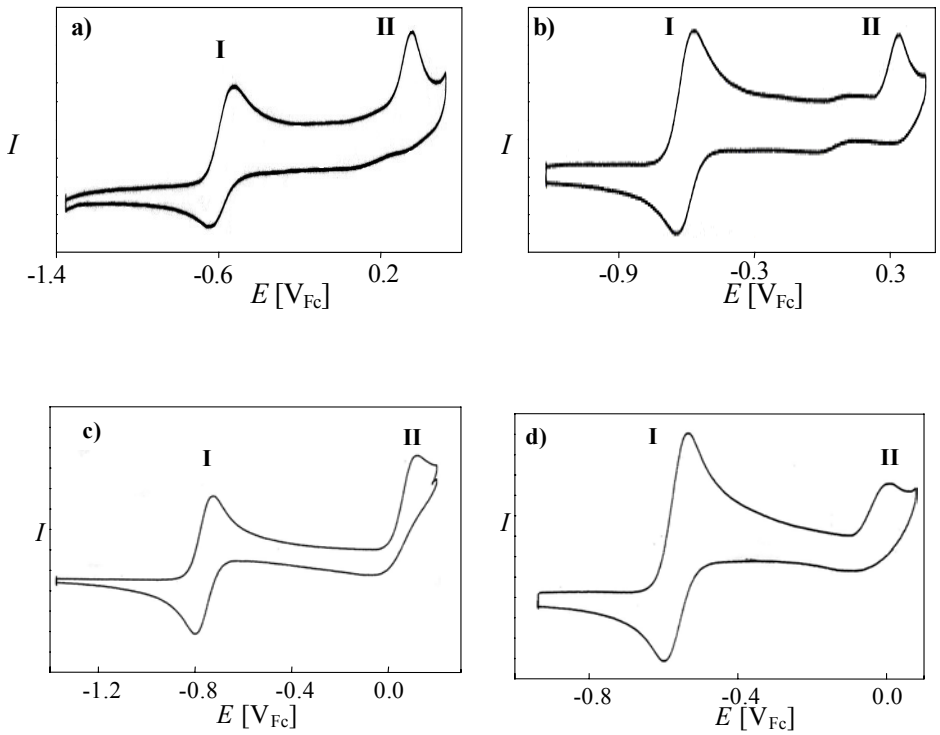

Figure 3–16: Cyclic voltammograms showing the waves for enolates (I) and α-carbonyl radicals (II) in acetonitrile at 100 mV/s scan rate formed by deprotonation of enols a) **E6**, b) **E9**, c) **E2**, d) **E4**.

3.7 Discussion

3.7.1 β,β-Dimesityl Enols with Six-membered Nitrogen Heterocylces in the α-Position (E2-E4)

Enols **E2-E4** were prepared in reasonable yields (29-44 %) starting from dimesityl ketene and the corresponding lithiated heterocycle. Solid state structure of all the enols **E2-E4** showed OH···N hydrogen bonding. The hydrogen bonding in **E2** and **E3** were intermolecular while in E4 it was intramolecular. Solution studies with ^{1}H-NMR dilution and solvent dependence however, indicated intramolecular hydrogen bonding in **E2** and **E4** while in **E3** it was intermolecular.

UV-Vis spectroscopic investigations revealed that the λ_{max} of **E4** (379 nm) was much more bathochromically shifted than **E2** (320 nm) and **E3** (340). The λ_{max} of quinoline (313 nm) and completely protonated quinoline was 433 nm. This suggested a partial proton transfer for **E4**.

Thus, enols **E2-E4** constitute three different hydrogen bonded enolic systems. **E2** forms an intramolecularly hydrogen bonded species as depicted in **E2´**; **E3** forms an intermolecularly hydrogen bonded dimer **E3´**and **E4** forms an intramolecularly hydrogen bonded system with partial proton transfer **E4´**.

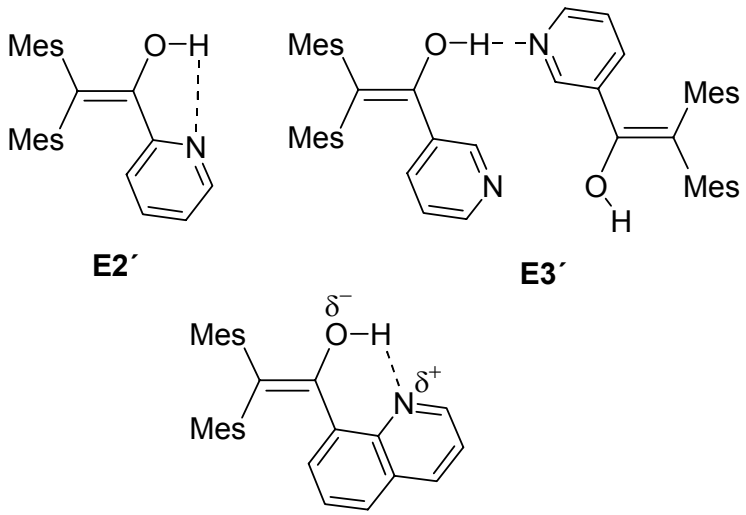

Cyclic voltammetric investigation both in DCM and acetonitrile revealed that unlike the normal β,β-dimesityl enols all the enols **E2-E4** had more than two irreversible oxidation waves for the enols. For **E2** two (0.53 V_{Fc}, 1.20 V_{Fc}), **E3** (0.36 V_{Fc}, 0.76 V_{Fc} and 1.04 V_{Fc}) and **E4** (0.02 V_{Fc}, 0.27 V_{Fc} and 0.80 V_{Fc}) had three irreversible oxidation waves for enols. Acid addition experiments shifted the oxidation wave in **E2** from 0.53 V_{Fc} to 0.75 V_{Fc} that finally merged with wave **III**. Dilution experiments in **E3** showed a decrease for the peak

current of the oxidation wave at 0.34 V_{Fc} while the intensities of the other waves (0.76 V_{Fc} and 1.04 V_{Fc}) remained unchanged. Addition of a base such as pyridine led to complete diappearance of the wave **III**. In **E3** no change was observed on the relative intensities on dilution. However, a complete disappearence of the first two waves was observed upon addition of the acid. The first oxidation waves for each enol were analysed using the Nicholson-Shain criterion ($I_{pa}/V_{1/2}$ vs v), revealing a mechanism EC_{rev} for **E4** and a mechanism EC_{irr} for **E2** and **E3**, respectively.

The various CV experiments confirmed the fact that in all the systems the lowest oxidation wave E_{pa} = 0.46 V_{Fc} (**E2**), 0.36 V_{Fc} (**E3**) and 0.02 V_{Fc} (**E4**) correspond to the oxidation of OH···N hydrogen bonded enol. However, the above experiments could not explain the origin of the waves at E_{pa} = 0.76 V_{Fc} (**E3**) and 0.25 V_{Fc} (**E4**). Both waves showed up clearly upon dilution suggesting that they belonged to the free enol in equilibrium with the hydrogen bonded and protonated enol, although in minor concentration. In order to elucidate this phenomenon the oxidation potential of enols was approximated by determining the adiabatic ionisation potentials (IP_a) of various β,β-dimesitylenols (**E16-E20**) by AM1 (calculations were carried out with the help of Rupali Lal) whose oxidation potentials were determined in our laboratory (Table 3–9). For adiabatic ionisation potential calculations only non-hydrogen bonded conformers were considered.

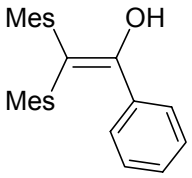

E16 (0.61 V_{Fc})

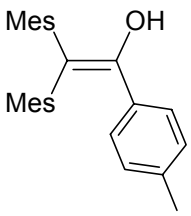

E17 (0.57 V_{Fc})

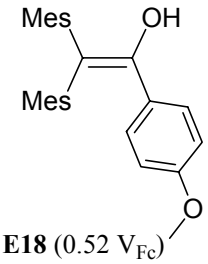

E18 (0.52 V_{Fc})

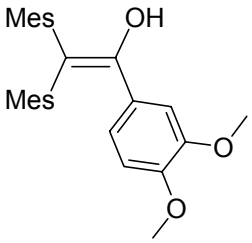

E19 (0.51 V_{Fc})

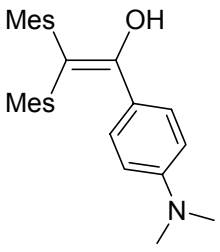

E20 (0.13 V_{Fc})

Table 3–9: Adiabatic ionisation potentials of various β,β-dimesitly enols obtained by AM1 calculation and their experimentally determined oxidation potentials.

$Mes_2C=C(OH)R$	IP_a (kcal/mol)	E_{pa} (V_{Fc})
E16	167.2	0.61
E17	165.3	0.57
E18	163.1	0.52
E19	163.9	0.51
E20	154.5	0.13

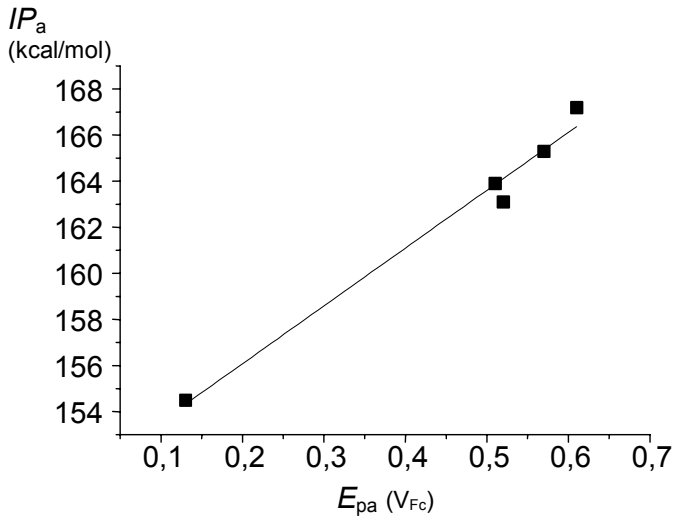

Figure 3–17: Plot of experimentally obtained oxidation potentials E_{pa} for enols **E16-E20** (in acetonitrile) *vs* the calculated IP_a by AM1 ($r^2 = 0.98$).

A good linear correlation ($IP_a = 25.1\ E_{pa} + 151.05$, $r^2 = 0.98$) between the adiabatic ionisation potential and the oxidation potential was observed for a small series of aryl substituted enols. The adiabatic ionisation potentials of the enols **E2-E4** was also determined by AM1 for the non hydrogen bond enol by using the above correlation and a prediction of their E_{pa} was also made from the above correlation.

Table 3–10: AM1 calculated and experimentally determined oxidation potentials E_{pa} (in acetonitrile) of **E2-E4**.

Enol	ΔH_f°(enol) (kcal mol^{-1})	$\Delta H_f^\circ(enol^{+\cdot})$ (kcal mol^{-1})	IP_a (kcal/mol)	E_{pa} (V_{Fc})[a] Without OH···N	E_{pa} (V_{Fc})[b] With OH···N
E2	41.2	211.1	169.9	0.75	0.46
E3	38.1	208.6	170.5	0.78	0.36
E4	61.7	226.0	164.3	0.53	0.02

With the oxidation potential of non hydrogen bonded enols at hand we examined whether their oxidation waves were detectable under cyclic voltammetric investigations. Indeed the additional waves at E_{pa} = 0.76 (**E3**, wave **II**) correspond to the free enol as predicted, which is in agreement with the dilution experiment performed by CV. For **E4** the situation is less clear, as the enol should only exist without the strong OH···N hydrogen bonding if a kinetically locked s-anti conformation at the enol-quionoline bond is possible. However, AM1 calculations, cannot reveal a small barrier for rotation. Thus, the wave at 0.25 V_{Fc} (**E4**, wave II) cannot correspond to the oxidation of the non-hydrogen bonded enol, but could be due to the protonated α-carbonyl radical **R4**.

What is the effect of hydrogen bonding on the oxidation potential? First of all, we have to realise that E_{pa} depends on the kinetics of the follow-up deprotonation (EC_{irr}). For enol radical cations the deprotonation rate constants and hence the kinetic contributions to the potential are rather similar. Thus, we can use E_{pa} instead of the thermochemically relevant $E_{1/2}$ for the ensuing analysis. The data in Table 3–10 suggests that the cathodic shift through hydrogen bonding can amount to a few hundred mV. One would expect $\Delta\Delta E_{pa}^{H} = \Delta E_{pa}$ (free enol) - ΔE_{pa} (H-bonded enol) to be more pronounced for **E4** ($\Delta\Delta E_{pa}^{H}$ = 510 mV) than for **E2** ($\Delta\Delta E_{pa}^{H}$ = 290 mV) because the geometric situation in a 6-membered ring is more favorable for hydrogen bonding than in a 5-membered ring. On the other side, intermolecular hydrogen bonding in **E3** accounts for $\Delta\Delta E_{pa}^{H}$ = 420 mV.

3.7.2 Effect of β,β-Dimesitylenols with 5-Membered Heterocycles in α-Position

Reactivity of enol and enol ether radical is being extensively investigated due to their pivotal role played in DNA damage, in important biological transformations carried out by coenzyme B_{12} dependent enzymes (such as diol dehydratase) and in ribonucleotide reductases. While enol ether radical cations can be easily prepared from their neutral precursors, such a simple oxidative strategy is precluded for enols as these constitute mostly fleetingly existing tautomers of carbonyl compounds. The two reactions that determine the fate of enol radical cations is the single electron reduction from a donor or deprotonation to α-carbonyl radical. α-carbonyl radicals themselves are good electron donors and can further be oxidised to the α-carbonyl cation, the fate of which has been rarely investigated.

A number of β,β-dimesityl enols with various α-substituted 5-membered heterocycles were synthesised in good yields **E5** (78 %) to investigate their effect on the stability of α-carbonyl cations formed. (**E13-E15** were prepared by Anja Langels Chart 3–2)

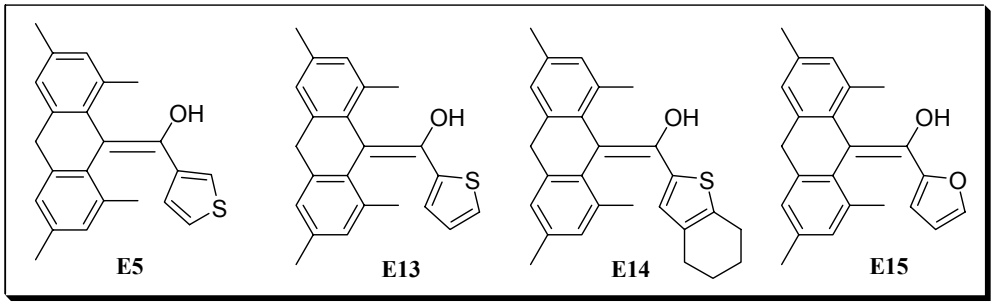

Chart 3–2: a) List of β, β-dimesityl enols with 5-membered heterocycles in the α-position **E5**, **E13-E15** (Anja, L.) and **E5** this work.

Cyclic voltammetric investigations on all these enols **E5**, **E13-E15** showed two irreversible oxidation waves. The first irreversible oxidation wave was assigned to the one-electron oxidation of the enol while the second oxidation wave was assigned to the oxidation of the dihydrofuranyl cations $\mathbf{X}^+$. The assignment of the second wave to $\mathbf{X}^+$ comes from the recent investigations on β,β-dimesityl enols containing electron donating groups in the α-position. The oxidation wave of **E5** was in the range of **E13-E15**. In general the oxidation potential for enol oxidation in these enols was 100-200 mV lower than simple phenyl substituted enols. Chemical oxidation of the enol **E5** with 1 eq. copper (II) triflate gave an intensly red coloured solution. UV-Vis investigation revealed a persistent species with λmax = 501 nm which was assigned to $\mathbf{X}^+$ based on earlier reports having a half life of $t_{1/2}$ = 7.2 min. An isosbestic point was observed under UV-Vis investigation for all the enols with the clean formation of the benzofuran derivative.

In conclusion, the presence of five membered heterocycle not only affects the oxidation potential of enols, but also plays a great role on the follow-up processes. The electron donating ability of the five membered heterocycles lowers the oxidation potential and also stabilises the $\mathbf{X5}^+$ to such an extent that other follow up reactions predominate leading to polymerisation rather than benzofuran formation.

3.7.3 β,β-Dimesityl Enols Containing Propargyl Alcohol and Homologues in the α-Position (E6-E11)

β,β-dimesitylenols bearing propargyl alcohol and homologues in the α-position were synthesised in reasonable yields (30-80 %). X-ray structure of **E6** and **E15** show an anti-conformation for the enolic OH group. The preference for the *anti*-conformation was mainly due to an OH···π inateraction between the triple bond and the hydrogen atom of the OH group. This OH···π interaction compensates for the similar interactions the OH group has with the mesityl ring in the *syn*-conformation.

Cyclic voltammetric investigations of these enols clearly indicated that for enols **E6**, **E7**, **E9**

and **E10** the electrochemical behaviour of these enols was similar to the β,β-dimesitylenols. Like β,β-dimesitylenols all the above enols showed two anodic waves of which the first irreversible oxidation wave was assigned to the oxidation of the enol while the second partially reversible wave was assigned to the oxidation of benzofuran derivative. This was further confirmed by quantitative formation of a band at $\lambda_{max} = 285$ nm for the benzofuran derivative upon oxidation of **E9-E10** with 3 eq. of copper (II) triflate or TBPA. Interestingly the cyclic voltammetric investigation of **E11** showed an abnormal behaviour. Unlike β,β-dimesitylenols two irreversible oxidation waves were observed ($E_{pa} = 0.74$ and 1.63 V_{Fc}). The first oxidation wave was assigned to the oxidation of the enol (**E9**, $E_{pa} = 0.84$ V_{Fc}, **E10** = $E_{pa} = 0.71$ V_{Fc}). However, the second oxidation wave could not be assigned to the oxidation of the benzofuran derivative since it was almost shifted by 600 mV anodically than expected for benzofuran derivatives. The oxidation potential was similar to the ones observed in β,β-dimesityl enols bearing electron donating groups or 5-membered heterocycles in the α-position. The second irreversible oxidation wave in **E11** ($E_{pa} = 1.63$ V_{Fc}) can also be assigned to an allene which have a similar oxidation potential ($E_{pa} = 1.0$ to 1.3 V_{Fc}).[141]

The presence of β,β-dimesityl groups, a triple bond and hydroxyl groups are features that are common to all the enols **E9-E11** differing in the number of bridging methylene groups. A closer analysis of the enols **E9-E11** indicate that upon oxidation and deprotonatin of the enol the resulting α-carbonyl radical ($E_{pa} = 0.34$, 0.31 and 0.30 V_{Fc}) would immediately be oxidised to the α-carbonyl cation. Stabilisation of the α-carbonyl cation by the triple bond would lead to the formation of a vinylic cation, such carbocations have indeed been reported earlier[†,142] however, their preparation in solution require harsh conditions.

Presence of OH group in these enols **E9-E11** can act as intra or intermolecular nucleophiles. Intramolecular nucleophilic attack in **E9** and **E10** was ruled out as it would require a strained 3 and 4 membered allenic product (Ring strain for cycloproane = 27.6 *K*cal/mol and cyclobutane = 26.2 *K*cal/mol). While intermolecular attack could not be ruled out however, presence of no oxidation waves above 1.11 V_{Fc} further indicated that the follow-up reaction leading to the benzofuran formation was preferred (intramolecular processes). In **E11** such an

---

[†] Formation of vinylic cation from a carbocation with acetylene group attached is well documented in literature.[142]

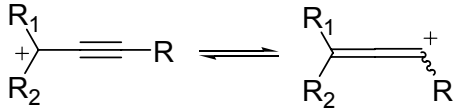

intramolecular nucleophilic attack would lead to a 5-membered ring (ring strain for cyclopentane = 6.3 *K*cal/mol) leading to an allenic product. Thus, such a mode would be a novel 5-exo-dig cyclisation rarely observed in the stabilisation of carbocation (Scheme 3–7, Chart 3–3).

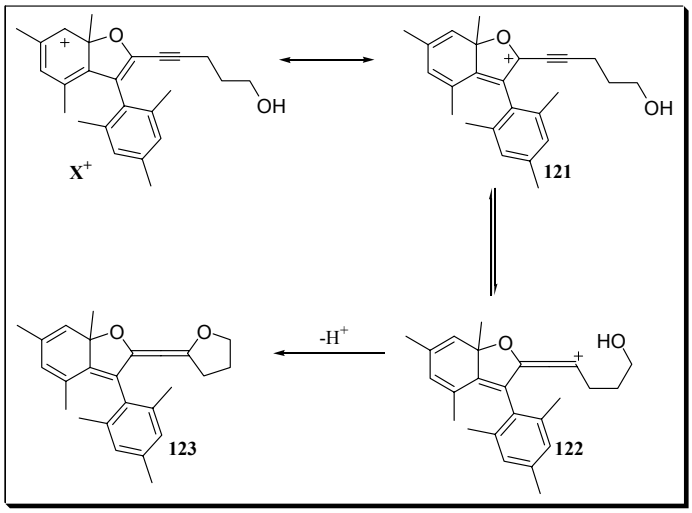

Scheme 3–7: Formation of **123** allene product via 5-exo-dig cyclisation of **121**.

To test the hypothesis of involvement of the OH group in the unusual behaviour of **E11**, the hydroxyl group was functionalised into an ester with pivaloylchloride. The bulky *t*-butyl group in the acid chloride prevents the esterification at the enolic position, thus furnishing **E12** in quantitative yield. The product was characterised by various spectroscopic methods. Cyclic voltammetric investigation of **E12** had two oxidation waves, the first of which at E_{pa} = 0.70 V_{Fc} was irreversible and the second (E_{pa} = 1.20 V_{Fc}) was partially reversible, as expected of a β,β-dimesityl enol (Figure 3–11).

The cyclic voltammetric investigations further confirm the hypothesis of formation of an allenic intermediate in the oxidative cyclisation of enol **E11**.

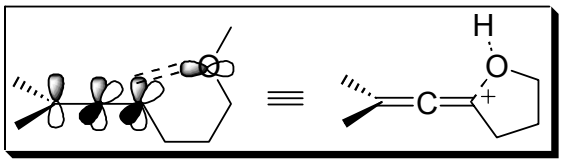

Chart 3–3: A probable 5-exo-dig cyclisation leading to formation of allene like structure upon oxidation of **E11**.

3.7.4 Comparison of Oxidation Potential of Enols and Enolates Derived from β,β-Dimesitylenols with Various Substitutents in α-Position

Enols and enolates are important in many reactions of chemical as well as biological origin. While enols of simple carbonyl compounds have fleeting existence in solution thus making it difficult to determine the electrochemical properties and reactivity in solution. Use of electron withdrawing groups or a bulky group in the β-position are the two main methods of stabilising enols in solution. Electrochemical properties of enols based on the latter approach has been extensively investigated by Schmittel *et. al*.[130,131] They were able to characterise for the first time an enol radical cation obtained after one-electron oxidation of β,β-dimesityl enol in solution.

β,β-Dimesityl enols Schmittel *et. al*.	**β-cyano enols** Orliac-Le Moing *et. al*.
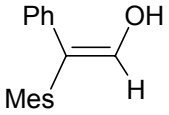 0.70 V_{Fc}	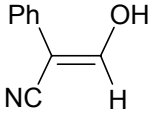 1.13 V_{Fc}
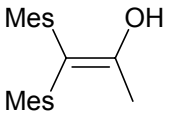 0.68 V_{Fc}	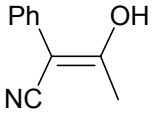 1.08 V_{Fc}
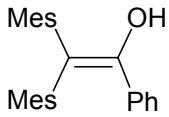 0.61 V_{Fc}	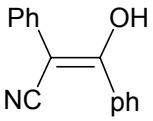 1.14 V_{Fc}

A comparison of the oxidation potentials of enols containing β,β-mesityl enols (Table 3–11, Chart 3–4) with that of β-cyano enols[143] clearly showed that the oxidation potentials of the enols with electron withdrawing group such as cyano in the β-position increased the oxidation potential of enols by about 400 mV.

No general trend in the oxidation potentials of the enols, enolates and α-carbonyl radicals derived with β,β-dimesityl enols were observed although, in general their oxidation potentials was lower than the corresponding enols, enolates and α-carbonyl radicals with electron withdrawing groups in the β-position. Overall the oxidation potentials of the enolates (**A**) derived from β,β-dimesityl enols were ~1.5 V_{Fc} lower than the enols (**E**). The corresponding α-carbonyl radicals **R** were ~1.0 V_{Fc} anodically shifted.

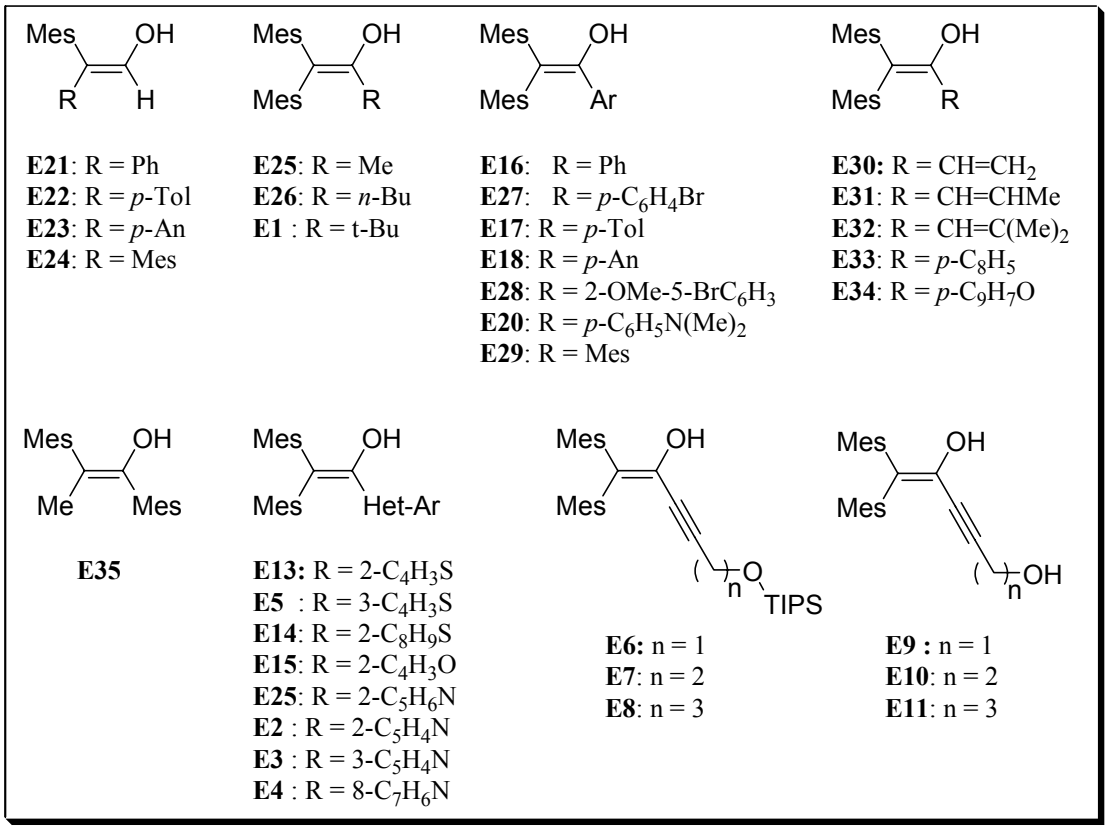

Chart 3–4: List of β,β-dimesityl enols, enolates and α-carbonyl radicals investigated by Schmittel *et. al*. in the last 1 decade.

Table 3–11: Oxidation potentials of enols, enolates and α-carbonyl radicals in solution by Schmittel *et. al*.[96,130,131,139] Except E2-E4, E5, E6-E12 the potentials of enols, enolates and α-carbonyl radicals were taken from the work of M. Röck, A. Langels.

model system	$E_{1/2}$ of enolates **A** [V_{Fc}]	E_{pa} of a-carbonyl radicals **R** [V_{Fc}]	E_p of enols **E** [V_{Fc}]
1	-1.02	+0.14	+0.64
2	-0.78	+0.11	+0.46
3	-0.72	+0.37	+0.36
4	-0.56	+0.01	+0.02
5	-0.99	Nd	+0.58
6	-0.61	+0.35	+0.69
7	-0.61	+0.32	+0.67
9	-0.55	+0.34	+0.84
10	-0.56	+0.31	+0.71
11	-0.63	+0.30	+0.74
13	-0.78	+0.24	+0.53
14	-0.77	+0.27	+0.46
15	-0.78	+0.27	+0.50
16	-0.83	+0.24	+0.61
17	-0.86	+0.22	+0.57
18	-0.875	+0.31	+0.52
20	-0.96	0.09	0.13
21	-0.66	+0.63	+0.70
22	n.d	n.d.	+0.64
23	n.d	n.d.	+0.48
24	-0.72	+0.37	+0.70
25	-0.89	+0.20	+0.68

26	-0.97	+0.14	+0.59
27	-0.78	+0.29 V	+0.58 V
28	n.d.[b]	n.d.[b]	0.61
29	-0.75 [c]	0.27 [c]	0.76[c]
30	-0.78	+0.27	+0.69[d]
31	-0.84	+0.23	+0.64[d]
32	-0.92	+0.14	+0.51[d]
33	-0.60	+0.38	+0.72[d]
34	-0.62	+0.31	+0.68[d]
35	-0.76	+1.38	+0.945

To our surprise enols **R2**, **R4**, **R26**, **R1** and **R20** had lower oxidation potential which can be attributed to the increased carbon-centred character of the SOMO.

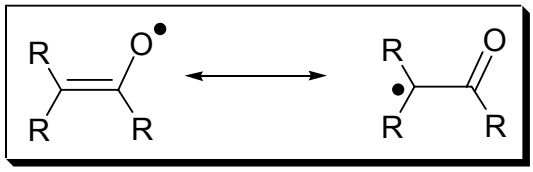

Interestingly the α-carbonyl radicals derived from enols bearing electron withdrawing group in the β-position have higher oxidation potentials (~700-800 mV_{Fc}) than enols bearing electron donating groups. This indicates that radical reactions predominate the chemistry of the α-carbonyl radicals derived from enols bearing electron withdrawing groups, while α-carbonyl cationic reactions predominate in the enols containing electron donating groups.

3.7.5 Comparison of Oxidation Potential of α-Carbonyl Radicals with Oxidation Potential of Carbon-Centred Radicals

α-Carbonyl radical are important intermediates in a number of reactions of chemical as well as biological origin. The low oxidation potentials of α-carbonyl radicals bearing electron donating group in the α–postion indicates a large contribution of the carbon centred radical in the SOMO of these enols.

Oxidation and reduction potentials of a number of carbon-centred radicals are known,[144] however, little is known about the oxidation potentials of α-carbonyl radicals derived from simple enols. While it is possible to compute the ionisation potentials (both gas phase as well as solvent corrected) of simple α-carbonyl radicals, the validity of the computed values can as well be misleading. Having been able to measure oxidation potential of α-carbonyl radicals with bulky groups in the α-position, we attempted to compare them with the known oxidation potentials of carbon-centred radicals.

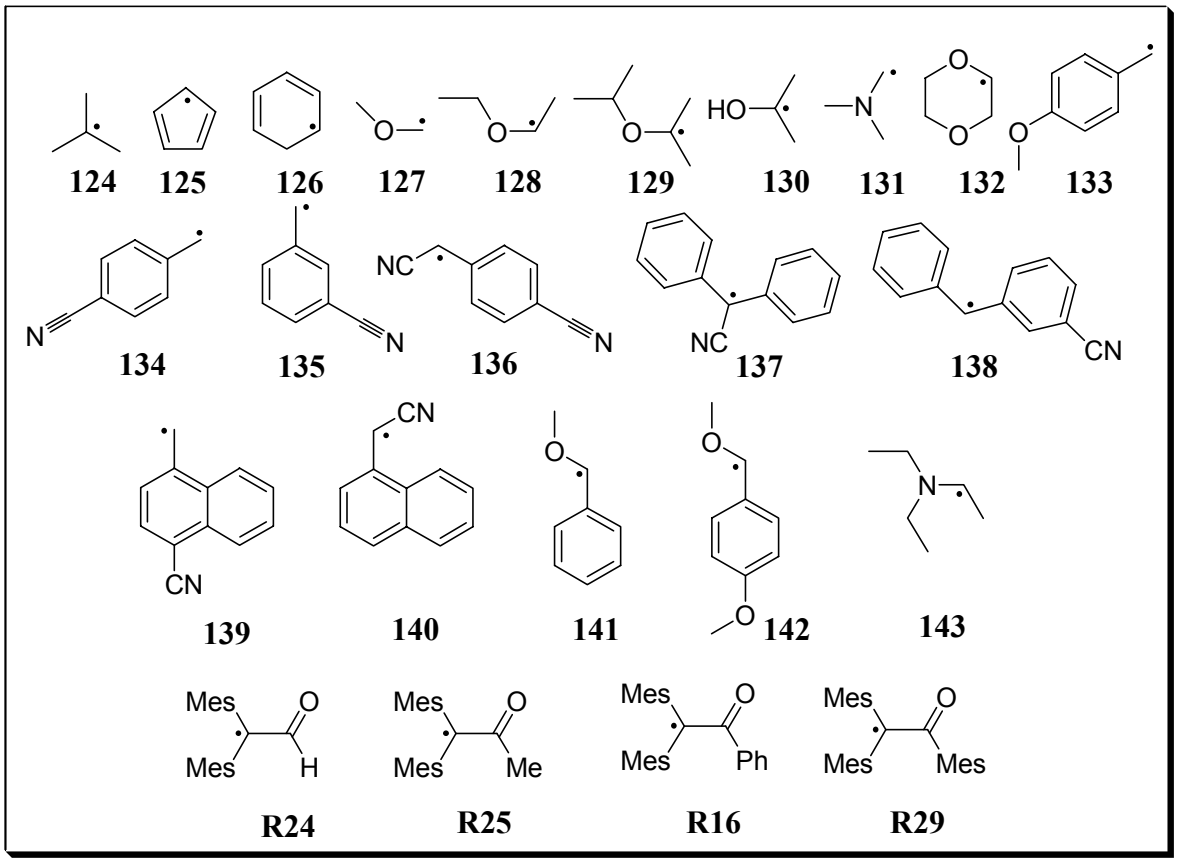

Chart 3–5: List of carbon-centred radicals used for correlation of solvent (acetonitrile) corrected ionisation potentials vs the measured oxidation potentials.

For a correlation the gas phase adiabatic ionisation potentials (IP_a^{gas}) of the carbon-centred radicals (Chart 3–5) were computed at AM1 level (Spartan).[145] Plotting of the calculated IP_a^{gas} against the experimental oxidation potential E_{pa}, gave a poor correlation with a correlation coefficient (R) = 0.86. However, when the IP_a^{gas} was corrected for the solvation term (for acetonitrile), a good correlation was obtained with a correlation coefficient of (R) = 0.96 (Figure 3–18). The correlation was given by the equation;

$$IP_a^{gas} - \Delta E_{solv}^{ACN} = 0.94 E_{pa} + 5.50$$

Interestingly, smaller the size of the carbon-centered radical, lower is its oxidation potential. The oxidation potential of carbon-centred radicals was found to increase with increased stabilisation effects such as resonance etc.

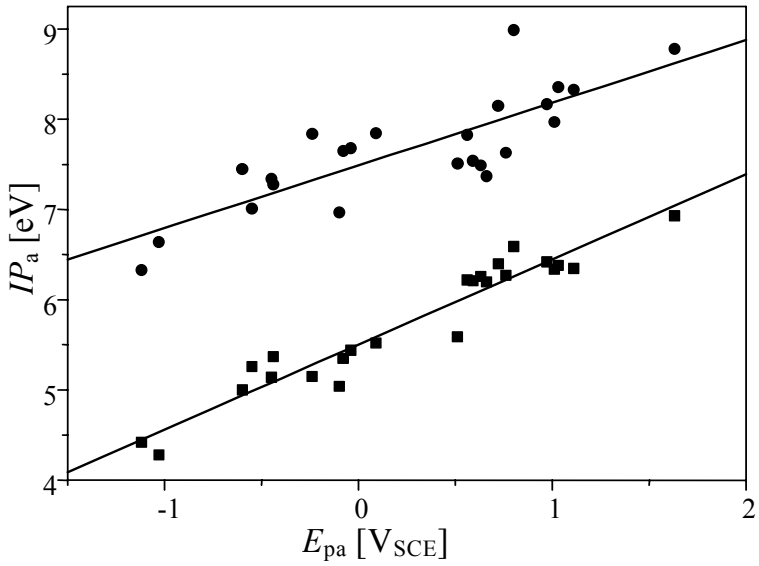

Figure 3–18: Plot of calculated IP_a^{gas} (eV, AM1, Spartan) against the experimentally determined E_{pa} (V_{SCE}) of α-carbonyl radicals, (●) represents the plot of IP_a^{gas} (eV) against the E_{pa} (V_{SCE}) while (■) is the plot of IP_a^{gas}-ΔE_{solv}^{ACN} (eV) against E_{pa} (V_{SCE}).

To our surprise not a very large difference in the gas phase adiabatic ionisation potentials was observed between various carbon-centred radicals. However, upon solvation correction the adiabatic ionisation potentials of small carbon-centred radicals decreased by ~2 eV. For large carbon-centred radicals the decrease was only about half the initial value (~1 eV). The trend could easily be explained by considering the solvation, the smaller the cation, more the stabilisation by solvation (Scheme 3–8).

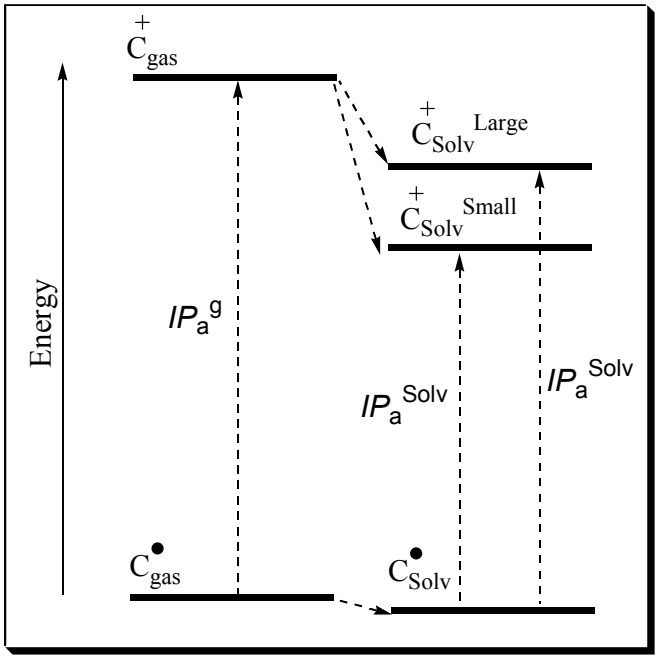

Scheme 3–8: Effect of solvation on carbocations in solution.

The validity of the equation was checked by predicting the oxidation potentials of α-carbonyl radicals with known oxidation potentials. The calculated oxidation potential using the above

equation was in close agreement with the experimentally determined values (Table 3–12). From the plot in Figure 3–18 the oxidation potentials of α-carbonyl radicals derived from β,β-dimesityl enols are in the range of benzyl radicals (simple as well as benzannulated).

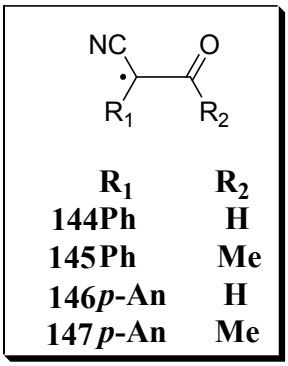

Table 3–12: Prediction of oxidation potentials of α-carbonyl radicals using the equation derived from the correlation. The solvation term was obtained using the classical Born equation.

System	IP_a^{gas} [eV]	ΔE_{Solv}^{ACN} [eV]	IP_a^{gas}-ΔE_{Solv}^{ACN} [eV]	Calculated $E_{1/2}$ (V_{SCE})	Experimental[143] $E_{1/2}$(V_{SCE})
144	8.80	1.87	6.93	1.50	1.52
145	8.56	1.77	6.79	1.35	1.48
146	8.30	1.72	6.58	1.14	1.19
147	8.09	1.64	6.45	0.99	1.15

3.7.6 Biological Relevance of Oxidation Potentials of Enols, Enolate and α-Carbonyl Radicals

Oxidation potentials for enols obtained from model compounds (with or without electron withdrawing group in the β-position) strongly indicate that biological oxidation of enols would not occur directly from the enol form (oxidation potentials of simple enols will be much higher than those of β,β-dimesityl enols) but can occur from the enolates which are more than 1.5 V (~35 *K*cal/mol) cathodically shifted from the enol forms. Additionally, formation of enolates has the added advantage in the fact that they are not only better electron donors, but also allows the system to selectively transfer one or two electrons (α-carbonyl radicals are ~0.9-1 V anodically shifted from the enolate, ~23.06 *K*cal/mol).

Flavin cofactors (FAD and FMN) are known to serve as biological oxidants and are involved in enzymatic reactions involving dehydrogenations[146] (D-lactate dehydrogenase, general acyl-

coenzyme A dehydrogenase, glutaryl-CoA and butyryl-CoA dehydrogenase). Enolates are known to be key intermediates in these transformations.

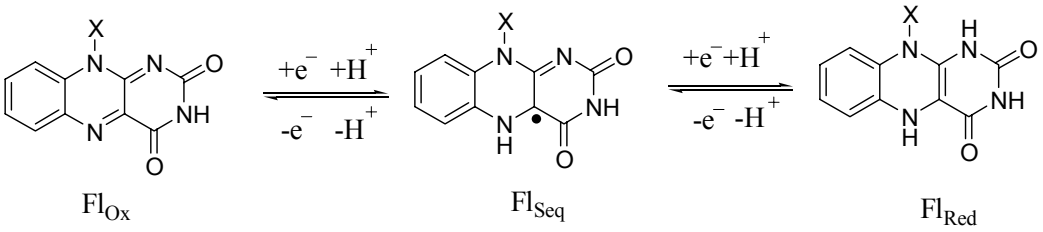

Fl_{Ox} Fl_{Seq} Fl_{Red}

Modulation of redox properties of these coenzymes by proteins has been a subject of intense investigation and persistent controversy. Investigations on the modulation of flavin redox properties were primarily concerned with protein conformation,[147] hydrogen bonding,[148] and π,π-stacking interactions,[149] reaffirmed by solution studies on model compounds.[150]

Solution investigations in fact show that oxidation of α-carbonyl radical could not proceed even in presence of electron rich α-carbonyl radical with β-mesityl groups.[151] The oxidation potential of the α-carbonyl radical derived from simple thioester **148** a mimick for the enzyme substrate for dehydrogenase, was predicted to be 1.92 V_{SCE} (from the correlation in Figure 3–18).

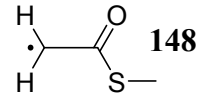

148

E_{pa} = **1.92** V_{SCE}

IP_{pa}^{gas} = **9.62** eV

ΔE_{solv}^{ACN} = **2.29** eV

Ascorbic acid (Vitamin C) an important two electron donor system is another biologically relevant enol (enediol) that has found wide application in various fields ranging from photographic developing plates, metal ion sensors, to as an antioxidant. While the electron donating ability of ascorbic acid is well accepted, the mechanism by which it donates the electron is not yet well understood.

Involvement of a radical anionic ascorbate has been invoked as an important intermediate after a one electron transfer, which was further supported by recent mechanistic investigations based on two dimensional voltammetry. The half wave potentials was found to be strongly dependent on pH (0.76 V_{SCE} at pH = 2.1 and 0.3 V_{SCE} at pH = 6.7, 1.13 V_{SCE} in DMF).

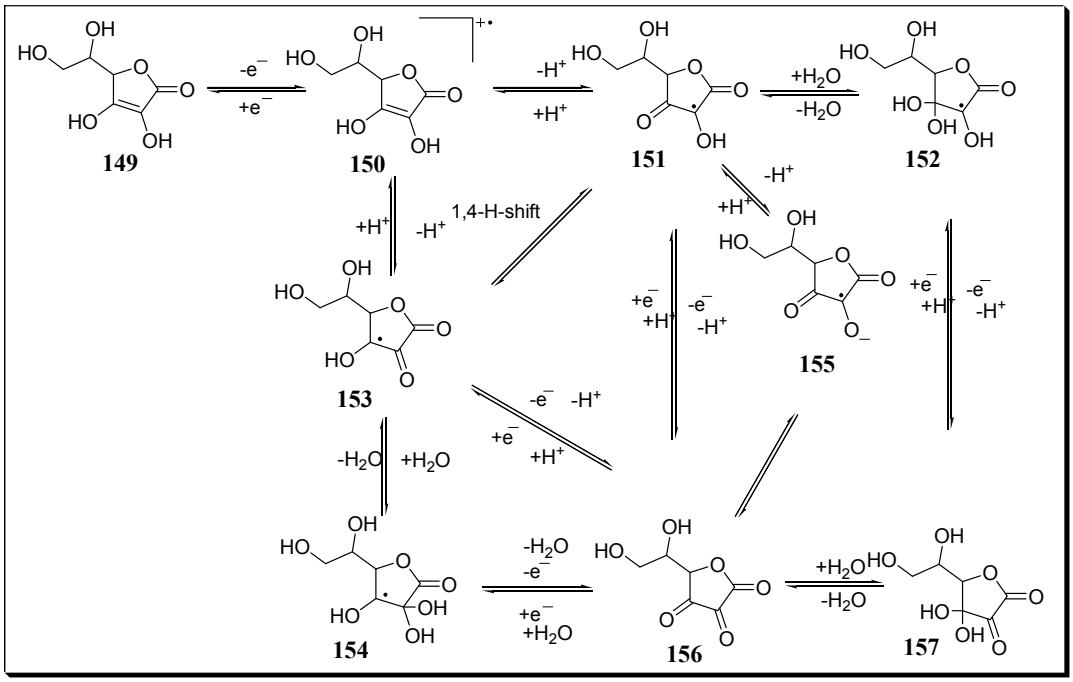

Scheme 3–9: Various possible radicals formed from oxidation of ascorbic acid **149**.

Recent theoretical calculations reveal that approximately 40 % of unpaired spin is found on O2 position in the ascorbic acid radical. It was also predicted that hydrogen bonding donation occuring at O2 and O3 atoms leads to a significant redistribution of spin density for the free radical. [152]

Interestingly presence of **153** was observed under pulse radiolytic conditions having an absorption at 290 nm which was 70 nm hypsochromically shifted in comparison to **151**.[153] Earlier pulse radiolytic investigations in nitrous oxide saturated solution between pH 3.0-4.5, showed two OH-radical adducts (**152** and **154**) in addition to the ascorbate radical anion.[154] The OH-radical adduct **152** formed by addition of hydroxyl radical to C3 position was found to exhibit a pair of lines in ESR that are pH dependent with a pK near 2.0 with a life time of 100μs. The adduct **154** formed by addition of hydroxyl radical at C2 position was found to be responsible for the formation of ascorbate radical anion. As it is apparent from the Scheme 3–9, a number of potential second electron donors (α-carbonyl radical and α,α′-dicarbonyl radical) can be written for ascorbic acid radical, some of which have been observed earlier. It would be of much interest to know which of these radicals participate in the second electron transfer.

To get a closer look we predicted the oxidation potentials of the radicals **151**-**154** by initially calculating the IP_a^{corr} based on AM1 method and equating it in equation 1. To our expectation **151** had a very high oxidation potential ~1.75 V_{SCE}. The oxidation potential of **151** was shifted 900 mV cathodically when compared to simple α,α′-dicarbonyl radical (2.72 V_{SCE} for

cyclohexanedione radical[‡]). The radical **153** (1.26 V_{SCE}) was found to be ~500 mV cathodically shifted in comparison to **151**, however, its oxidation potential is similar to the α-carbonyl radicals with α-electron withdrawing groups. The oxidation potential of radical **152** (1.37 V_{SCE}) was similar to **153** in line with our expectation, however, there was a 110 mV anodic shift of the oxidation potential which could be due to the fact that in **153**, the α-carbonyl radical is of ketone type while in **152** it is of ester type. The most interesting case is the oxidation potential of the radical **154** which from equation 4 was calculated to be 0.20 V_{SCE} in acetonitrile. The radical **154** is similar to an α-hydroxylalkyl radical. Oxidation potentials of some simple α-hydroxylalkyl radicals[155] in acetonitrile was reported recently by Wayner et al.,[156] which were in the range of -0.61 V_{SCE} to 0.38 V_{SCE} depending on the substituent. It was also noted that the oxidation potentials of α-hydroxylalkyl radicals are strongly dependent on the solvent used and are usually 1 V lower than those obtained in acetonitrile.[157] The main reason for the large solvent effect was attributed to the better ion solvation properties of water compared to that of acetonitrile. All the radicals **151**-**154** (pK = 4.25) can give the ascorbate radical anion by deprotonation however, its oxidation potential would be much more cathodically shifted than radicals **151**-**154**.

[‡] This work, The oxidation potential was obtained by calculating the IP_a^{corr} (8.03) of cyclohexanedione radical and equating in equation 4.

3.8 Conclusion

The synthesis and electrochemical investigations on simple enols, enolates and α-carbonyl radicals are impeded by their very existence in solution, model compounds based on electron withdrawing or electron donating groups have contributed much to the understanding of their reactivity pattern in solution.

Enols, enolates and α-carbonyl radicals derived from β,β-dimesityl enols can be used to model various scenarios both in biological systems as well as chemical systems. β,β-dimesityl enols bearing six membered nitrogen heterocylces in the α-position was an attempt to mimic the hydrogen bonding effect on the oxidation potential of enols at the active site of the enzyme. Cyclic voltammetric investigations indicated that hydrogen bonding of the enols would lower their oxidation potential and the reduction of the potential is directly proportional to the strength of the hydrogen bond. Oxidation potentials of the hydrogen bonded enols was about 300-500 mV lower than the non-hydrogen bonded enols.

The lowering of the oxidation potential is partly due to the stabilisation of the ground state and partly due to the stabilisation of the enol radical formed. Hydrogen bonding to enol radical cations would enhance the deprotonation step. This indicates that hydrogen bonded enol radical cations would be much weaker oxidants than non-hydorgen bonded ones.

While the deprotonation of enol radical cations reduces their oxidising power, in contrast hydrogen bonding to α-carbonyl radicals would enhance their oxidising power. Thus hydrogen bonded α-carbonyl radicals are expected to have higher oxidation potenital than the non-hydrogen bonded ones.

A change in reactivity of the α-carbonyl radicals derived from enols with β-electron withdrawing group to β-electron donating groups was observed. While the α-carbonyl radicals derived from enols with β-electron withdrawing groups undergo typical radical reactions, the α-carbonyl radicals derived from enols with β,β-dimesityl enols undergo reactions typical of carbocations, for example confirmed by formation of benzofuran derivatives and also UV-Vis spectroscopic studies on model compounds (**E5**). It was possible for the first time to measure the oxidation potentials of α-carbonyl radicals with electron donating group in the β-position. A correlation was obtained when calculated ionisation potentials corrected for the solvation terms were plotted against the experimentally determined oxidation potentials of α-cabonyl radicals.

The correlation was useful in predicting the oxidation potential of α-cabonyl radicals derived from simple thioesters, a mimick for the enzyme substrate in dehydrogenases. A difference in

$E_{1/2}$ of about 600 mV was found between the enolate A1 and the flavin, suggesting that the first electron transfer between the riboflavin derivatives (FAD or FMN) could occur which was indeed observed in solution (Thesis of M. Röck) however, the second electron transfer did not occur in solution. This could be due to the fact that the oxidation potential of the resulting α-carbonyl radical and the semiquinone form of flavin are similar thus making the process endergonic. Prediction of the oxidation potential of the α-carbonyl radical of the natural substrate (E_{pa} = 1.92 V_{SCE}) was in agreement with the solution results. However, in these enzymes after the first electron transfer the radical intermediate can undergo a hydrogen atom transfer or can undergo radical addition to the cofactor.

4 Design and Synthesis of Electroactive Surfactants to Modulate Surface Wetting Properties

4.1 Introduction to Wetting Phenomena

Wetting is a common phenomenon observed in our day to day life such as rain drops on a window or dispersing cocoa in milk, spreading of ink on paper, coatings and paints. The quantitative description of wetting phenomenon can be explained on the basis of Young's equation relating the contact angle to the interfacial tensions:

$$\gamma_L . \cos\theta = \gamma_S - \gamma_{SL} \qquad \text{Equation 4–1}$$

Rearranging the above equation:

$$\cos\theta = \frac{\gamma_S - \gamma_{SL}}{\gamma_L} \qquad \text{Equation 4–2}$$

When the interfacial tension of the bare solid surface is higher than that of the solid-liquid interface, then the contact angle is smaller than 90 °; partial wetting is observed. However, if the contact angle exceeds 90 °no wetting is observed. Complete wetting is observed when the numerator on the right hand side in the above equation is greater than the denominator.

A number of methods have been developed to investigate and measure the contact angle. The most common methods are the "sessile drop method", "captive or sessile bubble" method, "Wilhelmy plate method" and "capillary rise method".

The most important application of wetting phenomenon in recent times is moving small volumes of liquid on a surface popularly known as "microfluidics".

Microfluidics and reversible wetting

Exploration and exploitation of the physical, chemical and biological properties at dimensions comparable to the dimension of the structure has been the key to the development of nanotechnology. Nanotechnology has been recognised as one of the key research topics of the 21st century, whose potential relies on the development and manipulation of new tools at the atomic/ molecular scale. In recent years efforts are being made towards the development and miniaturisation of chemical[158] and biological[159] instruments with a net effect of creating highly integrated and automated "lab-on-a-chip" systems.

The advantages offered by such systems include, reduced reagent consumption, and reduced analysis volume, faster analysis times, high throughputs and automation. The added advantage of these systems also lies in their increased instrument portability.

While microfluidics is the driving force behind the "lab-on-a-chip" concept, handling capabilities of micro-liquids are still inflexible in comparison to their macrofluidic counterparts. Most of the microfluidic devices utilise closed channels permanently formed in glass, plastic or silicon. Depending on the flow of the fluid[160] in these channels microfluidic systems are broadly classified into two categories a) continuous flow and b) droplet-based architectures. The continuous flow systems rely on flow of liquid into the systems, the droplet-based systems utilise discrete volumes of liquid. With each flow system mixing is accomplished by active or passive means. While passive mixing is purely through diffusion without any external energy needed for mixing, active mixing can be achieved via actuation of some sort (turbulence).

Mixing in continuous flow systems are performed passively by merging two separate streams through etched micro-channels. A number of ways have been demonstrated to achieve passive mixing in flow systems. a) Passive mixing either by separating a pressure-driven main stream into a laterally alternating partial flows or superimposing two fluids by injection of one liquid into the other.[161] b) Serial mixing in electrokinetically driven flows,[162] c) creation of ridges and wells in the channels,[163] d) use of serpentine paths and interweaving channels.[164] Active mixing in continuous flow systems requires additional energy to create flow instabilities. It can be achieved by a) electrostatic actuators to achieve electrokinetic instabilities which stretch and fold the channel flow to promote mixing,[165] b) use of peristaltic pumps in continuous flow systems[166] or c) turbulent mixing using ultrasound by subjecting discrete mixing chambers to high frequency vibrations.[167]

The disadvantage of continuous flow systems is that liquid transport is physically confined to permanently etched structures and additional methods are required to enhance mixing. While transport mechanisms used are usually pressure-driven by external pumps or electrokinetically-driven. The approach requires use of valves and/or complex channeling, high-voltage supplies, large dead volumes and complicated integration and control.

An alternative approach to traditional continuous-flow systems is the one that manipulates discrete droplets.[168] This approach of micromanipulation of droplet allows one to perform complex procedures such as mixing, reaction, incubation, splitting or sensing of the droplets. It has an additional advantage over the continuous flow systems in that little or no excess fluid is required to fill micro-channels thus allowing higher utilisation of sample and reagent volumes. Another significant advantage of droplet-based systems are that they are compatible with wall-less structures where operations are carried out directly on the surface of the substrate, allowing easy fabrication, assembling and reconfiguration of the structures.

A wide range of methods are applied to achieve actuation in microfluidic droplets including use of air pressure,[169] thermocapillary effects,[170] structured surfaces,[171] Photochemical effects,[172] Dielectrophoresis (DEP),[173,159b] and electrowetting.[174]

4.2 Electroactive Surfactants

Surfactants are compounds when dissolved reduce the surface tension of liquids, or reduce interfacial tension between two liquids or a liquid and a solid. They are widely applied in various fields such as soaps, detergents, oil recovery, mineral floatation and medical applications (triton detergents,). Depending on the charge of the head group they are classified as follows,

a) Anionic surfactants: The head group has a negative charge (dodecylsulfate), b) cationic surfactants bearing a positive head group (cetylammoniumbromide), c) neutral surfactant: having no charge on the head group (alkylethyleneoxides), d) amphoteric bearing both a positive as well as a negative group in the molecule i.e. they are zwitterionic (phosphatidylcholine). A characteristic property of surfactants is that they spontaneously aggregate in water and form well-defined structures called micelles, cylinders, bilayers, etc.

Despite ample use of surfactants (Figure 4–1), their applications are limited to the anionic and neutral ones. The least applied surfactants are acidic and amphoteric surfactants, because of the environmental hazards and high costs. Search for new compounds having surfactant properties is continuously sought and has led to the development of switchable surfactants based on electrochemical properties. The advantage of electroactive surfactant over the conventional surfactant is that the switching is reversible, hence the surfactant property can be reversibly controlled. Under a given redox state they can be allowed to behave as cationic, anionic or a neutral surfactant.

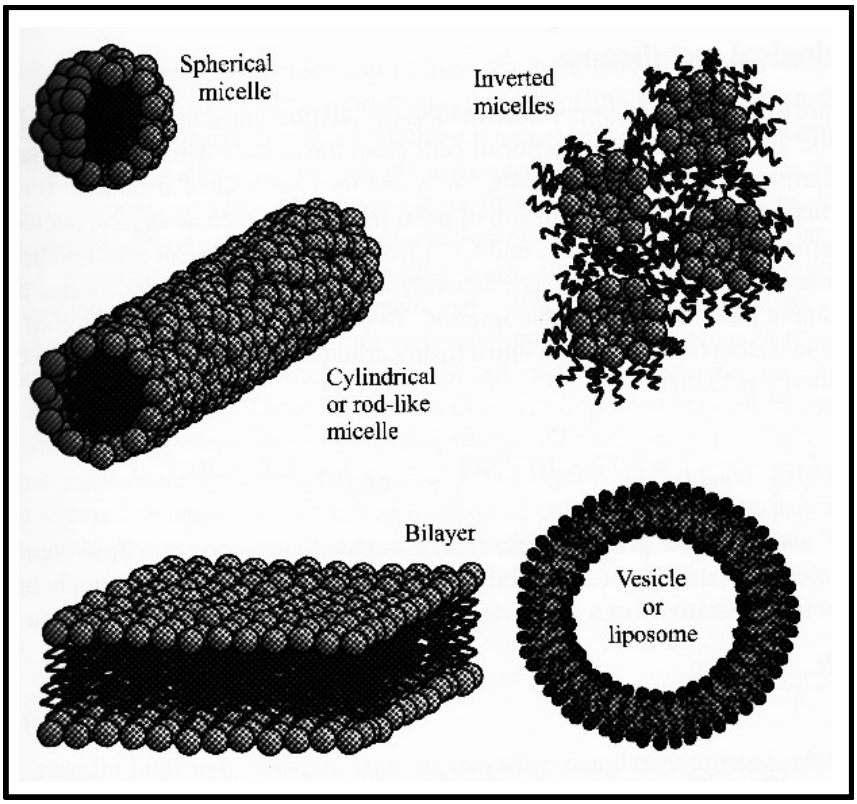

Figure 4–1: Various aggregates formed by surfactants.

Previous application of electroactive molecules was restricted to investigate the dynamics of micellar formation.[175] However, a number of redox active molecules are now being developed and investigated for application purposes. The most common electroactive molecules that are investigated were ferrocene, thiafulvene, quinones (anthraquinone), perylenes, porphyrins and viologens. They have been used to prepare thin films,[176] for reversible formation of micelles and vesicles[177] and also for surface modification.[178]

While electrowetting has been successfully applied to actuate microdroplets, electroactive surfactants are being extensively investigated for application to actuate microdroplets. The approach involves the utilisation of monolayer containing charged[179] (Figure 4–2)/ electroactive groups[180] (Figure 4–3) to modulate surface wetting behaviour.

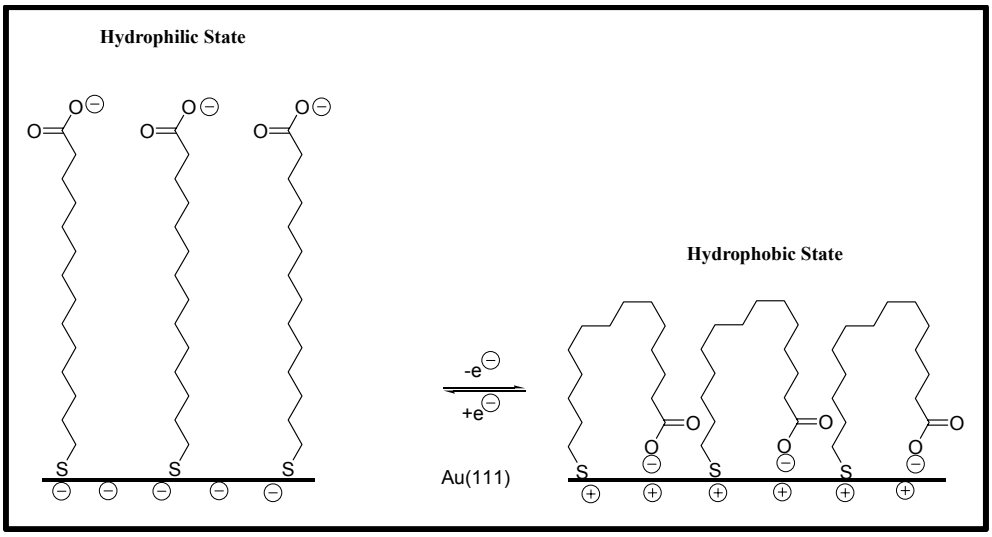

Figure 4–2: Changes associated with surface charge observed for the monolayer terminating with a carboxylate.

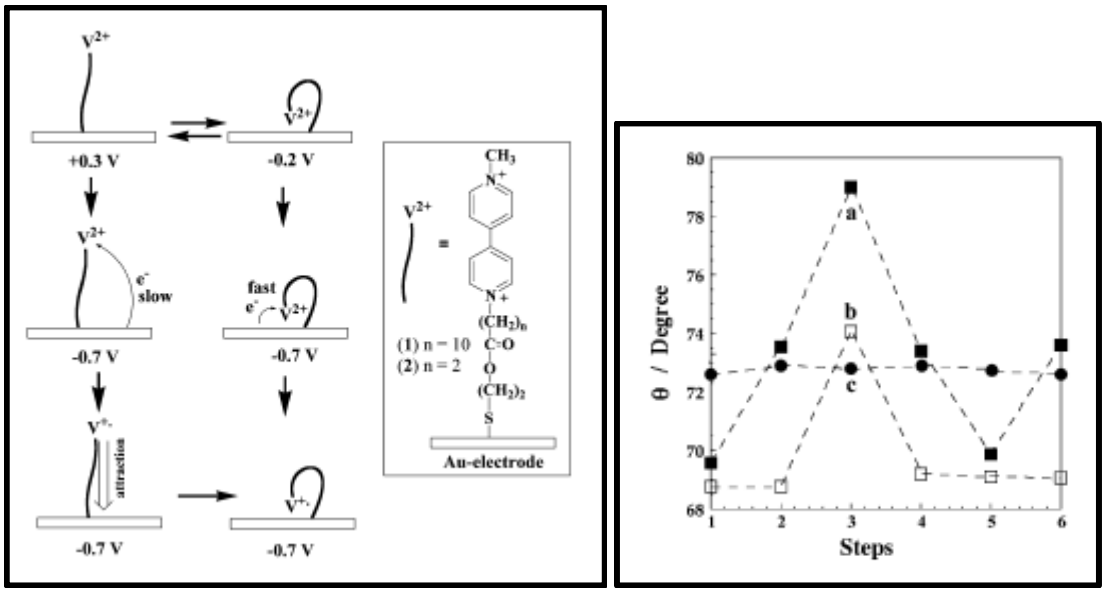

Figure 4–3: Change in wetting properties modulated by applied potential of a bipyridinium monolayer, a) cartoon representation of the electromodulation of surface properties, b) changes in contact angle observed upon change in potential.

With the above approach (Figure 4–3) a change in contact angle of about 6 ° was observed. The main advantage of the above system is that it reduces to a large extent the applied potential, allowing applications for various biological as well as chemical systems prone to changes (damages) caused by the applied voltage.

4.3 Objective

While a number of procedures are available to actuate droplets for microfluidic applications, electrowetting phenomena utilising monolayers with charged/electroactive group are appealing because of the advantages of fabrication and reconfiguration of surfaces. The additional advantage being that they can be operated at much lower voltages than the classical methods. Use of electroactive surfactants have the added advantage in the fact that it does not require prefabrication of microcapillaries to carry out operations such as transportation, droplet formation and mixing in addition to use of multicomponent system.

Electroactive head groups with multiple reversible redox-states further allow one to modulate the surface properties depending on the applied potential. The choice of electroactive head groups can be made from the list given in Chart 7-1.

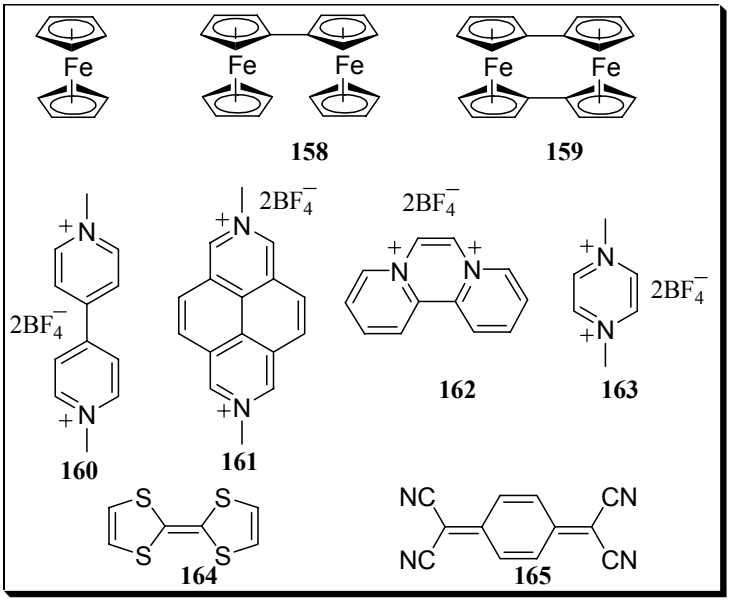

Chart 4–1: List of electrophores that can be used as head groups to modify surfaces for modulating the wetting properties.

The objective of the present work was:

a) to identify new electroactive head groups with multiple stable redox-states.
b) to develop and investigate the surfactants utilising the short listed electroactive groups.
c) finally to apply them to modify the electrode surface for surface wetting property and extend it for actuation of microdroplet.

4.3.1 Design of Electroactive Surfactants Based on 1,4-Dimethyl-2,3-dialkylpyrazinium Tetrafluoroborates

Diquaternary salts of pyrazines have attracted much attention for application as herbicides, as

electrographic inks, electrochromic materials and trapping solar energy.[181-184] These compounds are similar to their viologen counterparts. However, they differ from them in the fact that the charge density (less charge delocalisation than their benz annulated systems) is greater in diquaternary salts than the viologens (Scheme 4–1).

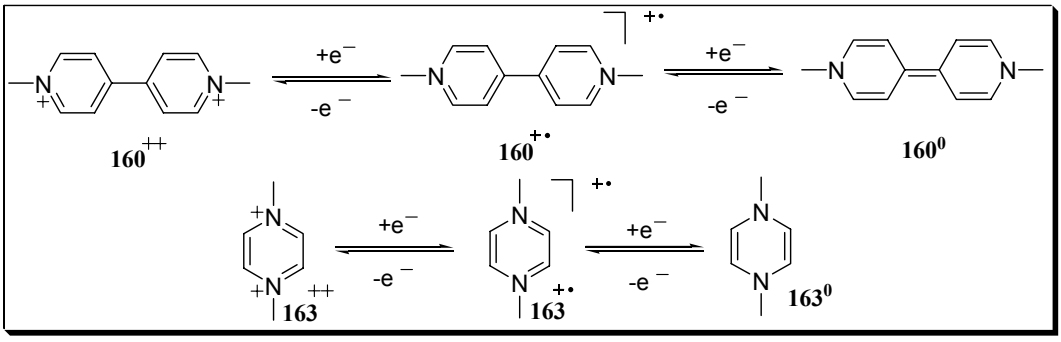

Scheme 4–1: Similarity between the two one-electron reduction processes in diquaternary salts of viologen and pyrazinium.

The diquaternary salts of pyrazinium derivatives are know to exhibit two reduction waves[181] similar to the viologens and are usually prepared by treatment of the corresponding derivative with Meerwein´s salt. In polar solvents the diquaternary salts of pyrazines exhibit polychromatic behaviour changing colour with time.[182] This was attributed to the formation of radical cationic species in polar solvents as confirmed by EPR with unusual spectra having more than 200 lines in water or alcohol.[182] The diquaternary salts were found to be stable in trifluoroacetic acid or a mixture of TFA and sulphuric acid. The radical cation formation in polar protic solvents was explained in the Scheme 4–2 below:

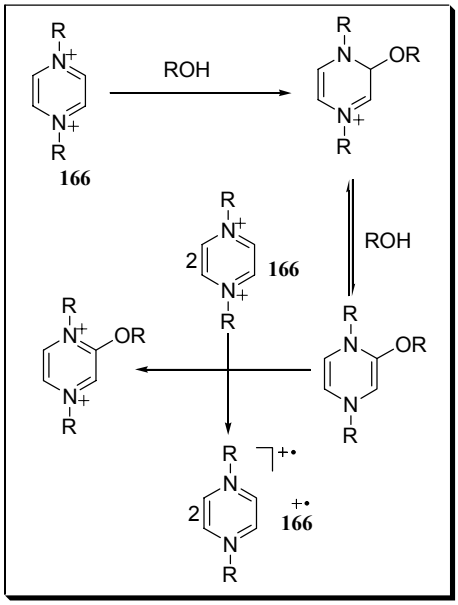

Scheme 4–2: Behaviour of pyrazinium salts in water, formation of dication and radical cations in water. number correction

Investigations by Hünig *et al*.[183] and Kaim *et al*.[184] on a number of Weitz-type redox systems indicate that the radical cations in these systems show extreme stability ($K_c = 10^{15}$, Scheme 4–3). EPR investigations on the radical cations indicate that it is not the extent but the effectiveness of cyclic spin delocalisation that ensures stability of a π-radical.

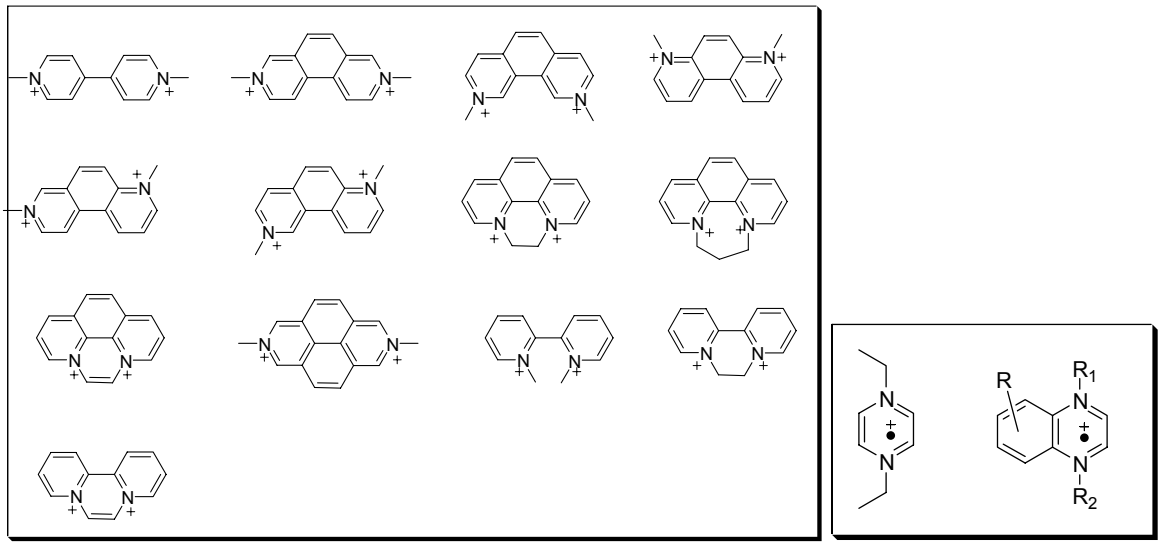

Scheme 4–3: List of diquatenary salts investigated by Hünig et. al.[183] and Kaim et. al.[184]

While viologens are extensively being used in various fields,[185] exhaustive literature on the application and electrochemical properties of diquaternary pyrazine salts are lacking. The high charge density on pyrazinium derivatives make them suitable candidates for application to modulate surface properties by applying a voltage.

Thus, we identified diquaternary pyrazinium derivative (**167**) as a suitable electrophore for modulating surface wetting and designed derivatives containing long alkyl chains based on a simple synthetic route.

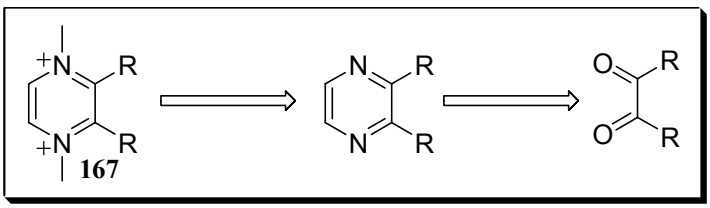

4.3.2 Design of Electroactive Surfactants Based on Ferrocene

Electroactive surfactants based on ferrocene are well known. They usually employ alkyl chains either directly attached to the ferrocene moiety or functionalised ferrocene derivatives with a charged amine group (Chart 4–2).

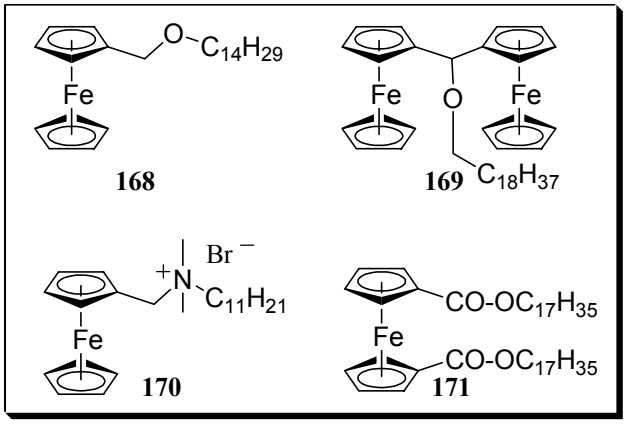

Chart 4–2: Some representative electroactive surfactants based on ferrocene as the electroactive group.

We decided to design and synthesise ferrocene based electroactive surfactants, the main orientation being application in addition to understand the film forming behaviour of the high order surfactants (Chart 4–3).

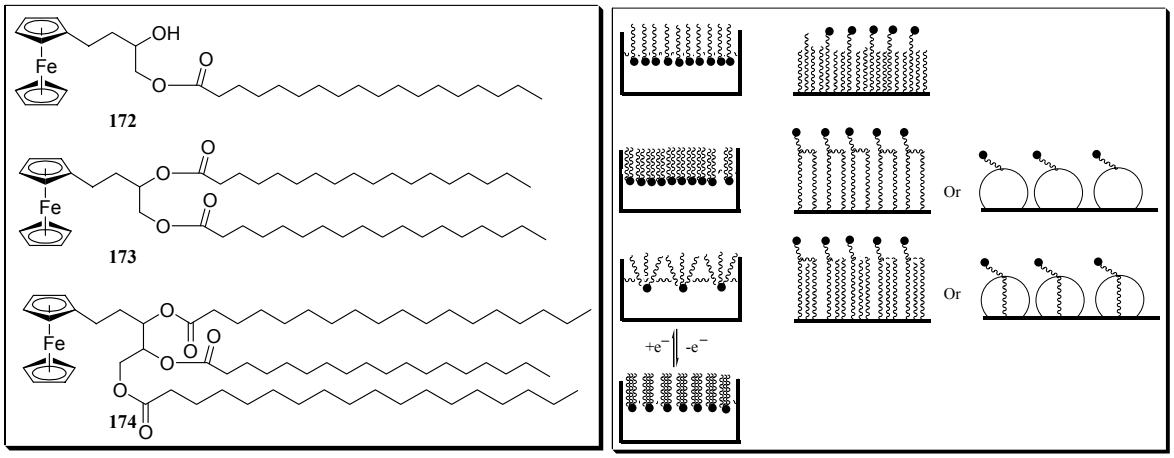

Chart 4–3: Ferrocene based electroactive surfactants a) list showing ferrocene surfactants with one two or three ester linkages, b) possible film forming ability of these surfactants at the water-air interface and monolayer formation on solid surfaces.

4.4 Results

4.4.1 Synthesis of Electroactive Surfactants

4.4.1.1 Synthesis of 1,4-Dimethyl-2,3-dialkylpyrazinium Tetrafluoroborates (167a-d)

The synthesis of pyrazinium derivative started with an initial Acyloin condensation of the ethyl esters in presence of sodium in refluxing toluene (Scheme 4–4). The acyloin products were trapped as trimethylsilylenediol ethers (**178a-d**). The trimethylsilylenediol ethers **178a-d** were obtained in 81-95% yield characterised by a band between 1676-1677 cm^{-1} (C=C) in the IR. The signal at 0.15 ppm (TMS) in ^{1}H-NMR and 134.2-134.4 in ^{13}C-NMR were characteristic for trimethylsilylenediol ethers.

Trimethylsilylenediol ethers **178a-d** when treated with 1 N HCl in THF at room temperature for 1.5 h gave the corresponding α-hydroxyketones **177a-d** in 71-85% yields. The α-hydroxyketones showed characteristic broad bands between 3338-3474 cm^{-1} (OH) and 1712-1713 cm^{-1} (C=O) in the IR. The presence of a signal between δ = 3.74-4.18 ppm in ^{1}H-NMR and at δ = 212.6 (C=O) in the ^{13}C-NMR confirmed the product formation.

Bismuth oxide oxidation of the α-hydroxyketones **177a-d** in glacial acetic acid gave the α-diketones **176a-d** in 44-86% yield. The α-diketones **176a-d** showed a strong band in the IR between 1713-1715 cm^{-1} (C=O) while the band characteristic for OH group for the starting material was not observed. In the ^{1}H-NMR the characteristic signal between 3.74-4.18 ppm (for CH-OH) was not observed and a shift of the (C=O) signal from 212 to 200 ppm in the^{13}C-NMR further confirmed our assignment for **176a-d**.

The α-diketones when refluxed with 1,2-diaminoethane in ethanol gave the Schiff bases (the signals at 4.16 ppm disappeared in the ^{1}H-NMR while signals at δ = 44.9 and 162.9 ppm appeared in the ^{13}C-NMR) which on reflux with KOH and MnO_2 for another 16 h furnished the desired pyrazine derivatives **175a-d** in 54-80% yield. The 2,3-dialkylpyrazines **175a-d** showed a characteristic weak band between 3041-3042 cm^{-1} (aromatic stretching) in the IR. New signals between δ = 8.30-8.31 ppm in the ^{1}H-NMR and δ = 141.1-143.0 ppm, 155.8-155.9 ppm in the ^{13}C-NMR confirmed product formation.

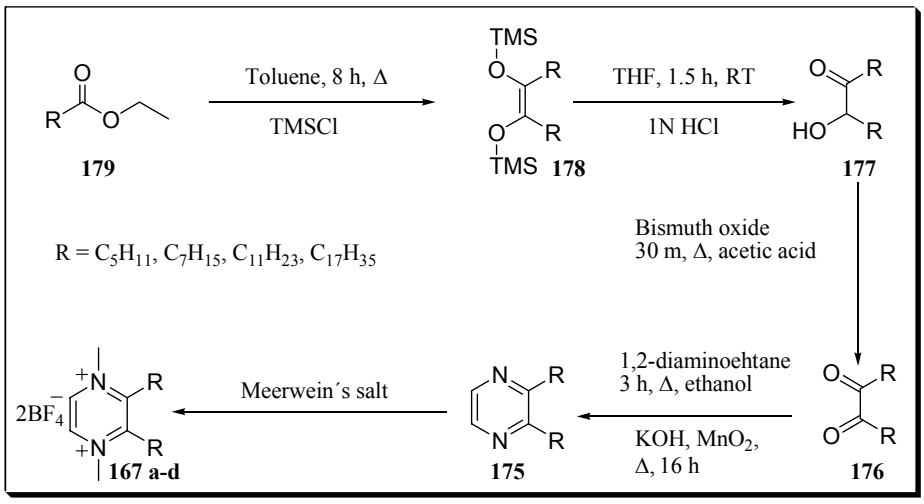

Scheme 4–4: Synthesis of *N*,*N*-dimethyl-2,3-dialkylpyrazinium tetrafluoroborates **167a-d** starting from the corresponding alkylesters **179a-d**.

Refluxing the pyrazine derivatives **175a-d** in 1,2-dichloroethane with trimethyloxonium tetrafluoroborate (Meerwein´s salt) gave the corresponding *N*,*N*-dimethyl-2,3-dialkyl-pyrazinium tetrafluoroborates **167a-d** in 18-91% yield. The products **167a-d** showed a strong shift of protons from δ = 8.30 ppm in the starting material to δ = 9.29 ppm (9.19-9.29 ppm) in the ^{1}H-NMR with appearance of a new signal at δ = 161.3-161.5 ppm in the ^{13}C-NMR.

When the dications **167a-d** were treated with solid KBr and KI an immediate colour change was observed (immediate formation of yellow colour with KBr and an initial violet colour followed by a reddish brown with KI). However when the salts were extracted with dichloromethane and their UV-Vis spectrum recorded, both showed the similar absorption bands, hence must involve same species. The dications **167a-d** were dissolved in dichloromethane and their ESI-MS (Figure 5–6, Figure 5–7) was recorded. In all cases, instead of a dicationic species only a monocationic species was observed which was assigned to the loss of a proton (M^{+}-1, Table 5–5). In addition to the radical cation the most predominant signal was that of a monocation formed by the loss of a methyl cation (M^{+}-15). In case of **167c** and **167d** water added products were also observed along with the radical cation (Scheme 5–1).

4.4.1.2 Synthesis of *N*-methyl-2,3-Dialkylpyrazinium Iodide

Synthesis involved refluxing of **175d** in methyl iodide for 12-15 h giving the pure product in quantitative yield, which after recrystallisation gave a yellowish-orange coloured solid (75%). The product had characteristic signal at 4.63, 9.09 and 9.47 ppm in ^{1}H-NMR, the product was further characterised by other spectroscopic techniques and by elemental analysis.

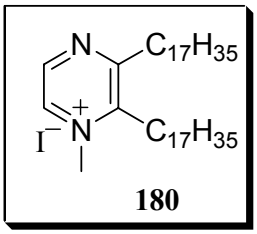

180

4.4.1.3 Synthesis of Ferrocene Based Electroactive Surfactants

The ferrocene-based surfactants were synthesised by esterification of the corresponding diol and triol **25** and **28** respectively. A typical synthesis involved treating the diol/triol with palmitoyl chloride and triethylamine in dichloromethane. For diol **25** a mixture of **172** (mono) and **173** (diester) was obtained in 38% and 48% yield, respectively. Triol **28**, when treated with an excess of palmitoyl chloride, gave **174** in 47% yield. A decrease in melting point was observed on going from the free alcohols **25** (92 °C)/**28** (71 °C) to the esters **172** (40 °C), **173** (48-50 °C) and **174** (44 °C). Interestingly, in the IR measurement **172** showed a single band at 3428 cm^{-1} (C=O), where in **173** and **174** two bands for C=O were observed at 1848 and 1736 (1723) cm^{-1}. The products were further characterised by ^{1}H-NMR, ^{13}C-NMR, elemental analysis and HRMS.

The esters **172** and **173** when oxidised with ferric chloride showed the protonated and oxidised esters $\mathbf{172}^{+\bullet}$ (750.9), $\mathbf{172} + \mathbf{H}^{+}$ (751.8) and $\mathbf{173}^{+\bullet}$ (1019), $\mathbf{173} + \mathbf{H}^{+}$ (1020) in the ESI-MS (Figure 5–9a). The calculated isotope splitting for the radical cation matched the experimentally determined ones (Figure 5–9b and c).

4.4.1.4 UV-Vis Spectroscopic Investigation

The pyrazine derivatives **175a-d** and the diquaternary salts of the pyrazinium derivatives **167a-d** were studied by UV-Vis spectroscopy. The pyrazine derivatives **175a-d** showed two absorption maximum at λ_{max} = 267-271 nm and λ_{max} = 308-310 nm. Diquaternary salts **167a-d** showed a bathochromic shift of the wave at λ_{max} = 308-310 nm (in **175a-d**) to λ_{max} = 317-318 nm. A complete disappearance of the band at λ_{max} = 267-271 nm and appearance of a new small band around λ_{max} = 228-229 nm was observed. The monomethylated **180d** showed a broad band at λ_{max} = 348 nm and two additional bands at λ_{max} = 229 and 258 nm (Figure 4–4).

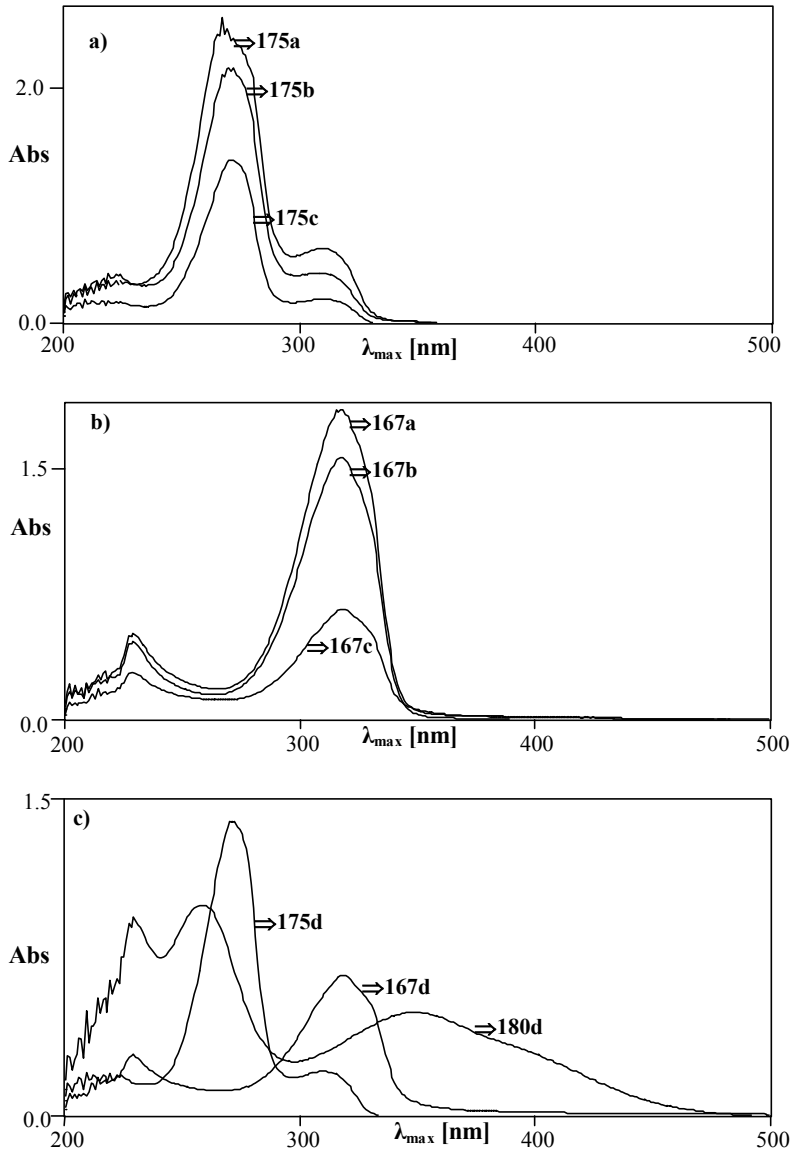

Figure 4–4: UV-Vis spectroscopic investigation in dichloromethane, a) overlay spectrum of pyrazine derivatives **175a-c**, b) overlay spectrum of diquaternary pyrazinium salts **167a-c**, c) overlay spectrum of **175d** (unmethylated), **167d** (dimethylated) and **180** (monomethylated).

Concentration dependence of the diquaternary salts with varying chain lengths was carried out for **167a** and **167d**. In both cases, a linear dependence of the absorption on the concentration was observed (Figure 5–8).

4.4.1.5 Cyclic Voltammetry Investigations

The diquaternary salts **167a-d** were investigated by cyclic voltammetry in acetonitrile and dichloromethane. As expected **167a-d** showed two completely reversible reduction waves at $E_{1/2}^{1} = -0.19$ to -0.20 V_{Fc} and $E_{1/2}^{2} = -1.14$ to -1.16 V_{Fc} (Figure 4–5,
Table 4–1). The first reduction wave was assigned to the one-electron reduction of the dication **167b** to **167b**$^{+\bullet}$ and the second reversible wave was assigned to the one-electron reduction of the radical cation into the p-quinoid type of the completely reduced product

167b^0.

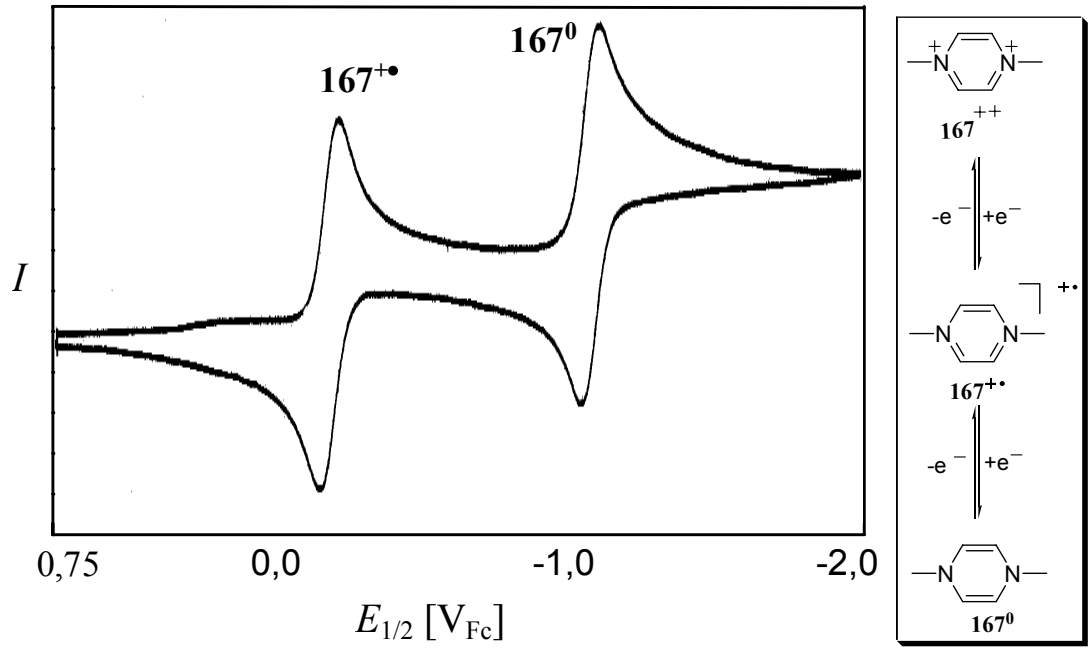

Figure 4–5: Cyclic voltammogram showing the two reversible reduction waves observed for **167b** in acetonitrile at 100 mV/s scan rate.

The difference in the anodic and the cathodic peak potential for both waves was found to be between 59-63 mV which was in agreement with the theoretical value (59 mV) for a reversible one-electron transfer. The ratio of the cathodic to anodic peak current was close to unity further indicating the reversible nature of the wave. Diagnostic criteria based on the Nicholson-Shain[123] procedure were evaluated to further determine the electrode kinetics. Scan rate dependence of the reduction waves was measured in acetonitrile over a range of scan rates starting from 20 mV/s to 500 mV/s (Figure 4–6).

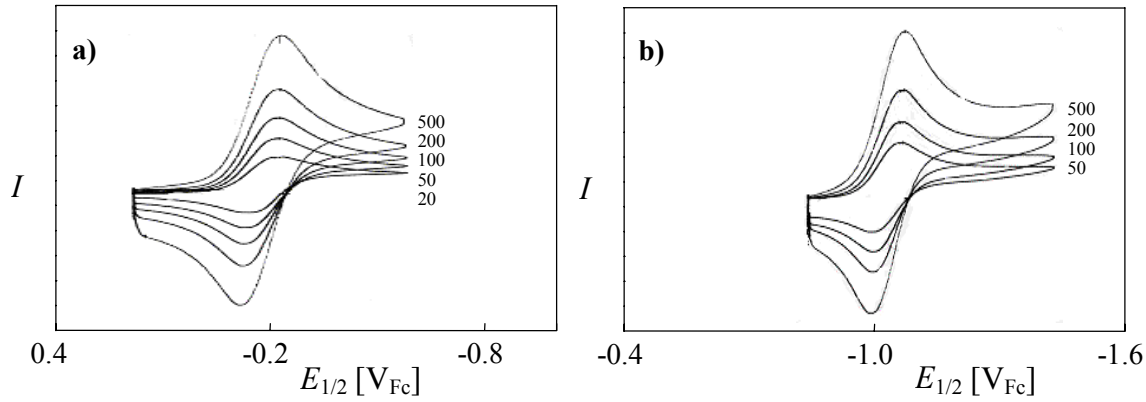

Figure 4–6: Scan rate dependence of a) first reduction wave and the b) second reduction wave in *N,N′*-dimethyl-2,3-dialkylpyrazinium tetrafluoroborates **167a-d**.

Completely reversible waves were observed at different scan rates for both reduction waves

of **167a-d**. A linear dependence of the cathodic current with the scan rate was observed for both waves (Figure 4–6a). Based on Nicholson-Shain criteria a plot of the current function (I_c/[scan rate]$^{1/2}$) vs. the scan rate supported an E_{rev} mechanism for the diquaternary salts **167a-d** in acetonitrile (Figure 4–7b).

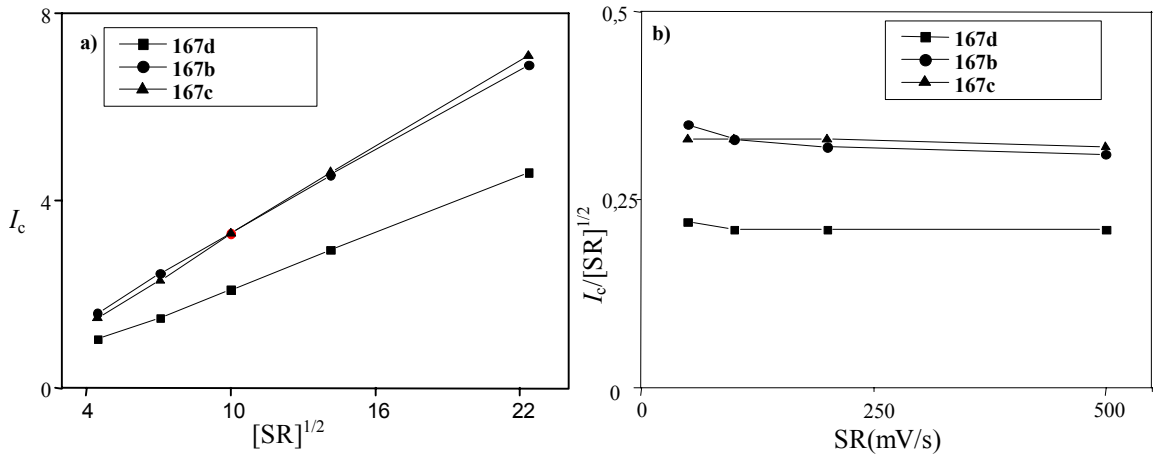

Figure 4–7: Scan rate dependence of the first reduction wave in **167b-d**, a) I_c vs. [SR]$^{1/2}$, b) current function (I_c/[SR]$^{1/2}$) vs. SR (scan rate).

Table 4–1: Electrochemical data with the $E_{1/2}$ for both the reduction waves for **167a-d** in acetonitrile (dichloromethane), stability constant for the radical cation ($K_c = 10^{\Delta E/59mV}$).

Pyrazinium derivative	$E_{1/2}$ [V_{Fc}]	$E_{1/2}$ [V_{Fc}]	K_c
167a	-0.20 (-0.12)	-1.16 (-1.18)	10^{20} (10^{18})
167b	-0.20 (-0.16)	-1.16 (-1.21)	10^{20} (10^{18})
167c	-0.19	-1.14	10^{16}
167d	-0.19 (-0.15)	-1.16 (-1.25)	10^{16} (10^{19})

High stability constants 10^{16}-10^{20} were obtained for radical cation **167$^{+\bullet}$a-d** in acetonitrile and dichloromethane. The radical cation with longer chain lengths **167$^{+\bullet}$c-d** are 4-orders of magnitude less stable in acetonitrile than those with smaller alkyl chains **167$^{+\bullet}$ a-b**.

4.4.1.6 Stability of *N*,*N*′-Dimethyl-2,3-dialkylpyrazinium Tetrafluoroborates 167a-d in Aqueous Solutions

N,*N*′-Dimethyl-2,3-dialkylpyrazinium tetrafluoroborates were found to turn brown or black when exposed to air. ^{1}H-NMR of the compounds exposed to air showed a broadening of the signals. This could be due to the presence of trace amounts of radical/ radical cations formed (further confirmed by EPR spectroscopy, Figure 4–12a). When a solution of **167b** in

acetonitrile was diluted with water an immediate colour change was observed (colour changes from golden yellow to violet and finally to reddish brown). After 4-5 h a precipitate was observed (~30%). After isolation the precipitate was found to be the diketone (**177b**, Scheme 4–5).

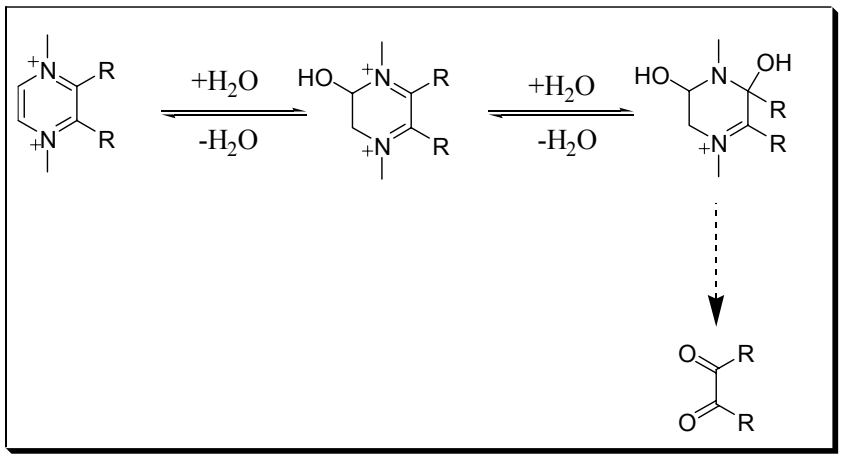

Scheme 4–5: Proposed mechanism for the degradation of *N*,*N*-dimethyl-2,3-dialkylpyrazinium tetrafluoroborates in presence of water.

The above result is in contrast to the earlier reports which suggest formation of radical cationic species. Cyclic voltammetric investigations were carried out with addition of increasing amount of water (doubly distilled and degassed) to a solution of **167b** (3.5 mM) in acetonitrile. Upon addition of 20 eq. of water, the *cathodic* current for the first and the second reduction wave remained the same (1 : 1). However, the *anodic* current for the first reduction wave increased dramatically (Figure 4–8a). This was accompanied by a change in colour of the solution from colourless to golden yellow. The colour of the solution darkened with addition of water however, the cyclic coltammetric behaviour remained unitl 800 eq. of water addition. When 2000 eq. of water had been added, after 10-15 min a completely reversible wave appearead at –0.27 V_{Fc} which was accompanied by a completely irreversible wave –0.88 V_{Fc} (Figure 4–8b and c).

The ratio of cathodic to anodic current for the new wave **I´** was found to be one and the difference E_{pc}-E_{pa} was 60 mV, which is close to a reversible system (59 mV) having Nernstian behaviour. The wave **I´** showed a linear dependence on the current height with the scan rate (Figure 4–8d, Figure 4–9a). Applying Nicholson-Shain criteria revealed an $E_{rev}C_{cat}$ mechanism for the electrode kinetics of wave **I´**(Figure 4–9b).

It has been reported earlier that the solutions of dimethylpyrazinium tetrafluoroborates can be stabilised in water containing trifluoroacetic acid.[182] Thus, the stability of pyrazinium salt **167b** (0.4 mM) was investigated in aqueous solution containing varying concentrations of

sulphuric acid (10 mM-10 M). The degradation was followed qualitatively by recording changes in colour observed over a period of time and comparing it with the sample containing only acetonitrile. Solutions with high concentration of acid (between 2 M-10 M) were stable even after 2 weeks time (no visible colour change was observed). Interestingly, the solutions were colourless in sulphuric acid solution in contrast to pure acetonitrile solution that changed to green after 1 h (and showed precipitation of material after 2 weeks). Solutions containing 0.5 -1 M sulphuric acid showed a slight green colouration after 4 h, while solutions containing lower concentrations (0.1 M-10 mM) showed an immediate green colouration (greener than the pure acetonitrile solution), which darkened with time. A precipitation was observed in solutions with lower concentrations of the acid.

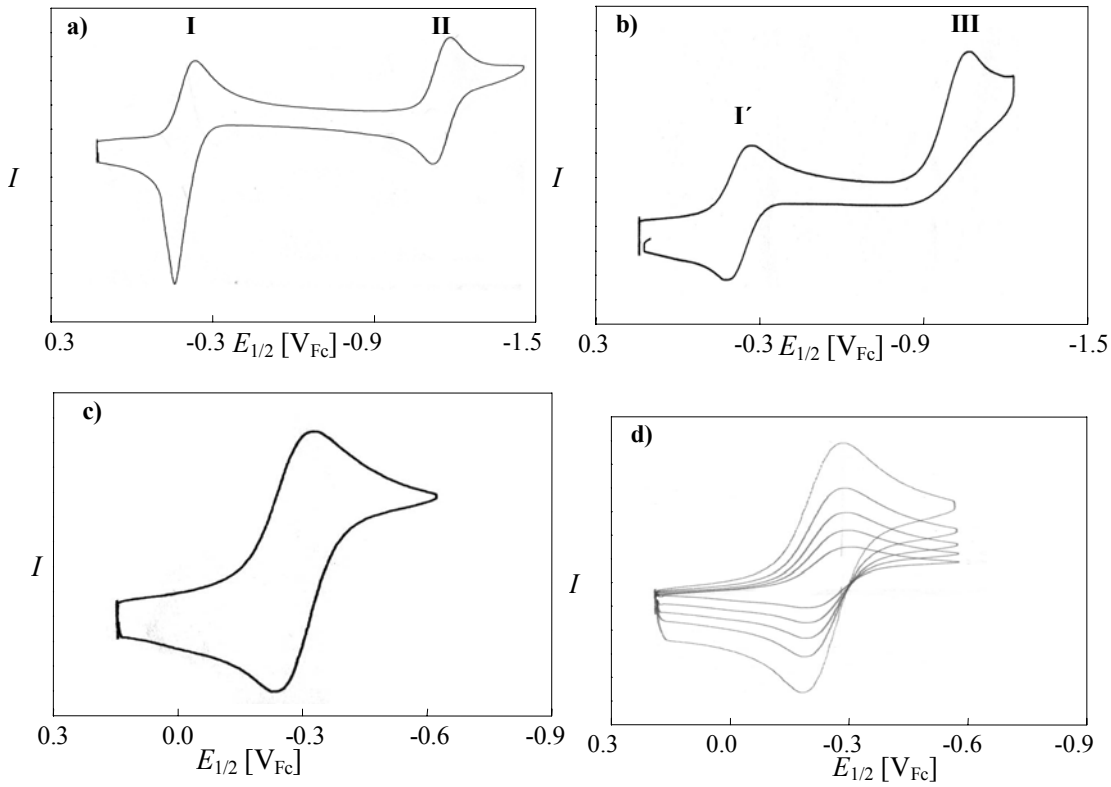

Figure 4–8: Cyclic voltammograms of **167b** (3.5 mM) in acetonitrile, a) after addition of 60 eq. of water, b) after 2000 eq. of water, showing the new wave I´, c) 2000 eq. water (I´) after 45 min, d) effect of scan rate on the peak current of I´ (20, 50, 100, 200 and 500 mV/s).

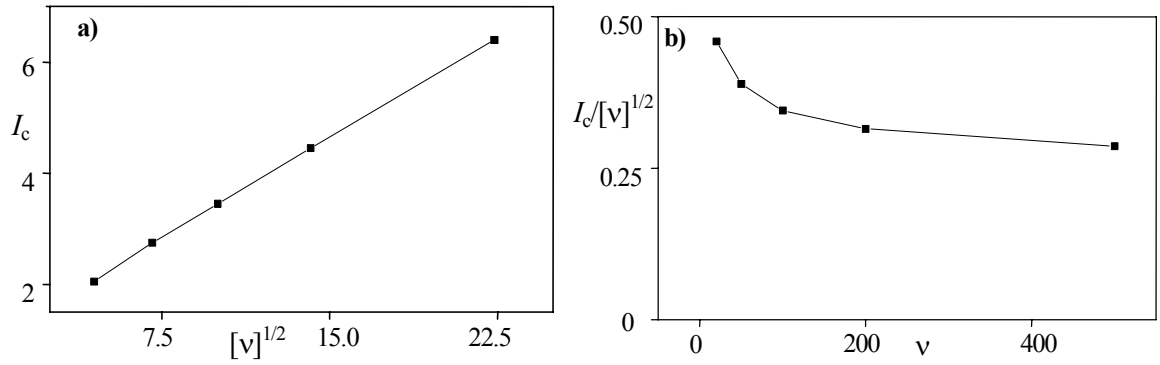

Figure 4–9: Scan rate dependence of wave I´ a) plot of cathodic current against the square root of scan rate, and b) plot of current function (cathodic current/square root of scan rate) against scan rate.

The stability of a solution of **167b** (0.5 M sulphuric acid) was monitored over a period of 11 h. The UV-Vis spectrum of the pyrazinium salt **167b** in sulphuric acid had a λ_{max} = 319 nm, which is similar to the one measured in dichloromethane (λ_{max} = 317-318 nm).

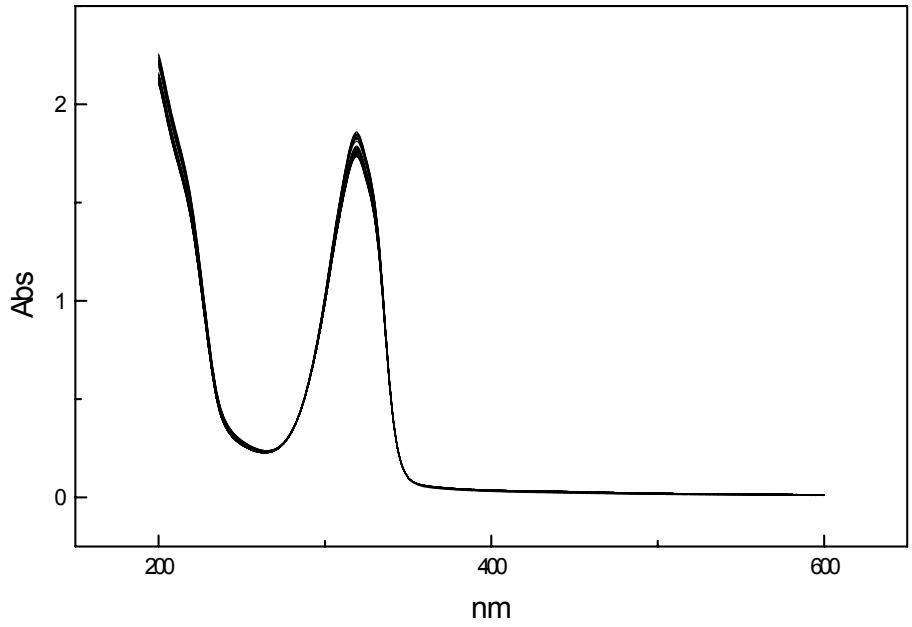

Figure 4–10: UV-Vis spectrum of **167b** in 0.5 M sulphuric acid. The spectrum is an overlay of 40 spectra measured over a period of 10 h with every measurement, every 15 min.

The UV-Vis spectral changes (Figure 4–10) were not very dramatic and indicate that the pyrazinium salt **167b** was quite stable to the above conditions in water.

4.4.1.7 Spectroelectrochemical Investigation

Spectroelectrochemical reduction of **167b** further confirmed the stability of all redox stages on the time scale of minutes (Figure 4–11). The recorded spectra showed two isosbestic points indicative for a clean conversion of the dication to radical cation. Upon further

reduction the completely reduced product emerged with no absorption above 250 nm.

An ESR spectrum of a fresh solution of **167d** in chloroform shows a multiplet with a g-value of 2.0032 typical for an organic compound (upper plot in Figure 4–12B). The multiplicity could arise due to the interaction of the radical cation with the hydrogen atoms and the methyl groups on the nitrogen. Within some hours a considerable broadening of the ESR spectrum was observed (lower plot Figure 4–12B) which could be due to intermolecular exchange broadening of radical cations coming close to each other. Such a process would depend on the extent of the radical cation aggregation into micelles and on temperature. ESR measurements on a sample **167c** kept for 1 year under cold condition further corroborated aggregate formation (Figure 4–12A). The solution was green and showed a broad spectrum with a line width of 2.2 mT (A).

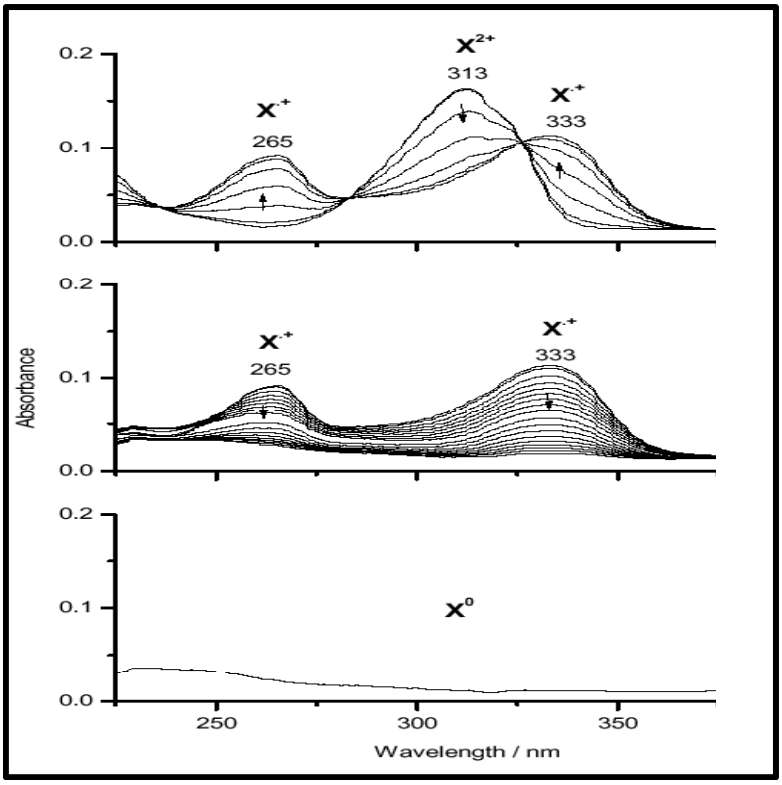

Figure 4–11: Spectroelectrochemical changes upon reduction of **167b** in acetonitrile.

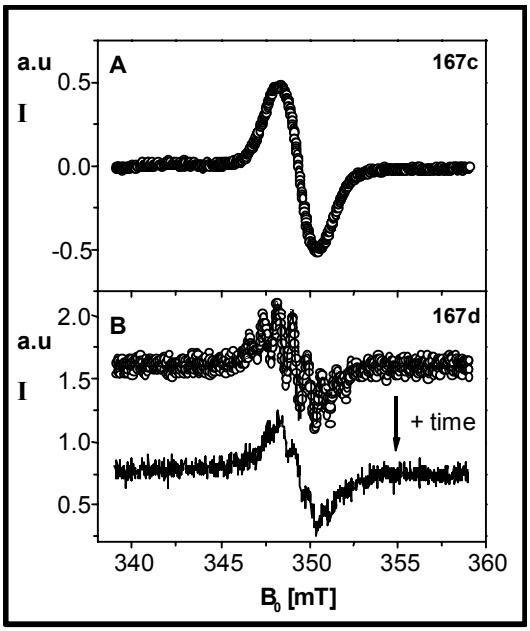

Figure 4–12: EPR spectrum of a) **167c** and b) **167d** in dichloromethane.

4.4.1.8 LB-Experiments

The most important tool for studying insoluble monolayers is the film balance method also called the Langmuir trough.[186] It consists of a temperature-controlled trough with the liquid called the "subphase" (usually water is used as a subphase). The lipids are dissolved in a volatile solvent (usually chloroform) which is immiscible with the subphase. Drops of the lipid solution are placed on the subphase, forming a lipid film after evaporation of the solvent. This process is called "spreading". The density of the molecules on the liquid surface can be balanced via movable barriers by compression or expansion.

The film pressure, also called the lateral pressure (π), is then defined as the difference between the surface tension of the bare subphase (γ_0) and the surface tension of the subphase covered with lipid (γ):

$$\pi = \gamma_0 - \gamma$$

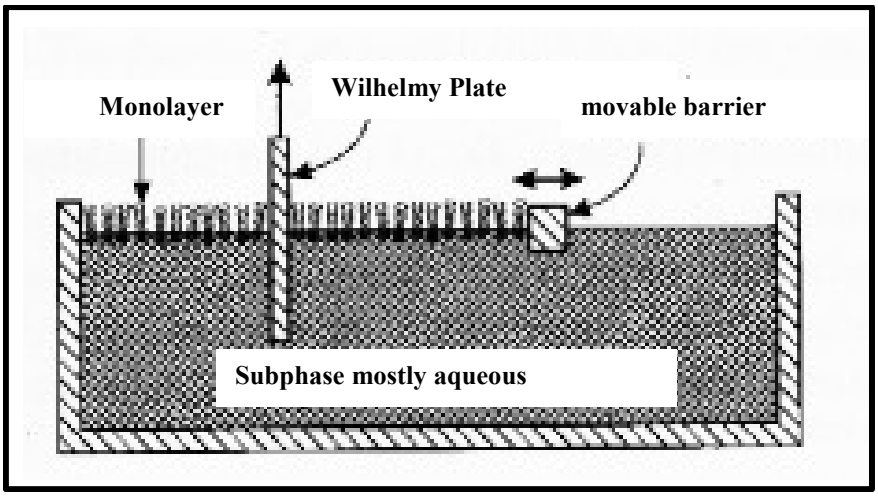

Figure 4–13: A typical Langmuir-trough depicting the subphase and a monolayer of amphiphilic molecules.

The film pressure is usually measured by the Wilhelmy plate method (Figure 4–13).[187] Molecular amphiphilic films show ordered phases that can be detected conveniently in the pressure-area isotherms (π-versus-σ_A).

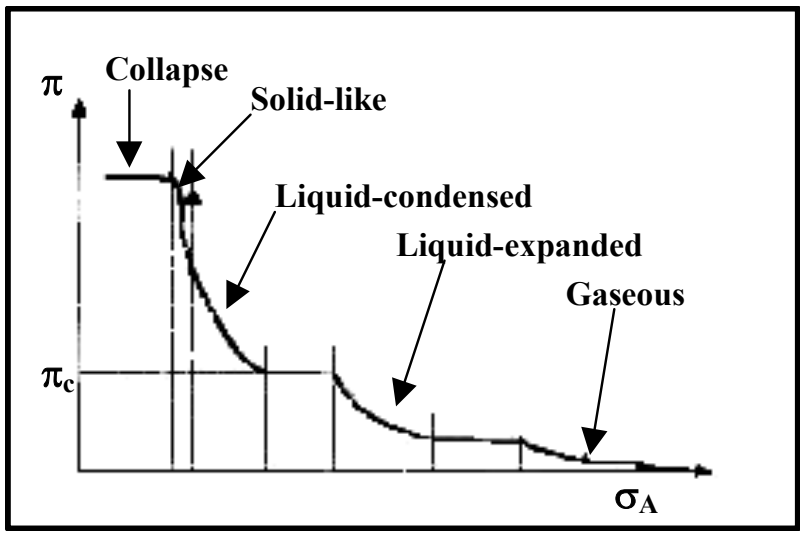

Figure 4–14: Typical plot representing the film pressure versus surface area per molecule showing the various phases.

The following phases have been observed for the fatty acids, phospholipids, etc., on water a) gaseous state (G, usually for large molecules), b) liquid (L) state usually characterised by a significant lateral interaction between the amphiphiles upon compression (first-order phase transition). It is characterised by two types, an expanded and a condensed phase. Moreover, there is the c) Solid state (S): characterised by a linear pressure-area isotherms. Extrapolation to zero film pressure results in an area corresponding to the molecular cross section (Figure 4–14).

4.4.1.9 Langmuir-Blodgett Film Balance Experiment for 167d

It was clear from the literature that the diquaternisation of pyrazines makes them very reactive towards water,[182] however, the radical cations of these quartenary salts have been a subject of intense investigation by EPR spectroscopy.[181] In order to apply **167d** as a redox switchable surfactant the phase behaviour of the quaternary salt **167d** was investigated with the well-known Langmuir-Blodgett (LB) technique. (Figure 4–15).

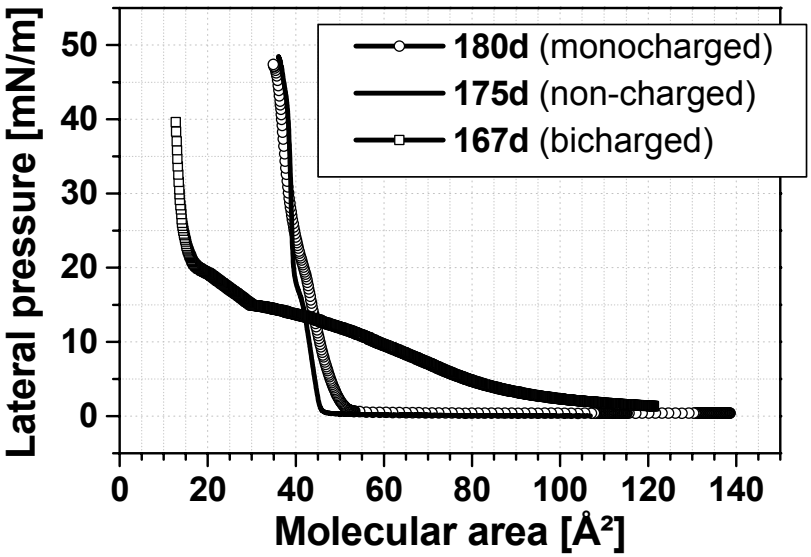

Figure 4–15: Film balance curve for **175d**, **167d** and **180d** obtained using the Wilhelmy plate method.

LB experiments were carried out in pure water at 20 °C. A solution of **167d** in dichloromethane of known concentration was spread over the aqueous layer. To our surprise it could be compressed to areas as low as 13 $Å^2$/molecule, passing two shoulders separated by a kink at 15 mN/m. A consecutive compression cycle shows a complete lack of the first broad shoulder but nearly the same smallest area. When a molar concentration of 1:1 salts such as NaCl was dissolved in the subphase the second shoulder develops into a plateau, entered via a sharp kink. In order to confirm that the behaviour is due to the radical cation of **167d**, quaternary monomethylated pyrazinium derivative **180d** was synthesised.

Langmuir-Blodgett film investigation for **180d** showed a steep isotherm with a low compressibility. The smallest area, which could be applied, was about 36 $Å^2$/molecule. Consecutive compression-expansion cycles showed complete reversibility in the isotherms. Isotherms for **175d** were also measured and were found to be nearly the same as **180d**. However, irreversible collapse at highest pressure (50 mN/m) was observed.

The series of LB-experiments on **175d**, **167d** and **180d** showed that the monocharged pyrazinium salt has amphiphilic character, most suitable to form an insoluble monolayer

similar to the ones known form lipids. The non-charged **175d** also tended to form an insoluble monolayer, but due to the missing charge in the head-group it showed a reduced tendency to stay coupled to the air-water interface, as the monolayer collapsed at high pressures. The most interesting and intriguing case is the one of **167d**, which would not exist as the dicationic form when exposed to water. The radical cation **167d**$^{+\bullet}$ would have had a similar behaviour as **180d**. The unusual behaviour of **167d** suggested that it may not be very stable to water and may be attacked by a nucleophile. It might even undergo disproportionation into the neutral species and the dication which would not allow the system to stabilise on the air-water interface. Film-balance experiments of **167d** in solutions containing sulphuric acid are in progress and would probably provide a useful insight into the film behaviour of these systems in acidic aqueous solutions.

4.4.1.10 Langmuir-Blodgette Film Balance Experiment on Ferrocene Based Electroactive Surfactant

Preliminary results of film-balance experiments carried out on **173** and **174** reveal that **173** (Figure 4–16a) forms a stable monolayer in pure water than **174** (Figure 4–16b). In **174** a broad wave was observed upon compression below a molecular area of 60 Å^2 and a complete collapse was observed below an area of 20 Å^2. Further investigations on the monocharged **173**$^{+\bullet}$ and **174**$^{+\bullet}$ is in progress.

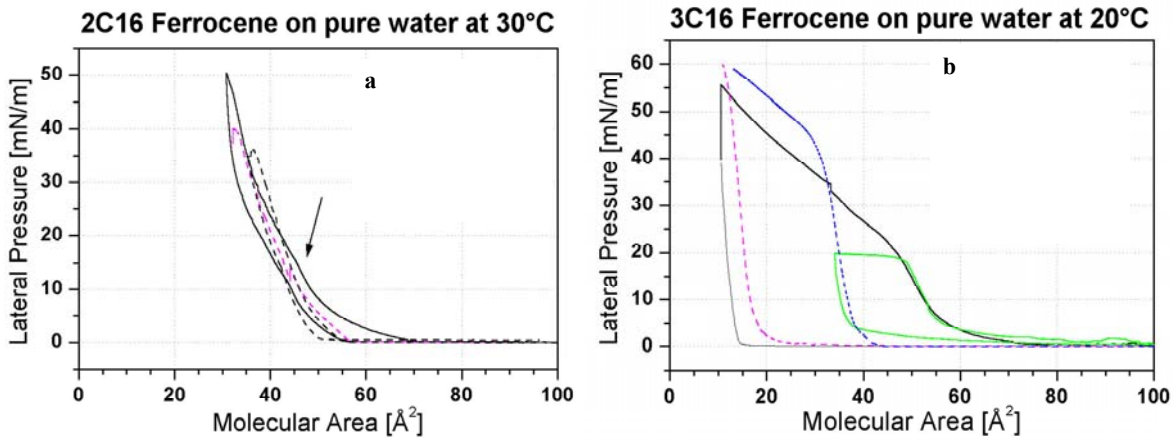

Figure 4–16: Film-Balance curves obtained for a) **173** and b) **174** with water as subphase.

4.5 Discussion and Conclusion

With the potential application of diquaternary ammonium salts in mind for material science, a number of systems having this feature have been synthesised and their chemical, stability and electrochemical properties have been investigated. Except for the viologen derivatives that are diquarternary salt, most of the quaternary ammonium salts that have found application are singly charged.

Although *N*,*N*′-dimethylpyrazinium and their benzannulated derivatives are known for quite sometime,[181] attempts to gain insight in their stability has usually been described as complex and confusing. While our results in nonpolar and aprotic solvents (cyclic voltammetry and UV-Vis. studies) are in good agreement with the earlier reports, the stability of these diquarternary salts in water was not well understood. Cyclic voltammetric investigation involving serial addition of water to a solution of **167b** in acetonitrile clearly showed that upon addition of water (excess) the first reduction wave shifts slightly, indicating formation of a newly formed dicationic species (**I**′). Further going to the cathodic side showed an irreversible reduction wave (**III**).

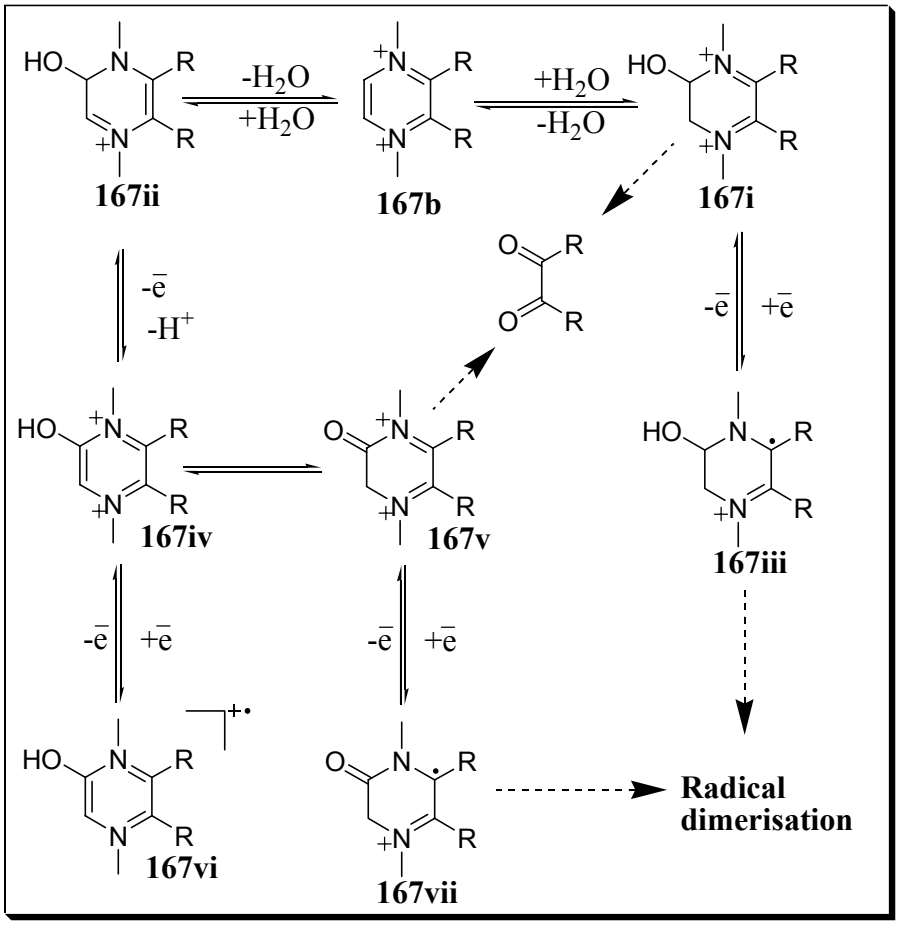

A nucleophilic attack of water on **167b** would lead to **167i** or **167ii**. **167i**, which is again a dicharged species, can lead to **167iii** upon one-electron reduction. The distonic radical cation **167iii** can undergo radical dimerisation or can be reduced to **167i**. One-electron oxidation of **167ii** followed by deprotonation would lead to **167iv**, which is a modified diquarternary pyarzinium salt. It can also show a similar behaviour as the parent diquaternary salt **167b**. Tautomerisation of **167iv** would give **167v** which would have a behaviour similar to **167ii** under electrochemical conditions.

^{1}H-NMR investigations indicate that upon addition of large excess of water (compared to the amount of pyrazinium salt) to **167b** an immediate formation of the diketone was observed, indicating that the most predominant pathway for degradation of **167b** is via **167i** rather than **167ii**. The reversible wave (**I´**) obtained after addition of excess of water to **167b** could be due to hydrogen bonded **167b** rather than **167vi**. This is further indicated by a decrease in the cathodic current with time (the cathodic current is decreased almost by 80-85% over a period of 18 h). The irreversible reduction wave (**III**) observed at higher cathodic potential could be due to the reduction of **167ii**.

Isolation of the diketone **176b** further confirmed that the main pathway for the degradation of pyrazinium salts in water is simple hydrolysis rather than radical cationic intermediates as previously suggested. This was further expressed in the film balance experiments on **167d**. Thus, for the first time it was possible to follow the degradation of diquarternary salts of pyrazine.

Radical cation stability of **167a-d** was found to be very high ($K_c = 10^{16}$-10^{20}) in non-polar or aprotic solvents they probably are not the important species in protic solvents or water. The LB-Film balance experiments on **167d** further confirmed our observeration. If the radical cation **167d**$^{+\bullet}$ was stable in water it would have given a stable and reversible monolayer. Instead the film balance experiment of **167d** was very complex showing a broadening and had a very low surface to area (13 Å/molecule) per molecule. The pyrazine derivative **175d** and the monocharged pyrazinium salt **180d** on the other hand formed a stable monolayer, the behaviour was similar to the arachidic acid (standard used).

The stability experiments in acidic solution however, clearly show that *N*,*N´*-dimethyl-2,3-dialkylpyrazinium tetrafluoroborates are stable and hence any practical applications of these pyrazinium salts would be limited to acidic solution below pH = 2.

With the limited application of pyrazinium tetrafluoroborates we further went on with the search of new electroactive materials for nanotechnological approach. The stable redox property of ferrocene makes it suitable for nanotechnological applications. Thus we designed

ferrocene based electroactive surfactants. The main advantage being in the fact that unlike diquaternary salts of pyrazine, ferrocene the surfactant would be neutral hence would have more pH tolerance. A number of ferrocene based electroactive surfactants **172-174** were synthesised by a simple esterification method of alcohols bearing ferrocenyl unit. A strong shift of the C=O bond stretching from 1728 to 1848 cm^{-1} in the IR was observed. LB-Film balance experiments indicated that the surfactant **173** showed a normal behaviour like the standard (arachidic acid), while an unusual behaviour for **174** was observed. The film balance experiment showed a broadening of the monolayer at low lateral pressure, however as the lateral pressure is increased the film collapsed. A clear understanding of which could be gained only after further experimentation.

4.6 Future perspective

The above results clearly indicate that diquarternary salts of pyrazinium derivatives cannot be applied for achieving electrowetting phenomenon on microchips. The main disadvantage of the above systems is their chemical stability (both the dication and the radical cation). However, ferrocene, thiafulvene or TCNQ based systems can provide systems that are not only electrochemically stable but also provide chemically stable redox states. Use of mixed valence compounds such as bisferrocene can also be used for modulating the wetting properties of surfaces.

5 Experimental Section

5.1 Instruments Used

Melting Point

Melting points of all the solids were determined on a Büchi SMP-20 (all the melting points are uncorrected).

IR-spectroscopy

Spectrometer 1750 FT-IR (Perkin-Elmer) was used for IR measurements. All the IR data are expressed in cm^{-1} and the intensities for the signals have been described, for eg. s (strong), m (medium), w (weak) etc.

UV-Vis spectroscopy

UV-Vis spectrometer Tidas II (J&M). All the kinetic measurements were carried out using an external optical dip probe. For preparing the solutions HPLC grade solvents were used (dried/distilled or degassed whenever required).

^{1}H, ^{13}C-NMR and DEPT-135 characterisation

^{1}H, ^{13}C-NMR and DEPT experiments were carried out on 200 MHz and 400 MHz machines (Bruker). All proton NMR spectras were calibrated to 7.26 ppm using $CDCl_3$, and the ^{13}C-NMR spectras were calibrated to 77.0 ppm. Appropriate calibration was done for other solvents.

Crystal structure analysis

Single crystal X-ray analysis was made in collaboration with Prof. H.-J. Deiseroth, M. Schlosser, J. Schlirf at University of Siegen and Dr. U. Florke from University of Padderborn. The machine used at Uni-Siegen was a STOE IPDS (Stoe Oxford cryostream 500).

Solvents for synthesis and chromatography

All the solvents used for synthesis and chromatography were predistilled before use (drying and degassing was carried out whenever required). Dry ether was prepared by distilling it over sodium wire under nitrogen atmosphere. Dry THF and benzene were prepared by distilling it over potassium under nitrogen atmosphere. Dry toluene was prepared by distilling the solvent over sodium in an inert atmosphere. Dry 1,2-dichloroethane and 1,2-dimethoxyethane were prepared by freshly distilling these solvents over calcium hydride.

Solvents for cyclic voltammetry

Dry DCM and acetonitrile were prepared by distilling the solvents over phosphorous pentoxide.

Cyclic voltammetry

CV measurements were carried out with a three electrode cell containing a platinum working electrode, a platinum counter electrode and a silver wire as *pseudo* reference electrode. All potentials are expressed with respect to ferrocene ($E_{1/2}$ =0.63 V_{NHE}, 0.39 V_{SCE}). Tetra-*n*-butylammonium hexafluorophosphate was used as electrolyte. In addition to ferrocene, tris-*p*-bromophenylamine and decamethylferrocene were also used as standards (only when the ferrocene was found to shift the potentials of the substrate waves).

Laser-Flash photolysis

LFP experiments were carried out in collaboration with Dr. G. Bucher from the University of Bochum. An inhouse assembled system was used for investigations.

Pulse-Radiolysis investigations

Pulse radiolysis investigations were carried out in collaboration with Dr. T. Mukherjee and Dr. S. Adhikari at Bhabha Atomic Research Centre, Mumbai, India. For preparing solution for pulse radiolysis, typically, a millimolar solution of the substrate was prepared in water (or a water acetonitrile mixture [15%]) and sonicated for 15 min. The solutions were then purged with N_2O for 30-45 min before making the measurements. Each sample was maximum exposed at best twice to the beam.

Enzyme investigations

Enzymatic investigation with Coenzyme B_{12} dependent diol and glycerol dehydratase were carried out in collaboration with Prof. J. Rétey at University of Karlsruhe. The enzymes were first overexpressed in *E. Coli*. Pure enzymes were obtained after a single HPLC purification. The enzymes were found to be stable to air and required 1,2-propanediol as the substrate.

Enzymatic investigations with phenoxyethanol dehydratase were carried out in collaboration with Prof. B. Schink and Britta Müller at University of Konstanz. The enzyme was obtained by harvesting the cells (after achieving a certain growth). The cells after centrifugation were resuspended in a phosphate buffer (pH 7.5) containing titanium citrate. The cells were then crushed under inert atmosphere using the French press technique. The crushed cells were then centrifuged to give the supernatant the “cell free extract”. The cell free extract was used as such without any further purification as the enzyme was found to be very unstable and decomposing completely within 12-15 hrs. All enzyme assays were prepared in an anoxic chamber. Due to the presence of titanium citrate the solubility of the enzyme probes designed for the investigations showed a decrease in solubility, especially with ferrocene containing probes. Thus, a small amount of ethanol was used to dissolve the compound in water. Then the solution was warmed to 50 °C for about 25-30 min. The supernatant was used for investigations. To check for the effect of ethanol, a similar quantity of ethanol was added to

solutions with a probe and the assay was made.

5.2 Synthesis

5.2.1 4-Ferrocenyl-1,2-dihydroxybutane (ML01161)

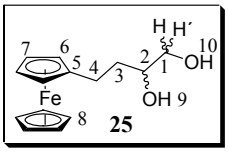

25

A solution of **30** (100 mg, 277 μmol) and palladium over charcoal (30.0 mg, 10% Pd) in 10 ml of methanol were stirred at room temperature under hydrogen pressure of 5-7 bar for 12 h. The reaction mixture was filtered concentrated. The crude product was purified by column chromatography with hexane:ether (50%) as eluent.

Yield: 62.4 mg (2.28 mmol) of a yellow solid, 82%.

Melting point: 92 °C (Lit:[188] 80-90 °C).

IR (KBr): $\tilde{\nu}$ (cm^{-1}) = 3327 (sb, OH), 2931 (s, CH), 2872 (m, CH), 1640, 1454, 1396, 1333, 1302, 1231, 1104, 1070, 1022, 997, 920, 875, 831, 806, 557, 510, 489.

^{1}H-NMR ($CDCl_3$, 400 MHz): δ (ppm) = 1.53-1.62 (m, 2H, 3-H), 1.81 (t, ^3J = 5.4 Hz, 1H, OH, 10-H), 2.05 (d, ^3J = 3.9 Hz, 1H, OH, 9-H), 2.31-2.39 (m, 1H, 4-H), 2.43-2.50 (m, 1H, 4-H), 3.37-3.41 (m, 1H, 1-H), 3.57-3.61 (m, 1H, 1′-H), 3.65-3.68 (m, 1H, 2-H), 3.99-4.04 (m, 9H, 6,7,8-H).

^{13}C-NMR ($CDCl_3$, 100 MHz): δ (ppm) = 26.0 (C-3), 34.9 (C-4), 67.2 (C-1), 67.7 (C-2), 68.3 (C-7), 68.6 (C-6), 68.93(C-8), 88.7 (C-5).

DEPT-135 ($CDCl_3$, 100 MHz): δ ppm = Positive signals: 67.7 (C-2), 68.3 (C-7), 68.6 (C-6), 68.9 (C-8), 72.3. Negative signals: 26.0 (C-3), 34.9 (C-4) and 67.2 (C-1) with disappearance of signals at 88.7 (C-5) as expected for a quaternary carbon.

Mass: (EI, 70 eV): (m/z) = 274 ($M^{+\bullet}$)

ESI-MS: (m/z) = 274 ($M^{+\bullet}$)

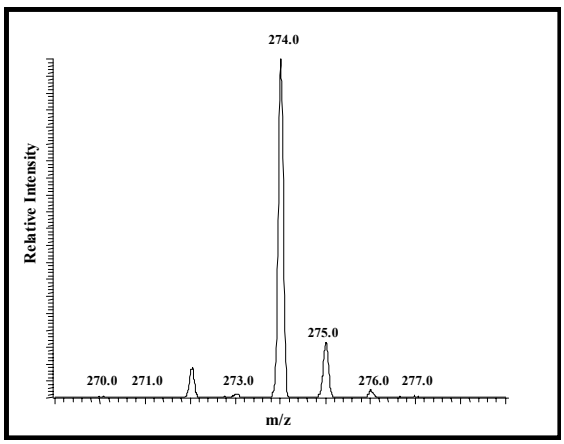

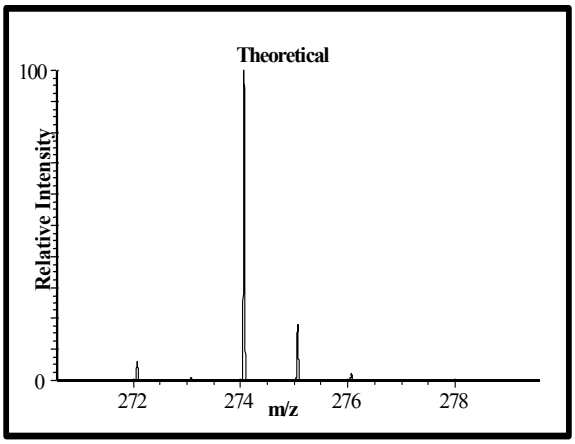

Elemental analysis: Calculated C = 61.34, H = 6.62
Found C = 61.26, H = 6.59

5.2.2 3-Ferrocenylpropan-1,2,3-triol (ML02062.1)

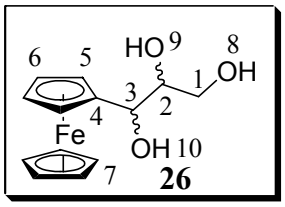

A solution of **61** (300 mg, 949 µmol) and H_2SO_4 (2 ml, 0.1 M) in 20 ml methanol was stirred at room temperature for 5 min. The reaction mixture was neutralised with saturated $NaHCO_3$ (10 ml) solution and extracted with ether. The combined organic layer was concentrated and chromatographed with hexane ether (40:60) as eluent yielding a red coloured oil.

Yield: trace of red oil sufficient for ^{1}H-NMR.

^{1}H-NMR ($CDCl_3$, 200 MHz): δ (ppm) = 3.43 (s, 2H, OH), 3.53 (s, 1H, OH), 3.68-4.03 (m, 4H, 1,2,3-H), 4.16 (s, 5H, 7-H), 4.18 (s, 4H, 5,6-H).

5.2.3 5-Ferrocenylpent-4-yne-1,2,3-triol (ML02063)

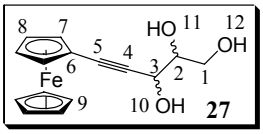

A solution of **31** (260 mg, 760 µmol) and H_2SO_4 (2 ml, 0.1 M) in 20 ml methanol was stirred at room temperature for 5 min. The reaction mixture was neutralised with saturated $NaHCO_3$ (10 ml) solution and extracted with ether. The combined organic layer was concentrated and chromatographed with hexane ether (40:60) as eluent yielding a red coloured solid.

Yield: 194 mg (0.650 mmol) of a red solid, 80%.

Melting point: 70 °C.

IR (KBr): $\tilde{\nu}$ (cm^{-1}) = 3369 (b, OH), 2227 (s, C≡C), 1655 (w, CH), 1410, 1105, 1067, 1025, 1001, 812, 486.

^{1}H-NMR ($CDCl_3$, 200 MHz): δ (ppm) = 3.50 (s, 1H, OH), 3.81-3.99 (m, 4H, 1,2,3-H), 4.19 (s, 2H, 8-H), 4.24 (s, 5H, 9-H), 4.5 (s, 2H, 7-H).

^{13}C-NMR ($CDCl_3$, 50 MHz): δ (ppm) = 64.3 (C-1,1´), 64.8 (C-2,2´), 66.1 (C-3,3´), 69.7 (C-8), 69.9 (C-8′), 70.9 (C-9), 71.1 (C-9′), 72.5 (C-7), 72.6 (C-7´), 74.9 (C-6), 76.2 (C-6´), 83.7 (C-4), 84.1 (C-4´), 86.7 (C-5), 87.0 (C-5´).

Mass (EI, 70 eV): (m/z) = 300 ($M^{+\bullet}$)

ESI-MS: (m/z) = 300.1 ($M^{+\bullet}$)

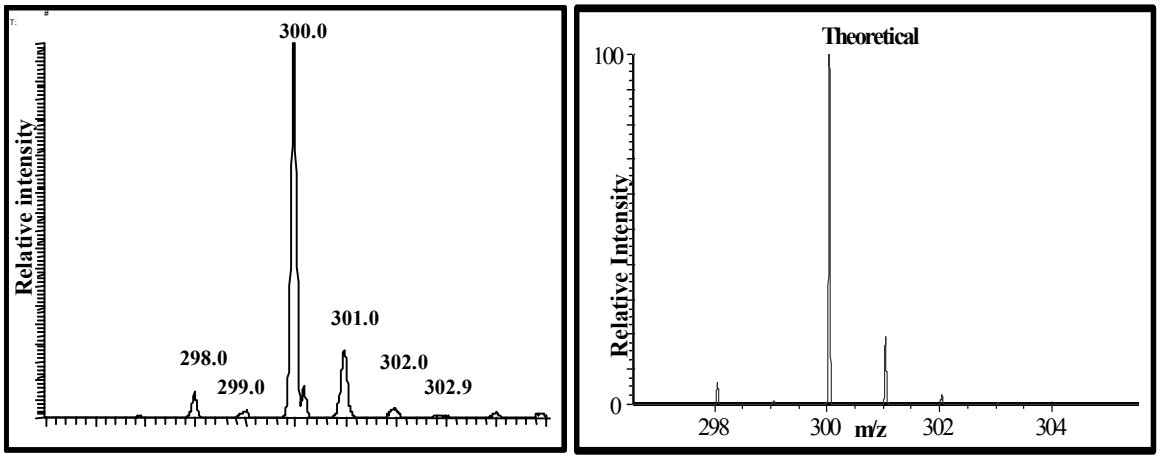

HRMS: Calculated for $C_{15}H_{16}FeO_3$: 300.045, Found: 300.046 ($M^{+\bullet}$)

5.2.4 5-Ferrocenylpentane-1,2,3-triol (ML02057)

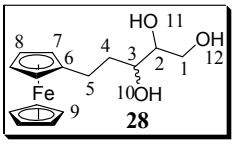

28

A solution of **59** (260 mg, 755 µmol) and H_2SO_4 (2 ml, 0.1 M) in 20 ml methanol were stirred at room temperature for 5 min. The reaction mixture was neutralised with saturated $NaHCO_3$ (10 ml) solution and extracted with ether. The combined organic layer was concentrated and chromatographed with hexane ether (60:40) as eluent, yielding a yellow solid as a mixture of diastereomers in equal amounts as characterised by ^{1}H-NMR

Yield: 184 mg (0.60 mmol) of a yellow solid, 80%.

Melting point: 71 °C.

IR (KBr): $\tilde{\nu}$ (cm^{-1}) = 3396 (b, OH), 3019 (s, CH), 2932 (w, CH), 1413, 1216, 1105, 1075, 1042, 1002, 927, 755, 669.

^{1}H-NMR ($CDCl_3$, 200 MHz): δ (ppm) = 1.57 (bs, 2H, 4-H), 2.35 (m, 2H, 5-H), 3.44 (m, 4H, 1,2,3-H), 4.19 (m, 12H, 7,8,9-H, OH).

^{13}C-NMR ($CDCl_3$, 50 MHz): δ (ppm) = 26.6 (C-4), 27.0 (C-4´), 35.3 (C-5), 35.9 (C-5´), 64.1 (C-1), 65.6 (C-1´), 68.4 (C-2), 68.5 (C-2´), 69.0 (C-3), 69.4 (C-3´), 69.7 (C-9, 9´), 73.0 (C-8), 74.1 (C-8´), 75.1 (C-7,7´), 88.5 (C-6, 6´).

Mass (EI, 70 eV): (m/z) = 304 ($M^{+\bullet}$)

ESI-MS: (m/z) = 304 ($M^{+\bullet}$)

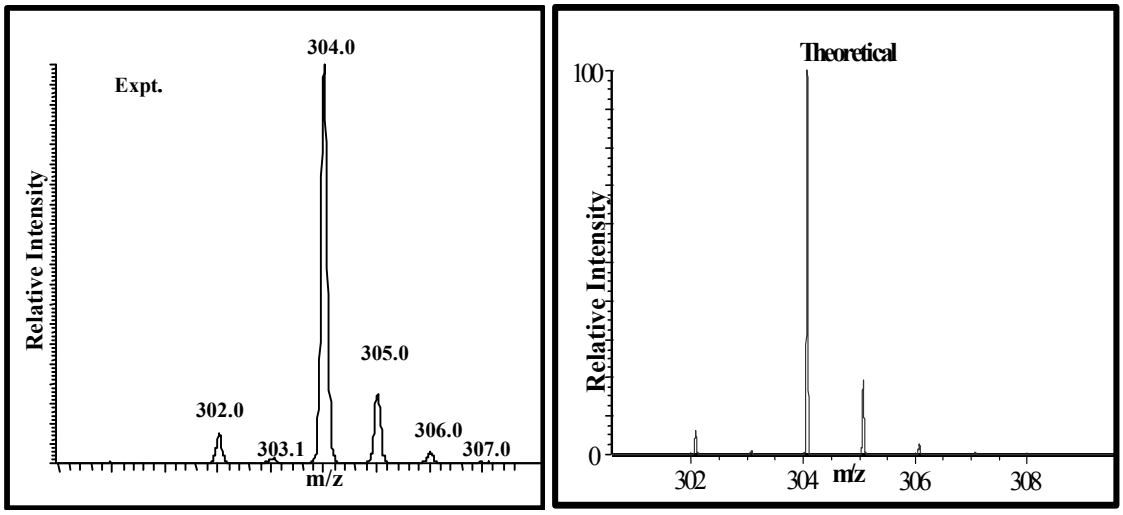

HRMS Calculated for $C_{15}H_{20}FeO_3$: 304.0762, Found: 304.0760 ($M^{+\bullet}$)

5.2.5 1,2-Diferrocenylethane-1,2-diol (ML01135)

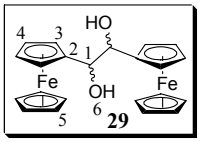

To ferrocenealdehyde (150 mg, 700 μmol) in 10 ml of THF, a solution of samarium iodide in THF (17.5 ml, 1.75 mmol) was added over a period of 20 min. After 30 min the reaction mixture was quenched with 10 ml of saturated ammonium chloride solution and extracted with ether (4 × 25 ml). The combined organic layer was dried over Na_2SO_4 (anhyd.) and concentrated at room temperature.

Yield: 140 mg (330 μmol) of a yellow solid, 93%.

Melting point: 71 °C

IR (KBr)**:** $\tilde{\nu}$ (cm^{-1}) = 3406 (b, OH), 3084 (s, CH), 2908 (w, CH), 1657, 1401, 1251, 1050, 923, 813, 490.

^{1}H-NMR ($CDCl_3$, 200 MHz): δ (ppm) = 2.55, (s, 1H, 6-H, OH), 3.90, (m, 1H, 1-H), 4.07-4.32 (m, 9H, 3,4,5-H).

Mass (EI, 70 eV): (m/z) = 430 ($M^{+\bullet}$).

Elemental analysis: Calculated C = 61.44, H = 5.16

Found C = 61.35, H = 5.18

5.2.6 1-Benzyloxy-4-ferrocenyl-but-3-yne-2-ol (ML01115.12)

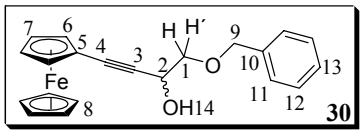

32 (700 mg, 3.30 mmol) dissolved in 15 ml of THF was added to ethylmagnesium bromide prepared from ethyl bromide (250 µl, 3.30 mmol) and magnesium (80.0 mg, 3.30 mmol) in 2 ml dry THF. After 15 minutes benzyloxyacetaldehyde (500 mg, 3.30 mmol) was added, and the reaction was monitored by TLC. It was quenched with saturated ammonium chloride solution (10 ml) after 30 min and extracted with ether (3 × 25 ml). The combined organic layer was dried over Na_2SO_4 (anhyd.) and concentrated. The crude product was purified by column chromatography with hexane:ether (80:20) as eluent.

Yield: 1.01 g (2.81 mmol) of a brown solid, 84%.

Melting point: 84-85 °C (recrystallised from hexane).

IR (KBr): $\tilde{\nu}$ (cm^{-1}) = 3391 (b, OH), 3112 (w, CH), 2924 (w, CH), 2860 (m, CH), 2226 (m, C≡C), 1493, 1453, 1366, 1257, 1103, 1078, 1010, 953, 833, 813, 741, 697, 613.

^{1}H-NMR ($CDCl_3$, 200 MHz): δ (ppm) = 2.56 (d, J = 4.7 Hz, 1H, OH, 14-H), 3.61 (dd, ^2J = 9.8 Hz, ^2J = 20.7 Hz, 1H, 1-H), 3.69 (dd, ^2J = 9.8 Hz, ^3J = 17.2 Hz, 1H, 1´-H), 4.17- 4.19 (m, 7H, 7,8-H), 4.41 (t, ^3J = 2.0 Hz, 2H, 6-H), 4.66 (s, 2H, 9-H), 4.68 (m, 1H, 2-H), 7.33 (m, 5H, 11,12,13-H).

^{13}C-NMR ($CDCl_3$, 50 MHz): δ (ppm) = 63.3 (C-2), 69.7 (C-6), 70.9 (C-8), 72.5 (C-7), 73.0 (C-5), 74.4 (C-1), 74.8 (C-9), 84.0 (C-3), 85.4 (C-4), 128.8 (C-11), 128.9 (C-13), 129.5 (C-12), 138.7 (C-10).

DEPT-135 (CDCl3, 50 MHz): δ (ppm) = Positive signals: 63.3 (C-2), 69.7 (C-6), 70.9 (C-8), 72.5 (C-7), 128.8 (C-11), 128.9 (C-13), 129.5 (C-12). Negative signals: 74.4 (C-1), 74.8 (C-9). Signals at 84.0 (C-3), 85.4 (C-4) and 138.7 (C-10) disappeared as expected for quaternary carbons.

Mass (EI, 70 eV): (m/z) = 360 ($M^{+\bullet}$)

ESI-MS: (m/z) = 360.1 ($M^{+\bullet}$)

Elemental analysis: Calculated C = 70.02, H = 5.06

Found C = 70.04, H = 5.70

5.2.7 1-Ferrocenyl-4,5-isopropylidene-pent-1-yne-3-ol (ML02042.2)

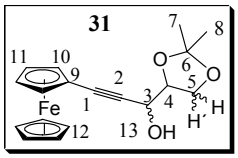

32 (760 mg, 3.62 mmol) in 15 ml of THF was added to ethyl magnesium bromide in 3 ml of dry THF, prepared from ethyl bromide (430 mg, 3.95 mmol) and magnesium (100 mg, 3.99 mmol). After 15 minutes [D]-2,3-isopropylidene glyceraldehyde (470 mg, 3.62 mmol)

was added. The reaction was monitored by TLC, quenched with saturated ammonium chloride solution (10 ml) and extracted with ether (3 × 25 ml). The combined extracts were dried over Na_2SO_4 (anhyd.) and concentrated. The crude product was purified by column chromatography with hexane:ether (80:20) as eluent, yielding a mixture of diastereomers in 1 : 0.8 ratio based on ^{1}H-NMR characterisation.

Yield: 820 mg (241 mmol) of a brown solid, 67%.

Melting point: 95 °C.

IR (KBr): $\tilde{\nu}$ (cm^{-1}) = 3389 (b, OH), 3088 (w, CH), 2987 (m, CH), 2231 (m, C≡C), 1762, 1458, 1376 (s), 1252, 1218, 1065, 841, 813, 523, 482.

^{1}H-NMR ($CDCl_3$, 200 MHz): δ (ppm) = 1.40 (s, 6H, 7,7′-H), 1.49 (s, 3H, 8-H), 1.52 (s, 3H, H-8′), 2.64 (dd, ^3J = 4.4 Hz, 1H, OH, 13-H), 2.70 (d, J = 4.18 Hz, 1H, 13′-OH), 3.92 (d, J = 5.16 Hz, 1H, 5-H), 3.98 (d, J = 5.16 Hz, 1H, 5′-H), 4.08-4.15 (m, 2H, 5,5′-H), 4.19 (s, 7H, 11,12-H), 4.20 (s, 7H, 11′,12′-H), 4.22-4.35 (m, 2H, 4,4′-H), 4.40 (s, 4H, 10,10′-H), 4.60 (t, J = 4.3 Hz, 2H, 3,3′-H).

^{13}C-NMR ($CDCl_3$, 50 MHz): δ (ppm) = 26.3 (C-7), 26.4 (C-7′), 27.5 (C-8), 27.9 (C-8′), 64.1 (C-3), 64.2 (C-3′), 64.8 (C-4), 65.0 (C-4′), 67.2 (C-5), 69.7 (C-5′), 69.8 (C-10), 69.9 (C-10′), 70.8, 70.9 (C-12), 71.0 (C-12′), 72.4 (C-11), 72.6 (C-11′), 79.1 (C-9), 80.0 (C-9′), (C-1), 83.5 (C-1′), 86.0 (C-2), 86.1 (C-2′), 111.1 (C-6), 111.4 (C-6′).

Mass (EI, 70 eV): (m/z) = 340 ($M^{+\bullet}$)

ESI-MS: (m/z) = 340.1 ($M^{+\bullet}$)

Elemental analysis: Calculated C = 63.55, H = 5.93

Found C = 63.54, H = 5.90

5.2.8 5-Ferrocenyl-1,2-isopropylidene-pentan-3-ol (ML02047)

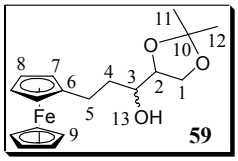

59

A solution of **31** (280 mg, 810 μmol) and palladium over charcoal (100 mg, 10% Pd) in 10 ml of methanol were stirred under hydrogen gas pressure 5-7 bar for 12 h. The reaction mixture was filtered and concentrated. The crude product was purified by column chromatography with hexane ether (80:20) as eluent yielding a yellowish brown liquid.

Yield: 260 mg (750 μmol) of a yellow liquid, 92%.

IR (KBr): $\tilde{\nu}$ (cm^{-1}) = 3477 (bs, OH), 3093, 2985, 2933, 1372, 1266, 1215, 1157, 1105, 856, 819, 737, 704.

^{1}H-NMR ($CDCl_3$, 200 MHz): δ (ppm) = 1.35 (s, 3H, 12-H), 1.43 (s, 3H, 11-H), 1.46-1.73 (m, 2H, 4-H), 2.35-2.60 (m, 3H, 5-H, OH), 3.45-3.53 (m, 1H, 3-H), 3.63-3.77 (m, 1H, 2-H), 3.92-3.98 (m, 2H, 1-H), 4.04-409 (m, 9H, 7,8,9-H).

^{13}C-NMR ($CDCl_3$, 50 MHz): δ (ppm) = 26.3 (C-4), 26.4 (C-4′), 26.5 (C-11), 26.8 (C-11′), 27.5 (C-12), 27.7 (C-12′), 35.1 (C-5), 36.1 (C-5′), 65.7 (C-3), 67.1 (C-3′), 68.3 (C-2, 2′), 68.8 (C-1, 1′), 69.3 (C-9), 69.5 (C-9′), 71.3 (C-8), 72.7 (C-8′), 79.6 (C-7), 80.1 (C-7′), 89.3 (C-6), 89.4 (C-6′), 109.9 (C-10), 110.35 (C-10′).

ESI-MS: (m/z) = 344.2 ($M^{+\bullet}$)

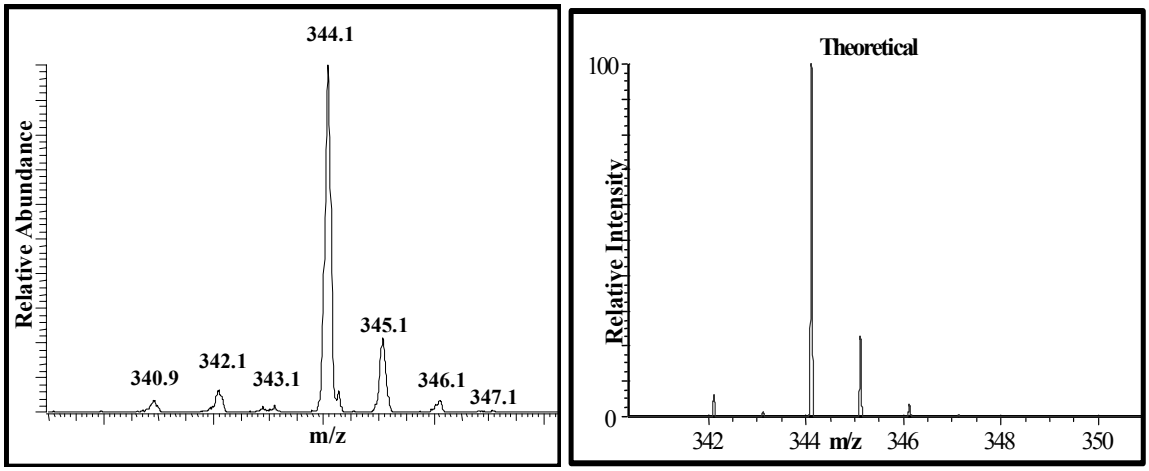

5.2.9 2-Benzyloxy-1-ferrocenylethan-1-ol (ML01119.2)

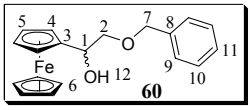

60

A solution of *tert.*-Butyllithium in hexane (2.90 ml, 4.30 mmol) was added slowly to ferrocene (930 mg, 4.90 mmol) in 20 ml dry THF. Benzyloxyacetaldehyde (470 µl, 3.30 mmol) was added after 15 minutes at room temperature. The reaction was monitored by TLC and quenched with saturated ammonium chloride solution (10 ml) and extracted with ether (3 × 25 ml). The combined organic layer was dried over Na_2SO_4 (anhyd.) and concentrated. The crude product was purified by column chromatography.

Yield: 360 mg (1.07 mmol) of a brown liquid, 32%.

^{1}H-NMR ($CDCl_3$, 200 MHz): δ (ppm) = 2.79 (d, *J* = 3.4 Hz, 12-H, OH), 3.56-3.72 (m, 2H, 2-H), 4.16-4.29 (m, 9H, 4,5,6-H), 4.61 (s, 2H, 7-H), 4.61 (m, 1H, 1-H), 7.30-7.38 (m, 5H, 9,10,11-H).

5.2.10 2,3-Isopropylidene-1-ferrocenylpropane-1-ol (ML01181)

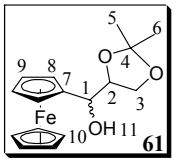

61

A solution of *tert.*-Butyllithium in hexane (6.70 ml, 16.7 mmol) was added slowly to ferrocene (2.15 g, 11.6 mmol) in 40 ml THF at 0 °C. [D]-2,3-Isopropylidene glyceraldehyde (1 g, 7.7 mmol) was added at room temperature after 15 min. The reaction was monitored by TLC and quenched with saturated ammonium chloride solution (15 ml) and extracted with ether (3 × 50 ml). The combined organic layer was dried over Na_2SO_4 (anhyd.) and concentrated. The crude product was purified by column chromatography with hexane:ether (20%) as the eluent.

Yield: 730 mg (0.23 mmol) of a brown solid, 30%.

IR (KBr): $\tilde{\nu}$ (cm^{-1}) = 3438 [1] (b, OH), 3016 (s, CH), 2989 (s, CH), 2936, 1455, 1382, 1373, 1216, 1156, 1066 (s, CH), 852, 759, 668.

^{1}H-NMR ($CDCl_3$, 200 MHz): δ (ppm) = 1.34 (s, 3H, 5-H), 1.37 (s, 3H, H-5′), 1.42 (s, 3H, 6-H), 1.44 (s, 3H, 6′-H), 2.24 (d, *J* = 2.5 Hz, 1H, OH), 2.45 (d, *J* = 3.5 Hz, 1H, OH), 3.68 (m, 6H, 2,2′,3,3′-H), 4.03 (s, 18H, 8,8′,9,9′,10,10′-H), 4.30 (m, 2H, 1,1′-H).

Elemental analysis: Calculated C = 60.78, H = 6.38

Found C = 61.19, H = 6.68

5.2.11 32-(2,3-Dihydroxy-propyl)-[1,4]benzoquinone (ML02054)

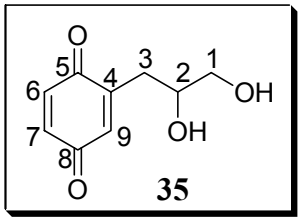

35

3-(2-Hydroxy-phenyl)-propane-1,2-diol (930 mg, 5.51 mmol) in 10 ml water was added to a solution of potassiumdihydrogen phosphate (3.80 g) in 150 ml water. Fremy′s salt (5.0 g) was added to the solution and after 1 hr the reaction mixture was saturated with ammonium sulphate. The resulting solution was extracted with ethylacetate (5 × 100 ml), the combined organic layer was dried over Na_2SO_4 (anhyd.) and concentrated. The crude product was obtained as deep red solid, and recrystallised from hot toluene.

Yield: 470 mg (2.58 mmol) of a yellow solid, 48% (recrystallised).

Melting Point: 79–80 °C (Lit**:**[63] 81–82 °C).

IR (KBr): $\tilde{\nu}$ (cm^{-1}) = 3327 (bs, OH), 2928 (m, CH), 2471 (s, CH), 1651 (vs, C=O), 1601, 1430, 1350, 1301, 1081, 1034, 1088, 913, 843, 630.

^{1}H-NMR (CD_3OD, 200 MHz): δ (ppm) = 2.24 (d, ^3J = 9.1 Hz, 1H, 1-H), 2.31 (d, ^3J = 9.1 Hz, 1H, 1-H), 2.60 (dd, ^2J = 1.2, ^3J = 2.7 Hz, 1H, 3-H), 2.67 (dd, ^2J = 1.2, ^3J = 2.7 Hz, 1H, 3-H), 3.18-3.21 (q, ^3J = 1.7 Hz, 1H, 2-H), 3.63-3.75 (m, 2H, OH), 6.61 (s, 1H, 9-H), 6.66-6.68 (m, 2H, 6,7-H).

^{13}C-NMR (CD_3OD, 50 MHz): δ (ppm) = 33.1(C-3), 65.7 (C-1), 70.0 (C-2), 133.8 (C-9), 135.8 (C-6), 136.5 (C-7), 146.1 (C-4), 187.3 (C-5), 187.6 (C-8).

Elemental analysis: Calculated C = 59.34, H = 5.53

Found C = 59.03, H = 5.53

5.2.12 3-3-(2-Hydroxy-phenyl)-propane-1,2-diol[63] (ML02048)

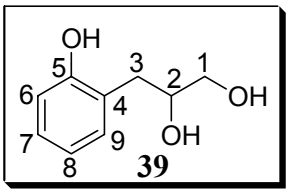

39

To a solution of hydrogen peroxide (81.6 ml, 30% solution in water) and formic acid (81.6 ml, 98%) maintained at 40-45 °C, 2-Allylphenylacetate (20.0 g, 120 mmol) was added dropwise over a period of 20 min. The temperature was held at 40 °C for 1 h, and the mixture was kept overnight at room temperature. The solvent was removed and the residue was heated with solution of sodium hydroxide (10 g) in water (150 ml). The solution was cooled and acidified to pH 1, and then extracted with ethylacetate (4 × 150 ml). The combined organic layer was washed with $NaHCO_3$ (3 × 100 ml), dried over Na_2SO_4 (anhyd.) and concentrated. The crude product was purified by column chromatography with dichloromethane and ether as eluent.

Yield: 2.24 g (13.3 mmol) of a colourless, water soluble liquid, 11%.

IR (NaCl): $\tilde{\nu}$ (cm^{-1}) = 3349 (bs, OH), 2482 (bvs), 2244, 2071, 1495, 1261, 1210, 1175, 1123, 997, 823.

^{1}H-NMR (CD_3OD, 200 MHz): δ (ppm) = 2.56-2.77 (m, 2H, 3-H), 3.27-3.45 (m, 3H, 1,2-H), 3.75-3.86 (m, 2H, OH), 6.59 (m, 2H, 7,8-H), 6.87 (m, 2H, 6,9-H).

^{13}C-NMR (CD_3OD, 50 MHz): δ (ppm) = 35.9 (C-3), 66.7 (C-1), 73.8 (C-2), 116.4 (C-4), 120.8 (C-8), 126.3 (C-9), 128.7 (C-7), 132.5 (C-6), 156.7 (C-5).

5.2.13 Acetic acid 2-allyl-phenyl ester (ML02045)

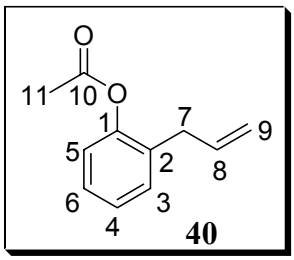

40

2-Allylphenol (19.6 ml, 150 mmol) was added to a mixture of pyridine (100 ml), acetic anhydride (200 ml) and catalytic amount of 4-*N*,*N*-dimethylaminopyridine. The reaction was stirred at room temperature for 1 d. The reaction mixture was washed with saturated solution of $KHSO_4$ (2 × 200 ml) and $NaHCO_3$ (2 × 200 ml). The organic layer was dried over Na_2SO_4 (anhyd.) and concentrated. The crude product was purified by distillation under reduced pressure.

Yield: 23.6 g (0.13 mol) of colourless liquid, 90%.

Boiling point: 62-65 °C / 2 mbar (Lit:[189] 123-124 °C/20 Torr).

IR (NaCl): $\tilde{\nu}$ (cm^{-1}) = 3079 (w, CH), 1762 (vs, C=O), 1639 (C=C), 1488, 1454, 1370, 1210, 1175, 1118, 1088, 1010, 917, 882, 796, 752.

^{1}H-NMR ($CDCl_3$, 200 MHz): δ (ppm) = 2.33 (s, 3H, 11-H), 3.34 (d, ^3J = 6.4 Hz, 2H, 7-H), 5.18-5.31 (m, 2H, 9-H), 5.99-6.19 (m, 1H, 8-H), 7.06 (m, 4H, 3,4,5,6-H).

5.2.14 4-(2,5-Dimethoxy-phenyl)-butane-1,2-diol (ML02022)

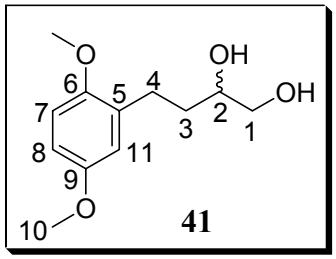

41

A solution of **42** (1.0 g, 3.2 mmol) and palladium over charcoal (30.0 mg, 10% Pd) in 10 ml of methanol were stirred at room temperature under hydrogen pressure of 5-7 bar for 12 h. The reaction mixture was filtered and concentrated. The crude product was purified by column chromatography with hexane:diethyl ether (50%) as eluent.

Yield: 610 mg (2.70 mmol) of white solid, 81%.

^{1}H-NMR ($CDCl_3$, 200 MHz): δ (ppm) = 1.61-1.72 (m, 2H, 3-H), 2.58-2.74 (m, 2H, 4-H), 3.39-3.67 (m, 3H, 1,2-H), 3.71 (s, 3H, 10-H), 3.74 (s, 3H, 10-H), 3.92 (b, 2H, OH) , 6.62-6.76 (m, 3H, 7,8,11-H).

5.2.15 1-Benzyloxy-4-(2,5-dimethoxy-phenyl)-but-3yn-2-ol (ML02021)

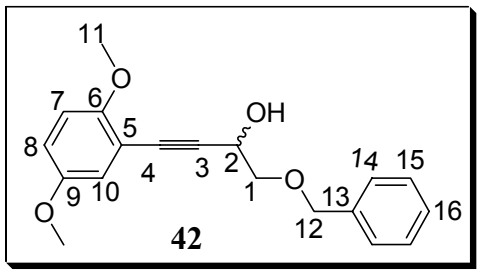

42

A solution of **43** (500 mg, 3.1 mmol) in 15 ml THF was added to ethylmagnesium bromide in 3 ml dry THF, prepared from ethyl bromide (400 mg, 3.3 mmol) and magnesium (100 mg, 3.3 mmol). After 15 minutes benzyloxyacetaldehyde (500 mg, 3.30 mmol) was added. The reaction was monitored by TLC and was quenched with saturated ammonium chloride solution (10 ml) and extracted with ether (3 × 25 ml). The combined organic layer was dried over Na_2SO_4 (anhyd.) and concentrated. The crude product was chromatographed with hexane:diethyl ether (20%).

Yield: 800 mg (2.56 mmol) of colourless liquid, 78%.

^{1}H-NMR ($CDCl_3$, 200 MHz): δ (ppm) = 3.74 (s, 3H, 11-H), 3.80 (s, 3H, 11-H), 4.66 (s, 2H, 1-H), 4.67 (s, 2H, 12-H), 4.83-4.89 (m, 1H, 2-H), 6.80 (s, 1H, 10-H), 6.83 (d, ^3J = 2.9 Hz, 1H, 8-H), 6.95 (d, ^3J = 2.9 Hz, 1H, 7-H), 7.30 (m, 5H, 14,15,16-H).

5.2.16 2-Ethynyl-1,4-dimethoxy-benzene (ML02015)

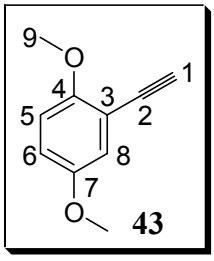

43

2-(1-Chloro-vinyl)-1,4-dimethoxy-benzene (4.4 g, 20.0 mmol) and potassium hydroxide (4 g, 70.0 mmol) in 20 ml ethanol were refluxed for 4 h. The solution was cooled, diluted with water (100 ml) and extracted with ether (3 × 100 ml). The combined organic layer was dried over Na_2SO_4 (anhyd.) and concentrated. The crude product was purified by column chromatography with hexane:diethyl ether (20%) as eluent.

Yield: 1.90 g (11.7 mmol) of white solid, 59%.

Melting point: 39-40 °C (Lit**:**[190] 39-40 °C).

IR (KBr): $\tilde{\nu}$ (cm^{-1}) = 3057 (w, CH), 3001, 2958, 2907, 2835, 2106 (m, C≡C), 1646, 1605, 1580, 1499, 1461, 1307, 1279, 1230, 1122, 1089, 1045, 1023, 926, 860, 807, 738, 617.

^{1}H-NMR ($CDCl_3$, 200 MHz): δ (ppm) = 3.31 (s, 1H, 1-H), 3.74 (s, 3H, 9-H), 3.83 (s, 3H, 9-

H), 6.80 (s, 1H, 8-H), 6.84 (d, ^3J = 3.0 Hz, 1H, 5-H), 6.99 (d, ^3J = 3.0 Hz, 1H, 6-H).

5.2.17 2-(1-Chloro-vinyl)-1,4-dimethoxy-benzene (ML02010)

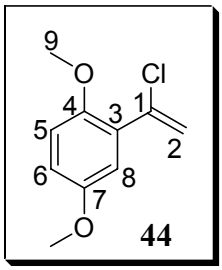

44

2,5-Dimethoxyacetophenone (5.0 g, 28 mmol) in 5 ml of benzene was added to a suspension of phosphorous pentachloride (5.8 g, 28 mmol) in 25 ml dry benzene and refluxed for 5 h. After cooling, the solution was poured into 50 ml of water extracted with ether (3 × 50 ml). The combined organic layer was dried over Na_2SO_4 (anhyd.) and concentrated. The crude product was purified by distillation under reduced pressure.

Yield: 4.40 g (22.2 mmol) of colourless liquid, 80%.

Boiling point: 84-87 °C/1 mbar.[191]

IR (NaCl): $\tilde{\nu}$ (cm^{-1}) = 2948 (w, CH), 2834 (w, CH), 1578 (m, C=C), 1499 (s), 1464, 1421 (s), 1278, 1229, 1171. 1053 (s, CH), 1024, 890, 806, 724.

^{1}H-NMR ($CDCl_3$, 200 MHz): δ (ppm) = 3.78 (s, 3H, 9-H), 3.82 (s, 3H, 9-H), 5.73 (d, ^2J = 1.0 Hz, 1H, 2-H), 5.79 (d, ^2J = 1.0 Hz, 1H, 2-H), 6.85 (d, ^4J = 1.72 Hz ,2H, 5,6-H)**,** 7.09 (t, ^4J = 1.72 Hz,1H, 8-H).

^{13}C-NMR ($CDCl_3$, 50 MHz): δ (ppm) = 56.6 (C-9), 57.2 (C-9), 113.6 (C-8), 116.0 (C-5), 116.8 (C-6), 118.6 (C-1), 128.5 (C-3), 136.9 (C-2), 151.9 (C-4), 154.2 (C-7).

DEPT-135 ($CDCl_3$, 50 MHz): δ (ppm) = 56.6 (C-9), 57.2 (C-9), 113.6 (C-8), 116.0 (C-5), 116.8 (C-6). Signals at 128.5 (C-3), 136.9 (C-1), 151.9 (C-4), 154.2 (C-7) disappeared due to the quaternary nature of the carbons, while the signal at 118.6 (C-2) inverted due to the secondary nature of the carbon.

5.2.18 2,4,5,7-Tetranitrofluorene[192] (ML02007)

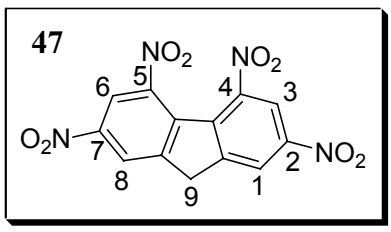

47

To a mixture of conc. nitric acid (65 ml) and conc. sulphuric acid, powdered fluorene (2.5 g, 15.0 mmol) was added in small portions at room temperature. The mixture was stirred and

warmed in a boiling water bath for 1.5 h. After cooling, the mixture was poured onto 400 g of ice. The precipitated powder was filtered, washed with large amount of water and dried. The crude product was purified by crystallisation from nitromethane.

Yield: 4.40 g (12.7 mmol) of cream colour solid, 84%.

Melting point: 260-261 °C.

IR (KBr): $\tilde{\nu}$ (cm^{-1}) = 3086 (CH), 2912, 1617, 1592, 1543, 1404, 1422, 1370, 1343, 1175, 1097 (CH), 949, 926, 912, 805, 742, 728, 689, 659, 640, 601.

^{1}H-NMR (CD_3OD, 200 MHz): δ (ppm) = 4.51 (s, 2H, 9-H), 8.80 (d, *J* = 2.1 Hz, 2H, 1,8-H), 8.86-8.87 (m, 2H, 3,6-H).

5.2.19 2-(2-Hydroxy-ethoxy)-isoindole-1,3-dione (ML02095)

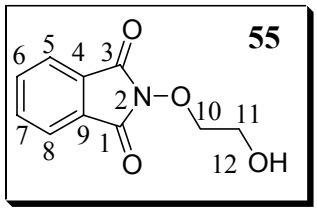

To a solution of *N*-hydroxyphthalimide (10 g, 61 mmol) in DMF (70 ml) was added sodium acetate (5.4 g, 66 mmol). The dark red solution was stirred for 15 min and then 2-bromoethanol (8.3 g, 66 mmol) was added via a syringe. The mixture was heated to 60 °C, stirred for 16 h, and then concentrated in vaccum. The residue was dissolved in ethyl acetate and washed with sodium bicarbonate till the red to yellow color of the *N*-hydroxyphthalimide anion remained in the aqueous layer. The organic phase was dried over Na_2SO_4 (anhyd.) and concentrated yielding a white coloured solid.

Yield: 3.8 g (18 mmol) solid 30% (lit.49 %)

M.P: 68-70 °C (Lit:[76] 73 °C)

IR (KBr): $\tilde{\nu}$ (cm^{-1}) = 3537 (s, OH), 3206, 2952 (s), 1793 (C=O), 1774 (C=O), 1736 (C=O), 1605, 1461, 1439, 1374, 1273, 1213, 1186, 1137, 1074, 1019, 1005, 949, 878, 824, 785, 701, 519, 490.

^{1}H-NMR (DMSO, 200 MHz): δ (ppm) = 3.68 (t, ^3J = 4.9 Hz, 2H, 10-H), 4.16 (t, ^3J = 4.9 Hz, 2H, 11-H), 4.80 (t, ^3J = 5.4 Hz, 1H, 12-H, OH), 7.82-7.85 (m, 4H, 5,6,7,8-H).

5.2.20 2,2,6,6-Tetramethyl-N-piperidinoxyl (ML02093)

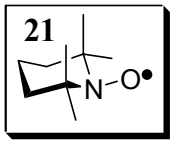

6.02 g (42.6 mmol) of 2,2,6,6-Tetramethylpiperine in 60.0 ml of benzene was cooled to 0 °C. 13.8 g (42.6 mmol, 70%) of MCPBA was added portion wise over a period of 10 min to the cooled amine solution. After complete addition the reaction mixture was warmed slowly to reflux temperature and held at that temperature for 12 h. After cooling the reaction mixture was concentrated and redissolved in hexane to precipitate MCBA. The filtrate was then concentrated and chromatographed on neutral alumina yielding a low melting red coloured solid.

Yield: 2.13 g (13.6 mmol) of red solid 32%

Melting point: 34-36 °C (Lit:[73] 36 °C).

Crystal Structure:[73]

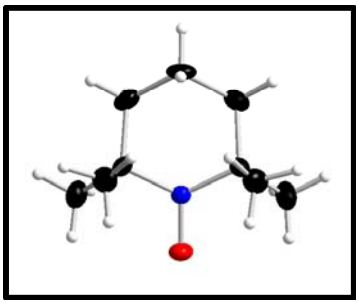

5.2.21 2,2,6,6-Tetramethyl-1-hydroxy-piperidine[74b] (ML02064)

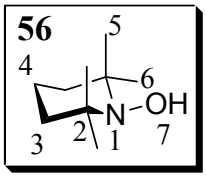

To a solution of 2,2,6,6-tetramethylpiperidinoxy radical (**21**) (34.4 mg, 0.22 mmol) in dry THF (5 ml), a saturated solution of ascorbic acid (0.80 g, 4.50 mmol) in distilled water (2 ml) was added. After 2-3 min of stirring at room temperature the colour of the solution changed from red to colourless. The reaction mixture was stirred for another min and extracted with dry ether (5 × 2 ml). The organic layers were collected and concentrated at room temperature under high vacuum.

Yield: 31.2-32.9 mg, 90-95%.

IR (KBr): $\tilde{\nu}$ (cm^{-1}) = 3440 (bs, OH), 2973 (s), 2936 (s), 1742(w), 1466, 1358, 1242, 1131, 938, 784.

^{1}H-NMR ($CDCl_3$, 200 MHz): δ (ppm) = 1,18 (s, 12H, 5,6-H), 1.56 (s, 6H, 3,4-H), 3.50 (s, 1H, OH).

^{13}C-NMR ($CDCl_3$, 50 MHz): δ (ppm) = 18.1 (C-5,6), 40.6, 59.8.

5.2.22 2-(2,2,6,6-Tetramethyl-piperidin-1-yloxy)-propane-1,3-diol (ML02134.22)

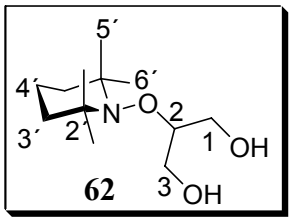

62

To a solution of **64** (410 mg, 1.30 mmol) in 5 ml of dry THF was added LAH (134 mg, 3.54 mmol) at 0 °C. The reaction mixture was stirred at that temperature for about 1 h and quenched with ethylacetate (2 ml) followed by dilution with 10 ml of water. The reaction mixture was extracted with ether (3 x 5 ml) and the combined organic layer was dried over Na_2SO_4 (anhyd.) and concentrated. The crude product was purified by chromatography with silica gel with hexane:ether (90:2 to 50:50) as the eluent.

Yield: 150 mg (0.65 mmol), 50%.

Melting point: 81 °C (85.4 °C = DSC).

IR (KBr)**:** $\tilde{\nu}$ (cm^{-1}) = 3310, 2920, 1360, 1244, 1133, 1112, 1094, 1039, 975, 959.

^{1}H-NMR ($CDCl_3$, 400 MHz): δ (ppm) = 1.15 (s, 6H, H-8´), 1.33 (s, 6H, 3´,4´,5´-H), 1.52 (s, 6H, 7´-H), 3.61, (m, 4H, 1,3-H, OH), 3.83 (t, ^{3}J = 7.1 Hz, 2H, 1,3-H), 4.38 (t, ^{3}J = 7.1 Hz, 1H, 2-H).

^{13}C-NMR ($CDCl_3$, 100 MHz): δ (ppm) = 18.0, 21.3, 34.5, 41.2, 61.9, 65.1, 82.0

Elemental analysis: Calculated C = 62.30, H = 10.89, N = 6.05

Found C = 61.70, H = 11.17, N = 5.99

5.2.23 2-Methyl-2-(2,2,6,6-tetramethyl-piperidin-1-yloxy)-propane-1,3-diol (ML05076.12)

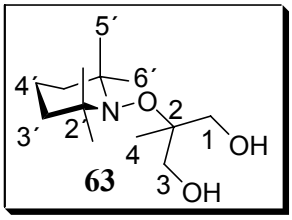

63

To a solution of **65** (510 mg, 1.55 mmol) in 5 ml of dry THF was added LAH (160 mg, 4.20 mmol) at 0 °C. The reaction mixture was stirred at that temperature for about 1 h and quenched with ethylacetate (2 ml) followed by dilution with 10 ml water. The reaction mixture was extracted with ether (3 × 5 ml) and the combined organic layer was dried over Na_2SO_4 (anhyd.) and concentrated. The crude product was purified by chromatography with

silica gel with hexane:ether (90:10 to 50:50) as the eluent.

Yield: 98.8 mg (0.40 mmol), 26%.

Melting point: 59-60 °C (62.9 °C = DSC).

IR (KBr): $\tilde{\nu}$ (cm^{-1}) = 3389, 2971, 1457, 1379, 1254, 1042, 919, 721.

^{1}H-NMR (CDCl3, 200 MHz): δ (ppm) = 1.15 (s, 6H, 6´-H), 1.23 (s, 3H, 4-H), 1.30 (s, 6H, H-5´), 1.46-1.61 (m, 6H, 3´,4´-H), 3.73-3.87 (m, 6H, 1,3-H, and 2H, OH).

^{13}C-NMR (CDCl3, 50 MHz): δ (ppm) = 17.8, 21.51, 21.9, 35.1, 41.8, 61.6, 68.0, 81.0

5.2.24 2-(2,2,6,6-Tetramethyl-piperidin-1-yloxy)-malonic acid diethyl ester[75] (ML02122.12)

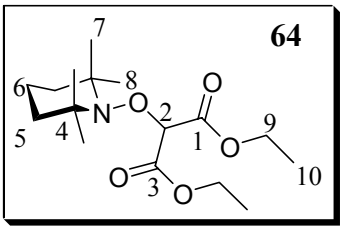

To a solution of LDA at -78 °C in 30 ml DME at 0 °C, diethyl malonate (240 mg, 1.50 mmol) was added. After 30 min, TEMPO (**21**) was added to the reaction mixture. Then the reaction mixture was warmed slowly to 0 °C. To this solution $CuCl_2$ (anhyd.) was added in small portions till the solution remained dark green. The reaction mixture was stirred for 2 h at 0 °C and quenched with water (10 ml). The aqueous layer was extracted with ether (3 × 15 ml), the combined organic layer was washed with water and dried over Na_2SO_4 (anhyd.). The crude product was purified with column chromatography on silica gel with hexane:ethylacetate (98:2).

Yield: 397 mg (1.26 mmol) 84%.

Melting point: 28-30 °C.

IR (KBr): $\tilde{\nu}$ (cm^{-1}) = 2977, 2935, 1767, 1746, 1468, 1367, 1213, 1183, 1097, 1028, 960.

^{1}H-NMR ($CDCl_3$, 200 MHz): δ (ppm) = 1.08 (s, 6H, 8-H), 1.20 (s, 6H, 7-H), 1.29 (t, J = 7.1 Hz, 6H, 5-H), 1.46 (bs, 6h, 3´,4´,5´-H), 4.20-4.27 (m, 4H, 4-H), 4.92 (s, 1H, 2-H).

^{13}C-NMR (CDCl3, 50 MHz): δ (ppm) = 15.1, 18.0, 21.2, 33.6, 41.1, 61.3, 62.6, 87.7, 168.3.

DEPT-135 ($CDCl_3$, 50 MHz): δ (ppm) = 15.0, 21.1, 33.6, 87.7. Signals at 18.0, 41.1 and 62.53 inverted due the secondary nature of the carbon while the signals at 61.3 and 168.3 disappeared due to the quaternary nature of the carbons.

Elemental analysis: Calculated C = 60.93, H = 9.27, N = 4.44

Found C = 61.04, H = 9.38, N = 4.57

5.2.25 2-Methyl-2-(2,2,6,6-tetramethyl-piperidin-1-yloxy)-malonic acid diethyl ester (ML05075.11)

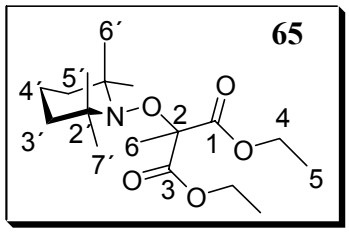

To a solution of LDA at –78 °C, in 30 ml DME at 0 °C diethyl-2-methylmalonate (261 mg, 1.50 mmol) was added. After 30 min to the reaction mixture TEMPO (**21**) was added and the reaction mixture was warmed slowly to 0 °C and $CuCl_2$ (anhyd.) was added in small portions till the solution remained dark green colour. The reaction mixture was stirred for 2 h at 0 °C and quenched with water (10 ml). The aqueous layer was extracted with ether (3 × 15 ml), the combined organic layer was washed with water and dried over Na_2SO_4 (anhyd.). The crude product was purified with column chromatography on silica gel with hexane:ethylacetate (98 : 2).

Yield: 296 mg (0.90 mmol), 60%.

Melting point: 76-78 °C (82.3 °C = DSC, Lit:[75] 76-77 °C).

IR (KBr): $\tilde{\nu}$ (cm^{-1}) = 2969, 1761, 1731, 1462, 1374, 1266, 1218, 1175, 1126, 1016, 928, 857, 802, 681, 563.

^{1}H-NMR ($CDCl_3$, 200 MHz): δ (ppm) = 1.03 (s, 6H, 7´-H), 1.23 (s, 6H, 6´-H), 1.27 (t, ^3J = 7.1 Hz, 6H, 5-H), 1.42-1.56 (m, 6H, 3´,4´,5´-H), 1.74 (s, 3H, 6-H), 4.10-4.35 (m, 4H, 4-H).

^{13}C-NMR ($CDCl_3$, 50 MHz): δ (ppm) = 14.0, 16.8, 17.8, 20.5, 32.9, 40.7, 60.2, 61.5, 85.4, 170.3.

Elemental analysis: Calculated C = 61.98, H = 9.48, N = 4.25

Found C = 61.95, H = 9.59, N = 4.21

5.2.26 General synthesis of substituted phenoxyethanols (57a-k)

Ethyl-2-phenoxyacetates (1 eq.) was dissolved in 10 ml of dry THF. To the above solution lithium aluminium hydride (1.1 eq.) was added portion wise over a period of 10 min at 0 °C. After 1 h the reaction mixture was quenched with 5 ml of ethylacetate followed by addition of water (10 ml) after 15 min. The reaction mixture was extracted with ether (2 x 20 ml) and the combined layer dried over Na_2SO_4 (anhyd.) and concentrated. The crude product was purified by column chromatography with hexane:ether (20%) as eluent.

5.2.26.1 2-(2,6-Dimethyl-phenoxy)-ethanol[78] (ML04109H)

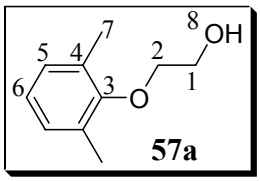

57a

Yield: 1.3 g (7.8 mmol) of colourless solid, 79%.

Melting point: 70 °C

IR (NaCl): $\tilde{\nu}$ (cm^{-1}) = 3312 (OH), 2963, 2926, 2867, 1591, 1476, 1357, 1263, 1203, 1164, 1079, 902, 812, 771, 673, 574.

^{1}H-NMR ($CDCl_3$, 400 MHz): δ (ppm) = 2.32 (s, 6H, 7-H), 3.31 (bs, 1H, OH, 8-H), 3.91 (bt, ^3J = 4.5 Hz, 2H, 1-H), 3.95-4.03 (m, 2H, 2-H), 6.95 – 7.05 (m, 3H, 5,6-H).

^{13}C-NMR ($CDCl_3$, 100 MHz): δ (ppm) = 16.0 (C-7), 62.0 (C-1), 72.9 (C-2), 123.8 (C-6), 128.7 (C-4), 130.6 (C-5), 155.2 (C-3).

Elemental analysis: Calculated C = 72.26, H = 8.49

Found C = 72.37, H = 8.41

5.2.26.2 2-(2,4-Dimethyl-phenoxy)-ethanol[78] (ML04109I)

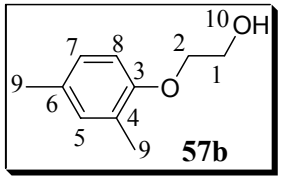

57b

Yield: 1.2 g (7.2 mmol) of colourless liquid, 75%.

IR (NaCl): $\tilde{\nu}$ (cm^{-1}) = 3428 (OH), 2922, 1595, 1456, 1323, 1166, 1068, 832.

^{1}H-NMR ($CDCl_3$, 400 MHz): δ (ppm) = 2.34 (s, 6H, 9-H), 3.60 (bs, 1H, OH, 10-H), 3.97 (t, ^3J = 4.6 Hz,2H, 1-H), 4.06 (t, ^3J = 4.6 Hz, 2H, 2-H), 6.61 (bs, 2H, 7,8-H), 6.66 (s, 1H, 5-H).

^{13}C-NMR ($CDCl_3$, 100 MHz): δ (ppm) = 21.1 (C-9), 60.9 (C-1), 68.1 (C-2), 112.1 (C-7,8), 122.5 (C-6), 138.9 (C-5), 158.4 (C-3).

Elemental analysis : Calculated C = 72.26, H = 8.49

Found C = 72.04, H = 8.69

5.2.26.3 2-(2,4,6-Trimethyl-phenoxy)-ethanol (ML04109G)

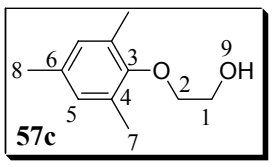

57c

Yield: 1.5 g (8.3 mmol) of colourless liquid, 92%.

Melting Point: 52-53 °C

IR (NaCl): $\tilde{\nu}$ (cm^{-1}) = 3520 (OH), 2921, 1485, 1373, 1308, 1245, 1213, 1149, 1053, 960, 897, 855.

^{1}H-NMR ($CDCl_3$, 200 MHz): δ (ppm) = 2.29 (s, 3H, 8-H), 2.30 (s, 6H, 7-H), 3.10 (bs, 1H, OH, 9-H), 3.89-3.91 (m, 2H, 1-H), 3.96-4.02 (m, 2H, 2-H), 6.87 (s, 2H, 5-H).

^{13}C-NMR ($CDCl_3$, 50 Hz): δ (ppm) = 15.9 (C-7), 20.5 (C-8), 62.0 (C-1), 73.0 (C-2), 129.3 (C-4), 130.2 (C-5), 133.1 (C-6), 152.9 (C-3).

5.2.26.4 2-(2-Propyl-phenoxy)-ethanol (ML0109D)

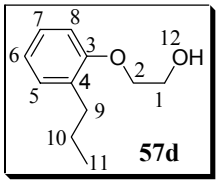

57d

Yield: 0.8 g (14 mmol) of colourless liquid, 49%.

IR (NaCl): $\tilde{\nu}$ (cm^{-1}) = 3401 (OH) cm^{-1}, 2959, 2931, 2871, 1600, 1493, 1452, 1377, 1243, 1180, 1128, 1080, 1050, 922, 752.

^{1}H-NMR ($CDCl_3$, 200 MHz): δ (ppm) = 0.94 (t, ^{3}J = 7.1 Hz, 3H, 11-H), 1.61 (sextet, ^{3}J = 7.1 Hz, ^{3}J = 7.4 Hz, 2H, 10-H), 2.25 (s, 1H, OH, 12-H), 2.60 (t, ^{3}J = 7.4 Hz, 2H, 9-H), 4.17 (t, ^{3}J = 4.4 Hz, 2H, 1-H), 4.45 (t, ^{3}J = 4.4 Hz, 2H, 2-H), 6.82 (d, ^{3}J = 7.6 Hz, 1H, 8-H), 6.91 (t, ^{3}J = 7.6 Hz, 1H, 6-H), 7.10 (d, ^{3}J = 7.6 Hz, 2H, 5,7-H).

^{13}C-NMR ($CDCl_3$, 50 MHz): δ (ppm) = 13.9 (C-11), 22.8 (C-10), 31.9 (C-9), 61.2 (C-1), 69.1 (C-2), 111.3 (C-8), 120.6 (C-6), 129.8 (C-5, 7), 131.0 (C-4), 155.8 (C-3).

5.2.26.5 2-(2-Isopropyl-phenoxy)-ethanol (ML04109F)

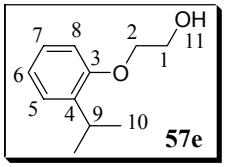

57e

Yield: 1.4 g (7.8 mmol) of colourless liquid, 86%.

IR (NaCl): $\tilde{\nu}$ (cm^{-1}) = 3374 (OH), 3033, 2962, 2870, 1599, 1584, 1493, 1449, 1362, 1240, 1195, 1147, 921, 752, 610, 490.

^{1}H-NMR ($CDCl_3$, 200 MHz): δ (ppm) = 1.23 (d, ^{3}J = 6.7 Hz, 6H, 10-H), 3.33 (q, ^{3}J = 6.7 Hz, 1H, 9-H), 4.18 (t, ^{3}J = 4.4 Hz, 2H, 1-H), 4.47 (t, ^{3}J = 4.4 Hz, 2H, 2-H), 6.83 (d, ^{3}J = 7.9 Hz, 1H, 8-H), 6.96 (t, ^{3}J = 7.4 Hz, 1H, 6-H), 7.16 (t, ^{3}J = 7.9 Hz, 1H, 7-H), 7.25 (d, ^{3}J = 7.4 Hz, 1H, 5-H).

^{13}C-NMR ($CDCl_3$, 50 MHz): δ (ppm) = 22.6 (C-10), 26.5 (C-9), 61.3 (C-1), 69.2 (C-2), 111.5

(C-8), 120.9 (C-6), 125.9 (C-7), 126.4 (C-5), 136.9 (C-4), 155.6 (C-3).

5.2.26.6 2-(2-*sec*-Butyl-phenoxy)-ethanol (ML04109E)

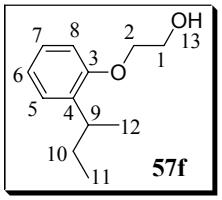

57f

Yield: 1.5 g (7.8 mmol) of colourless liquid, 92%.

IR (NaCl): $\tilde{\nu}$ (cm^{-1}) = 3391 (OH), 2961, 2931, 2873, 1484, 1599, 1585, 1239, 1153, 1096, 1050, 752.

^{1}H-NMR ($CDCl_3$, 200 MHz): δ (ppm) = 0.84 (t, ^3J = 7.4 Hz, 3H, 11-H), 1.20 (d, ^3J = 6.9 Hz, 3H, 12-H), 1.44-1.77 (m 2H, 10-H), 3.10 (sextet, ^3J = 6.9 Hz, ^3J = 7.4 Hz, 1H, 9-H), 4.17 (t, ^3J = 4.7 Hz, 2H, 1-H), 4.45 (t, ^3J = 4.7 Hz, 2H, 2-H), 6.83 (d, ^3J = 7.9 Hz, 1H, 8-H), 6.95 (t, ^3J = 7.6 Hz, 1H, 6-H), 7.19 (t, ^3J = 7.6 Hz, 2H, 5,7-H).

^{13}C-NMR ($CDCl_3$, 50 MHz): δ (ppm) = 12.0 (C-11), 20.4 (C-12), 29.7 (C-10), 33.4 (C-9), 61.3 (C-1), 69.3 (C-2), 111.7 (C-8), 120.9 (C-6), 126.3 (C-7), 126.7 (C-5), 135.8 (C-4), 155.9 (C-3).

5.2.26.7 2-(2-*tert*-Butyl-phenoxy)-ethanol[80] (ML04109C)

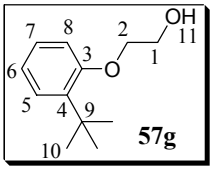

57g

Yield: 1.5 g (7.8 mmol) of colourless liquid, 91%.

IR (NaCl): $\tilde{\nu}$ (cm^{-1}) = 3400 (OH), 2955, 1595, 1488, 1443, 1235, 1093, 920, 750.

^{1}H-NMR ($CDCl_3$, 400 MHz): δ (ppm) = 1.50 (s, 9H, 10-H), 2.82 (bs, 1H, 11-H, OH), 4.07 (t, ^3J = 4.4 Hz, 2H, 1-H), 4.65 (dd, ^3J = 4.4 Hz, ^3J = 5.0 Hz, 2H, 2-H), 6.94 (dd, ^4J = 1.0 Hz, ^3J = 8.0 Hz, 1H, 8-H), 7.01 (dt, ^4J = 1.0 Hz, ^3J = 7.5 Hz, 1H, 6-H), 7.26 (dt, ^4J = 1.6 Hz, ^3J = 8.0 Hz, 1H, 7-H), 7.39 (dd, ^4J = 1.6 Hz, ^3J = 7.5 Hz, 1H, H-5).

^{13}C-NMR ($CDCl_3$, 100 MHz): δ (ppm) = 29.8 (C-10), 34.7 (C-9), 61.4 (C-1), 69.0 (C-2), 112.1 (C-8), 120.5 (C-6), 126.6 (C- 7), 126.9 (C-5), 137.9 (C-4), 157.3 (C-3).

5.2.26.8 2-(4-Methoxy-phenoxy)-ethanol[83] (ML05033)

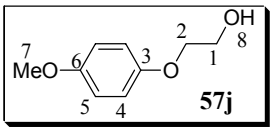

57j

Yield: 1.3 g (7.7 mmol) of colourless solid, 81%.

IR (NaCl): $\tilde{\nu}$ (cm^{-1}) = 3286 (OH), 2953, 2929, 1511, 1461, 1441, 1294, 1242, 1114, 1093, 1053, 1031, 921, 827.

^{1}H-NMR ($CDCl_3$, 400 MHz): δ (ppm) = 2.49 (bs, 1H, 8-H, OH), 3.77 (s, 3H, 7-H), 3.92-3.96 (m, 2H, 1-H), 4.01-4.05 (m, 2H, 2-H), 6.84 (s, 4H, 4,5-H).

^{13}C-NMR ($CDCl_3$, 100 MHz): δ (ppm) = 55.5 (C-7), 61.3 (C-1), 69.8 (C-2), 114.5 (C-4), 115.4 (C-5), 152.6 (C-3), 153.9 (C-6).

5.2.26.9 2-(4-Bromo-phenoxy)-ethanol

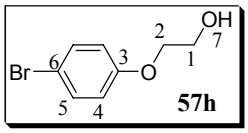

57h

Yield: 0.5 g (7.7 mmol) of colourless solid, 32%.

Melting Point: 48 °C

IR (NaCl): $\tilde{\nu}$ (cm^{-1}) = 3319 (OH), 2906, 1587, 1487, 1453, 1288, 1242, 1168, 1082, 1050, 999, 908, 822, 640, 508.

^{1}H-NMR ($CDCl_3$, 400 MHz): δ (ppm) = 2.14 (bs, 1H, 7-H, OH), 3.92-4.01 (m, 4H, 1,2-H), 6.79 (d, ^{3}J = 9.0 Hz, 2H, 4-H), 7.37 (d, ^{3}J = 9.0 Hz, 2H, 5-H).

^{13}C-NMR ($CDCl_3$, 100 MHz): δ (ppm) = 61.3 (C-1), 69.4 (C-2), 113.3 (C-6), 116.2 (C-4), 132.3 (C- 5), 157.7 (C-3).

Elemental analysis: Calculated C = 44.27, H = 4.18

Found C = 44.27, H = 4.18

5.2.26.9.1 2-(4-Nitro-phenoxy)-ethanol

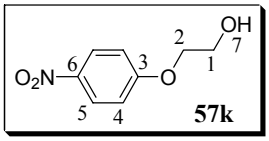

57k

Yield: 0.8 g (4.4 mmol) of colourless solid, 31%.

Melting Point: 87-88 °C

IR (NaCl): $\tilde{\nu}$ (cm^{-1}) = 3269 (OH), 1607, 1595, 1506, 1456, 1341, 1332, 1298, 1270, 1174, 1111, 1077, 1039, 917, 840, 752, 658.

^{1}H-NMR ($CDCl_3$, 200 MHz): δ (ppm) = 2.03-2.12 (m, 1H, 7-H, OH), 3.9-4.08 (m, 2H, 1-H), 4.19 (t, ^{3}J = 4.7 Hz, 2H, 2-H), 6.98 (d, ^{3}J = 9.1 Hz, 1H, 4-H), 8.21 (d, ^{3}J = 9.1 Hz, 1H, 5-H).

^{13}C-NMR ($CDCl_3$, 50 MHz): δ (ppm) = 61.0 (C-1), 69.9 (C-2), 114.4 (C-4), 125.9 (C-5), 141.7 (C-6), 163.6 (C-3).

5.2.27 General synthesis of substituted phenoxyesters (58a-k)

Various substituted phenols (1 eq.), ethylbromoacetate (1.1 eq.) and potassium carbonate (1.3 eq.)) were stirred for 2 days at room temperature. The reaction mixture was filtered through celite and concentrated. The crude product was purified by column chromatography with hexane: ether (20%) as eluent.

5.2.27.1 Ethyl-(2-nitro-phenoxy) acetate[81] (ML04107a)

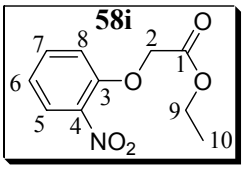

Yield: 5.6 g (25 mmol) of cream coloured solid, 87%.

Melting point: 38-40 °C

IR (NaCl): $\tilde{\nu}$ (cm^{-1}) = 2985, 1756 (s, C=O), 1607, 1586, 1527, 1488, 1355, 1296, 1206, 1168, 1098, 1065, 1026, 855, 774, 746, 664.

^{1}H-NMR ($CDCl_3$, 400 MHz): δ (ppm) = 1.26 (t, ^3J = 7.0 Hz, 3H, 10-H), 4.24 (q, ^3J = 7.0 Hz, 2H, 9-H), 4.76 (s, 2H, 2-H), 6.95 (d, ^3J = 7.0 Hz, 1H, 8-H), 7.12 (d, ^3J = 7.0 Hz, 1H, 6-H), 7.51 (t, J = 8.1 Hz, 1H, 7-H), 7.85 (d, J = 8.1 Hz, 1H, 5-H).

^{13}C-NMR ($CDCl_3$, 100 MHz): δ (ppm) = 14.0 (C-10), 61.6 (C-9), 66.5 (C-2), 115.1 (C-8), 121.6 (C-6), 125.7 (C-7), 134.0 (C-5), 140.0 (C-4), 151.2 (C-3), 167.7 (C-1).

Elemental analysis: Calculated C = 53.33, H = 4.92, N = 6.22

Found C = 53.26, H = 4.89, N = 6.17

5.2.27.2 Ethyl-(2,6-dimethyl-phenoxy) acetate[77] (ML04107H)

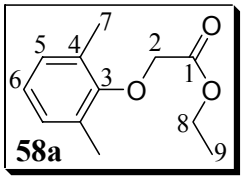

Yield: 5.5 g (26 mmol) of colourless liquid, 80%.

IR (NaCl): $\tilde{\nu}$ (cm^{-1}) = 2982, 1761 (s, C=O), 1477, 1379, 1282, 1191, 1096, 1071, 1031, 772.

^{1}H-NMR ($CDCl_3$, 200 MHz): δ (ppm) = 1.33 (t, ^3J = 6.9 Hz, 3H, 9-H), 2.30 (s, 6H, 7-H), 4.24 (q, ^3J = 6.8 Hz, 2H, 8-H), 4.40 (s, 2H, 2-H), 6.90 – 7.02 (m, 3H, 5,6-H).

^{13}C-NMR ($CDCl_3$, 50 MHz): δ (ppm) = 14.1 (C-9), 16.2 (C-7), 61.1 (C-8), 69.1 (C-2), 124.4 (C-6), 128.9 (C-4), 130.6 (C-5), 155.3 (C-3), 169.1 (C-1).

Elemental analysis: Calculated C = 69.21, H = 7.74

Found C = 69.65, H = 8.19

5.2.27.3 Ethyl-(2,4-dimethyl-phenoxy) acetate[77] (ML04107I)

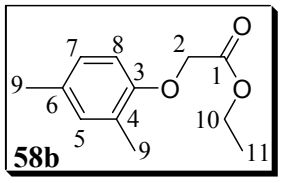

Yield: 5.9 g (28 mmol) of colourless liquid, 87%.

IR (NaCl): $\tilde{\nu}$ (cm^{-1}) = 2982, 2920, 1761 (s, C=O), 1614, 1596, 1474, 1379, 1324, 1299, 1280, 1172, 1097, 1033, 830, 687.

^{1}H-NMR ($CDCl_3$, 400 MHz): δ (ppm) = 1.30 (t, ^{3}J = 7.1 Hz, 3H, 11-H), 2.28 (s, 6H, 9-H), 4.27 (q, ^{3}J = 7.1 Hz, 2H, 10-H), 4.58 (s, 2H, 2-H), 6.54 (s, 2H, 5,7-H), 6.64 (s, 1H, 8-H).

^{13}C-NMR ($CDCl_3$, 100 MHz): δ (ppm) = 14.1 (C-11), 21.4 (C-9), 61.2 (C-10), 65.3 (C-2), 112.3 (C-8), 123.4 (C-6), 139.3 (C-5, 7), 157.8 (C-3), 169.1 (C-1).

5.2.27.4 Ethyl-(2, 4, 6-trimethyl-phenoxy) acetate[79] (ML04107G):

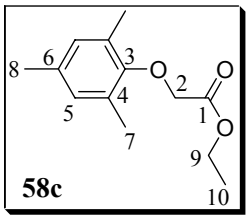

Yield: 5.8 g (26 mmol) of colourless liquid, 89%.

IR (NaCl): $\tilde{\nu}$ (cm^{-1}) = 2921, 1762 (s, C=O), 1484, 1378, 1283, 1196, 1150, 1075, 1033, 855.

^{1}H-NMR ($CDCl_3$, 200 MHz): δ (ppm) = 1.33 (t, ^{3}J = 7.1 Hz, 3H, 10-H), 2.23 (s, 3H, 8-H), 2.26 (s, 6H, 7-H), 4.30 (q, ^{3}J = 7.1 Hz, 2H, 9-H), 4.37 (s, 2H, 2-H), 6.81 (s, 2H, 5-H).

^{13}C-NMR ($CDCl_3$, 50 MHz): δ (ppm) = 14.1 (C-10), 16.1 (C-7), 20.6 (C-8), 61.1 (C-9), 69.2 (C-2), 129.4 (C-4), 130.2 (C-5), 133.7 (C-6), 153.1 (C-3), 169.2 (C-1).

5.2.27.5 Ethyl-(2-propyl-phenoxy) acetate (ML04107d)

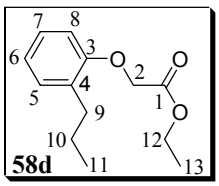

Yield: 3.1 g (14 mmol) of colourless liquid, 48%.

IR (NaCl): $\tilde{\nu}$ (cm^{-1}) = 2982, 2921, 1762 (s, C=O), 1484, 1446, 1378, 1283, 1196, 1150, 1075, 1033, 855.

^{1}H-NMR ($CDCl_3$, 200 MHz): δ (ppm) = 0.96 (t, ^{3}J = 7.1 Hz, 3H, 11-H), 1.29 (t, ^{3}J = 7.1 Hz, 3H, 13-H), 1.56-1.75 (m, 2H, 10-H), 2.67 (t, ^{3}J = 7.4 Hz, 2H, 9-H), 4.26 (q, ^{3}J = 7.1 Hz, 2H, 12-H), 4.63 (s, 2H, 2-H), 6.71 (d, ^{3}J = 7.6 Hz, 1H, 8-H), 6.92 (dt, ^{4}J = 1.0 Hz, ^{3}J = 7.6 Hz, 1H, 6-H), 7.14 (dt, ^{4}J = 1.0 Hz, ^{3}J = 7.6 Hz, 2H, 5,7-H).

^{13}C-NMR ($CDCl_3$, 50 MHz): δ (ppm) = 14.0 (C-11, 13), 23.0 (C-10), 32.3 (C-9), 61.2 (C-12), 65.5 (C-2), 111.1 (C-8), 121.4 (C-6), 126.7 (C-7), 130.2 (C-5), 131.7 (C-4), 155.8 (C-3), 169.2 (C-1).

5.2.27.6 Ethyl-(2-isopropyl-phenoxy) acetate (ML04107E)

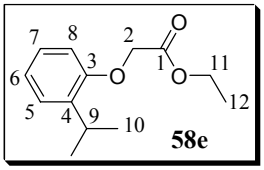

58e

Yield: 5.8 g (26 mmol) of colourless liquid, 89%.

IR (NaCl): $\tilde{\nu}$ (cm^{-1}) = 2963, 2870, 1762 (s, C=O), 1601, 1492, 1454, 1381, 1287, 1190, 1198, 1071, 1039, 800, 752.

^{1}H-NMR ($CDCl_3$, 200 MHz): δ (ppm) = 1.25 (d, ^{3}J = 6.9 Hz, 6H, 10-H), 1.29 (t, ^{3}J = 7.1 Hz, 3H, 11-H), 3.43 (q, ^{3}J = 6.9 Hz, 1H, 9-H), 4.26 (q, ^{3}J = 7.1 Hz, 2H, 11-H), 4.64 (s, 2H, 2-H), 6.72 (dd, ^{4}J = 1.0 Hz, ^{3}J = 7.9 Hz, 1H, 8-H), 6.97 (dt, ^{4}J = 1.0 Hz, ^{3}J = 7.4 Hz, 1H, H-6), 7.13 (dt, ^{4}J = 1.7 Hz, ^{3}J = 7.9 Hz, 1H, 7-H), 7.25 (dd, ^{4}J = 1.7 Hz, ^{3}J = 7.4 Hz, 1H, 5-H).

^{13}C-NMR ($CDCl_3$, 50 MHz): δ (ppm) = 14.1 (C-12), 22.6 (C-10), 26.9 (C-9), 61.2 (C-11), 65.6 (C-2), 111.2 (C-8), 121.7 (C-6), 126.4 (C-5, 7), 137.5 (C-4), 155.1 (C-3), 169.1 (C-1).

5.2.27.7 Ethyl-(2-*sec*-butyl-phenoxy) acetate (ML04107F)

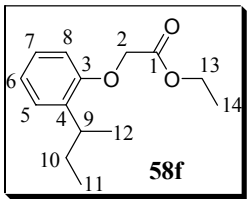

58f

Yield: 5.3 g (22 mmol) of colourless liquid, 84%.

IR (NaCl): $\tilde{\nu}$ (cm^{-1}) = 2963, 2932, 2873, 1761 (s, C=O), 1586, 1492, 1451, 1378, 1282, 1201, 1107, 1030, 752.

^{1}H-NMR ($CDCl_3$, 200 MHz): δ (ppm) = 0.86 (t, ^{3}J = 7.4 Hz, 3H, 11-H), 1.23 (d, ^{3}J = 7.0 Hz, 3H, 12-H), 1.29 (t, ^{3}J = 7.1 Hz, 3H, 14-H), 1.47-1.79 (m, 2H, 10-H), 3.20 (sextet, ^{3}J = 7.0 Hz, ^{3}J = 7.1 Hz, 1H, 9-H), 4.26 (q, ^{3}J = 7.1 Hz, 2H, 13-H), 4.63 (s, 2H, 2-H), 6.72 (dd, ^{4}J = 1.0 Hz, ^{3}J = 7.9 Hz, 1H, 8-H), 6.96 (dt, ^{4}J = 1.0 Hz, ^{3}J = 7.4 Hz, 1H, 6-H), 7.13 (dt,

^4J = 1.7 Hz, ^3J = 7.9 Hz, 1H, 7-H), 7.20 (dd, ^4J = 1.7 Hz, ^3J = 7.4 Hz, 1H, 5-H).

^{13}C-NMR ($CDCl_3$, 50 MHz): δ (ppm) = 12.1 (C-11), 14.1 (C-14), 20.4 (C-12), 29.8 (C-10), 33.7 (C-9), 61.2 (C-13), 65.7 (C-2), 111.3 (C-8), 121.6 (C-6), 126.4 (C-7), 127.2 (C-5), 136.4 (C-4), 155.4 (C-3), 169.1 (C-1).

5.2.27.8 Ethyl-(2-*tert*-butyl-phenoxy) acetate (ML04107C)

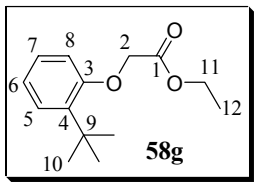

58g

Yield: 5.3 g (22 mmol) of colourless liquid, 84%.

IR (NaCl): $\tilde{\nu}$ (cm^{-1}) = 2958, 2912, 2870, 1762 (s, C=O), 1599, 1581, 1489, 1444, 1362, 1293, 1196, 1102, 1059, 1032, 791, 752.

^{1}H-NMR ($CDCl_3$, 200 MHz): δ (ppm) = 1.31 (t, ^3J = 7.0 Hz, 3H, 12-H), 1.44 (s, 9H, 10-H), 4.28 (q, ^3J = 7.1 Hz, 2H, 11-H), 4.65 (s, 2H, 2-H), 6.73 (dd, ^4J = 1.0 Hz, ^3J = 7.9 Hz, 1H, 8-H), 6.94 (dt, ^4J = 1.0 Hz, ^3J = 7.4 Hz, 1H, 6-H), 7.17 (dt, ^4J = 1.7 Hz, ^3J = 7.9 Hz, 1H, 7-H), 7.32 (dd, ^4J = 1.7 Hz, ^3J = 7.4 Hz, 1H, 5-H).

^{13}C-NMR ($CDCl_3$, 50 MHz): δ (ppm) = 14.1 (C-12), 29.6 (C-10), 34.8 (C-9), 61.2 (C-11), 65.2 (C-2), 111.7 (C-8), 121.2 (C-6), 126.9 (C-5, 7), 138.9 (C-4), 156.5 (C-3), 169.0 (C-1).

Elemental analysis: Calculated C = 71.16, H = 8.53

Found C = 70.66, H = 8.85

5.2.27.9 Ethyl-(4-methoxy-phenoxy) acetate (ML05029)

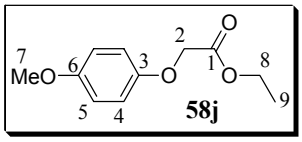

58j

Yield: 7.0 g (33 mmol) of colourless liquid, 83%.

IR (NaCl): $\tilde{\nu}$ (cm^{-1}) = 2982, 2936, 2909, 1757 (s, C=O), 1506, 1464, 1442, 1379, 1271, 1194, 1108, 1084, 1033, 826, 721.

^{1}H-NMR ($CDCl_3$, 200 MHz): δ (ppm) = 1.28 (t, ^3J = 7.1 Hz, 3H, 9-H), 3.75 (s, 3H, 7-H), 4.25 (q, ^3J = 7.1 Hz, 2H, 8-H), 4. 56 (s, 2H, 2-H), 6.84 (d, ^3J = 1.7 Hz, 4H, 4,5-H).

^{13}C-NMR ($CDCl_3$, 50 MHz): δ (ppm) = 14.0 (C-9), 55.4 (C-7), 34.8 (C-9), 61.1 (C-8), 66.1 (C-2), 114.5 (C-5), 115.7 (C-4), 151.8 (C-3), 154.3 (C-4), 169.1 (C-1).\

5.2.28 2,2-Dimethyl-[1,3]dioxolane-4-carboxylic acid 2-thio-2*H*-pyridin-1yl-ester (ML02020)

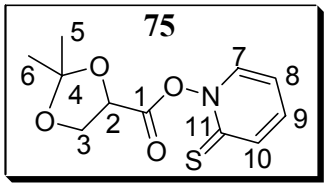

N-2-thiopyridineoxide sodium salt (1.67 g, 10 µmol), [D]-2,3-diisopropylideneglyceryl chloride (1.77 g, 10 µmol) and catalytic amount of DMAP were stirred in 50 ml dry ether was stirred for 30 minutes in dark. The reaction mixture was filtered through a bed of celite and concentrated below 45 °C.

Yield: 2.28 g (8.93 mmol) of a cream coloured solid, 83%.

Melting point: 62 °C

IR (NaCl): $\tilde{\nu}$ (cm^{-1}) = 3100 (w), 2992 (w), 1810 (s), 1736 (b), 1605 (s), 1527 (s), 1448 (s), 1372 (s), 1227 (b), 1132 (b), 1076 (bs), 963 (s), 840 (s), 740 (s).

^{1}H-NMR ($CDCl_3$, 200 MHz): δ (ppm) = 1.37 (s, 3H, 5-H), 1.49 (s, 3H, 6-H), 4.31 (dd, *J* = 9.1 Hz, *J* = 7.4 Hz 1H, 2-H), 4.65 (dd, *J* = 9.1 Hz, *J* = 4.7 Hz, 1H, 3-H), 4.86 (dd, *J* = 7.4 Hz, *J* = 4.7 Hz, 1H, 3-H), 6.67 (td, *J* = 6.9 Hz, *J* = 2.0 Hz, 1H, 8-H), 7.12-7.21 (m, 1H, 9-H), 7.58 (dd, *J* = 9.1 Hz, *J* = 2.0 Hz, 1H, 10-H), 7.66 (dd, *J* = 7.0 Hz, *J* = 1.6 Hz, 1H, 7-H).

^{13}C-NMR ($CDCl_3$, 50 MHz): δ (ppm) = 26.7 (C-5), 26.8 (C-6), 66.7 (C-4), 68.2 (C-3), 74.5 (C-2), 134.0 (C-10), 137.7 (C-7), 138.8 (C-8, 9), 171.2 (C-1), 172.9 (C-11).

DEPT-135 ($CDCl_3$, 50 MHz): δ (ppm) = 26.7 (C-5), 26.8 (C-6), 74.5 (C-2), 134.0 (C-10), 137.7 (C-7), 138.8 (C-8, 9). Signal at 68.2 (C-3) inverted due to the secondary nature of the carbon while signals at 66.7 (C-4), 171.2 (C-1) and 172.9 (C-11) disappeared due to the quaternary nature of the carbon.

Elemental analysis: Calculated C = 51.75, H = 5.13, N = 5.49, S = 12.56

Found C = 51.06, H = 5.15, N = 5.56, S = 13.18

5.2.29 2,2-Dimethyl-propanoic acid 2-thioxo-2*H*-pyridin-1-yl-ester[90] (ML02105/ML050-88.1)

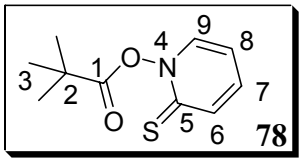

Pivalylchloride (2.0 g, 17 mmol) was added dropwise to a suspension of *N*-hydroxy-2-pyridinethione sodium salt (2.5 g, 17 mmol) in 50 ml of dry ether and catalytic amount DMAP (100 mg) at room temperature. After 45 min the reaction mixture was poured into water and extracted with ether (3 × 50 ml). The combined organic layer was then passed through celite (285) and washed with water (3 × 100 ml) and dried over Na_2SO_4 (anhyd.) and concentrated at 40 °C.

Yield: 3.1 g (15 mmol) of cream coloured solid, 93%.

Melting point: 93-94 °C

IR (NaCl): $\tilde{\nu}$ (cm^{-1}) = 3069, 2975, 2931, 1789 (C=O), 1606, 1526, 1452, 1414, 1368, 1285, 1227, 1176, 1137, 1092, 1057, 1015, 941, 864, 840, 797, 759, 711, 524, 502.

^{1}H-NMR ($CDCl_3$, 200 MHz): δ (ppm) = 1.45 (s, 9H, 3-H), 6.62 (td, *J* = 6.9 Hz, *J* = 1.7 Hz, 1H, 8-H), 7.19 (td, *J* = 6.9 Hz, *J* = 1.7 Hz, *J* = 1.5 Hz, 1H, 7-H), 7.48 (dd, *J* = 7.0 Hz, *J* = 1.5 Hz, 1H, H-6), 7.67 (dd, *J* = 7.0 Hz, *J* = 1.7 Hz, 1H, 9-H).

^{13}C-NMR ($CDCl_3$, 50 MHz): δ (ppm) = 27.1 (C-3), 38.8 (C-2), 112.6 (C-9), 133.4 (C-6), 137.4 (C-7), 137.6 (C-8).

HRMS: $C_{10}H_{13}NO_2S$, Calculated: 211.0667, Found: 211.0670

5.2.30 [D]-2,3-Isopropylideneglyceryl chloride (ML02050)

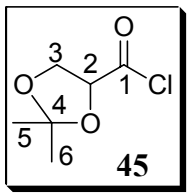

45

Oxalyl chloride (4.5 ml, 52.5 mmol), potassium [D]-2,3-isopropylideneglycerate (4.6 g, 24.8 mmol) and 100 µl of pyridine in 50 ml dry ether were stirred at room temperature for 20 h. The reaction mixture was then filtered and concentrated. The crude product was purified by distillation under reduced pressure.

Yield: 1.80 g (10.9 mmol) of a colourless liquid, 43%.

Boiling Point: 71-72 °C/25 mbar (Lit**:**[89] 70 °C/25 mbar).

IR (NaCl): $\tilde{\nu}$ (cm^{-1}) = 2992 (m), 2941, 2891, 1820 (s, C=O), 1777, 1456, 1385, 1226, 1113, 1074, 889, 839, 752, 642.

^{1}H-NMR ($CDCl_3$, 200 MHz): δ (ppm) = 1.38 (s, 3H, 5-H), 1.48 (s, 3H, H-6), 4.32 (d, *J* = 5.4 Hz, 2H, 3-H), 4.82 (t, *J* = 5.7 Hz, 1H, 2-H).

^{13}C-NMR ($CDCl_3$, 50 MHz): δ (ppm) = 26.3 (C-5), 26.6 (C-6), 67.9 (C-3), 82.1 (C-2), 114.0 (C-4), and 174.2 (C-1).

DEPT-135 ($CDCl_3$, 50 MHz): δ (ppm) = 26.3 (C-5), 26.6 (C-6), and 82.1 (C-2). Signal at 67.9 (C-3) inverted due to secondary nature of the carbon, while signals at 114.0 (C-4) and 174.2 (C-1) disappeared due to the quaternary nature of the carbons.

5.2.31 Potassium-[D]-2,3-isopropylideneglycerate[89] (ML02016)

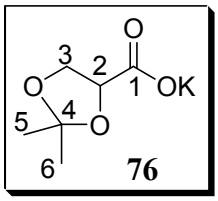

76

Potassium permanganate (10.27 g, 70.0 mmol) in 250 ml water was added slowly to crude [D]-2,3-isopropylideneglyceraldehyde (6.5 g, 49.9 mmol) and potassium hydroxide (5.70 g, 100 mmol) in 100 ml water at 0 °C. The solution was neutralized to pH 8 after 3 h. Water was removed by distillation producing a brown mass, which on extraction with hot ethanol yielded a yellow oil. The oil on precipitation with acetone 100 ml, gave a white solid.

Yield: 6.50 g (35.3 mmol) of a white solid, 46%.

Melting Point: softens above 60° C.

IR (NaCl): $\tilde{\nu}$ (cm^{-1}) = 2992 (m, CH), 2958, 2881, 1620 (bs, C=O), 1372, 1259, 1218, 1149, 1067, 970, 846, 788, 512.

^{1}H-NMR (D_2O, 200 MHz): δ (ppm) = 1.23 (s, 3H), 1.29 (s, 3H), 3.75 (dd, J = 8.2 Hz, J = 6.8 Hz, 1H, 2-H), 4.12 (t, J = 8.1 Hz, 1H, 3a-H), 4.31 (t, J = 7.4 Hz, 1H, 3b-H).

5.2.32 [D]-2,3-Isopropylideneglyceraldehyde[89] (ML02042.1)

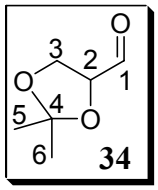

34

Sodium metaperiodate (12.5 g, 58.3 mmol) was added to [D]-1,2,5,6-diisopropyli-enemannitol (10.0 g, 38.1 mmol) in dichloromethane (100 ml) and 4.40 ml of saturated sodium bicarbonate. The reaction was stirred at room temperature for 5 h, filtered and concentrated at temperature lower than 45 °C. The crude product was purified by distillation under reduced pressure.

Yield: 6.20 g (47.6 mmol) of a colourless liquid, 62%.

Boiling Point: 42-44 °C/11 mbar (Lit:[193] 31 °C/1 torr)

IR (NaCl): $\tilde{\nu}$ (cm^{-1}) = 3451 (m, OH), 2990 (s, CH), 2892, 2819, 1735 (s, C=O), 1456, 1375, 1255, 1220, 1151, 1073, 842.

^{1}H-NMR ($CDCl_3$, 200 MHz): δ (ppm) = 1.39 (s, 3H, 5-H), 1.46 (s, 3H, H-6), 4.03-4.19 (m, 2H, 3-H), 4.33-4.40 (m, 1H, 2-H), 9.68 (s, 1H, 1-H).

^{13}C-NMR ($CDCl_3$, 50 MHz): δ (ppm) = 26.3 (C-5), 27.2 (C-6), 66.6 (C-3), 80.7 (C-2), 112.3 (C-4), and 202.8 (C-1).

5.2.33 [D]-1,2,5,6-Diisopropylidenemannitol (ML01173)

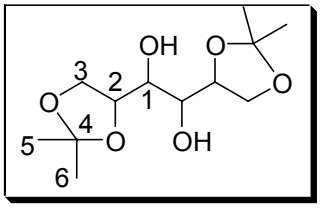

D-mannitol (36.0 g, 190 mmol) was added to a vigorously stirring dry acetone (150 ml) containing fused zinc chloride (75 g, 550 mmol) at 0 °C. A solution of potassium carbonate in water (100 g in 100 ml) was added slowly to the reaction mixture after 3 h. The precipitate was filtered out and the filtrate was extracted with chloroform (3 × 300 ml). The combined organic layer was dried over Na_2SO_4 (anhyd.) and concentrated.

Yield: 37.0 g (0.14 mol) of a white solid, 72%.

Melting Point: 120-122 °C (Lit:[194] 118-120 °C)

IR (NaCl): $\tilde{\nu}$ (cm^{-1}) = 3404 (b, OH), 3283, 2989 (s, CH), 2935, 2895, 1381, 1265, 1213, 1160, 1126, 1069, 1009, 943, 858, 800, 666, 516.

^{1}H-NMR ($CDCl_3$, 200 MHz): δ (ppm) = 1.34 (s, 6H, 5-H), 1.39 (s, 6H, 6-H), 2.82 (m, 2H, OH), 3.71 (t, *J* = 6.6 Hz, 2H, 1-H), 3.91-4.13 (m, 6H, 2,3-H).

5.2.34 2-(2,2-Dimethyl-[1,3]dioxolan-4-ylsulfanyl)-pyridine (ML05115.12)

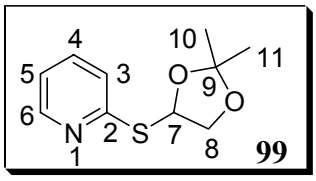

A solution of **75** (0.5 g, 2.0 mmol) in 25 ml benzene (dry) was photolysed (300 W UV-Lamp) for about 20 min. The reaction mixture was concentrated and purified by column chromatography with hexane ethyl acetate as eluent. The pure product was collected as second fraction with 20% ethyl acetate in hexane.

Yield: 0.3 g (1.4 mmol) of colourless oil, 73%.

IR (NaCl): $\tilde{\nu}$ (cm^{-1}) = 3046 (w), 2988 (m), 2937, 2872, 1578 (s), 1453 (s), 1417, 1374 (s), 1220 (b), 1148 (b), 1127, 1072 (bs), 989, 949, 838 (s), 760 (s), 725, 639, 514.

^{1}H-NMR ($CDCl_3$, 200 MHz): δ (ppm) = 1.44 (s, 3H, 10-H), 1.53 (s, 3H, 11-H), 4.12 (dd,

^3J = 9.4 Hz, ^2J = 4.7 Hz 1H, 8-H), 4.46 (dd, ^3J = 9.4 Hz, ^2J = 6.4 Hz, 1H, 8-H), 6.34 (dd, ^3J = 6.4 Hz, ^3J = 4.7 Hz, 1H, 7-H), 7.00-7.06 (m, 1H, 5-H), 7.24-7.29 (m, 1H, 3-H), 7.45-7.55 (m, 1H, 4-H), 8.44-8.49 (m, 1H, 6-H).

^{13}C-NMR ($CDCl_3$, 50 MHz): δ (ppm) = 26.0 (C-10), 26.0 (C-11), 70.0 (C-8), 80.1 (C-7), 115.5 (C-9), 120.2 (C-5), 122.1 (C-3), 136.4 (C-6,4), 149.7 (C-6).

5.2.35 2-*tert*-Butylsulphanyl-pyridine[90] (ML05114.11)

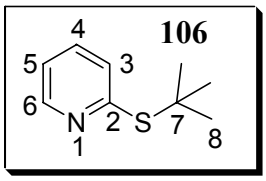

106

A solution of **78** (0.4 g, 2.0 mmol) in 25 ml benzene (dry) was photolysed (300 W UV-Lamp) for about 20 min. The reaction mixture was concentrated and purified by column chromatography with hexane ethyl acetate as eluent. The pure product was collected as second fraction with 20% ethyl acetate in hexane (R_f = 0.72).

Yield: 0.25 g (1.5 mmol) of colourless oil, 80%.

IR (NaCl): $\tilde{\nu}$ (cm^{-1}) = 3045 (w), 2961 (m), 2922, 1727, 1578 (s), 1556, 1449 (s), 1413, 1361 (s), 1278 (b), 1122 (b), 1072 (bs), 1044, 986, 758 (s), 724, 623.

^{1}H-NMR ($CDCl_3$, 200 MHz): δ (ppm) = 1.50 (s, 9H, 8-H), 7.04-7.10 (m, 1H, 5-H), 7.33 (dd, J = 7.9 Hz, J = 0.7 Hz, 1H, 3-H), 7.51 (td, J = 7.7 Hz, J = 2.0 Hz, 1H, 4-H), 8.51 (dt, J = 4.2 Hz, J = 0.7 Hz, 1H, 6-H).

^{13}C-NMR ($CDCl_3$, 50 MHz): δ (ppm) = 30.9 (C-8), 47.5 (C-7), 120.7 (C-5), 127.4 (C-3), 135.9 (C-6,4), 149.4 (C-2).

5.2.36 1-Bromo-3,3-dimethyl-2-butanone (ML01073)

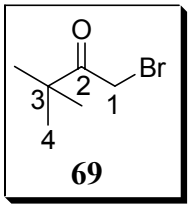

69

Bromine (12.0 ml, 240 mmol) was added to a solution of 3,3-dimethyl-2-butanone (30.0 ml, 240 mmol) in dry ether (200 ml) at 0 °C over a period of 30 minutes. After complete addition, the reaction mixture was poured into cold water (200 ml) and extracted with ether (2 × 100 ml). The combined organic extract was dried over Na_2SO_4 (anhyd.) and concentrated. The crude product was purified by distillation.

Yield: 32.0 g (0.179 mol) of colourless liquid, 74%.

Boiling point: 64-68 °C/15 mbar (Lit:[88] 78 °C/4 mmHg).

IR (NaCl): $\tilde{\nu}$ (cm^{-1}) = 2970 (s, CH), 1719 (s, C=O), 1478, 1395, 1368, 1226, 1057, 1003, 684.

^{1}H-NMR ($CDCl_3$, 200 MHz): δ (ppm) = 1.15 (s, 9H, 4-H), 4.13 (s, 2H, 1-H).

5.2.37 (2,2-Dimethyl-1-methylene-propoxy)-trimethylsilane[86] (ML01022)

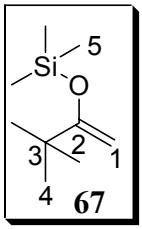

67

t-Butylmethyl ketone (31.1 ml, 300 mmol), DABCO (67.7 g, 600 mmol) and trimethylsilyl chloride (37.9 ml, 300 mmol) was refluxed for 4 h in dry DMF (100 ml). The reaction mixture was poured into water (100 ml) and extracted with pentane (5 × 100 ml). The combined organic layer was washed with 1.5 M HCl (2 × 100 ml), 10% $NaHCO_3$ (3 × 100 ml), dried over Na_2SO_4 (anhyd.) and concentrated. The crude product was purified by distillation under reduced pressure.

Yield: 32.1 g (186 mmol) of colourless liquid, 75%.

Boiling point: 45-48 °C / 19 mbar

IR (NaCl): $\tilde{\nu}$ (cm^{-1}) = 2961 (s, CH), 1619 (s, C=C), 1297, 1254, 1186, 1034, 1013, 881, 848.

^{1}H-NMR ($CDCl_3$, 200 MHz): δ (ppm) = 0.12 (s, 9H, 5-H), 1.09 (s, 9H, 4-H), 3.72 (s, 1H, 1-H), 3.90 (s, 1H, 1-H).

5.2.38 3,3-Dimethyl-1-trimethylsilanyloxy-butane-2-one[86] (ML01045.3)

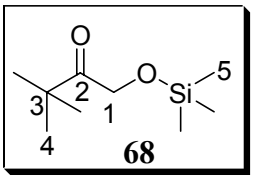

68

MCPBA (7.9 g, 31.8 mmol) was added portion wise over a period of 20 minutes to a mixture of 3,3-dimethyl-2-trimethylsilanyloxy-but-1-ene (5.0 g, 30.0 mmol) and sodium carbonate (3.1 g, 30.0 mmol) in dry dichloromethane (30 ml). After 1 h the excess of peroxide was decomposed with 10% Na_2SO_3 (4 × 100 ml) and the organic layer was washed with saturated $NaHCO_3$ (4 × 25 ml). The combined organic layer was dried over Na_2SO_4 (anhyd.) and concentrated. The crude product was purified by distillation.

Yield: 2.30 g (12.2 mmol) of a colourless liquid, 42%.

Boiling point: 60-62 °C/8 mbar

IR (NaCl): $\tilde{\nu}$ (cm^{-1}) = 2960 (s, CH), 1725 (s, C=O), 1480, 1368, 1251, 1173, 1056, 1000, 872, 844, 755.

^{1}H-NMR ($CDCl_3$, 200 MHz): δ (ppm) = 0.12 (s, 9H, 5-H), 1.19 (s, 9H, 4-H), 4.45 (s, 2H, 1-H).

5.2.39 1-Benzyloxy-3,3-dimethyl-2-butanone (ML01052.2)

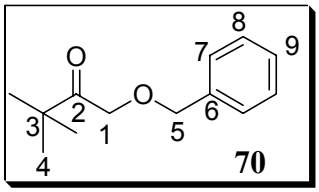

Benzylalcohol (100 ml, 924 mmol) was added to DMSO (200 ml) containing potassium hydroxide (51.8 g, 924 mmol) at room temperature. After 15 minutes, 1-bromo-3, 3-dimethyl-2-butanone (40.0 g, 223 mmol) was added. The reaction mixture was poured into water (1 L) after 30 minutes and extracted with dichloromethane (3 × 300 ml). The combined organic layer was dried over Na_2SO_4 (anhyd.) and concentrated. The crude product was purified by distillation under reduced pressure.

Yield: 27.6 g (133.8 mmol) of a colourless liquid, 60%.

Boiling point: 85-90 °C/5 mbar.

IR (NaCl): $\tilde{\nu}$ (cm^{-1}) = 3032 (w, CH), 2966 (s, CH), 2871, 1720 (s, C=O), 1497, 1478, 1455, 1393, 1367, 1204, 1141, 1057 (s, CH), 1005, 780, 738, 698.

^{1}H-NMR ($CDCl_3$, 200 MHz): δ (ppm) = 1.19 (s, 9H, 4-H), 4.31 (s, 2H, 1-H), 4.54 (s, 2H, 5-H), 7.20-7.35 (m, 5H, 7,8,9-H).

^{13}C-NMR ($CDCl_3$, 50 MHz): δ (ppm) = 27.1 (C-4), 43.7 (C-3), 71.4 (C-1), 73.9 (C-5), 128.5 (C-7), 128.8 (C-9), 129.3 (C-8), 138.4 (C-6), 212.5 (C-2).

5.2.40 2-Benzyloxy-1-ferrocenyl-1-hydroxy-4,4-dimethyl-3-pentanone (ML01059)

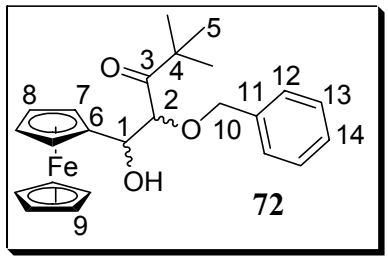

t-Butylbenzyloxy ketone **70** (200 mg, 1.00 mmol) dissolved in 1 ml dry THF was added to LDA in 15 ml THF, prepared from butyllithium (580 µl, 1.50 mmol) and diisopropylamine

(160 µl, 1.50 mmol) at – 40 °C. Ferrocenealdehyde (210 mg, 1.00 mmol) was added after 30 minutes. The reaction was warmed slowly to room temperature over a period of 2 h and stirred overnight. Reaction was quenched with 15 ml saturated ammonium chloride solution and extracted with ether (3 × 25 ml). The combined organic layer was dried over Na_2SO_4 (anhyd.) and concentrated. The crude product was isolated by column chromatography with hexane:diethyl ether (30%) as the eluent.

Yield: 21.3 mg (0.051 mmol) of a yellow solid, 5%.

Melting point: 157 °C.

IR (KBr): $\tilde{\nu}$ (cm^{-1}) = 3225 (bs, OH), 2955 (s, CH), 1700, 1452, 1380, 1354, 1236, 1190, 1104, 1040, 990, 923, 810, 741.

^{1}H-NMR ($CDCl_3$, 200 MHz): δ (ppm) = 0.88 (s, 18H, 5-H), 2.63 (d, *J* = 1.7 Hz, 1H, OH), 2.69 (d, *J* = 9.8 Hz, OH), 3.40 (d, *J* = 5.9 Hz, 1H, 2-H), 3.48 (d, *J* = 9.8 Hz, 1H, 2´-H), 4.22 (s, 9H, 7,8,9-H), 4.22 (s, 9H, 7´,8´,9´-H), 4.32 (d, *J* = 7.4 Hz, 2H, 10-H), 4.36-4.50 (m, 1H, 1-H), 4.59-4.63 (dd, *J* = 2.5 Hz, *J* = 3.0 Hz, 1H, 1´-H), 7.21-7.33 (m, 10H, Aromatic-H).

^{13}C-NMR ($CDCl_3$, 50 MHz): δ (ppm) = 27.2 (C-5, 5´), 35.7 (C-4), 66.2 (C-2, 2´), 69.0 (C-9), 69.4 (C-6), 69.5 (C-8), 69.6 (C-6´), 71.4 (C-7, 7´), 73.3 (C-10, 10´), 77.7 (C-1), 80.8 (C-1´), 128.8 (C-14, 14´), 129.1 (C-12, 12´), 129.3 (C-13, 13´), 138.6 (C-11, 11´), 200.2 (C-3).

Mass (EI, 70 eV): (m/z) = 422 ($M^{+\bullet}$)

5.2.41 (1-Benzyloxymethylene-2,2-dimethyl-propoxy)-trimethylsilane

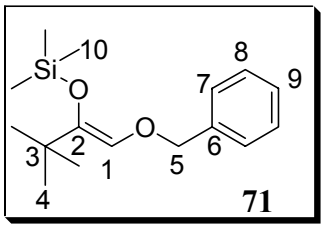

71

Diisopropylamine (180 µl, 1.33 mmol) was added to a solution of butyllithium (530 µl, 1.33 mmol, 2.5 M solution in THF) in dry THF (15 ml) at 0 °C. **70** (250 mg, 1.21 mmol) in 2 ml THF was added after 30 minutes at – 40 °C. The reaction was quenched with trimethylsilyl chloride (190 µl 1.50 mmol) followed by water (10 ml). The aqueous layer was extracted with ether (3 × 20 ml). The combined organic layer was washed twice with 10 ml 10% sodium bicarbonate solution, water and brine. The organic layer was dried over Na_2SO_4 (anhyd.) and concentrated, crude product was characterised by ^{1}H-NMR.

Yield: 310 mg (1.11 mmol) of a colourless liquid, 90%.

^{1}H-NMR ($CDCl_3$, 200 MHz): δ (ppm) = 0.07 (s, 9H, 10-H), 0.94 (s, 9H, 4-H), 4.61 (s, 2H, 5-H), 5.56 (s, 1H, 1-H), 7.22-7.28 (m, 5H, 7,8,9-H).

5.2.42 4,4-Dimethyl-1-ferrocenylpent-1-ene-3-one (ML01032.2)

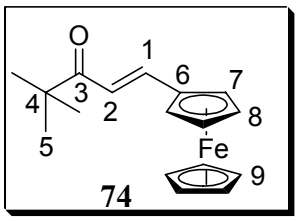

74

3,3-Dimethyl-2-butanone (100 µl, 800 µmol) was added to dry THF (10 ml) containing butyllithium (400 µl, 1.2 mmol) and diisopropylamine (140 µl, 1.2 mmol) at – 40 °C. After 15 minutes ferrocenealdehyde (171 mg, 800 µmol) dissolved in 1 ml dry THF was added. The reaction was monitored by TLC and was worked up with either dil. HCl (0.1 M, 1 ml) or was quenched with saturated ammonium chloride and left overnight. The reaction mixture was extracted with ether (4 × 10 ml), the combined organic layer was dried over Na_2SO_4 (anhyd.) and concentrated.

Yield: 240 mg (0.81 mmol) of a red solid, >99 %.

Melting point: 109-110 °C (Lit:[195] 108-109 °C)

IR (KBr): $\tilde{\nu}$ (cm^{-1}) = 2964 (s, CH), 1670 (s, C=C), 1595, 1473, 1394, 1362, 1287, 1179, 1081, 1044, 1006, 981, 807, 685, 524, 476.

^{1}H-NMR ($CDCl_3$, 200 MHz): δ (ppm) = 1.1 (s, 9H, 5-H), 4.2 (s, 7H, 8,9-H), 4.4 (d, 2H, 7-H), 6.7 (d, 1H, 2-H), 7.8 (d, 1H, 1-H).

^{13}C-NMR ($CDCl_3$, 50 MHz): δ (ppm) = 27.4 (C-5), 45.5 (C-4), 69.7 (C-9), 70.6 (C-7), 71.9 (C-8), 80.2 (C-6), 119.0 (C-2), 145.0 (C-1), 204.8 (C-3).

Elemental analysis: Calculated C = 68.94, H = 6.81

Found C = 69.17, H = 6.81

5.2.43 1-Ferrocenyl-1-hydroxy-4,4-dimethyl-3-pentanone (ML01034.1)

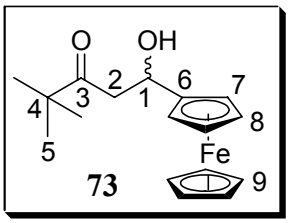

73

Butyllithium (1.1 ml, 2.5 M in THF, 2.7 mmol) was added to a solution of diisopropylamine (400 µl, 2.7 mmol) in 20 ml of dry THF at 0 °C. After 15 minutes, later 2,2-dimethyl-3-butanone (300 µl, 2.4 mmol) was added at – 40 °C. Ferrocenealdehyde (500 mg, 2.4 mmol) in THF 5 ml was added after 30 minutes. The reaction was quenched after 10-15 minutes with saturated ammonium chloride solution and extracted with ether (3 × 20 ml). The combined

organic layer was dried over Na_2SO_4 (anhyd.) and concentrated. The crude product containing the dehydrated Aldol was purified by column chromatography with hexane:diethyl ether (20%) as eluent.

Yield: 600 mg (1.90 mmol) of yellow solid, 81%.

Melting point: 104 °C.

IR (KBr): $\tilde{\nu}$ (cm^{-1}) = 3521 (s, OH), 3079 (w), 2965 (m), 1691 (s, C=O), 1478, 1388, 1358, 1297, 1255, 1224, 1189, 1089, 1060, 1009, 816, 692, 491.

^{1}H-NMR ($CDCl_3$, 200 MHz): δ (ppm) = 1.12 (s, 9H, 5-H), 2.90 (d, 2H, 2-H), 4.19 (s, 9H, 7,8,9-H), 4.8-4.9 (m, 1H, 1-H).

^{13}C-NMR ($CDCl_3$, 50 MHz): δ (ppm) = 27.1 (C-5), 45.3 (C-4), 66.8 (C-2), 67.2 (C-9), 67.6 (C-8), 68.8 (C-7), 68.9, 69.5 (C-6), 92.9 (C-1), 216.8 (C-3).

Elemental analysis: Calculated C = 64.98, H = 6.76

Found C = 65.15, H = 7.07

5.2.44 Fluorene-9-one *O*-(2-methoxyacetyl)-oxime (ML05034.1)

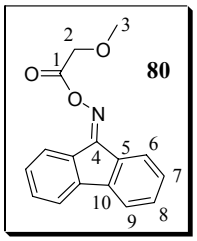

Methoxyacetylchloride (1.2 g, 11 mmol) was added dropwise to a solution of 9-fluorenoneoxime (2.0 g, 10 mmol) and triethylamine (1.2 g, 12 mmol) in 25 ml dry DCM at room temperature. After 12 h the reaction mixture was filtered through celite and concentrated yielding a pale yellow coloured solid.

Yield: 1.9 g (7.1 mmol) of a pale yellow solid, 69%.

Melting: **Point**: 73-74 °C

IR (NaCl): $\tilde{\nu}$ (cm^{-1}) = 1780 (s, C=O), 1449, 1201, 1172, 1120, 1102, 958, 940, 782, 725.

^{1}H-NMR ($CDCl_3$, 200 MHz): δ (ppm) = 3.58 (s, 3H, 3-H), 4.47 (s, 2H, 2-H), 7.33 (dt, ^3J = 7.4 Hz, ^4J = 1.2 Hz, 2H, 7-H), 7.46 (dq, ^3J = 7.6 Hz, ^4J = 1.2 Hz, 2H, 8-H), 7.61 (t, ^3J = 7.4 Hz, 2H, 9-H), 7.90 (d, ^3J = 7.4 Hz, 1H, 6-H), 8.30 (d, ^3J = 7.6 Hz, 1H, 6′-H).

5.2.45 Fluorene-9-one *O*-(2-methoxy-3-hydroxy-3-ferrocenylpropanyl)-oxime (ML05036.13)

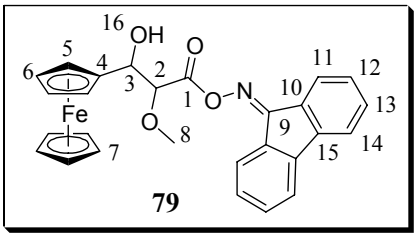

79

Butyllithium (1.0 ml, 2.3 mmol) was added to a solution of diisopropylamine (0.4 ml, 2.3 mmol) in 20 ml dry THF at 0 °C. After 15 min a solution of 9-fluorenoneoxime-2-methoxyacetate (0.6 g, 2.3 mmol) in 2 ml dry THF was added to the above solution at -70 °C. After 45 min a solution of ferrocenealdehyde (0.5 g, 2.6 mmol) was added to the reaction mixture. The reaction was quenched after 20 min with water (15 ml). The aqueous layer was extracted with ether and combined organic layer was dried over Na_2SO_4 (anhyd.) and concentrated below 40 °C. The pure product was isolated by column chromatography, starting initially with DCM (ferrocenealdehyde was collected) to 20% ether finally to 80% ether (product was collected).

Yield: 95 mg (0.2 mmol) of a brown solid, 9%.

Melting Point: Decomposes above 65 °C.

^{1}H-NMR ($CDCl_3$, 200 MHz): δ (ppm) = 2.75 (bs, 1H, OH, 16-H), 3.56 (s, 3H, 8-H), 4.08-4.18 (m, 4H, 5,6-H), 4.21 (s, 5H, 7-H), 4.38 (bs, 1H, 2-H), 4.83 (d, ^3J = 5.2 Hz, 1H, 3-H), 7.31 (d, ^3J = 7.4 Hz, 2H, 12-H), 7.46 (dq, ^3J = 7.6 Hz, ^4J = 1.0 Hz, 2H, 13-H), 7.59 (t, ^3J = 7.4 Hz, 2H, 14-H), 7.93 (d, ^3J = 7.4 Hz, 1H, 11-H), 8.14 (d, ^3J = 7.6 Hz, 1H, 11´-H).

^{13}C-NMR ($CDCl_3$, 50 MHz): δ (ppm) = 42.3 (C-8), 57.6 (C-3), 65.8 (C-2), 67.9 (C-5), 68.5 (C-6), 71.3 (C-7), 84.8 (C-4), 120.1 (C-14), 123.6 (C-12), 128.4 (C-11), 130.0 (C-13), 130.6 (C-15), 132.7 (C-10), 141.3 (C-9), 167.7 (C-1).

HRMS: $C_{27}H_{23}FeNO_4$, Calculated: 481.0976, Found: 481.0990

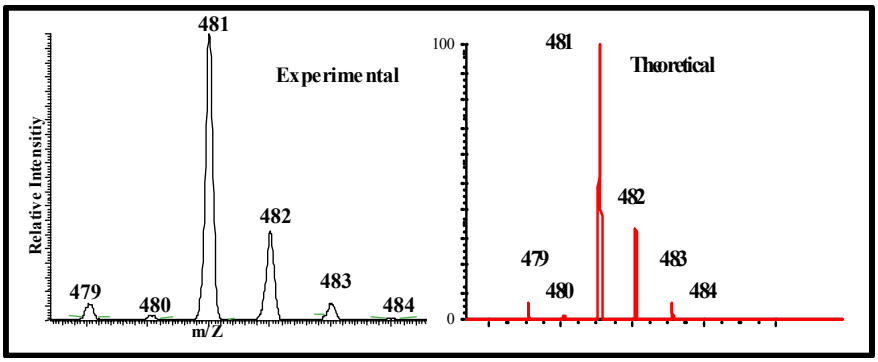

ESI-MS: (m/z) = 481.1 ($M^{+\bullet}$)

5.2.46 Dibromo-(dimethylglyoximato)-cobalt (III)[95] (ML05019)

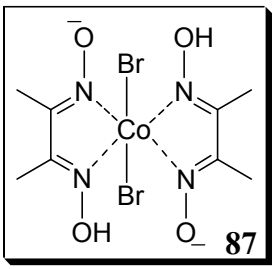

Dimethylglyoxime (2.2 g, 19 mmol) was added to a solution of cobalt(II) bromide (3.0 g, 9.2 mmol) in 50 ml acetone. A gentle stream of air was purged into the solution, leading to precipitation of a green coloured solid. After 30 min the reaction mixture was chilled on ice, filtered and washed with cold acetone (2 × 15 ml).

Yield: 3.5 g (7.8 mmol) of a yellow solid, 57%.

Melting point: decomposes above 212 °C.

IR (KBr): $\tilde{\nu}$ (cm^{-1}) = 2910 (s), 1604, 1537, 1530, 1512, 1503, 1494, 1472, 1454, 1440, 1418, 1383, 1220, 1192, 1115, 1102, 1069, 1051, 1014, 998, 969, 730, 717, 506.

Elemental analysis: Calculated C = 21.40, H = 3.14, N = 12.48

Found C = 21.54, H = 3.32, N = 12.18

5.2.47 Bromo-(4-*tert*-butyl-pyridine)-cobaloxime[95] (ML05020)

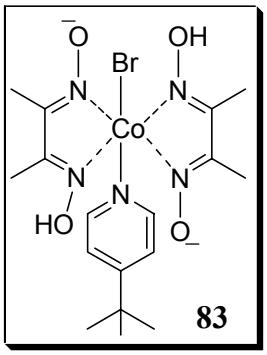

Dibromo-(dimethylglyoximato)cobalt (III) (3.0 g, 6.7 mmol) was suspended in 80 ml of methanol. To the above suspension 4-*tert*-butylpyridine (2.1 ml, 14 mmol) was added and the mixture was stirred until the green solid was replaced by a brown coloured crystalline solid (~25 min). To the above solution water was added with stirring and the suspension was cooled in ice bath for about 10 min and filtered yielding the desired product as a brown solid.

Yield: 3.3 g (6.5 mmol) of a brown solid, 98%.

Melting point: decomposes above 212 °C.

IR (KBr): $\tilde{\nu}$ (cm^{-1}) = 1618 (s), 1566, 1439, 1428, 1238, 1094, 1072, 1029, 978, 834.

^{1}H-NMR ($CDCl_3$, 200 MHz): δ (ppm) = 1.22 (s, 9H, 1-H), 2.39 (s, 12H, 4-H), 7.17 (d,

J = 5.4 Hz, 2H, 2-H), 8.05 (d, *J* = 5.4 Hz, 2H, 3-H).

Elemental analysis: Calculated C = 40.49, H = 5.40, N = 13.89

Found C = 40.38, H = 5.41, N = 13.75

5.2.48 4-Ferrocenyl-2-hydroxy-1-(2-iodobenzyloxy)-3-ethyne (ML01158.12)

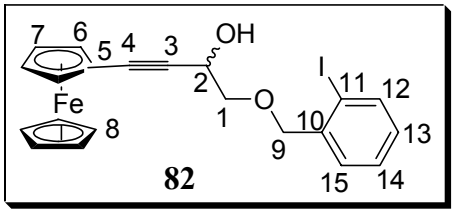

82

2-Ferrocenylethyne (290 mg, 1.42 mmol) in 2 ml dry THF was added to ethylmagnesium bromide prepared from ethyl bromide (110 µl, 1.47 mmol) and magnesium (34.5 mg, 1.42 mmol) in 1 ml of dry THF. *o*-Iodobenzyloxyacetaldehyde (390 mg, 1.42 mmol) was added after 15 minutes. Reaction was monitored by TLC, quenched with saturated ammonium chloride solution (10 ml) and extracted with ether (3 × 25 ml). The combined extracts were dried over Na_2SO_4 (anhyd.) and concentrated. The crude product was purified by column chromatography with hexane:diethyl ether (20%) as eluent.

Yield: 240 mg (0.49 mmol) of brown oil, 68%.

IR (NaCl): $\tilde{\nu}$ (cm^{-1}) = 3420 (b, OH), 3091 (w, CH), 2917 (m, CH), 2230 (s, C≡C), 1565, 1462, 1437, 1411, 1264, 1106, 1045, 1012, 903, 821, 751.

^{1}H-NMR ($CDCl_3$, 200 MHz): δ (ppm) = 3.03 (b, 1H, OH), 3.67-3.83 (m, 2H, 1-H), 4.18 (s, 7H, 7,8-H), 4.43 (s, 2H, 6-H), 4.62 (s, 2H, 9-H), 4.74 (t, ^3J = 3.5 Hz, 1H, 2-H), 6.95 (t, ^3J = 7.4 Hz, ^3J = 7.6 Hz, 1H, 14-H), 7.31 (t, ^3J = 7.4 Hz, ^3J = 7.6 Hz, 1H, 13-H), 7.46 (d, ^3J = 7.4 Hz, 1H, 12-H), 7.81 (d, ^3J = 7.9 Hz, 1H, 15-H).

^{13}C-NMR ($CDCl_3$, 50 MHz): δ (ppm) = 63.3 (C-6), 69.6 (C-5), 69.7 (C-7), 71.0(C-8), 72.5 (C-2), 75.3 (C-1), 78.0 (C-9), 83.9 (C-3), 85.5 (C-4), 99.0 (C-11), 129.3 (C-14), 130.1 (C-13), 130.5 (C-12), 140.3 (C-15), and 140.9 (C-10).

DEPT-135 ($CDCl_3$, 50 MHz): δ = 63.3, 69.7, 71.0, 72.5, 129.3, 130.1, 130.5, and 140.3. Signals at 75.3, 78.0 were inverted due to the secondary nature of the carbon while the signals at 83.9, 85.5, 99.0 and 140.5 disappeared due to the quaternary nature of the carbon.

5.2.49 (2-Iodo-benzyloxy)-acetaldehyde (ML01164.12)

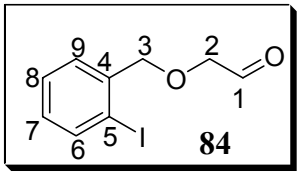

84

2-Iodobenzyloxyacetaldehyde diethylacetal (350 mg 1.00 mmol), 310 µl of trifluoroacetic acid in 10 ml chloroform was refluxed for nearly 2 h. The reaction mixture was stirred at room temperature for 16 h, diluted with 10 ml water and extracted with chloroform (3 × 15 ml). The combined organic layer was washed with saturated sodium bicarbonate solution (3 × 20 ml) and dried over Na_2SO_4 (anhyd.) and concentrated. The crude product was purified by column chromatography with hexane:diethyl ether (50%) as eluent.

Yield: 200 mg (0.73 mmol) of a colourless liquid, 71%.

IR (NaCl): $\tilde{\nu}$ (cm^{-1}) = 2920, 1736 (C=O), 1711 (C=O), 1565, 1438, 1363, 1222, 1107, 1045, 1014, 910, 752, 733, 648.

^{1}H-NMR ($CDCl_3$, 200 MHz): δ (ppm) = 4.19 (s, 2H, 2-H), 4.62 (s, 2H, 3-H), 6.97-7.05 (m, 1H, 6-H), 7.32-7.46 (m, 2H, 7,8-H), 7.83 (d, *J* = 7.9 Hz, 1H, 9-H), 9.77 (s, 1H, 1-H).

^{13}CNMR ($CDCl_3$, 50 MHz): δ (ppm) = 76.8 (C-2), 78.3 (C-3), 99.0 (C-5), 129.4 (C-6), 130.1 (C-7, 8), 130.6, 130.7 (C-9), 140.3 (C-4), 201.2 (C-1).

DEPT-135 ($CDCl_3$, 50 MHz): δ = 129.4, 130.1, 130.7, 140.3, and 201.3. Signals at 76.8 and 78.3 inverted due to the secondary nature of the carbons, signals at 99.0, 130.6 disappeared due to the quaternary nature of the carbons.

5.2.50 1-(2,2-Diethoxy-ethoxymethyl)-2-iodo-benzene (ML01152.22)

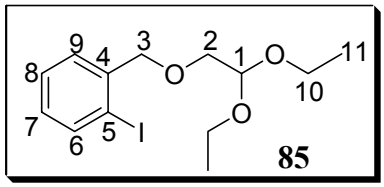

85

Bromoacetaldehyde diethylacetal (1.68 g, 8.52 mmol) was added to dry DMF (30 ml) containing sodium hydride (410 mg, 10 µmol, 60%) and 2-iodophenol (2.0 g, 8.52 mmol) at 0 °C. The reaction mixture was poured into water (50 ml) after 3 h and extracted with DCM (3 × 50 ml). The combined organic layer was dried over Na_2SO_4 (anhyd.) and concentrated. The crude product was purified by column chromatography yielding.

Yield: 1.33 g (3.80 mmol) of a colourless liquid, 45%.

IR (NaCl): $\tilde{\nu}$ (cm^{-1}) = 2975 (s), 2873, 1565, 1438, 1373, 1121, 1067 (s), 1013, 750.

^{1}H-NMR ($CDCl_3$, 200 MHz): δ (ppm) = 1.23 (t, ^3J = 7.1 Hz, 6H, 11-H), 3.51-3.80 (m, 6H, 10,2-H), 4.56 (s, 2H, 3-H), 4.71 (t, J = 5.2 Hz, 1H, 1-H), 6.95 (td, ^3J = 7.4 Hz, ^4J = 2.0 Hz, 1H, 8-H), 7.32 (td, ^3J = 7.4 Hz, ^4J = 1.2 Hz, 1H, 7-H), (t, ^3J = 7.4 Hz, 1H, 6-H), 7.37 (d, ^3J = 7.4 Hz, 1H, 9-H).

^{13}C-NMR ($CDCl_3$, 50 MHz): δ (ppm) = 16.4 (C-11), 63.2 (C-10), 72.1 (C-2), 77.9 (C-3), 98.5 (C-5), 102.0 (C-1), 129.1 (C-8), 129.6 (C-7), 130.1 (C-6), 140.0 (C-9), 141.4 (C-4).

DEPT-135 ($CDCl_3$, 50 MHz): δ (ppm) = 16.4, 102.0, 129.1, 129.6, 130.1, and 140.0. Signals at 63.2, 72.2 and 78.0 inverted due to the secondary nature of the carbons while signals at 98.5 and 141.4 disappeared due to their quaternary nature.

5.2.51 2-Bromo-1,1-diethoxy-ethane (ML01151)

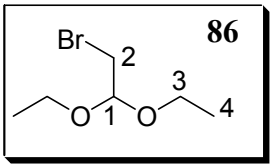

86

N-Bromosuccinamide (20.0 g, 110 mmol) was added slowly to an irradiating (300 W, UV lamp) acetaldehyde diethylacetal (13.3 g, 110 mmol) over a period of 30 min. After complete addition the reaction mixture was filtered. The crude product was purified by distillation under reduced pressure.

Yield: 10.2 g (52.0 mmol) of colourless liquid, 47%.

Boiling Point: 60-63 °C /16 mbar (Lit:[93] 67 °C/15 mbar).

IR (NaCl): $\tilde{\nu}$ (cm^{-1}) = 2977 (s, CH), 2882 (s, CH), 1739 (w, C-Br), 1444, 1373, 1348, 1128 (s), 1060 (s), 1016 (s), 888 (w), 811 (w), 683 (m).

^{1}H-NMR ($CDCl_3$, 200 MHz): δ (ppm) = 1.20 (t, J = 7.1 Hz, 6H, 4-H), 3.33 (d, J = 5.7 Hz, 2H, 2-H), 3.35-3.71 (m, 4H, 3-H), 4.63 (t, J = 5.7 Hz, 1H, 1-H).

5.2.52 (*E*/*Z*)-2-Chloro-1-ferrocenylethene[196] (ML02032.1)

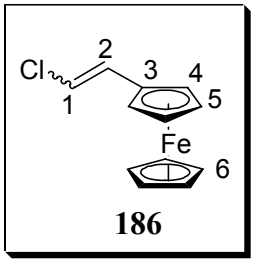

186

Potassium *t*-butoxide (11.2 g, 26.7 mmol) was added to a mixture of (chloromethyl) triphenylphosphonium chloride (7.9 g, 23.0 mmol) and ferrocenealdehyde (5.0 g, 23.0 mmol) in 100 ml dry THF at 0 °C. The reaction was stirred at room temperature for 15 h. Reaction

mixture was concentrated to obtain a brown solid, which was extracted with hexane. The combined organic layer was concentrated. The crude product was purified by column chromatography using hexane:DCM (3:1) as eluent.

Yield: 5.1 g (20.7 mmol) of brown oil, 87%.

IR (KBr): $\tilde{\nu}$ (cm^{-1}) = 3298 (s), 3094, 2109 (s, C≡C), 1632 (m, C=C), 1411, 1251, 1106, 1027, 1001, 930, 821, 733, 707, 645.

^{1}H-NMR ($CDCl_3$, 200 MHz): δ (ppm) = 4.15 (s, 10H, 6-H), 4.23 (m, 8H, 4,5-H), 6.04 (d, ^3J = 7.9 Hz, 1H, 1-H), 6.17 (d, ^3J = 13.3 Hz, 1H, 1-H), 6.35 (d, ^3J = 7.6 Hz, 1H, 2-H), 6.52 (d, ^3J = 13.5 Hz, 1H, 2-H).

5.2.53 1-Ferrocenylethyne[196] (ML02038)

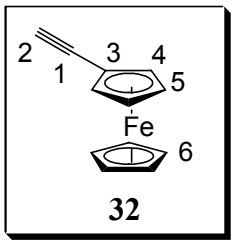

32

Potassium *t*-butoxide (1.8 g, 14.8 mmol) was added slowly to (E/Z)-2-chloro-1-ferrocenylethene in 30 ml of toluene at 0 °C. The reaction mixture was slowly warmed to room temperature and finally refluxed for 2 h. The reaction mixture was poured into water and extracted with hexane. The combined organic layer was dried over Na_2SO_4 (anhyd.) and concentrated.

Yield: 2.90 g (13.8 mmol) of a brown solid, 98%.

Melting point: 55 °C.

IR (KBr): $\tilde{\nu}$ (cm^{-1}) = 3327, 3280 (s), 3104, 2103 (s, C≡C), 1738, 1667, 1442, 1406, 1223, 1172, 1102, 1022, (s), 999, 913, 829, 662, 563.

^{1}H-NMR ($CDCl_3$, 200 MHz): δ (ppm) = 2.72 (s, 1H, 2-H), 4.19 (t, J = 2.0, 2H, 4-H), 4.22 (s, 5H, H-6), 4.46 (t, J = 2.0, 2H, 5-H).

Elemental analysis: Calculated C = 68.62, H = 4.80

Found C = 68.65, H = 4.79

5.2.54 2,2-Dimesityl-1-(2-pyridyl)-ethenol (ML03064.1)

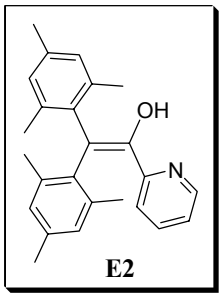

E2

To a solution of 2-bromopyridine (330 µl, 545 mg, 3.43 mol) in dry THF (20 ml) at – 78 °C, *n*-butyllithium (2.5 M in *n*-hexane, 1.22 ml, 3.7 mmol) was added dropwise. After 10 min a solution of dimesitylketene (960 mg, 3.43 mmol) in dry THF (20 ml) was added. The reaction mixture was stirred for 2 h at – 78°C and 12 h at room temp. After quenching with sat. aq. NH_4Cl solution (20 ml) and extraction with ether (3 × 20 ml) the combined organic layers were dried (Na_2SO_4). The solvent was removed in vacuum and the remaining brown oil was chromatographed on silica gel (hexane/ether 1:1, R_f = 0.6) yielding the desired enol **E2** as white solid.

Yield: 350 mg (1.0 mmol) of a white solid, 29%.

Melting Point: 168-170 °C.

IR (KBr): $\tilde{\nu}$ (cm^{-1}) = 3314 (bm, OH), 2918 (w), 2851 (m), 1609 (m), 1590 (s), 1564 (m), 1462 (s), 1436 (s), 1368 (m), 1276 (m), 1252 (m), 1197 (m), 1151 (m), 1084 (m), 900 (m), 856 (s).

^{1}H-NMR ($CDCl_3$, 200 MHz): δ (ppm) = 1.99, 2.15 and 2.27 (3s, coalescence, 18H, Mes-CH_3), 6.79 (s, 2H, Mes-H), 6.85 (s, 2H, Mes-H), 6.91 (d, 1H, ^3J = 7.8, 3′-H), 7.12 (m, 1H, 5′-H), 7.35 (dt, 1H, ^3J = 7.8, ^4J = 1.7, 4′-H), 8.44 (bs, 1H, OH), 8.53 (d, 1 H, ^3J = 4.7, 6′-H).

^{13}C-NMR ($CDCl_3$, 63 MHz): δ (ppm) = 20.8, 20.9, 21.0, 21.1, 114.8, 122.5, 129.1, 129.6, 129.7, 134.7, 135.6, 136.0, 136.1, 136.5, 138.1, 138.4, 146.4, 147.4, and 153.1.

Elemental analysis: Calculated C = 83.99, H = 7.61, N = 3.92

Found C = 83.86, H = 7.57, N = 3.92

5.2.55 2,2-Dimesityl-1-(3-pyridyl)-ethenol (ML03067.1)

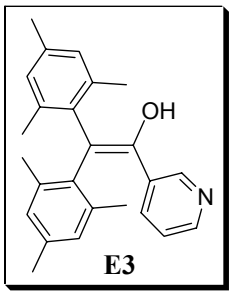

E3

To a solution of 3-bromopyridine (300 µl, 492 m g, 3.4 mol) in dry THF (20 ml) at –78 °C, *n*-butyllithium (2.5 M in *n*-hexane, 1.2 ml, 3.7 mmol) was added dropwise. After 10 min a solution of dimesitylketene (960 mg, 3.43 mmol) in dry THF (20 ml) was added. The reaction mixture was stirred for 2 h at 78 °C and 12 h at room temp. After quenching with sat. NH_4Cl solution (20 ml) and extraction with Et_2O (3 × 20 ml) the combined organic layers were dried (Na_2SO_4). The solvent was removed under *vacuum* and the remaining brown oil was chromatographed on silica gel (hexane/ether 1:1, R_f = 0.2) yielding the desired enol **E3** as a white solid.

Yield: 400 mg (1.12 mmol) of a white solid, 33%.

MP: 196-198 °C

IR (KBr): $\tilde{\nu}$ (cm^{-1}) = 3421 (bm, O-H), 2947 (C-H), 2919 (s), 2856 (m), 2617 (w), 1933 (vw), 1593 (s), 1560 (m), 1441 (s), 1155 (m), 1030 (s), 850 (s).

^{1}H-NMR ($CDCl_3$, 200 MHz): δ (ppm) = 1.91, 2.19 and 2.27 (3s, coalescence, 18H, Mes-CH_3), 5.61 (s, 1H, OH), 6.68 (s, 2H, Mes-H), 6.89 (bs, 2H, Mes-H), 7.07 (dd, 1H, *J* = 7.9, *J* = 4.9 , H-5´), 7.59 (dt, 1H, *J* = 7.9, *J* = 1.7, 6´-H), 8.31 (dd, 1H, *J* = 4.9, *J* = 1.7, H-4´), 8.48 (d, 1H, *J* = 1.7, 2-H´).

^{13}C-NMR ($CDCl_3$, 63 MHz): δ (ppm) = 21.7, 21.8, 21.9, 114.3, 123.8, 130.6, 133.1, 133.47, 135.5, 136.7, 137.4, 138.19, 138.8, 139.9, 148.7, 149.7, and 150.9.

Elemental analysis: Calculated C = 83.99, H = 7.61, N = 3.92

Found C = 83.82, H = 7.76, N = 3.89

5.2.56 2,2-Dimesityl-1-(8-quinolinyl)-ethenol (ML03081.1)

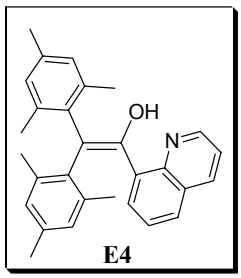

E4

To a solution of 8-bromoquinoline (0.5 g, 2.6 mmol) in dry THF (20 ml) at –78 °C, *sec*-butyllithium (2.5 M in *n*-hexane, 1.0 ml, 2.4 mmol) was added dropwise. After 10 min a solution of dimesitylketene (733 mg, 2.64 mmol) in dry THF (20 ml) was added. The reaction mixture was stirred for 2 h at -78 °C and 12 h at room temp.. After quenching with sat. aq. NH_4Cl solution (20 ml) and extraction with Et_2O (3 × 20 ml) the combined organic layers were dried (Na_2SO_4). The solvent was removed under *vacuum* and the remaining brown oil was chromatographed on silica gel (hexane/ether 1:1, R_f = 0.48) yielding the desired enol **E4** as an orange solid.

Yield: 475 mg (1.17 mmol) of orange solid, 44%.

Melting Point: 206-208 °C.

IR (KBr): $\tilde{\nu}$ (cm^{-1}) = 3389 (bm, O-H), 2953 (C-H), 2917 (s), 2857 (m), 1956 (vw), 1613 (s), 1408 (m), 1372 (s), 1311 (m), 1189 (m), 1014 (s), 900 (m), 852 (s), 790 (s).

^{1}H-NMR (DMSO-d_6, 400 MHz): δ (ppm) = 1.75, 2.05 and 2.21 (3s, coalescence, 18H, Mes-CH_3), 6.54 (bs, 2H, Mes-H), 6.77 (bs, 2 H, Mes-H), 7.28 (t, 1H, *J* = 8.0, 3′-H), 7.38 (dd, 1H, *J* = 8.0, *J* = 1.4, 6′-H), 7.57 (dd, 1H, *J* = 4.2, *J* = 8.4, 7′-H), 7.86 (dd, 1H, *J* = 1.4, *J* = 8.0, H-5′), 8.41 (dd, 1H, *J* = 1.7, *J* = 8.4, H-4′), 8.90 (dd, 1H, *J* = 1.7, *J* = 4.2, 1′-H), 9.84 (s, 1H, OH).

^{13}C-NMR (DMSO-d_6, 100 MHz): δ (ppm) = 20.3, 20.5, 114.4, 121.3, 125.7, 128.15, 128.6, 131.7, 134.2, 134.4, 135.7, 136.7, 137.2, 137.8, 145.5, 149.3, 151.2.

Elemental analysis: Calculated C = 85.47, H = 7.17, N = 3.44

Found C = 85.70, H = 7.22, N = 3.52

5.2.57 2,2-Dimesityl-1-(3′-thiophenyl)-ethene-1-ol (ML04031)

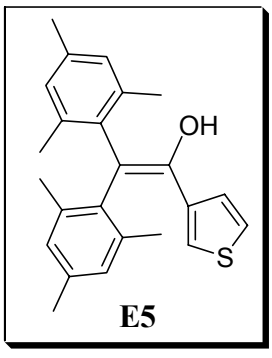

E5

n-Butyllithium (4.25 ml, 10.6 mmol) was added dropwise to a solution of 3-bromothiophene (1.72 g, 10.6 mmol) in 25 ml THF (dry) at –70 - –78 °C. After 2 h 25 ml solution of dimesityl keten (10.6 mmol) was added to the reaction mixture and the reaction was stirred for another 1 h at –78 C. The reaction was stirred at room temperature for another 12 h and quenched

with water and extracted with ether (3 × 25 ml), the combined organic layer was dried over Na_2SO_4 (anhyd.) and concentrated. The crude product was purified by column chromatography with hexane:ether (8:2) as eluent.

Yield: 3.1 g (8.6 mmol) of a colourless solid, 78%.

Melting point: 164-166 °C.

IR (NaCl): $\tilde{\nu}$ (cm^{-1}) = 3493 (s, OH), 3050, 2919, (alkyl), 1608 (C=C), 1441, 1238, 1169, 1060 (aromatic), 877, 854, 834, 791, 687, 497.

^{1}H-NMR ($CDCl_3$, 200 MHz): δ (ppm) = 2.17 (s, 12H, CH3), 2.23 (s, 3H, CH3), 2.27 (s, 3H, CH3), 5.09 (s, 1H, OH), 6.6 (dd, 1H), 6.73 (bs, 2H, CH), 6.88 (bs, 2H, CH), 6.99-7.04 (dd, 1H,), 7.34-7.36 (dd, 1H).

^{13}C-NMR ($CDCl_3$, 50 MHz): δ (ppm) = 20.68, 20.72, 20.80, 20.88, 20.91, 20.98, 111.13, 124.94, 127.36, 129.24, 132.38, 135.08, 136.05, 136.97, 137.49, 138.43, 139.11, 146.06.

Elemental Analysis: Calculated C = 79.51, H = 7.23, S = 8.85

Found C = 79.45, H = 7.70, S = 8.42

5.2.58 Trisiopropyl-prop-2-ynyloxy-silane (ML03099.1)

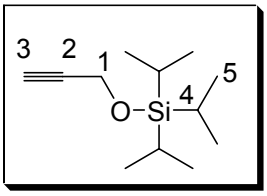

Propargyl alcohol (2,10 ml, 35,5 mmol), imidazole (3,60 g, 53,5 mmol) in 50 ml dichloromethane were stirred at 0 °C for 10-15 min. Triisopropylsilylchloride (7.60 g, 39.2 mmol) was added dropwise over a period of 5 min. The reaction mixture was stirred for another 30 min at 0 °C and at room temperature for 12 h. The reaction mixture was then filtered through celite and the filtrate was concentrated yielding a colourless liquid which was used as such without further purification.

Yield: 6.2 g (29 mmol) of a colourless liquid, 82%.

IR (NaCl): $\tilde{\nu}$ (cm^{-1}) = 3313, 2944, 2867, 2123 (alkyne), 1465, 1370, 1263, 1103, 1070, 1000, 921, 883, 774, 682, 660.

^{1}H-NMR ($CDCl_3$, 200 MHz): δ (ppm) = 1.08 (s, 5H, 18-H), 1.20-1.31 (m, 4H, 3-H), 2.40 (t, *J* = 2.2 Hz, 1H, 1-H), 4.38 (d, *J* = 2.2 Hz, 2H, 3-H).

^{13}C-NMR ($CDCl_3$, 50 MHz): δ (ppm) = 12.9 (C-5), 18.9 (C-4), 52.7 (C-3), 73.6 (C-1), 83.4 (C-2).

5.2.59 5-Triisopropylsilanyloxy-1,1-bis-(2,4,6-trimethyl-phenyl)-pent-1-en-3-yn-2-ol (ML03115.1)

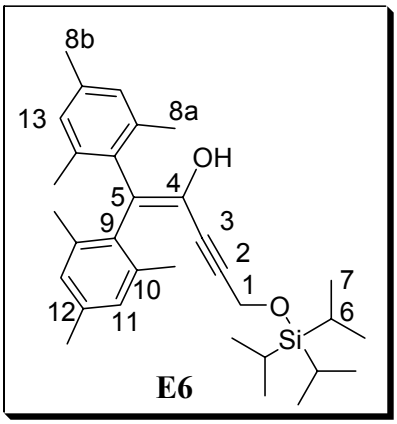

E6

Triisopropylsilyoxy-2-propyne (1.07 g, 4.70 mmol) was added to ethylmagnesium bromide generated by addition of ethyl bromide (0.6 g, 5.20 mmol) and magnesium (0.1 g, 5.20 mmol) in 10 ml THF (dry) at room temperature. After the effervescence of hydrogen gas stopped 15 ml THF solution of dimesitylketene (1.31 g, 4.70 mmol) was added. The reaction mixture was stirred at room temperature for 12 h and quenched with water. The reaction mixture was extracted with dichloromethane (2 × 25 ml), the combined organic layer was dried over Na_2SO_4 (anhyd.) and concentrated yielding a colourless solid which was recrystallised from hot pentane.

Yield: 0.9 g (1.8 mmol) of a colourless solid, 39%.

Melting Point: 98-99 °C

IR (NaCl): $\tilde{\nu}$ (cm^{-1}) = 3269 (bs, OH), 2919, 2864 (alkyl), 2214 (alkyne), 1612 (C=C), 1463, 1368, 1247, 1138, 1062 (aromatic), 1015, 882, 852, 725, 689, 584.

^{1}H-NMR ($CDCl_3$, 200 MHz): δ (ppm) = 0.98 (s, 21H, 7-H), 2.12-2.25 (bs, coalescence, 18H, 8-H), 4.43 (s, 2H, 1-H), 4.71 (bs, 1H, OH), 6.77 (bs, coalescence, 2H, 11-H), 6.86 (bs, coalescence, 2H, 13-H).

^{13}C-NMR ($CDCl_3$, 50 MHz): δ (ppm) = 12.9 (C-6), 18.9 (C-7), 21.8 (C-8a), 22.2 (C-8b), 53.3 (C-1), 81.6 (C-2), 91.6 (C-3), 122.2 (C-4), 130.0 (C-5), 130.1, 130.7, 132.3, 134.6, 135.1, 137.0, 138.3, 139.4.

Elemental analysis: Calculated C = 78.31, H = 9.45

Found C = 78.16, H = 9.70

5.2.60 5,5-Bis-(2,4,6-trimethyl-phenyl)-pent-4-en-2-yne-1,4-diol (ML04050.1)

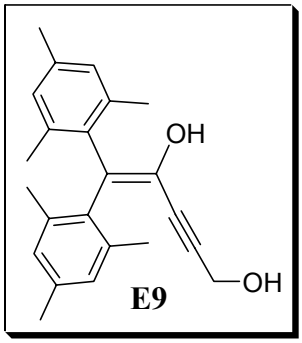

E9

E6 (0.4 g, 1.0 mmol) was added to a 20 ml solution of aqueous acidic methanol, prepared by dissolving 5 ml of 10% sulphuric acid to 15 ml methanol. The reaction mixture was stirred for 12-14 h and monitored by TLC. After complete consumption of starting material the reaction mixture was quenched with solid $NaHCO_3$ and concentrated. The residue was extracted with dichloromethane (2 × 25 ml), the combined organic layer was dried over Na_2SO_4 (anhyd.) and concentrated. The crude product was purified by column chromatography with 60:40 ether:hexane mixture as eluent (R_f = 0.5).

Yield: 225 mg (0.67 mmol) of colourless solid, 82%.

Melting point: 154 °C

IR (NaCl): $\tilde{\nu}$ (cm^{-1}) = 3413 (s, OH), 3197 (bs, OH), 2957, 2919, 2857 (alkyl), 2219 (alkyne), 1610 (C=C), 1474, 1445, 1375, 1262, 1203, 1178, 1097, 1046, 998, 967, 900, 856, 805, 594.

^{1}H-NMR ($CDCl_3$, 200 MHz): δ (ppm) = 1.60 (bs, 1H, OH), 2.17-2.24 (bs, coalescence, 18H, H-6a, 6b), 4.28 (s, 2H, 1-H), 4.85 (s, 1H, OH), 6.80 (bs, coalescence, 2H, 9-H), 6.86 (bs, coalescence, 2H, 10-H).

^{13}C-NMR ($CDCl_3$, 50 MHz): δ (ppm) = 21.8, 22.2, 52.4, 82.8, 90.9, 122.5, 130.0, 130.2, 130.8, 132.0, 134.6, 134.8, 137.4, 138.5, 139.4.

Elemental analysis: Calculated C = 82.60, H = 7.84

Found C = 82.25, H = 8.09

5.2.61 1-But-3-ynyloxy-triisopropyl-silane (ML03120.1)

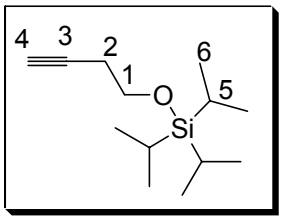

3-Butyne-1-ol (1,10 ml, 14,3 mmol), imidazole (1,50 g, 21,4 mmol) in 50 ml dichloromethane (dry) was stirred at 0 °C for 10-15 min. Triisopropylsilylchloride (3.03 g, 15.7 mmol) was

added dropwise over a period of 5 min. The reaction mixture was stirred for another 30 min at 0 °C and at room temperature for 12 h. The reaction mixture was then passed through celite and the filtrate was concentrated yielding a colourless liquid which was used as such without further purification.

Yield: 3.5 g (15.5 mmol) of a colourless liquid, 99%.

IR (NaCl): $\tilde{\nu}$ (cm^{-1}) = 3314, 2944, 2893, 2867, 2728, 2123 (alkyne), 1464, 1384, 1367, 1331, 1248, 1116, 1070, 1014, 996, 917, 883, 791, 736, 681, 658, 638.

^{1}H-NMR ($CDCl_3$, 200 MHz): δ (ppm) = 1.06 (s, 21H, TIPS), 1.94 (t, *J* = 2.7 Hz 1H, 4-H), 2.42 (dt, *J* = 2.7 Hz, *J* = 7.3 Hz, 2H, 2-H), 3.81 (d, *J* = 7.3 Hz, 2H, 1-H).

^{13}C-NMR ($CDCl_3$, 50 MHz): δ (ppm) = 13.0 (C-5), 18.9 (C-6), 23.9 (C-2), 63.0 (C-1), 70.2 (C-4), 82.4 (C-3).

5.2.62 6-Triisopropylsilanyloxy-1,1-bis-(2,4,6-trimethyl-phenyl)-hex-1-en-3-yn-2-ol (ML03124.1)

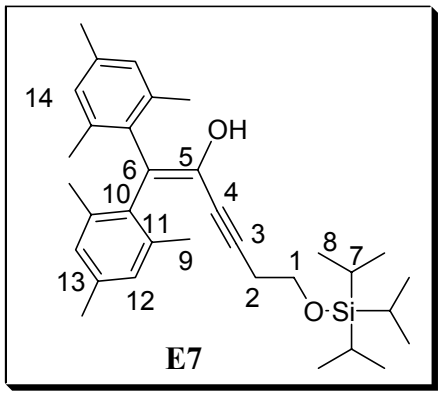

E7

Triisopropylsilyoxy-3-butyne (2.0 g, 8.8 mmol) was added to ethylmagnesium bromide generated by addition of ethyl bromide (1.1 g, 9.7 mmol) and magnesium (0.2 g, 9.7 mmol) in 20 ml THF (dry) at room temperature. After the effervescence of hydrogen gas stopped 25 ml THF solution of dimesitylketene (2.5 g, 8.8 mmol) was added. The reaction mixture was stirred at room temperature for 12 h and quenched with water. The reaction mixture was extracted with dichloromethane (2 × 25 ml), the combined organic layer was dried over Na_2SO_4 (anhyd.) and concentrated yielding a colourless crystalline solid, which was recrystallised from hot pentane.

Yield: 1.4 g (2.8 mmol) of a colourless crystalline solid, 31%.

Melting point: 126-128 °C

IR (NaCl): $\tilde{\nu}$ (cm^{-1}) = 3273 (bs, OH), 2956, 2916, 2863 (alkyl), 2727, 2214 (alkyne), 1721, 1610 (C=C), 1561, 1474, 1370, 1241, 1137, 1060 (aromatic), 1015, 965, 902, 885, 851, 828, 764, 696, 641, 567, 506.

^{1}H-NMR ($CDCl_3$, 200 MHz): δ (ppm) = 1.04 (s, 21H, 7,8-H), 2.12-2.25 (bs, coalescence, 18H, 9a,9b-H), 2.49 (t, *J* = 7.4 Hz, 2H, 2-H), 3.68 (t, *J* = 7.4 Hz, 2H, 1-H), 4.73 (bs, 1H, OH), 6.76 (bs, coalescence, 2H, 12-H), 6.86 (bs, coalescence, 2H, 14-H).

^{13}C-NMR ($CDCl_3$, 50 MHz): δ (ppm) = 12.9, 18.9, 21.8, 22.3, 24.9, 62.6, 91.1, 120.0, 129.9, 130.0, 130.7, 132.5, 135.0, 135.5, 136.9, 138.1, 138.3, 139.4.

5.2.63 6,6-Bis-(2,4,6-trimethyl-phenyl)-hex-5-ene-3-yne-1,5-diol (ML04051.1-3)

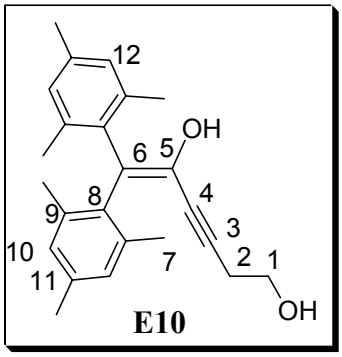

E10

6,6-Dimesityl-1-trisiopropylsilyloxhex-5-ene-3-yene-5-ol (0.6 g, 1.0 mmol) added to a 20 ml solution of aqueous acidic methanol, prepared by dissolving 5 ml of 10% sulphuric acid to 15 ml methanol. The reaction mixture was stirred for 12-14 h and monitored by TLC. After complete consumption of starting material the reaction mixture was quenched with solid $NaHCO_3$ and concentrated. The residue was extracted with dichloromethane (2 × 25 ml), the combined organic layer was dried over Na_2SO_4 (anhyd.) and concentrated. The crude product was purified by column chromatography with 60:40 ether:hexane mixture as eluent (R_f = 0.5).

Yield: 325 mg (0.93 mmol) of a colourless solid, 77%.

Melting point: 192-194 °C.

IR (NaCl): $\tilde{\nu}$ (cm^{-1}) = 3430 (s, OH), 3173 (bs, OH), 3017, 2995, 2958, 2916 (alkyl), 2853, 2214 (alkyne), 1611 (C=C), 1475, 1439, 1373, 1355, 1289, 1238, 1165, 1138, 1035, 902, 849, 821, 735, 683, 582.

^{1}H-NMR ($CDCl_3$, 200 MHz): δ (ppm) = 1.60 (bs, 1H, OH), 2.17-2.24 (bs, coalescence, 18H, 7a,7b-H), 2.49 (t, *J* = 5.8 Hz, 2H, 2-H), 3.57 (t, *J* = 5.8 Hz, 2H, 1-H), 4.88 (bs, 1H, OH), 6.82 (bs, coalescence, 2H, 10-H), 6.86, (bs, coalescence, 2H, 12-H).

^{13}C-NMR ($CDCl_3$, 50 MHz): δ (ppm) = 21.8, 25.0, 36.9, 61.7, 90.8, 121.4, 130.9, 132.1, 135.3, 135.4, 137.9, 138.3, 139.4, 139.6.

HRMS: Calculated for $C_{24}H_{28}O_2$: 348.2089, Found: 348.2093($M^{+\bullet}$).

5.2.64 Triisopropyl-pent-4-ynyloxy-silane (ML04057.1)

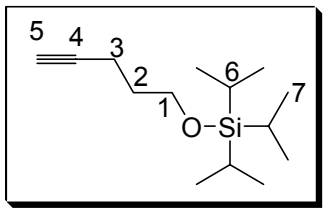

4-Pentyne-1-ol (1,82 g, 21,6 mmol), imidazole (2,21 g, 32,4 mmol) in 50 ml dichloromethane (dry) was stirred at 0 °C for 10-15 min. Triisopropylsilylchloride (5.01 g, 26.0 mmol) was added dropwise over a period of 5 min. The reaction mixture was stirred for another 30 min at 0 °C and at room temperature for 12 h. The reaction mixture was then passed through celite and the filtrate was concentrated yielding a colourless liquid which was used as such without further purification.

Yield: 3.6 g (15 mmol) of a colourless liquid, 70%.

IR (NaCl): $\tilde{\nu}$ (cm^{-1}) = 3314, 2944, 2893, 2867, 2727, 2121 (alkyne), 1464, 1385, 1247, 1111, 1070, 982, 948, 882, 797, 725, 680, 634.

^{1}H-NMR ($CDCl_3$, 200 MHz):δ (ppm) = 1.06 (s, 21H, 6 & 7-H), 1.75 (q, *J* = 6.1 Hz, 2H, 2-H) 1.92 (t, *J* = 2.7 Hz, 1H, 5-H), 2.30 (dt, *J* = 2.7 Hz, *J* = 7.1 Hz, 2H, 3-H), 3.77 (t, *J* = 6.1 Hz, 2H, 2-H).

^{13}C-NMR ($CDCl_3$, 50 MHz): δ (ppm) = 13.0 (C-6), 15.9 (C-2), 18.9 (C-7), 32.8 (C-3), 62.7 (C-1), 69.2 (C-5), 85.4 (C-4).

5.2.65 7-Triisopropylsilanyloxy-1,1-bis-(2,4,6-trimethyl-phenyl)-hept-1-en-3-yn-2-ol (ML04059.1)

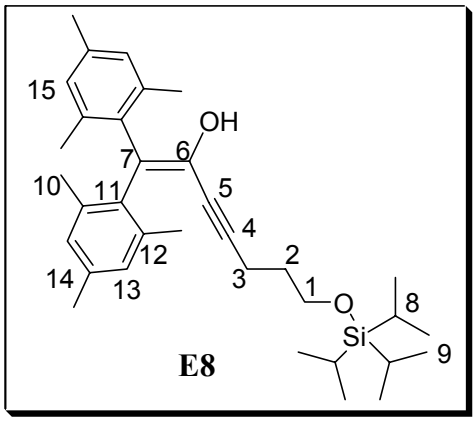

Triisopropylsilyoxy-4-pentyne (2.0 g, 8.3 mmol) was added to ethylmagnesium bromide generated by addition of ethyl bromide (1.0 g, 8.3 mmol) and magnesium (0.2 g, 9.7 mmol) in 20 ml THF (dry) at room temperature. After the effervescence of hydrogen gas stopped 25 ml THF solution of dimesitylketen (2.5 g, 8.8 mmol) was added. The reaction mixture was stirred

at room temperature for 12 h and quenched with water. The reaction mixture was extracted with dichloromethane (2 × 25 ml), the combined organic layer was dried over Na_2SO_4 (anhyd.) and concentrated yielding a brown oil.

Yield: 3.73 g (7.19 mmol) of brown oil, 80%.

^{1}H-NMR ($CDCl_3$, 200 MHz): δ (ppm) = 1.03 (s, 21H, 8,9-H), 1.64 (q, ^3J = 5.8 Hz, 2H, 2-H) 1.99-2.28 (bs, coalescence, 18H, 10a,10b-H), 2.38 (t, ^3J = 7.0 Hz, 2H, 3-H), 3.53 (t, ^3J = 5.8 Hz, 2H, 1-H), 4.72 (bs, 1H, OH), 6.77 (bs, coalescence, 2H, 14-H), 6.86 (bs, coalescence, 2H, 15-H).

^{13}C-NMR ($CDCl_3$, 50 MHz): δ (ppm) = 12.9, 16.8, 19.0, 21.8, 21.9, 32.4, 62.4, 94.2, 120.5, 129.9, 130.0, 130.7, 132.65, 135.1, 135.7, 136.8, 138.1, 139.5.

5.2.66 7,7-Bis-(2,4,6-trimethyl-phenyl)-hept-6-en-4-yne-1,6-diol (ML04096.1-b)

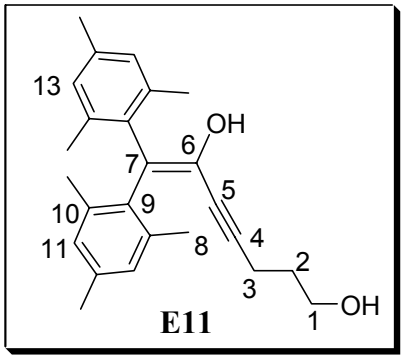

E11

Enol **E8** (2.0 g, 3.9 mmol) was added to a 20 ml solution of aqueous acidic methanol, prepared by dissolving 5 ml of 10% sulphuric acid to 15 ml methanol. The reaction mixture was stirred for 12-14 h and monitored by TLC. After complete consumption of starting material the reaction mixture was quenched with solid $NaHCO_3$ and concentrated. The residue was extracted with dichloromethane (2 × 25 ml), the combined organic layer was dried over Na_2SO_4 (anhyd.) and concentrated. The crude product was purified by column chromatography with 90:10 DCM:ether mixture as eluent (R_f = 0.7).

Yield: 1.2 g (3.3 mmol) of colourless solid, 84%.

M.P: 141-142 °C

IR (NaCl): $\tilde{\nu}$ (cm^{-1}) = 3435 (s, OH), 2952, 2223 (alkyne), 1609 (C=C), 1474, 1454, 1350, 1239, 1193, 1137, 1054, 1032, 993, 899, 849, 819, 733, 564.

^{1}H-NMR ($CDCl_3$, 200 MHz): δ (ppm) = 1.21 (bs, 1h, OH), 1.63 (q J = 6.4 Hz, 2H, 2-H) 2.12-2.25 (bs, coalescence, 18H, 8a,8b-H), 2.36 (t, J = 6.4 Hz, 2H, 3-H), 3.45 (t, J = 6.1 Hz, 2H, 1-H), 4.84 (bs, 1H, OH), 6.80 (bs, coalescence, 2H, 12-H), 6.86, (bs, coalescence, 2H, 13-H).

^{13}C-NMR ($CDCl_3$, 50 MHz): δ (ppm) = 21.9, 22.1, 31.5, 62.2, 78.3, 93.4, 120.8, 129.8, 130.7,

132.4, 135.3, 135.7, 137.0, 138.2, 139.4.

Elemental analysis: Calculated: C = 82.83, H = 8.34

Found: C = 82.30, H = 8.66

5.2.67 6,7-Bis-trimethylsilanyloxy-dodec-6-ene (ML03071a)

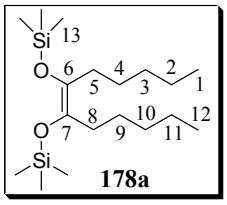

178a

A solution of ethylcaproate (3.40 g, 22.6 mmol) and trimethylsilyl chloride (72.4 ml, 566 mmol) in 150 ml dry toluene was added dropwise to a suspension of sodium (2.30 g, 100 mmol) in toluene at 110 °C, over a period of 8 h. The reaction was cooled in an ice bath and filtered under nitrogen atmosphere. The filtrate was concentrated yielding the crude product which was used as such without further purification.

Crude Yield: 3.23 g (9.37 mmol) of a colourless liquid, 95%.

IR (NaCl): $\tilde{\nu}$ (cm^{-1}) = 2957, 2929, 2860, 1677 (C=C), 1460, 1378, 1338, 1250, 1213, 1127, 1097, 1045, 983, 940, 843, 750, 687.

^{1}H-NMR ($CDCl_3$, 200 MHz): δ (ppm) = 0.15 (s, 18H, 13-H), 0.87 (t, ^{3}J = 6.6 Hz, 6H, 1,12-H), 1.25-1.29 (m, 8H, 2-H, 4, 9, 11), 1.37-1.47 (m, 4H, 3,10-H), 2.01 (t, ^{3}J = 7.4 Hz, 4H, 5,8-H).

^{13}C-NMR ($CDCl_3$, 50 MHz): δ (ppm) = 0.83 (C-13), 14.1 (C-1, 12), 22.5 (C-2, 11), 27.3 (C-5, 8), 31.5 (C-3, 4, 9, 10), 134.4 (C-6, 7).

DEPT-135 ($CDCl_3$, 50 MHz): δ (ppm) = Signals at 0.83 (C-13) and 14.1 (C-1, 12) remained positive (1°-C), signals at 22.5 (C-2, 11), 27.3 (C-5, 8), 31.5 (C-3, 4, 9, 10) were inverted (2°-C) and signal at 134.4 (C-6, 7) disappeared (4°-C).

5.2.68 7-Hydroxy-dodecan-6-one (ML03071b)

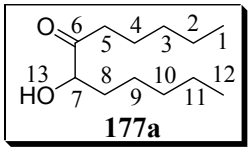

177a

Hydrochloric acid (15 ml, 1 *N*) was added to a solution of **178a** (3.0 g, 8.7 mmol) in 150 ml of THF. The reaction mixture was stirred for 1.5 h followed by addition of 2 g of $NaHCO_3$. The organic layer was concentrated and extracted with chloroform (3 × 25 ml). The combined organic layer was dried over Na_2SO_4 (anhyd.) and concentrated yielding the crude product,

which was purified by column chromatography with hexane diethyl ether (20%) as eluent.

Yield: 1.4 g (6.9 mmol) of a colourless liquid (76%)

IR (KBr): $\tilde{\nu}$ (cm^{-1}) = 3469 (OH), 2956, 2931, 2860, 1712 (C=O), 1466, 1378,1251, 1124, 1057, 530.

^{1}H-NMR ($CDCl_3$, 200 MHz): δ (ppm) = 0.88 (t, ^3J = 6.6 Hz, 6H, H-1, 12), 1.30 (s, 8H, 2-H, 3, 10, 11), 1.45-1.69 (m, 4H, H-4, 9), 1.76-1.93 (m, 2H, 8-H), 2.44 (dt, ^3J = 7.4 Hz, ^3J = 2.7 Hz, 2H, 5-H), 3.51 (d, ^3J = 4.7 Hz, 1H, OH, 13-H), 4.12-4.18 (m, 1H,7-H).

^{13}C-NMR ($CDCl_3$, 50 MHz): δ (ppm) = 14.0 (C-1, 12), 22.4 (C-8), 22.5 (C-2, 11), 23.3 (C-4), 24.5 (C-9), 31.3 (C-3), 31.6 (C-10), 33.7 (C-7), 37.8 (C-5), 212.6 (C-6).

5.2.69 Dodecane-6,7-dione[197] (ML03074.11)

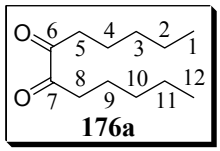

176a

The hydroxyketone **177a** (0.54 g, 2.50 mmol) and bismuth oxide (0.60 g, 1.2 mmol) in 5 ml acetic acid was refluxed for 30 min. The reaction mixture was filtered and the precipitate extracted with hot benzene. The filtrate was washed with water (2 × 10 ml), saturated $NaHCO_3$ solution (2 × 10 ml). The combined organic layer was dried over Na_2SO_4 (anhyd.) and concentrated yielding the crude product which was purified by column chromatography with hexane ether as eluent (20%).

Yield: 0.46 g (2.32 mmol) of a yellow coloured liquid (86%)

IR (KBr): $\tilde{\nu}$ (cm^{-1}) = 2958, 2931, 2861, 1713 (C=O), 1466, 1402, 1379, 1248, 1121, 730.

^{1}H-NMR ($CDCl_3$, 200 MHz): δ (ppm) = 0.88 (t, ^3J = 6.6 Hz, 6H, 1,12-H), 1.29 (m, ^3J = 4.1 Hz, ^3J = 6.6, 7.4 Hz, 8H, 2,3,10,11-H), 1.57 (q, ^3J = 4.1 Hz, ^3J = 7.4 Hz, 4H, 2, H-4, 9), 2.72 (t, J = 7.4 Hz, 4H, 5,8-H).

^{13}C-NMR ($CDCl_3$, 50 MHz): δ (ppm) = 13.8 (C-1, 12), 22.4 (C-2, 11), 22.7 (C-4, 9), 31.3 (C-3, 10), 36.2 (C-5, 8), 200.2 (C-6,7).

DEPT-135 ($CDCl_3$, 50 MHz): δ (ppm) = Signal at 13.8 remained positive (1°-C) while signals at 22.4, 22.7, 31.3, 36.2 inverted (2°-C) and signal at 200.2 disappeared (4°-C).

5.2.70 2,3-Dipentyl-pyrazine (ML03076.11)

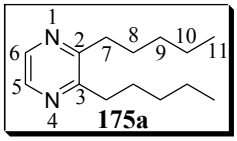

175a

A solution of the dione **176a** (0.8 g, 4.0 mmol) and ethylenediammine (0.3 ml, 4.4 mmol) in 20 ml ethanol was refluxed for 3-4 h, the reaction was monitored by TLC (50% hexane:ether). After complete conversion of the starting material potassium hydroxide (0.2 g, 4.4 mmol) and manganese dioxide (1.2 g, 13 mmol) was added and refluxed for 16 h. The reaction mixture was filtered through celite and concentrated. The crude product was chromatographed on silica gel with 60% ethylacetate in hexane, yielding a yellow coloured liquid.

Yield: 0.7 g (3.2 mmol) of yellow oil 80%

IR (KBr): $\tilde{\nu}$ (cm^{-1}) = 3042 (CH, aromatic), 2956, 2928, 2860, 1461, 1407, 1153, 1056, 855.

^{1}H-NMR ($CDCl_3$, 200 MHz): δ (ppm) = 0.90 (t, ^3J = 6.6 Hz, 6H, 11-H), 1.34-1.39 (m, ^3J = 4.2 Hz, ^3J = 6.6 Hz, ^3J = 7.4 Hz, 8H, 9,10-H), 1.67-1.75 (m, 4H, 8-H), 2.80 (t, J = 7.9 Hz, 4H, 7-H), 8.30 (s, 2H, 5,6-H).

^{13}C-NMR ($CDCl_3$, 50 MHz): δ (ppm) = 14.0 (C-11), 22.5 (C-10), 28.6 (C-8), 31.8 (C-9), 34.5 (C-7), 141.2 (C-5, 6), 155.8 (C-2, 3).

HRMS: $C_{14}H_{24}N_2$, Calculated: 220.1940, Found: 220.1934

5.2.71 1,4-Dimethyl-2,3-dipentyl-pyrazinium tetrafluoroborate (ML03078)

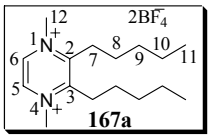

167a

(2,3-Dipentyl)-pyrazine (0.7 g, 3.2 mmol) and trimethyloxonium tetrafluoroborate (1.2 g, 7.9 mmol) was refluxed in 25 ml 1,2-dichloroethane for 2 h. The reaction mixture was cooled and filtered. The filtrate was washed with dry THF (3 × 25 ml) followed by dry pentane (3 × 25 ml). After drying a colourless solid was obtained that turned grey upon exposure to air.

Yield: 0.8 g (1.9 mmol) of a colourless solid 59%.

M.P: 102 °C with decomposition

^{1}H-NMR ($CDCl_3$, 400 MHz): δ (ppm) = 0.93 (t, ^3J = 6.8 Hz, 6H, 11-H), 1.40 (h, ^3J = 6.8 Hz, ^3J = 7.1 Hz, 4H, 10-H), 1.53 (q, ^3J = 7.1 Hz, 4H, 9-H), 1-76-1.78 (m, 4H, 8-H), 3.19 (bs, 4H, 7-H), 4.53 (bs, 6H, 12-H), 9.24 (s, 2H, 5,6-H).

^{13}C-NMR ($CDCl_3$, 100 MHz): δ (ppm) = 13.7 (C-11), 21.8 (C-8, 10), 25.4 (C-7), 31.8 (C-9), 142.9 (C-5, 6), 161.5 (C-2, 3).

HRMS: $C_{16}H_{30}N_2^{+\bullet}$, Calculated: 250.2409, Found: 250.2403.

5.2.72 8,9-Bis-trimethylsilanyloxy-hexadec-8-ene (ML03072a)

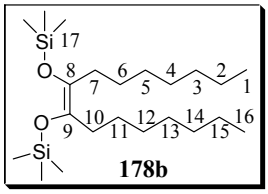

178b

A solution of ethylcaprylate (8.70 ml, 50.5 mmol) and trimethylsilyl chloride (72.4 ml, 566 mmol) in 150 ml dry toluene was added dropwise to a suspension of sodium (2.3 g, 100 mmol) in toluene at 110 °C, over a period of 8 h. The reaction was cooled in an ice bath and then filtered under nitrogen atmosphere. The filtrate was concentrated yielding the crude product which was used as such without further purification.

Crude Yield: 8.20 g (20.4 mmol) of colourless oil 81%

IR (NaCl): $\tilde{\nu}$ (cm^{-1}) = 2956, 2927, 2855, 1676 (C=C), 1460, 1378, 1338, 1250, 1213, 1128, 1103, 1054, 1027, 844, 758, 728, 694.

^{1}H-NMR ($CDCl_3$, 200 MHz): δ (ppm) = 0.15 (s, 18H, H-), 0.88 (t, ^3J = 6.6 Hz, 6H, 1,16-H), 1.27 (s, 16H, 2 to 5,12 to 15-H), 1.43 (m, 4H, 6,11-H), 2.01 (t, ^3J = 7.3 Hz, 4H, 7,10-H).

^{13}C-NMR ($CDCl_3$, 50 MHz): δ (ppm) = 0.83 (C-17), 14.1 (C-1,16), 22.7 (C-2, 15), 27. 6 (C-4, 13), 29.2 (C-5, 6, 11, 12), 31.6 (C-7, 10), 31.9 (C-3, 14), 134.4 (C-8, 9).

5.2.73 9-Hydroxy-hexadecan-8-one (ML03072b)

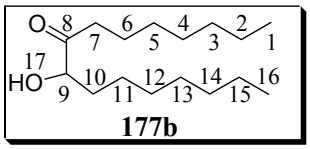

177b

To a solution of **178b** (7.00 g, 17.5 mmol) in 150 ml of THF was added 30 ml of 1*N* HCl. The reaction mixture was stirred for 1.5 h followed by addition of 2 g of $NaHCO_3$. The organic layer was concentrated and extracted with chloroform (3 × 25 ml). The combined organic layer was dried over Na_2SO_4 (anhyd.) and concentrated yielding the crude product. Purification by column chromatography with hexane diethyl ether (20%) as eluent gave a colourless liquid.

Yield: 3.8 g (10 mmol) of a colourless liquid (85%)

IR (KBr): $\tilde{\nu}$ (cm^{-1}) = 3474 (OH), 2927, 2856, 1712 (C=O), 1465, 1403, 1377, 1250, 1125, 1068, 895, 842, 738.

^{1}H-NMR ($CDCl_3$, 200 MHz): δ (ppm) = 0.87 (t, ^3J = 6.6 Hz, 6H, 1,16-H), 1.27 (s, 16H, 2 to 5,12 to 15-H), 1.47-1.64 (m, 4H, 6,11-H), 1.84 (q, 2H, ^3J = 6.4 Hz, 3.0 Hz, 10-H), 2.44 (dt, ^3J = 7.4 Hz, ^3J = 3.0 Hz, 2H, 7-H), 3.74 (t, ^3J = 6.4 Hz, 1H, 17-H, OH), 4.16 (dd, ^3J = 6.4 Hz,

^{3}J = 3.4 Hz, 1H, 9-H).

^{13}C-NMR ($CDCl_3$, 50 MHz): δ (ppm) = 14.0 (C-1, 16), 22.6 (C-2, 10, 15), 23.6 (C-6), 24.8 (C-4), 29.0 (C-11, 15), 29.1 (C-12), 29.4 (C-13), 31.6 (C-3), 31.7 (C-14), 33.7 (C-9), 37.8 (C-7), 212.6 (C-8).

5.2.74 Hexadecan-8,9-dione[198] (ML03075.1)

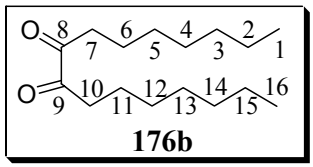

176b

A solution of **177b** (0.69 g, 2.69 mmol) and bismuth oxide (0.60 g, 1.29 mmol) in 5 ml acetic acid was refluxed for 30 min. The reaction mixture was filtered and the precipitate extracted with hot benzene. The filtrate was washed with water (2 × 10 ml), saturated $NaHCO_3$ solution (2 × 10 ml). The combined organic layer was dried over Na_2SO_4 (anhyd) and concentrated to yield the crude product which was purified by column chromatography with hexane ether as eluent (20%) yielding a yellow, low melting solid.

Yield: 300 mg (1.17 mmol) of a yellow solid 44%

Melting Point: 40 °C

IR (KBr): $\tilde{\nu}$ (cm^{-1}) = 2934, 2849, 1715 (C=O), 1466, 1408, 1373, 1350, 1265, 1125, 916, 713.

^{1}H-NMR ($CDCl_3$, 200 MHz): δ (ppm) = 0.87 (t, ^{3}J = 6.6 Hz, 6H, 1,16-H), 1.26 (s, 16H, 2 to 5,12 to 15-H), 1.56 (q, ^{3}J = 7.4 Hz, 4H, 6,11-H), 2.72 (t, ^{3}J = 7.4 Hz, 4H, 7,10-H).

^{13}C-NMR ($CDCl_3$, 50 MHz): δ (ppm) = 13.8 (C-1, 12), 22.4, 22.7, 31.3, 36.2, 127.1, 200.2 (C-6,7).

5.2.75 2,3-Diheptyl-pyrazine (ML03077.1)

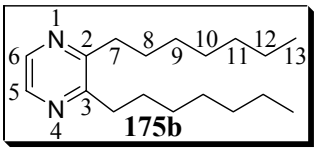

175b

A solution of **176b** (1.0 g, 3.9 mmol) and ethylenediammine (0.3 ml, 4.40 mmol) in 20 ml ethanol was refluxed for 3-4 h. After complete consumption of the starting material, potassium hydroxide (0.3 g, 4.46 mmol) and manganese dioxide (1.2 g, 13 mmol) were added and refluxed for 16 h. The reaction mixture was filtered through celite and concentrated. The crude product was chromatographed on silica gel with 60% ethylacetate in hexane, yielding a yellow coloured oil.

Yield: 0.7 g (2.5 mmol) of a yellow oil 63%

IR (KBr): $\tilde{\nu}$ (cm^{-1}) = 3043 (CH, aromatic), 2956, 2927, 2855, 1465, 1407, 1378, 1232, 1148, 1073, 852, 714.

^{1}H-NMR ($CDCl_3$, 200 MHz): δ (ppm) = 0.87 (t, ^3J = 6.6 Hz, 6H, 13-H), 1.28 (s, 16H, H- 9-12), 1.63-1.74 (m, 4H, 8-H), 2.80 (t, ^3J = 7.6 Hz, 4H, 7-H), 8.30 (s, 2H, 5,6-H).

^{13}C-NMR ($CDCl_3$, 50 MHz): δ (ppm) = 14.1 (C-13), 22.6 (C-12), 28.9 (C-8), 29.1 (C-9) 29.6 (C-10), 31.7 (C-11), 34.5 (C-7), 141.2 (C-5, 6), 155.9 (C-2, 3).

HRMS: $C_{18}H_{32}N_2$, Calculated: 276.2566, Found: 276.2559

5.2.76 1,4-Dimethyl-2,3-diheptyl-pyrazinium tetrafluoroborate

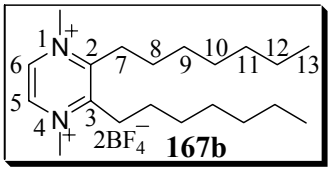

167b

2,3-Di-heptyl-pyrazine (0.7 g, 2.5 mmol) and trimethyloxonium tetrafluoroborate (1,0 g, 6.3 mmol) was refluxed in 25 ml 1,2-dichloroethane for 2 h. The reaction mixture was cooled and filtered. The filtrate was washed with dry THF (3 × 25 ml) followed by dry pentane (3 × 25 ml) yielding a colourless solid which turned grey-black upon exposure to air.

Yield: 1.1 g (2.3 mmol) of a colourless solid 91%.

Melting Point: 178 °C with decomposition.

^{1}H-NMR ($CDCl_3$, 400 MHz): δ (ppm) = 0.88 (t, ^3J = 6.6 Hz, 6H, 13-H), 1.29 (s, 8H, 11,12-H), 1.36 (m, 4H, 10-H), 1.54 (t, ^3J = 6.6 Hz, 4H, 9-H), 1.77 (bs, 4H, 8-H), 3.18 (bs, 4H, 7-H), 4.54 (bs, 6H, 14-H), 9.27 (s, 2H, 5,6-H).

^{13}C-NMR ($CDCl_3$, 100 MHz): δ (ppm) = 14.0 (C-13), 22.5 (C-11, 12), 28.4 (C-9, 10), 29.8 (C-7, 8), 31.5 (C-14), 143.0 (C-5, 6), 161.3 (C-2, 3).

Elemental analysis: Calculated C = 49.93, H = 8.17, N = 5.82

Found C = 49.35, H = 7.68, N = 5.79

HRMS: ($C_{20}H_{38}N_2$) Calculated: 306.3035, Found: 306.3041

5.2.77 12,13- Bis-trimethylsilanyloxy-tetracos-12-ene[199] (ML03016.11)

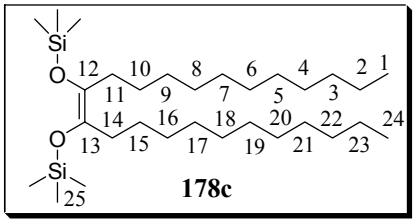

178c

A solution of ethyllaurate (4.30 g, 18.8 mmol) and trimethylsilyl chloride (60.0 ml, 471 mmol) in 150 ml dry toluene was added dropwise to a suspension of sodium (1.94 g, 84.7 mmol) in toluene at 110 °C, over a period of 8 h. The reaction was cooled in an ice bath and then filtered under nitrogen atmosphere. The filtrate was concentrated yielding the crude product which was used as such without further purification.

Crude Yield: 4.15 g (8.09 mmol) of a colourless liquid, 86%.

IR (NaCl): $\tilde{\nu}$ (cm^{-1}) = 2926, 2854, 1711 (C=C), 1466, 1265, 1039, 846, 742, 706.

^{1}H-NMR ($CDCl_3$, 200 MHz): δ (ppm) = 0.15 (s, 18H, 25-H), 0.88 (t, *J* = 7.0 Hz, 6H, 1, 24H), 1.26 (s, 32H, H- 2-9, 16-23), 1.40-1.46 (m, 4H, 10,15-H), 2.01 (t, *J* = 7.4 Hz, 4H, 11,14-H).

^{13}C-NMR ($CDCl_3$, 50 MHz): δ (ppm) = 0.9 (C-25), 14.1 (C-1, 24), 22.7 (C-2, 23), 23.9 (C-10, 15), 27.6 (C-9, 16), 29.2 (C-4, 21), 29.7 (C- 5-8, 17-20), 31.5 (C-11, 14), 31.9 (C-3, 22), 134.4 (C-12,13).

5.2.78 13-Hydroxy-tetracosan-12-one[199] (ML03016.12)

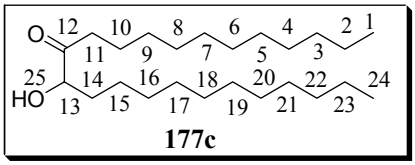

177c

15 ml of 1*N* HCl was added to a solution of **178c** (4.15 g, 8.09 mmol) in 150 ml of THF. The reaction mixture was stirred for 1.5 h followed by addition of 2 g of $NaHCO_3$. The organic layer was concentrated and extracted with chloroform (3 × 25 ml). The combined organic layer was dried over Na_2SO_4 (anhyd.) and concentrated to yield the crude product, which was purified by column chromatography with benzene as eluent (R_f = 0.35).

Yield: 2.5 g (6.8 mmol) of a colourless solid (71%)

M.P: 56-58 C

IR (KBr): $\tilde{\nu}$ (cm^{-1}) = υ 3359 (OH), 2956, 2918, 2849, 1712 (C=O), 1465, 1377,1103, 1069, 842, 724.

^{1}H-NMR ($CDCl_3$, 200 MHz): δ (ppm) = 0.88 (t, *J* = 6.6 Hz, 6H, 1,24-H), 1.26 (s, 32H, H- 2-9, 16-23), 1.47-1.61 (m, 4H, 10,15-H), 1.81-1.91 (m, 2H, 14-H) 2.35-2.50 (m, 2H, 11-H), 3.50 (d, *J* = 5.0 Hz, 1H, OH, 25-H), 3.74 (t, *J* = 6.6 Hz, 1H, 12-H).

5.2.79 Tetracosane-12,13-dione[200] (ML03028.1)

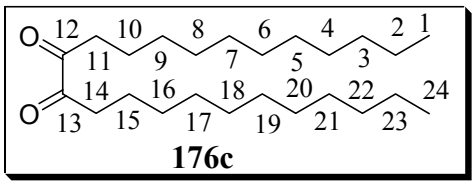

176c

Tetracosane-13-Hydroxy-12-one (0.5 g, 1.4 mmol) and bismuth oxide (0.3 g, 0.6 mmol) in 5 ml acetic acid was refluxed for 30 min. The reaction mixture was filtered (hot) and the precipitate extracted with hot benzene. The filtrate was washed with water (2 × 10 ml), saturated $NaHCO_3$ solution (2 × 10 ml). The combined organic layer was dried over Na_2SO_4 (anhyd.) and concentrated yielding the crude product. Purification was carried out by column chromatography with benzene as eluent (R_f = 0.74).

Yield: 0.3 g (0.9 mmol) of a cream coloured solid (66%)

Melting point: 71-72 C (Lit:[200b] 61-62 °C).

IR (KBr): $\tilde{\nu}$ (cm^{-1}) = 2955, 2918, 2849, 1717 (C=O), 1473, 1462, 1407, 915, 715.

^{1}H-NMR ($CDCl_3$, 200 MHz): δ (ppm) = 0.86 (t, *J* = 6.6 Hz, 6H, 1,24-H), 1.25 (s, 32H, H- 2-9, 16-23), 1.52-1.56 (m, 4H, 10,15-H), 2.70 (t, *J* = 7.4 Hz, 4H, 11,14-H).

^{13}C-NMR ($CDCl_3$, 50 MHz): δ (ppm) = 14.1 (C-1, 24), 22.7 (C-2, 23), 23.0 (C-10, 15), 29.1 (C-9, 16), 29.3 (C-8, 17), 29.4 (C-4, 21), 29.6 (C- 5-7, 18-20), 31.9 (C-3, 22), 36.0 (11, 14), 200.1 (C-12, 13).

Elemental Analysis: Calculated C = 78.63, H = 12.65

Found C = 78.93, H = 13.43

5.2.80 5,6-Diundecyl-2,3-dihydro-pyrazine (ML03030.12)[201]

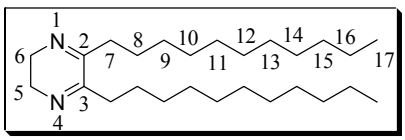

Tetracosane-12,13-dione (0.1 g, 0.3 mmol) and ethylenediammine (18 mg, 0.3 mmol) was refluxed in 5 ml dry toluene for 45 min. The reaction mixture was concentrated and chromatographed with 50% ether in hexane (R_f = 0.1) yielding a yellow coloured waxy material.

Yield: 20 mg (51 μmol) of a waxy material, 19%.

IR (KBr): $\tilde{\nu}$ (cm^{-1}) = 2924, 2853, 1646, 1593, 1465, 1377, 1192, 976, 721.

^{1}H-NMR ($CDCl_3$, 200 MHz): δ (ppm) = 0.86 (t, ^3J = 6.6 Hz, 6H, 17-H), 1.24 (s, 32H, H- 9-16), 1.48-1.55 (m, 4H, 8-H), 2.40 (t, ^3J = 7.8 Hz, 4H, 7-H), 3.30 (s, 4H, 5,6-H).

^{13}C-NMR ($CDCl_3$, 50 MHz): δ (ppm) = 14.1 (C-17), 22.7 (C-16), 26.2 (C-8), 29.3 (C-14), 29.4 (C-13), 29.5 (C-11, 12), 29.6 (C-9, 10), 31.9 (C-7), 35.5 (C-15), 44.9 (C-5, 6), 163.0 (C-2, 3).

DEPT-135 ($CDCl_3$, 50 MHz): δ (ppm) = Signal at 14.1 (C-17) remained positive (1°-C) while signals at 22.7, 26.2, 29.3, 29.4, 29.5, 29.6, 31.9, 35.5 inverted (2°-C) and signal at 164.0 (C-2, 3) disappeared (4°-C).

5.2.81 2,3-Diundecyl-pyrazine (ML03062)

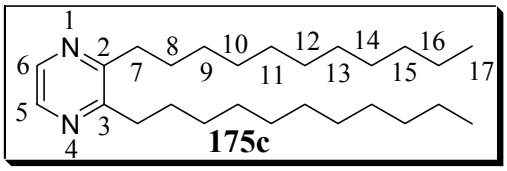

175c

A solution of 5,6-diundecyl-2,3-dihydro-pyrazine (0.4 g, 1.0 mmol), potassium hydroxide (0.3 g, 3.3 mmol) and manganese dioxide (62 mg, 1.1 mmol) in 20 ml ethanol was refluxed for 16 h. The reaction mixture was filtered through celite and concentrated. The crude product was chromatographed on silica gel with 60% ethylacetate in hexane, yielding a yellow coloured liquid.

Yield: 0.2 g (0.5 mmol) of a yellow coloured liquid, 50%.

***R*$_f$:** 0.89 (60:40, ethylacetate:hexane).

IR (KBr): $\tilde{\nu}$ (cm^{-1}) = 3042 (CH, aromatic), 2924, 2853, 1465, 1407, 1138, 851, 721.

^{1}H-NMR ($CDCl_3$, 200 MHz): δ (ppm) = 0.87 (t, *J* = 6.6 Hz, 6H, 17-H), 1.26 (s, 32H, H- 9-16), 1.62-1.74 (m, 4H, 8-H), 2.81 (t, *J* = 7.6 Hz, 4H, 7-H), 8.31 (s, 2H, 5,6-H).

^{13}C-NMR ($CDCl_3$, 50 MHz): δ (ppm) = 14.1 (C-17), 22.7 (C-16), 29.0 (C-8), 29.6 (C- 9-14), 31.9 (C-15), 34.5 (C-7), 141.2 (C-5, 6), 155.9 (C-2, 3).

HRMS: $C_{26}H_{48}N_2$ Calculated: 388.3818, Found: 388.3826.

5.2.82 1,4-Dimethyl-2,3-diundecyl-pyrazinium tetrafluoroborate (ML030-80)

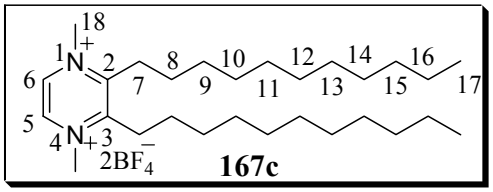

167c

2,3-Diundecyl-1,4-pyrazine (0.7 g, 1.8 mmol) and trimethyloxonium tetrafluoroborate (0.7 g, 4.4 mmol) in 20 ml dry 1,2-dichloroethane was refluxed for 2 h, cooled and filtered. The precipitate was washed with dry diethyl ether (3 × 25 ml) followed by dry pentane (3 × 25 ml) yielding a white solid that turned grey upon exposure to air.

Yield: 0.25 g, 50%.

^{1}H-NMR ($CDCl_3$, 200 MHz):δ (ppm) = 0.88 (t, *J* = 7.6 Hz, 6H, 17-H), 1.26 (s, 32H, 8,15-H), 1.62-1.74 (m, 4H, 16-H), 2.81 (t, *J* = 7.6 Hz, 4H, 7-H), 8.31 (s, 2H, 5,6-H).

^{13}C-NMR ($CDCl_3$, 50 MHz): δ (ppm) = 15.1 (C-17), 23.7, 29.9, 30.3, 30.6, 32.9, 35.5(C-7), 142.2 (C-5, 6), 156.8 (C-2, 3).

HRMS: $C_{28}H_{54}N_2$ Calculated: 418.430, Found: 418.425.

5.2.83 18,19-Bis-trimethylsilanyloxy-hexatriacont-18-ene (ML03086a)

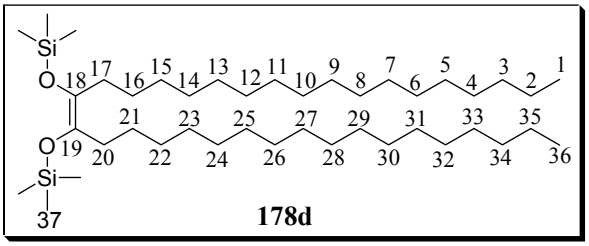

178d

A solution of ethylstearate (10.0 g, 32.0 mmol) and trimethylsilyl chloride (102 ml, 800 mmol) in 150 ml dry toluene was added dropwise to a suspension of sodium (3.70 g, 100 mmol) in toluene at 110 °C, over a period of 8 h. The reaction was cooled in an ice bath and then filtered under nitrogen atmosphere. The filtrate was concentrated yielding the crude product which was used as such without further purification.

Crude Yield: 10.1 g (14.8) of a low melting solid, 93%.

IR (NaCl): $\tilde{\nu}$ (cm^{-1}) = 2923, 2853, 1676 (C=C), 1465, 1250, 1213, 1040, 844, 750, 720.

^{1}H-NMR ($CDCl_3$, 200 MHz): δ (ppm) = 0.15 (s, 18H, 37-H), 0.89 (t, *J* = 6.4 Hz, 6H, 1,36-H), 1.26 (s, 56H, CH_2), 1.37-1.43 (m, 4H, 2,35-H), 2.01 (t, *J* = 6.4 Hz, 4H, 17-H, 20).

^{13}C-NMR ($CDCl_3$, 50 MHz): δ (ppm) = 0.85 (C-37), 14.1 (C-1,36), 22.7 (C-2, 35), 23.9 (C-16, 21), 27.6 (C-3, 32), 29.7 (C- 4-15, 22-33), 31.5, 31.9 (C-17, 20), 134.3 (C-18, 19).

5.2.84 19-Hydroxy-hexatriacontan-18-one (ML03086.12)

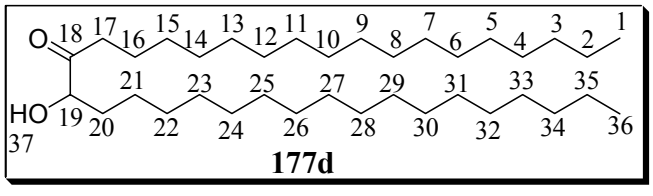

177d

To a solution of **178d** (10.1 g, 14.8 mmol) in 150 ml of THF was added 15 ml of 1*N* HCl. The reaction mixture was stirred for 1.5 h followed by addition of 2 g of $NaHCO_3$. The organic layer was concentrated and extracted with chloroform (3 × 25 ml). The combined organic layer was dried over Na_2SO_4 (anhyd) and concentrated to yield the crude product, which was purified by column chromatography with hexane diethyl ether (20%) as eluent yielding a

colourless solid.

Yield: 6.5 g (12.1) of a colourless solid, 76%.

Melting Point: 85 °C (Lit: 82-83 C)

IR (KBr): $\tilde{\nu}$ (cm^{-1}) = 3338 (OH), 2955, 2915, 2847, 1713 (C=O), 1464, 1404, 1377,1113, 1089, 927, 903, 805, 720.

^{1}H-NMR ($CDCl_3$, 200 MHz): δ (ppm) = 0.88 (t, ^3J = 6.9 Hz, 6H, C-1), 1.25 (s, 56H, C- 3-16, 21-34), 1.55-1.59 (m, 4H, 2,35-H), 1.76-1-94 (m, 2H, 20-H), 2.44 (dt, ^3J = 7.5 Hz, ^3J = 3.0 Hz, 2H, 17-H), 3.50 (d, J = 4.9 Hz, 1H, OH, 37-H), 4.13-4.16 (m, 1H, 19-H).

Elemental analysis: Calculated C = 80.53, H = 13.52

Found C = 80.21, H = 13.71

5.2.85 Hexatriacontane-18,19-dione (ML03103.1)

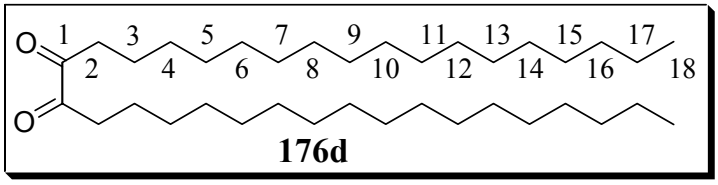

176d

19-Hydroxy-hexatriacontan-18-one (0.5 g, 0.9 mmol) and bismuth oxide (0.2 g, 0.4 mmol) in 5 ml acetic acid was refluxed for 30 min. The reaction mixture was filtered and the precipitate extracted with hot benzene. The filtrate was washed with water (2 × 10 ml), saturated $NaHCO_3$ solution (2 × 10 ml). The combined organic layer was dried over Na_2SO_4 (anhyd) and concentrated to yield the crude product which was purified by column chromatography with hexane ether as eluent (20%) yielding a cream coloured solid.

Yield: 360 mg (0.67 mmol) of a cream coloured solid, 72%.

Boiling point: 90-92 C (Lit:[200b] 82-83 °C)

IR: (KBr): $\tilde{\nu}$ (cm^{-1}) = 2955, 2920, 2847, 1714 (C=O), 1525, 1463, 1408, 1373, 1008, 915, 718.

^{1}H-NMR (C_6D_6, 400 MHz): δ (ppm) = 1.07 (t, ^3J = 7.0 Hz, 6H, 18-H), 1.44 (s, 56H, H-), 1.64 (q, ^3J = 7.4 Hz, 4-H, 3-H), 2.67 (t, ^3J = 7.4 Hz, 4H, 2-H).

^{13}C-NMR (C_6D_6, 100 MHz): δ (ppm) = 14.2 (C-18), 23.0 (C-17), 23.6, 29.5, 29.7, 29.8, 30.0, 30.1 (C-16), 32.3 (C-3), 36.2 (C-2), 199.7 (C-1).

Elemental analysis: Calculated C = 80.83, H = 13.19

Found C = 81.26, H = 13.72

5.2.86 2,3-Diheptadecyl-pyrazine (ML03126.12)

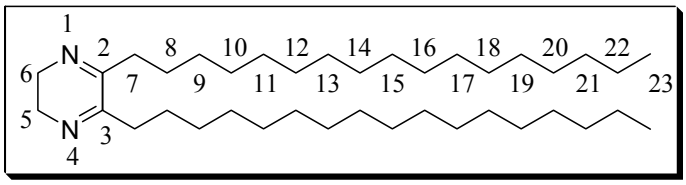

Hexatriacontane-18,19-dione (1.0 g, 1.9 mmol), ethylenediamine (0.2 ml, 2.1 mmol) was refluxed for 3 h in 15 ml ethanol and 5 ml benzene. The reaction was monitored by TLC, when all the starting material was consumed the reaction was cooled and sample was taken out for NMR measurements.

^{1}H-NMR ($CDCl_3$, 200 MHz): δ (ppm) = 0.87 (t, ^{3}J = 6.6 Hz, 6H, 23-H), 1.24 (s, 56H, 8,21-H), 1.49-1.56 (m, 4H, 8-H), 2.40 (t, ^{3}J = 7.1 Hz, 4H, 7-H), 3.30 (s, 4H, 5,6-H).

^{13}C-NMR ($CDCl_3$, 50 MHz): δ (ppm) = 14.1 (C-23), 22.7 (C-22), 26.1 (C-8), 29.7 (C-9-20), 31.9 (C-21), 35.5 (C-7), 44.9 (C-5, 6), 162.9 (C-2).

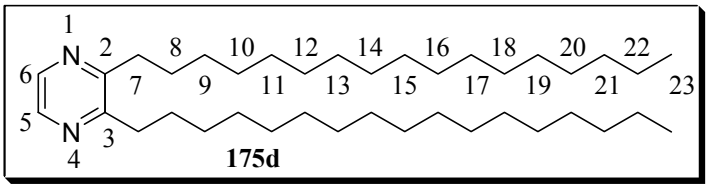

175d

For preparation of **175d** to the above reaction mixture was then added MnO_2 (0.5 g, 6.0 mmol) and potassium hydroxide (0.1 g, 2.5 mmol) and the reaction mixture was refluxed for another 14-15 h. The reaction mixture was cooled, filtered through celite and concentrated. The crude product was purified by column chromatography with hexane:ethyl acetate (50%).

Yield: 0.8 g (1.4 mmol) of a white solid 72%

Melting Point: 43-44 °C

IR (KBr): $\tilde{\nu}$ (cm^{-1}) = 2954, 2915, 2849, 1472, 1411, 1156, 1135, 1069, 872, 716.

^{1}H-NMR ($CDCl_3$, 200 MHz): δ (ppm) = 0.87 (t, *J* = 6.6 Hz, 6H, 23-H), 1.25 (s, 56H, 9,22-H), 1.63-1.74 (m, 4H, 8-H), 2.80 (t, *J* = 7.8 Hz, 4H, 7-H), 8.30 (s, 2H, 5,6-H).

^{13}C-NMR ($CDCl_3$, 50 MHz): δ (ppm) = 14.1 (C-23), 22.7 (C-22), 29.7 (C- 9-21), 31.9 (C-8), 34.5 (C-7), 141.2 (C-2, 3), 155.9 (C-5, 6).

HRMS: $C_{38}H_{72}N_2$, Calculated: 556.5696, Found: 556.5685.

5.2.87 2,3-Diheptadecyl-1-methyl-pyrazinium iodide (ML05038.1)

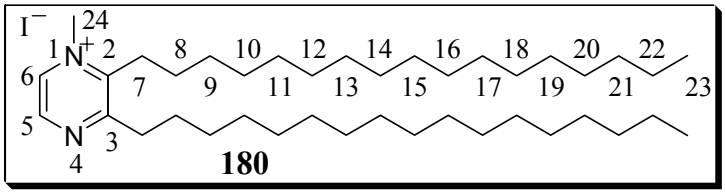

180

2,3-Diheptadecyl-pyrazine (150 mg, 0.27 mmol) was refluxed in 15 ml of methyl iodide for 12 h. The reaction mixture was concentrated yielding a yellow solid containing pure product in quantitative yield.

Melting Point: 95-96 °C

IR (KBr): $\tilde{\nu}$ (cm^{-1}) = 2921, 1691, 1609, 1449, 1371, 1265, 1216, 1156, 1059, 1006, 848, 568.

^{1}H-NMR ($CDCl_3$, 200 MHz): δ (ppm) = 0.87 (t, ^3J = 6.2 Hz, 6H, 23-H), 1.25 (s, 52H, H- 10-22), 1.54-1.85 (m, 8H, 8,9-H), 3.03 (t, ^3J = 7.6 Hz, 2H, 7′-H), 3.19 (t, ^3J = 8.4 Hz, 2H, 7-H), 4.63 (s, 3H, 24-H), 9.09 (d, ^3J = 3.0 Hz, 1H, 5-H), 9.47 (d, ^3J = 3.0 Hz, 1H, 6-H).

Elemental Analysis: Calculated C = 67.02, H = 10.82, N = 4.01

Found C = 67.40, H = 10.88 , N = 3.87

5.2.88 2,3-Dihetadecyl-1,4-dimethyl-pyrazinium tetrafluoroborate (ML0401-4.1)

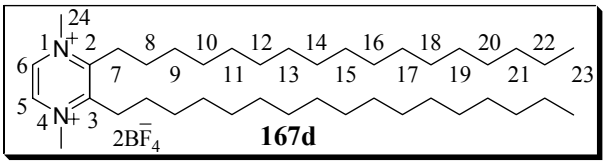

167d

2,3-Diheptadecyl-pyrazine (600 mg, 1.08 mmol), trimethyloxonium tetrafluoroborate (400 mg, 2.69 mmol) in 25 ml dry 1,2-dichloroethane was refluxed for 2 h. The solvent was evaporated and the residue was treated with dry diethyl ether yielding a white precipitate which was collected by filtration under nitrogen.

Yield: 150 mg (1.20 mmol) of a white solid, 18%.

Melting Point: 192 °C with decomposition.

^{1}H-NMR ($CDCl_3$, 200 MHz): δ (ppm) = 0.88 (t, J = 6.6 Hz, 6H, 23-H), 1.26 (s, 56H, 9,22-H), 1.61-1.76 (m, 4H, 8-H), 3.16 (m, 4H, 7-H), 4.54 (bs, 6H, 24-H), 9.29 (s, 2H, 5,6-H).

^{13}C-NMR ($CDCl_3$, 50 MHz): δ (ppm) = 14.1 (C-23), 22.7 (C-22), 26.5 (C-21), 28.8 (C-9), 29.7 (C- 10-20), 31.9 (C-8), 36.0 (C-7), 70.6 (C-24), 161.3 (C-5, 6).

HRMS: $C_{40}H_{78}N_2^{+\bullet}$, Calculated: 586.6165, Found: 586.6156.

5.2.89 Butyl-(4-ferrocenyl-2-hydroxy)-hexadecanoate (ML04068.12)

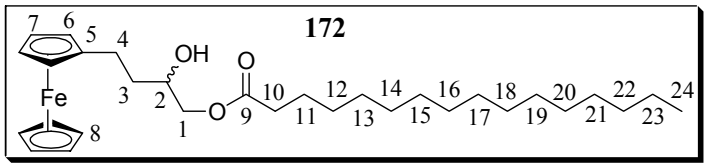

To a mixture of 4-ferrocenyl-butane-1,2-diol (**25**) (100 mg, 0.37 mmol) and triethylamine (130 mg, 1.28 mmol) in 10 ml dry dichloromethane was added palmitoyl chloride (275 mg, 1.00 mmol). The reaction was stirred at room temperature for 12 h, filtered through a pad of celite and concentrated. The pure product was obtained as a yellow solid by column chromatography with hexane:ether (20%) as eluent.

Yield: 70 mg (0.1 mmol) of a yellow solid, 38%.

Melting point: 40°C

IR (NaCl)**:** $\tilde{\nu}$ (cm^{-1}) = 3428 cm^{-1} (b, OH), 2920 (s), 2851, 1727 (s, C=O), 1465 (s), 1179 (b), 1103, 815 (s), 487 (s).

^{1}H-NMR ($CDCl_3$, 200 MHz): δ (ppm) = 0.88 (t, ^{3}J = 6.6 Hz, 3H, 24-H), 1.25 (s, 24H, 12 to 23-H), 1.60 – 1.73 (m, 4H, 3,11-H), 2.35 (t, ^{3}J = 7.4 Hz, 2H, 10-H), 2.41 – 2.505 (m, 2H, 4-H), 3.85 – 4.02 (m, 3H, 1,2-H) 4.06-4.19 (m, 9H, 6,7,8-H).

^{13}C-NMR ($CDCl_3$, 50 MHz): δ (ppm) = 14.1 (C-24), 22.7 (C-23, 11), 25.0 (C-3), 29.4 (C-12), 29.5 (C-13, 21), 29.7 (C-14-20), 31.9 (C-22), 34.2 (C-10) 34.6 (C-4), 67.2 (C-8), 68.5 (C-6), 68.6 (C-7), 69.6 (C-1, 2), 88.1 (C-5), 174.1 (C-9).

Elemental analysis: Calculated C = 70.30, H = 9.44

Found C = 70.61, H = 9.82

5.2.90 Bis-([4-ferrocenyl]-butyl) hexadecanoate (ML04068.11)

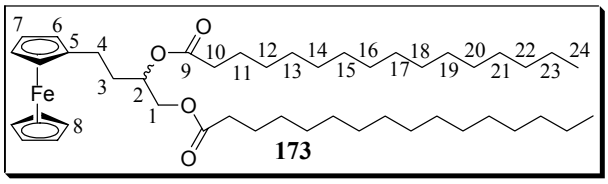

To a mixture of 4-ferrocenyl-butane-1,2-diol (**25**) (100 mg, 0.37 mmol) and triethylamine (130 mg, 1.28 mmol) in 10 ml of dry dichloromethane was added palmitoyl chloride (275 mg, 1.00 mmol). The reaction was stirred at room temperature for 12 h, filtered through a pad of celite and concentrated. The pure product was obtained as a cream solid by column chromatography with hexane:ether (30%) as eluent.

Yield: 130 mg (8.93 mmol) of cream coloured solid, 48%.

Melting point: 48-50 °C

IR (NaCl): $\tilde{\nu}$ (cm^{-1}) = 2917 cm^{-1} (s), 2849, 1848 (w, C=O), 1736 (s, C=O), 1468 (s), 1178 (b), 1104, 839, 822 (s), 720, 484 (s).

^{1}H-NMR ($CDCl_3$, 200 MHz): δ (ppm) = 0.88 (t, ^{3}J = 6.6 Hz, 6H, 24-H), 1.25 (s, 50H, CH_2), 1.56 – 1.84 (m, 7H), 2.06 – 2.44 (m, 6H), 4.05 (s, 4H, 6,7-H), 4.09 (s, 5H, 8-H).

^{13}C-NMR ($CDCl_3$, 50 MHz): δ (ppm) = 14.1 (C-24), 22.7 (C-23, 11), 25.1 (C-3), 29.2 (C-12), 29.4 (C-13, 21), 29.7 (C-14-20), 31.9 (C-22), 34.2 (C-10), 34.5 (C-4), 64.8 (C-2), 67.4 (C-8), 67.9 (C-1), 68.6 (C-6), 71.0 (C-7), 87.9 (C-5), 173.4 (C-9).

5.2.91 Bis-([4-ferrocenyl]-butyl) hexadecanoate (ML04070.1)

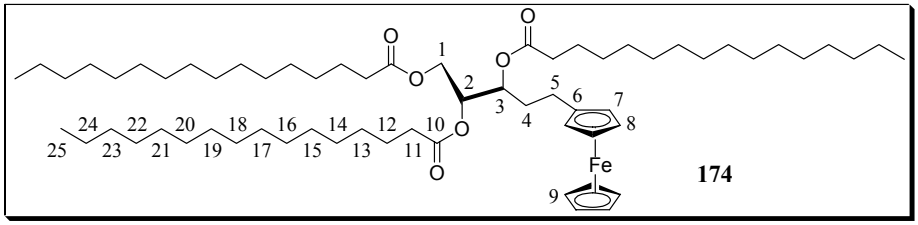

174

To a mixture of 5-ferrocenyl-pentane-1,2,3-triol (50 mg, 0.2 mmol) and triethylamine (97 mg, 1.0mmol) in 10 ml dry dichloromethane was added palmitoyl chloride (0.2 g, 0.7 mmol). The reaction was stirred at room temperature for 12 h, filtered through a pad of celite and concentrated. The pure product was obtained as a yellow solid by column chromatography with hexane:ether (50%) as eluent.

Yield: 120 g (0.12 mmol) of cream coloured solid, 71%.

Melting point: 44 °C

IR (NaCl): $\tilde{\nu}$ (cm^{-1}) = 2952 cm^{-1}, 2917 (s), 2849, 1848 (s, C=O), 1723 (s, C=O), 1469 (s), 1378, 1181 (b), 1096, 940, 905, 871, 839, 823 (s), 720.

^{1}H-NMR ($CDCl_3$, 200 MHz): δ (ppm) = 0.88 (t, ^{3}J = 6.9 Hz, 9H, 25-H), 1.25 (s, 76H, CH_2), 1.57 – 1.65 (m, 4H), 1.71-1.82 (m, 4H), 2.06 – 2.17 (m, 4H), 3.29-2.48 (m, 4H), 3.93 (t, J = 7.6 Hz, 2H, H), 4.04-4.08 (s, 5H), 4.69 (t, J = 7.6 Hz, 2H,).

^{13}C-NMR ($CDCl_3$, 50 MHz): δ (ppm) = 14.1 (C-25), 22.7, 24.6, 26.3, 27.5, 29.7, 31.9, 53.6, 53.7, 68.4, 68.5, 101.7, 101.8, 145.5 (C-10´), 169.8 (C-10).

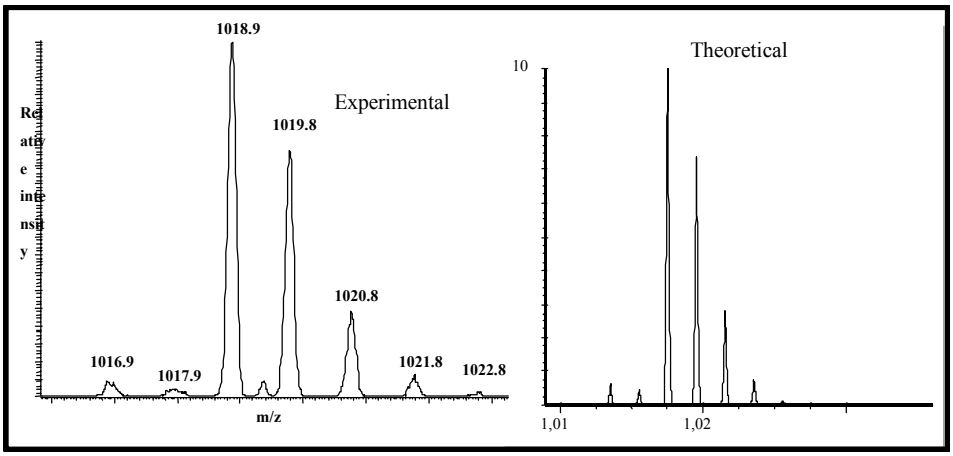

ESI-MS: (m/z) $C_{63}H_{110}FeO_6$ = 1019.0 ($M^{+\bullet}$)

5.2.92 HPLC-DATA for photolysis of 75 and 78

For HPLC investigations, initially calibration plots for **98** (R_t = 9.21 min Figure 5–1a) and **99** (R_t = 4.67 min, Figure 5–1c) were made with hexane (85%)-ethyl acetate (15%) [Figure 2–21]. The HPLC chromatograms were followed at two wavelengths 260 and 290 nm, respectively. For the calibration curve, the peak area at 290 nm was plotted against concentration (average of two measurements).

Table 5–1: Data for the calibration curve obtained from HPLC for **98** and **99** at 290 nm. The peak area presented here are average of two measurements.

Conc. of **98** [mM]	Peak area	Conc. of **99** [mM]	Peak area
0.39	52.85	0.33	24.8
1.54	399.46	1.66	127.16
3.09	723.01	3.31	253.69
6.17	1246.75	6.62	515.61
9.26	1685.23	9.94	789.29

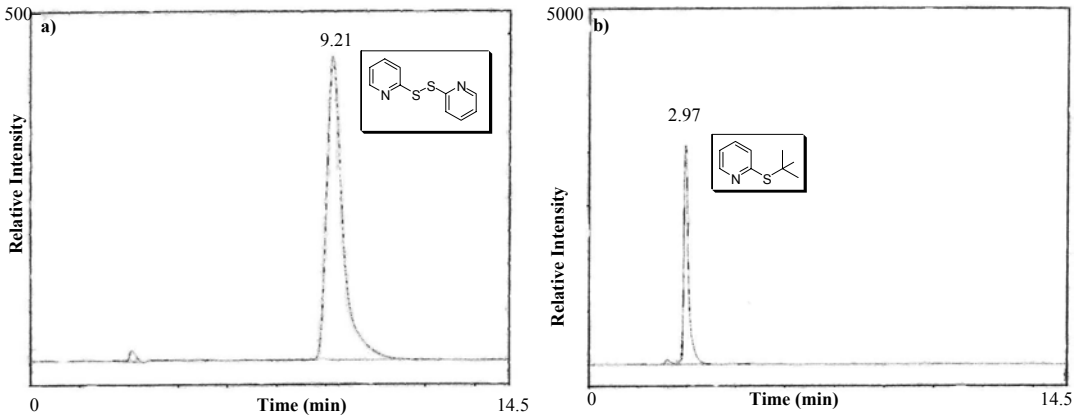

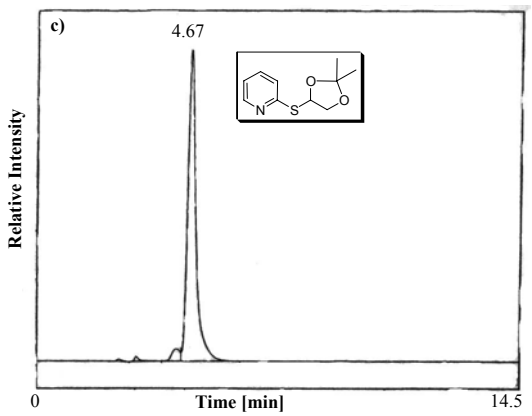

Figure 5–1: HPLC chromatograms of **98**, **106** and **99** observed at 290 nm with hexane (85%) and ethylacetate (15%) as eluent.

A linear relationship was observed for both **98** and **99** between the peak area and the concentration of the sample injected (200µl, correlation coeff. R = 0.99).

Table 5–2: HPLC data of photoproducts of **75** in presence as well as in absence of TFA with hexane (85%) and ethyl acetate (15%) as eluent.

Photolysis Experiment	Peak area **98**	Peak area **99**
	Without TFA	
1	218.99	103.61
	229.08	107.08
	With TFA [1.57 mM]	
2	209.52	66.52
	217.84	68.43

Table 5–3: HPLC data for the photoproducts of **99** with hexane (85%) and ethyl acetate (15%) as eluent.

Photolysis of **99**	Peak area (1^{st} measurement)	Peak area(2^{nd} measurement)
with TFA	470.24	468.94
without TFA	482.12	487.31

5.2.92.1 ESI-MS Spectrum of 79

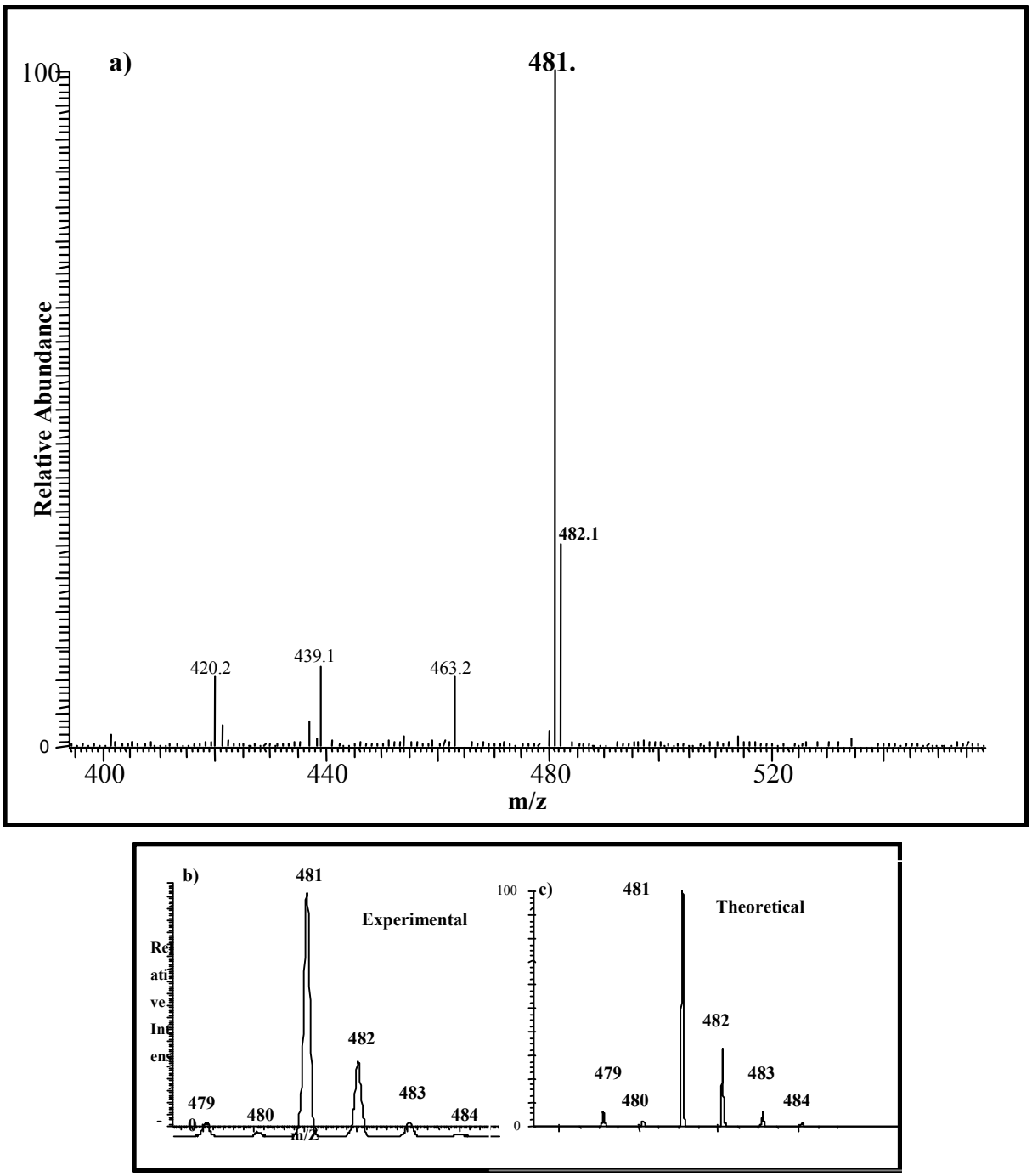

Figure 5–2: ESI-MS spectrum of oxidised form of **79** in dichloromethane, a) Complete ESI spectrum, b) experimentally determined isotope splitting and c) theoretically calculated isotope splitting.

5.2.92.2 Kinetics of $X5^+$ decay as observed by UV-Vis spectroscopy

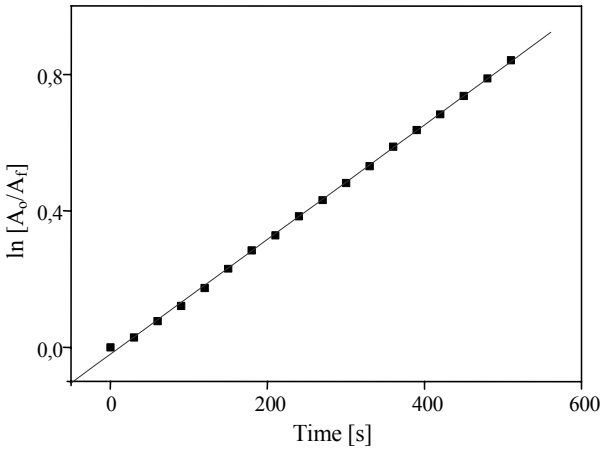

Figure 5–3: First order decay of $\mathbf{X5}^+$ as observed by UV-Vis spectroscopy at λ_{max} = 501 nm.

Table 5–4: UV-Vis spectral changes (λ_{max} = 501 nm) observed during the decay of $\mathbf{X5}^+$ generated by oxidation of **E5** with copper (II) triflate.

Abs	time (sec)	Change	time	$\log A_0/A_f$
$4{,}62e^{-01}$	$3{,}00e^{+01}$	$0{,}00e^{+00}$	$0{,}00e^{+00}$	$0{,}00e^{+00}$
$4{,}49e^{-01}$	$6{,}00e^{+01}$	$1{,}03e^{+00}$	$3{,}00e^{+01}$	$2{,}96e^{-02}$
$4{,}29e^{-01}$	$9{,}00e^{+01}$	$1{,}08e^{+00}$	$6{,}00e^{+01}$	$7{,}70e^{-02}$
$4{,}09e^{-01}$	$1{,}20e^{+02}$	$1{,}13e^{+00}$	$9{,}00e^{+01}$	$1{,}22e^{-01}$
$3{,}87e^{-01}$	$1{,}50e^{+02}$	$1{,}19e^{+00}$	$1{,}20e^{+02}$	$1{,}74e^{-01}$
$3{,}67e^{-01}$	$1{,}80e^{+02}$	$1{,}26e^{+00}$	$1{,}50e^{+02}$	$2{,}31e^{-01}$
$3{,}48e^{-01}$	$2{,}10e^{+02}$	$1{,}33e^{+00}$	$1{,}80e^{+02}$	$2{,}85e^{-01}$
$3{,}32e^{-01}$	$2{,}40e^{+02}$	$1{,}39e^{+00}$	$2{,}10e^{+02}$	$3{,}29e^{-01}$
$3{,}14e^{-01}$	$2{,}70e^{+02}$	$1{,}47e^{+00}$	$2{,}40e^{+02}$	$3{,}85e^{-01}$
$3{,}00e^{-01}$	$3{,}00e^{+02}$	$1{,}54e^{+00}$	$2{,}70e^{+02}$	$4{,}32e^{-01}$
$2{,}85e^{-01}$	$3{,}30e^{+02}$	$1{,}62e^{+00}$	$3{,}00e^{+02}$	$4{,}82e^{-01}$
$2{,}72e^{-01}$	$3{,}60e^{+02}$	$1{,}70e^{+00}$	$3{,}30e^{+02}$	$5{,}31e^{-01}$
$2{,}57e^{-01}$	$3{,}90e^{+02}$	$1{,}80e^{+00}$	$3{,}60e^{+02}$	$5{,}88e^{-01}$
$2{,}45e^{-01}$	$4{,}20e^{+02}$	$1{,}89e^{+00}$	$3{,}90e^{+02}$	$6{,}37e^{-01}$
$2{,}33e^{-01}$	$4{,}50e^{+02}$	$1{,}98e^{+00}$	$4{,}20e^{+02}$	$6{,}83e^{-01}$
$2{,}21e^{-01}$	$4{,}80e^{+02}$	$2{,}09e^{+00}$	$4{,}50e^{+02}$	$7{,}37e^{-01}$
$2{,}10e^{-01}$	$5{,}10e^{+02}$	$2{,}20e^{+00}$	$4{,}80e^{+02}$	$7{,}88e^{-01}$
$1{,}99e^{-01}$	$5{,}40e^{+02}$	$2{,}32e^{+00}$	$5{,}10e^{+02}$	$8{,}42e^{-01}$

5.2.92.3 Cyclic-Voltammograms of Enolates

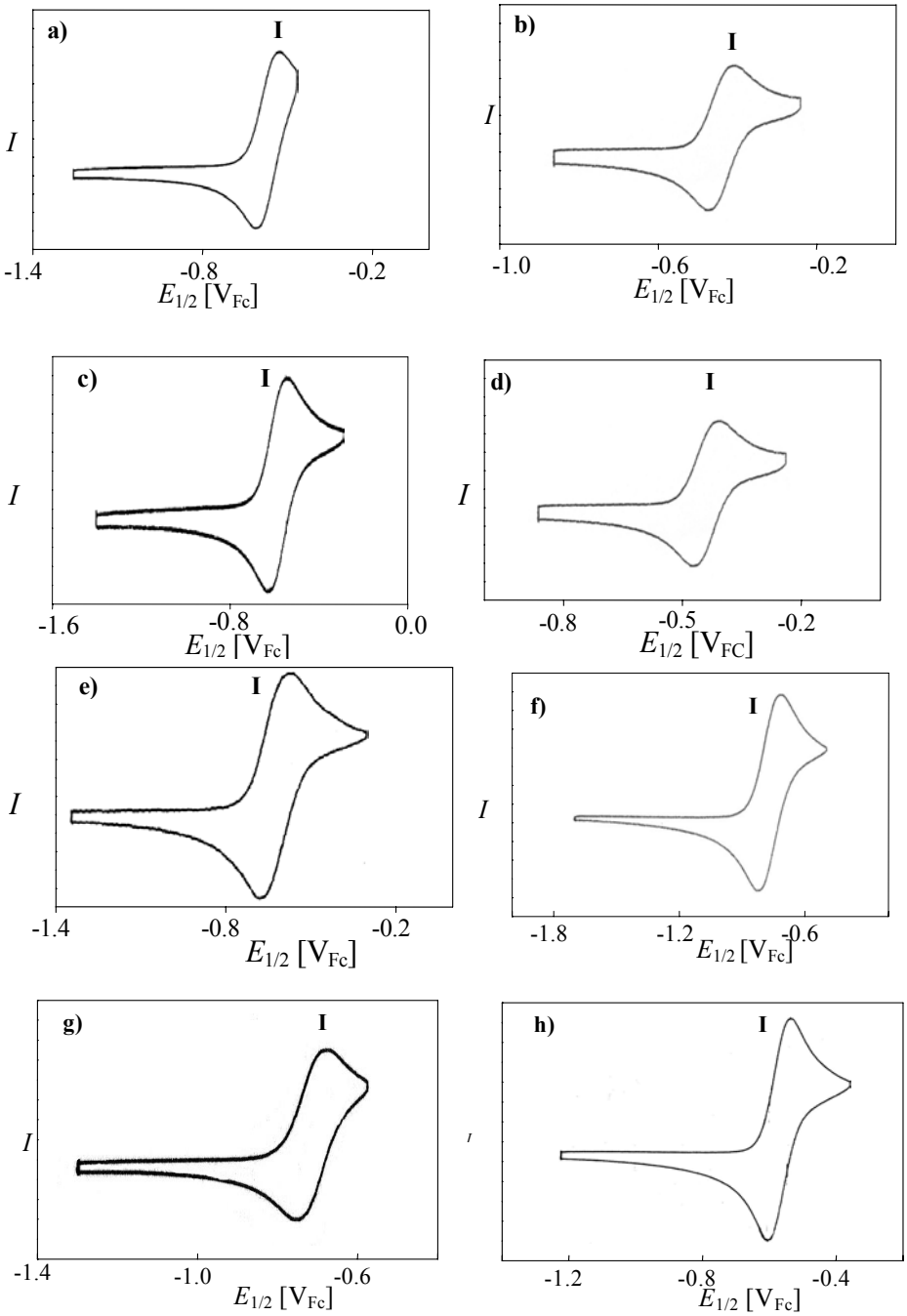

Figure 5–4: Cyclic voltammograms showing the enolate wave upon addition of 1 eq. base to the enols in acetonitrile at 100 mV/s scan rate, a) **A6**, b) **A7**, C) **A9**, d) **A10**, e) **A11**, f) **A2**, g) **A3**, h) **A4**.

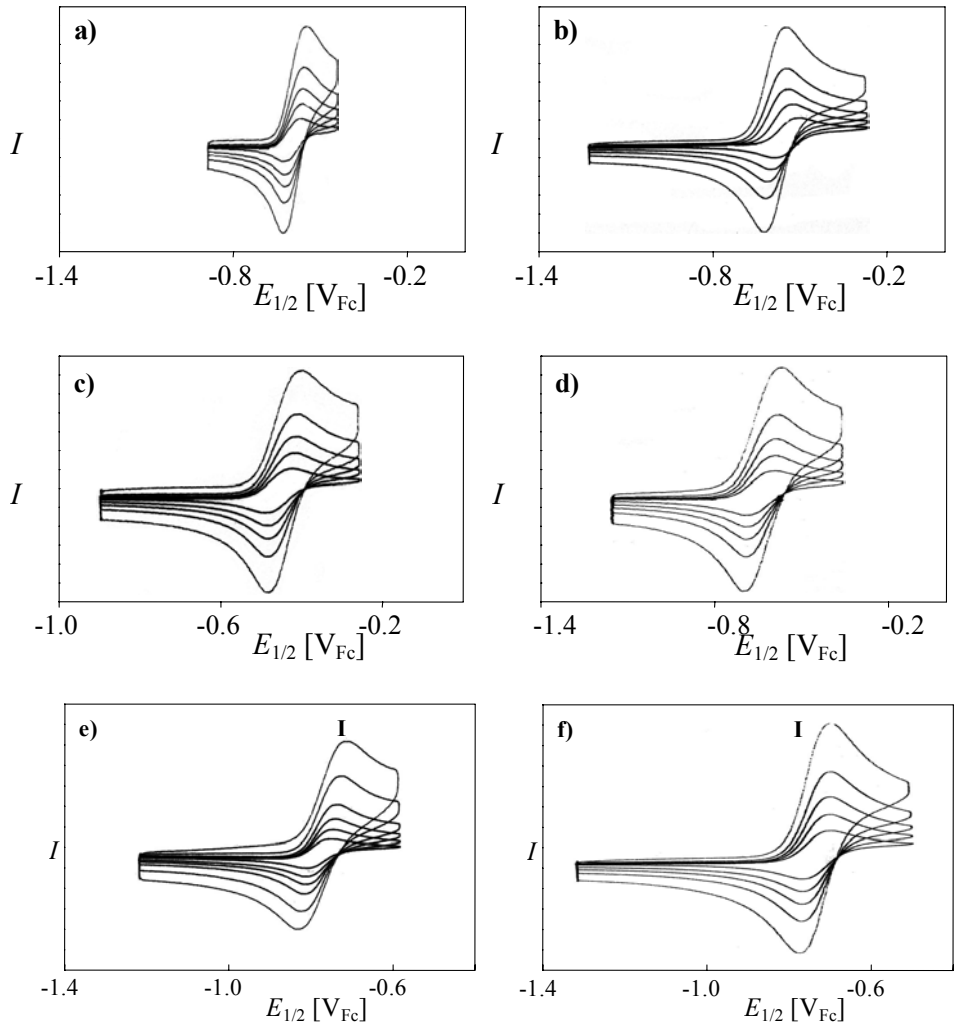

Figure 5–5: Cyclic voltammograms showing the anodic current dependence of enolates on the scan rate, a) **A6**, b) **A9**, c) **A10**, d) **A11**, e) **A2**, f) **A3** in acetonitrile. Every scan represents a different scan rate starting with the lowest 20 mV, 50 mV, 100 mV, 200 mV and 500 mV.

5.2.92.4 ESI-MS Characterisation of 2,3-dialkylpyrazinium Tetrafluoroborates 167a-d

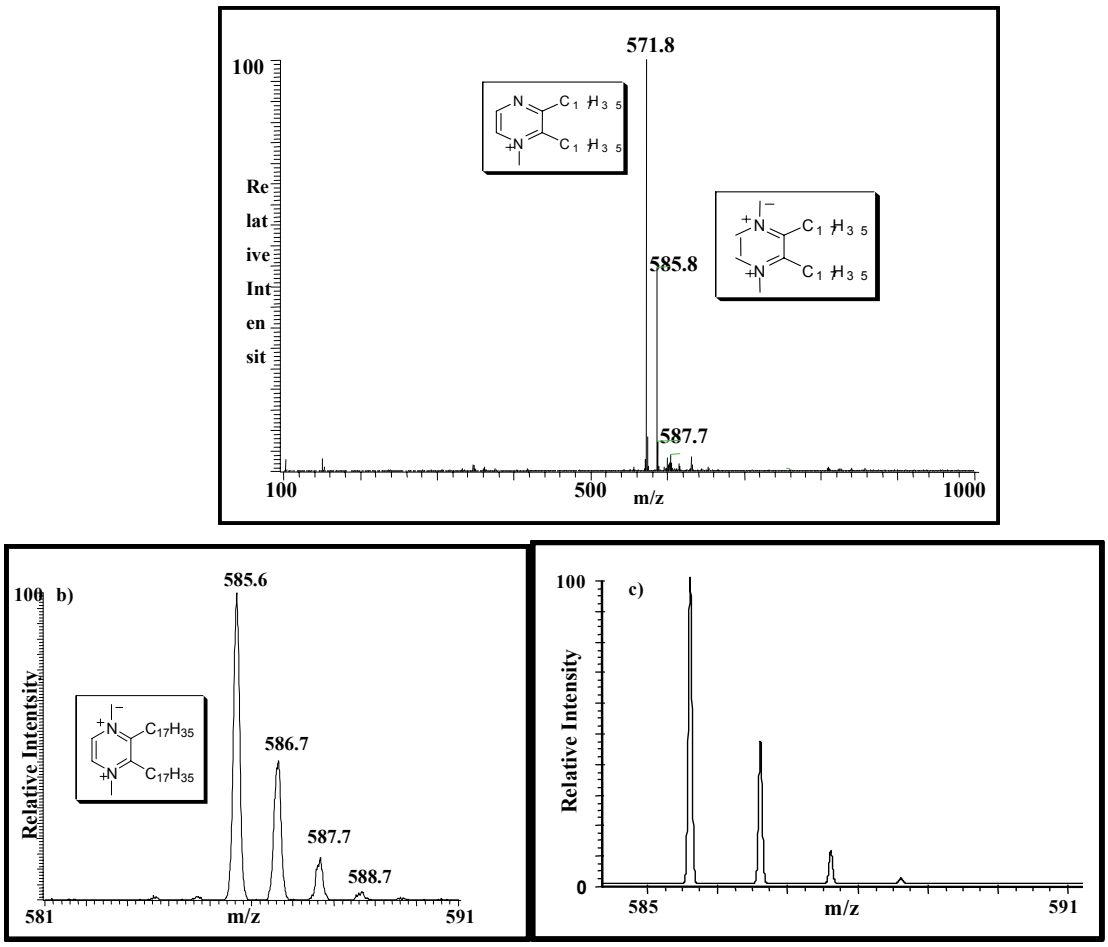

Figure 5–6: ESI-MS spectroscopic investigation of **167a-d**, a) typical spectrum showing the $\mathbf{M^+ - 1}$ fragment for **167d**, b) experimentally obtained isotope splitting for $\mathbf{M^+ - 1}$ fragment, c) theoretically obtained isotope splitting for $\mathbf{M^+ - 1}$ fragment.

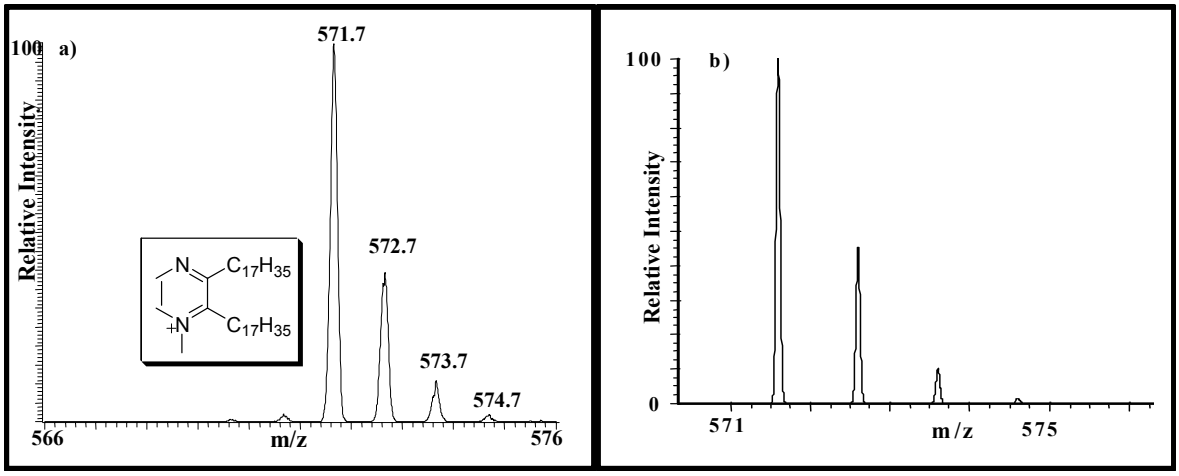

Figure 5–7: Isotope splitting patterns for $\mathbf{M^+ - 15}$ observed for **167d** a) experimental and b) theoretically calculated.

Table 5–5: ESI-MS investigation of **167a-d** in dichloromethane showing the characteristic fragmentation pattern.

m/z (RI)	**167a**	**167b**	**167c**	**167d**
M^+-1	249.3 (48%)	-	417.6 (50%)	585.8 (50%)
M^+-15	235.4 (100%)	291.5 (88%)	403.6 (100%)	571.8 (100%)
$M^{+\bullet}$	-	306.4 (100%)	418.6 (48%)	-
MH^+ + 18	-	325.4 (23%)	437.5 (8%)	-
M^+ + 17	-	-	435.5 (17%)	-

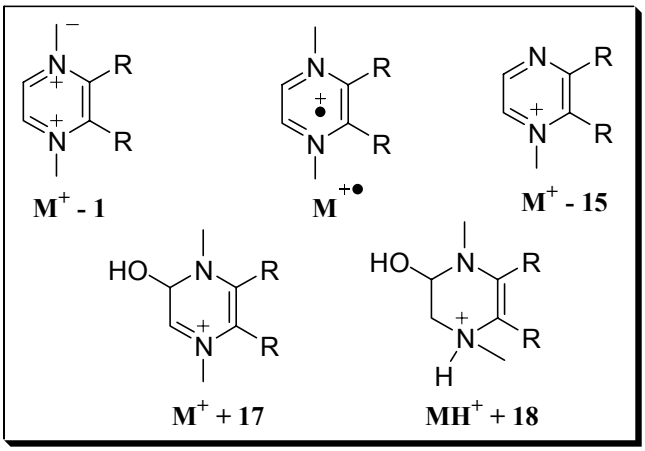

Scheme 5–1: Type of fragments observed in the ESI-MS investigation of **167a-d** in dichloromethane.

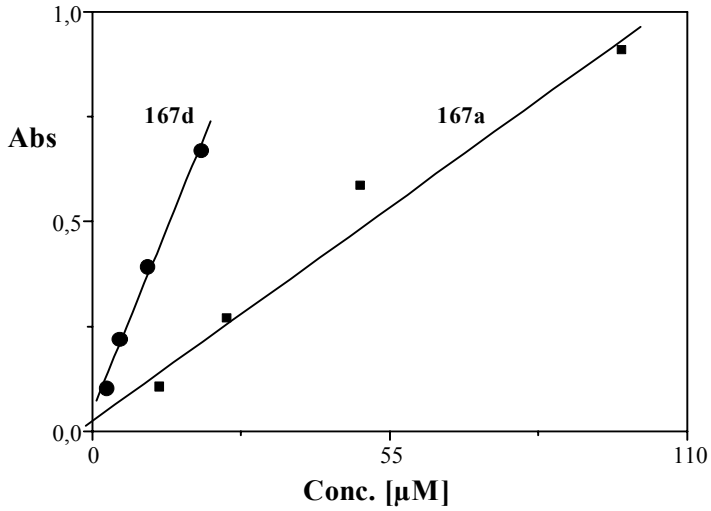

Figure 5–8: Concentration dependence of absorption in **167a** and **167d** investigated by UV-Vis spectroscopy.

5.2.92.5 ESI-MS Characterisation of 172 a Ferrocene-based Electroactive Surfactant

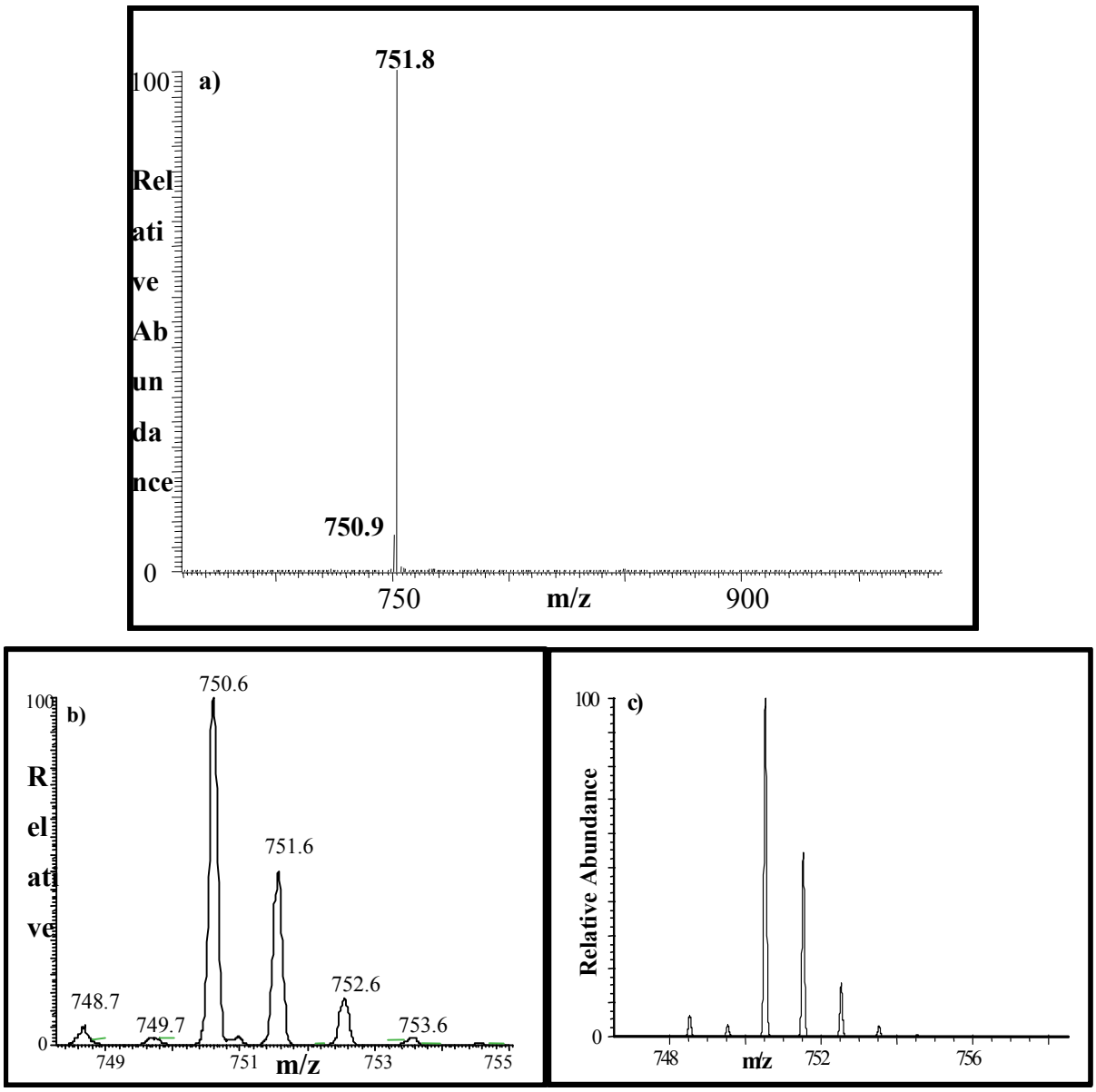

Figure 5–9: Representative ESI-MS spectrum for the electroactive surfactants, a) ESI-MS spectrum for **172** after oxidation by ferric chloride, b) experimentally determined isotope splitting and c) theoretically calculated isotope splitting.

6 Crystal Structures

6.1 Crystal Structure Analysis of Racemic 4-Ferrocenylbutan-1,2-diol (25)

Suitable single crystals of **25** were obtained and analysed by X-ray crystallography. Single crystal analysis indicates that **25** crystallises in monoclinic system with the space group P21/c, with one molecule in the formula unit. The two cyclopentadienyl groups were found in almost eclipsed conformation (deviation of about 1.6-2.1° was observed). The Cp rings were characterised by C-C bond distances in the range of 1.419 (2) to 1.434 (2) Å, with the iron well centred in the sandwich structure. Fe-Cp distances were ca. 2.04 Å. An average bond distance of about 1.52 Å between the sp3 hybrid carbons while a slightly shorter bond distance between a sp3-sp2 bonded carbons (1.50 Å) (Figure 6–1).

Additionally in the crystal structure intermolecular hydrogen bonding networks were observed. At a supramolecular level a ladder arrangement resulted due to co-operative effects of complimentary intermolecular bifurcated hydrogen bonding interactions. The hydroxyl group acts as both hydrogen bond donor and acceptor for the intermolecular hydrogen bonding.

The primary hydrogen bonding interactions lead to a dimeric arrangement of (*R*)-**25** and (*S*)-**25** due to intermolecular O1-H1···O2 interactions with a distance of 1.91 Å (between O2 and H1). The distance between the donor O1 and H1 is 0.84 Å, and the donor to acceptor oxygen (O1--O2) is about 2.752(1) Å. Only the primary alcoholic functionality (O1H1) acts as the acceptor. Secondary hydrogen bonding interactions of the O-H···O type, leading to the already mentioned 2D network, are observed between O2H2 and O1 with the O2H2 hydroxyl group exclusively acting as donor and O1 acting as acceptor. The secondary hydrogen bonding interaction leads to a chain C (5) like pattern. The secondary interactions are as strong as the primary ones as judged by the various distances: O2-H2 (0.84 Å), H2···O1 (1.94 Å), and O2···O1 (2.770 Å) in the vertical direction.

At a supramolecular level, the co-operative effects of the H-bonding in the two dimension *i.e.* R_2^2 (10) and C (5) yield a staircase ladder like arrangement making **25** the first vicinal diol having a staircase arrangement. The O···O intrastrand, interstrand and intramolecular distances were found to be 2.770(1) Å, 2.752(1) Å and 2.97 Å, respectively.

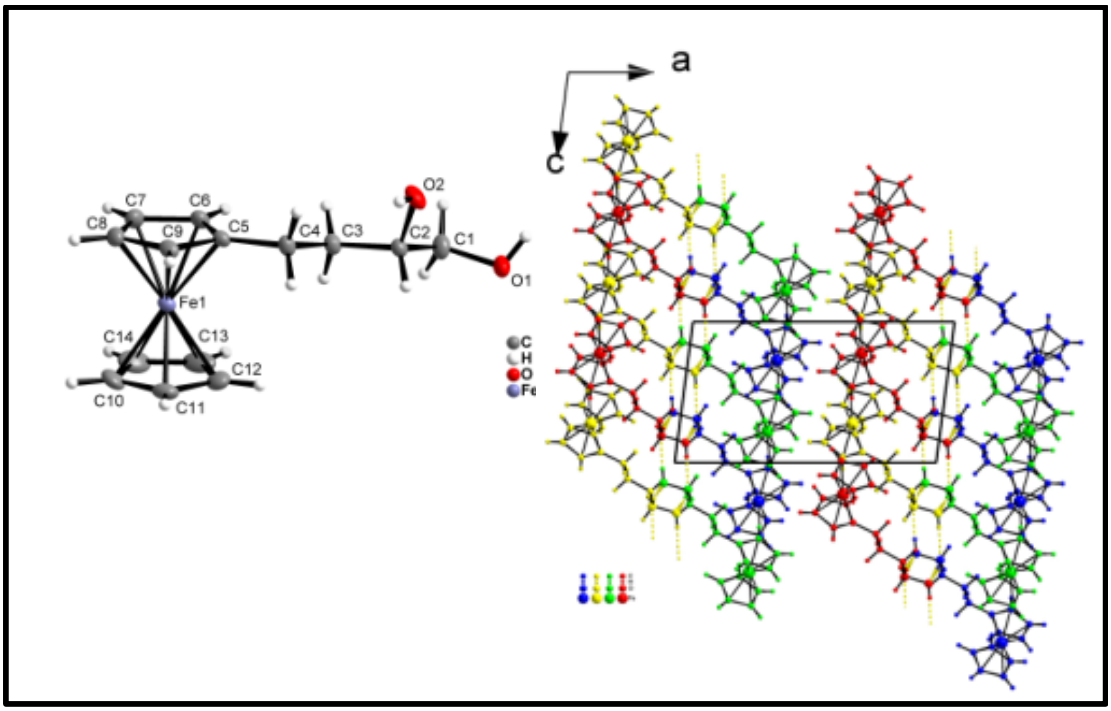

Figure 6–1: Molecular drawing of **25** depicting a single molecule and a supramolecular ladder arrangement (50%-probability displacement ellipsoids).

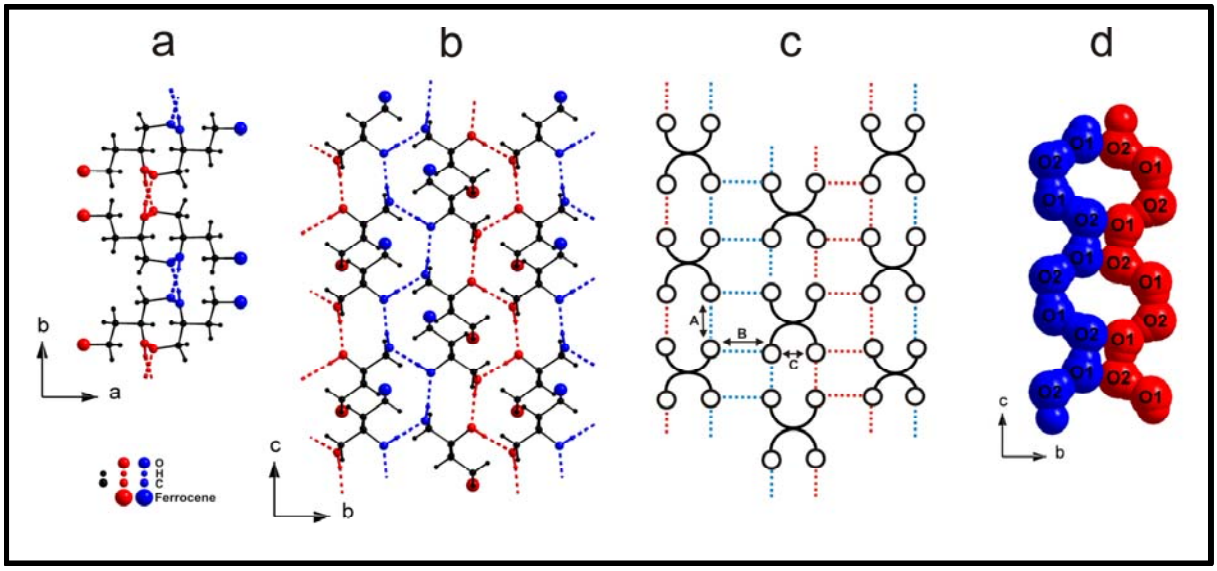

Figure 6–2: Hydrogen bond-connected secondary structure of **25** showing duplex staircase ladder arrangement in different perspectives.

Interestingly, two such staircase ladders run parallel to each other thus making a racemic duplex staircase. Unlike in the usual step and staircase ladders where both the hydroxy groups are involved in the same ladder, in **25** however each of the hydroxy group of the diol gives rise to a staircase ladder, thus leading to the duplex form (Figure 6–2). Interestingly the rung region of **25** is quite unique in the fact that like the step ladder oxygen atoms of four different molecules are involved. However instead of forming $(OH)_4$ cycles they form $(OH)_n$ chains involving only 3 molecules in the $(OH)_n$ chains rather than 4 molecules in the usual step-ladders (Figure 6–2).

Dilution experiments by ^{1}H-NMR to study hydrogen bonding in solution indicated that upon. A 10 fold dilution of **25** in $CDCl_3$ induced a shift of the signals (bs) at 2.17 and 2.33 ppm to 2.05 ppm and 1.81 ppm respectively. For both signals, this shift was further accompanied by a distinct change in the splitting of the signals, as the broad singlets developed in a relatively sharp triplet and doublet, respectively. From the data in table 1 it becomes clear that the O1H1 group (δ_{O1H1}) is most affected by the dilution, while the shift (δ_{O2H2}) of the hydroxy O2H2 group is rather modest. At 96.9 mM (relative concentration = 1) the intermolecular exchange of hydrogen via hydrogen bridged systems is so rapid that only broad singlets are observed.

The effect of dilution is most pronounced when going to 0.1 relative concentrations, whereas further dilution only brings about a minor shift at both hydroxy groups. Such a behaviour indicates a strong intramolecular hydrogen bonding at low concentration but suggests at 96.9 mM a bifurcated hydrogen bonded dimer for which structure **25A** is plausible due to the stronger hydrogen donor character of the O1H1 (Scheme 6–1). Upon dilution the O1H1 should keep acting as hydrogen donor as in 1C. Such a scenario would be in line with the observed NMR shifts.

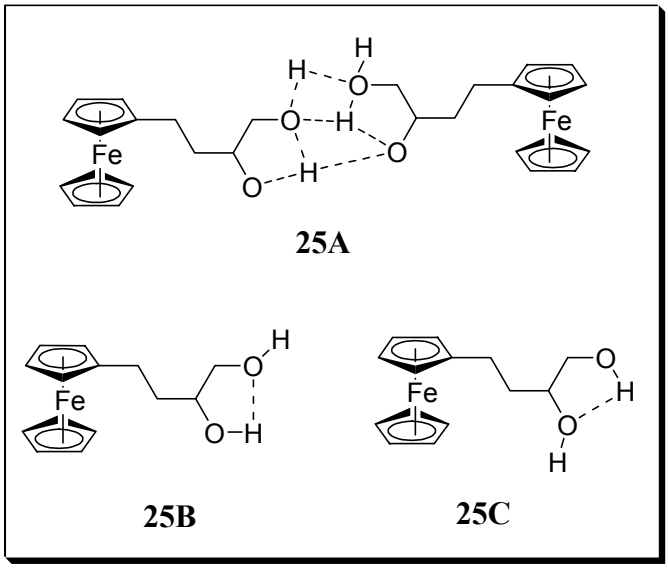

Scheme 6–1: Possible intra and intermolecular hydrogen bonded forms of **25** in solution based on 1H-NMR

investigations.

The structure refinement and measurement parameters are tabulated below, the crystal structure data have been summarised in Appendix (Table 9–1 and Table 9–2):

Table 6–1: Crystal data and structure refinement for **25**.[a]

Substance, Pearson symbol	*4-ferrocenyl-1,2-dihydroxybutane*, *m*P140
Empirical formula	$C_{14}H_{18}FeO_2$
Formula weight /g·mol^{-1}	274.13
Temperature /K	173(1)
Wavelength /pm	71.073
Crystal system, space group	monoclinic, $P2_1/c$ (no. 14)
Unit cell dimensions	a = 1525.9(1)
/pm, /°	b = 976.26(8), β = 97.460(8)
	c = 829.40(5)
Volume /nm^3	1.2250(2)
Z, Calculated density /Mg·m^{-3}	4, 1.486
Absorption coefficient /mm^{-1}	1.217
F(000)	576
Crystal size /mm^3	0.47 × 0.24 × 0.17
Θ-range for data collection /°	3.24 – 31.65
Limiting indices	$-22 \le h \le 22$, $-14 \le k \le 14$, $-12 \le l \le 12$
Reflections collected / unique / significant	17434 / 3912 / 3211
R_{int}, R_σ	0.0294, 0.0216
Completeness to Θ = 31.65	94.5
Absorption correction	numerical, crystal description with 16 faces, shape-optimised with [9]
Max. and min. transmission	0.8898 and 0.6787
Refinement method	Full-matrix least-squares on F^2
Data / restraints / parameters	3912 / 0 / 159
Goodness-of-fit on F^2	1.050
Final *R* indices [I>2σ(I)]	*R*1 = 0.0270, *wR*2 = 0.0674
R indices (all data)	*R*1 = 0.0354, *wR*2 = 0.0697
Extinction coefficient	0.0039(7)
$\Delta\rho_{min.}$, $\Delta\rho_{max.}$ /10^{-6}e·pm^{-3}	-0.41(6), 0.43(6)

6.2 Crystal Structure of 2,2,6,6-Tetramethylpiperidin-1-oxyl (21)

The crystal structure data are summarised in Appendix (Table 9–3 to Table 9–6).

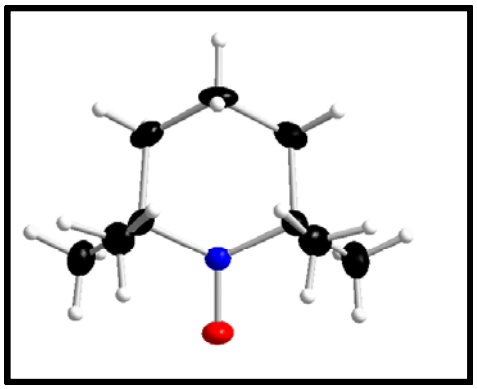

Figure 6–3: Molecular structure of **21** as obtained by X-ray single crystal analysis.

Table 6–2: Crystal data and structural refinement for **21**.

Substance, Pearson symbol	*2,2,6,6-tetramethylpiperidin-1-yloxy*
Empirical formula	$C_9H_{18}NO$
Formula weight	156.24
Temperature	173(2) K
Wavelength	71.073 pm
Crystal system	orthorhombic
Space group	Fdd2
Unit cell dimensions	a = 2117.2(4) pm, α= 90°.
	b = 2275.7(5) pm, β= 90°.
	c = 788.89(16) pm, γ = 90°.
Volume	3.8009(13) nm^3
Z	16
Density (calculated)	1.092 Mg/m^3
Absorption coefficient	0.070 mm^{-1}
F(000)	1392
Crystal size	0.4 x 0.3 x 0.2 mm^3
Theta range for data collection	2.63 to 29.19°.
Index ranges	-28<=h<=28, -31<=k<=30, -10<=l<=10
Reflections collected	5777

Independent reflections	1230 [R(int) = 0.0505]
Completeness to theta = 29.19°	89.1 %
Absorption correction	None
Refinement method	Full-matrix least-squares on F^2
Data / restraints / parameters	1230 / 1 / 107
Goodness-of-fit on F^2	0.985
Final R indices [I>2sigma(I)]	R1 = 0.0360, wR2 = 0.0841
R indices (all data)	R1 = 0.0470, wR2 = 0.0867
Absolute structure parameter	10(10)
Extinction coefficient	0.0026(4)
Largest diff. peak and hole	0.176 and -0.146 e Å $^{-3}$

6.3 Crystal Structure Analysis of 2-(2,2,6,6-Tetramethylpiperidin-1-yloxy) propane diol (62)

2-(2,2,6,6-Tetramethylpiperidin-1-yloxy) propane-1, 3-diol crystallises in the space group XYZ with one molecule in the formula unit. The piperidinoxyl ring adopts the usual chair conformation. Atom O1 is anti-periplanar with O2 (-178.12[7] Å), while it is synclinal with atom O3 (-58.52[9] Å) in the solid state. Intermolecular CH···O interactions (H···O = 2.44 Å) were observed between the axial methyl groups of the piperidinoxyl group (C10 and C12) with oxygen atom O1. Intermolecular OH···O hydrogen bonding interactions predominates in the crystal structure of **62**. Interestingly the hydrogen bonding was bifurcated with each primary oxygen (O2 and O3) acting as both intermolecular hydrogen bond donor and acceptor. Along the [001] direction the OH···O hydrogen bonding gives rise to a chain like structure with a C_1^1 (6) descriptor. Two such C_1^1 (6) chains form a 2D hydrogen bonded network giving rise to a ladder arrangement at a supramolecular level. The ladder arrangement in **62** shows $(OH)_4$ cycles in the rung region thus representing a step ladder which was expected of a symmetrically substituted achiral 1,3-diol (Figure 6–4).[202]

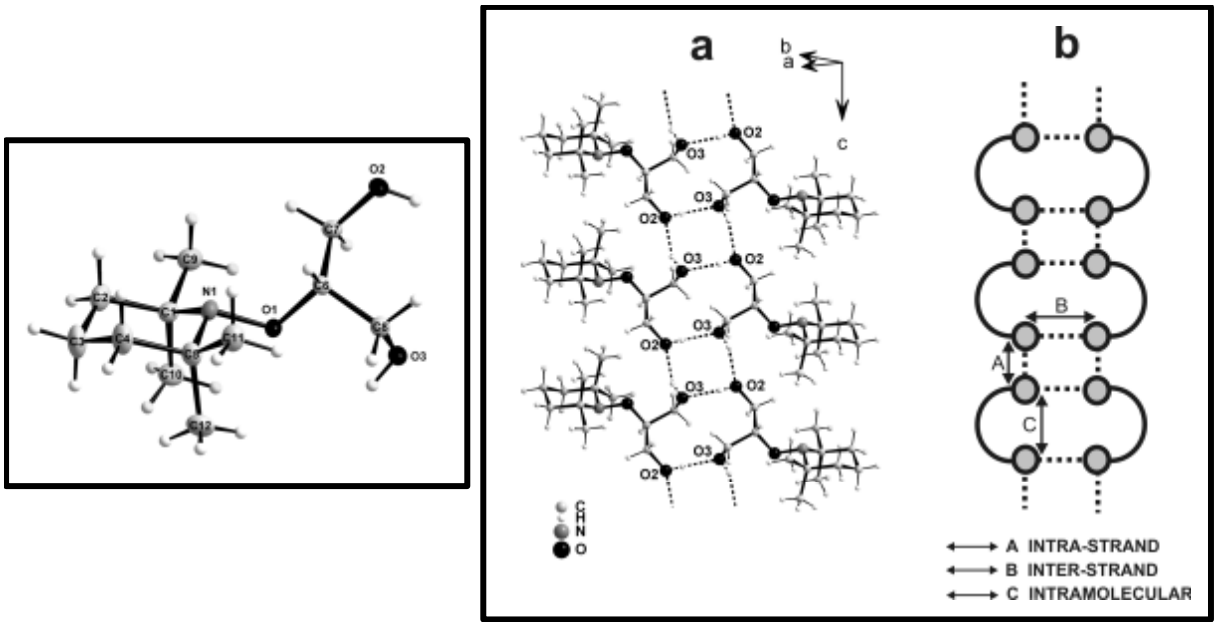

Figure 6–4: I) Molecular structure of **62** with 50% displacement of ellipsoids, II) Hydrogen bonded secondary structure of **62**, showing the step-ladder arrangement in different representations, *viz*. (a) a ball-and-stick model and (b) a schematic representation.

The intrastrand O···O distance with 2.75 Å was slightly longer than the interstrand O...O distance (2.71 Å) resulting in a slightly stronger interstrand hydrogen bonding interaction (1.88 Å for interstrand O-H···O) than the intrastrand hydrogen bonding (1.95 Å for intrastrand O-H···O). The intramolecular O···O distance was found to be 3.64 Å. The crystal refinement and data (Appendix , Table 9–7 to Table 9–12) are tabulated below in the following tables:

Table 6–3: Crystal data and structure refinement for **62**.

Substance, Pearson symbol	*2-(2,2,6,6-tetramethylpiperidin-1-yloxy)propane-1,2-diol*
Empirical formula	$C_{12}H_{25}NO_3$
Formula weight	231.33
Temperature	173(2) K
Wavelength	71.073 pm
Crystal system	monoclinic
Space group	$P2_1/n$
Unit cell dimensions	a = 1465.25(13) pm α = 90°
	b = 1463.57(8) pm β = 93.801(10)°.
	c = 617.93(5) pm γ = 90°.
Volume	1.32223(17) nm^3
Z	4
Density (calculated)	1.162 Mg/m^3
Absorption coefficient	0.082 mm^{-1}
F(000)	512

Crystal size	0.2 x 0.1 x 0.08 mm^3
Theta range for data collection	3.11 to 30.46°.
Index ranges	-20<=h<=20, -20<=k<=19, -8<=l<=8
Reflections collected	15527
Independent reflections	3992 [R(int) = 0.0428]
Completeness to theta = 30.46°	99.3 %
Absorption correction	None
Refinement method	Full-matrix least-squares on F^2
Data / restraints / parameters	3992 / 0 / 158
Goodness-of-fit on F^2	0.926
Final R indices [I>2sigma(I)]	R1 = 0.0364, wR2 = 0.0846
R indices (all data)	R1 = 0.0663, wR2 = 0.0930
Extinction coefficient	0.019(2)
Largest diff. peak and hole	0.253 and -0.191 e $Å^{-3}$

6.4 Crystal Structure Analysis of Diethyl-2-(2,2,6,6-tetramethylpiperidin-1-yloxy)malonate (65)

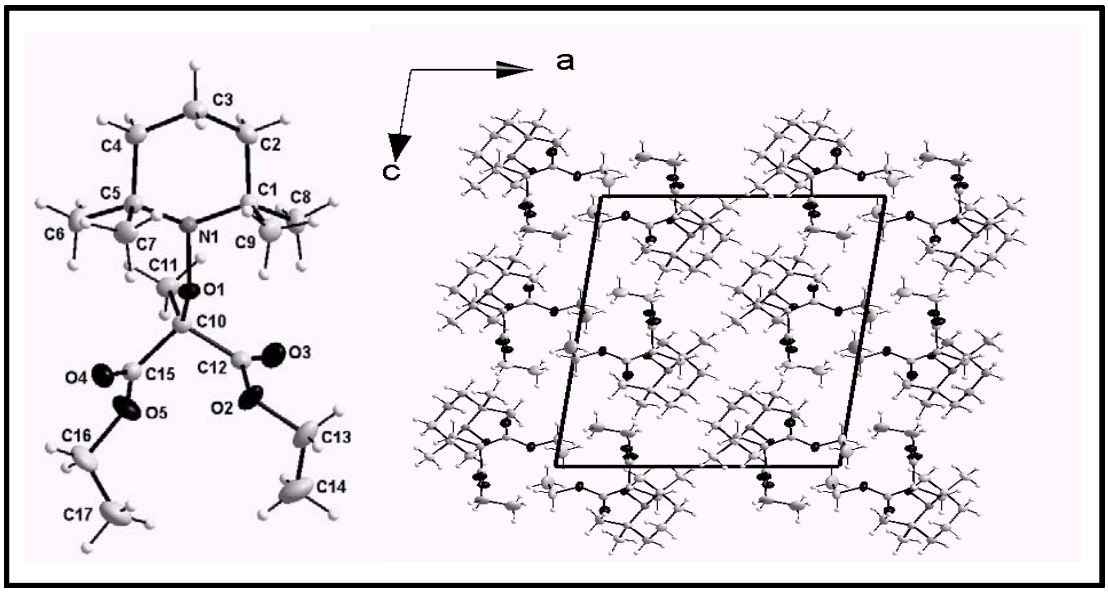

Figure 6–5: Figure showing the molecular structure of **65** (left) with a probability of 50 %.

The crystal structure data have been summarised in Appendix (Table 9–13 to Table 9–15).

Table 6–4: Crystal data and refinement details for **65**.

Substance, Pearson symbol	*Diethyl-2-(2,2,6,6-tetramethyl-piperidin-1-yloxy)malonate*

Empirical formula	$C_{17}H_{31}NO_5$
Formula weight /g mol^{-1}	M = 329.43
Temperature /K	T = 173(2)
Colour,	colourless,
Wavelength /pm	Mockα, γ = 71.073
Crystal System	monoclinic
Space group	$P2_1/c$(No. 14)
Cell dimensions /pm /°	a = 1309.2(1)
	b = 859.60(4)
	c = 1641.8(1)
	β = 97.435(9)
Volume /10^6 pm^3	V = 1832.2(2)
Formula units per unit cell	Z = 4
Density(calc.) /g cm^{-3}	ρ = 1.194
Absorption coefficient /mm^{-1}	μ = 0.087
F(000)	720
Diffractometer	IPDS(Stoe), oriented graphite monochromator
Scan type	φ
Measured θ range	$3.68° \leq \theta \leq 29.16°$
Index ranges	$-17 \leq h \leq 17$; $-11 \leq k \leq 11$; $-22 \leq l \leq 22$
Measured reflections	19144
Independent reflections	4925(R_{int} = 0.0527)
Completeness to θ	99.4 %
Absorption correction	Numerical [X-SHAPE]
Max, min. transmission	T_{max} = 0.8061, T_{min} = 0.5609
Crystal dimension /mm	0.95 × 0.42 × 0.16
Structure solution	Direct methods [SHELXS-97]
Structure refinement	Full-matrix least-squares on F^2 [SHELXL-97]
Data/restraints/parameters	4925 / 0 / 216
Goodness-of-Fit on F^2	0.992
Weighting Scheme [a)]	A = 0.0568; B = 0
R values [$I \geq 2\sigma(I)$]	R_1 = 0.0369; wR_2 = 0.0935
R values(all data)	R_1 = 0.0574; wR_2 = 0.0994
Difference Fourier residuals /e 10^{-6} pm^{-3}	$\rho_{max.}$ = 0.289; $\rho_{min.}$ = -0.231

[a)] $w = 1/[\sigma^2(F_0^2) + (AP)^2 + BP)]$, $P = (F_0^2 + 2F_c^2)/3$

6.5 Crystal Structure Analysis of 2,2-Dimesityl-ethanols with Various Six Membered Nitrogen Heterocycles (E2, E3, E4)

The single crystal measurement was carried out on a STOE IPDS one-circle image-plate diffractometer equipped with an Oxford Cryostream liquid-nitrogen cooling device. Because of the $\mu \cdot x < 0.1$ criterion no absorption correction was necessary. Crystal structure solution and refinement based on F^2 were performed by direct methods and subsequent Fourier syntheses with anisotropic displacement parameters for all non hydrogen atoms using SHELXS-97 and SHELXL-97.[203]

*Crystal structure description Basic structural features of **E2-E4***:

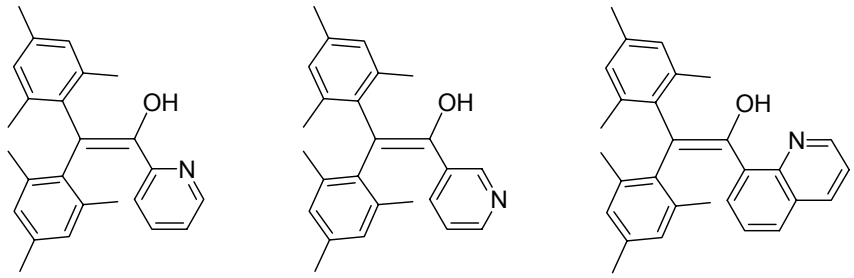

E2 **E3** **E4**

In the solid state **E2** and crystallises in the space group P_1 (triclinic) and **E3** (*o*P432) crystallises orthorhombic in the space group *Pbca*. Single crystal measurements of **E2**-**E4** suggest that despite the difference in substitution, the hydrocarbon skeletons of these enols adopt a helical propeller conformation similar to various aryl substituted enols.[204] The enols display a C=C bond length of about 135 pm Although α_5, α_6 remained constant for **E2** and **E3,** a slight (α_5 ~3° higher, and α_6 ~6° lower) deviation was observed for **E4**. The effect was more pronounced in α_6 thus bringing the enolic OH and the α aryl substituent closer to each other, this was further expressed in an increase of α_4 from **E2**-**E4**. As a consequence α_2 also increased in the order **E3 < E2 < E4** and α_3 decreased in the order **E3 > E2 > E4** (Table 6–5).

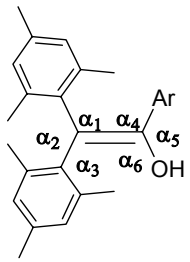

Table 6–5: Some important bond angles (α/°) and (d/pm) bond distances as observed in the solid state for **E2**, **E3** and **E4**.

Bond angle/distance	**E2**	**E3**	**E3**
α_1	120(0)	121(0)	122(0)

α_2	120(0)	118(0)	120(0)
α_3	120(0)	121(0)	118(0)
α_4	124(0)	125(0)	127(0)
α_5	111(0)	110(0)	114(0)
α_6	125(0)	125(0)	119(0)
C=C	134(1)	135(0)	135(3)
C-O	136(0)	136(0)	138(2)
=C-mes (β)	150(0)	151(0)	149(1)
=C-mes (β′)	150(1)	150(0)	149(2)
=C-Ar (α)	149(1)	148(0)	149(2)

N···H-O hydrogen bonding and π-π interactions:

The directionality of hydrogen bonding interactions enables one to design molecules to study specific interactions (including hydrogen bonding), both in solution as well as in solid state.

Thus enols **E2-E4** were designed so as to study hydrogen bonding interactions between the nitrogen of the aromatic ring acting as acceptor and the OH of the enol as donor. Intramolecular N···HO hydrogen bonding was expected for **E2** and **E3** via five and six membered ring, while intermolecular for **E4**.

Solution studies by ^{1}H-NMR both the dilution and solvent dependence (based on δ_{OH} ppm shifts, Table 6–5) were in line with the design i.e., intramolecular hydrogen bonding in **E2** and **E4** and intermolecular in **E3**, however the solid state structure of these enols were quite surprising.

Interestingly in the solid state **E2** existed as dimer R_2^2 (10)[205,206] stabilised by intermolecular N···H-O hydrogen bonding [192(1) pm], with a synclinal orientation of the enolic OH. While an intramolecular hydrogen bonding was observed in solution would demand an anticlinal orientation of the enolic OH. **E3** to our expectation had a chain C_1^1 (6) like structure having N···H-O hydrogen bonding [187(0) pm] and **E4** which also was dimeric actually had intramolecular hydrogen bonding D_1^1 (6) with the dimer formed by π-π stacking interaction between quinoline units of two enols [357 pm] (Figure 6–6).The donor to acceptor distances were found to be between 264.0 - 271.1 pm, with **E3** and **E4** having short donor to acceptor distance than **E2**.

Table 6–6: Comparison of Inter and Intramolecular N···HO hydrogen bonding interactions for enols **E2-E4** in solution and solid state.

Enol	Hydrogen bonding in solution	Hydrogen bonding in solid	O···N distance (/pm)	H···N distance (/pm)
E2	Intramolecular (strong)	Intermolecular (dimer)	271.1 (15)	192(1)

E3	Intermolecular (weak)	Intermolecular (chain)	264.4 (1)	187(0)
E4	Intramolecular (partial proton transfer)	Intramolecular (dimer)	264.0 (43)	193(3)

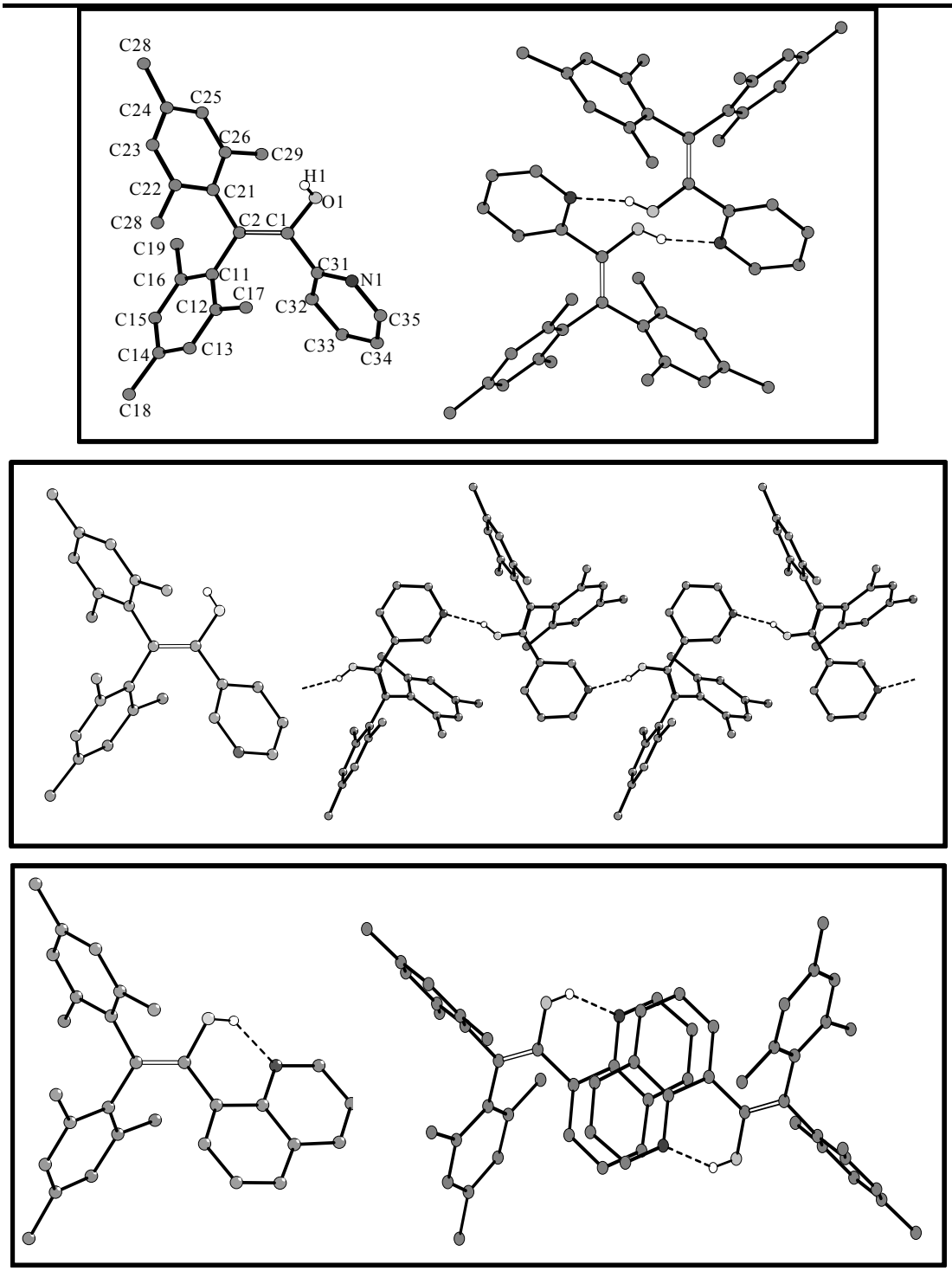

Figure 6–6: Figures shows the molecular structure of enols **E2**, **E3** and **E4** (left) and the hydrogen bonded motifs (right) observed in the solid state.

OH-π and CH-π interactions:

The synclinal orientation of the OH groups of enols in **E2** and **E3** stabilised by OH-π

interactions between the alkene backbone and also with the mesityl rings, with the former interaction being stronger (Table 6–7).

Table 6–7: Non-covalent interactions (OH···π) observed in the crystal structure of **E2** and **E3**.

Enol	OH-π interaction	
	Alkene backbone(pm)	Mesityl ring (pm)
E2	254(1)	271(1) and 295(2)
E3	247(0)	261(0) and 291(0)

In addition to the OH-π interactions several C···H interactions between the π-electron rich system and the hydrogens of the Methyl-units or the heterocyclic system were found in each of these enols. The interactions were similar to the ones observed in triptycenes[207] and substituted aromatic compounds.[208] The calculated distances between the fixed hydrogens and the π-electron rich systems were in the range of 259 up to 297 pm (Table 6–8, Figure 6–7). The crystal structure data are summarised in Appendix (Table 9–16 to Table 9–24).

Table 6–8: Intramolecular CH···π interactions observed in the solid state structures of enols **E2-E4**.

Enol	CH-π interacting atoms	distance (pm)	CH-π interacting atoms	distance (pm)
E2	C1-H17B	263(2)	C2-H27B	284(1)
	C1-H29B	264(2)	C11-H27C	267(1)
	C2-H17B	259(2)	C11-H32	277(1)
	C2-H19B	282(0)	C21-H19C	269(1)
	C2-H29B	260(2)	C2-H29C	257(0)
E3	C1-H17B	265(0)		
	C1-H29C	257(0)	C11-H27C	266(0)
	C2-H17B	261(0)	C11-H32	273(0)
	C2-H19C	290(0)	C21-H19A	262(0)
	C2-H27B	282(0)		
E4	C1-H17B	269(4)	C11-H27A	278(4)
	C1-H29B	266(2)	C11-H27B	297(2)
	C1-H32	263(3)	C11-H32	266(4)
	C2-H17B	267(2)	C21-H19B	269(5)
	C2-H19C	278(4)	C21-H19C	288(4)
	C2-H27B	278(4)	C26-H19C	291(4)

C2-H29B	260(4)	C31-H17A	261(4)
C2-H32	282(1)	C39-H17A	287(4)

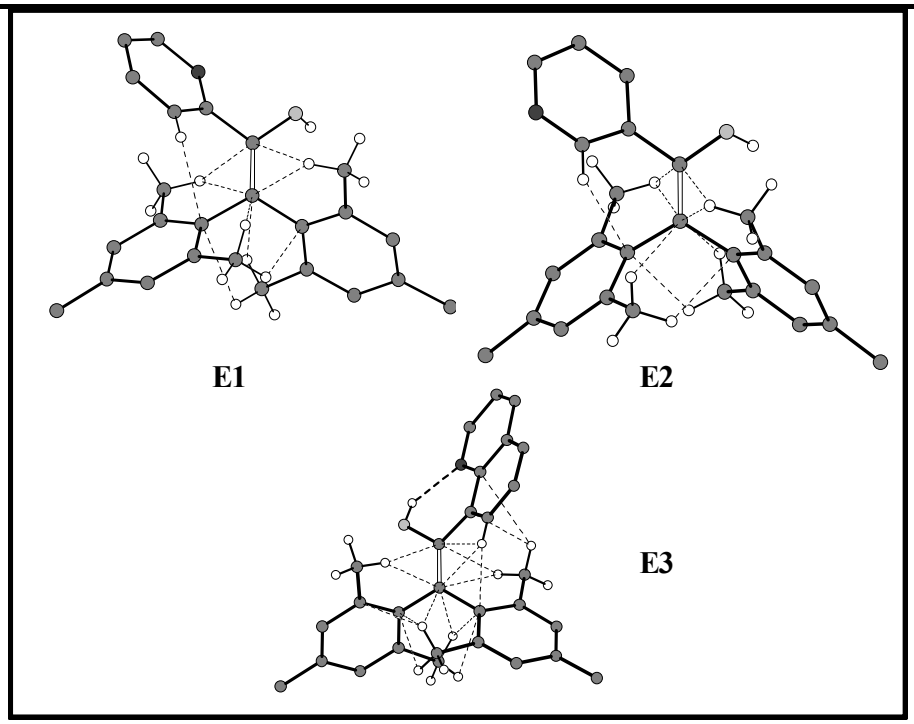

Figure 6–7: Structures showing the CH···π interaction motifs in the solid state structures of **E2**, **E3** and **E4**.

Table 6–9: Crystal data and structure refinement for enols **E2-E4**.

Substance, Pearson symbol	**E2**, *a*P108	**E3**, *o*P432	**E4**, *a*P120
Empirical formula	$C_{25}H_{27}NO$	$C_{25}H_{27}NO$	$C_{29}H_{29}NO$
Formula weight /g·mol^{-1}	357.48	357.48	407.53
Temperature /K	170(1)	173(2)	173(2)
Wavelength /pm	71.073	71.073	71.073
Crystal system, space group	triclinic, P-1	orthorhombic, *Pbca*	triclinic, P-1
Unit cell dimensions	a = 836.6(1),	a = 1254.4(3),	a = 793.7(2), α =
	α = 106.11(1)	α = 90.0	78.06(3)
/pm, /°	b = 1117.9(1),	b = 1707.2(3),	b = 857.8(2),
	β = 109.50(1)	β = 90.0	β = 79.69(3)
	c = 1186.0(1),	c = 1921.1(4),	c = 1688.2(3),
	γ = 92.59(1)	γ = 90.0	γ = 89.75(3)
Volume /nm^3	0.993(5)	4.1141(15)	1.1057(4)
Z, Calculated density /Mg·m^{-3}	2, 1.196	8, 1.154	2, 1.224
Absorption coefficient /mm^{-1}	0.072	0.069	0.073
F(000)	384	1536	436
Crystal size /mm^3	0.3 · 0.3 · 0.1	0.70 · 0.24 · 0.06	0.70 · 0.56 · 0.05

Θ-range for data collection /°	2.61 – 27.16	2.93 – 30.50	2.43 – 27.08
Limiting indices	-10 ≤ h ≤ 9, -14 ≤ k ≤ 14, -15 ≤ l ≤ 15	-17 ≤ h ≤ 17, -24 ≤ k ≤ 24, -27 ≤ l ≤ 27	-10 ≤ h ≤ 10, -10 ≤ k ≤ 10, -21 ≤ l ≤ 21
Reflections collected / unique / significant	10838 / 4016 / 3003	47040 / 6241 / 3179	12316 / 4485 / 3329
R_{int}, R_{σ}	0.0320, 0.0346	0.1134, 0.0764	0.0532, 0.0458
Completeness to Θ_{max}	90.9	99.5	92.4
Absorption correction	none (μ·x < 0.1)	None (μ·x < 0.1)	None (μ·x < 0.1)
Refinement method	Full-matrix least-squares on F^2	Full-matrix least-squares on F^2	Full-matrix least-squares on F^2
Data / restraints / parameters	4016 / 0 / 254	6241 / 0 / 254	4485 / 0 / 290
Goodness-of-fit on F^2	1.049	0.889	1.022
Final R indices [I>2σ(I)]	R1 = 0.042, wR2 = 0.110	R1 = 0.0468, wR2 = 0.1026	R1 = 0.0453, wR2 = 0.1234
R indices (all data)	R1 = 0.058, wR2 = 0.118	R1 = 0.1087, wR2 = 0.1204	R1 = 0.0603, wR2 = 0.1319
$\Delta\rho_{min.}$, $\Delta\rho_{max.}$ /10^{-6}e·pm^{-3}		-0.223, 0.221	-0.263, 0.260

6.6 Crystal Structure Determination of E6

The single crystal measurement was carried out on a STOE IPDS one-circle image-plate diffractometer equipped with an Oxford Cryostream liquid-nitrogen cooling device. Further details on measurement, refinement and crystal data are summarized in Table 6–10. Because of the μ·x < 0.1 criterion no absorption correction was necessary. Crystal structure solution and refinement based on F^2 were performed by direct methods and subsequent Fourier syntheses with anisotropic displacement parameters for all non hydrogen atoms using SHELXS-97 and SHELXL-97.[203] The coordinates of the hydrogen atoms were placed and refined for idealized geometries with isotropic displacement.

Crystal structure description **E6**:

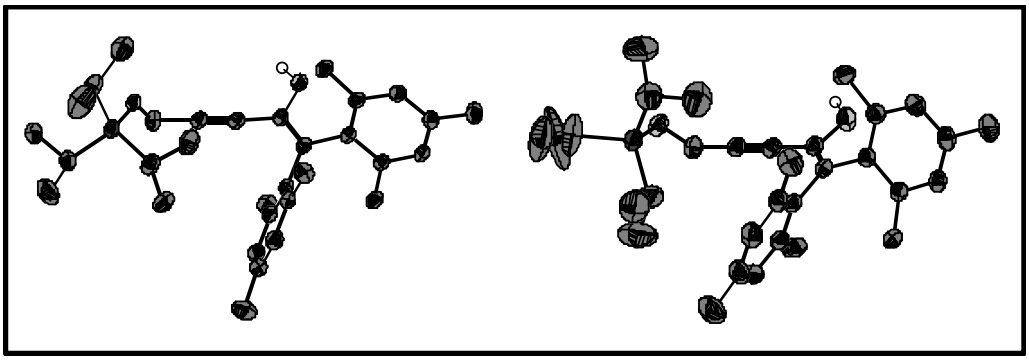

Figure 6–8: Molecular structure of **E6** showing the thermal ellipsoid of the two molecules with 50% probability distribution.

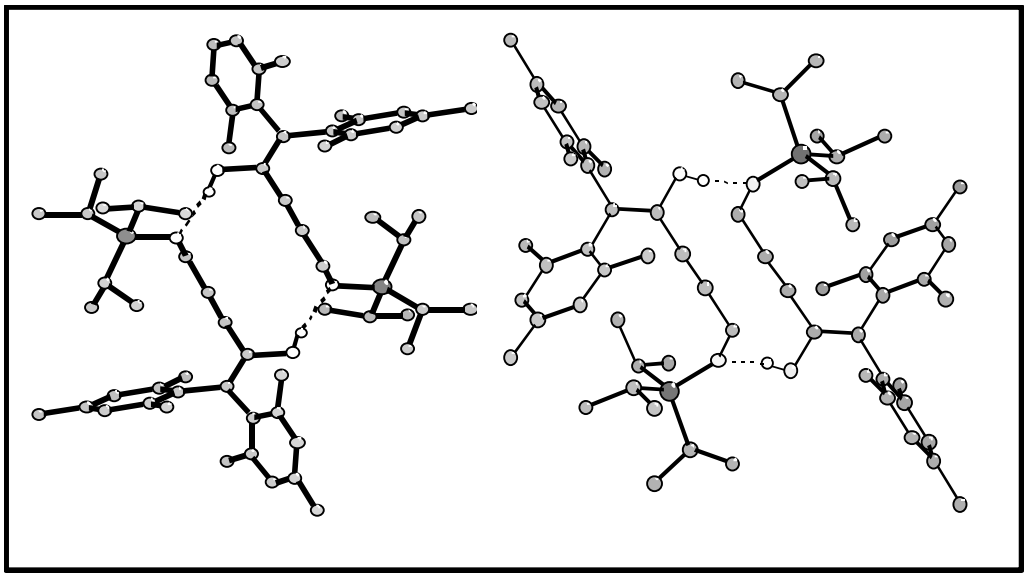

Figure 6–9: Molecular structure of **E6** showing the formation of dimers due to intermolecular hydrogen bonding interaction.

E6 (*a*P324) crystallises triclinic in the space group P_1 with two formula unit in the asymmetric unit (Figure 6–8). All atoms of **E6** are placed on general positions 2*i*. Intermolecular hydrogen bonds leading to dimers were observed in the solid state structure of interestingly dimers were formed between molecules of the same type Si1Si1 or Si2Si2 and no mixed dimers were observed. In **E6** the oxygen atom of enol acts as OH···O hydrogen bond donor and the oxygen atom connected to the silicon acts as acceptor (Figure 6–9). The H···A distance was found to be about 1.95 Å. The crystal structure data have been summarised in Appendix (Table 9–25 to Table 9–27).

Table 6–10: Crystal data and structure refinement for **E6**[a].

Substance, Pearson symbol	*5-Triisopropylsilanyloxy-1,1-bis-(2,4,6-trimethyl-phenyl)-pent-1-en-3yn-2-ol* *a*P324
Empirical formula	$C_{32}H_{46}O_2Si$
Formula weight /g·mol^{-1}	490.8

Temperature /K	173(2)
Wavelength /pm	71.073
Crystal system, space group	triclinic, P-1
Unit cell dimensions	a = 840.7(2), α = 80.63(3)
/pm, /°	b = 1495.7(3), β = 80.70(3)
	c = 2512.4(5), γ = 74.22(3)
Volume /nm^3	2.9766(11)
Z, Calculated density /$Mg \cdot m^{-3}$	4, 1.095
Absorption coefficient /mm^{-1}	0.1095
F(000)	1072
Crystal size /mm^3	1.60 · 0.90 · 0.70
Θ-range for data collection /°	2.48 – 28.08
Limiting indices	$-11 \le h \le 11$, $-19 \le k \le 19$, $-33 \le l \le 33$
Reflections collected / unique / significant	36317 / 13315 / 9629
R_{int}, R_σ	0.0427, 0.0419
Completeness to Θ = 28.08	92.0
Absorption correction	None ($\mu \cdot x < 0.1$)
Refinement method	Full-matrix least-squares on F^2
Data / restraints / parameters	13315 / 0 / 660
Goodness-of-fit on F^2	1.069
Final R indices [$I>2\sigma(I)$]	R1 = 0.0535, wR2 = 0.1609
R indices (all data)	R1 = 0.0721, wR2 = 0.1712
$\Delta\rho_{min.}$, $\Delta\rho_{max.}$ /$10^{-6} e \cdot pm^{-3}$	-0.497, 0.763

6.7 Crystal Structure Analysis of 1,1-Dimesityl-5-hydroxypentane-1-ene-2-ol (E11)

Suitable single crystals for **E11** were obtained and solved by X-ray single crystal analysis. **E11** was found to crystallise as triclinic with one molecule in the formula unit. A small deviation of the triple bond from planarity was observed (178.57[14] Å), with the overall propeller orientation of the enol. Interestingly the orientation of the enolic OH was anticlinal instead of the usual synclinal due to the OH···π interaction between the enolic OH and the π bond of the triple bond. Intermolecular hydrogen bonding interactions were observed in the crystal structure of **E11** leading to step ladder like arrangement. The hydrogen bonding is bifurcated with the enolic as well as the alcohol oxygen atom acting both as donor as well as acceptor. The step-ladder has $(OH)_4$ cycles with the rung region made up of the hydrocarbon part (Figure 6–10). The crystal structure data have been summarised in Table 9–28 to Table 9–31 (Appendix).

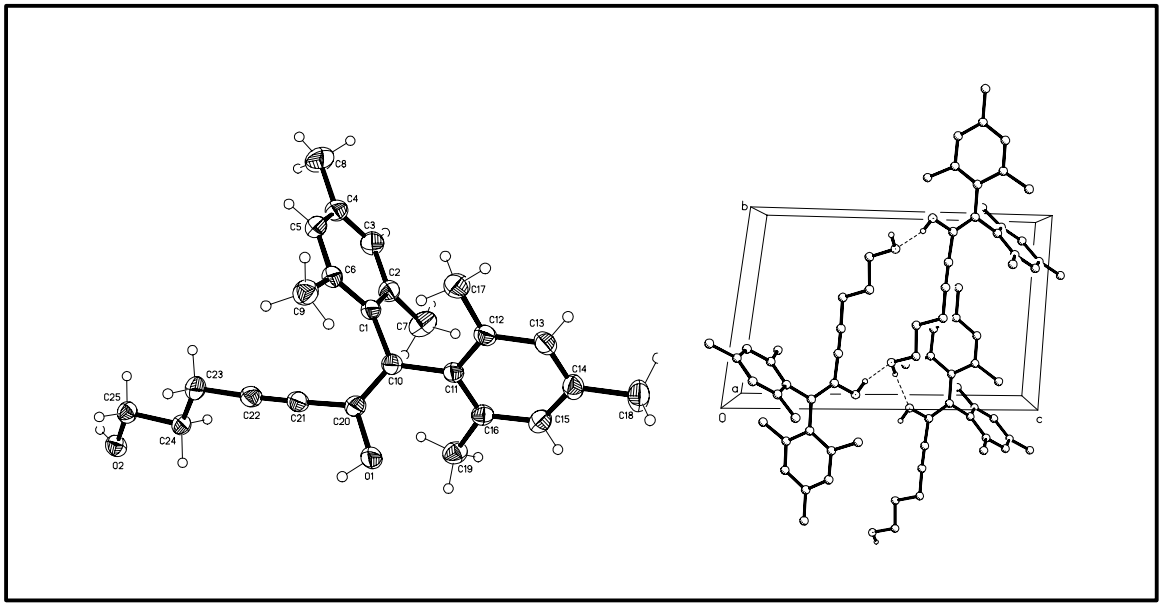

Figure 6–10: Molecular structure of **E11** showing the thermal ellipsoid with 50 % probability distribution, towards the right shows the hydrogen bonding interaction observed in the crystal structure giving rise to a ladder arrangement.

Table 6–11: Crystal data and structure refinement for **E11**.

Identification code	s1006
Empirical formula	C25 H30 O2
Formula weight	362.49
Temperature	150(2) K
Wavelength	0.71073 Å
Crystal system	Triclinic
Space group	P-1

Unit cell dimensions	a = 8.0809(6) Å α= 82.184(2)°. b = 9.7154(7) Å β= 81.136(1)°. c = 14.4476(11) Å γ = 69.744(1)°.
Volume	1047.22(13) $Å^3$
Z	2
Density (calculated)	1.150 Mg/m^3
Absorption coefficient	0.071 mm^{-1}
F(000)	392
Crystal size	0.40 x 0.35 x 0.35 mm^3
Theta range for data collection	2.24 to 26.37°.
Index ranges	-8<=h<=10, -7<=k<=12, -18<=l<=17
Reflections collected	6148
Independent reflections	4168 [R(int) = 0.0119]
Completeness to theta = 26.37°	97.5 %
Absorption correction	Semi-empirical from equivalents
Max. and min. transmission	0.990 and 0.908
Refinement method	Full-matrix least-squares on F^2
Data / restraints / parameters	4168 / 0 / 252
Goodness-of-fit on F^2	1.039
Final R indices [I>2sigma(I)]	R1 = 0.0426, wR2 = 0.1152
R indices (all data)	R1 = 0.0492, wR2 = 0.1206
Largest diff. peak and hole	0.216 and -0.177 e $Å^{-3}$

7 Appendix I

7.1 Methods of Determining Enzyme Inhibition[209]

A variety of ways are known to explore the various aspects of enzyme-catalysed reactions. Steady state enzyme kinetics has been used as a means of defining catalytic efficiency and substrate affinity of simple enzymes given by the well known Henri-Michaelis-Menten[210] equation relating the velocity of enzyme catalysed reaction to the substrate concentration:

$$\upsilon = \frac{V_{\max}[S]}{K_m + [S]} \qquad \text{Equation 7–1}$$

Lineweaver-Burk (1934)[211] developed a method called the double - reciprocal plot used for linearising enzyme kinetic data starting from the same steady state assumption. Rearrangement of the Henri-Michaelis-Menten equation leads to the equation formulated by Lineweaver-Burk given below:

$$\frac{1}{\upsilon} = \left(\frac{K_m}{V_{\max}}\frac{1}{[S]}\right) + \frac{1}{V_{\max}} \qquad \text{Equation 7–2}$$

This equation is similar to the equation of a straight line (y = mx + c), where m stands for the slope of the equation and c for the y intercept. Thus, by plotting a graph between the $1/\nu$ Vs $1/[S]$ one gets a straight line with slope = K_m/V_{max} with a y intercept $1/V_{max}$. These plots are extremely useful in diagnosing the mechanistic details of multi-substrate enzyme and also for determining the mode of interaction between an enzyme and an inhibitor.

Enzyme inhibition by an inhibitor can occur in a number of ways. First the inhibitor can bind irreversibly to the enzyme rendering it inactive (through covalent bond formation etc.). Second, it can tightlybind to the enzyme rendering it inactive or it can have a reversible binding with the enzyme.

The equilibrium between the enzyme, substrate and inhibitor can provide useful insights into the molecular basis of reversible inhibition. In the Scheme 7–1 K_S represents the equilibrium constant for the formation of the enzyme-substrate complex (**ES**) from a free enzyme and the substrate, K_i is the dissociation constant for the enzyme-inhibitor constant (**EI**) and k_p is the rate constant for the product formation from **ES** or **ESI** complexes. The factors α and β reflect the affinity of the enzyme for the substrate and the modification of the rate of product formation by the inhibitor respectively. While the value of α remains unchanged, the value of β reflects the effect of the inhibitor (e.g. $\beta = 0$ for complete inhibition, β is between 0 and 1 for partial inhibition, for enzyme activators $\beta > 0$).

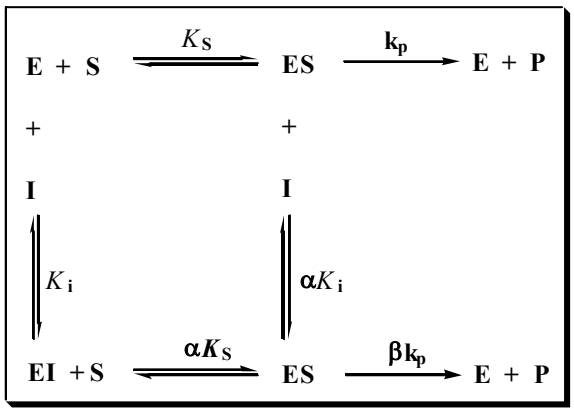

Scheme 7–1: Depicts the various modes in which an inhibitor affects the enzyme catalysis.

The various modes of reversible inhibition are; a) competitive inhibition, b) non-competitive inhibition, c) un-competitive inhibition, d) mixed inhibition and e) partial inhibition.

Competitive inhibition: is observed when the substrate as well the inhibitor competes for the same binding site leading to a decrease in the initial velocity of the catalytic reaction. Competitive inhibition thus affects the apparent K_m value of the enzyme for their substrates while the V_{max} remain unchanged. Since competitive inhibitors compete for the substrate-binding site, they are usually structural mimics of the reaction substrate or transition state. Competitive inhibition can be overcome by increasing the substrate concentration (Scheme 7–2).

Non-competitive inhibition: this is observed when the inhibitors bind to the enzyme at a site that is distinct from the substrate binding site and inhibit the enzyme by a number of different mechanisms. This type of inhibition cannot be overcome by increasing the substrate concentration. Non-competitive inhibition decreases the V_{max} of the enzyme without affecting the apparent K_m.

Un-competitive inhibition: is observed upon binding of the inhibitor to the enzyme at a site, which is distinct. This occurs exclusively to the enzyme-substrate complex (**ES**), and as a result both the V_{max} and K_m values decrease.

Mixed inhibition and *partial inhibition* are the types of inhibition that are seldomly observed. In mixed inhibition, a decrease in both the V_{max} and K_m values is observed; however, one needs to determine the K_i for the inhibitor having affinity for both the free as well as the substrate bound enzyme. The most distinguishing feature of partial inhibition is that the activity of the enzyme cannot be driven to zero even at very high concentrations of the inhibitor.

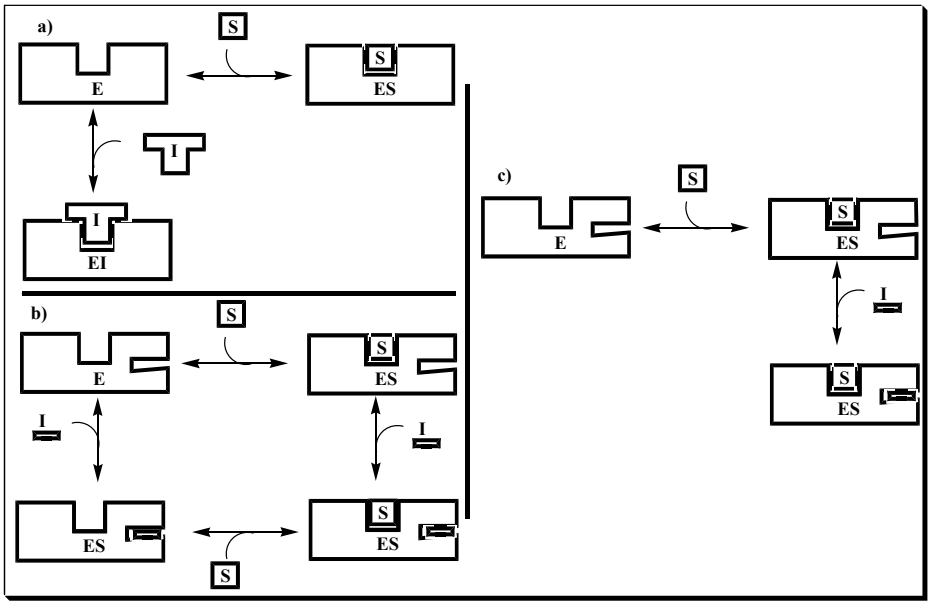

Scheme 7–2: Pictorial representation of various modes of enzyme inhibition, a) competitive, b) non-competitive and c) un-competitive inhibition.

Graphical Determination of Inhibitor Type

A number of graphical methods are known for determining the mode of inhibition in enzymatic catalysis. The most straightforward and diagnostic ones are the double reciprocal plots or the Lineweaver-Burk plot.

Patterns of straight lines intersecting at “y” intercept are characteristic of a competitive inhibitor. The intersection at the y-axes is due to the fact that competitive inhibition does not affect the apparent V_{max} value. The degree of perturbation of K_m varies with inhibitor concentration and also on the K_i for a particular inhibitor (Table 7–1).

Double reciprocal plots for varying a non-competitive inhibitor gives a nest of lines that intersect at the "*x*" intercept of the graph. Similarly, a double reciprocal plot for an un-competitive inhibition has a set of parallel lines and is independent of inhibitor concentration. The "*y*" intercept increases with increasing inhibitor concentration. For mixed inhibition, the double reciprocal plots depends on the value of α, when $\alpha > 1$ the lines intersect at a value of 1/[*S*] lower than zero. When $\alpha < 1$ the lines then intersect below the value of "x" and "y", at negative values of 1/[*S*] and 1/[v].

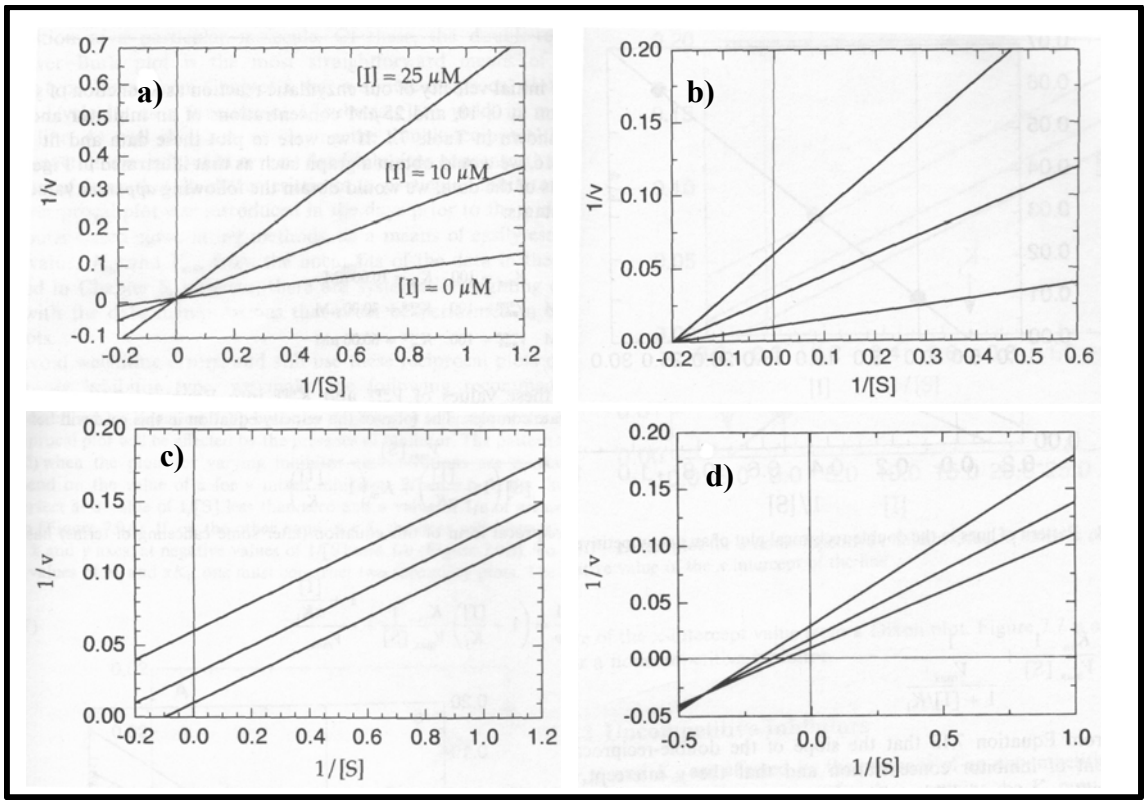

Figure 7–1: Diagnostic Lineweaver-Burk plot for determining the mode of inhibition for a given inhibitor on enzyme activity, a) competitive inhibition, b) non-competitive inhibition, c) un-competitive inhibition and d) mixed inhibition.

Table 7–1: Velocity equations used for double reciprocal plots for distinguishing enzyme inhibitions.

Inhibition type	Velocity equation for double reciprocal plots
Competitive inhibition	$\frac{1}{\upsilon} = \frac{1}{V_{\max}} + \frac{1}{[S]}\frac{K_m}{V_{\max}}\left(1 + \frac{[I]}{K_i}\right)$
Non-competitive inhibition	$\frac{1}{\upsilon} = \left(\frac{1}{V_{\max}} + \frac{K_m}{V_{\max}}\frac{1}{[S]}\right)\left(1 + \frac{[I]}{K_i}\right)$
Un-competitive inhibition	$\frac{1}{\upsilon} = \frac{K_m}{V_{\max}}\frac{1}{[S]} + \frac{\frac{1}{V_{\max}}}{1 + [I]/K_i}$
Mixed inhibition	$\frac{1}{\upsilon} = \left(1 + \frac{[I]}{K_i}\right)\frac{K_m}{V_{\max}}\frac{1}{[S]} + \frac{1 + \frac{[I]}{\alpha K_i}}{V_{\max}}$

8 Appendix II

The adiabatic ionisation potentials were obtained using AM1 level of computation. For solvent (acetonitrile) correction of the gas phase adiabatic ionisation potential the Born equation was used:

$$\Delta E_{solv}^{ACN} = \frac{-N_L Z^2 e^2}{2r}\left[1-\frac{1}{\varepsilon}\right]$$

Table 8–1: Calculation of gas phase adiabatic ionisation potential of various radicals and their corresponding cations using semiemperical method (AM1 Spartan).[155]

Radical	Radical (R) ΔH_f (Kcal/mol)	Cation (C) ΔH_f (Kcal/mol)	IP_a^{gas} = (C-R) (kcal/mol)	IP_a^{gas} in eV
124	-6.1	174.8	180.9	7.85
125	61.9	269.2	207.3	8.99
126	28.8	206.0	177.2	7.68
127	-22.8	158.0	180.8	7.84
128	-38.2	131.0	169.2	7.34
129	-49.2	111.6	160.8	6.97
130	-46.2	125.5	171.7	7.45
131	21.6	174.7	153.1	6.64
132	-67.3	109.1	176.4	7.65
133	0.0	173.2	173.2	7.51
134	69.6	262.3	192.7	8.36
135	70.0	262.0	192	8.33
136	98.2	300.7	202.5	8.78
137	97.9	281.6	183.7	7.97
138	89.7	270.3	180.6	7.83
139	86.1	274.0	187.9	8.15
140	82.3	270.6	188.3	8.17
141	-5.9	161.9	167.8	7.28
142	-44.3	117.3	161.6	7.01
143	0.3	146.2	145.9	6.33
R24	-2.8	173.1	175.9	7.63
R25	-8.0	165.8	173.8	7.54
R16	27.3	200.0	172.7	7.45
R29	13.8	183.8	170	7.37

Table 8–2: Solvent corrected (for acetonitrile) adiabatic ionisation potential of various radicals using the Born equation method. The last column represents the experimentally determined oxidation potential of these radicals in acetonitrile.[155]

Radical	Surface area (S.A.) Å^2	Radius (r) Å	ΔE_{solv}^{ACN} = 159.1326/r (kcal/mol)	ΔE_{solv}^{ACN}= 159.1326/r (eV)	(IP_a^{gas} -ΔE_{solv}^{ACN}) eV	$E_{1/2}^{ox}$ V_{SCE}
124	110.5	2.97	53.58	2.32	5.52	0.09
125	103.6	2.87	55.45	2.402	6.59	0.80
126	118.5	3.07	51.84	2.25	5.44	-0.04
127	82.8	2.57	61.92	2.69	5.16	-0.24
128	124.2	3.14	50.68	2.20	5.14	-0.45
129	160.3	3.57	44.586	1.93	5.04	-0.10
130	99.9	2.827	56.29	2.445	5.01	-0.60
131	107.3	2.921	54.48	2.36	4.28	-1.03
132	113.0	3.00	53.04	2.30	5.35	-0.08
133	163.3	3.60	44.20	1.921	5.59	0.51
134	154.0	3.50	45.47	1.97	6.39	1.03
135	154.0	3.50	45.47	1.97	6.36	1.11
136	173.5	3.728	42.69	1.85	6.93	1.63
137	224.9	4.23	37.62	1.63	6.34	1.01
138	231.4	4.29	37.09	1.61	6.22	0.56
139	196.3	3.95	40.29	1.75	6.40	0.72
140	196.9	3.96	40.19	1.74	6.42	0.97
141	165.1	3.62	43.96	1.91	5.37	-0.44
142	195.0	3.94	40.39	1.75	5.26	-0.55
143	163.4	3.61	44.08	1.91	4.42	-1.12
R24	325.4	5.09	31.26	1.36	6.27	0.76
R25	342.2	5.23	30.43	1.32	6.22	0.59
R16	396.8	5.62	28.32	1.23	6.26	0.63
R29	438.4	5.91	26.93	1.17	6.20	0.66

9 Appendix III

9.1 Crystal Structure Data of 25

Table 9–1: Positional and equivalent isotropic displacement parameters (U_{eq} /pm^2) of **25**.

Atom	WS	x	y	z	U_{eq}
Fe1	4*e*	0.66061(1)	0.98679(2)	0.22362(2)	156.7(6)
O1	4*e*	1.03194(6)	1.1483(1)	0.8569(1)	277(2)
H1	4*e*	1.0431	1.1332	0.9571	420
O2	4*e*	0.93529(7)	0.88412(9)	0.8112(1)	248(2)
H2	4*e*	0.9389	0.8124	0.7565	370
C1	4*e*	0.93987(8)	1.1279(1)	0.8061(2)	247(3)
H1A	4*e*	0.9159	1.2082	0.7421	300
H1B	4*e*	0.9086	1.1208	0.9032	300
C2	4*e*	0.92232(8)	0.9996(1)	0.7039(2)	185(2)
H2A	4*e*	0.9655	0.9948	0.6231	220
C3	4*e*	0.82847(8)	1.0023(1)	0.6136(2)	195(2)
H3A	4*e*	0.7861	1.0083	0.6942	230
H3B	4*e*	0.8212	1.0856	0.5452	230
C4	4*e*	0.80562(8)	0.8770(1)	0.5059(2)	191(2)
H4A	4*e*	0.8458	0.8738	0.4214	230
H4B	4*e*	0.8158	0.7933	0.5731	230
C5	4*e*	0.71169(7)	0.8771(1)	0.4244(1)	162(2)
C6	4*e*	0.64060(8)	0.9630(1)	0.4610(2)	196(2)
H6	4*e*	0.6445	1.0323	0.5420	240
C7	4*e*	0.56275(8)	0.9263(1)	0.3545(2)	239(2)
H7	4*e*	0.5061	0.9674	0.3519	290
C8	4*e*	0.58487(8)	0.8175(1)	0.2530(2)	233(2)
H8	4*e*	0.5457	0.7729	0.1713	280
C9	4*e*	0.67640(8)	0.7875(1)	0.2960(1)	191(2)
H9	4*e*	0.7086	0.7192	0.2472	230
C10	4*e*	0.6357 (1)	1.0451(2)	-0.0144(2)	309(3)
H10	4*e*	0.5952	1.0028	-0.0960	370
C11	4*e*	0.7263(1)	1.0110(1)	0.0261(2)	255(3)
H11	4*e*	0.7572	0.9422	-0.0246	310
C12	4*e*	0.7630(1)	1.0973(1)	0.1553(2)	287(3)

H12	4*e*	0.8224	1.0959	0.2064	340
C13	4*e*	0.6952(1)	1.1862(1)	0.1948(2)	354(3)
H13	4*e*	0.7013	1.2548	0.2767	420
C14	4*e*	0.6167(1)	1.1542(2)	0.0897(2)	372(4)
H14	4*e*	0.5610	1.1980	0.0890	450

Table 9–2: Anisotropic displacement parameters (Uij/pm^2) of **25**.

Atom	U_{11}	U_{22}	U_{33}	U_{12}	U_{13}	U_{23}
Fe1	193.6(9)	142.5(8)	132.5(9)	11.6(5)	15.7(6)	2.3(5)
O1	266(4)	307(4)	231(5)	41(4)	-69(4)	-110(4)
O2	357(5)	184(4)	178(4)	4(3)	-61(4)	35(3)
C1	236(6)	201(5)	281(7)	-26(4)	-55(5)	-22(4)
C2	185(5)	200(5)	160(5)	16(4)	-14(4)	-12(4)
C3	196(5)	189(5)	187(5)	-5(4)	-22(4)	5(4)
C4	186(5)	200(5)	178(6)	-21(4)	-14(4)	20(4)
C5	196(5)	164(4)	124(5)	11(3)	8(4)	-3(3)
C6	200(5)	250(5)	142(5)	-4(4)	29(4)	12(4)
C7	175(5)	331(6)	213(6)	31(5)	27(5)	-15(4)
C8	242(5)	240(5)	207(6)	23(4)	-15(5)	-87(4)
C9	266(5)	134(4)	169(5)	11(3)	6(4)	-23(4)
C10	392(7)	334(6)	182(6)	104(5)	-29(6)	-19(5)
C11	379(7)	209(5)	198(6)	27(4)	115(5)	-14(4)
C12	326(7)	255(6)	284(7)	40(5)	60(6)	-116(5)
C13	630(1)	135(5)	331(8)	-2(5)	173(7)	-60(5)
C14	446(8)	286(6)	400(9)	188(6)	113(7)	158(6)

9.2 Crystal Structure Data of 21

Table 9–3: Atomic coordinates ($\times 10^4$) and equivalent isotropic displacement parameters ($pm^2 \times 10^{-1}$) for **21**. U (eq.) is defined as one third of the trace of the orthogonolised U^{ij} tensor.

	x	y	z	U(eq)
N(1)	1252(1)	1191(1)	7239(2)	19(1)
O(1)	874(1)	1624(1)	7496(2)	29(1)
C(1)	1773(1)	1298(1)	6004(2)	23(1)
C(2)	2055(1)	706(1)	5474(3)	31(1)
C(3)	2199(1)	303(1)	6950(3)	33(1)
C(4)	1588(1)	182(1)	7902(3)	29(1)
C(5)	1273(1)	733(1)	8595(2)	22(1)
C(6)	2268(1)	1696(1)	6814(3)	33(1)
C(7)	1487(1)	1608(1)	4476(3)	35(1)
C(8)	1624(1)	977(1)	10134(3)	32(1)
C(9)	594(1)	600(1)	9093(3)	38(1)

Table 9–4: Anisotropic displacement parameters ($pm^2 \times 10^{-1}$) for **21**. The anisotropic displacement factor exponent takes the form: $-2\pi^2[h^2a^{*2}U^{11} + ... + 2 h k a^* b^* U^{12}]$

	U_{11}	U_{22}	U_{33}	U_{23}	U_{13}	U_{12}
N(1)	18(1)	19(1)	19(1)	-1(1)	-1(1)	1(1)
O(1)	29(1)	26(1)	32(1)	1(1)	4(1)	12(1)
C(1)	21(1)	26(1)	22(1)	-1(1)	4(1)	-1(1)
C(2)	30(1)	33(1)	31(1)	-9(1)	7(1)	5(1)
C(3)	29(1)	24(1)	45(1)	-8(1)	1(1)	9(1)
C(4)	30(1)	19(1)	36(1)	-1(1)	-4(1)	1(1)
C(5)	22(1)	22(1)	23(1)	3(1)	-1(1)	0(1)
C(6)	28(1)	29(1)	43(1)	-1(1)	2(1)	-8(1)
C(7)	32(1)	48(1)	26(1)	9(1)	4(1)	1(1)
C(8)	42(1)	33(1)	21(1)	-1(1)	-6(1)	5(1)
C(9)	29(1)	43(1)	41(1)	17(1)	4(1)	-1(1)

Table 9–5: Bond lengths [pm] and angles [°] for **21**.

Bond angle	Bond angle (deg)	Bond angle	Bond angle (deg)	Bond angle	Bond angle (deg)
O(1)-N(1)-C(1)	116.01(13)	C(4)-C(3)-H(3B)	110.0	H(6B)-C(6)-H(6C)	109.5
O(1)-N(1)-C(5)	116.15(13)	H(3A)-C(3)-H(3B)	108.3	C(1)-C(7)-H(7A)	109.5
C(1)-N(1)-C(5)	123.93(13)	C(3)-C(4)-C(5)	113.48(15)	C(1)-C(7)-H(7B)	109.5
N(1)-C(1)-C(7)	107.30(14)	C(3)-C(4)-H(4A)	108.9	H(7A)-C(7)-H(7B)	109.5
N(1)-C(1)-C(6)	109.36(15)	C(5)-C(4)-H(4A)	108.9	C(1)-C(7)-H(7C)	109.5
C(7)-C(1)-C(6)	109.28(15)	C(3)-C(4)-H(4B)	108.9	H(7A)-C(7)-H(7C)	109.5
N(1)-C(1)-C(2)	108.86(14)	C(5)-C(4)-H(4B)	108.9	H(7B)-C(7)-H(7C)	109.5
C(7)-C(1)-C(2)	110.25(15)	H(4A)-C(4)-H(4B)	107.7	C(5)-C(8)-H(8A)	109.5
C(6)-C(1)-C(2)	111.68(15)	N(1)-C(5)-C(9)	107.13(14)	C(5)-C(8)-H(8B)	109.5
C(3)-C(2)-C(1)	113.63(16)	N(1)-C(5)-C(4)	109.33(14)	H(8A)-C(8)-H(8B)	109.5
C(3)-C(2)-H(2A)	108.8	C(9)-C(5)-C(4)	109.97(15)	C(5)-C(8)-H(8C)	109.5
C(1)-C(2)-H(2A)	108.8	N(1)-C(5)-C(8)	109.33(14)	H(8A)-C(8)-H(8C)	109.5
C(3)-C(2)-H(2B)	108.8	C(9)-C(5)-C(8)	109.08(16)	H(8B)-C(8)-H(8C)	109.5
C(1)-C(2)-H(2B)	108.8	C(4)-C(5)-C(8)	111.87(15)	C(5)-C(9)-H(9A)	109.5
H(2A)-C(2)-H(2B)	107.7	C(1)-C(6)-H(6A)	109.5	C(5)-C(9)-H(9B)	109.5
C(2)-C(3)-C(4)	108.63(15)	C(1)-C(6)-H(6B)	109.5	H(9A)-C(9)-H(9B)	109.5
C(2)-C(3)-H(3A)	110.0	H(6A)-C(6)-H(6B)	109.5	C(5)-C(9)-H(9C)	109.5
C(4)-C(3)-H(3A)	110.0	C(1)-C(6)-H(6C)	109.5	H(9A)-C(9)-H(9C)	109.5
C(2)-C(3)-H(3B)	110.0	H(6A)-C(6)-H(6C)	109.5	H(9B)-C(9)-H(9C)	109.5

Table 9–6: Hydrogen coordinates ($\times 10^4$) and isotropic displacement parameters ($pm^2 \times 10^{-1}$) for **21**.

	x	y	z	U(eq)
H(2A)	1755	506	4704	45(2)
H(2A)	1755	506	4704	45(2)
H(2B)	2449	778	4834	45(2)
H(3A)	2509	492	7716	45(2)
H(3B)	2382	-70	6531	45(2)
H(4A)	1678	-88	8856	45(2)
H(4B)	1289	-20	7130	45(2)

H(6A)	2062	2045	7285	45(2)
H(6B)	2577	1816	5955	45(2)
H(6C)	2485	1482	7723	45(2)
H(7A)	1129	1378	4049	45(2)
H(7B)	1806	1645	3584	45(2)
H(7C)	1341	1999	4811	45(2)
H(8A)	2076	1005	9876	45(2)
H(8B)	1562	714	11103	45(2)
H(8C)	1460	1368	10409	45(2)
H(9A)	398	955	9560	45(2)
H(9B)	589	288	9948	45(2)
H(9C)	358	472	8091	45(2)

9.3 Crystal Structure Data of 62

Table 9–7: Atomic coordinates (10^4) and equivalent isotropic displacement parameters ($pm^2 \times 10^{-1}$) for **62**. U (eq.) is defined as one third of the trace of the orthogonalized U^{ij} tensor.

	x	y	z	U(eq)
N(1)	8370(1)	1945(1)	946(1)	19(1)
O(1)	8790(1)	2824(1)	1509(1)	19(1)
O(2)	9333(1)	4040(1)	-3509(1)	28(1)
O(3)	9708(1)	4438(1)	2292(1)	23(1)
C(1)	7381(1)	2029(1)	1424(2)	23(1)
C(2)	6946(1)	1086(1)	970(2)	31(1)
C(3)	7431(1)	320(1)	2232(2)	39(1)
C(4)	8432(1)	310(1)	1719(2)	36(1)
C(5)	8921(1)	1225(1)	2183(2)	25(1)
C(6)	9334(1)	3173(1)	-172(1)	19(1)
C(7)	8772(1)	3736(1)	-1846(2)	23(1)
C(8)	10080(1)	3726(1)	1044(2)	21(1)
C(9)	6923(1)	2712(1)	-168(2)	28(1)
C(10)	7204(1)	2365(1)	3720(2)	30(1)
C(11)	9857(1)	1166(1)	1218(2)	29(1)
C(12)	9096(1)	1394(1)	4636(2)	35(1)

Table 9–8: Bond lengths [pm] and angles [°] for **62**.

Bond	Bond Length pm	Bond	Bond Length pm	Bond	Bond Length pm
N(1)-O(1)	145.91(9)	C(3)-C(4)	152.01(16)	C(8)-H(8B)	99.00
N(1)-C(1)	150.24(12)	C(3)-H(3A)	99.00	C(9)-H(9A)	98.00
N(1)-C(5)	150.50(13)	C(3)-H(3B)	99.00	C(9)-H(9B)	98.00
O(1)-C(6)	144.38(10)	C(4)-C(5)	153.74(14)	C(9)-H(9C)	98.00
O(2)-C(7)	142.93(12)	C(4)-H(4A)	99.00	C(10)-H(10A)	98.00
O(2)-H(2)	87.3(15)	C(4)-H(4B)	99.00	C(10)-H(10B)	98.00
O(3)-C(8)	142.63(12)	C(5)-C(11)	153.30(14)	C(10)-H(10C)	98.00
O(3)-H(3)	85.5(15)	C(5)-C(12)	154.03(16)	C(11)-H(11A)	98.00
C(1)-C(9)	152.66(14)	C(6)-C(8)	151.87(13)	C(11)-H(11B)	98.00
C(1)-C(2)	153.80(14)	C(6)-C(7)	152.09(13)	C(11)-H(11C)	98.00
C(1)-C(10)	153.97(14)	C(6)-H(6)	100.00	C(12)-H(12A)	98.00
C(2)-C(3)	151.55(17)	C(7)-H(7A)	99.00	C(12)-H(12B)	98.00
C(2)-H(2A)	99.00	C(7)-H(7B)	99.00	C(12)-H(12C)	98.00
C(2)-H(2B)	99.00	C(8)-H(8A)	99.00		

Table 9–9: Bond lengths [pm] and angles [°] for **62**.

Angle	bond angle in degrees	Angle	bond angle in degrees	Angle	bond angle in degrees
O(1)-N(1)-C(1)	106.12(6)	C(5)-C(4)-H(4A)	108.9	C(6)-C(8)-H(8B)	109.3
O(1)-N(1)-C(5)	107.00(7)	C(3)-C(4)-H(4B)	108.9	H(8A)-C(8)-H(8B)	108.0
C(1)-N(1)-C(5)	116.76(7)	C(5)-C(4)-H(4B)	108.9	C(1)-C(9)-H(9A)	109.5
C(6)-O(1)-N(1)	112.64(6)	H(4A)-C(4)-H(4B)	107.7	C(1)-C(9)-H(9B)	109.5
C(7)-O(2)-H(2)	107.2(10)	N(1)-C(5)-C(11)	107.81(8)	H(9A)-C(9)-H(9B)	109.5
C(8)-O(3)-H(3)	107.8(9)	N(1)-C(5)-C(4)	106.65(8)	C(1)-C(9)-H(9C)	109.5
N(1)-C(1)-C(9)	108.39(7)	C(11)-C(5)-C(4)	107.27(9)	H(9A)-C(9)-H(9C)	109.5
N(1)-C(1)-C(2)	106.46(8)	N(1)-C(5)-C(12)	115.86(8)	H(9B)-C(9)-H(9C)	109.5
C(9)-C(1)-C(2)	108.14(8)	C(11)-C(5)-C(12)	107.31(8)	C(1)-C(10)-H(10A)	109.5
N(1)-C(1)-C(10)	115.51(8)	C(4)-C(5)-C(12)	111.59(9)	C(1)-C(10)-H(10B)	109.5

C(9)-C(1)-C(10)	106.91(8)	O(1)-C(6)-C(8)	104.26(7)	H(10A)-C(10)-H(10B)	109.5
C(2)-C(1)-C(10)	111.21(8)	O(1)-C(6)-C(7)	112.41(7)	C(1)-C(10)-H(10C)	109.5
C(3)-C(2)-C(1)	113.30(9)	C(8)-C(6)-C(7)	112.81(8)	H(10A)-C(10)-H(10C)	109.5
C(3)-C(2)-H(2A)	108.9	O(1)-C(6)-H(6)	109.1	H(10B)-C(10)-H(10C)	109.5
C(1)-C(2)-H(2A)	108.9	C(8)-C(6)-H(6)	109.1	C(5)-C(11)-H(11A)	109.5
C(3)-C(2)-H(2B)	108.9	C(7)-C(6)-H(6)	109.1	C(5)-C(11)-H(11B)	109.5
C(1)-C(2)-H(2B)	108.9	O(2)-C(7)-C(6)	110.25(8)	H(11A)-C(11)-H(11B)	109.5
H(2A)-C(2)-H(2B)	107.7	O(2)-C(7)-H(7A)	109.6	C(5)-C(11)-H(11C)	109.5
C(2)-C(3)-C(4)	109.01(9)	C(6)-C(7)-H(7A)	109.6	H(11A)-C(11)-H(11C	109.5
C(2)-C(3)-H(3A)	109.9	O(2)-C(7)-H(7B)	109.6	H(11B)-C(11)-H(11C)	109.5
C(4)-C(3)-H(3A)	109.9	C(6)-C(7)-H(7B)	109.6	C(5)-C(12)-H(12A)	109.5
C(2)-C(3)-H(3B)	109.9	H(7A)-C(7)-H(7B)	108.1	C(5)-C(12)-H(12B)	109.5
C(4)-C(3)-H(3B)	109.9	O(3)-C(8)-C(6)	111.57(7)	H(12A)-C(12)-H(12B)	109.5
H(3A)-C(3)-H(3B)	108.3	O(3)-C(8)-H(8A)	109.3	C(5)-C(12)-H(12C)	109.5
C(3)-C(4)-C(5)	113.41(9)	C(6)-C(8)-H(8A)	109.3	H(12A)-C(12)-H(12C)	109.5
C(3)-C(4)-H(4A)	108.9	O(3)-C(8)-H(8B)	109.3	H(12B)-C(12)-H(12C)	109.5

Table 9–10: Hydrogen coordinates ($\times 10^4$) and isotropic displacement parameters ($pm^2 \times 10^{-1}$) of **62**.

H(2)	9614(10)	4535(10)	-3030(20)	42	H(8B)	10485	3996	-8	25
H(3)	9485(9)	4193(9)	3400(20)	35	H(9A)	7163	3326	152	34
H(2A)	6300	1105	1342	38	H(9B)	6261	2707	-27	34
H(2B)	6953	953	-600	38	H(9C)	7051	2542	-1652	34
H(3A)	7143	-273	1826	47	H(10A)	7340	1872	4765	36
H(3B)	7382	415	3806	47	H(10B)	6562	2546	3765	36
H(4A)	8472	155	169	43	H(10C)	7598	2891	4089	36
H(4B)	8753	-175	2589	43	H(11A)	9771	1122	-365	35
H(6)	9619	2649	-916	23	H(11B)	10184	624	1789	35
H(7A)	8262	3361	-2497	28	H(11C)	10214	1715	1613	35
H(7B)	8507	4271	-1133	28	H(12A)	9248	2039	4890	42
H(8A)	10455	3316	2017	25	H(12B)	9606	1011	5203	42
H(8B)	10485	3996	-8	25	H(12C)	8545	1239	5375	42

Table 9–11: Anisotropic displacement parameters ($pm^2 \times 10^{-1}$) for **62**. The anisotropic displacement factor exponent takes the form: $2\pi^2[h^2a^{*2}U^{11} + ... + 2 h k a^* b^* U^{12}]$

	U_{11}	U_{22}	U_{33}	U_{23}	U_{13}	U_{12}
N(1)	19(1)	19(1)	20(1)	-3(1)	2(1)	-5(1)
O(1)	23(1)	19(1)	16(1)	-3(1)	4(1)	-7(1)
O(2)	40(1)	29(1)	16(1)	-1(1)	5(1)	-14(1)
O(3)	31(1)	23(1)	17(1)	-2(1)	5(1)	-9(1)
C(1)	19(1)	29(1)	20(1)	-2(1)	3(1)	-4(1)
C(2)	23(1)	35(1)	36(1)	-4(1)	4(1)	-11(1)
C(3)	34(1)	29(1)	55(1)	4(1)	7(1)	-13(1)
C(4)	33(1)	23(1)	51(1)	3(1)	4(1)	-5(1)
C(5)	24(1)	22(1)	28(1)	3(1)	2(1)	-2(1)
C(6)	21(1)	21(1)	17(1)	-1(1)	5(1)	-4(1)
C(7)	25(1)	29(1)	16(1)	0(1)	1(1)	-6(1)
C(8)	19(1)	24(1)	20(1)	1(1)	1(1)	-2(1)
C(9)	20(1)	38(1)	26(1)	0(1)	1(1)	0(1)
C(10)	28(1)	41(1)	23(1)	-3(1)	8(1)	-3(1)
C(11)	25(1)	24(1)	38(1)	0(1)	2(1)	1(1)
C(12)	35(1)	42(1)	26(1)	9(1)	-2(1)	1(1)

Table 9–12: Hydrogen bond lengths and bond angles observed in the crystal structure of **62** [pm and °].

D-H...A	d(D-H)	d(H...A)	d(D...A)	<(DHA)
O(2)-H(2)...O(3)	87.3(15)	328.7(15)	363.71(10)	106.8(11)
C(10)-H(10C)...O(1)	98	244	285.24(12)	104.6
C(12)-H(12A)...O(1)	98	244	286.45(13)	105.6
O(2)-H(2)...O(3)#1	87.3(15)	184.4(15)	271.33(10)	173.3(14)
O(3)-H(3)...O(2)#2	85.5(15)	195.2(15)	274.94(10)	154.8(13)

9.4 Crystal Structure Data of 65

Table 9–13: Atomic coordinates Wyckoff notations and equivalent isotropic displacement parameters U_{eq} /10^4 pm^2 for **65**. U_{eq} is defined as one-third of the trace of the orthogonalised U_{ij} tensor; *s.o.f.* = 1.

Atom	x	y	z	U_{eq}
N1	0.33962(3)	0.70734(5)	0.14515(3)	0.01768(11)
O1	0.25901(3)	0.62909(4)	0.09049(2)	0.01948(9)
O2	0.09708(3)	0.42592(5)	0.07322(3)	0.03069(11)
O3	0.20040(3)	0.27995(5)	0.16168(3)	0.03075(11)
O4	0.24018(3)	0.55028(5)	-0.06715(3)	0.02973(11)
O5	0.25954(4)	0.29685(5)	-0.03686(3)	0.03539(12)
C1	0.28997(4)	0.76269(6)	0.21713(3)	0.02055(13)
C2	0.36989(5)	0.86078(7)	0.27061(4)	0.02430(14)
H2A	0.3382	0.9031	0.3175	0.029
H2B	0.4280	0.7931	0.2930	0.029
C3	0.41121(5)	0.99432(7)	0.22426(4)	0.02582(14)
H3A	0.3546	1.0665	0.2040	0.031
H3B	0.4636	1.0528	0.2610	0.031
C4	0.45883(4)	0.92722(7)	0.15281(4)	0.02523(14)
H4A	0.5186	0.8622	0.1746	0.030
H4B	0.4848	1.0138	0.1214	0.030
C5	0.38460(4)	0.82830(7)	0.09405(4)	0.02147(13)
C6	0.44885(5)	0.74446(8)	0.03652(4)	0.03044(16)
H6A	0.4991	0.6767	0.0686	0.046
H6B	0.4852	0.8212	0.0067	0.046
H6C	0.4036	0.6817	-0.0028	0.046
C7	0.30586(5)	0.93060(7)	0.04152(4)	0.02975(15)
H7A	0.2527	0.8646	0.0114	0.045
H7B	0.3407	0.9904	0.0024	0.045
H7C	0.2738	1.0022	0.0771	0.045
C8	0.26748(5)	0.61965(7)	0.26681(4)	0.02903(15)
H8A	0.2107	0.5607	0.2366	0.044
H8B	0.2483	0.6525	0.3199	0.044
H8C	0.3291	0.5539	0.2758	0.044
C9	0.18855(5)	0.85265(7)	0.19653(4)	0.02921(15)
H9A	0.2031	0.9567	0.1765	0.044

H9B	0.1543	0.8619	0.2460	0.044
H9C	0.1435	0.7967	0.1540	0.044
C10	0.27526(4)	0.46718(6)	0.07562(3)	0.01826(12)
C11	0.37776(4)	0.39811(7)	0.11114(4)	0.02367(14)
H11A	0.4334	0.4514	0.0878	0.036
H11B	0.3789	0.2871	0.0977	0.036
H11C	0.3873	0.4111	0.1709	0.036
C12	0.18791(4)	0.37778(6)	0.10959(3)	0.01966(13)
C13	0.00673(5)	0.35265(9)	0.09981(5)	0.03794(18)
H13A	-0.0531	0.4232	0.0881	0.046
H13B	0.0190	0.3353	0.1599	0.046
C14	-0.01726(6)	0.20162(10)	0.05757(7)	0.0606(3)
H14A	-0.0295	0.2185	-0.0019	0.091
H14B	-0.0790	0.1565	0.0761	0.091
H14C	0.0409	0.1302	0.0707	0.091
C15	0.25637(4)	0.44752(6)	-0.01838(4)	0.02153(13)
C16	0.23587(6)	0.25442(9)	-0.12320(4)	0.03976(19)
H16A	0.2761	0.1612	-0.1345	0.048
H16B	0.2559	0.3405	-0.1579	0.048
C17	0.12492(7)	0.22183(12)	-0.14410(5)	0.0585(3)
H17A	0.1047	0.1390	-0.1084	0.088
H17B	0.1110	0.1886	-0.2016	0.088
H17C	0.0854	0.3162	-0.1362	0.088

Table 9–14: Anisotropic displacement parameters U_{ij} /Å^2 for **65**. The anisotropic displacement factor is defined as: exp $\{-2\pi^2[U_{11}(ha^*)^2 + \ldots + 2U_{12}hka^*b^*]\}$.

Atom	U_{11}	U_{22}	U_{33}	U_{23}	U_{13}	U_{12}
N1	0.01746(19)	0.0174(2)	0.0181(2)	-0.00236(18)	0.00191(17)	-0.00348(17)
O1	0.01732(16)	0.01563(16)	0.0242(2)	-0.00195(15)	-0.00226(15)	-0.00031(14)
O2	0.01688(17)	0.0322(2)	0.0421(2)	0.0123(2)	0.00025(17)	-0.00177(17)
O3	0.0299(2)	0.0284(2)	0.0333(2)	0.01185(19)	0.00161(18)	-0.00225(18)
O4	0.0382(2)	0.0294(2)	0.0217(2)	0.00222(18)	0.00405(18)	-0.00259(18)
O5	0.0550(3)	0.0246(2)	0.0252(2)	-0.00804(18)	-0.0001(2)	0.0043(2)
C1	0.0227(2)	0.0192(2)	0.0206(3)	-0.0010(2)	0.0058(2)	0.0008(2)
C2	0.0291(3)	0.0226(3)	0.0207(3)	-0.0037(2)	0.0015(2)	0.0014(2)
C3	0.0280(3)	0.0196(2)	0.0286(3)	-0.0029(2)	-0.0013(2)	-0.0028(2)
C4	0.0243(3)	0.0223(3)	0.0289(3)	0.0009(2)	0.0026(2)	-0.0058(2)
C5	0.0229(2)	0.0199(2)	0.0220(3)	0.0024(2)	0.0043(2)	-0.0039(2)

C6	0.0318(3)	0.0323(3)	0.0300(3)	-0.0025(3)	0.0144(2)	-0.0089(3)
C7	0.0345(3)	0.0261(3)	0.0272(3)	0.0080(3)	-0.0012(3)	-0.0037(3)
C8	0.0376(3)	0.0264(3)	0.0252(3)	0.0017(3)	0.0123(2)	-0.0033(3)
C9	0.0228(2)	0.0288(3)	0.0368(3)	-0.0042(3)	0.0070(2)	0.0047(2)
C10	0.0187(2)	0.0156(2)	0.0201(3)	-0.0007(2)	0.0014(2)	-0.00002(19)
C11	0.0203(2)	0.0202(3)	0.0297(3)	-0.0009(2)	0.0005(2)	0.0028(2)
C12	0.0209(2)	0.0169(2)	0.0208(3)	-0.0019(2)	0.0012(2)	0.0001(2)
C13	0.0192(3)	0.0457(4)	0.0494(4)	0.0108(3)	0.0065(3)	-0.0047(3)
C14	0.0405(4)	0.0626(5)	0.0776(6)	-0.0058(5)	0.0034(4)	-0.0261(4)
C15	0.0193(2)	0.0228(3)	0.0229(3)	-0.0031(2)	0.0039(2)	-0.0018(2)
C16	0.0578(4)	0.0356(3)	0.0265(3)	-0.0145(3)	0.0080(3)	0.0004(3)
C17	0.0623(5)	0.0731(6)	0.0390(4)	-0.0254(4)	0.0027(4)	-0.0114(4)

Table 9–15: Selected geometric parameters for **65**.

N1—O1	1.4582(6)	C15—O5—C16	117.11(5)
N1—C1	1.4981(8)	N1—C1—C8	107.42(5)
N1—C5	1.5032(7)	N1—C1—C2	107.07(5)
O1—C10	1.4337(6)	C8—C1—C2	107.60(5)
O2—C12	1.3260(7)	N1—C1—C9	115.92(5)
O2—C13	1.4560(8)	C8—C1—C9	107.60(5)
O3—C12	1.1955(7)	C2—C1—C9	110.89(5)
O4—C15	1.1926(7)	C3—C2—C1	113.05(5)
O5—C15	1.3321(7)	C3—C2—H2A	109.0
O5—C16	1.4578(8)	C1—C2—H2A	109.0
C1—C8	1.5252(8)	C3—C2—H2B	109.0
C1—C2	1.5294(8)	C1—C2—H2B	109.0
C1—C9	1.5359(8)	H2A—C2—H2B	107.8
C2—C3	1.5152(9)	C4—C3—C2	108.09(5)
C2—H2A	0.9900	C4—C3—H3A	110.1
C2—H2B	0.9900	C2—C3—H3A	110.1
C3—C4	1.5123(9)	C4—C3—H3B	110.1
C3—H3A	0.9900	C2—C3—H3B	110.1
C3—H3B	0.9900	H3A—C3—H3B	108.4
C4—C5	1.5347(8)	C3—C4—C5	114.07(5)
C4—H4A	0.9900	C3—C4—H4A	108.7

C4—H4B	0.9900	C5—C4—H4A	108.7
C5—C6	1.5246(9)	C3—C4—H4B	108.7
C5—C7	1.5330(8)	C5—C4—H4B	108.7
C6—H6A	0.9800	H4A—C4—H4B	107.6
C6—H6B	0.9800	N1—C5—C6	107.83(5)
C6—H6C	0.9800	N1—C5—C7	115.30(5)
C7—H7A	0.9800	C6—C5—C7	107.90(5)
C7—H7B	0.9800	N1—C5—C4	107.12(4)
C7—H7C	0.9800	C6—C5—C4	107.22(5)
C8—H8A	0.9800	C7—C5—C4	111.15(5)
C8—H8B	0.9800	C5—C6—H6A	109.5
C8—H8C	0.9800	C5—C6—H6B	109.5
C9—H9A	0.9800	H6A—C6—H6B	109.5
C9—H9B	0.9800	C5—C6—H6C	109.5
C9—H9C	0.9800	H6A—C6—H6C	109.5
C10—C11	1.5136(7)	H6B—C6—H6C	109.5
C10—C15	1.5403(8)	C5—C7—H7A	109.5
C10—C12	1.5409(8)	C5—C7—H7B	109.5
C11—H11A	0.9800	H7A—C7—H7B	109.5
C11—H11B	0.9800	C5—C7—H7C	109.5
C11—H11C	0.9800	H7A—C7—H7C	109.5
C13—C14	1.4861(12)	H7B—C7—H7C	109.5
C13—H13A	0.9900	C1—C8—H8A	109.5
C13—H13B	0.9900	C1—C8—H8B	109.5
C14—H14A	0.9800	H8A—C8—H8B	109.5
C14—H14B	0.9800	C1—C8—H8C	109.5
C14—H14C	0.9800	H8A—C8—H8C	109.5
C16—C17	1.4755(12)	H8B—C8—H8C	109.5
C16—H16A	0.9900	C1—C9—H9A	109.5
C16—H16B	0.9900	C1—C9—H9B	109.5
C17—H17A	0.9800	H9A—C9—H9B	109.5
C17—H17B	0.9800	C1—C9—H9C	109.5
C17—H17C	0.9800	H9A—C9—H9C	109.5
O1—N1—C1	106.18(4)	H9B—C9—H9C	109.5
O1—N1—C5	106.27(4)	O1—C10—C11	117.31(4)
C1—N1—C5	117.51(4)	O1—C10—C15	105.60(4)
C10—O1—N1	116.17(4)	C11—C10—C15	111.25(5)

C12—O2—C13	116.49(5)	O1—C10—C12	106.81(4)
C11—C10—C12	109.12(4)	C5—N1—C1—C8	-170.46(4)
C15—C10—C12	106.11(4)	O1—N1—C1—C2	-173.81(4)
C10—C11—H11A	109.5	C5—N1—C1—C2	-55.12(6)
C10—C11—H11B	109.5	O1—N1—C1—C9	-49.47(6)
H11A—C11—H11B	109.5	C5—N1—C1—C9	69.21(6)
C10—C11—H11C	109.5	N1—C1—C2—C3	56.14(6)
H11A—C11—H11C	109.5	C8—C1—C2—C3	171.36(5)
H11B—C11—H11C	109.5	C9—C1—C2—C3	-71.21(7)
O3—C12—O2	124.99(5)	C1—C2—C3—C4	-58.49(6)
O3—C12—C10	124.79(5)	C2—C3—C4—C5	57.30(6)
O2—C12—C10	110.22(5)	O1—N1—C5—C6	-72.70(5)
O2—C13—C14	111.64(7)	C1—N1—C5—C6	168.66(4)
O2—C13—H13A	109.3	O1—N1—C5—C7	47.90(6)
C14—C13—H13A	109.3	C1—N1—C5—C7	-70.74(6)
O2—C13—H13B	109.3	O1—N1—C5—C4	172.18(4)
C14—C13—H13B	109.3	C1—N1—C5—C4	53.54(6)
H13A—C13—H13B	108.0	C3—C4—C5—N1	-53.44(6)
C13—C14—H14A	109.5	C3—C4—C5—C6	-168.96(5)
C13—C14—H14B	109.5	C3—C4—C5—C7	73.33(6)
H14A—C14—H14B	109.5	N1—O1—C10—C11	-5.63(7)
C13—C14—H14C	109.5	N1—O1—C10—C15	-130.22(4)
H14A—C14—H14C	109.5	N1—O1—C10—C12	117.12(4)
H14B—C14—H14C	109.5	C13—O2—C12—O3	0.11(9)
O4—C15—O5	125.12(5)	C13—O2—C12—C10	-179.37(5)
O4—C15—C10	125.66(5)	O1—C10—C12—O3	-121.06(6)
O5—C15—C10	109.21(5)	C11—C10—C12—O3	6.67(8)
O5—C16—C17	110.65(7)	C15—C10—C12—O3	126.62(6)
O5—C16—H16A	109.5	O1—C10—C12—O2	58.42(6)
C17—C16—H16A	109.5	C11—C10—C12—O2	-173.85(5)
O5—C16—H16B	109.5	C15—C10—C12—O2	-53.90(6)
C17—C16—H16B	109.5	C12—O2—C13—C14	-82.82(8)
H16A—C16—H16B	108.1	C16—O5—C15—O4	-3.47(9)
C16—C17—H17A	109.5	C16—O5—C15—C10	175.69(5)
C16—C17—H17B	109.5	O1—C10—C15—O4	5.55(7)
H17A—C17—H17B	109.5	C11—C10—C15—O4	-122.74(6)
C16—C17—H17C	109.5	C12—C10—C15—O4	118.70(6)

H17A—C17—H17C	109.5	O1—C10—C15—O5	-173.61(4)
H17B—C17—H17C	109.5	C11—C10—C15—O5	58.10(6)
C1—N1—O1—C10	-118.32(5)	C12—C10—C15—O5	-60.46(6)
C5—N1—O1—C10	115.84(5)	O1—N1—C1—C8	70.85(5)

9.5 Crystal Data of E2-E4

Table 9–16: Positional and equivalent isotropic displacement parameters of **E2**.

Atom	WS	x	y	z	$U_{eq.}$
O1	2*i*	-0.00982(14)	0.86697(10)	0.93228(8)	265(2)
H1	2*i*	-0.0885	0.9042	0.9042	627(15)
N1	2*i*	0.21762(17)	0.98292(12)	1.17200(10)	278(3)
C1	2*i*	-0.02985(19)	0.83295(12)	1.02892(12)	226(3)
C2	2*i*	-0.17653(19)	0.77542(12)	1.02566(11)	219(3)
C11	2*i*	-0.18862(18)	0.75532(13)	1.14241(12)	217(3)
C12	2*i*	-0.15731(19)	0.85752(13)	1.25233(12)	242(3)
C13	2*i*	-0.1707(2)	0.83459(14)	1.35856(12)	285(3)
H13	2*i*	-0.1472	0.9022	1.4313	368(17)
C14	2*i*	-0.2177(2)	0.71546(15)	1.35992(13)	308(4)
C15	2*i*	-0.2489(2)	0.61570(15)	1.25139(14)	314(4)
H15	2*i*	-0.2806	0.5346	1.2508	368(17)
C16	2*i*	-0.23429(19)	0.63298(13)	1.14350(12)	256(3)
C17	2*i*	-0.1163(2)	0.99315(14)	1.26151(13)	315(4)
H17A	2*i*	-0.1849	1.0429	1.3010	627(15)
H17B	2*i*	-0.1408	0.9999	1.1787	627(15)
H17C	2*i*	0.0030	1.0231	1.3108	627(15)
C18	2*i*	-0.2403(3)	0.69580(19)	1.47540(15)	446(5)
H18A	2*i*	-0.1396	0.6685	1.5228	627(15)
H18B	2*i*	-0.3383	0.6329	1.4499	627(15)
H18C	2*i*	-0.2574	0.7736	1.5266	627(15)
C19	2*i*	-0.2626(2)	0.51902(14)	1.03133(14)	338(4)
H19A	2*i*	-0.2785	0.4440	1.0532	627(15)
H19B	2*i*	-0.1646	0.5190	1.0064	627(15)

H19C	2*i*	-0.3628	0.5214	0.9629	627(15)
C21	2*i*	-0.33128(19)	0.73651(12)	0.90633(11)	219(3)
C22	2*i*	-0.48957(19)	0.77382(13)	0.90458(12)	245(3)
C23	2*i*	-0.6291(2)	0.74277(14)	0.79169(13)	291(3)
H23	2*i*	-0.7334	0.7680	0.7921	368(17)
C24	2*i*	-0.6160(2)	0.67485(14)	0.67825(13)	320(4)
C25	2*i*	-0.4628(2)	0.63337(14)	0.68198(13)	309(4)
H25	2*i*	-0.4542	0.5846	0.6073	368(17)
C26	2*i*	-0.3192(2)	0.66104(13)	0.79295(12)	261(3)
C27	2*i*	-0.5185(2)	0.84963(16)	1.02100(14)	331(4)
H27A	2*i*	-0.6296	0.8755	0.9974	627(15)
H27B	2*i*	-0.4319	0.9227	1.0644	627(15)
H27C	2*i*	-0.5125	0.7989	1.0753	627(15)
C28	2*i*	-0.7666(3)	0.64998(19)	0.55625(16)	508(5)
H28A	2*i*	-0.7344	0.6061	0.4871	627(15)
H28B	2*i*	-0.7999	0.7286	0.5462	627(15)
H28C	2*i*	-0.8611	0.5994	0.5579	627(15)
C29	2*i*	-0.1618(2)	0.60576(15)	0.78484(14)	342(4)
H29A	2*i*	-0.1948	0.5213	0.7279	627(15)
H29B	2*i*	-0.0901	0.6046	0.8667	627(15)
H29C	2*i*	-0.0997	0.6560	0.7547	627(15)
C31	2*i*	0.13496(19)	0.86545(13)	1.13874(12)	245(3)
C32	2*i*	0.2005(2)	0.78000(15)	1.20018(14)	319(4)
H32	2*i*	0.1404	0.6994	1.1755	368(17)
C33	2*i*	0.3567(2)	0.81621(18)	1.29892(15)	407(4)
H33	2*i*	0.4038	0.7603	1.3414	368(17)
C34	2*i*	0.4413(2)	0.93655(18)	1.33326(14)	397(4)
H34	2*i*	0.5464	0.9633	1.3995	368(17)
C35	2*i*	0.3682(2)	1.01669(16)	1.26834(13)	338(4)
H35	2*i*	0.4259	1.0980	1.2924	368(17)

Table 9–17: Anisotropic displacement parameters (U_{ij}/pm^2) of **E2**.

Atom	U_{11}	U_{22}	U_{33}	U_{12}	U_{13}	U_{23}
O1	282(6)	334(6)	228(5)	125(4)	128(4)	23(4)
N1	269(7)	318(7)	242(6)	69(5)	106(5)	-11(5)
C1	281(8)	225(7)	195(6)	73(5)	109(5)	36(5)
C2	283(8)	196(6)	182(6)	45(5)	102(5)	20(5)
C11	219(7)	250(7)	206(6)	82(5)	100(5)	25(5)
C12	242(8)	276(7)	211(6)	69(5)	97(5)	10(6)
C13	295(9)	353(8)	199(6)	65(6)	98(6)	20(6)
C14	296(9)	434(9)	258(7)	182(6)	121(6)	47(7)
C15	333(9)	316(8)	334(7)	169(6)	123(6)	-6(6)
C16	245(8)	264(7)	261(7)	91(5)	91(6)	6(6)
C17	433(10)	259(7)	262(7)	36(6)	178(6)	3(6)
C18	550(12)	557(11)	319(8)	234(8)	195(8)	31(9)
C19	453(10)	238(7)	338(8)	82(6)	171(7)	0(7)
C21	258(8)	211(6)	202(6)	69(5)	101(5)	-11(5)
C22	282(8)	228(7)	242(6)	73(5)	122(6)	-15(6)
C23	259(8)	281(7)	322(7)	99(6)	93(6)	-9(6)
C24	337(9)	286(8)	257(7)	62(6)	39(6)	-60(6)
C25	395(10)	281(7)	208(6)	21(5)	111(6)	-37(6)
C26	322(9)	245(7)	222(6)	54(5)	127(6)	-11(6)
C27	318(9)	408(9)	300(7)	91(6)	164(6)	87(7)
C28	474(12)	512(11)	331(8)	37(8)	-32(8)	21(9)
C29	394(10)	356(8)	264(7)	23(6)	160(6)	68(7)
C31	246(8)	299(7)	220(6)	73(5)	131(5)	24(6)
C32	313(9)	363(8)	332(7)	149(6)	144(6)	59(6)
C33	342(10)	579(11)	355(8)	236(8)	112(7)	141(8)
C34	263(9)	622(11)	257(7)	96(7)	69(6)	28(8)
C35	288(9)	398(9)	274(7)	32(6)	104(6)	-44(7)

Table 9–18: Selected bond lengths (pm) and angles (degrees) of **E2**.

Mesityl-I		**Mesityl-II**	
C11-C12	141.1(11)	C21-C22	140.2(4)
C12-C13	139.2(2)	C22-C23	139.2(11)
C13-C14	137.7(4)	C23-C24	139.2(7)
C14-C15	138.6(10)	C24-C25	137.3(4)
C15-C16	138.9(2)	C25-C26	139.9(11)
C16-C11	140.8(4)	C26-C21	141.4(8)
C12-C17	150.5(4)	C22-C27	150.9(8)
C14-C18	151.5(3)	C24-C28	151.2(12)
C16-C19	150.7(11)	C26-C29	150.0(5)
Pyridyl-I		**Ethylene-bridge**	
C31-C32	138.2(7)	C1-O1	136.0(3)
C32-C33	138.2(12)	C1-C2	134.3(6)
C33-C34	137.6(8)	C1-C31	149.1(12)
C34-C35	137.4(7)	C2-C11	149.7(2)
C35-N1	133.9(11)	C2-C21	150.1(13)
N1-C31	134.4(8)		
H-bonds		H···N	191.9(10)
O1-H1	82.0(4)	O1···N1	271.1(15)
Angles			
C11-C2-C1	120.16(1)	C31-C1-C2	124.28(1)
C21-C2-C1	119.99(1)	O1-C1-C2	124.99(1)
O1-C1-C2-C21	3.94(2)	C11-C2-C1-C31	8.33(2)
C1-C2-C21-C22	-126.54(1)	C1-C2-C11-C16	-123.10(1)
C2-C1-C31-N1	-133.38(1)	H1-O1-C1-C2	48.15(2)
O1-H1-N1	162.09(2)		

Table 9–19: Positional and equivalent isotropic displacement parameters of **E3**.

Atom	WS	X	y	z	$U_{eq.}$
O1	8*c*	0.66015(8)	0.18605(7)	0.71479(6)	341(3)
H1	8*c*	0.6124	0.1708	0.6890	642(14)
N1	8*c*	0.97304(10)	0.14279(8)	0.83559(7)	322(3)
C1	8*c*	0.74619(11)	0.13817(8)	0.70824(7)	266(3)
C2	8*c*	0.77355(11)	0.10047(8)	0.64916(7)	250(3)
C11	8*c*	0.85983(11)	0.03884(8)	0.64912(7)	254(3)
C12	8*c*	0.85045(12)	-0.02954(8)	0.69000(7)	291(3)

C13	8*c*	0.92841(13)	-0.08809(9)	0.68425(8)	335(3)
H13	8*c*	0.9215	-0.1331	0.7111	417(17)
C14	8*c*	1.01512(13)	-0.08151(9)	0.64020(8)	344(4)
C15	8*c*	1.02440(12)	-0.01297(9)	0.60159(8)	329(3)
H15	8*c*	1.0829	-0.0069	0.5724	417(17)
C16	8*c*	0.94932(11)	0.04679(8)	0.60516(7)	276(3)
C17	8*c*	0.75914(14)	-0.04549(10)	0.73888(9)	394(4)
H17A	8*c*	0.7376	-0.0992	0.7346	642(14)
H17B	8*c*	0.7003	-0.0120	0.7273	642(14)
H17C	8*c*	0.7813	-0.0354	0.7859	642(14)
C18	8*c*	1.09442(16)	-0.14731(11)	0.63243(11)	484(5)
H18A	8*c*	1.1066	-0.1712	0.6770	642(14)
H18B	8*c*	1.1603	-0.1269	0.6147	642(14)
H18C	8*c*	1.0668	-0.1857	0.6007	642(14)
C19	8*c*	0.96792(13)	0.12015(9)	0.56374(9)	360(4)
H19A	8*c*	0.9104	0.1274	0.5314	642(14)
H19B	8*c*	1.0339	0.1157	0.5387	642(14)
H19C	8*c*	0.9713	0.1643	0.5946	642(14)
C21	8*c*	0.71733(11)	0.11701(8)	0.58175(7)	248(3)
C22	8*c*	0.67041(11)	0.05601(8)	0.54270(8)	273(3)
C23	8*c*	0.62630(12)	0.07163(8)	0.47780(8)	299(3)
H23	8*c*	0.5980	0.0303	0.4522	417(17)
C24	8*c*	0.62283(12)	0.14661(9)	0.44977(8)	304(3)
C25	8*c*	0.66562(12)	0.20646(9)	0.48965(8)	315(3)
H25	8*c*	0.6623	0.2574	0.4726	417(17)
C26	8*c*	0.71345(12)	0.19388(8)	0.55420(8)	287(3)
C27	8*c*	0.66373(15)	-0.02639(9)	0.57021(9)	403(4)
H27A	8*c*	0.6170	-0.0567	0.5412	642(14)
H27B	8*c*	0.6364	-0.0255	0.6169	642(14)
H27C	8*c*	0.7335	-0.0495	0.5701	642(14)
C28	8*c*	0.57527(15)	0.16220(11)	0.37900(9)	417(4)
H28A	8*c*	0.5067	0.1865	0.3844	642(14)
H28B	8*c*	0.5674	0.1136	0.3543	642(14)
H28C	8*c*	0.6215	0.1964	0.3532	642(14)
C29	8*c*	0.76179(14)	0.26367(9)	0.59040(9)	393(4)
H29A	8*c*	0.7064	0.2939	0.6120	642(14)
H29B	8*c*	0.7987	0.2955	0.5570	642(14)

H29C	8*c*	0.8110	0.2460	0.6253	642(14)
C31	8*c*	0.80605(11)	0.13485(8)	0.77452(8)	271(3)
C32	8*c*	0.91603(11)	0.14186(9)	0.77686(8)	291(3)
H32	8*c*	0.9525	0.1462	0.7349	417(17)
C33	8*c*	0.92048(13)	0.13527(9)	0.89570(8)	336(3)
H33	8*c*	0.9592	0.1352	0.9370	417(17)
C34	8*c*	0.81120(13)	0.12765(10)	0.89898(8)	364(4)
H34	8*c*	0.7771	0.1219	0.9417	417(17)
C35	8*c*	0.75314(12)	0.12874(9)	0.83795(8)	334(3)
H35	8*c*	0.6792	0.1254	0.8392	417(17)

Table 9–20: Anisotropic displacement parameters (U_{ij}/pm^2) of **E3**.

Atom	U_{11}	U_{22}	U_{33}	U_{12}	U_{13}	U_{23}
O1	255(5)	442(6)	328(6)	-88(5)	-29(5)	67(4)
N1	278(6)	406(7)	284(6)	-26(5)	-36(5)	5(5)
C1	215(6)	300(7)	283(7)	-22(6)	-13(6)	-3(6)
C2	253(7)	243(6)	252(7)	1(5)	-6(6)	-41(5)
C11	270(7)	257(6)	235(6)	-34(5)	-28(6)	-10(5)
C12	346(8)	286(7)	239(7)	-5(6)	-33(6)	-18(6)
C13	453(9)	261(7)	291(8)	19(6)	-73(7)	15(6)
C14	373(8)	326(8)	333(8)	-79(6)	-84(7)	51(7)
C15	296(7)	342(8)	349(8)	-68(6)	20(7)	8(6)
C16	280(7)	286(7)	263(7)	-56(6)	-12(6)	-24(5)
C17	473(10)	355(8)	355(9)	84(7)	42(8)	-34(7)
C18	533(11)	398(9)	520(11)	-60(8)	-58(9)	132(8)
C19	366(8)	326(8)	389(9)	9(6)	103(7)	-21(6)
C21	240(6)	251(6)	255(7)	-10(5)	18(6)	5(5)
C22	286(7)	260(6)	274(7)	-19(5)	-19(6)	7(5)
C23	322(8)	294(7)	282(7)	-61(6)	-36(6)	7(6)
C24	297(7)	354(8)	261(7)	2(6)	7(6)	64(6)
C25	343(8)	277(7)	326(8)	46(6)	14(7)	38(6)
C26	303(7)	249(6)	309(7)	-6(6)	11(6)	5(5)
C27	537(10)	267(7)	406(9)	13(7)	-169(8)	-79(7)
C28	471(10)	463(10)	317(9)	24(7)	-43(8)	82(8)
C29	476(9)	256(7)	447(9)	3(6)	-52(8)	-40(7)

C31	253(7)	295(7)	265(7)	-44(6)	4(6)	3(6)
C32	255(7)	369(8)	248(7)	-29(6)	5(6)	-21(6)
C33	353(8)	413(8)	243(7)	-18(6)	-36(6)	55(7)
C34	371(8)	482(9)	239(7)	-13(7)	41(7)	50(7)
C35	254(7)	450(9)	299(8)	-39(7)	30(6)	18(6)

Table 9–21: Selected bond distances (pm) and bond angles (degrees) of **E3**.

Mesityl-I		**Mesityl-II**		
C11-C12	141.2(0)	C21-C22		141.2(0)
C12-C13	140.3(0)	C22-C23		139()
C13-C14	138.3(0)	C23-C24		138.9(0)
C14-C15	139()	C24-C25		138.5(0)
C15-C16	139()	C25-C26		139.4(0)
C16-C11	141.1(0)	C26-C21		141.6(0)
C12-C17	150.6(0)	C22-C27		150.5(0)
C14-C18	150.8(0)	C24-C28		150.8(0)
C16-C19	150.2(0)	C26-C29		150.7(0)
Pyridyl-I		**Etylene-bridge**		
C31-C32	138.6(0)	C1-O1		136()
C32-N1	133.6(0)	C1-C2		134.9(0)
N1-C33	133.6(0)	C1-C31		147.9(0)
C33-C34	137.8(0)	C2-C11		151()
C34-C35	138()	C2-C21		150.1(0)
C35-C31	139.1(0)			
Angles				
C11-C2-C1	121.02(1)	C31-C1-C2		125.23(1)
C21-C2-C1	121.09(1)	O1-C1-C2		124.51(1)
O1-C1-C2-C21	8.07(2)	C11-C2-C1-C31		10.92(2)
C1-C2-C21-C22	-125.55(1)	C1-C2-C11-C12		60.55(2)
C2-C1-C31-C32	44.92(2)	H1-O1-C1-C2		31.49(2)
H-bonds	**d(D-H)**	**d(H···A)**	**d(D···A)**	**∠(DHA)**
O1-H1···N1	82()	187.3(0)	264.4(1)	156.33(2)

Table 9–22: Positional and equivalent isotropic distribution parameters of **E4**.

Atom	WS	x	Y	z	$U_{eq.}$
O1	2*i*	0.45351(14)	0.65421(13)	0.39239(6)	369(3)
H1	2*i*	0.4379	0.5677	0.4247	633(14)
N1	2*i*	0.31411(16)	0.36482(14)	0.44991(7)	339(3)
C1	2*i*	0.37385(17)	0.65129(16)	0.32676(8)	275(3)
C2	2*i*	0.44360(16)	0.73782(15)	0.25209(8)	260(3)
C11	2*i*	0.38385(16)	0.71655(16)	0.17588(8)	255(3)
C12	2*i*	0.37388(17)	0.56354(17)	0.15833(8)	293(3)
C13	2*i*	0.31742(18)	0.54627(18)	0.08693(9)	336(3)
H13	2*i*	0.3104	0.4447	0.0761	479(16)
C14	2*i*	0.27156(19)	0.6745(2)	0.03173(9)	351(3)
C15	2*i*	0.28768(17)	0.82491(18)	0.04794(8)	323(3)
H15	2*i*	0.2595	0.9128	0.0108	479(16)
C16	2*i*	0.34449(16)	0.84899(17)	0.11784(8)	271(3)
C17	2*i*	0.4230(2)	0.41405(17)	0.21236(10)	371(3)
H17A	2*i*	0.3255	0.3701	0.2533	633(14)
H17B	2*i*	0.5137	0.4390	0.2390	633(14)
H17C	2*i*	0.4613	0.3377	0.1793	633(14)
C18	2*i*	0.2044(3)	0.6512(2)	-0.04306(10)	514(4)
H18A	2*i*	0.2532	0.7326	-0.0896	633(14)
H18B	2*i*	0.0819	0.6578	-0.0333	633(14)
H18C	2*i*	0.2352	0.5484	-0.0540	633(14)
C19	2*i*	0.35974(19)	1.01715(17)	0.12935(9)	337(3)
H19A	2*i*	0.3035	1.0870	0.0908	633(14)
H19B	2*i*	0.4786	1.0492	0.1202	633(14)
H19C	2*i*	0.3069	1.0227	0.1844	633(14)
C21	2*i*	0.58614(16)	0.85487(16)	0.24652(8)	257(3)
C22	2*i*	0.74500(17)	0.85182(16)	0.19414(8)	283(3)
C23	2*i*	0.87183(17)	0.96606(17)	0.18941(9)	313(3)
H23	2*i*	0.9765	0.9622	0.1550	479(16)
C24	2*i*	0.84860(17)	1.08547(17)	0.23394(9)	304(3)
C25	2*i*	0.69157(17)	1.08814(16)	0.28466(8)	291(3)
H25	2*i*	0.6732	1.1673	0.3152	479(16)
C26	2*i*	0.56045(17)	0.97678(16)	0.29161(8)	273(3)
C27	2*i*	0.78287(19)	0.7269(2)	0.14290(10)	385(4)
H27A	2*i*	0.7240	0.7503	0.0971	633(14)

H27B	2*i*	0.7448	0.6240	0.1760	633(14)
H27C	2*i*	0.9040	0.7270	0.1230	633(14)
C28	2*i*	0.9851(2)	1.2105(2)	0.22748(11)	423(4)
H28A	2*i*	1.0502	1.1779	0.2705	633(14)
H28B	2*i*	0.9327	1.3097	0.2328	633(14)
H28C	2*i*	1.0598	1.2236	0.1749	633(14)
C29	2*i*	0.39347(18)	0.99647(18)	0.34650(9)	339(3)
H29A	2*i*	0.3956	0.9398	0.4016	633(14)
H29B	2*i*	0.3009	0.9546	0.3267	633(14)
H29C	2*i*	0.3775	1.1076	0.3462	633(14)
C31	2*i*	0.20606(17)	0.56239(16)	0.34989(8)	274(3)
C32	2*i*	0.06739(18)	0.62259(18)	0.31674(9)	316(3)
H32	2*i*	0.0828	0.7139	0.2751	479(16)
C33	2*i*	-0.09714(18)	0.5502(2)	0.34385(10)	372(3)
H33	2*i*	-0.1886	0.5950	0.3207	479(16)
C34	2*i*	-0.12355(19)	0.4152(2)	0.40367(10)	382(4)
H34	2*i*	-0.2327	0.3677	0.4209	479(16)
C35	2*i*	0.01363(19)	0.34700(18)	0.43973(9)	334(3)
C36	2*i*	-0.0056(2)	0.2094(2)	0.50307(9)	422(4)
H36	2*i*	-0.1120	0.1567	0.5215	479(16)
C37	2*i*	0.1303(3)	0.1537(2)	0.53719(10)	464(4)
H37	2*i*	0.1188	0.0620	0.5785	479(16)
C38	2*i*	0.2877(2)	0.23590(18)	0.50946(9)	411(4)
H38	2*i*	0.3795	0.1978	0.5343	479(16)
C39	2*i*	0.17916(18)	0.42185(16)	0.41365(8)	284(3)

Table 9–23: Anisotropic displacement parameters (U_{ij}/pm^2) of **E4**.

Atom	U_{11}	U_{22}	U_{33}	U_{12}	U_{13}	U_{23}
O1	463(6)	343(6)	309(5)	9(4)	-179(5)	-114(5)
N1	494(7)	262(6)	281(6)	-44(5)	-139(5)	-26(6)
C1	316(7)	249(7)	273(6)	-44(5)	-99(5)	-20(6)
C2	279(6)	217(7)	287(6)	-53(5)	-60(5)	-1(5)
C11	251(6)	252(7)	253(6)	-45(5)	-30(5)	-24(5)
C12	303(6)	269(7)	295(7)	-60(6)	-22(5)	-38(6)
C13	400(7)	302(8)	309(7)	-105(6)	-21(6)	-86(6)
C14	373(7)	416(9)	260(7)	-77(6)	-39(6)	-72(7)
C15	348(7)	348(8)	242(6)	-8(6)	-35(5)	-26(6)
C16	261(6)	272(7)	255(6)	-30(5)	-6(5)	-29(5)
C17	471(8)	228(7)	425(8)	-75(6)	-104(7)	1(7)
C18	675(11)	574(11)	325(8)	-110(8)	-153(8)	-108(9)
C19	403(8)	252(7)	342(7)	-16(6)	-85(6)	9(6)
C21	289(6)	215(7)	268(6)	-30(5)	-79(5)	-14(5)
C22	292(6)	255(7)	306(7)	-62(6)	-64(5)	7(6)
C23	261(6)	307(8)	365(7)	-68(6)	-46(5)	-11(6)
C24	316(7)	264(7)	342(7)	-43(6)	-107(6)	-32(6)
C25	368(7)	229(7)	292(7)	-61(6)	-95(6)	-5(6)
C26	321(7)	238(7)	254(6)	-25(5)	-65(5)	-2(6)
C27	335(7)	381(9)	464(9)	-195(7)	-13(6)	-26(7)
C28	372(8)	392(9)	531(10)	-168(8)	-69(7)	-77(7)
C29	380(7)	292(8)	332(7)	-80(6)	-12(6)	-18(6)
C31	338(7)	249(7)	240(6)	-61(5)	-51(5)	-30(6)
C32	339(7)	303(8)	302(7)	-50(6)	-66(6)	-16(6)
C33	320(7)	415(9)	395(8)	-114(7)	-71(6)	-21(7)
C34	348(7)	425(9)	369(8)	-134(7)	7(6)	-120(7)
C35	429(8)	316(8)	254(7)	-109(6)	2(6)	-106(6)
C36	584(10)	361(9)	289(7)	-74(7)	21(7)	-196(8)
C37	813(12)	295(8)	261(7)	5(6)	-102(8)	-168(9)
C38	680(10)	279(8)	304(7)	-28(6)	-205(7)	-38(8)
C39	392(7)	251(7)	222(6)	-78(5)	-55(5)	-37(6)

Table 9–24: Selected bond distances (pm) and angles (degrees) of **E4**.

Mesityl-I		**Mesityl-II**	
C11-C12	141.0(9)	C21-C22	140.8(23)
C12-C13	139.4(12)	C22-C23	138.8(22)
C13-C14	138.0(25)	C23-C24	138.4(17)
C14-C15	138.4(9)	C24-C25	138.3(23)
C15-C16	138.9(13)	C25-C26	138.8(22)
C16-C11	141.2(25)	C26-C21	140.9(18)
C12-C17	150.6(26)	C22-C27	150.8(20)
C14-C18	150.5(14)	C24-C28	150.2(25)
C16-C19	150.3(7)	C26-C29	150.6(25)
Quinolinyl-I		**Etylene-bridge**	
C31-C32	137.4(19)	C1-O1	137.5(15)
C32-C33	140.6(22)	C1-C2	134.7(27)
C33-C34	135.9(26)	C1-C31	148.6(24)
C34-C35	140.8(21)	C2-C11	149.3(13)
C35-C36	140.7(27)	C2-C21	149.3(23)
C36-C37	135.2(19)		
C37-C38	139.2(24)		
C38-N1	132.1(26)		
N1-C39	136.7(19)		
C39-C31	142.9(28)		
C39-C35	142.0(22)		
Angles			
O1-C1-C2-C11	168.20(12)	C1-C2-C11	121.53(12)
O1-C1-C2-C21	-10.6(2)	C1-C2-C21	118.37(12)
C11-C2-C1-C31	-18.68(22)	C2-C1-C31	126.99(13)
C21-C2-C1-C31	162.52(13)	C2-C1-O1	118.92(12)
C1-C2-C11-C12	-51.71(19)		
C1-C2-C21-C22	125.43(15)		
C2-C1-C31-C32	-36.86(22)		
C2-C1-O1-H1	-147.90(13)		
π-π interaction: Quinolinyl-I / Quinolinyl-I			
Distances			
C31-C36	361.9(57)	C34-N1	353.9(55)
C32-C37	357.4(56)	C35-C39	361.2(56)
C33-C38	350.7(55)		

H-bonds	**d(D-H)**	**d(H⋯A)**	**d(D⋯A)**	**∠(DHA)**
O1-H1⋯N1	82.0(15)	193.2(30)	264.0(43)	144.01(9)

9.6 Crystal Structure Data of E6

Table 9–25: Positional and equivalent isotropic displacement parameters of **E6**.

Atom	WS	x	y	z	$U_{eq.}$
			1st Molecule		
Si1	2i	0.16071(7)	0.89363(3)	0.355245(18)	291.3(13)
O1	2i	-0.01786(17)	1.23263(8)	0.51177(5)	318(3)
H1	2i	-0.0342	1.1840	0.5293	850(12)
O2	2i	0.12715(16)	0.90830(7)	0.42104(4)	272(3)
C1	2i	0.1195(2)	1.28228(11)	0.42705(6)	249(3)
C2	2i	0.0859(2)	1.21240(11)	0.46494(6)	259(3)
C3	2i	0.1480(2)	1.11506(11)	0.45895(6)	270(3)
C4	2i	0.1877(2)	1.03314(11)	0.45586(7)	285(4)
C5	2i	0.2383(2)	0.93312(11)	0.45008(7)	318(4)
H5A	2i	0.3501	0.9178	0.4309	518(16)
H5B	2i	0.2400	0.8970	0.4858	518(16)
C6	2i	0.2529(2)	1.26210(10)	0.38036(7)	252(3)
C7	2i	0.4182(2)	1.21547(11)	0.38897(7)	282(4)
C8	2i	0.5408(2)	1.20428(12)	0.34458(8)	344(4)
H8	2i	0.6494	1.1731	0.3506	518(16)
C9	2i	0.5083(3)	1.23740(13)	0.29177(8)	366(4)
C10	2i	0.3455(3)	1.28272(12)	0.28373(7)	354(4)
H10	2i	0.3209	1.3053	0.2485	518(16)
C11	2i	0.2173(2)	1.29567(11)	0.32652(7)	282(3)
C12	2i	0.4744(2)	1.17812(13)	0.44415(8)	348(4)
H12A	2i	0.4812	1.1122	0.4514	850(12)
H12B	2i	0.3958	1.2100	0.4714	850(12)
H12C	2i	0.5819	1.1883	0.4448	850(12)
C13	2i	0.6445(3)	1.22467(19)	0.24473(10)	566(6)
H13A	2i	0.6818	1.1596	0.2397	850(12)
H13B	2i	0.7359	1.2458	0.2521	850(12)
H13C	2i	0.6027	1.2605	0.2123	850(12)
C14	2i	0.0444(3)	1.34396(13)	0.31312(8)	372(4)
H14A	2i	0.0097	1.4041	0.3260	850(12)
H14B	2i	-0.0307	1.3067	0.3303	850(12)

H14C	2i	0.0437	1.3519	0.2745	850(12)
C15	2i	0.0222(2)	1.38136(10)	0.43110(6)	240(3)
C16	2i	0.1043(2)	1.45250(11)	0.42982(6)	249(3)
C17	2i	0.0121(2)	1.54496(11)	0.42989(7)	281(4)
H17	2i	0.0673	1.5910	0.4300	518(16)
C18	2i	-0.1587(2)	1.57082(11)	0.42984(7)	294(4)
C19	2i	-0.2386(2)	1.50007(12)	0.43213(7)	299(4)
H19	2i	-0.3538	1.5160	0.4330	518(16)
C20	2i	-0.1526(2)	1.40641(11)	0.43314(7)	273(3)
C21	2i	0.2897(2)	1.43100(12)	0.42979(8)	314(4)
H21A	2i	0.3447	1.4144	0.3949	850(12)
H21B	2i	0.3238	1.3797	0.4573	850(12)
H21C	2i	0.3189	1.4851	0.4371	850(12)
C22	2i	-0.2531(3)	1.67219(12)	0.42677(9)	404(4)
H22A	2i	-0.3654	1.6769	0.4437	850(12)
H22B	2i	-0.2539	1.6991	0.3894	850(12)
H22C	2i	-0.2001	1.7053	0.4453	850(12)
C23	2i	-0.2537(2)	1.33638(12)	0.43465(8)	347(4)
H23A	2i	-0.3487	1.3651	0.4156	850(12)
H23B	2i	-0.2904	1.3161	0.4717	850(12)
H23C	2i	-0.1861	1.2834	0.4176	850(12)
C24	2i	-0.0348(3)	0.86345(14)	0.34542(9)	435(5)
H24	2i	-0.0222	0.7975	0.3603	518(16)
C25	2i	-0.1947(3)	0.91831(17)	0.37618(12)	572(6)
H25A	2i	-0.2232	0.9817	0.3589	850(12)
H25B	2i	-0.1774	0.9180	0.4131	850(12)
H25C	2i	-0.2837	0.8896	0.3759	850(12)
C26	2i	-0.0539(5)	0.8698(2)	0.28538(12)	807(10)
H26A	2i	-0.1465	0.8460	0.2821	850(12)
H26B	2i	0.0460	0.8335	0.2670	850(12)
H26C	2i	-0.0732	0.9340	0.2693	850(12)
C27	2i	0.3516(3)	0.79362(13)	0.34689(8)	417(5)
H27	2i	0.4393	0.8100	0.3618	518(16)
C28	2i	0.3275(3)	0.70204(13)	0.38023(10)	461(5)
H28A	2i	0.2443	0.6822	0.3665	850(12)
H28B	2i	0.2923	0.7117	0.4176	850(12)
H28C	2i	0.4309	0.6548	0.3775	850(12)

C29	2i	0.4193(5)	0.7769(2)	0.28852(12)	791(10)
H29A	2i	0.5185	0.7265	0.2881	850(12)
H29B	2i	0.4448	0.8327	0.2686	850(12)
H29C	2i	0.3372	0.7608	0.2720	850(12)
C30	2i	0.1968(3)	1.00043(13)	0.30954(8)	395(4)
H30	2i	0.2026	0.9867	0.2723	518(16)
C31	2i	0.3627(3)	1.02188(15)	0.31289(10)	516(6)
H31A	2i	0.3804	1.0710	0.2846	850(12)
H31B	2i	0.4518	0.9667	0.3085	850(12)
H31C	2i	0.3600	1.0414	0.3477	850(12)
C32	2i	0.0531(3)	1.08803(14)	0.31578(10)	525(6)
H32A	2i	0.0413	1.1046	0.3518	850(12)
H32B	2i	-0.0483	1.0756	0.3097	850(12)
H32C	2i	0.0762	1.1388	0.2897	850(12)
			2^{nd} Molekule		
Si2	2i	0.13606(7)	0.23140(3)	0.05620(2)	352.0(14)
O3	2i	-0.1210(2)	0.55795(9)	-0.13226(6)	417(3)
H3	2i	-0.1192	0.5831	-0.1058	850(12)
O4	2i	0.16816(19)	0.33848(9)	0.04774(5)	377(3)
C41	2i	-0.0821(2)	0.40447(12)	-0.15192(6)	278(3)
C42	2i	-0.0500(2)	0.46356(12)	-0.12241(7)	307(4)
C43	2i	0.0548(2)	0.43488(12)	-0.08006(7)	320(4)
C44	2i	0.1372(2)	0.41524(12)	-0.04314(7)	321(4)
C45	2i	0.2405(3)	0.38784(13)	0.00090(7)	362(4)
H45A	2i	0.3477	0.3486	-0.0120	518(16)
H45B	2i	0.2598	0.4435	0.0111	518(16)
C46	2i	0.0125(2)	0.30390(12)	-0.14898(6)	289(4)
C47	2i	0.1874(2)	0.27798(13)	-0.15985(7)	348(4)
C48	2i	0.2706(3)	0.18382(15)	-0.16026(8)	454(5)
H48	2i	0.3862	0.1676	-0.1674	518(16)
C49	2i	0.1873(4)	0.11353(15)	-0.15032(9)	525(6)
C50	2i	0.0166(3)	0.13920(14)	-0.13905(9)	477(5)
H50	2i	-0.0411	0.0927	-0.1317	518(16)
C51	2i	-0.0731(3)	0.23257(13)	-0.13831(8)	363(4)
C52	2i	0.2933(3)	0.34718(16)	-0.17378(9)	442(5)
H52A	2i	0.3371	0.3527	-0.1418	850(12)
H52B	2i	0.2267	0.4071	-0.1873	850(12)

H52C	2i	0.3836	0.3258	-0.2011	850(12)
C53	2i	0.2817(5)	0.01214(17)	-0.15298(14)	810(10)
H53A	2i	0.2677	-0.0069	-0.1863	850(12)
H53B	2i	0.2392	-0.0265	-0.1227	850(12)
H53C	2i	0.3978	0.0056	-0.1517	850(12)
C54	2i	-0.2591(3)	0.25248(16)	-0.12588(11)	515(6)
H54A	2i	-0.3091	0.2825	-0.1581	850(12)
H54B	2i	-0.2965	0.2929	-0.0979	850(12)
H54C	2i	-0.2907	0.1948	-0.1137	850(12)
C55	2i	-0.2145(2)	0.44134(11)	-0.18868(7)	287(4)
C56	2i	-0.1771(2)	0.43310(11)	-0.24492(7)	297(4)
C57	2i	-0.3041(3)	0.46457(12)	-0.27773(7)	339(4)
H57	2i	-0.2788	0.4591	-0.3147	518(16)
C58	2i	-0.4668(3)	0.50379(12)	-0.25752(8)	369(4)
C59	2i	-0.5011(3)	0.51319(13)	-0.20250(8)	379(4)
H59	2i	-0.6093	0.5411	-0.1884	518(16)
C60	2i	-0.3789(2)	0.48227(12)	-0.16786(7)	338(4)
C61	2i	-0.0029(3)	0.39422(14)	-0.27049(7)	392(4)
H61A	2i	0.0302	0.3280	-0.2593	850(12)
H61B	2i	0.0714	0.4241	-0.2592	850(12)
H61C	2i	0.0011	0.4057	-0.3093	850(12)
C62	2i	-0.6031(3)	0.53744(16)	-0.29384(10)	496(5)
H62A	2i	-0.5973	0.5974	-0.3135	850(12)
H62B	2i	-0.7095	0.5430	-0.2721	850(12)
H62C	2i	-0.5893	0.4934	-0.3191	850(12)
C63	2i	-0.4317(3)	0.49390(17)	-0.10837(8)	471(5)
H63A	2i	-0.4247	0.5543	-0.1022	850(12)
H63B	2i	-0.3596	0.4460	-0.0867	850(12)
H63C	2i	-0.5444	0.4888	-0.0985	850(12)
C64	2i	0.2242(6)	0.1755(3)	0.12063(14)	945(12)
H64	2i	0.1326	0.2117	0.1440	518(16)
C65	2i	0.3436(9)	0.2049(3)	0.1380(3)	1970(40)
H65A	2i	0.3271	0.2711	0.1275	850(12)
H65B	2i	0.4512	0.1727	0.1219	850(12)
H65C	2i	0.3371	0.1916	0.1768	850(12)
C66	2i	0.1894(7)	0.0834(3)	0.14387(16)	1252(18)
H66A	2i	0.2405	0.0383	0.1190	850(12)

H66B	2i	0.0712	0.0902	0.1496	850(12)
H66C	2i	0.2340	0.0626	0.1779	850(12)
C67	2i	0.2317(4)	0.16740(17)	-0.00315(11)	637(7)
H67	2i	0.1893	0.2081	-0.0352	518(16)
C68	2i	0.4166(6)	0.1453(3)	-0.01428(19)	1084(14)
H68A	2i	0.4640	0.1088	0.0171	850(12)
H68B	2i	0.4518	0.2024	-0.0223	850(12)
H68C	2i	0.4532	0.1103	-0.0448	850(12)
C69	2i	0.1745(6)	0.0772(2)	0.00036(14)	882(11)
H69A	2i	0.2164	0.0493	-0.0326	850(12)
H69B	2i	0.0550	0.0919	0.0052	850(12)
H69C	2i	0.2164	0.0342	0.0306	850(12)
C70	2i	-0.0962(4)	0.2474(2)	0.06691(11)	617(7)
H70	2i	-0.1174	0.1856	0.0792	518(16)
C71	2i	-0.1772(4)	0.2862(3)	0.01673(15)	949(12)
H71A	2i	-0.2925	0.2853	0.0238	850(12)
H71B	2i	-0.1227	0.2488	-0.0118	850(12)
H71C	2i	-0.1686	0.3494	0.0058	850(12)
C72	2i	-0.1802(5)	0.3100(3)	0.11105(16)	961(11)
H72A	2i	-0.1596	0.3708	0.1004	850(12)
H72B	2i	-0.1358	0.2828	0.1446	850(12)
H72C	2i	-0.2980	0.3157	0.1159	850(12)

Table 9–26: Anisotropic displacement parameters (U_{ij}/pm^2) of **E6**.

Atom	U_{11}	U_{22}	U_{33}	U_{12}	U_{13}	U_{23}
			1st Molecule			
Si1	401(3)	252(2)	247(2)	-35.4(16)	-38.4(19)	-125(2)
O1	408(8)	265(5)	288(6)	-40(5)	18(5)	-129(6)
O2	342(7)	241(5)	264(6)	-52(4)	-36(5)	-113(5)
C1	254(9)	240(7)	283(8)	-31(6)	-70(6)	-93(7)
C2	283(9)	248(7)	272(8)	-44(6)	-51(6)	-95(7)
C3	308(10)	267(7)	259(8)	-17(6)	-58(7)	-109(7)
C4	351(10)	274(8)	259(8)	-23(6)	-53(7)	-126(7)
C5	385(11)	242(7)	347(9)	-49(6)	-126(8)	-60(7)
C6	277(9)	202(7)	298(8)	-19(6)	-54(7)	-94(7)
C7	283(9)	231(7)	356(9)	-25(6)	-71(7)	-93(7)

C8	279(10)	307(8)	456(10)	-69(7)	-35(8)	-82(8)
C9	361(11)	328(9)	411(10)	-81(7)	39(8)	-121(8)
C10	447(12)	313(8)	311(9)	-27(7)	-42(8)	-121(8)
C11	322(10)	226(7)	311(8)	-29(6)	-57(7)	-85(7)
C12	284(10)	351(9)	429(10)	-1(7)	-134(8)	-88(8)
C13	499(15)	682(15)	466(12)	-104(11)	101(11)	-137(13)
C14	380(11)	386(9)	328(9)	-27(7)	-117(8)	-28(8)
C15	262(9)	230(7)	252(7)	-22(6)	-49(6)	-98(7)
C16	269(9)	265(7)	241(7)	-26(6)	-40(6)	-114(7)
C17	335(10)	250(7)	296(8)	-21(6)	-55(7)	-133(7)
C18	331(10)	248(7)	298(8)	-33(6)	-57(7)	-56(7)
C19	250(9)	303(8)	348(9)	-39(7)	-52(7)	-67(7)
C20	261(9)	272(7)	311(8)	-33(6)	-50(7)	-105(7)
C21	284(10)	301(8)	397(9)	-24(7)	-76(7)	-135(7)
C22	424(12)	269(8)	512(11)	-57(8)	-95(9)	-47(8)
C23	278(10)	331(8)	479(10)	-40(7)	-86(8)	-137(8)
C24	550(14)	367(9)	471(11)	-10(8)	-187(10)	-209(10)
C25	416(14)	509(12)	831(18)	3(12)	-258(13)	-128(11)
C26	1190(30)	87(2)	629(17)	-80(14)	-465(18)	-520(20)
C27	517(14)	319(9)	406(10)	-114(8)	67(9)	-125(9)
C28	492(14)	295(9)	555(12)	-80(8)	-6(10)	-50(9)
C29	1070(30)	551(14)	575(16)	-191(12)	332(16)	-98(16)
C30	577(14)	339(9)	291(9)	14(7)	-51(8)	-186(9)
C31	599(15)	419(11)	546(13)	29(9)	19(11)	-262(11)
C32	680(16)	336(10)	559(13)	90(9)	-209(12)	-135(10)
			2^{nd} Molecule			
Si2	435(3)	332(2)	300(2)	-26.5(19)	-76(2)	-106(2)
O3	623(10)	289(6)	372(7)	-75(5)	-207(7)	-67(6)
O4	547(9)	359(6)	257(6)	-52(5)	-59(6)	-155(6)
C41	308(10)	309(8)	232(7)	-35(6)	-41(7)	-99(7)
C42	370(11)	301(8)	262(8)	-47(6)	-64(7)	-84(8)
C43	392(11)	325(8)	273(8)	-66(6)	-46(7)	-121(8)
C44	382(11)	315(8)	281(8)	-45(6)	-58(7)	-103(8)
C45	405(11)	388(9)	320(9)	3(7)	-103(8)	-139(9)
C46	356(10)	306(8)	220(7)	-48(6)	-63(7)	-83(7)
C47	357(11)	422(9)	267(8)	-80(7)	-59(7)	-65(8)
C48	435(13)	488(11)	367(10)	-110(9)	-77(9)	52(10)

C49	723(18)	355(10)	451(12)	-85(9)	-188(11)	29(11)
C50	670(17)	320(9)	478(11)	-51(8)	-158(11)	-135(10)
C51	454(12)	341(9)	334(9)	-33(7)	-114(8)	-132(9)
C52	325(12)	617(13)	405(10)	-139(9)	22(8)	-147(10)
C53	1040(30)	410(13)	86(2)	-158(13)	-237(19)	117(14)
C54	464(14)	458(11)	683(15)	17(10)	-106(11)	-245(11)
C55	351(10)	264(7)	265(8)	-44(6)	-79(7)	-81(7)
C56	381(11)	263(7)	269(8)	-35(6)	-59(7)	-105(7)
C57	456(12)	299(8)	298(8)	-17(7)	-121(8)	-121(8)
C58	427(12)	319(8)	409(10)	28(7)	-180(9)	-143(9)
C59	325(11)	368(9)	450(11)	-29(8)	-84(8)	-92(8)
C60	354(11)	339(8)	331(9)	-52(7)	-56(8)	-86(8)
C61	443(12)	431(10)	263(8)	-64(7)	-29(8)	-43(9)
C62	473(14)	529(12)	525(12)	34(10)	-239(11)	-149(11)
C63	392(13)	621(13)	350(10)	-128(9)	-2(9)	-28(11)
C64	1320(30)	1010(20)	626(18)	361(17)	-470(20)	-570(20)
C65	3430(90)	586(19)	2340(60)	110(30)	-2530(70)	-180(30)
C66	2210(60)	88(2)	72(2)	349(19)	-500(30)	-540(30)
C67	88(2)	428(12)	521(14)	-115(10)	48(13)	-65(13)
C68	1090(30)	674(19)	1290(30)	-290(20)	400(30)	-100(20)
C69	1360(30)	567(15)	78(2)	-236(14)	-220(20)	-215(18)
C70	585(17)	651(15)	627(15)	-2(12)	-51(13)	-237(14)
C71	59(2)	1380(30)	87(2)	160(20)	-195(17)	-350(20)
C72	69(2)	1140(30)	93(3)	-21(2)	216(19)	-150(20)

Table 9–27: Selected bond distances (pm) and angles (°) of **E6**.

1st molecule		2nd molecule	
distances (/pm)		distances (/pm)	
C1-C2	135.2(23)	C41-C42	134.6(16)
C2-C3	143.1(16)	C42-C43	142.8(23)
C3-C4	119.1(10)	C43-C44	119.8(18)
C4-C5	146.4(13)	C44-C45	145.5(23)
C5-O2	142.8(17)	C45-O4	142.5(25)
O2-SI1	167.2(11)	O4-SI2	167(1)
SI1-C24	188.1(13)	SI2-C64	186.5(30)
SI1-C27	188.3(38)	SI2-C67	185.6(32)

SI1-C30	187.5(30)	SI2-C70	188.1(11)
C2-O1	137.0(24)	C42-O3	137.4(20)
O1-H1	82.0(12)	O3-H3	82.0(9)
C1-C15	149.6(24)	C41-C55	149.3(26)
C15-C16	141.1(15)	C55-C56	141.5(10)
C16-C17	138.9(22)	C56-C57	138.8(23)
C17-C18	138.2(12)	C57-C58	138.1(23)
C18-C19	138.9(15)	C58-C59	138.8(10)
C19-C20	138.9(21)	C59-C60	138.8(23)
C20-C15	140.9(11)	C60-C55	140.3(24)
C16-C21	150.3(10)	C56-C61	150.0(26)
C18-C22	150.4(23)	C58-C62	150.8(25)
C20-C23	151.0(17)	C60-C63	151.3(14)
C1-C6	149.4(28)	C41-C46	149.4(23)
C6-C7	140.9(21)	C46-C47	140.8(15)
C7-C8	138.9(25)	C47-C48	139.3(20)
C8-C9	138.2(16)	C48-C49	138.5(17)
C9-C10	138.3(20)	C49-C50	137.5(15)
C10-C11	139.1(25)	C50-C51	139.7(22)
C11-C6	141.4(17)	C51-C46	141.1(17)
C7-C12	150.7(21)	C47-C52	150.6(20)
C9-C13	150.4(27)	C49-C53	151.5(23)
C11-C14	150.2(23)	C51-C54	150.0(13)
C24-C25	153.3(31)	C64-C65	135.4(14)
C24-C26	152.8(5)	C64-C66	149.2(18)
C27-C28	153.0(23)	C67-C68	148.8(13)
C27-C29	152.0(18)	C67-C69	153.6(12)
C30-C31	153.2(9)	C70-C71	148.8(24)
C30-C32	153.1(30)	C70-C72	152.7(28)
H1-O2	194.5(34)	H3-O4	194.2(29)
O1-O2	274.4(47)	O3-O4	274.4(37)
angles (/°)		angles (/°)	
C1-C2-C3	124.00(7)	C41-C42-C43	124.22(4)
C2-C3-C4	174.84(10)	C42-C43-C44	176.20(5)
C3-C4-C5	178.06(10)	C43-C44-C45	177.71(5)
C1-C2-O1	120.26(4)	C41-C42-O3	119.70(8)
C3-C2-O1	115.70(5)	C43-C42-O3	116.08(5)

C2-O1-H1	109.47(5)	C42-O3-H3	109.47(10)
C2-C1-C6	120.81(4)	C42-C41-C46	121.52(7)
C2-C1-C15	120.29(6)	C42-C41-C55	118.70(4)
O1-H1-O2	164.55(7)	O3-H3-O4	165.77(5)
O2-SI1-C24	102.21(4)	O4-SI2-C64	103.46(4)
O2-SI1-C27	106.41(4)	O4-SI2-C67	112.12(5)
O2-SI1-C30	112.81(3)	O4-SI2-C70	106.53(6)
C26-C24-C25	110.61(3)	C65-C64-C66	120.91(8)
C28-C27-C29	109.61(3)	C68-C67-C69	109.22(7)
C31-C30-C32	110.33(8)	C71-C70-C72	108.58(3)
torsion angles (/°)		torsion angles (/°)	
C7-C6-C1-C2	-56.94(11)	C47-C46-C41-C42	-56.13(11)
C16-C15-C1-C2	126.71(9)	C56-C55-C41-C42	122.96(9)
H1-O1-C2-C3	-3.52(13)	H3-O3-C42-C43	-19.34(13)
O1-C2-C1-C6	169.88(7)	O3-C42-C41-C46	170.07(7)
O1-C2-C1-C15	-10.58(12)	O3-C42-C41-C55	-9.33(12)
C3-C2-C1-C6	-12.48(12)	C43-C42-C41-C46	-10.30(13)
C3-C2-C1-C15	167.07(7)	C43-C42-C41-C55	170.30(7)

9.7 Crystal Structure Data of E11

Table 9–28: Bond distances [pm] observed for **E11**.

Atom	x	y	z	U(eq)
O(1)	13377(1)	457(1)	4069(1)	37(1)
O(2)	5766(1)	7938(1)	4866(1)	34(1)
C(1)	11244(2)	1065(1)	1863(1)	26(1)
C(2)	9793(2)	691(2)	1686(1)	31(1)
C(3)	8906(2)	1365(2)	911(1)	37(1)
C(4)	9373(2)	2438(2)	299(1)	37(1)
C(5)	10768(2)	2822(2)	490(1)	34(1)
C(6)	11728(2)	2161(1)	1252(1)	29(1)
C(7)	9092(2)	-362(2)	2357(1)	44(1)
C(8)	8367(3)	3156(2)	-536(1)	57(1)
C(9)	13250(2)	2668(2)	1361(1)	36(1)
C(10)	12260(2)	287(1)	2679(1)	25(1)
C(11)	13188(2)	-1346(1)	2728(1)	25(1)
C(12)	14439(2)	-1990(1)	1976(1)	28(1)
C(13)	15284(2)	-3510(2)	2027(1)	32(1)
C(14)	14951(2)	-4439(1)	2795(1)	33(1)
C(15)	13722(2)	-3797(2)	3525(1)	32(1)
C(16)	12832(2)	-2282(1)	3512(1)	28(1)
C(17)	14941(2)	-1080(2)	1121(1)	38(1)
C(18)	15920(2)	-6082(2)	2841(1)	46(1)
C(19)	11506(2)	-1735(2)	4350(1)	35(1)
C(20)	12342(2)	1085(1)	3353(1)	28(1)
C(21)	11358(2)	2624(1)	3382(1)	29(1)
C(22)	10543(2)	3909(1)	3385(1)	30(1)
C(23)	9516(2)	5484(1)	3345(1)	32(1)
C(24)	8093(2)	5913(1)	4179(1)	28(1)
C(25)	7069(2)	7536(1)	4071(1)	30(1)

Table 9–29: Anisotropic displacement parameters (U_{ij}/pm^2) of **E11**.

Atom	U_{11}	U_{22}	U_{33}	U_{23}	U_{13}	U_{12}
O(1)	45(1)	26(1)	37(1)	-8(1)	-21(1)	-1(1)
O(2)	32(1)	30(1)	36(1)	-9(1)	-7(1)	-1(1)
C(1)	27(1)	24(1)	24(1)	-4(1)	-4(1)	-4(1)
C(2)	31(1)	29(1)	32(1)	-2(1)	-7(1)	-8(1)
C(3)	35(1)	37(1)	40(1)	-3(1)	-15(1)	-10(1)
C(4)	43(1)	33(1)	32(1)	-2(1)	-14(1)	-4(1)
C(5)	42(1)	27(1)	29(1)	1(1)	-5(1)	-7(1)
C(6)	31(1)	26(1)	27(1)	-5(1)	-3(1)	-6(1)
C(7)	39(1)	50(1)	50(1)	10(1)	-15(1)	-23(1)
C(8)	70(1)	53(1)	47(1)	9(1)	-32(1)	-16(1)
C(9)	39(1)	35(1)	35(1)	1(1)	-5(1)	-15(1)
C(10)	23(1)	26(1)	25(1)	-3(1)	-3(1)	-6(1)
C(11)	25(1)	25(1)	25(1)	-4(1)	-7(1)	-7(1)
C(12)	29(1)	30(1)	25(1)	-6(1)	-6(1)	-7(1)
C(13)	32(1)	32(1)	31(1)	-11(1)	-6(1)	-4(1)
C(14)	32(1)	26(1)	41(1)	-6(1)	-13(1)	-7(1)
C(15)	32(1)	30(1)	35(1)	3(1)	-10(1)	-12(1)
C(16)	25(1)	30(1)	28(1)	-2(1)	-7(1)	-9(1)
C(17)	40(1)	37(1)	29(1)	-5(1)	4(1)	-5(1)
C(18)	48(1)	26(1)	62(1)	-8(1)	-16(1)	-6(1)
C(19)	33(1)	39(1)	30(1)	1(1)	-1(1)	-10(1)
C(20)	27(1)	26(1)	27(1)	-2(1)	-7(1)	-3(1)
C(21)	30(1)	29(1)	26(1)	-6(1)	-6(1)	-5(1)
C(22)	29(1)	30(1)	28(1)	-5(1)	-6(1)	-5(1)
C(23)	33(1)	25(1)	35(1)	-2(1)	-5(1)	-5(1)
C(24)	30(1)	24(1)	30(1)	-2(1)	-9(1)	-5(1)
C(25)	29(1)	26(1)	34(1)	-2(1)	-7(1)	-5(1)

Table 9–30: Positional and equivalent isotropic displacement parameters of **E11**.

	x	y	z	U(eq)
H(1)	13520	1121	4332	55
H(2)	4850	8594	4690	51
H(3A)	7948	1083	794	44
H(5A)	11091	3567	86	41
H(7A)	8662	46	2967	66
H(7B)	10045	-1309	2437	66
H(7C)	8114	-508	2104	66
H(8A)	8251	2394	-877	85
H(8B)	9014	3727	-956	85
H(8C)	7184	3812	-317	85
H(9A)	13933	2751	746	54
H(9B)	14023	1952	1791	54
H(9C)	12783	3630	1618	54
H(13A)	16120	-3926	1517	38
H(15A)	13473	-4414	4058	38
H(17A)	15998	-1694	754	57
H(17B)	15195	-255	1319	57
H(17C)	13957	-698	733	57
H(18A)	16109	-6418	2212	69
H(18B)	15209	-6591	3269	69
H(18C)	17070	-6301	3073	69
H(19A)	10843	-2418	4557	53
H(19B)	10679	-757	4174	53
H(19C)	12134	-1674	4864	53
H(23A)	8940	5770	2758	39
H(23B)	10339	6046	3318	39
H(24A)	7271	5347	4219	34
H(24B)	8658	5670	4769	34
H(25A)	7893	8104	4016	36
H(25B)	6478	7777	3490	36

Table 9–31: Some important bond distances and bond angles in **E11**.

Parameter	Value	Parameter	Value
O(1)-C(20)	1.3727(15)	C(11)-C(12)	1.4147(18)
O(2)-C(25)	1.4296(16)	C(12)-C(13)	1.3930(18)
C(1)-C(2)	1.4081(19)	C(12)-C(17)	1.5065(19)
C(1)-C(6)	1.4116(18)	C(13)-C(14)	1.386(2)
C(1)-C(10)	1.5038(17)	C(14)-C(15)	1.384(2)
C(2)-C(3)	1.3861(19)	C(14)-C(18)	1.5124(19)
C(2)-C(7)	1.507(2)	C(15)-C(16)	1.3957(18)
C(3)-C(4)	1.389(2)	C(16)-C(19)	1.5094(18)
C(4)-C(5)	1.379(2)	C(20)-C(21)	1.4327(17)
C(4)-C(8)	1.511(2)	C(21)-C(22)	1.1929(19)
C(5)-C(6)	1.3973(19)	C(22)-C(23)	1.4649(17)
C(6)-C(9)	1.5106(19)	C(23)-C(24)	1.5255(19)
C(10)-C(20)	1.3473(18)	C(24)-C(25)	1.5051(17)
C(10)-C(11)	1.4986(17)	C(11)-C(16)	1.4126(18)
Bond angles	(in degrees)	C(20)-C(10)-C(11)	120.89(11)
C(2)-C(1)-C(6)	118.55(12)	C(20)-C(10)-C(1)	118.91(11)
C(2)-C(1)-C(10)	120.13(11)	C(11)-C(10)-C(1)	120.19(10)
C(6)-C(1)-C(10)	121.31(11)	C(16)-C(11)-C(12)	118.26(11)
C(3)-C(2)-C(1)	120.04(13)	C(16)-C(11)-C(10)	121.39(11)
C(3)-C(2)-C(7)	118.32(13)	C(12)-C(11)-C(10)	120.35(11)
C(1)-C(2)-C(7)	121.52(12)	C(13)-C(12)-C(11)	119.75(12)
C(2)-C(3)-C(4)	122.12(13)	C(13)-C(12)-C(17)	118.06(12)
C(5)-C(4)-C(3)	117.45(12)	C(11)-C(12)-C(17)	122.17(12)
C(5)-C(4)-C(8)	121.89(14)	C(14)-C(13)-C(12)	122.51(12)
C(3)-C(4)-C(8)	120.66(14)	C(15)-C(14)-C(13)	117.22(12)
C(4)-C(5)-C(6)	122.81(13)	C(15)-C(14)-C(18)	121.43(13)
C(5)-C(6)-C(1)	119.00(12)	C(13)-C(14)-C(18)	121.34(13)
C(5)-C(6)-C(9)	116.98(12)	C(14)-C(15)-C(16)	122.82(13)
C(1)-C(6)-C(9)	124.02(12)	C(15)-C(16)-C(11)	119.44(12)
C(15)-C(16)-C(19)	117.17(12)	C(22)-C(21)-C(20)	178.57(14)
C(11)-C(16)-C(19)	123.39(12)	C(21)-C(22)-C(23)	177.22(14)
C(10)-C(20)-O(1)	121.43(11)	C(22)-C(23)-C(24)	113.66(11)
C(10)-C(20)-C(21)	123.02(11)	C(25)-C(24)-C(23)	110.32(11)
O(1)-C(20)-C(21)	115.55(11)	O(2)-C(25)-C(24)	110.06(11)

10 Reference

[1] a) S. W. Ragsdale, "Pyruvate ferredoxin oxidoreductase and its radical intermediate", *Chem. Rev*. **2003**, *103*, 2333-2346, b) A. V. Bogachev, Y. V. Bertsova, B. Barquera, M. I. Verkhovsky, "Sodium-dependent steps in the redox reactions of the Na^+-motive NADH: quinone oxidoreductase from *Vibrio harveyi*", *Biochemistry* **2001**, *40*, 7318-7323, c) X. Lu, R. B. Silverman, "Monoamine oxidase B-catalysed reactions of *cis*-and *trans*-5-aminomethyl-3-(4-Methoxyphenyl)dihydrofuran-2(3*H*)-ones. Evidence for a reversible redox reaction", *J. Am. Chem. Soc*. **1998**, *120*, 10583-10587.

[2] a) M. Garcia-Viloca, J. Gao, M. Karplus, D. G. Truhlar, "How enzymes work: Analysis by modern rate theory and computational simulations", *Science* **2004**, *303*, 186-195, b) K. H. G. Verschueren, F. Seljee, H. J. Roseboom, K. H. Kalk, B. W. Dijkstra, "Crystallographic analysis of the catalytic mechanism of haloalkane dehalogenase", *Nature* **1993**, *363*, 693-698.

[3] C.-H. Tai, P. F. Cook, "Pyridoxal-5´-phosphate-dependent α,β-elimination reactions: Mechanism of *o*-acetylserine sulfhydrylase, *Acc. Chem. Res*. **2001**, *34*, 49-59.

[4] a) B. Ruma, "Radical carbon skeleton rearrangements: Catalysis by coenzyme B_{12} dependent mutase", *Chem. Rev*. **2003**, *103*, 2083-2094. b) T. Toraya, "Radical catalysis in coenzyme B_{12}-dependent isomerisation (eliminating) reactions", *Chem. Rev*. **2003**, *103*, 2095-2128. c) P. A. Frey, O. Th. Magnusson,"S-Adenosylmetheonine: A wolf in sheep´s clothing, or a rich man´s adenosylcobalamine?", *Chem. Rev*. **2003**, *103*, 2129-2148. d) M. Fontecave, S. Ollagnier-de-Chaudens, E. Mulliez, "Biological radical sulfur insertion reactions", *Chem. Rev*. **2003**, *103*, 2149-2166.

[5] a) J. Stubbe, D. G. Nocera, C. S. Yee, M. C. Y. Chang, "Radical initiation in class I ribonucleotide reductase: Long-range proton coupled electron transfer?" *Chem. Rev*. **2003**, *103*, 2167-2202. b) J. W. Whittaker, "Free radical catalysis by galactose oxidase", *Chem. Rev*. **2003**, *103*, 2347-2364. c) T. Borowski, E. Broclawik, "Catalytic reaction mechanism of lipoxygenase. A density functional theory study, *J. Phys. Chem. B* **2003**, *107*, 4639-4646.

[6] J. Stubbe, W. A. Van der Donk, "Protein radical in enzyme catalysis", *Chem. Rev*. **1998**,

98, 705-762.

[7] M. Schmittel, M. K. Ghorai, *Electron Transfer in Chemistry*, Balzani, V., Ed., Wiley-VCH, Weinheim, 2001, *Vol 2*, pp 5-54.

[8] R. A. Rossi, "Phenomenon of radical-anion fragmentation in the course of aromatic SRN1 reactions", *Acc. Chem. Res.* **1982**, *15*, 164-170.

[9] a) A. Jordan, E. Torrents, C. Jeanthon, R. Eliasson, U. Hellman, C. Wernstedt, J. Barbe, I. Gibert, P. Reichard, "B_{12}-dependent ribonucleotide reductases from deeply rooted eubacteria are structurally related to the aerobic enzyme from *Escherichia coli*", *Proc. Natl. Acad. Sci.* USA. **1997**, *94*, 13487-13492. b) J. Stubbe, "Ribonucleotide reductases in the twenty-first century", *Proc. Natl. Acad. Sci.* USA. **1998**, *95*, 2723-2724.

[10] P. Reichard, B. Estborn, "Utilisation of deoxyribosides in the synthesis of poly-nucleotides", *J. Biol. Chem*. **1951**, *188*, 839-846.

[11] R. L. Blakley, H. A. Barker, "Cobamide stimulation of reduction of ribotides to deoxyribotides in *Lactobacillus Leichmannii*", *Biochem. Biophys. Res. Commun*. **1964**, *16*, 391-397.

[12] W. S. Beck, J. Hardy, "Requirement of ribonucleotide reductases for cobamide coenzyme a product of ribosomal activity", *Proc. Natl. Acad. Sci. U. S. A*. **1965**, *54*, 286-293.

[13] M. Fontecave, R. Eliasson, P. Reichard, "Oxygen sensitive ribonucleoside triphosphate reductase is present in anaerobic *Escherichia-Coli*", *Proc. Natl. Acad. Sci. U. S. A*. **1989**, *86*, 2147-2151.

[14] A. Willing, H. Follman, G. Auling, "Ribonucleotide reductase of *Brevibacterium-Ammoniagenes* is a manganese enzyme", *Eur. J. Biochem*. **1988**, *178*, 603-611.

[15] H. Zipse, "The addition of water to ethylene and trans-butene radical cation. Model system for the reaction of alkene radical cations with nucleophiles", *J. Am. Chem. Soc*. **1995**, *117*, 11798-11806.

[16] A. L. J. Beckwith, D. Crich, P. J. Duggan, Q. Yao, "Chemistry of β-(acyloxy)alkyl and β-(phosphotoxy)alkyl radicals and related species: Radical and radical ionic migrations and fragmentations of carbon-oxygen bonds", *Chem. Rev*. **1997**. *97*, 3273-3312.

[17] A. I. Lin, G. W. Ashley, J. Stubbe, "Location of the redox-active thiols of

ribonucleotide reductases: Sequence similarity between the *Escherichia coli* and *Lactobacillus leichmannii* enzymes", *Biochemistry* **1987**, *26*, 6905-6909.

[18] W. A. Van der Donk, G. Yu, D. J. Silva, J. Stubbe, J. R. McCarthy, E. T. Jarvi, D. P. Matthews, R. J. Resvick, E. Wagner, "Inactivation of ribonucleotide reductase by (*E*)-2′-fluoromethylene-2′-deoxycytidine-5′-diphosphate: A paradigm for nucleotide mechanism-based inhibition", *Biochemistry* **1996**, *35*, 8381-8391.

[19] S. S. Mao, T. P. Holler, G. X. Yu, J. Jr. M. Bollinger, S. Booker, M. I. Johnston, S, J. tubbe, "A model for the role of multiple cysteine residues involved in ribonucleotide reduction: Amazing and still confusing", *Biochemistry*. **1992**, *31*, 9733-9743.

[20] S. Booker, S. Licht, J. Broderick, J. Stubbe, "Coenzyme B_{12}-dependent ribonucleotide reductase: Evidence for the participation of five cysteine residues in ribonucleotide reduction", *Biochemsitry.* **1994**, *33*, 12676-12685.

[21] R. Lenz, B. Giese, "Studies on the mechanism of ribonucleotide reductases", *J. Am. Chem. Soc.* **1997**, *119*, 2784-2794.

[22] U. Uhlin, H. Eklund, "Structure of ribonucleotide reductase protein R1", *Nature* **1994**, *370*, 533-539.

[23] P. E. M. Siegbahn, "Theoretical study of the substrate mechanism of ribonucleotide reductase", *J. Am. Chem. Soc.* **1998**, *120*, 8417-8429.

[24] H. Zipse, M. Mohr, "C-H bond activation in ribonucleotide reductases-do short, strong hydrogen bonds play a role", *Chem. Eur. J.* **1999**, *5*, 3046-3054.

[25] Folkers, K. *Vitamin B_{12}*, Zagalak, B.; Friedrich, W., Ed., Walter de Gruyter, Berlin, 1979, pp 7-18.

[26] B. M. Babior, *BioFactors* **1988**, *1*, 21.

[27] W. Buckel, B. T. Golding, "Glutamate and 2-methyleneglutarate mutase: From microbial curiosities to paradigms for coenzyme B_{12}-dependent enzymes", *Chem. Soc. Rev*. **1996**, *26*, 329-337.

[28] a) J. G. Lawrence, J. R. Roth, "Evolution of coenzyme B_{12} synthesis among enteric bacteria: Evidence for loss and reacquisition of multigene complex", *Genetics*, , **1996**, *142*, 11-24. b) J. Frings, B. Schink, "Fermentation of phenoxyethanol to phenol and acetate by a homoacetogenic bacterium", *Arch. Microbiol*. **1994**, *162*, 199-204. c) J.

Frings, C. Wondrak, B. Schink, "Fermentation of phenoxyethanol to phenol and acetate by a homoacetogenic bacterium", *Arch. Microbiol*. **1994**, *162*, 103-107.

[29] a) T. Toraya, S. Kuno, S. Fukui, "Distribution of coenzyme B_{12}-dependent diol Dehydratase and glycerol dehydratase in selected genera of enterobacteriaceae and propionibacteraceae", *J. Bacteriol*. **1980**, *141*, 1439. b) R. G. Forage, M. A. Foster, "Resolution of the coenzyme B_{12}-dependent dehydratases of *Klebsiella Sp.* and *Citrobacter-freundii*", *Biochim. Biophys. Acta* **1979**, *569*, 249. c) T. Toraya, S. Honda, S. Kuno, S. Fukui, Coenzyme B_{12}-dependent diol dehydratase. 10. Regulation of apoenzyme synthesis in *Klebsiella pneumoniae* (*Aerobacter-Aerogenes*)", *J. Bacteriol*. **1978**, *135*, 726-729.

[30] a) M. G. N. Hartmanis, T. C. Stadtman, "Diol metabolism and diol dehydratase in *Clostridium-Glycolicum*", *Arch. Biochem. Biophys*. **1986**, *245*, 144-152. b) M. G. N. Hartmanis, T. C. Stadtman, "Solubilisation of a membrane-bound diol dehydratase with retention of electron-paramagnetic-res G = 2.02 signal by using 2-(N-cyclohexylamino)ethanesulfonic acid buffer", *Proc. Natl. Acad. Sci*. U. S. A. **1987**, *84*, 76-79. c) M. G. N. Hartmanis, "Diol dehydrase from *Clostridium-Glycolicum*-the-non-B_{12}-dependent enzyme", *Met. Ions Biol. Sys*. **1994**, *30*, 201-215.

[31] T. Toraya, "The structure and mechanism of action of coenzyme B_{12}-dependent diol dehydratases", *J. Mol. Catal. B Enzym*. **2000**, *10*, 87-106.

[32] N. Shibata, J. Masuda, T. Tobimatsu, T. Toraya, K. Suto, Y. Morimoto, N. Yasuoka, "A new mode of B_{12} binding and direct participation of a potassium ion in enzyme catalysis: X-ray structure of diol dehydratase", *Structure Fold. Des.* **1999**, *7*, 997-1008.

[33] F. Mancia, N. H. Keep, A. Nakagawa, P. F. Leadlay, S. McSweeney, B. Rasmussen, P. Böecke, O. Diat, P. R. Evans, "How conenzyme-B_{12} radicals are generated: The crystal structure of methylmalonyl-coenzyme A mutase at 2Å resolution", *Structure* **1996**, *4*, 339-350.

[34] a) H. A. Lee, R. H. Abeles, "Purification and properties of dioldehydrase, an enzyme requiring a cobamide coenzyme", *J. Biol. Chem*. **1963**, *238*, 2367. b) T. Toraya, M. Uesaka, S. Fukui, "Coenzyme B_{12} dependent diol dehydratase system-dissociation of enzyme into 2 different protein components and some properties of components",

Biochemistry **1974**, *13*, 3895-3899. c) J. Masuda, Y. Yamaguchi, T. Tobimatsu, T. Toraya, K. Suto, N. Shibata, Y. Morimoto, Y. Higuchi, N. Yasuoka, "Crystallisation and preliminary X-ray study of two crystal forms of *Klebsiella oxytoca* diol dehydratase-cyanocobalamin complex", *Acta Crystallogr., Sect. D* **1999**, *55*, 907-909.

[35] B. Zagalak, P. A. Frey, G. L. Karabatsos, R. H. Abeles, "Stereochemistry of coversion of D and L 1,2-propanediols to propionaldehyde", *J. Biol. Chem*. **1966**, *241*, 3028.

[36] A. Ishida, T. Toraya, "Adenosylcobinamide methyl phosphate as a pseudocoenzyme for diol dehydrase", *Biochemistry* **1993**, *32*, 1535-1540.

[37] K. L. Schepler, W. R. Dunham, R. H. Sands, J. A. Fee, R. H. Abeles, "Physical explanation of EPR-spectrum observed during catalysis by enzymes utilising coenzyme-B_{12}*", Biochim. Biophys. Acta* **1975**, *397*, 510-518.

[38] P. Manitto, G. Speranza, G. Fontana, A. Galli, "Stereochemistry and fate of hydrogen atoms in the diol-dehydratase-catalysed dehydration of meso-butane-2,3-diol", *Helv. Chim. Acta* **1998**, *81*, 2005-2016.

[39] G. Speranza, C. E. Morelli, M. Orlandi, M. Scarpellini, P. Manitto, "Fate of oxygen atoms in the diol-dehydratase-catalysed dehydration of meso-butane-2,3-diol", *Helv. Chim. Acta* **2001**, *84*, 335-344.

[40] a) B. T. Golding, L. Radom, "On the mechanism of action of adenosylcobalamin"*, J. Am. Chem. Soc*. **1976**, *98*, 6331-6338. b) P. George, J. P. Glusker, C. W. Bock, "An *ab Initio* computational molecular orbital study of radical, protonated radical (radical cation), and carbocation species that have been proposed in mechanisms for the transfer process in the enzyme-coenzyme B_{12}-catalyzed dehydration of 1,2-dihydroxyethane", *J. Am. Chem. Soc*. **1997**, *119*, 7065-7074. c) M. Eda, T. Kamachi, K. Yoshizawa, T. Toraya, "Theoretical study on the mechanism of catalysis of coenzyme B_{12}-dependent diol dehydratase", *Bull. Chem. Soc. Jpn*. **2002**, *75*, 1469-1481. d) E. Hayon, M. Simic, "Acid-base properties of free Radicals in solution"*, Acc. Chem. Res*. **1974**, *7*, 114-119. e) V. N. Belevskii, D. A. Tyurin, N. D. Chuvylkin, "The role of radical cations in the radiation chemistry of aldehydes: An ESR study and a quantum chemical analysis", *High Energ. Chem*. **1998**, *32*, 424-435. f) M. Semialjac, H. Schwarz, "Computational exploration of rearrangements related to the vitamin B_{12}-dependent ethanolamine ammonialyase

catalysed transformation", *J. Am. Chem. Soc.* **2002**, *124*, 8974-8983. g) D. M. Smith, B. T: Golding, L. Radom, "Understanding the mechanism of B_{12}-dependent diol dehydratase: A synergistic retro-push-pull proposal", *J. Am. Chem. Soc.* **2001**, *123*, 1664-1675.

[41] A. Abend, V. Bandarian, G. H. Reed, P. A. Frey, "Identification of cis-ethanesemidione as the organic radical derived from glycolaldehyde in the suicide inactivation of dioldehydrase and of ethanolamine ammonia-lyase", *Biochemistry* **2000**, *39*, 6250-6257.

[42] a) R. J. Anderson, S. Ashwell, I. Garnett, B. T. Golding, "Intramoleculer functionalisation by a methylene radical of a 1,2-diol and a vicianl amino alcohol: Models for coenzyme B_{12} dependent diol dehydratase and ethanolamine ammonialyase", *J. Chem. Soc., Perkin Trans. 1,* **2000**, *24*, 4488-4498, b) D. M. Smith, B. T. Golding, L. Random, "Understanding the mechanism of B_{12}-dependent methymalonyl -CoA mutase: Partial prorton transfer in action", *J. Am. Chem. Soc.* **1999**, *121*, 5700-5704, c) R. J. Anderson, S. Ashwell, R. M. Dixon, B. T. Golding, "An improved model for B_{12}-dependent diol dehydrase", *J. Chem. Soc., Chem. Commun*. **1990**, 70-72.

[43] a) G. F. White, "Bacterial scission of ether bonds", *Microbiol. Rev*. **1996**, *60*, 216-232, b) S. Wagener, B. Schink, "Fermentative degradation of nonionic surfactants and polyethylene glycol by enrichment cultures and by pure cultures of homoacetogenic and propionate-forming bacteria", *Appl. Environ. Microbiol*. **1988**, *54*, 561-565, c) E. Schramm, B. Schink, "Ether-cleaving enzyme and diol dehydratase involved in anaerobic polyethylene glycol degradation by a new Acetobacterium sp.", *Biodegradation* **1991**, *2*, 71-79.

[44] a) D. I. Stirling, H. Daltonm, "Oxidation of dimethyl ether, methylformate and bromomethane by *Methylococcus Capsulatus* (Bath)", *J. Gen. Microbiol*. **1980**, *116*, 277-283, b) U. Karlson, D. F. Dwyer, S. W. Hooper, E. R. B. Moore, K. N. Timmis, L. D. Eltis, "Two independently regulated cytochormes P-450 in a *Rhodococcus rhodochrous* strain that degrades 2-ethoxyphenol and 4-methoxybenzoate", *J. Bacteriol*. **1993**, *175*, 1467-1464, c) I. G. Young, F. Gibson, "Regulation of enzymes involved in the biosynthesis of 2,3-dDihydroxybenzoic acid in *Aerobacter aerogenes* and *E. Coli*",

Biochim. Biophs. Acta **1969**, *177*, 401-411, d) F. Kawai, T. Kimura, M. Fukaya, Y. Tani, K. Ogata, T. Ueno, H. Fukami, "Bacterial oxidation of polyethylene glycol", *Appl. Environ. Microbiol*. **1978**, *40*, 701-705, e) E. Masai, Y. Katayama, S. Nishikawa, M. Yamasaki, N. Morohoshi, T. Haraguchi, "Detection and localisation of a new enzyme catalysisng the β-arylether cleavage in the soil bacterium *Pseudomonas paucimobilis* SYK-6", *FEBS lett*. **1993**, *249*, 348-352.

[45] M. Newcomb, "Competition methods and scales for alkyl radical reaction kinetics", *Tetrahedron* **1993**, *49*, 1151-1176.

[46] a) H. G. Kuivila, *Synthesis* **1970**, 499-509, b) C. Walling, J. H. Cooley, A. Á. Ponares, E. J. Racah, "Radical cyclisations in reactions of trialkyltin hydrides with alkenyl halides", *J. Am. Chem. Soc*. **1966**, *88*, 5361-5363, c) C. Chatgilialoglu, K. U. Ingold, J. C. Scaiano, "Rate constants and Arrhenius parameters for the reactions of primary, secondary, and tertiary alkyl radicals with tri-normal-butyltin hydride", *J. Am. Chem. Soc*. **1981**, *103*, 7739-7742, d) L. J. Johnston, J. Lusztyk, D. D. M. Wayner, A. N. Abeywickreyama, A. L. J. Beckwith, J. C. Scaiano, K. U. Ingold, "Absolute rate constants for reaction of phenyl-2,2-dimethylvinyl, cycloproyl and neopentyl radicals with tri-normal-butylstannane-comparison of the radical trapping abilities of tri-normal-butylstannane and germane", *J. Am. Chem. Soc*. **1985**, *107*, 4594-4596.

[47] a) M. Newcomb, S. U. Park, "N-Hydroxypyridine-2-thione esters as radical precursors in kinetic-studies-measurements of rate constants for hydrogen atom abstraction reactions", *J. Am. Chem. Soc*. **1986**, *108*, 4132-4134, b) M. Newcomb, A. G. Glenn, "A convenient method for kinetic-studies of fast radical rearrangements-rate constants and Arrhenius functions for the cyclopropylcarbinyl radical ring-opening", *J. Am. Chem. Soc*. **1989**, *111*, 275-277, c) D. H. R. Barton, D. Crich, W. B. Motherwell, "The invention of new radical chain reactions. 8. Radical chemistry of thiohydroxamic esters. A new method for the generation of carbon radicals from carboxylic-acids", *Tetrahedron* **1985**, *41*, 3901-3924, d) D. P. Curran, E.Bosch, J. Kaplan, M. Newcomb, "Rate constants for halogen atom transfer from representative alpha-halocarbonyl compounds to primary alkyl radicals", *J. Org. Chem*. **1989**, *54*, 1826-1831.

[48] a) A. L. J. Beckwith, , V. W. Bowry, K. U. Ingold, "Kinetics of nitroxide radical

trapping.1.Solvent effects", *J. Am. Chem. Soc*. **1992**, *114*, 4983-4992, b) V. W. Bowry, K. U. Ingold, "Kinetics of nitroxide radical trapping.2.Structural effects", *J. Am. Chem. Soc*. **1992**, *114*, 4992-4996.

[49] a) J. Lusztyk, B. Maillard, S. Deycard, D. A. Lindsay, K. U. Ingold, "Kinetics for the reaction of a secondary alkyl Radical with tri-*N*-butylgermanium hydride and caliberation of a secondary alkyl radical clock reaction", *J. Org. Chem*. **1987**, *52*, 3509-3514, b) C. Chatgilialoglu, J. Dickhaut, B. Giese, "Rate constants and Arrhenius parameters for the reactions of some carbon-centered radicals with tris(trimethylsilyl)silane", *J. Org. Chem*. **1991**, *56*, 6399-6403.

[50] a) D. Griller, K. U. Ingold, "Free-radical clocks", *Acc. Chem. Res*. **1980**, *13*, 317-323, b) R. Hollis, L. Hughes, V. W. Bowry, K. U. Ingold, "Calibration of a fast benzylic radical clock reaction", *J. Org. Chem*. **1992**, *57*, 4284-4287.

[51] D. C. Nonhebel, "The chemistry of the cyclopropymethyl and related radicals", *Chem. Soc. Rev*. **1993**, *22*, 347-359.

[52] V. W. Bowry, K. U. Ingold, "A radical clock investigation of microsomal cytochrome P-450 hydroxylation of hydrocarbons-rate of oxygen rebound", *J. Am. Chem. Soc*. **1991**, *113*, 5699-5707.

[53] a) A. J. Castellino, T. C. Bruice, "Intermediates in the epoxidation of alkenes by cytochrome P-450 models.2. Use of the trans-2, trans-3-diphenylcyclopropy substitutents in a search for radical intermediates", *J. Am. Chem. Soc*. **1988**, *110*, 7512-7519, b) T. G. Traylor, A. R. Miksztal, "Mechanisms of hemin-catalysed epoxidations-electron-transfer from alkenes", *J. Am. Chem. Soc*. **1987**, *109*, 2770-2774.

[54] a) J.-M. Kim, M. A. Bogdan, P. S. Mariano, "SET photochemistry of flavin cyclopropylamin systems-models for proposed monoamine-oxidase inhibition mechanism", *J. Am. Chem. Soc*. **1991**, *113*, 9251-9257, b) R. B. Silverman, Y Zelechonok, "Evidence for hydrogen atom transfer mechanism or a proton coupled fast electron-transfer mechanism for monoamine-oxidase", *J. Org. Chem*. **1992**, *57*, 6373-6374.

[55] a) I. McInnes, D. C. Nonhebel, S. T. Orszulik, C. J. Suckling, "On the mechanism of hydrogen transfer by nicotinamide coenzymes and alcohol dehydrogenase", *J. Chem.*

Soc., Perkin Trans. **1983**, 2777-2779, b) D. Laurie, E. Lucas, D. C. Nonhebel, C. J. Suckling, "On the mechanism of hydrongen transfer by nicotinamide coenzymes and alcohol dehydrogenase", *Tetrahedron* **1986**, *42*, 1035-1045.

[56] J. E. Baldwin, R. M. Adlington, D. G. Marquess, A. R. Pitt, A. T. Russell, "Evidence for an insertion homolysis mechanism for carbon sulfur bond formation in penicillin biosynthesis", *J. Chem. Soc. Chem. Commun.* **1991**, 856-858.

[57] S.-H. Kim, H. L. Chen, N. Feilchenfeld, J. Halpern, "Thermal decomposition and cobalt carbon bond-dissociation energies of organocobalamines-neopentyl, (cyclopentylmethyl), (cyclohexylmethyl), (tetrahydrofurfuryl), and (tetrahydropyryl)-methyl) cobalamin", *J. Am. Chem. Soc*. **1988**, *110*, 3120-3126.

[58] L. Z. Avila, J. W. Frost, "Monomeric meta-phosphate formation during radical-based dephosphorylation", *J. Am. Chem. Soc*. **1988**, *110*, 7904-7906.

[59] a) N. J. Forrow, S. J. Walters, "Transition metal half sandwich complexs as redox mediators to glucose oxidase", *Biosensors Bioelectron*. **2004**, *19*, 763-770, b) A. D. Ryabov, E. S. Ryabova, M. D. Reshetova, "Enzymatic chemistry of ferrocenes: micellar tuning of the glucose oxidase reactivity towards solubilized electrochemically generated n-alkylferro-cenium cations", *J. Organomet*. *Chem*. **2001**, *637*, 469-475.

[60] a) T. Kijima, T. Suzuki, T. Izumi, "Electrical communication between NAD-dependent enzyme and metal electrode using ferrocene-labelled NAD derivatives", *J. BioSci. BioEng.*, **2003**, *96*, 585-587, b) J. Razumiene, A. Vilkanauskyte, V. Gureviciene, V. Lurinavicius, N. V. Roznyatovskaya, Y. V. Ageeva, M. D. Reshetova, A. D. Ryabov, "New bioorganometallic ferrocene derivatives as efficient mediators for glucose and ethanol biosensors based on PPQ dependent dehydrogenases", *J. Organomet*. *Chem*. **2003**, *668*, 83-90.

[61] W. A. Wlassoff, G. C. King, "Ferrocene conjugates of dUTP for enzymatic redox labelling of DNA" *Nucleic Acid Res*. **2002**, *30*, 58.

[62] S.-J. Jong, J.-M. Fang, C.-H. Lin, "Reactions of acylferrocenes with samarium diiodide: reduction , deoxygenation, reductive coupling and rearrangment" *J. Organomet*. *Chem*. **1999**, *590*, 42-45.

[63] J. M. Bruce, D. Creed, "Light-induced and related reaction of quinones VI. Reactions

of some p-quinones carrying formyl groups", *J. Chem. Soc. C: Org*. **1970**, *5*, 649-653.

[64] S. Ohnishi, H. M. McConnell, "Interaction of the radical ion of chlorpromazine with deoxyribonucleic acid", *J. Am. Chem. Soc*. **1965**, *87*, 2293.

[65] J. F. W. Keana, "Newer aspects of the synthesis and chemistry of nitroxide spin labels", *Chem. Rev*. **1978**, *78*, 37-64.

[66] a) D. F. Bowman, T. Gillan, K. U. Ingold, "Kinetic applications of electron paramagnetic resonance spectroscopy. III. Self reactions of dialkyl nitroxide radicals", *J. Am. Chem. Soc*. **1971**, *93*, 6555, b) J. Martinie-Hombrouck, A. Rassat, "Nitroxides. 60. Isolation and autodecomposition of *N*-methyl 2, 4, 6-*N*-tri-t-butylphenyl nitroxide", *Tetrahedron* **1974**, *30*, 433.

[67] N. R. Cameron, A. J. Reid, P. Span, S. A. F. Bon, J. J. G. Steven van Es, A. L. German, "Studies on controlled radical polymerisation using 5-membered cyclic PROXYL nitroxides and corresponding alkoxyamines", *Macromol. Chem. Phys*. **2000**, *201*, 2510-2518.

[68] W. S. Gump, E. J. Nikawitz, "Adrenergic blocking agents.II. *N*-(2-chloroethyl)-*N*-(phenoxyethyl)-amine hydrochlorides", *J. Am. Chem. Soc*. **1950**, *72*, 3846-3851.

[69] K. C. Frisch, "Derivatives of *o*-and p-(α-phenylethyl)phenol", *J. Org. Chem*. **1950**, *15*, 587-592.

[70] E. Dyer, H. Scott, "Preparation of polymeric and cyclic urethanes and ureas from ethylene carbonate and amines", *J. Am. Chem. Soc*. **1957**, *79*, 672-675.

[71] P. L. Beaulieu, P. C. Anderson, D. R. Cameron, G. Corteau, V. Gorys, C. Grand-Maitre, D. Lamarre, F. Liard, W. Paris, L. Plamondon, F. Soucy, D. Thibeault, D. Wernic, C Yoakim, "2′-6′-Dimethoxyphenoxy acetyl: A new achiral high affinity P_3-P_2 ligand for peptidomimetic-based HIV protease inhibitors", *J. Med. Chem*. **2000**, *43*, 1094-1108.

[72] D. W. Robertson, E. E. Beedle, R. Lawson, J. D. Leander, "Imidazole anticonvulsants: structure-activity relationships of [(bipheylyloxy)alkyl]imidazoles", *J. Med. Chem*. **1987**, *30*, 939-943.

[73] A. Capiomont, J. Lajzerowicz-Bonneteau, "Study of the 2,26,6-tetramethyl-1-piperidine 1-oxyl nitroxide radical on tannane. II. Refining the crystallographic structure

of the disordered quadratic form", *Acta Crystallogr. Sect. B* **1974**, 2160-2166.

[74] a) J. Sobek, R. Martschke, H. Fischer, "Entropy control of the cross-reaction between carbon-centered and nitroxide radicals", *J. Am. Chem. Soc*. **2001**, *123*, 2489-2857, b) S. Marque, H. Fischer, E. Baier, A. Studer, "Factors influencing the C-O bond homolysis of alkoxyamines: Effects of H-bonding and polar substituents", *J. Org. Chem*. **2001**, *66*, 1146-1156, c) S. Marque, C. le Mercier, P. Tordo, H. Fischer, "Factors influencing the C-O bond homolysis of trialkylhydroxylamines", *Macromolecules* **2000**, *33*, 4403-4410.

[75] a) U. Jahn, P. Hartmann, I. Dix, P. G. Jones, "Lithium malonate enolates as prescursors for radical reactions-convenient induction of radical cyclisations with either radical or cationic termination", *Eur. J. Org. Chem*. **2001**, 3333-3355, b) U. Jahn, "Highly efficient generation of radicals from ester enolates by the ferrocenium ion. Application to selective alpha oxygenation and dimeristaion reactions of esters", *J. Org. Chem*. **1999**, *63*, 7130-7131.

[76] D. Dashyant, C. B. Reese, "Synthesis of [6][2,4]pyridinophanes", *J. Chem. Soc. Perkin Trans. 1* **1987**, 2829-2832.

[77] A. N. Osman, S. Botros, M. M. Kandeel, N. A. Khalil, H. A. Abdel El-Latif, "Synthesis and screening of certain aryloxyacetylaminoguanidines as potential antihypertensive agents", *Ind. J. Chem. Section B* **1996**, *35B*, 446-455.

[78] E. Elhalem, B. N. Bailey, R. Docampo, I. Ujváry, S. H. Szajnmann, J. B. Rodriguez, "Design, synthesis, and biological evaluation of arlyoxyethyl thiocyanate derivatives against *Trypanosoma Cruzi*", *J. Med. Chem*. **2002**, *45*, 3984-3999.

[79] H. L. Sham, D. A. Betebenner, X. Chen, A. Saldivar, S. Vasavanonda, D. J. Kempf, J. J. Plattner, D. N. Nortseck, "Synthesis and structure-activity relationships of a noval series of HIV-1 protease inhibitors encompassing ABT-378 (Lopinavir)", *Bioorg. Med. Chem. Lett*. **2002**, *12*, 1185-1187.

[80] S. L. Aleksandrova, E. A. Viktorova, "Oxyethylation of ortho-substituted phenols by ethylene oxide", *Vertnik Moskovskogo Univeristeta, Seriya 2: Khimiya* **1967**, *22*, 79-82.

[81] J. Atkinson, P. Morand, J. T. Arnason, "Analogues of the cyclic hydroxamic acid 2,4-dihydroxy-7-methoxy-2*H*-1,4-benzoxazin-3-one: Decomposition to benzoxazolinones and reaction with β-mercaptoethanol", *J. Org. Chem*. **1991**, *56*, 1788-1800.

[82] K. Wünsche, U. Schwaneberg, U. T. Bornscheuer, H. H. Meyer, "Chemoezymatic route to β-blockers via 3-hydroxy esters", *Tetrahedron: Asymmetry* **1996**, *7*, 2017-2022.

[83] M. P. Capparelli, R. E. DeSchepper, J. S. Swenton, "Structural and solvent/electrolyte effects on the selectivity and efficiency of the anodic oxidation of p-susbtituted aromatic ethers. An efficient route to quinol ether ketals and quinol ethers", *J. Org. Chem*. **1987**, *52*, 4953-4961.

[84] X. Zhang, W. H. Steel, R. A. Walker, "Probing solvent polarity across strongly associating solid/liquid interface using molecular rulers", *J. Phys. Chem. B* **2003**, *107*, 3829-3836.

[85] a) S. N. Müller, R. Batra, M. Senn, B. Giese, M. Kisel, O. Shadyro, "Chemsitry of C-2 glyceryl radicals: Indications for a new mechanism of lipid damage", *J. Am. Chem. Soc*. **1997**, *119*, 2795-2803, b) S. Peukert, R. Batra, B. Giese, "ESR evidence for a heterolytic C,O-bond cleavage in models of 4′-DNA radicals", *Tetrahedron Lett*. **1997**, *38*, 3507-3510, c) A. Dussy, E. Meggers, B. Giese, "Spontaneous cleavage of 4′-DNA radicals under aerobic conditions: Apparent discrepancy between trapping rates and cleavage products", *J. Am. Chem. Soc*. **1998**, *120*, 7399-7403.

[86] A. Hassner, R. H. Reuss, H. W. Pinnick, "Hydroxylation of carbonyl compounds via silylenol ethers", *J. Org. chem*. **1975**, *40*, 3427-3429, b) H. O. House, L. J. Czuba, M. Gall, H. D. Olmstead, "The chemistry of cananions. XVIII. Preparation of trimethylsilylenol ethers", *J. Org. chem*. **1975**, *34*, 2324--2336.

[87] G. M. Anantharamaiah, K. M. Sivanandaiah, "Transfer hydrogenation; a convenient method for removal of some commonly used protecting groups in peptide synthesis", *J. Chem. Soc. Perkin Trans. 1*, **1977**, 490-491.

[88] C. F. Tormena, R. Rittner, R. J. Abraham, "An NMR, IR and theoretical investigation of the methyl effect on conformational isomerism in 3-fluoro-3-methyl-2-butanone and 1-fluoro-3,3-dimethyl-2-butanone", *J. Phys. Org. Chem*. **2002**, *15*, 211-217.

[89] M. J. Earle, A. Abdur-Rashid, N. D. Priestley, "Large scale synthesis of cyclodiphospho-D-glycerate", *J. Org. Chem*. **1996**, *61*, 5697-5700.

[90] D. H. R. Barton, D. Crich, G. Kretzsehmar, "Formation of carbon-carbon bonds with radicals derived from the esters of thiohydroxamic acids", *Tetrahedron Lett*. **1984**, *25*,

1055-1058,

[91] a) C. Kolano, G. Bucher, H. H. Wenk, M. Jäger, O. Schade, W. Sander, "Photochemistry of 9-fluorenoneoxime phenylglyoxalate: a combined TRIR, TREPR and *ab initio* study", *J. Phys. Org. Chem*. **2004**, *17*, 207-214, b) G. Bucher, J. C. Sciano, R. Sinta, G. Barclay, J. Cameron, "Laser flash photolysis of carbamates derived from 9-fluorenone oxime", *J. Am. Chem. Soc*. **1995**, *117*, 3848-3855, c) G. Bucher, M. Halupka, C. Kolano, O. Schade, W. Sander, "Characterisation of alkoxycarbonyl radicals by step-scan time-resolved infrared spectroscopy", *Eur. J. Org. Chem*. **2001**, 545-552.

[92] a) H. Bhandal, V. F. Patel, G. Pattenden, J. J. Russel, "Cobalt-mediated radical reactions in organic synthesis. Oxidative cyclisations of aryl and alkyl halides leading to functionalised reduced heterocycles and butyrolactones", *J. Chem. Soc. Perkin Trans. 1*, **1990**, 2691-2701, b) H. Bhandal, A. R: Howell, V. F. Patel, G. Pattenden, "Cobalt-mediated intermolecular radical additions to carbon-to-carbon double bonds leading to a new functionalised alkenes", *J. Chem. Soc. Perkin Trans. 1*, **1990**, 2709-2714, c) G. Pattenden, "Cobalt-mediated radical reactions in organic synthesis", *Chem. Soc. Rev*. **1988**, *17*, 361-382.

[93] E. N. Marvell, M. J. Joncich, "The preparations of α-bromoacetals", *J. Am. Chem. Soc*. **1951**, *73*, 973-975.

[94] L.-Y. Hsu, C.-H. Lin, "Synthesis and biological evaluation of 3-hydroxymethylpyrimido-[1,6-c]oxazine derivatives", *Heterocycles* **1996**, *43*, 2687-2699.

[95] D. L. Jameson, J. J. Grzybowski, D. E. Hammels, R. K. Castellano, M. E. Hoke, K. Freed, S. Basquill, A. Mendel, W. J. Shoemaker, "Synthesis of some cobaloxime derivatives: a demonstration of "umpolung" in the reactivity of an organometallic complex", *J. Chem. Edu*. **1998**, *75*, 447-450.

[96] M. Schmittel, G. Gescheidt, M. Röck, "First Spectroscopic Identification of an Enol Radical Cation in Solution: The Anisyl-Dimesitylethenol Radical Cation", *Angew. Chem. Int. Ed*. **1994**, *106*, 1961-1963.

[97] a) D. H. R. Barton, C. Y. Chern, J. C. Jaszberenyi, "The Invention of Radical Reactions. 34. Homologation of Carboxylic-Acids to Alpha-Keto Carboxylic-Acids by Barton-Ester Based Radical-Chain Chemistry", *Tetrahedron* **1995**, *51*, 1867-1886, b) D.

H. R. Barton, J. C. Jaszberenyi, W. S. Liu, "The Invention of Radical Reactions. 36. Synthetic studies related to 3-deoxy-D-manno-2-octulosonic acid (KDO)", *Tetrahedron* **1996**, *52*, 2717-2726, c) P. O. Whitted, J. H. Horner, M. Newcomb, D. Crich, "Heterolytic cleavage of a beta-phosphatoxyalkyl radical resulting in phosphate migration or radical cation formation as a function of solvent polarity", *Org. Lett*. **1999**, *1*, 153-156, d) M. Newcomb, N. Miranda, X. Huang, D. Crich, "Laser flash photolysis kinetic studies of alpha-methoxy-beta-phosphatoxyalkyl radical heterolysis reactions: A method for alkoxyalkyl radical cation detection", *J. Am. Chem. Soc*. **2000**, *122*, 6128-6129, f) D. H. R. Barton, D. Crich, P. Potier, "On the Mechanism of the Decarboxylative Rearrangement of Thiohydroxamic Esters", *Tetrahedron Lett*. **1985**, *26*, 5943-5946.

[98] M. Newcomb, J. Kaplan, "Rate constants and Arrhenius function for scanvenging of octyl radical by an N-hydroxypyridine-2-thione ester", *Tetrahedron Lett*. **1987**, *27*, 1615-1618.

[99] M. M. Alam, A. Watanabe, O. Ito, "Laser flash photolysis of dithio-2,2′-dipyridine; Structure and reactivity of pyridyl-2-thio radical", *J. Org. Chem*. **1995**, *60*, 3440-3444.

[100] B. M. Aveline, I. E. Kochevar, R. W. Redmond, "Photochemistry of N-hydroxypyridine-2-thione derivatives: involvement of the 2-pyridylthiyl radical in the radical chain reaction mechanism", *J. Am. Chem. Soc*. **1995**, *117*, 9699-9708.

[101] a) K. H. Lee, K.-L. Chin, "Electron spin resonance spectra of free radicals. Part 3. 2,2-Disubstituted 1,3-dioxolan-4-yl radicals", *J. Chem. Soc. Perkin Trans. 2*, **1985**, 161-164, b) G. Behrens, E. Bothe, G. Koltzenburg, D. Schulte-Frohlinde, "Formation and structure of 1,1-dialkoxyalkene radical cations in aqueous solution. An in situ electron spin resonance and pulse conductivity study", *J. Chem. Soc. Perkin Trans. 2*, **1980**, 883-889, c) G. Trampe, J. Mattay, S. Steenken, "Ionisation of 1,3-dioxoles in aqueous solution by 248-nm laser flash photolysis characterisation of the radical cations", *J. Phys. Chem*. **1989**, *93*, 7157-7160.

[102] R. V. Bensasson, E. J. Land, T. G. Truscott, "Flash Photolysis and Pulse Radiolysis", 1983, Pregamon Press, Oxford.

[103] a) M. Anbar, M. Bambenek, A. B. Ross, *Nat. Stand. Ref. Data Ser. Nat. Bur. Stand*. **1973**, 43, b) M. Anbar, A. B. Farhataziz, A. B. Ross, *Nat. Stand. Ref. Data Ser. Nat. Bur.*

Stand. **1975**, 51.

[104] a) H. Scherz, "Formation of deoxycompounds and malondialdehyde in irradiated aqueous solution of carbohydrates and related compounds", *Radiat. Res*. **1970**, *43*, 12-24, b) P. J. Baugh, J. S. Moore, A. F: Norris, C. von Sonntag, "γ-Radiolysis of N2O-saturated aqueous glycerol solution: Product yields and free radical mechanism", *Radiat. Phys. Chem*. **1982**, *20*, 215-222, c) S. Kawakishi, Y. Kito, M. Namiki, "Formation of 1-deoxy-D-threo-2,5-hexodiulose by radication induced chain reaction in crystalline D-fructose", *Agr. Bio. Chem*. **1975**, *39*, 1897-1898, d) M. Dizdaroglu, H. Scherz, C. von Sonntag, "γ-Radiolysis von meso-Erythrit in wäßriger lösung", *Z. Naturforsch*. **1972**, *27b*, 29-41.

[105] a) K. M. Bansal, M. Grätzel, A. Henglein, E. Janata, "Polarographic and optical absorption studies of radicals produced in the pulse radiolysis of aqueous solution of ethylene glycol", *J. Phys. Chem*. **1973**, *77*, 16-19, b) S. Steenken, M. J. Davis, B. C. Gilbert, "Pulse radiolysis and electron spin resonance studies of the dehydration of radicals from 1,2-diols and related compounds", *J. Chem. Soc. Perkin Trans. 2* **1986**, 1003-1010, c) B. C. Gilbert, J. P. Larkin, R. O. C. Norman, "Electron spin resonance studies. Part XXXIII. Evidence for heterolytic and homolytic transformations of radicals from 1,2-diols and related compounds", *J. Chem. Soc. Perkin Trans. 2* **1972**, 794-802.

[106] S. Steenken, "Oxidation of phenolates and phenylenediamines by 2-alkanonyl radicals produced from 1,2-dihydroxy- and 1-hydroxy-2-alkoxyl radicals", *J. Phys. Chem.* **1979**, *83*, 595-599.

[107] M. Dixon, E. C. Webb, Enzymes, 3rd. Ed., 1979, Academic Press, New York.

[108] M. L. Andersen, N. Mathivanan, D. D. M. Wayner, "Electrochemistry of electron-transfer probes. The role of the leaving group in the cleavage of radical anions of α-aryloxyacetophenones", *J. Am. Chem. Soc*. **1996**, *118*, 4871-4879, b) C. Vannuci, P. Fornier de Violet, H. Bouas-Laurent, A. Castellan, "Photochemical degradation of lignin: a photophysical and photochemical study of a nonphenollic α-carbonyl β-*O*-4-lignin model dimer, 3,4-dimethoxy-α-(2′-methoxyphenoxy)acetophenone", *J. Photochem. Photobiol. A: Chemistry* **1988**, *41*, 251-265, c) D. D. Tanner, J. J. Chen, L. Chen, C. Luelo, "Fragmentation of substituted acetophenone and halobenzophenone ketyls. Calibration of a mechanistic probe *J. Am. Chem. Soc*. **1991**, *113*, 8074-8081, c) J. M.

Tanko, R. E. Drumright, N. K. Suleman, L. E. Brammer, "Radical ion probes 3. The importance of resonance vs. strain energy in the design of SET probes based upon the cyclopropycarbinyl-to-homoallyl radical rearragement", *J. Am. Chem. Soc*. **1994**, *113*, 8074-8081.

[109] a) G. Speranza, B. Müller, M. Orlandi, C. F. Morelli, P. Manitto, B. Schink, "Mechanism of anaerobic ether cleavage", *J. Biol. Chem*. **2002**, *277*, 11684-11690, b) G. Speranza, B. Müller, M. Orlandi, C. F. Morelli, P. Manitto, B. Schink, "Stereochemistry of the conversion of 2-phenoxyethanol into phenol and acetaldehyde by *Acetobacterium* sp.", *Helv. Chim. Acta* **2003**, *86*, 2629-2636.

[110] a) H. D. Zook, W. E. Smith, J. L. Greene, "Rearrangement of ketones in acid media", *J. Am. Chem. Soc*. **1957**, *79*, 4436-4439, b) L. W. Kendrick Jr., B. M. Benjamin, C. J. Collins, "Molecular reararangements. XIII. Additional evidence for the mechanism of the aldehyde-ketone rearrangement", *J. Am. Chem. Soc*. **1958**, *80*, 4057-4065

[111] Y. Apeloig, M. Karni, B. Ciommer, G. Depke, G. Frenking, S. Meyn, J. Schmidt, H. Shwarz, "Mechanism of keto-reversible –enol tautomerism of ionised vinylalcohol versus acetaldehyde and their dissociation to $C_2H_3O^+$and H. An ab initio molecular-orbital study", *Int. J. Mass Spectrom.Ion Phys*. **1984**, *59*, 21-37.

[112] W. J. Bouma, J. K. Macleod, L. Radom, "An ab initio molecular orbital study of the structures and stabilities of the $C_2H_4^{+\bullet}$ isomers", *J. Am. Chem. Soc*. **1979**, *101*, 5540-5545.

[113] a) B. Albrecht, M. Allan, E. Haselbach and L. Neuhaus, "Molecular ions of transient species-vinyl alcohol cation", *Helv. Chim. Acta*, **1984**, *67*, 216-219, b) N. Heinrich, J. Schmidt, H. Schwarz, Y. Apeloig, "On the mechanism of $(C,H_3,O)\bullet$ loss from ionised methyl acetate. An ab initio molecular orbital study", *J. Am. Chem. Soc*. **1987**, *109*, 1317-1322.

[114] a) J. L. Holmes, J. K. Terlouw, F. P. Lossing, "The thermochemistry of $C_2H_4O^+$ ions", *J. Phys. Chem*. **1976**, *80*, 2860, b) F. Turecek, V. Hanus, "Mass-spectra of ethenol and its deuteron analogs", *Org. Mass Spectrom*. **1984**, *19*, 423-427.

[115] N. P. Schepp, "Generation and Absolute Reactivity of an Aryl Enol Radical cation in Solution", *J. Org. Chem*. **2004**, *69*, 4931-4935.

[116] B. Capon, C. Zucco, "Simple Enols. 2. Kinetics and Mechanism of the Ketonisation of Vinyl Alcohol", *J. Am. Chem. Soc*. **1982**, *104*, 7567-7572.

[117] a) J. H. Horner, E. Taxil, M. Newcomb, "Laser Flash Photolysis Kinetic Studies of Enol Ether Radical Cations. Rate Constants for Heterolysis of α-Methoxy-β-phosphatoxyalkyl Radicals and for Cylcisations of Enol Ether Radical Cations", *J. Am. Chem. Soc*. **2002**, *124*, 5402-5410, b) B. C. Bales, J. H. Horner, X. Huang, M. Newcomb, D. Crich, M. M. Greenberg, "Product Studies and Laser Flash Photolysis on Alkyl Radicals Containing Two Different β-Leaving Groups Are Consonant with the Formation of an Olefin Cation Radical", *J. Am. Chem. Soc*. **2001**, *123*, 3623-3629, c) E. Taxil, L. Bagnol, J. H. Horner, M. Newcomb, "Efficient Production of Enol Ether Radical Cations by Heterolytic Cleavage of β-Mesylate Radicals", *Org. Lett*. **2003**, *5*, 827-830.

[118] a) L. L. Schaleger, C. N. Richards, "Medium Effects on the Activation Parameters for A-1 Dioxolane Hydrolysis in Water-Glycerol Mixtures", *J. Am. Chem. Soc*. **1970**, *92*, 5565-5570, b) M. M. Kreevoy, R. Taft Jr., "Acid Catalysed Hydrolysis of Acetal and Chloroacetal", *J. Am. Chem. Soc*. **1955**, *77*, 3146-3148.

[119] M. O. F. Goulart, J. H. P. Utley, "Electroorganic reactions. 31. Quinonemethide radical anions and dianions. Their cathodic generation and reactivity", *J. Org. Chem*. **1988**, *53*, 2520-2525.

[120] H.-D. Becker, K. Gustafsson, "Preparations and reactions of 2,6-di-tert-butyl-4-(9-fluorenylidene)-1,4-benzoquinone", *J. Org. Chem*. **1976**, *41*, 214-221.

[121] K. Yoshida, "Electrooxidation in Orgainc Chemistry" Wiley-Interscience, New York (1984).

[122] H. R. Thirsk, J. A. Harrison, "Electrode Kinetics", Academic Press, London (1972).

[123] a) R. S. Nicholson, I. Shain, "Theory of Stationary Electrode Polarograophy" *Anal. Chem*. **1964**, *36*, 706-723, b) R. S. Nicholson, I. Shain, "Semiempirical Procedure for Measuring with Stationary Electrode Polarography Rates of Chemical Reactions Involving the Product of Electron Transfer", *Anal. Chem*. **1966**, *38*, 1406.

[124] C. Bohne, D. MacDonald, H. B. Dunford, "Measurements of rates and equilibria for keto-enol tautomerism of aldehydes using horseradish peroxidase compound I", *J. Am. Chem. Soc*. **1986**, *108*, 7867-7868.

[125] J. F. G. Barrett, A. Rasheed, D. L. Corina, "Partial reactions of D-glucose-6-phosphate-1L-mayoinositol-1-phosphate cyclase", *J. Biochem.* **1973**, *131*, 21-30.

[126] a) F. Westheimer, "Mechanism of enzymic decarboxylation of acetoacetic acid", *Proc. Chem. Soc*. **1963**, 253, b) D. L. Leussing, M. Emly, "Application of Marcus theory to metal ion catalysed group transfer reactions", *J. Am. Chem. Soc*. **1984**, *106*, 443.

[127] a) R. L. Hill, J. W. Teipel, in *The Enzymes*, 3rd ed. Vol. V (Ed. P. Boyer), Academic Press, New York, 1971, 539-571, b) J. P. Glusker, in *The Enzymes*, 3rd ed. Vol. V (Ed. P. Boyer), Academic Press, New York, 1971, 413-439, c) S. M. Afrin, "Evidence for an enol intermediate in the enzymatic conversion of α, β-dihydroxyisovalerate to α-ketoisovalerate", *J. Biol. Chem*. **1969**, *244*, 2250.

[128] a) S. Ghisla, C. Thorpe, V. Massey, "Mechanistic studies with general acyl-CoA dehydrogenase and butyryl-CoA dehydrogenase: evidence for the transfer of the β-hydrogen to flavin position (N5) as a hydride", *Biochemistry* **1984**, *23*, 3154-3161, b) G. Fendrich, R. H. Abeles, "Mechanism of action of butyryl-CoA dehydrogenase: reactions with acetylenic, olefinic and fluorinated substrate analogs", *Biochemistry* **1982**, *23*, 6685-6695.

[129] a) H. Hart, Z. Rappoport, S. E. Biali, *The Chemistry of Enols*, S. Patai, Z. Rappoport (eds), Wiley, Chichester, 1990; 481-589, b) Z. Rappoport, S. E. Biali, *Acc. Chem. Res.* 1988, 21, 442-449, c) A. F. Hegarty, P. O´Neill, *The Chemistry of Enols*, S. Patai, Z. Rappoport (eds), Wiley, Chichester, 1990; 639-650.

[130] a) M. Schmittel, A. Burghart, "Understanding reactivity patterns of radical cations", *Angew. Chem.* **1997**, *109*, 2659-2699, b) M. Schmittel, M. Keller, A. Burghart, Z. Rappoport, A. Langels, "Electronic effects in polyarylvinyl propellars. Solid state structures and dynamic behaviour in solution of several crowded enol derivatives", *J. Chem. Soc. Perkin Trans. 2* **1998**, 869-875, c) M. Schmittel, G. Gescheidt, L. Eberson, H. Trenkle, "Persistent benzofuran radical cations in solution. A cyclic voltammetry and EPR/ENDOR study", *J. Chem. Soc. Perkin Trans. 2* **1997**, 2145-2150.

[131] a) M. Schmittel, A. Langels, "Enol radical cations in solution part 13. First example of radical dication rearrangement. One-electron oxidation of dihydrobenzofuranyl cations leads to drastic rate enhancement in the oxidative benzofuran formation from enols", *J.*

Org. Chem. **1998**, *63*, 7328-7337, b) M. Schmittel, M. Röck, "Enol radical cations in solution, 3. Reaction of enol radical cations in the presence of nucleophiles", *Chem. Ber*. **1992**, *125*, 1611-1620, c) M. Röck, M. Schmittel, "α-Carbonyl cation chemistry from enolate oxidation", *J. Chem. Soc. Chem. Commun*. **1993**, 1739-1741, d) M. Röck, M. Schmittel, "A new efficient synthesis of 4,6,7-trimethylbenzofurans by oxidation of β-mesityl substituted enols", *J. Prakt. Chem*. **1994**, *336*, 325-329.

[132] a) T. Maki, Y. Araki, Y. Ishida, O. Onomura, A. Matsumura, "Construction of persistent phenoxy radical with intramolecular hydrogen bonding", *J. Am. Chem. Soc*. **2001**, *123*, 3371-3372, b) N. Gupta, H. Linschitz, "Hydrogen-bonding and protonations effects in electrochemistry of quinones in aprotic solvents", *J. Am. Chem. Soc*. **1997**, *119*, 6384-6391.

[133] a) T. Kajiki, H. Moriya, K. Hoshino, T. Kuroi, S.-I. Kondo, T. Nabeshima, Y. Yano, "Functionalized flavin receptors. Regulation of redox properties of 6-azaflavin via hydrogen bondings with melamine derivatives bearing guanidinium ion(s) in organic solvents", *J. Org. Chem*. **1999**, *64*, 9679-9689, b) L. H. Bradley, R. P. Swenson, "Role of hydrogen bonding interactions to N(3) H of the flavin mononucleotide cofactor in the modulation of redox potentials of the *Clostridium beijerinckii* flavodoxin", *Biochemistry* **2001**, *40*, 8686-8695.

[134] a) M. Oelgemöller, A. G. Griesbeck, J. Lex, A. Haeuseler, M. Schmittel, M. Niki, D. Hesek, Y. Inoue, "Structural, Cyclic Voltammetric and IR-Spectral Evidences for Preorientation in PET-Active Phthalimido Carboxylic Acids", *Org. Lett.* **2001**, 3, 1593-1596, b) M. Oelgemöller, A. Haeuseler, M. Schmittel, A. G. Griesbeck, J. Lex, Y. Inoue, "Hydrogen Bonding in Phthalimido Carboxylic Acids: Cyclic Voltammography Study and Correlation with Photochemical Reactivity. Part 2. Aliphatic and Aromatic Acids", *J. Chem. Soc. Perkin Trans. 2* **2002**, 676-86.

[135] R. C. Fuson, J. Crose, C. H. McKeever, "A stable vinyl alcohol, 1, 2-dimesityl-1-propen-1-ol", *J. Am. Chem. Soc*. **1940**, *62*, 3250.

[136] M. Kaftory, S. E. Biali, Z. Rappoport, "Stable simple enols 9. Solid-state structures and conformations of several simple enols and their keto tautomers", *J. Am. Chem. Soc*. **1985**, *107*, 1701-1709.

[137] a) Jr, J. C. Davis, K. S. Pitzer, C. N. R. Rao, "Nuclear magnetic resonance studies of hydrogen bonding II. Alcohols", *J. Phys. Chem.* **1960**, *64*, 1744-1747, b) C. M. Huggins, G. C. Pimentel, J. N. Shoolery, "Proton magnetic resonance studies of the hydrogen bonding of phenol, substituted phenols and acetic acid. *J. Phys. Chem.* **1956**, *60*, 1311-1314, c) C. Beeson, N. Pham, Jr, G. Shipps, T. A. Dix, "A comprehensive description of the free energy of an intramolecular hydrogen bond as a function of solvatin: nmr study", *J. Am. Chem. Soc*. **1993**, *115*, 6803-6812.

[138] a) S. E. Biali, Z. Rappoport, "Stable simple enols. 5. Solvent dependence of the conformation of the OH group in 2, 2-dimesitylethenol and several 1, 2, 2-triarylethenols", *J. Am. Chem. Soc*. **1984**, *106*, 5641-5653, b) Z. Rappoport, D. A. Nugiel, S. E. Biali, "Association of α-alkyl-β, β-dimesitylethenols hydrogen-bond-accepting solvents", *J. Org. Chem*. **1988**, *53*, 4814-4821.

[139] M. Schmittel, A. Langels, "A short-lived radical dication as a key intermediate in the rearrangement of persistent cation. The oxidative cyclisation of 2,2-dimesityl-1-(4-N,N-dimethylaminophenyl)ethenol", *Angew. Chem., Int. Ed. Engl*. **1997**, *34*, 392-395.

[140] N. P. Schepp, "Generation and absolute reactivity of an aryl enol radical cation in solution", *J. Org. Chem*. **2004**, *69*, 4931-4935.

[141] a) B. Zinger, J. Y. Becker, "Anodic oxidation of allenic hydrocarbons in methanol", *Electrochim. Acta* **1980**, *25*, 791-793, b) J. Y. Becker, B. Zinger, "Electrochemical oxidation of alkyl-substituted allenes in methanol", *Tetrahedron* **1982**, *38*, 1677-1682, c) J. Y. Becker, B. Zinger, "Electrochemical oxidation of allenic hydrocarbons in acetonitrile", *J. Chem. Soc. Perkin Trans. 2* **1982**, 395-401.

[142] a) H.-U. Siehl, "Excursions into Long-Lived Vinyl Cations: NMR Spectroscopic Characterisation of α-Aryl Vinyl Cations", Stable Carbocation Chemistry, G. K. Suryaprakash, P. v. R. Schleyer (eds), John Wiley and Sons, New York, 1997, 165-196, b) H.-U. Siehl, *J. Chem. Soc. Chem. Commun*. **1984**, 635, c) G. A. Olah, R.-J. Spear, P. W. Westerman, J. M. Denis, "Stable carbocations. CLXXIII. C-13 nuclear magnetic resonance studies of alkylnylcarbenium ions and alkynoyl cations. Relative importance of mesomeric vinylic (allenylic) cation forms", *J. Am. Chem. Soc*. **1974**, *96*, 5855, d) G. A. Olah, A. L. Barrier, L. D. Field, G. K. S. Prakash, "Stable carbocations. 238. Two and

three fold degenrate rearragements in di and trimethylcyclopropylcarbinyl cations", *J. Am. Chem. Soc*. **1982**, *104*, 5855.

[143] M.-A. Orliac-Le Moing, G. Le Guillanton, "Anodic behaviour of unsaturated systems-II. An evidence of a specific oxidation step for enols", *Electrochim. Acta* **1982**, *27*, 1775-1780.

[144] a) D. D. M. Wayner, D. Griller, "Oxidation and reduction potentials of transient free-radicals", *J. Am. Chem. Soc*. **1985**, *107*, 7764-7765, b) D. D. M. Wayner, D. J. MacPhee, D. Griller, "Oxidation and reduction potentials of transient free-radicals", *J. Am. Chem. Soc*. **1988**, *110*, 132-137, c) B. A. Sim, P. H. Milne, D. Griller, D. D. M. Wayner, "Thermodynamic significance of RHO^+ and RHO^- from substituent effects on the redox potentials of arylmethyl radicals", *J. Am. Chem. Soc*. **1990**, *112*, 6635-6638, d) D. D. M. Wayner, B. A. Sim, "Thermodynamic properties of carbocations and carbanions-solvation effects from an electrochemical and theoretical (AM1) study of some substituted benzyl radicals", *J. Org. Chem*. **1991**, *56*, 4853-4858, e) T. Nagaoka, D. Griller, D. D. M. Wayner, "Digital-simulation of photomodulation voltammograms-reactivity of the diphenylmethyl carbanion and carbocation in acetonitrile", *J. Phys. Chem*. **1991**, *95*, 6264-6270.

[145] a) G. D. Hawkins, C. J. Cramer, D. G. Truhlar, "Parametrized models of aqueous free energies of solvation based on pairwise descreening of solute atomic charges from a dielectric medium", *J. Phys. Chem*. **1996**, *100*, 19824-19839, b) C. J. Crammer, D. G. Truhlar, "Implicit solvation models: Equilibria, structure, spectra and dynamics", *Chem. Rev*. **1999**, *99*, 2161-2200.

[146] K. H. Diêp Lê, F. Lederer, "Amino acid sequence of long chain α-hydroxy acid oxidase from rat kidney, a member of the family of FMN-dependent α-hydroxyacid-oxidising enzymes", *J. Biol. Chem*. **1991**, *266*, 20877-20881.

[147] a) J. J. Hasford, W. Kemnitzer, C. J. Rizzo, "Conformational effects on flavin redox chemistry", *J. Org. Chem*. **1997**, *62*, 5244-5245, b) D. H. Evansm, N. Xie, "Electron transfer reactions and associated conformational changes. Studies of bianthrone reduction via homegenous catalysis", *J. Am. Chem. Soc*. **1983**, *105*, 315.

[148] a) F.-C. C. Chang, R. P. Swenson, "The midpoint potentials for the oxidised-

semiquinone couple for Gly57 mutants of the *Clostridium beijerinckii* flavodoxin correlate with changes in the hydrogen bonding interaction with the proton on N(5) of the reduced flavin mononucleotide cofactor as measured by NMR chemical shift temperature dependencies", *Biochemistry* **1999**, *38*, 7168-7176, b) S. Shinkai, N. Honda, Y. Ishikawa, O. Manabe, "Coenzyme models. 41. On the unusual reactivities of N(5)-hydrogen-bonded flavin. An approach to regiospecific flavin activation through hydrogen bonding", *J. Am. Chem. Soc*. **1985**, *117*, 6286-6292.

[149] L. J. Druhan, R. P. Swenson, "Role of methionine 56 in the control of oxidation-reduction potentials of the *Clostridium beijerinckii* flavodoxin: effects of substitutions by aliphatic amino acid and evidence for a role of sulphur flavin interactions", *Biochemistry* **1998**, *37*, 9668-9678.

[150] J. J. Hasford, C. J. Rizzo, "Reduction of Hg (II) EDTA by conformationally biased flavins", *Tetrahedron Lett*. **1998**, *39*, 1317-1320.

[151] M. Schmittel, M. Lal, R. Lal, Z. Rappoport, J. Schlirf, H. –J. Deiseroth, manuscript in prepartation.

[152] Patric, J. O´Malley, "Density functional calculations modelling the spin density distribution , hyperfine couplings, and hydrogen bonding environment of the ascorbate (Vitamin C) free radical", *J. Phys. Chem. B* **2001**, *105*, 11290-11293.

[153] J. B. H. Bielski, D. A. Comstok, R. A. Bowen, "Ascorbic acid free radicals. 1. Pulse radiolysis study of optical absorption and kinetic properties", *J. Am. Chem. Soc*. **1971**, *93*, 5624-5629.

[154] a) Y. Kirino, T. Kwan, "Free radicals formed during oxidation of L-ascorbic acid or hydroxytetronic acid with hydrogen peroxide and titanium (III) ions", *Chem. Pharm. Bull*. **1971**, *19*, 718-, b) Y. Kirino, T. Kwan, "ESR studies of ascorbic acid free radicals", *Chem. Pharm. Bull*. **1972**, *20*, 2651-2660, c) G. P. Laroff, R. W. Fessenden, R. H. Schuler, "Electron spin resonance spectra of radical intermediates in the oxidation of ascorbic acid and related substances", *J. Am. Chem. Soc*. **1972**, *94*, 9062.

[155] a) R. J. Kolt, D. D. M.Wayner, D. Griller, "Using electron-transfer reactions to propagate radical chain processes", *J. Org. Chem*. **1989**, *54*, 4259, b) V. J. Lilie, G. Beck, A. Henglein, "Pulse radiolysis and polarography -half-wave potentials for oxidation and

reduction of short-lived organic radicals on Hg electrode", *Ber. Bunsen-Ges. Phys. Chem*. **1971**, *75*, 458.

[156] T. Lund, D. D. M. Wayner, M. Jonsson, A. G. Larsen, K. Daasbjerg, "Oxidation potentials of α-hydroxyalkyl radicals in acetonitrile obtained by photomodulated voltammetry", *J. Am. Chem. Soc*. **2001**, *123*, 12590-12595.

[157] D. D. M. Wayner, A. Houmam, "Redox properties of free radicals", *Acta Chem. Scand.* **1998**, *52*, 377-384.

[158] a) J. B. Edel, R. Fortt, J. C. deMello, A. J. deMello, "Microfluidi routes to the controlled production of nanoparticles", *Chem. Commun*. **2002**, 1136-1137, b) T. Funii, Y. Sando, K. Higashino, Y. Fujii, "A plug and play microfluidic device", *Lab Chip* **2003**, *3*, 193-197, c) P. He, S. J. Haswell, P. D. I. Fletcher, "Microwave heating of heterogenously catalysed Suzuki reactions in a micro reactor", *Lab Chip* **2004**, *4*, 38-41, d) J. deMello, A. deMello, "Microscale reactors: nanoscale products", *Lab Chip* **2004**, 4, 11N-15N, e) C. Wiles, P. Watts,, S. J. Haswell, E. Pombo-Villar, "Steroselective alkylation of an Evans auxilliary derivative with a pressure-driven micro reactor", *Lab Chip* **2004**, *4*, 171-173.

[159] a) Y.-X. Wang, J. W. Cooper, C. S. Lee, D. L. DeVoe, "Efficient electrospray ionisation from polymer microchannels using integrated hydrophobic memberanes", *Lab Chip* **2004**, *4*, 363-367, b) J. A. Schwartz, J. V. Vykoukal, R. C. Gascoyne, "Droplet-based chemistry on a programmable micro-chip", *Lab Chip* **2004**, *4*, 11-17, c) M. K. Runyoun, B. L. Johnson-Kerner, R. F. Ismagilov, "Minimal Functional Model of Hemostasis in a Biomimetic Microfluidic System", *Angew. Chem. Int. Ed*. **2004**, *43*, 1531-1536.

[160] P. Paik, V. M. Pamula, M. G. Pollack, R. B. Fair, "Elecrtowetting-based droplet mixers for microfluidic systems", *Lab Chip* **2003**, *3*, 28-33.

[161] M. Koch, D. Chatelain, A. G. R. Evans, A. Brunnschweiler, "Two simple micromixers based on silicon", *J. Micromech. Microeng*. **1998**, *8*, 123-126.

[162] S. C. Jacobson, T. E. Mcknight, J. M. Ramsey, "Microfluidic Devices for Electrokinetically Driven Parllel and Serial Mixing", *Anal. Chem.* **1999**, *71*, 4455-4459.

[163] a) T. J. Johnson, D. Ross, L. E. Locascio, "Rapid microfluidic mixing", *Anal. Chem.*

2002, *74*, 45-51, b) A. D. Stroock, S. K. W. Dertinger, A. Ajdari, I. Mezic, H. A. Stone, G. M. Whitesides, "Chaotic Mixer for Microchannels", *Science* **2002**, *295*, 647-651.

[164] R. H. Liu, M. A. Stremler, K. V. Sharp, M. G. Olsen, J. G. Santiago, R. J. Adrian, H. Aref, D. J. Beebe, "Passive Mixing in a Three Dimensional Serpentine Microchannel", *J. Microelectromech. Syst*. **2000**, *9*, 190-197, b) B. He, B. J. Burke, X. Zhang, R. Zhang, F. E. Regnier, "A Picoliter Volume Mixer for Microfluidic Analytical Systems", *Anal. Chem.* **2001**, *73*, 1942-1947, c) C. Erbacher, F. Bessoth, M. Busch, E. Verpoorte, A. Manz, "Towards Integrated Continous-Flow Chemical Reactors", *Microchim. Acta*, **1999**, *131*, 19-24.

[165] M. H. Oddy, J. G. Santiago, J. C. Mikkelsen, "Electrokinetic instability micromixing", *Anal. Chem.* **2001**, *73*, 5822-5832.

[166] H.-P. Chou, M. A. Unger, S. R. Quake, "A microfabricated rotary pump", *Biomed. Microdev.* **2001**, *3*, 323-330.

[167] a) Z. Yang, S. Matsumoto, H. Goto, M. Matsumoto, R. Maeda, "Ultrasonic micromixer for microfluidic systems", *Sens. Actuators A* **2001**, *93*, 266-272, b) J. C. Rife, M. I. Bell, J. S. Horwitz, M. N. Kabler, R. C. Y. Auyeung, W. J. Kim, "Miniature valveless utrasonic pumps and miers", *Sens. Actuators A* **2000**, *86*, 135-140.

[168] R. F. Ismagilov, "Integrated Microfluidic Systems", *Angew. Chem. Int. Ed.* **2003**, *42*, 4130-4132.

[169] a) K. Handique, D. T. Burk, C. H. Mastrangelo, M. A. Burns, "On-Chip Thermopneumatic Pressure for Discrete Drop Pumping", *Anal. Chem.* **2001**, *73*, 1831-1838, b) K. Hosokawa, T. Fujii, I. Endo, "Handling of Picoliter Liquid Samples in a Poly(dimethylsiloxane)-based Microfluidic Device", *Anal. Chem.* **1999**, *71*, 4781-4785, c) K. Handique, D. T. Burke, C. H. Mastrangelo, M. A. Burns, "Nanoliter Liquid Metering in Microchannels Using Hydrophobic Patterns", *Anal. Chem.* **2000**, *72*, 4100-4109.

[170] M. A. Burns, C. H. Matrangelo, T. S. Sammarco, F. P. Man, J. R. Webster, B. N. Johnson, B. Foerster, D. Jones, Y. Fields, A. Kaiser, D. T. Burke, "Microfabricated structures for integrated DNA analysis", *Proc. Natl. Acad. Sci. USA*, **1996**, *93*, 5556-5561.

[171] O. Sandre, L. Gorre-Talini, A. Ajdari, J. Prost, P. Silberzan, "Moving droplets on asymmetrically structured surfaces", *Phys. Rev. E* **1999**, *60*, 2964-2972.

[172] a) R. Rosario, D. Gust, M. Hayes, F. Jahnke, J. Springer, A. A. Garcia, "Photon-Modulated Wettability Changes on Spiropyran-Coated Surfaces", *Langmuir* **2002**, *18*, 8062-8069, b) J. Y. Shin, N. L. Abbott, "Using light to control dynamic surface tensions of aqueous solution of water soluble surfactants", *Langmuir* **1999**, *15*, 4404.

[173] T. B.Jones, M. Gunki, M. Washizu, M. J. Feldman, "Dielectrophoretic liquid actuation and nanodroplet formation", *J. Appl. Phys.* **2001**, *89*, 1441-1448.

[174] a) M. G. Pollack, A. D. Shenderov, R. B. Fair, "Electrowetting-based actuation of droplets for integrated microfluidics", *Lab Chip* **2002**, *2*, 96-101, b) P. Haik, V. K. Pamula, M. G. Pollack, R. B. Fair, "Electrowetting-based droplet mixers for microfluidic systems", *Lab Chip* **2003**, *3*, 28-33, c) M. G. Pollack, R. B. Fair, A. D. Shenderov, "Electrowetting-based actuation of liquid droplets for microfluidic applications", *Appl. Phys. Lett.* **2000**, *77*, 1725-1726, d) H. J. J. Verheijen, M. W. J. Prins, *Langmuir* **1999**, *15*, 6616, M. W. J. Prins, W. J. J. Welters, J. M. Weekemp, *Science* **2001**, *291*, 277, E. Seyart, R. A. Hayes, "Amorphous fluoropolymers as insulators for reversible low-voltage electrowetting", *J. Appl. Phys.* **2001**, *90*, 1383.

[175] a) X. Zu, J. F. Rusling, "Amphiphilic Ferrocene Alcohols as Electroactive Probes in Micerllar Solutions and Microemulsions", *Langmuir*, **1997**, *13*, 3693-3699, b) A. P. Abbott, G. Gounili, J. M. Bobbitt, J. F. Rusling, "Electron Transfer between Amphiphilic Ferrocenes and Electrodes in Cationinc Micellar Solution", *J. Phys. Chem.* **1992**, *96*, 11091-11095.

[176] a) T. Saji, K. Hoshino, Y. Ishii, M. Goto, "Formation of Organic Thin Films by Electrolysis of Surfactants with the Ferrocenyl Moiety", *J. Am. Chem. Soc.* **1991**, *113*, 450-456, b) P. Anton, J. Heinze, A. Laschewsky, "Redox-Active Monomeric and Polymeric Surfactants", *Langmuir* **1993**, *9*, 77-85.

[177] a) K. Wang, G. W. Gokel, "Redox-Switched Amphiphiles: Oxidised Ferrocene Derivatives Form Stable Vesicles when either one or two Alkyl tairs are Present", *J. Phys. Org. Chem.* **1997**, *10*, 323-334, b) K. Wang, S. Muñoz, L. Zhang, R. Castro, A. E. Kaifer, G. W. Gokel, "Organometallic Amphiphiles: Oxidized Ferrocene as Headgroup

for Redox-Swtiched Bilayer and Monolayer Membranes", *J. Am. Chem. Soc.* **1996**, *118*, 6707-6715.

[178] a) M. Subramanian, S. K. Mandal, S. Bhattacharya, "Electroactive Depostis of Anthraquionone- Attached Micelle and Vesicle-Forming Surfactant Assemblies on Glassy Carbon Surfaces", *Langmuir* **1997**, *13*, 153-160, b) M. Gomez, J. Li, A. E. Kaifer, "Surfactant Monolayers on Electrode Surfaces: Self-Assembly of a Series of Amphiphilic Viologens on Gold and Tin Oxide", *Langmuir*, **1991** *7*, 1797-1806, c) J. Li, A. E. Kaifer, "Surfactant Monolayers on Electrode Surfaces: Self-Assembly of a Viologen Derivative Having a Cholesteryl Hydrophobic Residue", *Langmuir* **1993**, *9*, 591-596.

[179] J. Lahann, S. Mitragotri, T.-N. Tran, H. Kaido, J. Sundaram, I. S. Choi, S. Hoffer, G. A. Somorjai, R. Langer, "A Reversibly Switching Surface", *Science* **2003**, *299*, 371-374.

[180] X. Wang, A. B. Kharitonov, E. Katz, I. Willner, "Potential-controlled molecular machinery of bipyridinium monolayer-functionalized surfaces: an electrochemical and contact angle analysis", *Chem. Commun*. **2003**, 1542-1543.

[181] A. Schulz, W. Kaim, "Elektrochemische und spekroskopische Charakterisierung von N, N´-Dialkylchinoxalinium-Redoxsystemen", *Chem. Ber*. **1991**, *124*, 129-139.

[182] T. J. Curphey, K. S. Prasad, "Diquartenary Salts. I. Preparation and Characterisation of Diquartenary Salts of some Diazines and Diazoles", *J. Org. Chem*. **1972**, *37*, 2259-2266.

[183] S. Hunig, J. Groß, "Reversible redox system of Weitz-Type", *Tetetrahedron Lett*. **1968**, 2599-2604.

[184] A. Schulz, W. Kaim, H.-D. Hausen, "Crystalline heterocyclic radical cation salts as stable intermediates of new redox-mediating systems", *J. Chem. Soc. Faraday Trans. I* **1988**, *84*, 3207-3214.

[185] a) F. P. Nicoletta, D. Cupelli, G. De Filpo, G. Chidichimo, "Electrochromism in switchable nematic emulsions", *Appl. Phys. Lett*. **2004**, *84*, 4260-4262, b) H. Karatani, W. Naohisa, T. Sugimoto, "Voltammetric and spectroelectrochemical characterisation of a water-soluble viologen polymer and its application to electron-transfer mediator for enzyme free regeneration of NADH", *Bioelectrochem*. **2003**, *60*, 57-64.

[186] a) I. Langmuir, "The constitution and fundamental properties of solids and liquids. II.

Liquids", *J. Am. Chem. Soc*. **1917**, *39*, 1848-1906, b) K. B. Blodgett, "Films built by depositing successive monomolecular layers on a solid surface", *J. Am. Chem. Soc*. **1935**, *57*, 1007-1022.

[187] G. Roberts (ed), *Langmuir-Blodgett Films*, Plenium Press, New York, 1990

[188] G. J. Walther, J. Baumgartner, "Asymmetric dihydroxylation reactions leading to novel chiral ferrocene derivatives", *Tetrahedron Asymmetry* **1998**, *9*, 2081-2085.

[189] R. Adams, R. E. Rindfusz, "Cyclic ethers from o-allylphenols; methylene coumaranes", *J. Am. Chem. Soc.* **1919**, 648-665.

[190] A. G. M. Barrett, B. T. Hopkins, A. C. Love, L. Tedeschi, "Parellel synthesis of terminal alkynes using a ROMPgel-supported ethyl 1-diazo-2-oxopropylphonate", *Org. Lett.* **2004**, *6*, 835-837.

[191] D. R. Buckle, C. J. M. Rockell, "A versatile two-stage synthesis of 2-susbtituted benzo[*b*]furans from (2-methoxyphenyl)ethynes", *J. Chem. Soc. Perkin Trans. 1*, **1985**, 2433-2447.

[192] P. J. Skabara, I. M. Serebryakov, I. F. Perpichka, "Electron acceptors of the fluorene series. Part 8. Electrochemical and intramolecular charge transfer studies of thiophene functionalised fluorenes", *J. Chem. Soc. Perkin Trans. 2* **1999**, 505-513.

[193] D. Horton, J. B. Hughes, J. K. Thomson, "Extension of sugar chains through acetylenic intermediates. IV. Derivatives of 1-pentyne-D-erythro(and D-threo)-3,4,5-triol", *J. Org. Chem.* **1968**, *33*, 728-734.

[194] K. Danielmeier, E. Steckhan, "Efficient pathways to (*R*)- and (*S*)-5-hydroxymethyl-2-oxazolidinone and some derivatives", *Tetrahedron Asymmetry* **1995**, *6*, 1181-1190.

[195] K. Shibata, I. Katsuyama, M. Matsui, H. Muramatsu, "Synthesis of ferrocenyl-substituted 3-cyano-2-methylpyridines", *Bull. Chem. Soc. Jpn.* **1990**, *63*, 3710-3712.

[196] J. G. Rodriguez, A. Onate, R. M. Martin-Villamil, I. Fonseca, "A practical synthesis of ethynylferrocene from ferrocenecarboxaldehyde: structure of 1,4-ferrocenyl-1,3-butadiyne", *J. Organomet. Chem.* **1996**, *513*, 71-76.

[197] T. Inokuchi, S. Matsumoto, S. Torii, "Indirect electrooxidation of alcohols by a double mediatory system with two redox couples of $[R_2N^+=O]$/R2NO$^\bullet$ and $[Br^\bullet$ pr $Br^+]/Br^-$ in an organic-aqueous two-phase solution", *J. Org. Chem.* **1991**, *56*, 2416-2421.

[198] B. Bhatia, T. punniyamurthy, J. Iqbal, "Cobalt [II]-catalyzed reaction of aldehydes with acetic anhydride under an oxygen atmosphere: Scope and mechanism", *J. Org. Chem.* **1993**, *58*, 5518-5523.

[199] A. Natarajan, J. D. Ferrara, W. J. Youngs, C. H. Sukenik, "Micellar control of organic reactions: propellane substrates as a streochemical probes for micellar binding", *J. Am. Chem. Soc.* **1987**, *109*, 7477-7483.

[200] a) D. E. Ames, G. Hall, B. T. Warren, "Long-chain acyloins and vicinal diketones", *J. Chem. Soc. C* **1968**, 2617-2621, b) V. L. Hansley, "The preparation of high molecular weight acycloins", *J. Am. Chem. Soc.* **1935**, 2303-2305.

[201] R. M. Adlington, J. E. Baldwin, D. Catterick, G. J. Pritchard, "The, efficient enantioselective synthesis of quinoxalin, pyrazine and 1, 2, 4-triazine substituted α-amino acids from vicinal tricarbonyls", *J. Chem. Soc. Perkin Trans. 1* **2001**, 668-679.

[202] V. T. Nguyen, P. D. Ahn, R. Bishop, M. L. Scudder, D. C. Craig, "Molecular solids formed by the self organisation of dialcohols into hydrogen-bonded ladders", *Eur. J. Org. Chem.* **2001** 4489-4499.

[203] a) G. M. Sheldrick, *SHELEX-97*, "A programme for crystal solution", University of Göttingen, Germany, 1997, b) G. M. Sheldrick, *SHELEX-97/2*, "A programme for the refinement of crystal structures", University of Göttingen, Germany, 1997

[204] M. Kaftory, S. E. Biali, Z. Rappoport, "Stable simple enols. 9. Solid state structures and conformations of several simple enols and their keto tautomers", *J. Am. Chem. Soc.* **1985**, *107*, 1701-1709.

[205] M. C. Etter, "Encoding and decoding hydrogen-bond patterns of organic compounds", *Acc. Chem. Res*. **1990**, *23*, 120-126.

[206] F. H. Allen, S. W. D. Motherwell, P. R. Raithby, G. P. Shields, R. Taylor, "Systematic analysis of the probabilities of formation of bimolecular hydrogen-bonded ring motifs in organic crystal structures", *New J. Chem*. **1999**, 25-34.

[207] M. Öki, "1,9-Disubstituted triptycenes: an excellent probe for weak molecular interactions", *Acc. Chem. Res*. **1990**, *23*, 351-356.

[208] Y. Kodama, K. Nishihata, M. Nishio, Y. Iitaka, "X-ray study of (α-SS, α-SR)-1-(*p*-bromophenyl)ethyl-t-butyl sulfoxide and conformational-analysis of diasteromeric pairs

of 1-phenylethyl-t-butyl sulfoxides", *J chem. Soc. Perkin Trans. 2*, **1976**, 1490-1495.

[209] a) R. A. Copeland, "Enzymes-A Practical Introduction to Structure, Mechanism, and Data Analysis", 1996, Wiley-VCH, New York, b) R. B. Silverman, "The Organic Chemistry of Enzyme-Catalysed Reactions", **2000**, Academic Press, San Diego, California.

[210] a) V. Henri, *Lois Générales de l'actiondes diastases*, 1903, Hermann, Paris, b) L. Michaelis, M. L. Menten, *Biochem. Z.* **1913**, *49*, 333-369.

[211] H. Lineweaver, J. Burk, "The determination of enzyme dissociation constants", *J. Am. Chem. Soc.* **1934**, *56*, 658-666.

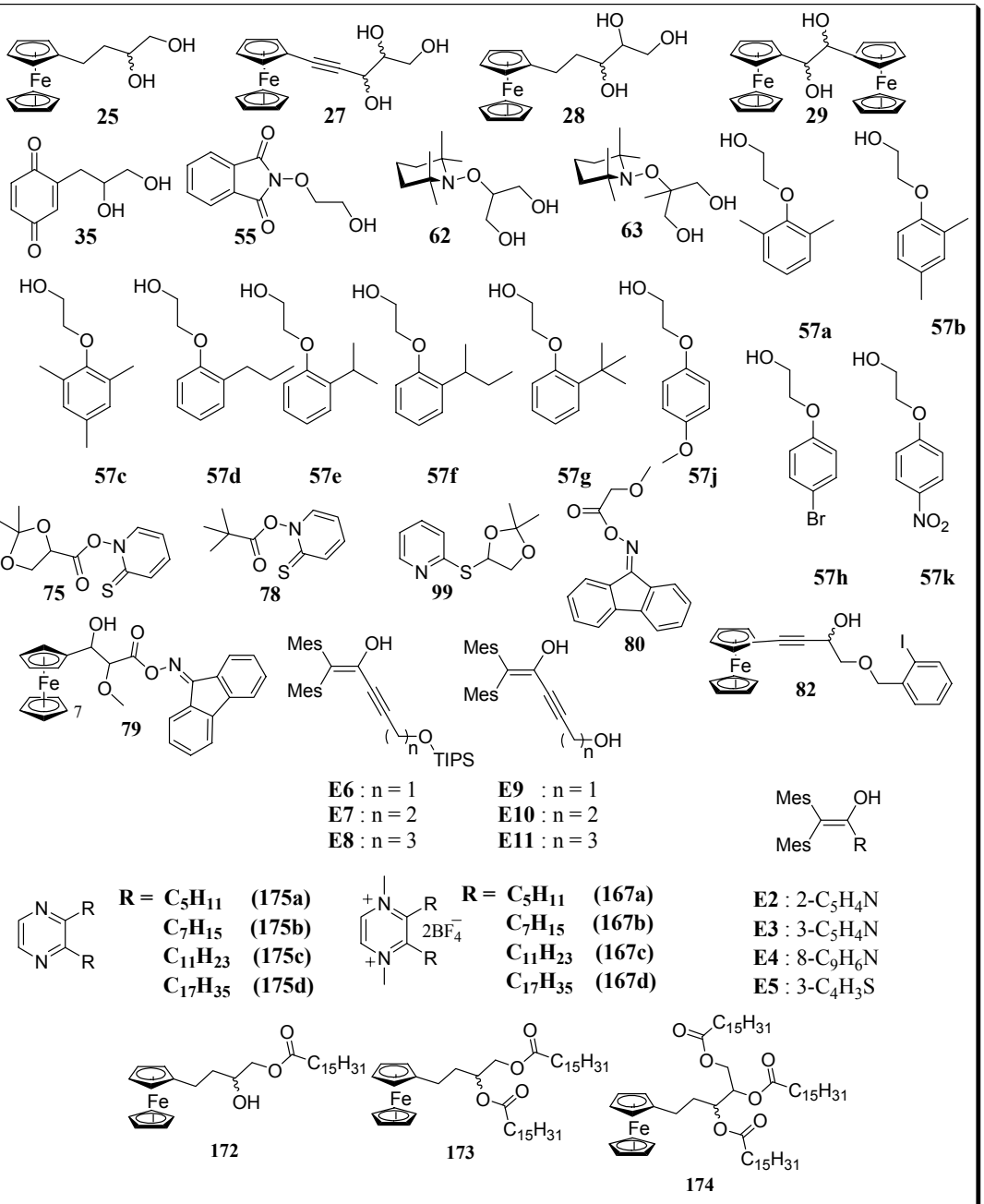
25
27
28
29
35
55
62
63
57a
57b
57c
57d
57e
57f
57g
57j
57h
57k
75
78
99
80
82
79
E6 : n = 1
E7 : n = 2
E8 : n = 3
E9 : n = 1
E10 : n = 2
E11 : n = 3
R = C5H11 (175a)
C7H15 (175b)
C11H23 (175c)
C17H35 (175d)
R = C5H11 (167a)
C7H15 (167b)
C11H23 (167c)
C17H35 (167d)
E2 : 2-C5H4N
E3 : 3-C5H4N
E4 : 8-C9H6N
E5 : 3-C4H3S
172
173
174